GEOCHEMICAL AND THERMODYNAMIC CONTROLS IN THE FORMATION OF MINERAL ASSEMBLAGES FROM THE METAMORPHIC AUREOLE OF THE BUSHVELD COMPLEX IN THE POTGIETERSRUS AREA

BY

JOHANNES NELL

Submitted in partial fulfilment of
the requirements for the degree of
MASTER OF SCIENCE
in the Faculty of Science,
University of Pretoria.

DECEMBER 1984

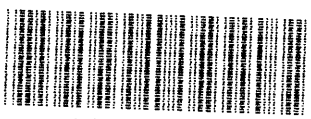

Study and in general
the pursuit of truth
and beauty is a sphere
of activity in which we
are permitted to remain
children all our lives

Albert Einstein

ABSTRACT

The metamorphic aureole of the Bushveld Complex in the Potgietersrus area was created in a two-stage metamorphic event. In the first stage which was related to the intrusion of the lower zone magma, maximum temperatures of 750°C were attained at 1,5 kbar pressure. Pressure estimates are based on the rare cordierite + olivine + orthopyroxene $\pm$ spinel $\pm$ quartz assemblage. At lower temperatures the cordierite + chloritoid assemblage also appears to have been stable.

Equilibrium temperatures and pressures during the second stage, which was brought about by the intrusion of more voluminous gabbroic liquids that gave rise to the upper critical, main and upper zones were considerably higher at 900°C and 4 to 5 kbar pressure. Geothermobarometry is based on the garnet + cordierite + orthopyroxene + biotite; clinopyroxene + plagioclase + quartz and cordierite + spinel $\pm$ sillimanite $\pm$ corundum $\pm$ orthopyroxene $\pm$ olivine assemblages. The temperature dependence of the Mg-Fe exchange reaction between cordierite and spinel was used as the basis of a geothermometer calibrated against published data for natural mineral assemblages. High alumina (44 wt. percent), low silica (36 wt. percent) and low alkali pelites from the Timeball Hill Formation also originated during this stage through the removal of about 65 percent granitic melt from normal pelites.

The maximum pressures calculated for the second stage of the metamorphic event are about 2 kbar higher than the lithostatic pressure that could have been exercised by the presently exposed succession of layered- and roof-rocks. This difference can be accounted for by a directed stress contribution, which there is evidence for in the form of a large fold in the floor rocks, and by assuming that the lithostatic pressure during the second stage of the metamorphic event was about 1,0 kbar higher than the value suggested by the current field relations, brought about by a superincumbent load of layered rocks.

SAMEVATTING

Die kontakoureool van die Bosveldkompleks in die omgewing van Potgietersrus het deur 'n tweefase metamorfe episode ontstaan. Gedurende die eerste fase, wat deur die inplasing van die laersone magma veroorsaak is, is temperature van 750°C onder 'n druk van 1,5 kbar behaal. Die berekening van druk is gebaseer op die seldsame kordiëriet + olivien + ortopirokseen ± spinel ± kwarts assosiasie. By laer temperature was die kordiëriet + chloritoïed assosiasie skynbaar stabiel.

Ewewigstemperature en -drukke gedurende die tweede fase, wat veroorsaak is deur die inplasing van 'n groter volume gabroïese magma waaruit die kritieke-, hoof- en bosones gekristalliseer het, was aansienlik hoër teen 900°C en 4 tot 5 kbar druk. Geotermobarometrie is gebaseer op die granaat + kordiëriet + ortopirokseen + biotiet; klinopirokseen + plagioklaas + kwarts en kordiëriet + spinel ± sillimaniet ± korundum ± ortopirokseen ± olivien assosiasies. Die temperatuursensitiewe Mg - Fe uitruilreaksie tussen kordiëriet en spinel is as 'n geotermometer gekalibreer deur die data van natuurlike mineraalassosiasies te gebruik. Hoë alumina (44 gewigspersentasie), lae silika (36 gewigspersentasie) en lae alkali pelitiese gesteentes van die Timeball Hillformasie het ook gedurende die fase deur die onttrekking van ongeveer 65 persent granitiese materiaal vanuit gewone pelitiese gesteentes ontstaan.

Die maksimum druk wat vir die tweede fase van die metamorfe episode bereken is, is ongeveer 2 kbar hoër as die litostatiese druk wat deur die huidiglik blootgestelde opeenvolging van gelaagde- en dakgesteentes uitgeoefen kon word. Die verskil kan verklaar word deur 'n gerigte druk bydrae, waarvoor 'n groot plooi in die vloergesteentes as bewys dien, en deur aan te neem dat die litostatiese druk gedurende die tweede fase van die metamorfe episode ongeveer 1,0 kbar hoër was as die waarde wat tans deur die veldverhoudings gesuggereer word, as gevolg van 'n bykomstige hoeveelheid gelaagde gesteentes.

CONTENTS

LIST OF FIGURES IN THE TEXT

LIST OF TABLES IN TEXT

1. INTRODUCTION

1.1 General background

The metamorphic aureole of the Bushveld Complex provides a unique opportunity to study a variety of metamorphic assemblages which crystallized at intermediate pressures and a range of temperatures between about 400°C and 1200°C.

This thesis contains the results of an investigation of the metamorphosed rocks of the Transvaal Sequence bordering the Potgietersrus limb of the Bushveld Complex. The study area proved particularly rewarding since a number of mineral assemblages were encountered of which the experimentally determined stability conditions have been published in the literature, thus making the calculation of physical conditions of metamorphism possible. The transgression of the Bushveld Complex across the Transvaal Sequence in the area furthermore allowed the investigation of metamorphic reactions in calcareous- and pelitic rocks of divergent chemical composition and at a wide range of metamorphic temperatures.

The investigation was initiated as part of a honours project during July 1980. Further mapping and sampling was undertaken during the summer months of 1980 - 1981. In the process, a total area of about 320 sq. km. was mapped on aerial photographs on a scale of 1 : 30 000 and subsequently reduced to a scale of 1 : 50 000. A total of 450 samples were collected of which 300 were examined in thin section. This led to the selection of samples for mineral chemical investigations, as well as for whole-rock analyses.

1.2 Location and physiography

A simplified geological map which shows the location of the study area relative to the Bushveld Complex is presented in Figure 1.

The morphology of the region is a direct expression of the geology. Quartzites form prominent north-south trending

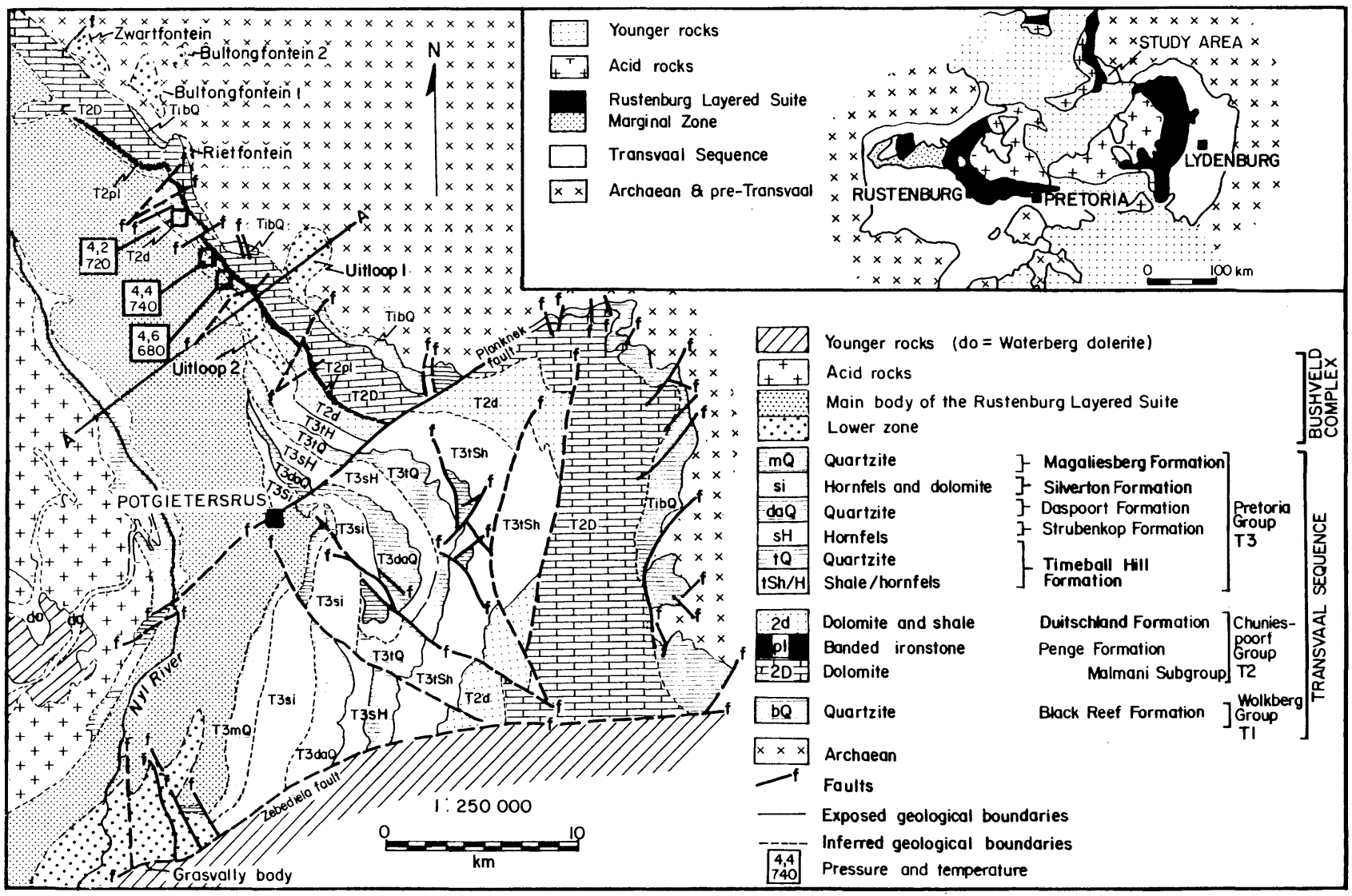

Fig. 1: Simplified geological map of the Rustenburg Layered Suite and metamorphosed Transvaal Sequence in the Potgietersrus area.

ridges with barren dip slopes. Less resistant shales or hornfelses form the easterly slopes of the ridges. Dolomites crop out as rounded hills with gentle slopes.

Outcrops of the layered rocks of the Bushveld Complex are very poor and occupy a broad valley flanked by sediments of the Transvaal Sequence to the east and by a continuous series of steep hills comprising the acid roof-rocks to the west. The northward draining Nyl River in the valley is the only major river in the area.

1.3 Previous work in the area

The geology of the area surrounding Potgietersrus first received the attention of Molengraaff in 1901 when he investigated roof-rocks of the Bushveld Complex near Potgietersrus. In 1909 Hall described the dolomite member of the Silverton Formation and concluded that these rocks were actually marls. Subsequent to that Hall and Gardthausen (1911) investigated xenoliths of Pretoria Group rocks in the layered rocks south of the Potgietersrus station. The paper contains the first, and so far only description of kyanite from the Bushveld aureole. In the same year (1911) Kynaston and Hall wrote an explanation for the first published geological map of the Potgietersrus area.

Zagt (1942) investigated the relationship between the Bushveld Complex and the Transvaal Sequence, while Truter (1947) concluded that a certain quartzite block occurring in the Pretoria Group and previously considered to be part of the Waterberg Group belongs to the Timeball Hill Formation and that it reached its present position through transcurrent faulting. He also examined a fold in the Daspoort Formation and presented a structural analysis of the area.

In 1954 Van Rooyen revised the existing geological map of the area. This map proved extremely useful during this investigation. Van der Merwe (1978) examined the layered rocks of the Bushveld Complex along the Potgietersrus limb, although he also mapped the adjacent Transvaal Sequence rocks.

Various other workers, for example Hulbert (1983) concentrated on certain aspects of the layered igneous rocks but paid little attention to the metamorphosed floor rocks.

2. STRATIGRAPHY

2.1 General Geology

The Transvaal Sequence in the study area can be divided into two sectors separated by the Planknek fault. There is a distinct difference in the thickness and general strike of the various lithological units in the two sectors (Fig. 1, Folder 1).

South of the Planknek fault the Transvaal Sequence covers an area of about 500 sq. km. that is bounded by the Bushveld Complex to the west, the Pietersburg Group and the Archaean granites to the east and the Zebediela fault to the south. The Wolkberg- and Chuniespoort Groups are fully developed in this sector and the Magaliesberg Quartzite forms the highest stratigraphic unit in the Pretoria Group that is in contact with the Bushveld Complex. North of the Planknek fault rocks of the Wolkberg Group are absent and the Chuniespoort- and Pretoria Groups are considerably reduced in thickness. The transgression of the Bushveld Complex across the floor rocks leads to the complete elimination of the Transvaal Sequence about 30 km north of the fault.

The layered rocks of the Bushveld Complex form an S-shaped body with its strongest curvature towards the south where it is in contact with the Transvaal Sequence. In the north, where rocks of the Transvaal Sequence have been completely overstepped, the layered rocks are in contact with Archaean granites. To the west the layered rocks are overlain by the various acid rocks of the Bushveld Complex while the Zebediela fault truncates the layered rocks to the south.

2.2 The Transvaal Sequence

2.2.1 The Black Reef Quartzite

This unit has been examined only in the northern sector of the study area since it has not been significantly affected by the thermal metamorphism in the southern sector.

Button (1973) expressed the view that the quartzite north of the Planknek fault belongs to the Wolkberg Group because it bears no resemblance to the true Black Reef Quartzite developed to the south of the Planknek fault. This implies that the Black Reef Quartzite must have pinched out in the vicinity of the Planknek fault, a feature that was ascribed by Button (1973) to the presence of the Uitloop Platform to the north. This structurally positive feature probably resulted through the Planknek fault that was active in early Transvaal times.

The basal quartzite in the northern sector received little attention in the study and despite Button's doubt, the name Black Reef Quartzite was retained in order to conform to the nomenclature used on the 2428 Nylstroom 1 : 250 000 geological map. The quartzite thins rapidly towards the north until only a thin sliver is present between the Malmani Subgroup and Archaean granite on the farm Tweefontein 238 KR.

2.2.2 The Chuniespoort Group

2.2.2.1 The Malmani Subgroup

The Malmani Subgroup was only examined in the northern sector because no metamorphic minerals are developed in this unit south of the Planknek fault. No attempt was made to distinguish the various formations of the subgroup (Folder 1) because the thinning of the subgroup towards the north and the transgression of the Bushveld Complex preclude the identification of the various formations.

The Malmani Subgroup comprises relatively chert-rich and chert-poor units. Carbonaceous shale layers are common throughout the subgroup and a few quartzite beds occur near the base. The top of the subgroup is characterized by a heterogeneity of lithologies which include dolomite, chert, limestone and ferruginous chert. Ferruginous chert

oolites are present in iron-rich dolomite directly underlying the Penge Formation. At low metamorphic grades radial amphibole prisms developed around the oolites and amphibole bundles occur on the contacts between chert and dolomite layers. The ferruginous chert oolites may be related to Button's "Iron Formation Precursor" which is an assemblage of iron-rich dolomite with layers of chert, iron-rich amphibole and iron oxides (Button, 1973).

Dolomites from the chert-poor units are dark brown in colour on weathered surface while dolomites from the chert-rich units assume a grey colour on weathered surface. Sedimentary structures are present in the form of domical stromatolites, crinkly algal laminations and rare oolites occurring in granular dolomite.

Tremolite, clinopyroxene and olivine are typical minerals that appear with increasing metamorphic grade. Wollastonite is rare while idocrase and grossularite occur in dolomites of the impure upper unit of the subgroup.

2.2.2.2 The Penge Formation

The Penge Formation was only examined north of the Planknek fault where it is sporadically exposed from the farm Planknek 43 KS in the south to Tweefontein 238 KR in the north. There is a gradational contact between the Penge Formation and the Malmani Subgroup. The ferruginous chert oolites near the top of the Malmani Subgroup are thought to represent the first stage in the gradation. Interlaminated layers of iron silicates, chert and iron oxides constitute the principal iron formation which is overlain by carbonaceous shale. The chemical sediments are extremely unstable when exposed to oxidizing atmospheric conditions. The components decompose to hydrous iron oxides and clays which are subsequently silicified to produce the hard resistant rocks observed in outcrop today.
It is therefore impossible to obtain fresh samples and the principal iron formation has received little attention in the course of this study.

Quartzo - feldspathic rocks of uncertain origin are developed within the Penge Formation on the farm Rietfontein 2 KS. Van Rooyen (1950) argued in favour of a sedimentary origin for these rocks but the matter is not satisfactoraly resolved yet.

2.2.2.3 The Duitschland Formation

The dolomites of this formation represent the lowest stratigraphic level in the southern sector that have been metamorphosed by the Bushveld Complex. Despite poor exposures in the northern sector, the formation can be traced from its type locality, the farm Duitschland 95 KS in the southern sector, to the farm Tweefontein 238KR where it is finally truncated by the Bushveld Complex.

In general, the Duitschland Formation is a heterogeneous unit in which shale and dolomite are approximately equally abundant while quartzite, chert and diamictite are sporadically developed. The basal member of the Duitschland Formation is a diamictite that has its greatest development on the farm Amatava 41 KS and in the Potgietersrus Townlands. The clasts are unsorted and angular in shape and comprise chert and iron formation set in a dark, clay-rich matrix. The diamictite suggests a period of non-deposition or erosion prior to the deposition of the Duitschland Formation.

Overlying the diamictite is a carbonaceous lower shale member that is well developed throughout the area. The shale is often laminated as expressed by alternating calcareous and argillaceous layers. Pyrite is common in the unmetamorphosed rock while cordierite,biotite and orthopyroxene developed with increasing metamorphic grade.

The lower shale member is overlain by a dolomite member which is characterized by a chert breccia near the top. Algal laminations and oolites are common while metamorphosed stromatolites were observed on the farm Rietfontein 2 KS.

A second shale member overlies the dolomite member. The lower part of this member is calcareous while the top is carbonaceous and resembles the lower shale member in appearance. A few thin quartzite beds occur near the base of this member. Typical metamorphic minerals include biotite, hornblende, clinopyroxene, orthopyroxene and plagioclase.

The upper dolomite member constitutes the top of the Duitschland Formation. This member is similar in appearance to the lower dolomite member. A copper-bearing limestone that can be traced from the type locality to the farm Macalacaskop 243 KR is present in the top half of the member. The mineralization is considered to be of syngenetic origin (Martini, 1977). A cherty dolomite forms the top of this member.

2.2.3 The Pretoria Group

2.2.3.1 The Rooihoogte Formation

The Rooihoogte Formation rests unconformably on the Chuniespoort Group (Button, 1973) and marks the base of the Pretoria Group. It consists, to a large extent, of the detritus left upon the Chuniespoort erosion surface and the thickness of the formation changes considerably over short distances along strike.

The Rooihoogte Formation has its best development where it overlies the Duitschland Formation in the southern sector. The thickness of the formation decreases rapidly in a northerly direction and it is absent or very poorly developed in the northern sector. The formation consists of a chert breccia. The lack of contrast between matrix and clasts makes identification in the field difficult.

2.2.3.2 The Timeball Hill Formation

The formation has its best exposure in the southern sector where it can be divided into a lower shale member, a

quartzite member and an upper shale member, attaining thicknesses of about 1400, 100 and 180 metres respectively. The thickness of the formation decreases rapidly towards the north and the lower shale member is only about 300 metres thick immediately south of the Planknek fault. In the northern sector this member was only observed in the northern corner of the farm Macalacaskop 243 KR beyond which the formation is completely transgressed by the Bushveld Complex. Similarly the quartzite member is poorly exposed in the northern sector while the upper shale member is not exposed at all.

The shale members consist of shale, mudstone and siltstone. A carbonaceous shale is found near the base, and a thin quartzite layer is sometimes developed near the top of the lower shale member. Intercalated in the upper shale member is an arkosic quartzite that attains a maximum thickness of about 80 metres at its northernmost exposure and thins rapidly towards the south until it pinches out on the farm Doornfontein 98 KS.

The metamorphic grade increases to the north. Isolated chloritoid and andalusite crystals are present in the southernmost part of the southern sector, while andalusite, cordierite and biotite are developed at higher metamorphic grades. The northernmost outcrop of the lower shale member forms a glassy rock that contains cordierite, sillimanite, spinel and sometimes also corundum. It will be shown later that this rock probably underwent extensive anatexis.

2.2.3.3 The Dwaalheuwel Formation

Before discussing this formation it must be stated that the Hekpoort Formation could not be identified in the study area.

The Dwaalheuwel Formation, which has its best development in the southern sector, rests unconformably on the Timeball Hill Formation. It consists of a basal conglomerate and quartzite

in which a thin shale layer occurs intercalated on the farms Witpoort 96 KS and Pruissen 48 KS.

The conglomerate is a useful marker and indicated folded quartzite on the farm Vier-en-Twintig Rivier 49 KS to belong to this formation. Neither the conglomerate, nor the shale is well developed in the northern sector.

2.2.3.4 The Strubenkop Formation

The Strubenkop Formation consists of shale and mudstone and has its best development in the southern sector. In the northern sector it crops out over 4 kilometres of strike length with a greatly reduced thickness.

In the southern part of the southern sector the shale is poorly recrystallized and has a spotted appearance due to the presence of isolated chlorite, biotite and cordierite crystals. With increasing metamorphic grade to the north andalusite, cordierite, biotite and K - feldspar are commonly developed.

2.2.3.5 The Daspoort Formation

This formation consists of quartzite with a few poorly exposed shale intercalations. In the northern sector the formation is greatly reduced in thickness and the shale intercalations are absent.

The quartzite is generally pure except for a ferruginous quartzite that is developed on the farm Vier-en-Twintig Rivier 49 KS. Cordierite and biotite are developed in the northernmost exposures of the shale intercalations.

2.2.3.6 The Silverton Formation

Only the Boven Shale Member of the Silverton Formation is present in the study area. It has a sharp basal contact and comprises a dolomite- and two shale units. The lower shale unit is metamorphosed over its entire strike lenght and contains the minerals cordierite, biotite, anthophyllite and cummingtonite.

The basal shale unit is overlain by a dolomite that contains a few shale intercalations. Algal laminations and stromatolites are sporadically developed, while tremolite, clinopyroxene, olivine and spinel appear with increasing metamorphic grade, from south to north, in this unit.

The upper shale unit has its best development on the farm Rooipoort 46 KS. Amphiboles are present in the southernmost exposures while orthopyroxene and clinopyroxene are developed where the unit is in contact with the Bushveld Complex.

2.2.3.7 The Magaliesberg Formation

This formation is only exposed in the southern part of the southern sector before it is transgressed by the Bushveld Complex. Pyrite was the only impurity detected in the typical orthoquartzite.

2.3 The Rustenburg Layered Suite

A description of the Rustenburg Layered Suite is beyond the scope of this investigation and the interested reader is referred to Van der Merwe (1978) and Hulbert (1983). It is important, however, to pay attention to the relationship between the lower zone, which crops out as six distinct ultramafic satellite bodies intrusive into the floor rocks of the Complex to the north of Potgietersrus and as a large upfaulted body within the main body of the Complex south of Potgietersrus, and the critical -, main- and upper zones of the Bushveld Complex (Fig.1).

The Grasvally body is transgressed by the main body of the Bushveld Complex and Hulbert (1983) noted the presence of lower zone xenoliths in critical zone rocks. Field relations and mineral geochemistry suggest a hiatus between the emplacement of the lower zone and the critical-, main- and upper zones (Van der Merwe,1978; Hulbert, 1983). It will later be shown that this hiatus is also evident from the metamorphic mineral assemblages.

2.4 Structure

2.4.1 The Structural setting of the Bushveld Complex

The structural features of the Potgietersrus area may be related to prominent north-northwest and east-northeast structures that dominated the Kaapvaal craton from the earliest Precambrian to Transvaal times (Hunter, 1975). The siting of the Potgietersrus limb of the Bushveld Complex is considered by Van der Merwe (1978) to have been influenced by three tectonic lineaments, viz. the east-northeast trending Pietersburg Greenstone belt direction which coincides with the tectonically buoyant Eersteling basin (Button, 1973), the north,northwesterly trending Usushwana lineament (Hunter, 1970) and the Bushveld - Great Dyke lineament (Cousins, 1959). The three lineaments intersect to the west of Potgietersrus in close proximity to a gravity high, the postulated feeder to the Potgietersrus limb (Smit et al., 1962).

2.4.2 Faults

The first and apparently oldest set of faults strike northeast to east-northeast, approximately parallel to the Pietersburg Greenstone belt. The Planknek fault and a number of faults on the farms Rietfontein 2 KS and Tweefontein 238 KR belong to this type. These faults are either transcurrent or normal faults with downthrows to the southeast.

A second set of faults strike north and northwest, approximately parallel to the Usushwana lineament (Hunter 1975). These faults are especially abundant in the southern portion of the southern sector where the transcurrent faults described by Truter (1947) cut through the Timeball Hill- and Duitschland Formations. According to Hulbert (1983) these faults are post Rustenburg Layered Suite in age although they may be related to the emplacement of the Bushveld granite.

Strauss (1954) reported that large dolerite dykes have intruded along the fault planes of some north-east trending faults in the Moordkopje area, suggesting that these faults could be of Karoo age. Similarly the Zebediela fault is believed to be of post-Karoo age (Van der Merwe, 1978).

2.4.3 Structural features within the Transvaal Sequence

Two interesting structures occur in the Transvaal Sequence. One is the dolomite tongue on the farms Sandsloot 236 KR and Vaalkop 819 LR (Folder 1). The tongue truncates the layering of the Bushveld Complex and is believed to represent a paleoridge or antiform in the pre-Bushveld Transvaal Sequence (Van der Merwe, 1978).

The second feature is a fold in the Dwaalheuwel Formation on the farm Vier-en-Twintig Rivier 49 KS. It has a fold-axis parallel to the contact between the Transvaal Sequence and the Bushveld Complex. Faults separate the fold from the over- and underlying sedimentary rocks to the north, east and west while a lack of outcrop obscures the relationship between the fold and the associated rocks to the south. Truter (1947) proposed a complicated mechanism involving faulting to explain the fold but Sharpe (pers.comm.) considers that directed stress was responsible for the folding in the quartzite.

3. PETROGRAPHY

3.1 Introduction

Approximately 300 thin sections were examined in the course of the investigation. Subsequently 70 pelitic - and 62 calcareous rocks, representative of the mineral assemblages encountered, were selected for mineral chemical studies. Assemblages were divided into 14 pelitic (Table 1) and 11 calcareous (Table 2) assemblage groups. The sample numbers of each assemblage group together with available essential chemical data is presented in Tables 3 and 4 while the sample localities of representative samples from the various assemblage groups are indicated on Folder 1. The choice of the assemblage groups is to a certain extent arbitrary. In general, however, assemblage groups were selected to portray changes in the metamorphic grade while mineralogical differences due to slight variations in bulk composition were not taken into consideration.

3.2 Pelitic mineral assemblages

3.2.1 Assemblage group 1: chlorite + muscovite (sericite) + quartz ± chloritoid ± andalusite.

This assemblage group defines the lowest recorded metamorphic grade in the study area. The rocks are poorly recrystallized and quartz, feldspars and opaque minerals are of detrital origin. Sedimentary textures are well preserved.

Chlorite occurs as subidioblastic to xenoblastic grains and forms the matrix of the detrital minerals in the rock, thereby giving it a web texture (Fig. 2A). Subidioblastic chloritoid crystals are commonly twinned and contain many inclusions of what is suspected to be quartz. Andalusite crystals have idioblastic to subidioblastic outlines and are riddled with inclusions. Completely seritisized crystals, rimmed by chlorite, are also common (PH - 144).

TABLE 1 LIST OF THE ASSEMBLAGE GROUPS IN PELITIC ROCKS FROM THE POTGIETERSRUS AREA.

NUMBER	ASSEMBLAGE GROUP °
1	chlorite + muscovite (sericite) + quartz ± chloritoid ± andalusite
2	chlorite + muscovite (sericite) + cordierite + biotite + quartz ± chloritoid ± andalusite
3	cordierite + biotite + quartz ± andalusite ± muscovite ± K - feldspar
4	orthoamphibole + cordierite + quartz ± garnet ± biotite
5	cummingtonite + plagioclase + quartz ± cordierite ± garnet
6	hornblende + biotite + plagioclase + quartz ± K - feldspar
7	orthopyroxene + plagioclase + quartz ± clinopyroxene ± hornblende ± biotite
8	orthopyroxene + cordierite + quartz ± garnet ± biotite ± orthoamphibole ± plagioclase
9	cordierite + spinel ± sillimanite ± biotite ± corundum ± K - feldspar
10	orthopyroxene + cordierite + spinel ± biotite ± quartz
11	olivine + cordierite + orthopyroxene + biotite + quartz
12	olivine + cordierite + orthopyroxene + spinel + K - feldspar
13	olivine + clinopyroxene + plagioclase
14	garnet + sphene + quartz

° All assemblage groups may coexist with one or more opaque minerals

TABLE 2 LIST OF THE ASSEMBLAGE GROUPS IN CALCAREOUS ROCKS FROM THE POTGIETERSRUS AREA

NUMBER	ASSEMBLAGE GROUP
1	clinochlore + dolomite + calcite + quartz ± phlogopite
2	tremolite + dolomite + calcite ± clinochlore ± phlogopite ± quartz
3	clinopyroxene + calcite ± dolomite ± tremolite ± phlogopite ± quartz ± K - feldspar
4	forsterite + calcite + dolomite ± clinopyroxene ± tremolite ± phlogopite
5	spinel + forsterite + calcite ± phlogopite ± clinopyroxene
6	garnet ± clinopyroxene ± calcite ± plagioclase ± idocrase ± quartz
7	clinopyroxene ± calcite ± quartz
8	clinopyroxene ± amphibole ± plagioclase ± biotite ± calcite ± idocrase
9	clinopyroxene + spinel ± calcite
10	wollastonite + clinopyroxene + calcite ± monticellite ± garnet
11	Ti-garnet + clinopyroxene + biotite + plagioclase + sphene + apatite + magnetite

Table 3: List of samples comprising the various pelitic assemblage groups and summary of available mineral chemical data.

Assemblage group 1: chlorite + muscovite (sericite) + quartz ± chloritoid ± andalusite.
Feldspars and opaque minerals present as detrital grains.

Sample #	Formation	Mg/(Mg+Fe) ratio of ferromagnesian minerals			Al_2SiO_5
		chlorite	chloritoid	muscovite	polymorph
PH - 105	T2d.m3	0,307	-	n.d.	-
PH - 109	T3tSh	0,285	0,083	n.d.	-
PH - 133	T3tH	n.d.	-	n.d.	andalusite
PH - 144	T3tH	n.d.	-	n.d.	andalusite

Assemblage group 2: chlorite + muscovite (sericite) + cordierite + biotite + quartz ± chloritoid ± andalusite.
Feldspars and opaque minerals present as detrital grains.

Sample #	Formation	Mg/(Mg+Fe) ratio of ferromagnesian minerals					Al_2SiO_5
		chlorite	chloritoid	cordierite	biotite	muscovite	polymorph
PH - 34	T3sSh	n.d.	-	n.d.	n.d.	n.d.	-
PH - 45	T3sSh	n.d.	-	n.d.	n.d.	n.d.	-
PH - 75	T3sSh	0,294	-	0,421 core 0,337 rim	0,263	n.d.	-
PH - 76	T3sSh	0,422	-	0,539	0,403	n.d.	-
PH - 122	TstH	0,231	0,083	n.d.	0,233	n.d.	andalusite
PH - 143	T3tH	n.d.	0,065	0,281	0,202	0,451	andalusite

1. Crystals completely seritisized.

Assemblage group 3: cordierite + biotite + quartz ± andalusite ± muscovite ± K-feldspar.

Sample #	Formation	Mg/(Mg+Fe) ratio of ferromagnesian minerals			Al_2SiO_5			
		cordierite	biotite	muscovite	Polymorph	K-feldspar	opaque minerals	plagioclase
PH - 14	T3sH	0,783	0,815	-	andalusite	86% Or	magnetite	-
PH - 16	T3siH	0,814	0,802	-	andalusite	87% Or	magnetite	-
PH - 31	T3siH	n.d.	0,637	0,297	andalusite	-	magnetite	-
PH - 40	T3sSH	0,345	0,255	0,401	andalusite	92% Or	ilmenite	n.d.
PH - 41	T3daH	0,465	0,331	0,292	-	-	magnetite, ilmenite [2]	n.d.
PH - 42	T3siH	n.d.	0,647	0,278	andalusite	89% Or	magnetite	-
PH - 48	T3tH	0,567	0,426	0,266	andalusite	91% Or	magnetite	-
PH - 117	T3tH	0,253	0,202	0,208	andalusite	-	magnetite, ilmenite [2]	-
PH - 220	T3siH	0,572	0,409	-	andalusite	n.d.	magnetite, ilmenite [2]	48% An

Assemblage group 4: orthoamphibole + cordierite + quartz ± garnet ± biotite

Sample #	Formation	Mg/(Mg+Fe) ratio of ferromagnesian minerals.					
		gedrite	anthophylllite	cordierite	garnet	biotite	opaque minerals
PH - 8	T3siH	-	0,394	0,553	-	0,359	magnetite
PH - 21	T3siH	-	0,567	0,728	-	0,594	ilmenite
PH - 116	T3tH	0,220	-	0,369	0,054	-	ilmenite
PH - 151	T2pH	0,229	-	0,408	0,072	-	ilmenite
PH - 152	T2pH	0,274	-	0,428	0,078	-	ilmenite
PH - 157	T2pH	-	0,579	0,789	-	-	ilmenite
PH - 320	T2pH	0,231	-	0,441	-	0,305	magnetite
PH - 335	T2pH	0,180	-	0,405	-	-	ilmenite

2: These opaque minerals may be of detrital origin.

Assemblage group 5: cummingtonite + plagioclase + quartz ± cordierite ± garnet.

Sample #	Formation	Mg/(Mg+Fe) ratio of ferromagnesian minerals				
		cummingtonite	cordierite	garnet	opaque minerals	plagioclase
PH - 85	T3siH	0,495	-	-	ilmenite	37% An
PH - 312	T2pH	0,393	n.d.	0,103	ilmenite	52% An
PH - 313	T2pH	0,407	0,557	0,136	ilmenite	n.d.

Assemblage group 6: hornblende + biotite + plagioclase + quartz ± K-feldspar.

Sample #	Formation	Mg/(Mg+Fe) ratio of ferromagnesian minerals				
		hornblende	biotite	opaque minerals	plagioclase	K-feldspar
PH - 19	T3siH	0,804	0,783	magnetite	80% An	-
PH - 80	T3siH	0,721	0,616	-	n.d.	95% Or
PH - 16	T3siH	0,819	0,721	magnetite	33% An	-

Assemblage group 7: orthopyroxene + plagioclase + quartz ± clinopyroxene ± hornblende ± biotite

Sample #	Formation	Mg/(Mg+Fe) ratio of ferromagnesian minerals					
		orthopyroxene	clinopyroxene	hornblende	biotite	plagioclase	opaque minerals
PH - 88	T3siH	0,454	0,597	0,546	-	49% An	ilmenite
PH - 181	T2dH.m3	0,262	0,352	n.d.	-	n.d.	-
PH - 182	T2dH.m3	0,412	0,517	-	0,526	84% An	magnetite ilmenite
PH - 316	T2dH.m3	0,346	-	0,778	-	90% An	magnetite

Assemblage group 8: orthopyroxene + cordierite + quartz ± garnet ± biotite ± orthoamphibole ± plagioclase

Sample #	Formation	Mg/(Mg+Fe) ratio of ferromagnesian minerals							
		orthopyroxene	cordierite	garnet	biotite	gedrite	anthophyllite	plagioclase	opaque minerals
PH - 170	T2pH	0,328	0,56	0,137	0,366	-	-	30% An	-
PH - 176	T2pH	0,309	0,467	-	0,339	-	-	n.d.	magnetite
PH - 177	T2dH.ml	0,488	0,687	-	0,573	-	-	40% An	ilmenite
PH - 178	T2dH.ml	0,437	0,625	-	-	-	-	53% An	magnetite
PH - 188	T2pH	0,294	0,482	0,123	0,456	-	-	n.d.	magnetite ilmenite
PH - 191	T2dH.ml	0,490	0,698	-	0,521	-	-	-	magnetite
PH - 196	T2pH	0,294	0,458	-	-	-	-	-	-
PH - 321	T2pH	0,385	0,582	0,150	0,350	0,359	0,421	n.d.	magnetite ilmenite
PH - 324	T2pH	0,283	0,449	0,144	0,364	-	-	n.d.	magnetite
PH - 325	T2pH	0,307	0,495	0,125	0,371	-	-	n.d.	magnetite
PH - 326	T2pH	0,304	0,466	0,126	0,332	-	-	-	magnetite
PH - 330	T2pH	0,397	0,585	0,178	0,368	-	-	-	-

Assemblage group 9: cordierite + spinel ± sillimanite ± biotite ± corundum ± K-feldspar

Sample #	Formation	Mg/(Mg+Fe) ratio of ferromagnesian minerals			Al_2SiO_5		
		cordierite	spinel	biotite	polymorph	corundum	opaque minerals
PH - 168	T3tH	0,582	0,140	n.d.	-	-	ilmenite
PH - 169	T3tH	0,667	0,281	-	sillimanite	n.d.	-
PH - 173	T3tH	0,601	0,236	-	sillimanite	-	-
PH - 183	T3tH	0,382	-	-	sillimanite andalusite	-	magnetite
PH - 184	T3tH	0,513	0,140	n.d.	sillimanite	-	ilmenite
PH - 189	T2dH.ml	0,829	n.d.	n.d.	-	-	magnetite
PH - 334	T3tH	0,636	0,224	-	sillimanite	n.d.	-
1H - 4	T2dH.ml						

Assemblage group 10: orthopyroxene + cordierite + spinel ± biotite ± quartz

Sample #	Formation	Mg/(Mg+Fe) ratio of ferromagnesian minerals					
		orthopyroxene	cordierite	spinel	biotite	opaque minerals	textural type
PH - 195	T2pH	0,539	0,720	0,190	0,544	magnetite	1
PH - 199	T2pH	0,688	0,836	0,421	0,698	magnetite	1
PH - 201	T2pH	0,477	0,672	0,155	-	magnetite	2
PH - 204	T2pH	0,588	0,773	0,269	-	magnetite	3
PH - 208	T2pH	0,687	0,853	0,406	n.d.	magnetite	1
PH - 212	T2pH	0,434	0,636	0,132	-	magnetite	3
PH - 214	T2pH	0,710	0,871	0,241	n.d.	magnetite	2
PH - 215	T2pH	0,740	0,873	0,531	n.d.	magnetite	2

Assemblage group 11: olivine + cordierite + orthopyroxene + biotite + quartz

Sample #	Formation	Mg/(Mg+Fe) ratio of ferromagnesian minerals				
		olivine	cordierite	orthopyroxene	biotite	opaque minerals
PH - 197	T2pH	0,185	0,562	0,359	0,404	magnetite
PH - 328	T2pH	0,113	0,432	0,273	0,293	ilmenite

Assemblage group 12: olivine + cordierite + orthopyroxene + spinel $\pm$ K-feldspar.

Sample #	Formation	olivine	cordierite	orthopyroxene	spinel	opaque minerals	K-feldspar
PH - 202	T2pH	0,379	0,725	0,502	0,253	-	94% Or
PH - 203	T2pH	0,349	0,665	0,492	0,196	magnetite	98% Or
PH - 206	T2pH	0,339	0,653	0,464	0,176	magnetite	-
PH - 209	T2pH	0,254	0,586	0,422	0,118	magnetite	-
PH - 219	T2pH	0,340	0,620	0,462	0,199	-	-

Assemblage group 13: olivine + clinopyroxene + plagioclase

Sample #	Formation	Mg/(Mg+Fe) ratio of ferromagnesian minerals			
		olivine	clinopyroxene	plagioclase	opaque minerals
PH - 213	T2dH.ml	0,450	0,659	90% An	magnetite ilmenite

Assemblage group 14: garnet + sphene + quartz

Sample #	Formation	garnet composition
PH - L[3]	T2dH.ml	63% spess; 17% alm.+py.; 20% gross.+andr.

3: contains pumpellyite and chlorite as retrograde minerals.

Table 4: List of samples comprising the various calcareous assemblage groups and summary of available mineral chemical data

Assemblage group 1: clinochlore + dolomite + calcite + quartz + phlogopite

Sample #	Formation	Mg/(Mg+Fe) ratio of ferromagnesian minerals	
		clinochlore	phlogopite
PD - 8	T2dD. m4	n.d.	-
PD - 10	T2dD. m4	0,831	0,873
PD - 18	T2dD. m4	0,224	0,882
PD - 29	T2dD. m4	n.d.	n.d.
PD - 35	T2D	0,981	0,980

Assemblage group 2: tremolite + dolomite + calcite $\pm$ clinochlore $\pm$ phlogopite $\pm$ quartz

Sample #	Formation	Mg/(Mg+Fe) ratio of ferromagnesian minerals			
		tremolite	phlogopite	clinochlore	quartz
PD - 34	T2D	0,981	-	-	n.d.
PD - 56	T2D	0,968	0,945	0,962	n.d.
PD - 57	T2D	n.d.	n.d.	-	-
PC - 14	T3siD	0,967	0,969	-	-

Assemblage group 3: clinopyroxene ± calcite ± dolomite ± tremolite ± phlogopite ± quartz ± K-feldspar

Sample #	Formation	Mg/(Mg+ Fe) ratio of ferromagnesian minerals			carbonates
		clinopyroxene	tremolite	phlogopite	
PD - 38	T2D	0,959	0,905	-	calcite
PD - 48	T2D	0,988	0,990	n.d.	calcite, dolomite
PD - 50	T2D	0,978	0,983	n.d.	calcite, dolomite
PD - 53	T2D	0,973	0,974	-	calcite
PD - 70	T2D	0,970	0,982	-	calcite, dolomite
PD - 128	T2D	0,977	-	-	calcite
PD - 130	T2D	0,784	0,987	-	calcite
PD - 131	T2dD. m2	0,726	-	-	calcite
PD - 157	T2dD. m4	0,717	-	-	calcite
PD - 166	T2D	0,977	0,921	-	calcite
PD - 30	T3siD	0,549	0,478	-	calcite

Assemblage group 4: forsterite + calcite + dolomite ± clinopyroxene ± tremolite ± phlogopite

Sample #	Formation	Mg/(Mg+ Fe) ratio of ferromagnesian minerals			
		forsterite	clinopyroxene	tremolite	phlogopite
PD - 140	T2D	0,967	n.d.	-	n.d.
PD - 216	T2D	0,896	0,888	-	0,871
PC - 27	T3siD	0,965	0,930	0,889	n.d.
PC - 34	T3siD	0,985	-	-	n.d.
PC - 36	T3siD	0,965	0,961	-	n.d.

Assemblage group 5: spinel + forsterite + calcite + phlogopite ± clinopyroxene

Sample #	Formation	Mg/(Mg+Fe) ratio of ferromagnesian minerals			
		spinel	forsterite	phlogopite	clinopyroxene
PD - 208	T2D	0,974	0,988	n.d.	n.d.
PD - 214	T2D	0,686	0,894	0,932	0,859
PC - 1	T3siD	0,803	0,990	-	-
PC - 10	T3siD	0,768	0,960	-	-

Assemblage group 6: garnet ± clinopyroxene ± calcite ± plagioclase ± idocrase ± quartz

Sample #	Formation	Mg/(Mg+Fe) ratio of clinopyroxene				
			garnet	plagioclase	calcite	idocrase
PD - 19	T2dD. m4	0,771	44% Gross	-	n.d.	-
PD - 152	T2dD. m4	0,770	63% Gross	n.d.	n.d.	-
PD - 158[a]	T2dD. m4	0,607	40% Gross	n.d.	n.d.	n.d.
PD - 162[a,b]	T2dD. m4	0,823	68% Gross	-	n.d.	-
PD - 171	T2dD. m2	0,790	58% Gross	-	n.d.	-
PD - 176[a]	T2dD. m4	0,760	64% Gross	-	n.d.	-
PC - 13	T3siD	0,717	72% Gross	-	n.d.	-
PC - 25[a]	T3siD	-	10% Gross	-	n.d.	-
PC - 52	T3siD	0,846	74% Gross	-	-	-
OV - 4C	T2D	0,951	24% Gross	-	-	-

a: contains clinozoisite or epidote as a retrograde mineral.

b: contains prehnite as a retrograde mineral.

Assemblage group 7: clinopyroxere ± calcite ± quartz

Sample #	Formation	Mg/(Mg+Fe) ratio of clinopyroxene	calcite
PH - 161	T2dH. m1	0,321	-
PH - 166	T2dH. m3	0,437	-
PH - 192[a]	T2dH. m3	0,174	-
PH - 207	T2dH. m3	0,634	n.d.
PH - 315	T2dH. m3	0,228	-

a: contains magnetite as an accessory mineral.

Assemblage group 8: clinopyroxene ± amphibole ± plagioclase ± biotite ± calcite ± idocrase

Sample #	Formation	Mg/(Mg+Fe) ratio of ferromagnesian minerals					
		clinopyroxene	amphibole	biotite	plagioclase	calcite	idocrase
PH - 186	T2dH. m1	0,420	-	0,392	88% An	-	-
PD - 81	T2D	0,548	-	-	n.d.	n.d.	-
PD - 82[a]	T2dD. m2	0,871	n.d.	-	n.d.	-	-
PD - 83[b]	T2dD. m2	-	0,750	-	-	-	-
PD - 89[b]	T2D	-	0,853	-	-	-	-
PD - 96	T2D	0,886	-	-	-	-	-
PD - 97	T2D	0,946	-	-	-	n.d.	n.d.
PD - 124	T2dD. m4	0,669	-	0,592	44% An	-	-
PD - 125	T2dD. m4	0,881	0,766	-	-	-	-
PD - 178[a,b,c]	T2dD. m4	0,800	0,700	-	n.d.	-	-
PD - 205	T2D	0,870	-	-	-	-	-
PC - 12[a]	T3siD	0,783	-	-	n.d.	-	-
PC - 20	T3siD	0,951	0,509	-	-	n.d.	-
PC - 30	T3siD	0,549	0,478	-	n.d.	n.d.	-
PC - 32	T3siD	0,582	-	-	n.d.	-	-

a: contains epidote as a retrograde mineral.

b: contains prehnite as a retrograde mineral.

c: contains Ni - minnesotaite as an accessory mineral.

Assemblage group 9: clinopyroxene + spinel ± calcite

Sample #	Formation	Mg/(Mg+Fe) ratio of ferromagnesian minerals		
		clinopyroxene	spinel	calcite
PD - 148	T2dD. m4	0,828	0,744	-
PD - 174[a]	T2dD. m4	0,770	0,761	-
PD - 177	T2dD. m4	0,821	0,772	n.d.
PD - 184[a]	T2dD. m4	0,681	0,754	n.d.

a: contains clinozoisite as a retrograde mineral.

Assemblage group 10: wollastonite + clinopyroxene + calcite ± monticellite ± garnet

Sample #	Formation	Mg/(Mg+Fe) ratio of ferromagnesian minerals			
		wollastonite	clinopyroxene	monticellite	garnet
PD - 191	T2D	0,396	0,591	-	-
PD - 194	T2D	0,675	0,741	0,885	69% Gross

Assemblage group 11: Ti-garnet + clinopyroxene + biotite + plagioclase + sphene + apatite + magnetite

Sample #	Formation	Mg/(Mg+Fe) ratio of ferromagnesian minerals			
		clinopyroxene	biotite	garnet	plagioclase
PH - 79	T3siD	0,64	0,69	34% schl. 48% andr.	3% An[a]; 17% An[b]

a: plagioclase aggregates.

b: subidioblastic matrix crystals.

3.2.2 Assemblage group 2: chlorite + muscovite (sericite) + cordierite + biotite + quartz ± chloritoid ± andalusite.

Rocks belonging to this assemblage group have a spotted appearance. Original sedimentary textures are still visible and detrital quartz, feldspar and opaque minerals are common. Xenoblastic or subidioblastic chlorite crystals occur in the matrix of the samples although chlorite rims between andalusite and biotite are also developed (PH - 122). The cordierite crystals in fine-grained argillaceous layers in some samples are idioblastic with pseudohexagonal crystal outlines (Fig. 2 C and D). The crystals are zoned with a sectorially twinned core relatively free from inclusions and a MgO /(MgO + FeO_T) ratio of 0,42. The core is surrounded by an inclusion-rich zone, which in turn, is enclosed by a relatively inclusion-free rim with a MgO /(MgO + FeO_T) ratio of 0,34. Inclusions consist mostly of quartz and sericite although rare biotite and chlorite inclusions are also present. Cordierite in the coarse-grained siliceous layers are xenoblastic and contain many inclusions of detrital minerals, biotite and chlorite (Fig. 2 B).

Two samples contain the assemblage chloritoid + cordierite. Chloritoid crystals are subidioblastic and contain quartz inclusions. In cases where it is in contact with, or included in cordierite, it has a resorbed appearance.

Andalusite forms small poikiloblastic grains (Fig. 2 B) or subidioblastic to idioblastic chiastolite crystals (PH - 122). Inclusions are mostly quartz and biotite, while chlorite can occur along crystal boundaries.

3.2.3 Assemblage group 3: cordierite + biotite + quartz ± andalusite ± muscovite ± K - feldspar.

Rocks belonging to this assemblage group are completely re-crystallized, have a glassy appearance and break with a conchoidal fracture. Cordierite forms either large

xenoblastic crystals with a poikiloblastic appearance (Fig. 2 E) or small granular crystals free from inclusions (PH - 16).

In samples where muscovite has reacted to give andalusite and K - feldspar, biotite forms rims around magnetite grains in the vicinity of andalusite - K-feldspar intergrowths (Fig. 2 F). Biotite in this case may represent the hydration product of opaque minerals as the water could have been supplied by the muscovite - breakdown reaction. Andalusite crystals are normally subidioblastic to idioblastic (Fig. 2 E) but when it is intergrown with K-feldspar the grains are rounded, giving rise to a nodular texture (Fig. 2 F). The K-feldspar grains in these intergrowths are large and xenoblastic in contrast to the small granular crystals in the groundmass of the other samples from this assemblage group.

3.2.4 Assemblage group 4: orthoamphibole + cordierite + quartz ± garnet ± biotite.

The rocks comprising this assemblage group are completely recrystallized and original sedimentary features are destroyed. Orthoamphibole crystals occur as bow-ties (Fig. 2 G) or crystal mats (Fig. 2 H). The crystals are relatively inclusion-free although some biotite and magnetite inclusions were observed.

Two different textural types of cordierite can be identified in two samples from this assemblage group (Fig. 3 A). The first type has subidioblastic, rounded crystal outlines and is almost completely devoid of magnetite and biotite inclusions although rare quartz inclusions may be present. This type is further characterized by a high concentration of opaque minerals in the matrix adjacent to the crystal outlines. The second type forms smaller, xenoblastic grains and is frequently found to be intergrown with orthoamphibole. It also contains numerous magnetite, biotite and quartz inclusions. The first type of cordierite possibly formed through a reaction such as the one responsible for cordierite in

Figure 2. Photomicrographs of pelitic metamorphic mineral assemblage groups 1 to 4. Abbreviations: chl = chlorite; ctd = chloritoid; bi = biotite; and = andalusite; cord = cordierite; mag = magnetite; K-spar = K-feldspar; gar = garnet; ged = gedrite; ilm = ilmenite. Sections A,F,G and H have been photographed in plane polarized light and the remaining sections under crossed nicols. Sample numbers are indicated in brackets.

(A) Chloritoid porphyroblasts in a chlorite and quartz matrix (PH - 109)

(B) The chloritoid + cordierite + andalusite + biotite assemblage (PH - 143)

(C) and (D) Zoned cordierite porphyroblasts with pseudohexagonal crystal outlines (PH - 75)

(E) Idioblastic chiastolite crystals together with cordierite and biotite in a fine-grained, poorly recrystallized matrix (PH - 124)

(F) Andalusite - K-feldspar intergrowth. Biotite forms rims around magnetite grains in the immediate vicinity of the intergrowth (PH - 16)

(G) Gedrite bow-ties in a poorly recrystallized, quartz-rich matrix (PH - 116)

(H) Gedrite - cordierite intergrowth (PH - 335)

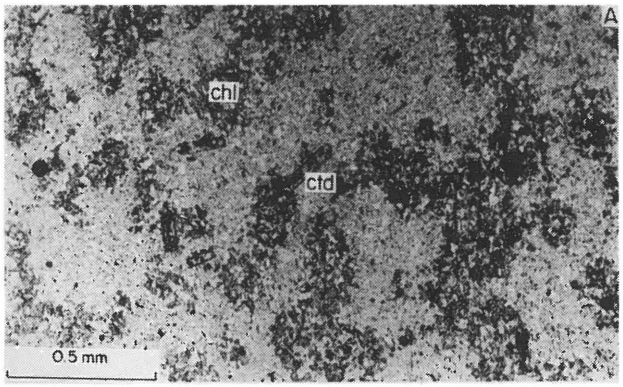

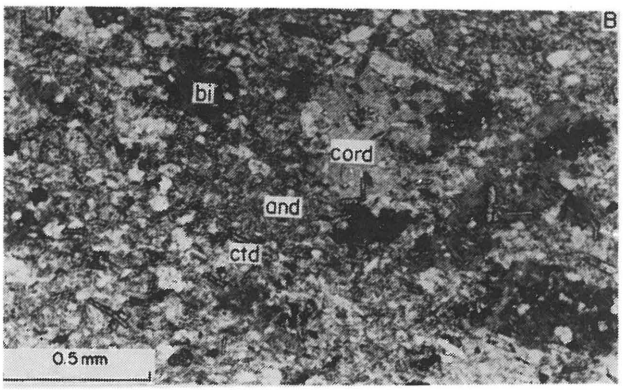

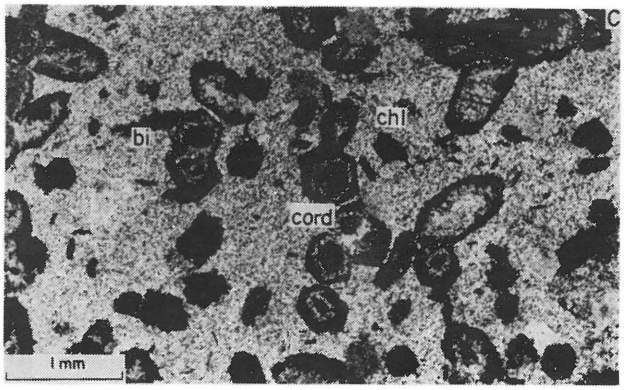

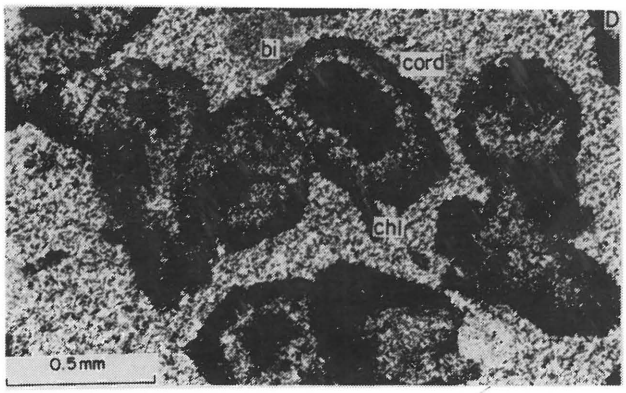

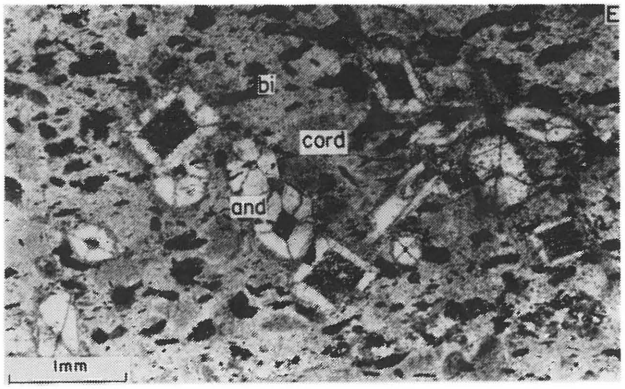

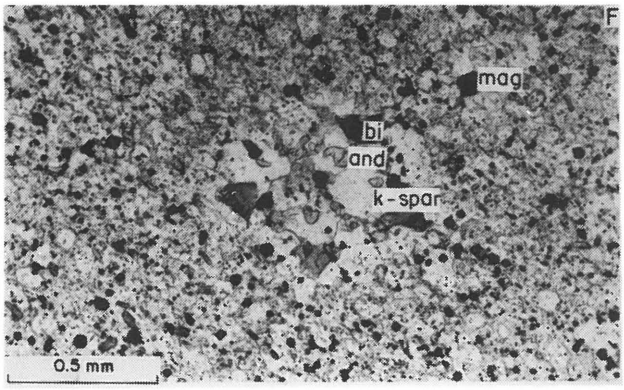

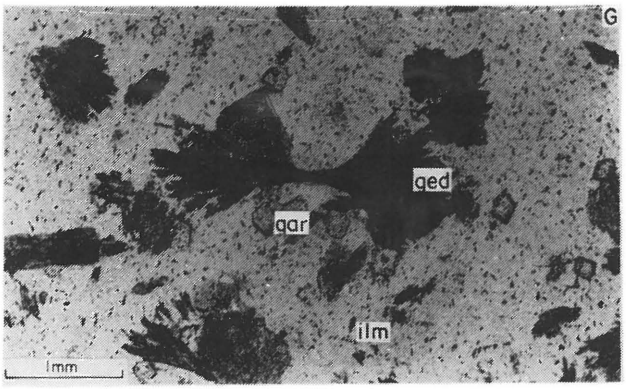

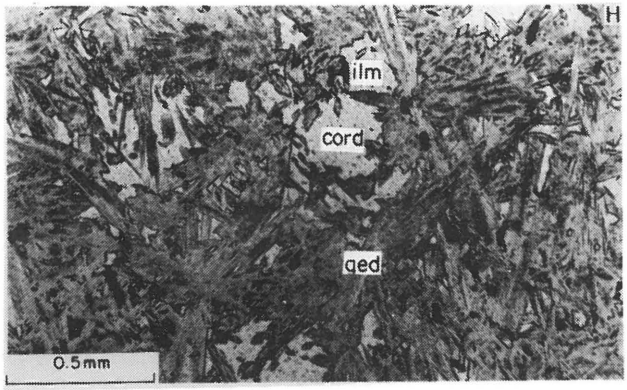

assemblage group 2, while the second type, as well as the orthoamphibole, formed as the result of a different reaction that probably took place at a higher temperature.

Both types of cordierite have the same $MgO/(MgO + FeO_T)$ ratio of about 0,55 indicating chemical equilibrium in the sample. In the remaining samples from this assemblage group subidioblastic to xenoblastic cordierite crystals, riddled with inclusions, are often intergrown with orthoamphibole (Fig. 3 B).

Where garnet occurs together with gedrite it can be present either as small idioblastic crystals (Fig. 2 G) or as large grains with inclusions of gedrite and opaque minerals (Fig. 3 B). The absence of K-feldspar from this assemblage is also noteworthy.

3.2.5 Assemblage group 5: cummingtonite + plagioclase + quartz ± cordierite ± garnet.

Samples from this assemblage group are closely related to the samples from the previous assemblage group in the field. Acicular cummingtonite crystals form star-like textures or densely packed mats (Fig. 3 C). Garnet crystals are idioblastic to subidioblastic and contain many quartz, amphibole and ilmenite inclusions. Plagioclase and cordierite form small crystals in the matrix of the samples.

3.2.6 Assemblage group 6: hornblende + biotite + plagioclase + quartz ± K-feldspar.

Hornblende occurs as subidioblastic to idioblastic crystals with a poikiloblastic nature due to quartz inclusions (PH - 19, PH - 80). Where the crystals merge together (PC - 16) the rock assumes an overall web texture. Biotite crystals are xenoblastic to subidioblastic and are free from inclusions.

3.2.7 Assemblage group 7: orthopyroxene + plagioclase + quartz ± clinopyroxene ± hornblende ± biotite.

Orthopyroxene crystals are short and stubby (PH - 88) or elongated with a quasi - parallel arrangement (PH - 316)

and contain quartz and feldspar inclusions. The same type of inclusions also occur in xenoblastic clinopyroxene grains. Hornblende may form xenoblastic grains interstitial to orthopyroxene- and clinopyroxene grains (PH - 181) or small subidioblastic crystals (PH - 88).

3.2.8 Assemblage group 8: orthopyroxene + cordierite + quartz ± garnet ± biotite ± orthoamphibole ± plagioclase

Both orthopyroxene and orthoamphibole are present in one sample that contains thus both the reactants and products of the orthopyroxene - forming reaction (Fig. 3 D). Orthopyroxene forms small (< 0,05 mm) xenoblastic grains while gedrite and anthophyllite occur as large idioblastic crystals. The textural relationship between the two orthoamphiboles is not clear, although immiscibility is expected.

The mineral textures in this assemblage group changes with metamorphic grade. There is a tendency to form more idioblastic crystals as well as a marked increase in the grain size of orthopyroxene, garnet, cordierite and biotite from the orthoamphibole-bearing sample (Fig. 3 D) through a sample collected in close proximity to sample PH - 321 (Fig. 3 E) to the higher grade samples (Fig. 3 F). Orthopyroxene crystals are often prismatic and contain numerous inclusions of cordierite, biotite and quartz (Fig. 3 F). The same minerals also occur included in garnet while orthoamphibole and rare orthopyroxene inclusions have also been observed in the orthoamphibole-bearing sample, suggesting the contemporaneous growth of garnet and orthopyroxene.

Cordierite contains orthopyroxene and orthoamphibole inclusions in the lower grade sample (PH - 321, PH - 330) while the sectorially twinned crystals in the higher grade samples are devoid of inclusions (Fig. 3 F). Biotite crystals are always relatively inclusion-free although an intergrowth between biotite and plagioclase has been noted where two biotite crystals are surrounded by plagioclase (Fig. 3 G). The biotite crystals have been penetrated by parallel plagioclase "fingers" along the basal pinacoid. As replacement of biotite by plagioclase or vice versa is

unlikely, the two minerals probably crystallized together. Another possible explanation is that the plagioclase inclusions may be elongated and aligned parallel to the basal pinacoid in order to produce a boundary of relatively low interfacial energy, analogous to a similar biotite-quartz intergrowth described by Kretz (1966).

It is important to note that garnet-bearing samples contain less biotite than garnet-free samples, while a thin layer of quartz is often developed between orthopyroxene and cordierite in the immediate vicinity of a garnet grain.

3.2.9 Assemblage group 9: cordierite + spinel ± sillimanite ± biotite ± corundum ± K-feldspar.

Two textural types of cordierite can be identified in most samples. The first type forms small xenoblastic crystals that comprise the bulk of the matrix of most samples and give the rocks a granoblastic polygonal texture. The second type forms large subidioblastic crystals that may replace spinel porphyroblasts (Fig. 3 H). Both types of cordierite have similar $MgO/(MgO + FeO_T)$ ratios, indicating chemical equilibrium in the samples.

Both green and brown spinel occur in this assemblage group, the difference in colour is probably due to differences in their Fe_2O_3 / FeO ratio. Spinel crystals have idioblastic to subidioblastic outlines and contain rare cordierite and K-feldspar inclusions. Alteration to diaspore has also been observed in a few crystals. In corundum-bearing samples spinel grains have a resorbed appearance where the crystals are in contact with cordierite while corundum laths cut into and even through spinel grains (Fig. 4 A). In other samples two generations of spinel are present, one as isolated idioblastic crystals in a plagioclase and cordierite matrix and the other replacing corundum laths (Fig. 4 B). The latter group of samples does not, however, contain sillimanite and different reactions are thus responsible for the textures in the two groups of samples.

Figure 3. Photomicrographs of pelitic metamorphic mineral assemblage groups 4 to 9. Abbreviations: cord = cordierite; anth = anthophyllite; gar = garnet; ged = gedrite; ilm = ilmenite; cumm = cummingtonite; bi = biotite; opx = orthopyroxene; plag = plagioclase; sp = spinel; sill = sillimanite. All sections have been photographed in plane polarized light. Sample numbers are indicated in brackets.

(A) Two generations of cordierite in assemblage group 4. "Cord I" forms rounded, inclusion-free crystals rimmed by magnetite grains, while "cord II" occurs as xenoblastic grains riddled with inclusions (PH - 8)

(B) The garnet + cordierite + gedrite assemblage (PH - 152)

(C) Garnet crystals in a cummingtonite-plagioclase matrix (PH - 313)

(D) The orthopyroxene - gedrite assemblage on the orthopyroxene - in isoreactiongrad (PH - 321)

(E) Small xenoblastic orthopyroxene grains that crystallized at a slightly higher grade than the orthopyroxene - in isoreactiongrad (PH - 330)

(F) The orthopyroxene - cordierite - garnet assemblage. Note the increase in grain size of the minerals as well as the better recrystallization relative to Fig. 3 E (PH - 188).

(G) Biotite (dark) -plagioclase (light) intergrowth. Plagioclase forms fingers along the basal pinacoid of biotite (PH - 170).

(H) Cordierite porphyroblast replacing spinel (PH - 173)

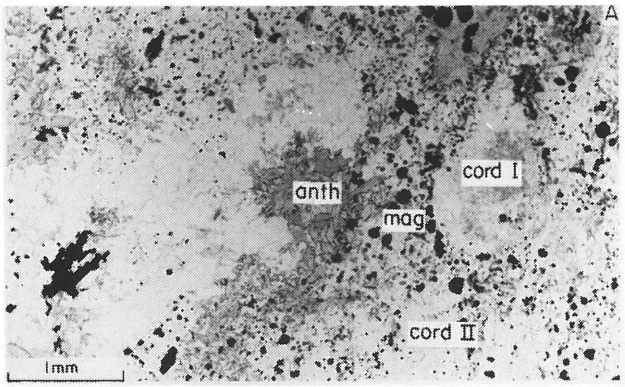

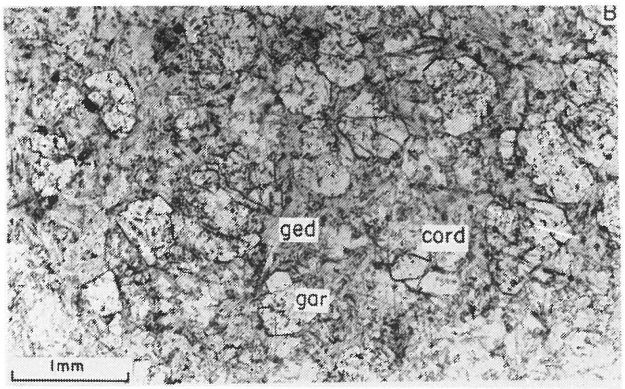

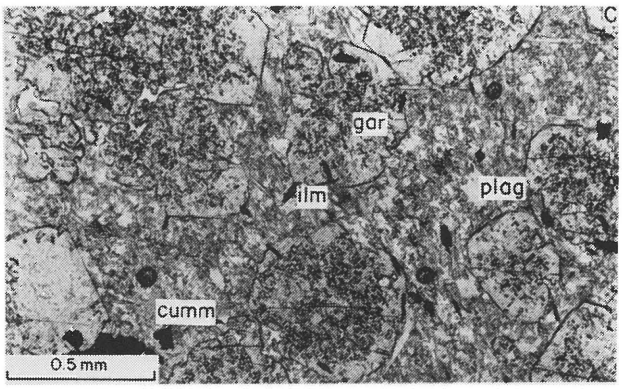

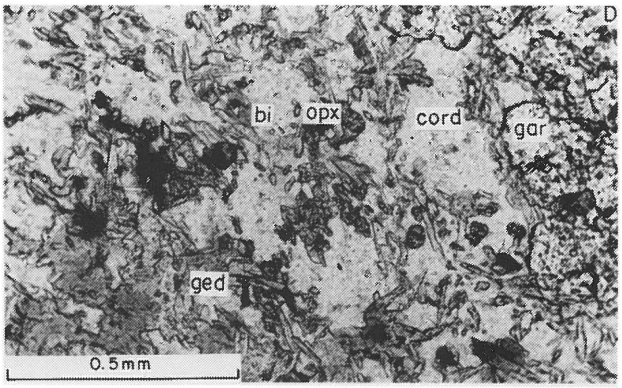

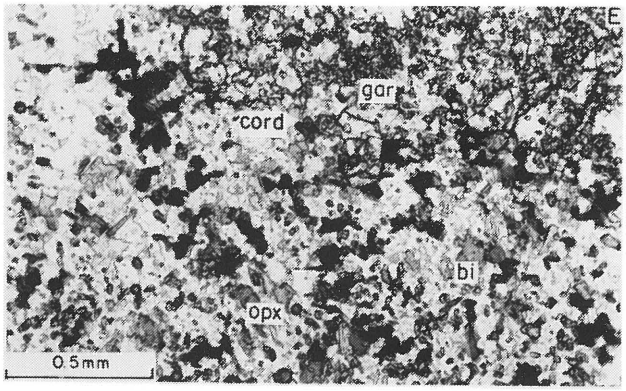

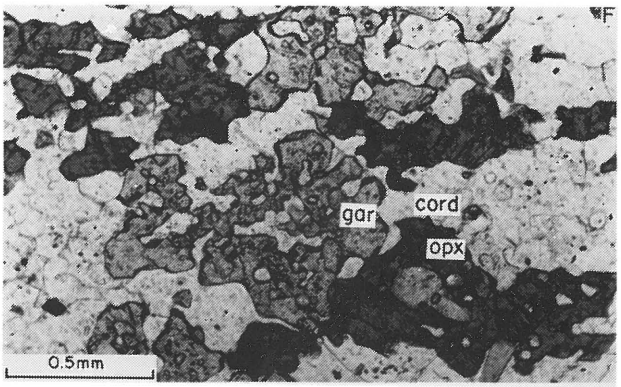

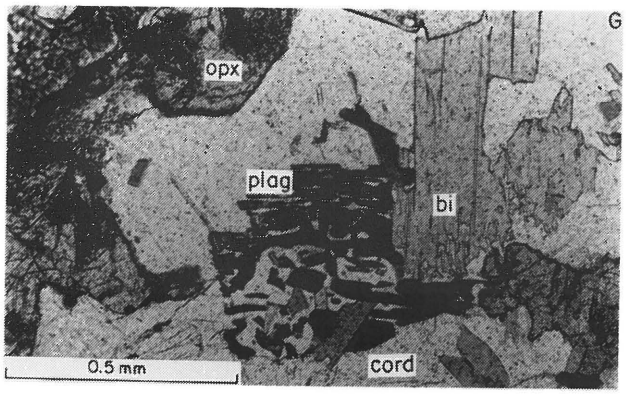

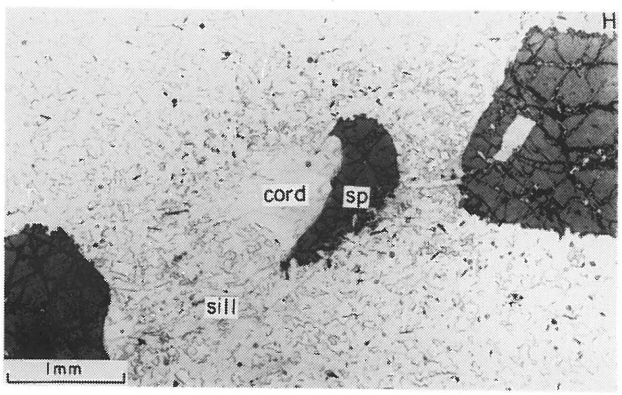

Only rare xenoblastic biotite flakes rimming magnetite were found. Sillimanite usually forms idioblastic crystals (Fig. 4 A) although whispy patches have also been observed (PH - 183). Andalusite porphyroblasts, rimmed by chlorite, occur in a sillimanite - cordierite matrix in sample PH - 184 while large K-feldspar grains sometimes appear to be replacing spinel (PH - 173).

3.2.10 Assemblage group 10: orthopyroxene + cordierite + spinel $\pm$ biotite $\pm$ quartz.

Three general textures between orthopyroxene, magnetite and spinel were distinguished. In the first type orthopyroxene is never in contact with either magnetite, spinel or composite oxide grains (Fig. 4 D and E). Large xenoblastic orthopyroxene crystals contain inclusions of cordierite, magnetite and spinel, but cordierite is invariably developed between the orthopyroxene and oxide grains. Oxide grains enclosed by orthopyroxene contain numerous cordierite inclusions and embayments whereas oxide grains some distance away from the orthopyroxene crystals are more subidioblastic. Magnetite and spinel are always intergrown in the form of exsolution lamellae or rims of the one phase around the other.

In the second textural type orthopyroxene is freely in contact with both magnetite and spinel, while both minerals together with cordierite also occur included in orthopyroxene (Fig. 4 F).

The third textural type is characterized by orthopyroxene intergrowths with large magnetite, spinel or composite oxide grains (Fig. 4 G). The oxide grains have a skeletal appearance due to cordierite and orthopyroxene inclusions. The latter is often optically discontinuous with the large enclosing orthopyroxene grain, suggesting that the inclusions belong to an earlier orthopyroxene generation and that they were trapped by oxide grains which grew similtaneously with a second orthopyroxene generation. Oxide grains in the matrix of the sample are smaller and are normally devoid of inclusions.

Biotite is rare in this assemblage group and it only occurs as rims around magnetite grains (Fig. 4 D).

3.2.11 Assemblage group 11: olivine + cordierite + orthopyroxene + biotite + quartz.

Orthopyroxene forms subidioblastic, elongated crystals that sometimes contain olivine and cordierite inclusions (Fig. 4 H and 5 A). Olivine is present as rounded grains that may be partially serpentenized. Biotite forms rims around magnetite and ilmenite grains and also occur as xenoblastic flakes that may be partially enclosed by orthopyroxene. Subidioblastic cordierite crystals give the samples a granoblastic polygonal appearance.

3.2.12 Assemblage group 12: olivine + cordierite + orthopyroxene + spinel + K-feldspar.

Intergrowths between olivine and K-feldspar commonly surround spinel grains which have a resorbed appearance (Fig. 5 B and C). Irregular blebs of spinel are often enclosed by the symplectite (Fig. 5B) suggesting the replacement of spinel by the olivine K-feldspar intergrowth. A thin layer of quartz sometimes separates orthopyroxene and cordierite in the vicinity of these intergrowths (Fig. 5 C). Spinel boundaries with orthopyroxene are smooth, suggesting textural equilibrium between the two minerals. Small spinel grains are often rimmed by orthopyroxene where these grains occur in a cordierite matrix, and cordierite is rarely in contact with spinel.

Intergrowths between spinel and orthopyroxene occur locally in large orthopyroxene crystals, although entire crystals may consist of the symplectite (Fig. 5 D). The intergrowth probably resulted from the exsolution of spinel from an initially high Al-orthopyroxene. The exsolution might have been controlled by the following reaction suggested by Obata (1976) :

Figure 4. Photomicrographs of pelitic metamorphic mineral assemblage groups 9 to 11. Abbreviations: sp = spinel; cor = corundum; sill = sillimanite; cord = cordierite; and = andalusite; chl = chlorite; opx = orthopyroxene; ol = olivine; mag = magnetite; bi = biotite. All sections have been photographed in plane polarized light. Sample numbers are indicated in brackets.

(A) Corundum laths cutting into spinel porphyroblasts. Note the resorbed appearance of spinel (PH - 334)

(B) Two textural types of spinel. One replaces corundum laths while the other type forms idioblastic crystals (1 H 4)

(C) The andalusite - sillimanite - cordierite - spinel assemblage on the andalusite - sillimanite reaction boundary

(D) and (E) The first textural type of assemblage group 10. Orthopyroxene is never in contact with spinel. Spinel grains in the vicinity of orthopyroxene contain inclusions and embayments of cordierite (PH - 195 and PH - 199)

(F) The second textural type of assemblage group 10. Orthopyroxene is freely in contact with spinel (PH - 214)

(G) The third textural type of assemblage group 10. Orthopyroxene is intergrown with spinel. Orthopyroxene inclusions in spinel are often optically discontinuous with the enclosing orthopyroxene grain (PH - 204)

(H) The olivine - orthopyroxene - cordierite assemblage (PH - 328)

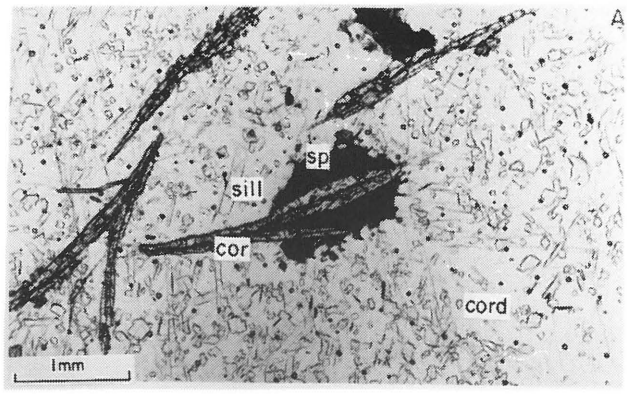

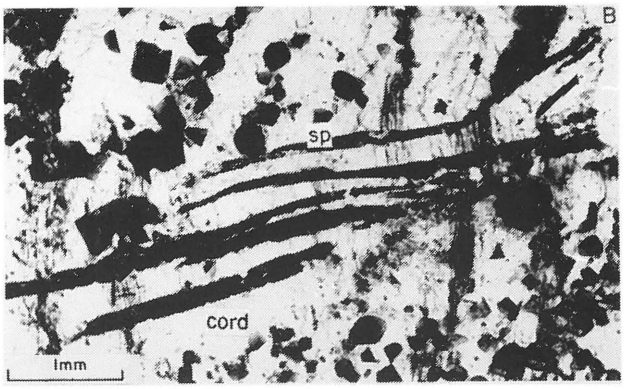

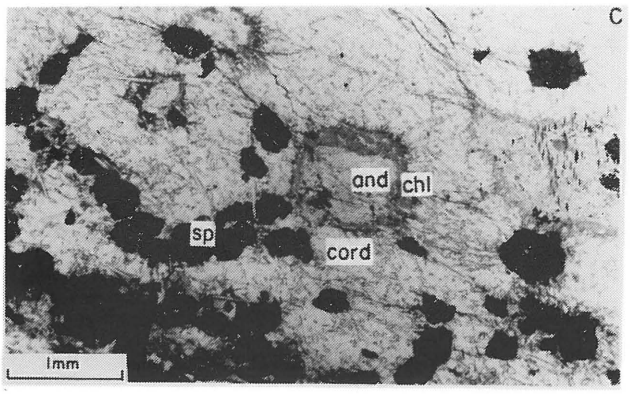

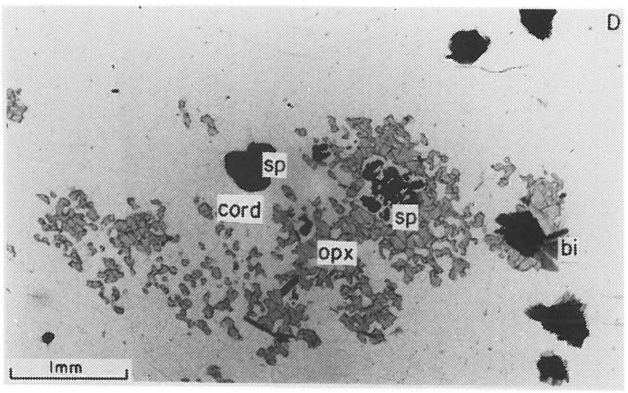

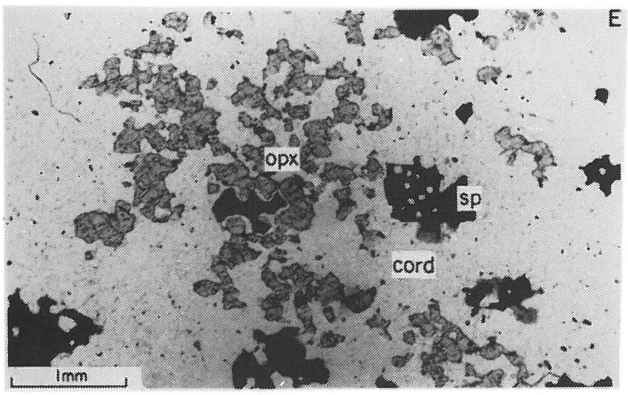

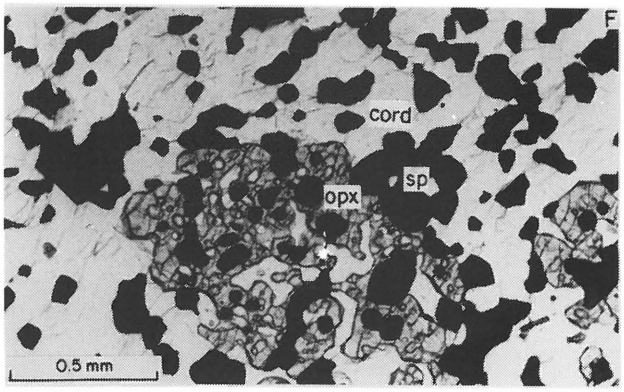

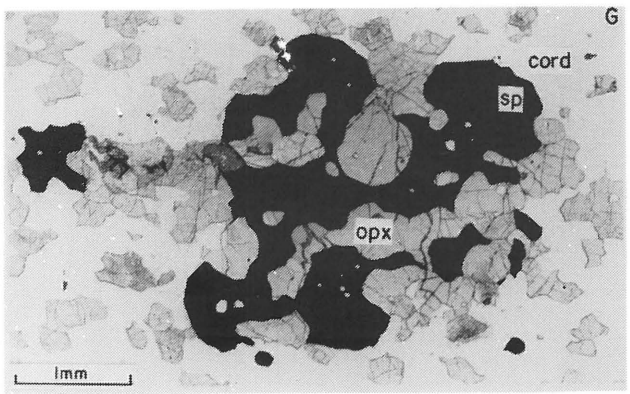

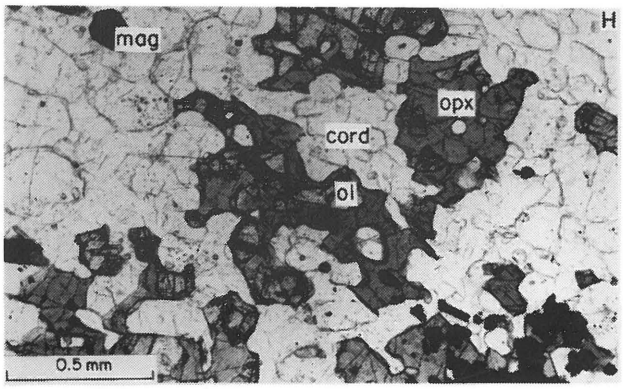

Mg_2SiO_4 + $MgAl_2SiO_6$ ⇌ Mg_2SiO_6 + $MgAl_2O_4$ ....3(1)
forsterite Al-opx enstatite spinel

In some samples olivine is only present as small inclusions in orthopyroxene and spinel porphyroblasts (Fig. 5 E and F). The absence of olivine from the matrix of these samples indicate that olivine was a reactant in some reaction that produced spinel and orthopyroxene. Where spinel grains with orthopyroxene inclusions are, in turn, included by orthopyroxene, the inclusions do not have the same optical orientation as the enclosing grains thereby suggesting two stages of orthopyroxene growth.

3.2.13 Assemblage group 13: olivine + clinopyroxene + plagioclase.

Subidioblastic olivine crystals, containing rounded plagioclase inclusions, occur in a plagioclase and clinopyroxene matrix (Fig. 5 G). Thin exsolution lamellae parallel to the {001} crystal planes are present in the small matrix pyroxenes, while coarse-grained pyroxenes that occur in a layer cutting the sample have exsolution lamellae parallel to both the {001} and {100} crystal planes.

3.2.14 Assemblage group 14: garnet (spessartine) + sphene + quartz.

Large (up to 1,5 cm in diameter), subidioblastic garnet crystals, containing quartz inclusions, are anisotropic and display complex extinction patterns (Fig. 9 E). The resulting pattern is almost similar to a laminated texture observed in anisotropic garnets from Japan for which the word "tatami" (meaning rice straw mat) texture is used (Takēuchi et al., 1982). Although the crystals are roughly zoned with respect to sectors of similar optical orientation, no general pattern could be detected. An attempt will be made in a later chapter to explain the anisotropism.

Subidioblastic to idioblastic pumpellyite crystals occur together with chlorite and quartz in the matrix of the rock. Both minerals are however absent from quartz halos around garnet porphyroblasts which formed as the result

Figure 5. Photomicrographs of pelitic metamorphic mineral assemblage groups 11 to 13. Abbreviations: ol = olivine; opx = orthopyroxene; mag = magnetite; sp = spinel; K-spar = K-feldspar; cord = cordierite; qz = quartz; cpx = clinopyroxene; plag = plagioclase. All sections have been photographed in plane polarized light. Sample numbers are indicated in brackets.

(A) The olivine - cordierite - orthopyroxene assemblage (PH - 197)

(B) The olivine - K-feldspar intergrowth that appears to be replacing spinel. Note the remnant spinel fragment enclosed by the intergrowth (PH - 202).

(C) The olivine - K-feldspar intergrowth replacing both orthopyroxene and spinel. Note the quartz rim between cordierite and orthopyroxene (PH - 203)

(D) Spinel - orthopyroxene symplectite (PH - 202)

(E) and (F) Olivine and cordierite enclosed by spinel and orthopyroxene porphyroblasts. Olivine is completely absent from the matrix in Figure 5 E (PH - 206 and PH - 219)

(G) The olivine - clinopyroxene - plagioclase assemblage (PH - 213)

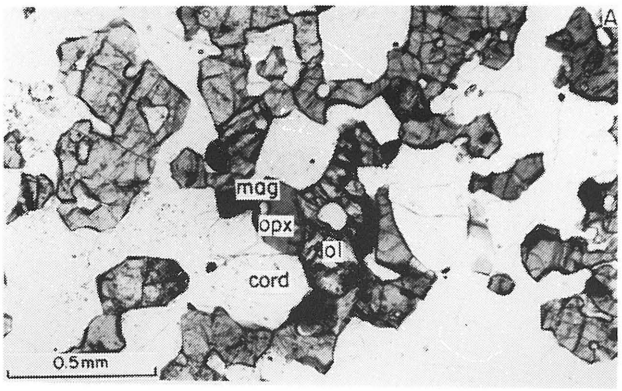

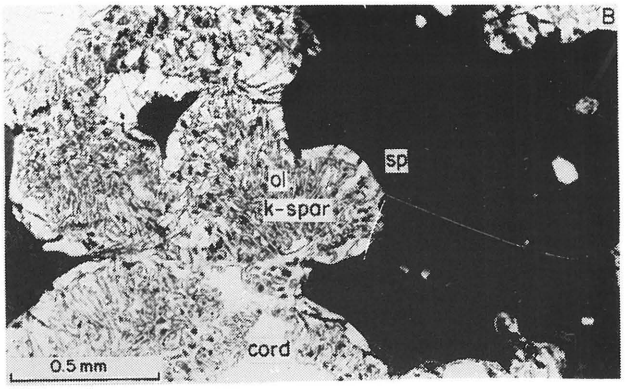

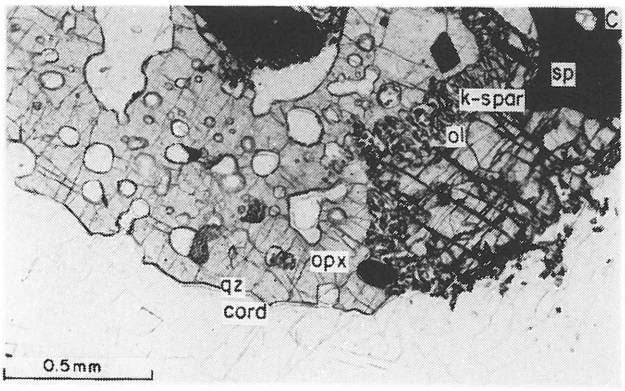

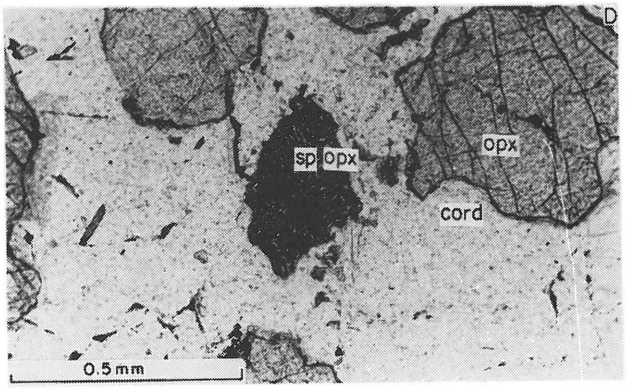

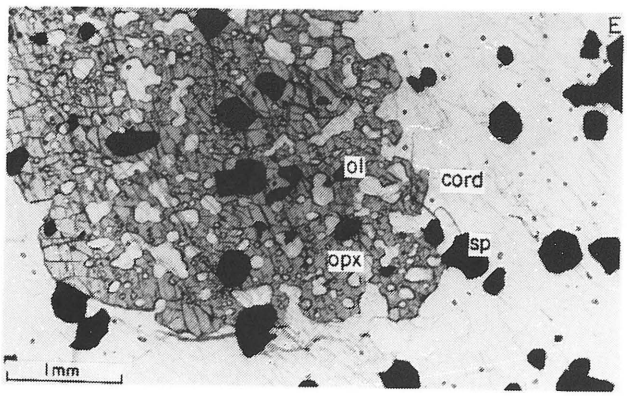

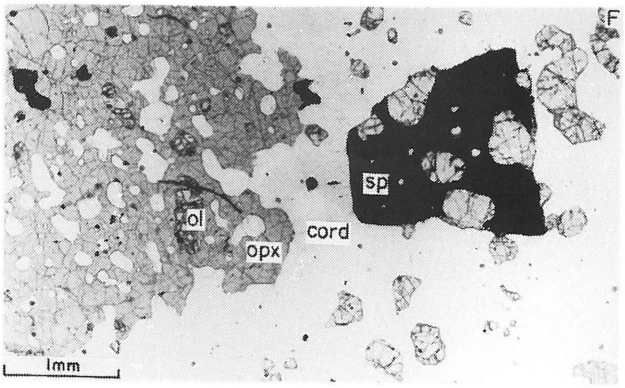

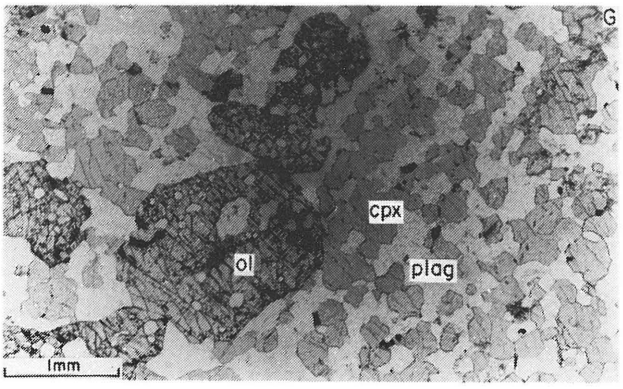

of the depletion of Mg, Fe, Ca and Al in the immediate vicinity of the porphyroblasts. Both pumpellyite and chlorite are believed to be of retrograde origin since the sample was collected within metres from the contact of the Bushveld Complex where the peak metamorphic temperature must have exceeded the upper temperature stability limits of both minerals.

3.3 Calcareous mineral assemblages

3.3.1 Assemblage group 1: clinochlore + dolomite + calcite + quartz ± phlogopite.

This assemblage group represents the lowest metamorphic grade observed in calcareous rocks from the study area. The samples are poorly recrystallized and large detrital quartz and feldspar grains occur in a predominantly dolomite matrix.

Subidioblastic clinochlore crystals are commonly twinned. The crystals are usually warped (Fig. 6 A) and may contain rare phlogopite and quartz inclusions. Subidioblastic phlogopite crystals are free from inclusions and show a faint yellowish pleochroism. Small amounts of calcite are present in the vicinity of phlogopite and clinochlore grains.

3.3.2 Assemblage group 2: tremolite + dolomite + calcite ± clinochlore ± phlogopite ± quartz.

Tremolite forms idioblastic to subidioblastic crystals that may contain carbonate and phlogopite inclusions (Fig. 6 B). Phlogopite inclusions in tremolite (PD - 57) are notably larger than the flakes in the matrix of the sample. Calcite is in contact with tremolite although dolomite is still the most important carbonate mineral.

3.3.3 Assemblage group 3: clinopyroxene + calcite ± dolomite ± tremolite ± phlogopite ± quartz ± K-feldspar.

Clinopyroxene occurs as granoblastic polygonal aggregates (PD - 130) or as subidioblastic (Fig. 6 C) to idioblastic (Fig. 6 D) crystals in a calcite matrix. The latter type often contains large inclusions of optically continuous tremolite (Fig. 6 E), while some crystals also

contain exsolution lamellae parallel to the c - pinacoid. Clinopyroxene layers which occur in a chert matrix consist of a core where the crystals are aligned parallel to the layers, and edges where the crystals have grown perpendicular to the layers to give rise to a comb texture (Fig. 6 F).

Tremolite and phlogopite occur as subidioblastic crystals or as inclusions in clinopyroxene. In samples where both calcite and dolomite are present, the former is associated with clinopyroxene. K-feldspar has only been observed in one sample (Fig. 6 C).

3.3.4 Assemblage group 4: forsterite + calcite + dolomite ± clinopyroxene ± tremolite ± phlogopite.

Partially or completely serpentenized olivine forms elongated crystals (Fig. 6 G) or rounded grains (Fig. 6 H) in a carbonate matrix. Xenoblastic to subidioblastic clinopyroxene crystals usually occur together with olivine, although some samples (PC - 36) are laminated with layers consisting of olivine and carbonates alternating with clinopyroxene or tremolite-rich layers. Both clinopyroxene and tremolite may occur together with olivine in a carbonate matrix (PC - 27). This assemblage may be genetically important as will be shown later.

Subidioblastic phlogopite crystals are common while dolomite is never in contact with forsterite.

3.3.5 Assemblage group 5: spinel + forsterite + calcite ± phlogopite ± clinopyroxene.

Spinel occurs as relatively large subidioblastic crystals with a dark green colour (Fig. 6 H) or as small colourless (PD - 208) to light apple green (PC - 10) idioblastic crystals. Where the spinel grains of the first type is included by forsterite a thin corona of clinochlore (retrograde origin) is developed around them. Such spinel grains have a resorbed appearance whereas spinels in contact with calcite or phlogopite have smooth crystal outlines. The colour appears to be related to the MgO /(MgO +FeO_T) ratio, with the colourless spinels having a ratio of up to 0,97.

Figure 6 Photomicrographs of calcareous metamorphic mineral assemblage groups 1 to 5. Abbreviations: dol = dolomite; cal = calcite; phlog = phlogopite; chl = chlorite (clinoclore); trem = tremolite; cpx = clinopyroxene; K-spar = K-feldspar; qz = quartz; sp = spinel; ol = olivine. Sections B,C,D and H have been photographed in plane polarized light and the remaining sections under crossed nicols. Sample numbers are indicated in brackets.

(A) Phlogopite and warped clinochlore crystals in a dolomite matrix (PD - 29)

(B) Subidioblastic tremolite crystals in a calcite matrix (PD - 57)

(C) Clinopyroxene and K-feldspar in a calcite matrix (PD - 157)

(D) Idioblastic clinopyroxene crystals in a calcite matrix (PD - 48)

(E) Optically continuous tremolite inclusions (black) in a clinopyroxene (light) crystal (PD - 162 a)

(F) Clinopyroxene layer in a chert matrix. Crystals near the middle of the layer have their c - axes parallel to the layer, while those near the rims have their c - axes perpendicular to the layer (PD - 166)

(G) Elongated forsterite crystals together with tremolite in a calcite matrix (PC - 27)

(H) Spinel inclusions in phlogopite from an olivine plus clinopyroxene-bearing assemblage (PD- 214)

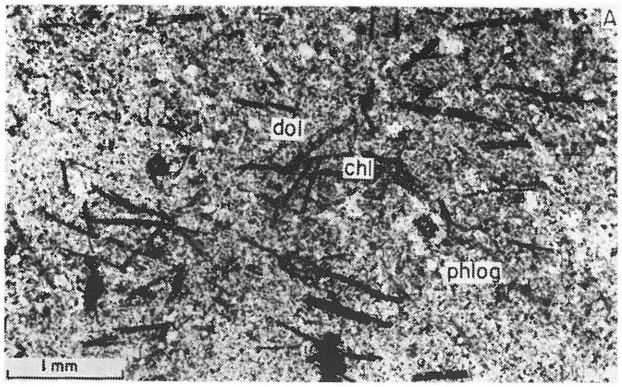

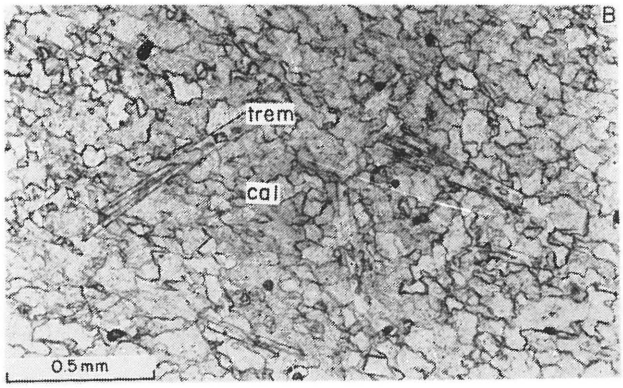

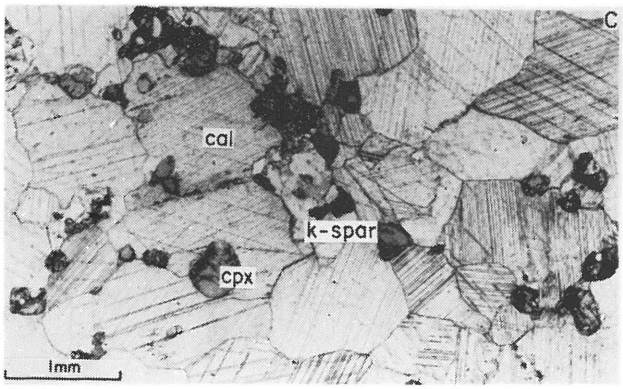

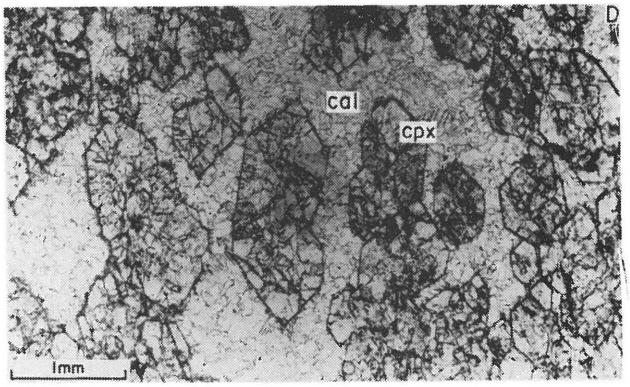

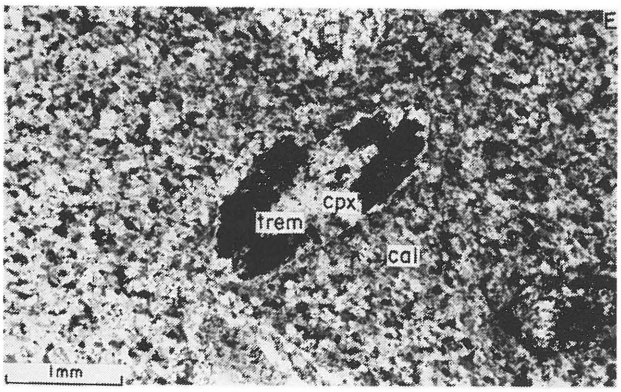

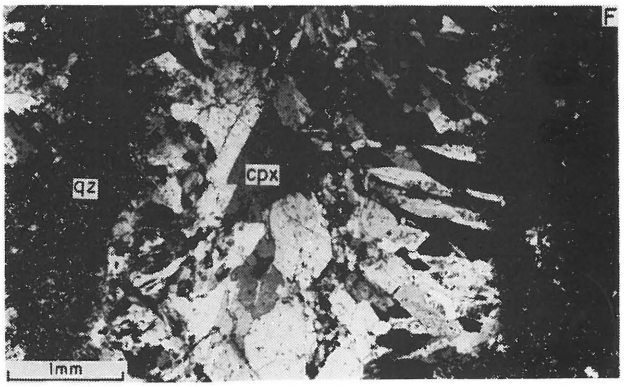

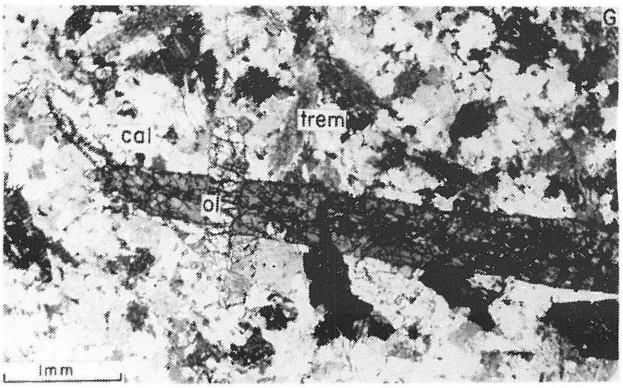

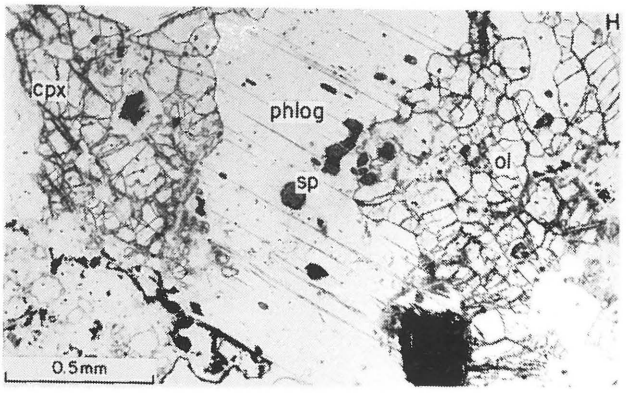

Forsterite grains are granular and are usually serpentenized Phlogopite crystals, up to 1,5 mm thick, were observed to include spinel and even forsterite.

3.3.6 Assemblage group 6: garnet ± clinopyroxene ± calcite ± plagioclase ± idocrase ± quartz.

Three textural types of garnet can be distinguished in this assemblage group. The first type forms isolated crystals in a calcite matrix (Fig. 7 A). Calcite and clinopyroxene inclusions are common and small crystals have an atoll texture due to garnet growth along calcite grain boundaries.

The second type of garnet forms massive layers that may contain many calcite inclusions in which case a web texture is formed (Fig. 7 B). The garnet layers often appear to separate calcite - from clinopyroxene - rich layers. The layering is probably caused by original differences in bulk composition.

The third type of garnet forms a symplectic intergrowth with clinopyroxene and occur together with larger sub-idioblastic clinopyroxene and garnet crystals (Fig. 7 C and D). The clinopyroxene is locally replaced by prehnite, which is of retrograde origin (Fig. 7 E). The garnet single crystals have identical compositions to the garnet intergrown with clinopyroxene while the clinopyroxene single crystals have considerably higher Al_2O_3 concentrations (13 wt. percent in PD -176) than the clinopyroxene intergrown with garnet (9 wt. percent in PD - 176).

A different relationship between clinopyroxene and garnet is displayed by one sample (Fig. 7 F) where irregular garnet crystals have grown along clinopyroxene grain boundaries, while garnet blebs may also be included by clinopyroxene. Clinozoisite and epidote appears to be replacing garnet and or clinopyroxene in a few samples. Similar to prehnite these minerals are considered to be of retrograde origin.

3.3.7 Assemblage group 7: clinopyroxene ± calcite ± quartz.

These samples are virtually monomineralic and comprise granular clinopyroxene crystals that may contain interstitial calcite, quartz and magnetite grains . Clinozoisite may be present as a retrograde alteration product.

3.3.8 Assemblage group 8: clinopyroxene ± amphibole ± plagioclase ± biotite ± calcite ± idocrase.

Subidioblastic clinopyroxene crystals usually approach diopside in composition. One sample, however, (PD - 96) contains crystals which have cores containing about 12 wt. percent Al_2O_3 and 4 wt. percent TiO_2 and rims containing about 7 wt. percent Al_2O_3 and 0,3 wt. percent TiO_2. The cores of these crystals display strong dispersion of the optical axes , which fades away towards the rims.

Amphibole occurs as subidioblastic crystals while idocrase either forms turbid xenoblastic grains or intergrowths with clinopyroxene. Plagioclase grains are usually sericitized.

Prehnite, epidote and clinozoisite are present as retrograde minerals. Prehnite either forms pseudomorphs after clinopyroxene, garnet and plagioclase or elongated idioblastic crystals enclosed in quartz aggregates (Fig. 7 G). The quartz aggregates occur in a clinopyroxene-rich matrix and it is suggested that these aggregates represent veins or cracks that developed in the rock as a result of volume reduction caused by degassing reactions. A siliceous, water-rich fluid then filled the cracks and the quartz-prehnite assemblage crystallized from this fluid.

An epidote-prehnite assemblage, in which the epidote forms large, zoned, idioblastic crystals (Fig. 7 H and 8 A) is also believed to have crystallized from a water-rich fluid that filled a crack in a clinopyroxene-rich rock upon cooling. Epidote and clinozoisite in the remaining samples replaces plagioclase and clinopyroxene.

Figure 7 Photomicrographs of calcareous metamorphic mineral assemblage groups 6 to 8. Abbreviations: cal = calcite; gar = garnet; cpx = clinopyroxene; qz = quartz; prh = prehnite ; ep = epidote. All sections have been photographed under crossed nicols. Sample numbers are indicated in brackets.

(A) Sieved garnet crystals in a calcite matrix (PC - 13)

(B) Garnet layer with web-texture due to calcite inclusions separating a clinopyroxene-rich layer from a calcite-rich layer (PD - 176)

(C) Two textural types of clinopyroxene and garnet. "gar I" and"cpx I" form subidioblastic crystals while "gar II" and "cpx II" are intergrown with one another (PD - 162 a)

(D) The garnet-clinopyroxene intergrowth at a higher magnification (PD - 176)

(E) Massive garnet, subidioblastic garnet crystals ("gar I") and garnet intergrown with clinopyroxene ("gar II") on a millimetre scale. Prehnite is of retrograde origin, probably after clinopyroxene (PD - 162 a)

(F) Garnet growing along clinopyroxene grain boundaries (OV - 4C)

(G) Quartz aggregate containing idioblastic prehnite crystals in a clinopyroxene and amphibole matrix (PD - 125)

(H) Prehnite showing typical weavy extinction (PD - 158)

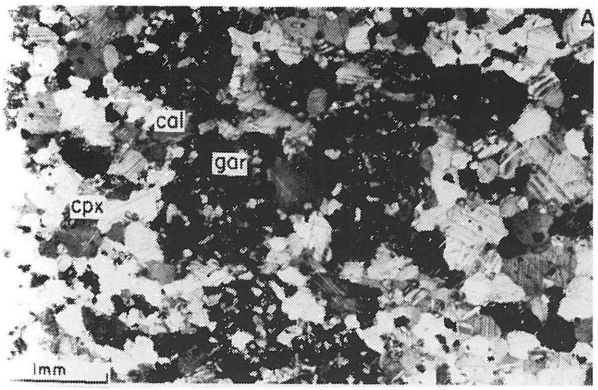

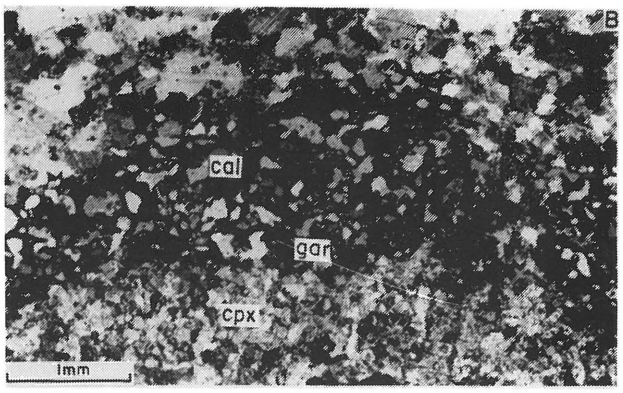

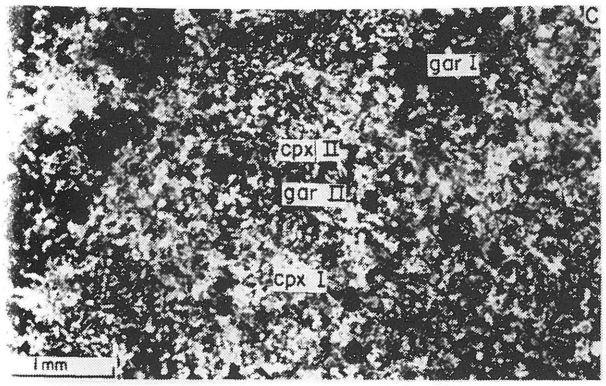

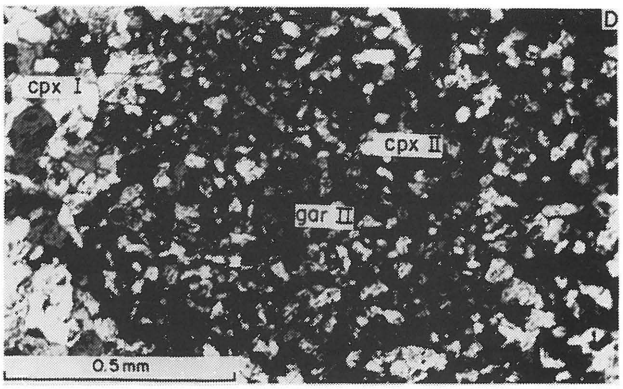

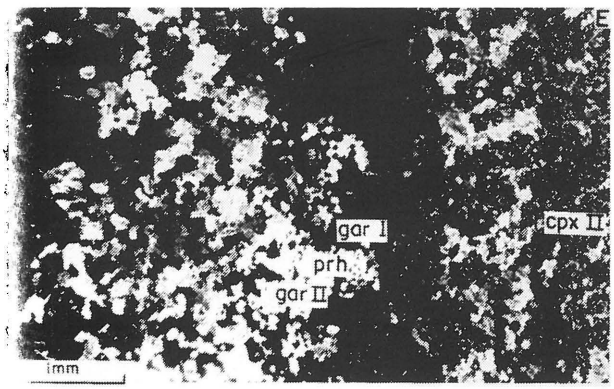

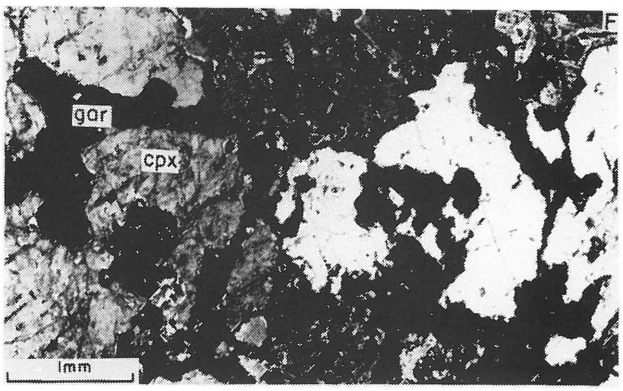

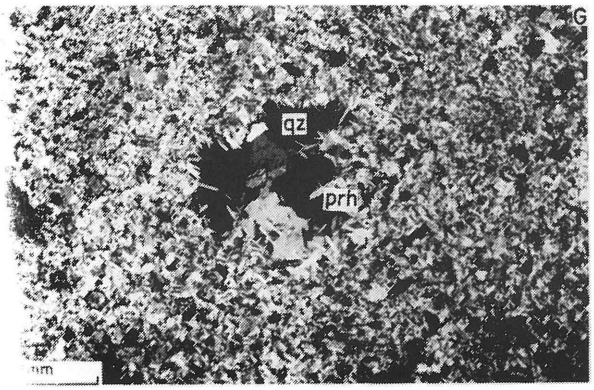

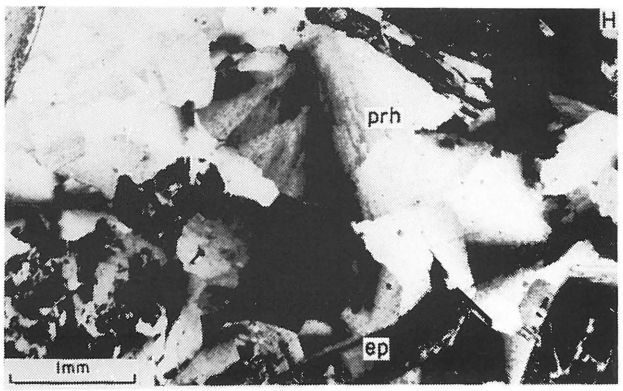

3.3.9 Assemblage group 9: clinopyroxene + spinel ± calcite.

Spinel crystals are idioblastic in outline and have a light green colour (Fig. 8 B). Subidioblastic clinopyroxene crystals are fassaitic in composition and together with spinel, give the samples a granoblastic polygonal appearance. Clinozoisite may be present as a retrograde mineral.

3.3.10 Assemblage group 10: wollastonite + clinopyroxene + calcite ± monticellite ± garnet.

Small subidioblastic wollastonite and clinopyroxene crystals give the rock a granoblastic appearance (Fig. 8 C) but when monticellite is present, an interesting intergrowth between wollastonite, monticellite and garnet is developed (Fig. 8 D-F). Groups of large wollastonite crystals may include small calcite grains in atoll-like fashion (Fig. 8 D) but more commonly it contains worm-like inclusions of monticellite or garnet or both minerals (Fig. 8 E and F). Garnet is usually present in larger quantities where both garnet and monticellite are present as inclusions. In such cases garnet appears to post-date monticellite as it can be seen cutting through monticellite inclusions. The monticellite has an unusually high birefringance and relief which is due to the high Mn concentration (7,0 wt. percent MnO) and low $MgO/(MgO + Feo_T)$ ratio (about 0,59).

3.3.11 Assemblage group 11: Ti-garnet + clinopyroxene + biotite + plagioclase + sphene + apatite + magnetite.

Orange-brown Ti-garnet crystals have idioblastic outlines and are strongly zoned (Fig. 9 A). The crystals contain rare inclusions of apatite, plagioclase, calcite and rutile that are sometimes concentrated near the rims of the crystals and that tend to be elongated in a direction parallel to the crystal faces, thereby giving rise to an atoll texture (Fig. 9 A).

Complete replacement of garnet is suggested by an aggregate of clinopyroxene, magnetite, sphene, calcite, plagioclase and tiny garnet remnants which shows a distinct pseudohexagonal

Figure 8 Photomicrographs of calcareous metamorphic mineral assemblage groups 8 to 10. Abbreviations: ep = epidote; prh = prehnite; sp = spinel; cpx = clinopyroxene; wo = wollastonite; cal = calcite; monti = monticellite; gar = garnet. Sections B,C and D have been photographed in plane polarized light and the remaining sections under crossed nicols. Sample numbers are indicated in brackets.

(A) Idioblastic zoned epidote crystal surrounded by prehnite (PD - 158)

(B) Spinel-clinopyroxene assemblage displaying a granoblastic polygonal texture (PD - 177)

(C) Wollastonite and clinopyroxene in a calcite matrix (PD - 191)

(D) Wollastonite - monticellite intergrowth in a calcite matrix (PD - 194)

(E) and (F) Intergrowths between wollastonite, monticellite and garnet in a calcite matrix (PD - 194)

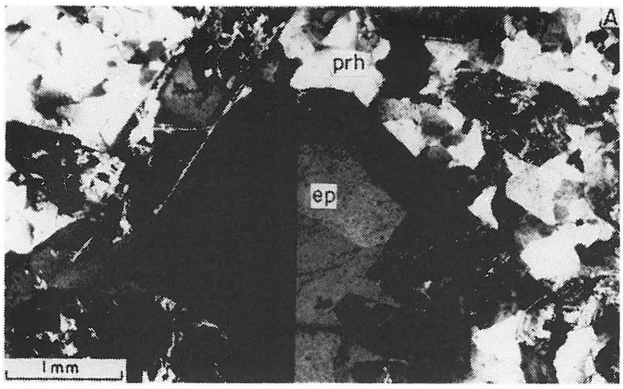

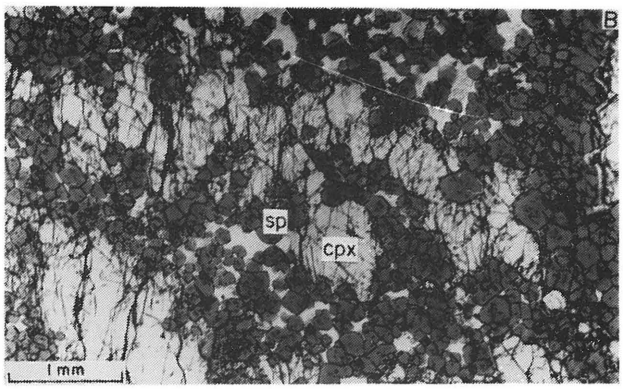

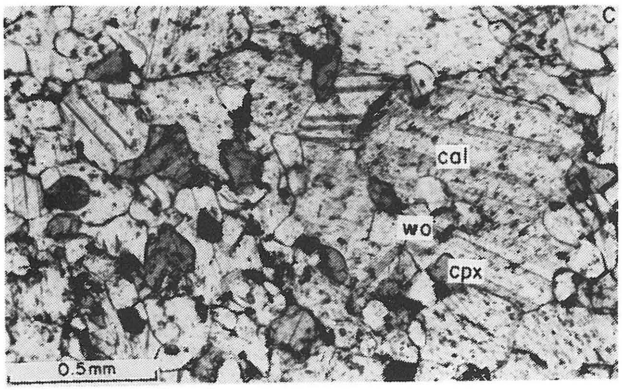

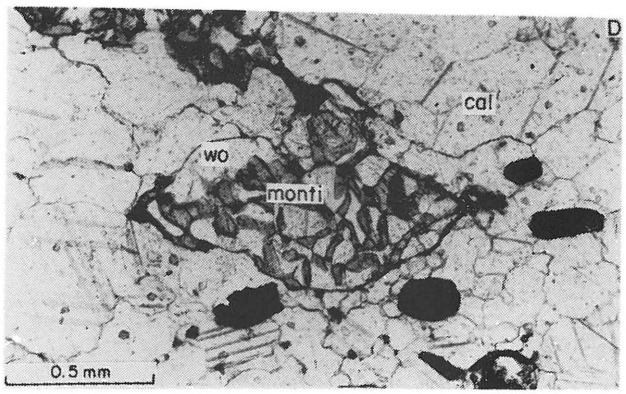

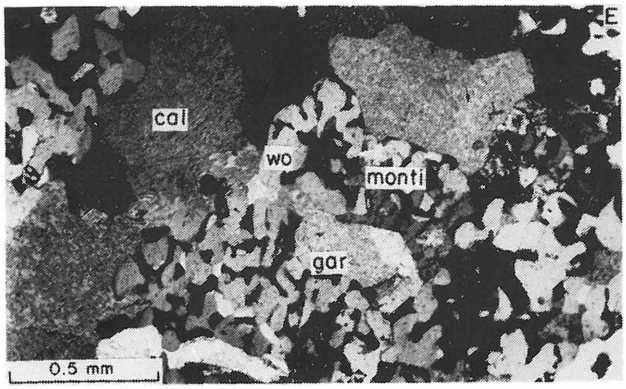

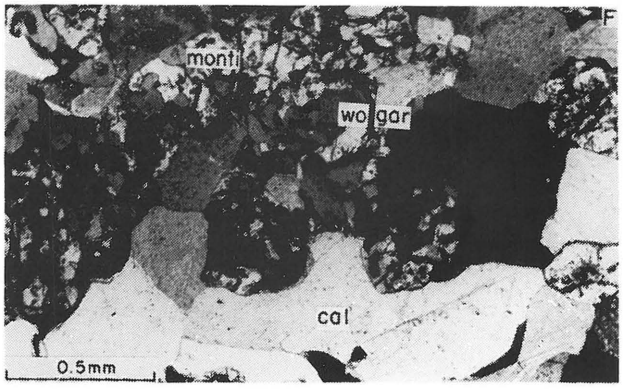

outline similar to that of the garnet crystals, (Fig. 9 B)

A second clinopyroxene textural type consists of an intergrowth between calcite and optically continuous, elongated clinopyroxene "islands" in a calcite matrix (Fig. 9 C). The intergrowth displays an overall idioblastic outline that is elongated in a direction parallel to the C - axes of the clinopyroxene fragments. Magnetite and biotite are often concentrated outside the boundaries of the intergrowths. The texture probably resulted from the retrograde replacement of clinopyroxene by a calcite-producing reaction.

Two textural and chemical types of plagioclase are also present. The first type forms small, slender subidioblastic crystals which form, together with magnetite, sphene and clinopyroxene the matrix of the rock. The second type forms relatively large crystals that occur in rounded aggregates in the matrix (Fig. 9 D). The peripheral crystals in the aggregates are orientated with their C - axes perpendicular to the perimeter, while those near the core have a random orientation. The composition of the two types corresponds to the peristerite gap; the first type having an anorthite content of about 17 percent compared to 3 percent of the latter type.

Figure 9 Photomicrographs of pelitic metamorphic mineral assemblage group 14 and calcareous metamorphic mineral assemblage group 11. Abbreviations: gar = garnet; mag = magnetite; sph = sphene; cpx = clinopyroxene; cal = calcite; bi = biotite; ap = apatite; plag = plagioclase; chl = chlorite; qz = quartz. All sections, except E, have been photographed in plane polarized light. Sample numbers are indicated in brackets.

(A) Idioblastic Ti-garnet crystal containing inclusions which have their c - axes parallel to the crystal boundaries (PH - 79)

(B) Aggregate of magnetite, sphene, clinopyroxene, calcite and plagioclase replacing garnet. The pseudohexagonal outline of the original garnet crystal is clearly visible (PH - 79)

(C) Optically continuous clinopyroxene fragments enclosed by calcite. The calcite has been produced by a clinopyroxene breakdown reaction. The original clinopyroxene crystal outline is visible due to a concentration of tiny opaque minerals outside the original crystal boundaries (PH - 79)

(D) Two textural types of plagioclase. "plag I" forms aggregates and has the composition An_3 while "plag II" forms tiny subidioblastic crystals with the composition An_{17} (PH - 79)

(E) Large anisotropic garnet crystal surrounded by quartz and some chlorite (PH - L)

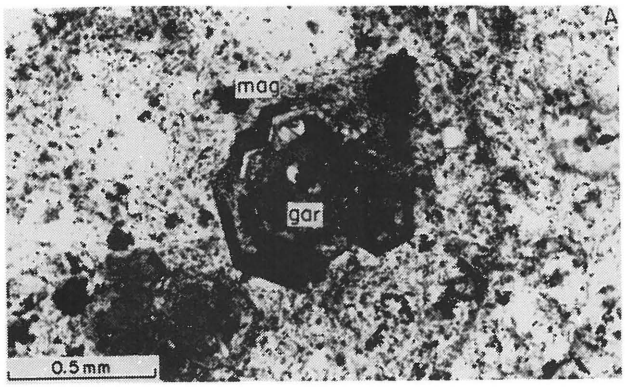

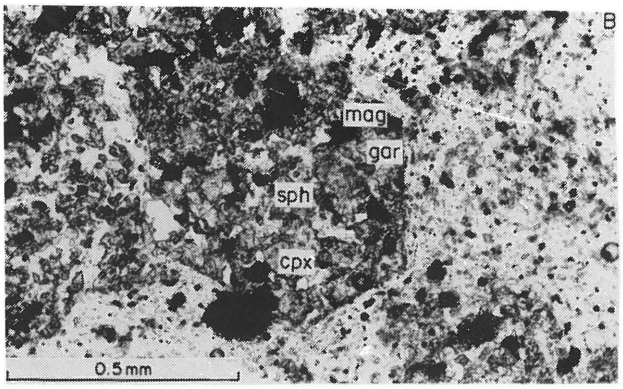

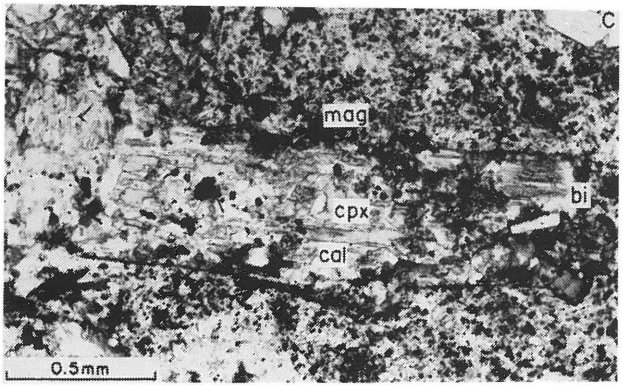

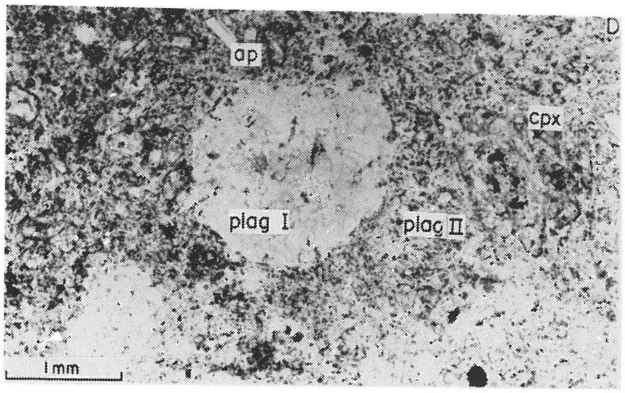

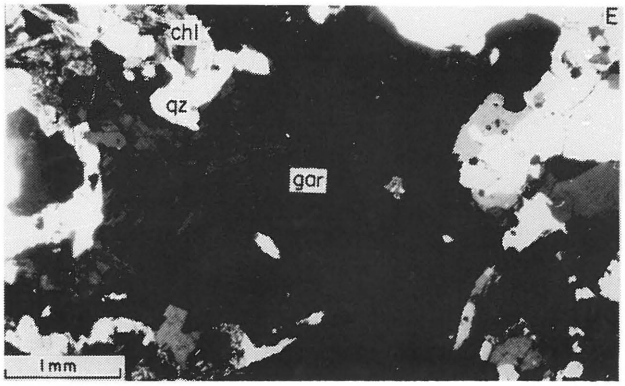

4 GEOCHEMISTRY

4.1 Introduction

Bulk rock analyses were carried out to determine whether the presence of certain minerals in a sample could be related to the composition of the rock, and to compare the chemistry of the various pelitic and calcareous formations with one another.

4.2 Analytical procedures

4.2.1 Sample preparation

Most of the samples selected for chemical analyses were sufficiently fine-grained to permit the use of relatively small amounts of material. Where original bedding was discernable in the specimen, the material required for chemical analyses was cut from the sample parallel to the sedimentary bedding in order to avoid chemical differences that may exist between the layers. Large specimens were collected in the field in the case of coarse-grained rocks with large porphyroblasts.

The material was crushed to chips smaller than about 5 mm in diameter with the aid of primary and secondary steel-faced jaw crushers. The chips were then reduced to -300 mesh powder in a chrome steel disc mill.

4.2.2 Major and trace element analyses by X.R.F.

Glass discs, prepared according to the method of Norrish and Hutton (1969) as modified by the University of Cape Town, were analysed for major elements (Si, Ti, Al, Fe, Mn, Mg, Ca, K, P, Cr and Ni). Sodium was analysed in powder pellets. Analyses were performed in duplicate on 103 of the samples, while single analyses were performed on the remaining 26 samples. Total Fe was expressed as Fe^{2+}. The Geological Survey laboratory determined the CO_2 concentrations in

27 calcareous rock samples.

The trace elements Nb, Zr, Y, Sr, Rb, Cu and Zn were determined for all samples in compressed powder pellets. Ga and Hf were only determined for the pelitic rock samples.

Accuracy of the major element analyses is estimated to be better than one percent relative for elements in concentrations greater than one percent, and better than two percent relative at lower concentrations. Accuracy of trace element analyses is approximately ± 5 percent relative for concentrations below 20 ppm and ± 2 percent above 50 ppm. Precision of major and trace element analyses is similar to their accuracy at low levels but is better than ± 0,5 percent at concentrations of more than 5 percent or 50 ppm for major and trace elements respectively.

Major and trace element concentrations, as well as the mineral assemblages of the analysed samples are given in Appendix 1.

4.3 Chemistry of the pelitic formations.

For the purpose of comparing the chemistry of the pelitic formations some commonly used diagrams, or modifications of such diagrams were used (Figs. 10,11). The ACF and AKF diagrams are usually constructed for rocks that contain excess SiO_2 (Winkler, 1979; Hutchison, 1974) but this condition is not fulfilled by all the samples plotted in Figure 10. Seeing that Fe_2O_3 was not determined and modal analyses were not performed the A,C,F and K points in the ACF, AKF and AFM diagrams were modified as follows:

$A = Al_2O_3$ $\quad\quad$ $C = CaO$

$F = FeO_T + MgO + MnO$ $\quad\quad$ $K = K_2O$

The omittance of the corrections of the A,C and F components for interference minerals does not introduce serious errors in the modified diagrams since these minerals are present in very small quantities in most samples. The most serious difference between the conventional ACF, AKF and AFM diagrams and the ones used in this study is the omission of Fe_2O_3 from point A

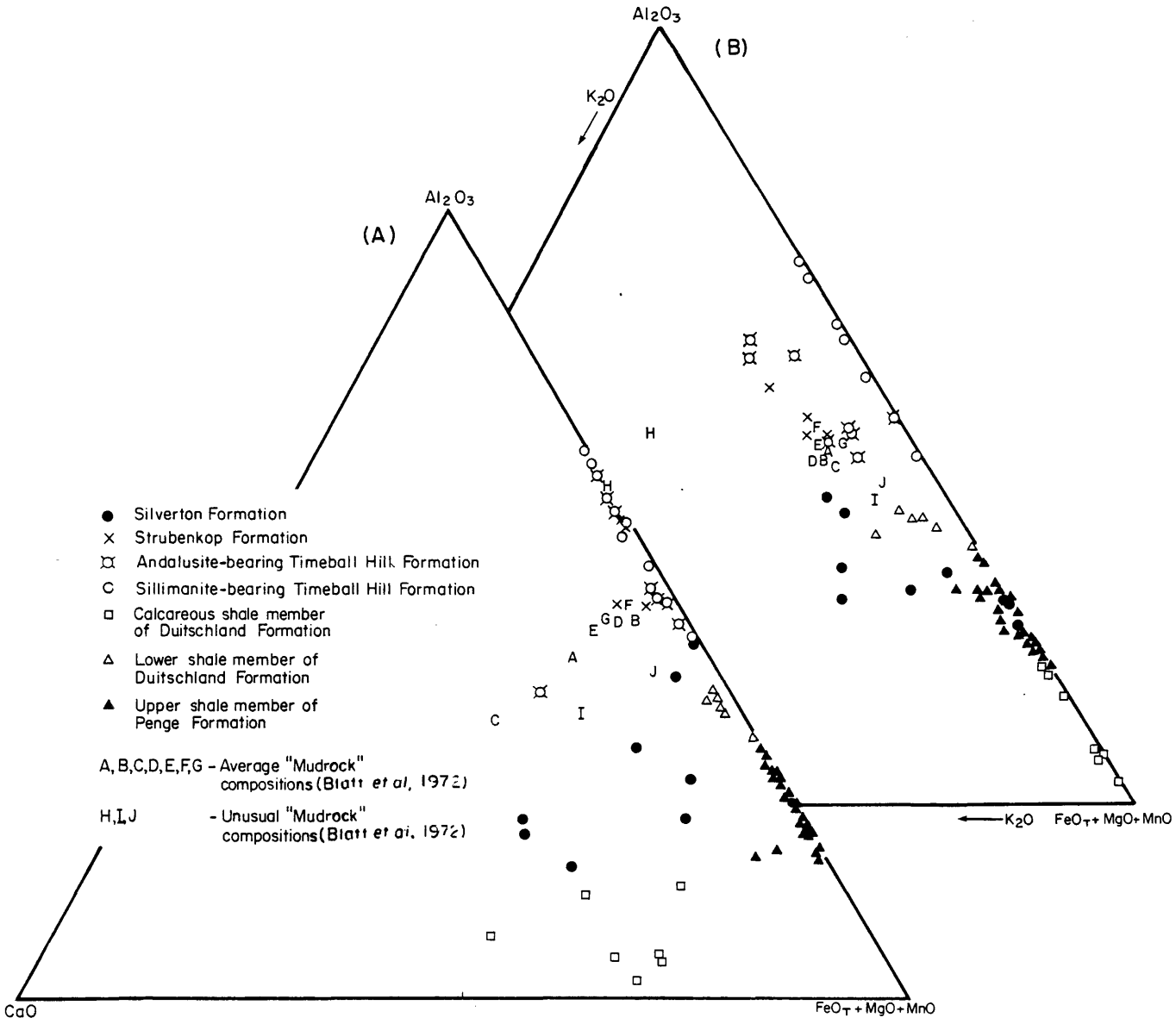

Fig. 10: Composition of the pelitic units from the Potgietersrus area compared to average- and unusual-mudrock compositions cited in the literature

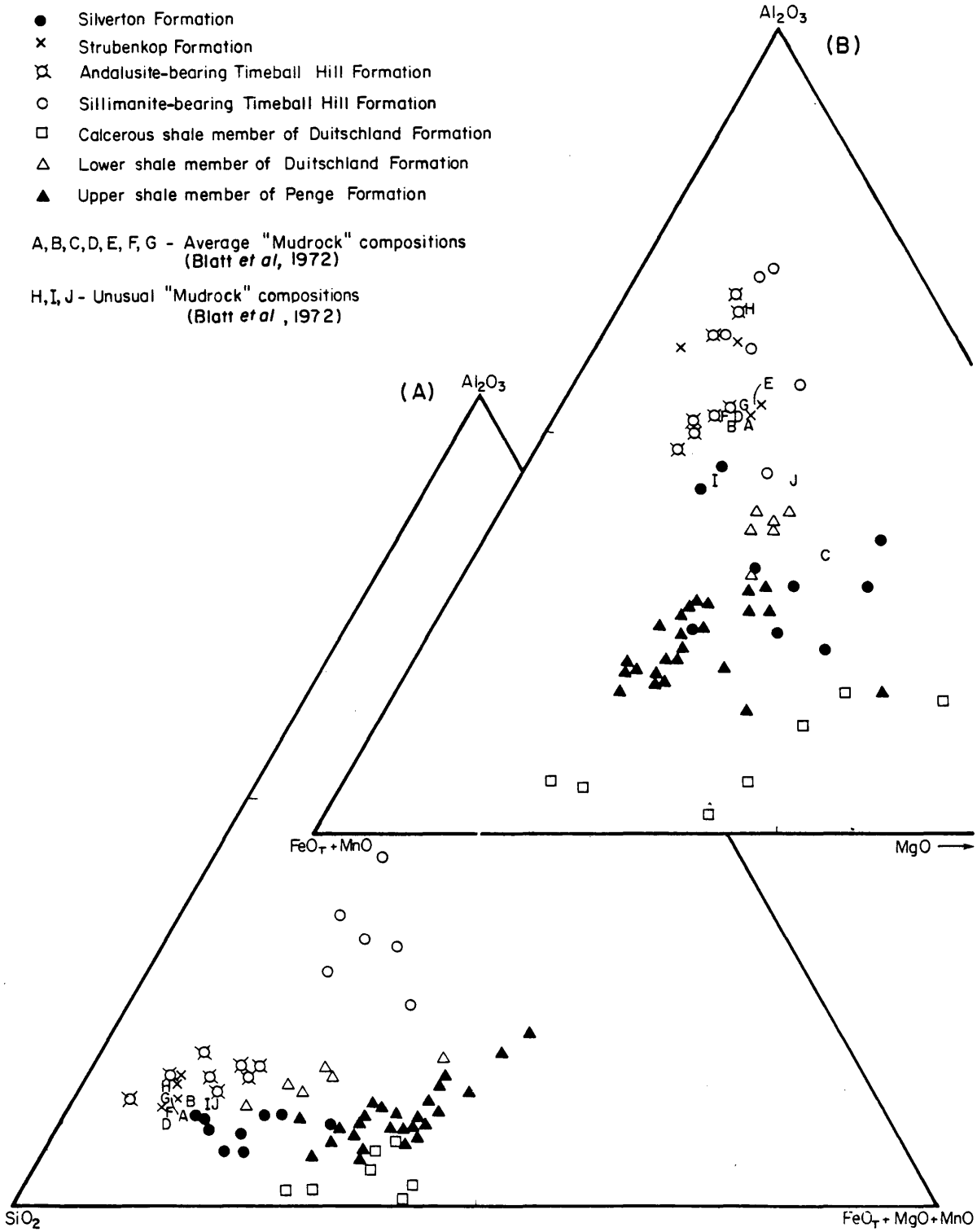

Fig. 11: Composition of the pelitic units from the Potgietersrus area compared to average- and unusual-mudrock compositions cited in the literature

The SiO_2 - Al_2O_3 - FeO_T +MgO +MnO diagram (Fig. 11) is based on the Si - Al - Fe_T diagram of Moore and Dennen (1970) who used it for the classification of sedimentary rocks. MgO and MnO were included in Figure 11 because of the high concentration of the former element in some of the pelitic formations. Analyses of average pelites as well as pelites with uncommonly high percentages of particular oxides (Blatt et al., 1972) are also plotted on Figures 10 and 11 for comparative purposes.

A plot of the mean concentrations of the most important major elements in the pelitic units, relative to the average shale composition (Shaw, 1956) (Fig. 12) reveals the following trends regarding the evolution of these units:

1) The mean SiO_2 concentration of the Pretoria Group formations is much higher than that of the Chuniespoort Group formations and there is a distinct compositional break between the two groups.
2) The upward increase in the SiO_2 content is accompanied by a concomitant decrease in FeO_T.
3) Formations with a relatively high CaO content are depleted in Al_2O_3.

4.3.1 The evolution of the pelitic formations

4.3.1.1 The shale member of the Penge Formation.

Rocks with a similar enrichment in FeO_T and MgO and depletion in SiO_2 and alkalis are rare in nature. Davidson and Mathison (1974) reported orthopyroxene + cordierite + garnet + biotite rocks from Western Australia with a similar composition, while Lal and Moorhouse (1969) as well as Lal and Shukla (1975) suggested that high FeO_T + MgO and low SiO_2 rocks may form through the metasomatic introduction of MgO and FeO and the simultaneous removal of alkalis by hydrothermal fluids generated by the magma that caused the metamorphism. Another explanation calls on the enrichment of MgO and FeO as the result of the removal of a granitic fraction from the parent rock during differential anatexis. These processes can, however, not be invoked to explain the

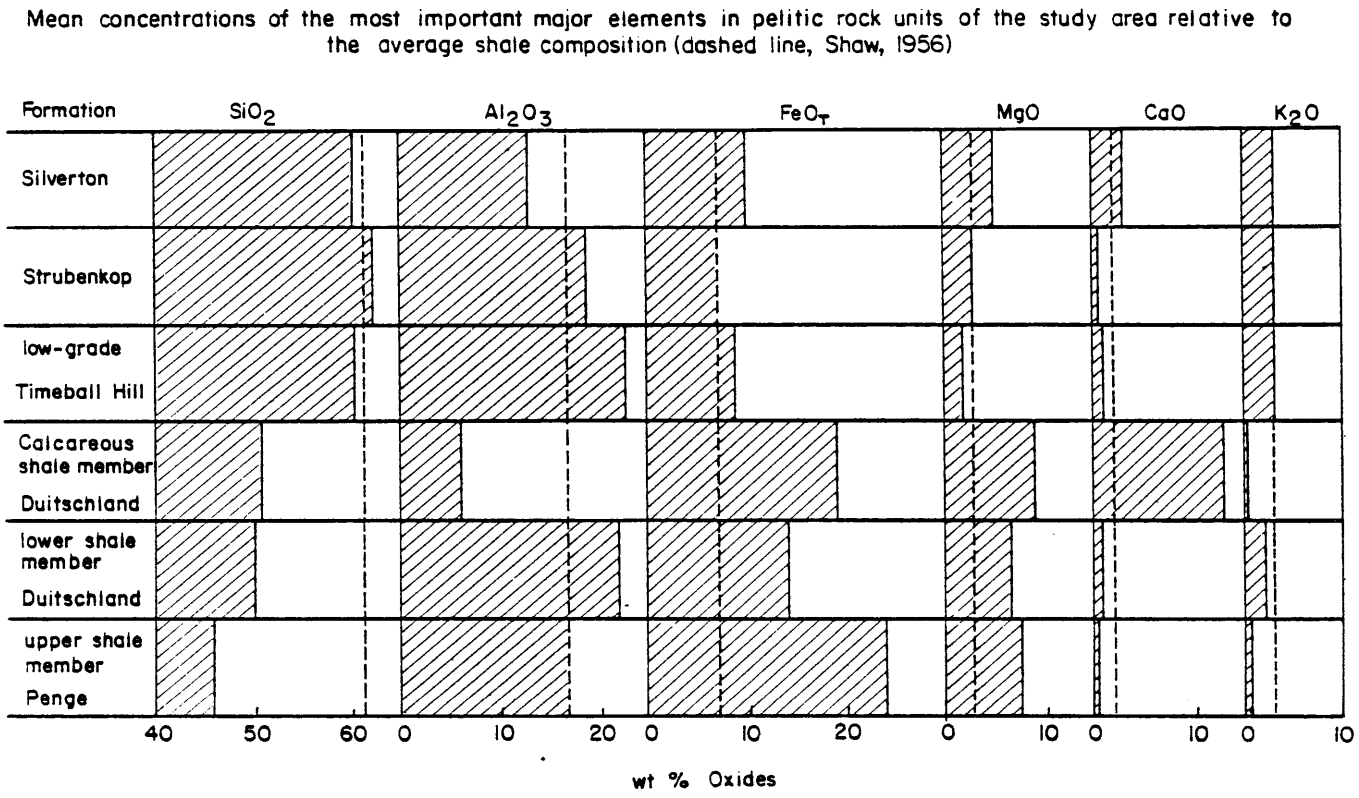

Fig. 12: Variation in the mean concentrations of the most important major elements in the pelitic units, illustrating the chemical evolution of these units

abnormal composition of the shales of the Penge Formation since the shales of the overlying Duitschland Formation do not show similar chemical features in proximity of the Bushveld Complex.

It is believed that the underlying ferruginous sedimentary rocks controlled the chemistry of the shales at the time of their deposition. The presence of berthierine (chamosite) in the Penge Formation (James, 1966), as well as the similarity in the composition of berthierine as given by Iijima and Matsumoto (1982) and Rohrlich et al. (1969) to the bulk composition of the Penge Formation shales suggest that these shales represent original chamosite-rich rocks. This theory is substantiated by the presence of 7 Å and 14 Å reflections in two samples of the Penge Formation shales (D. Bühmann, pers. comm.). The high MgO content of the shales, compared to the average chamosite composition, points to the formation of chamosite in a shallow marine, rather than a continental environment (D. Bühmann, pers. comm.), in which case the Mg could have been derived from seawater trapped in sediment pores.

The berthierine is believed to have formed through a reaction similar to the one proposed by Iijima and Matsumoto (1982) for berthierine occurrences in freshwater, sideritic, kaolinitic shales in coal swamps, because both the coal swamps and the Penge Formation formed under reducing conditions. The presence of shale beds indicate that clays and silt were introduced into the Penge basin so that the berthierine - producing reaction could be

$$\underset{\text{kaolinite}}{Al_2Si_2O_5(OH)_4} + 2\,FeCO_3 \rightleftharpoons \underset{\text{berthierine}}{Fe_2Al_2SiO_5(OH)_4} + SiO_2 + 2CO_2 \quad ...4\,(1)$$
$$\text{siderite}$$

as was suggested by Iijima and Matsumoto (1982). The reaction can be slightly modified to account for the higher MgO content of the Penge Formation shales:

$$Mg^{2+} + Al_2Si_2O_5(OH)_4 + FeCO_3 \rightleftharpoons (Fe,Mg)_2Al_2SiO_5(OH)_4 + SiO_2 + CO_2 \quad ..4\,(2)$$

A further point in support for this reaction is the relatively high Al content of the Penge Formation shales. According to Iijima and Matsumoto (1982) the berthierines derived from kaolinite are aluminous with Si/Al ratios < 1.

The model proposed for the genesis of the shale member of the Penge Formation is modified from Button (1973). Fresh water carried silt and clay into the Penge basin. Gradual mixing of fresh and saline water resulted in the cessation of chemical sedimentation (by dilution) and in the flocculation and settling of the clay and silt. The saline water trapped in the silt and clay layer subsequently crystallized minerals such as siderite that reacted with kaolinite to porduce berthierine during early diagenesis. This reaction can proceed at temperatures as low as 65°C (Iijima and Matsumoto, 1982).

4.3.1.2 The lower shale member of the Duitschland Formation

The FeO_T and MgO values in this member are still relatively high, but this is to be expected since the formation overlies very FeO-rich rocks. The increase in the K_2O concentration is accompanied by a relatively small increase in SiO_2 and a relatively large increase in Al_2O_3 compared to the Penge shales, suggesting that illite and kaolinite were more important constituents than K-feldspar in these shales since K-feldspar contains about 30 percent more SiO_2 in its formula than average illite.

It is suggested that this unit derived its FeO and MgO from the underlying Penge Formation at a time of non-deposition that preceded the deposition of the Duitschland Formation of which the basal diamictite is an indication. The sediments that were transported into the basin contained silt, kaolinite and illite, while the carbonaceous nature of the shales indicates reducing conditions in the basin.

4.3.1.3 The calcareous shale member of the Duitschland Formation

The high CaO and low Al_2O_3 concentrations indicate that this member is not a true pelite but a rock intermediate between a shale and a limestone. The low Al_2O_3 and K_2O

concentrations are probably caused by a decrease in the clay component, while the high CaO and MgO content is due to the presence of calcite and or dolomite. The high SiO_2 content can be ascribed to a large silt component in the original rock.

The high FeO_T content is problematic since this member does not overly ferruginous lithologies from which the Fe could have been derived. It is suggested that the Fe is of similar origin as the Fe of the Penge Formation and the ferruginous dolomites in the Malmani Subgroup, i.e. that it was precipitated as ferruginous carbonates or even oxides similar to Button's (1973) "Iron Formation Precursor". The source of the Fe for the ferruginous lithologies of the Chuniespoort Group may be unique to Chuniespoort Group times as suggested by the sharp drop in the average Fe content of the Pretoria Group sediments compared to the formations of the Chuniespoort Group (Fig. 12). Another distinctive feature of the Chuniespoort Group is its low average SiO_2 content when compared to the shales of the Pretoria Group. On chemical ground, therefore, the Duitschland Formation should be included in the Chuniespoort, rather than the Pretoria Group.

4.3.1.4 The "low-grade" Timeball Hill and Strubenkop Formations

Except for relatively low CaO and high Al_2O_3 concentrations, both formations have compositions very similar to the average shale (Fig. 12).

4.3.1.5 The Silverton Formation

The presence of calcite and or dolomite may explain the relatively high CaO and MgO concentrations in this formation. The K_2O content is the same as the average shale and the decrease in the Al_2O_3 concentration is therefore probably the result of a decrease in the kaolinite component in the original rock.

4.3.1.6 The "high-grade" Timeball Hill Formation

The samples from the Timeball Hill Formation can be divided into "low-grade" (andalusite-bearing) and "high-grade"

(sillimanite + spinel ± corundum - bearing) groups. The high-grade samples are further characterized by the absence of free quartz. The low-grade group has a mean composition similar to that of the average shales, while the high-grade group shows a strong depletion in SiO_2 and alkalis that is compensated for by a significant increase in the Al_2O_3 concentration (Table 5). The peculiar composition of these rocks can either be ascribed to a very unusual original rock composition or to modification of the composition during metamorphism. It is considered very unlikely that the pre-metamorphic composition of the pelitic member of the Timeball Hill Formation changed so drastically after remaining constant over more than 25 km strike length. A very unusual bulk composition is therefore discarded.

All the high-grade samples were collected within metres from the contact with the Bushveld Complex and it will later be shown that temperatures exceeded 800°C at these localities. The enrichment in Al_2O_3, FeO_T and MgO and the depletion in SiO_2 and alkalis, as well as the higher MgO /(MgO + FeO_T) ratio in the high-grade samples is consistent with the removal of a granitic melt (Brown and Fyfe, 1970) and such a mechanism is therefore postulated for the formation of these samples.

In order to semiquantatively evaluate the partial melting process the compositions of the low-and high-grade Timeball Hill shales were plotted on a variation diagram as suggested by Bowen (1928) (Fig. 13). The two points indicating the proportions of each oxide are joined by straight lines, and these lines are produced in both directions. Any material that is more siliceous than the low-grade Timeball Hill shales has a composition such that, if it were subtracted from the low-grade Timeball Hill shales, the high-grade Timeball Hill shales would result. The MgO line falls to zero at 71 wt percent SiO_2 and this is therefore the most siliceous possible material that could be subtracted to produce the high-grade Timeball Hill shales. The proportions of all other oxides are fixed by their ordinates above this point, C in Figure 13. The MgO curve is not known accurately enough to fix its intersection

TABLE 5 Mean compositions and standard deviations of the low- and high-grade Timeball Hill shales and the composition of the material subtracted from the former to produce the latter

	Low -grade Timeball Hill shales		High-grade Timeball Hill shales		subtracted material
	Mean [a]	S[c]	Mean[b]	S[c]	
SiO_2	58,76	5,21	35,80	4,22	71,0
TiO_2	0,83	0,13	0,34	0,61	-
Al_2O_3	21,50	2,27	44,18	7,99	9,0
FeO_T	7,60	2,78	10,98	2,78	5,5
MgO	2,12	0,59	5,79	1,62	-
MnO	0,05	0,02	0,07	0,01	-
CaO	0,27	0,16	0,27	0,26	-
Na_2O	0,98	0,10	0,58	0,29	1,5
K_2O	3,22	0,55	0,31	0,19	4,5
L.O.I.	3,96	1,26	1,89	0,97	-
H_2O^-	0,36	0,28	0,11	0,03	-
TOTAL	99,65		100,32		91,5 [d]
$MgO/(MgO + FeO_T)$	0,333		0,485		

	CIPW norm
Q	40,4
or	26,7
ab	12,6
C	1,6
hy	10,2

a: Arithmetic mean of 6 analyses

b: Arithmetic mean of 5 analyses

c: S = standard deviation

d: The summation is not to 100 percent because H_2O; TiO_2; CaO; MnO and minor constituents are omitted and because of uncertainties in the positions of the lines for the various oxides.

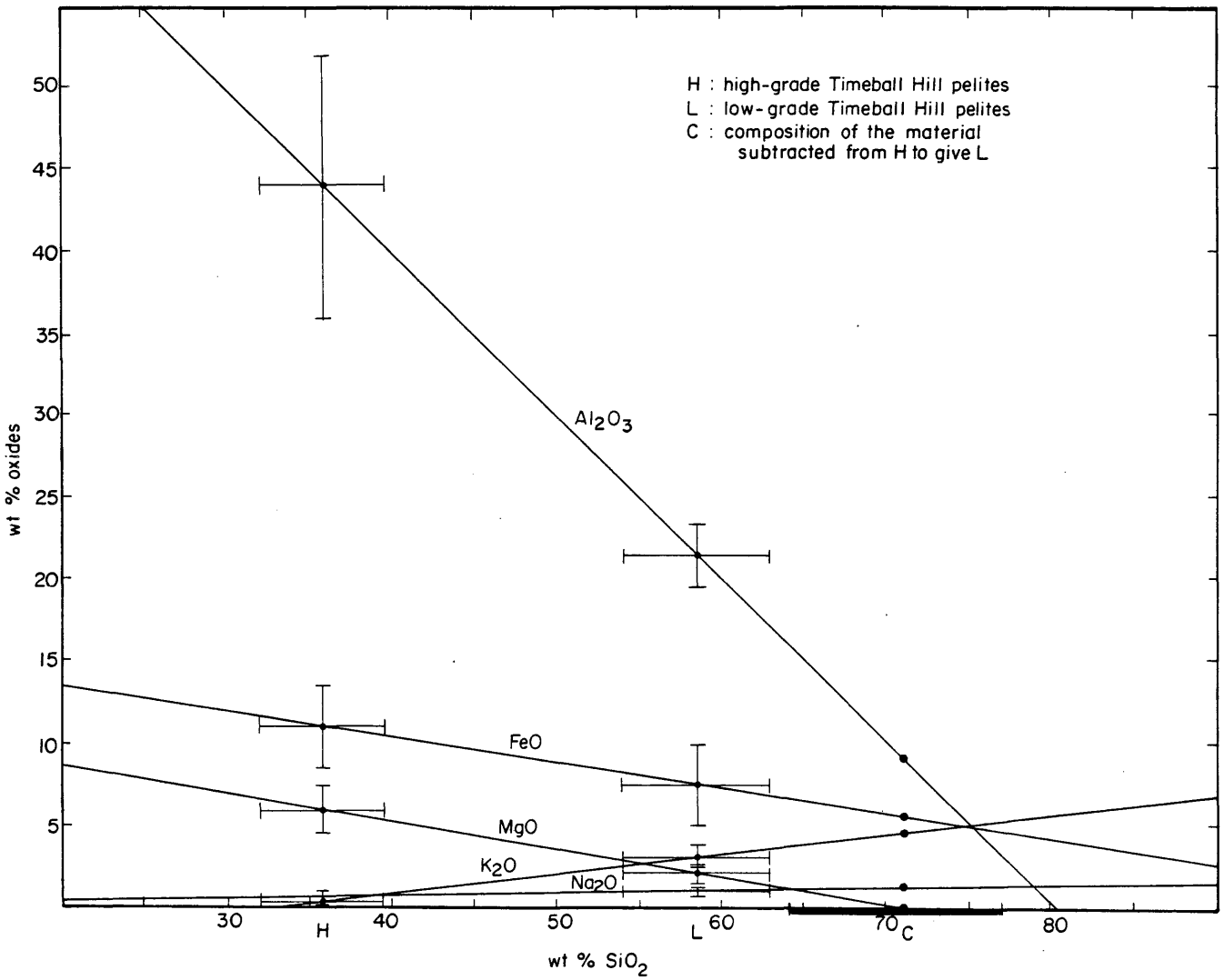

Fig. 13: Graphical solution of the nature of the material subtracted from the low-grade Timeball Hill pelites to produce the high-grade Timeball Hill pelites. Heavy bar at composition C represents the range over which the MgO curve may fall to zero, based on the standard deviations of the two MgO points

with the axis of abscissae exactly at 71 wt percent SiO_2 and the standard deviations for the two MgO points were therefore used to obtain a range (71 $\pm$ 6 wt percent SiO_2) over which the MgO line may fall to zero.

The subtracted material (Table 5) has a granitic norm. When 65 percent of composition C is subtracted from the low-grade Timeball Hill shales the composition of the high-grade Timeball Hill shales is obtained.

Due to poor outcrops no granitic material was found in the area. Some samples (PH - 190) show a texture that resembles flow banding. This texture may be the result of plastic deformation of the rock during anatexis.

4.3.2 Trace element distribution between the low- and high-grade Timeball Hill Formations

Support for the removal of a granitic melt from the high-grade Timeball Hill Formation is also provided by the trace element distribution between this lithology and its low-grade equivalent. A large depletion in Rb, Sr, Y, Zr, Nb and Hf and an enrichment in Ga in the high-grade samples relative to the low-grade samples was detected (Fig. 14).

The mean Rb concentration of about 170 ppm in the low-grade samples is similar to the value reported for shales (Wedepohl, 1978), while the high-grade samples have values below 30 ppm. The decrease in Rb is linked to the decrease in K_2O in the high-grade samples with which it has a positive correlation (Wedepohl, 1978). Several workers e.g. Lambert and Heier (1968) as well as Heier (1960) noted a depletion in Rb in medium to high pressure granulites in Australia and Norway respectively, but the depletion is never as extensive as in the case of the high-grade Timeball Hill pelites.

The mean Sr concentration in the low-grade samples (about 125 ppm) is slightly lower than the 130 - 280 ppm recorded for carbonate-poor argillaceous rocks (Wedepohl, 1978). Although Sr normally substitutes for Ca, the decrease to 5 - 35 ppm in the high-grade samples is apparently related to the drop in the K_2O concentration with which Sr may be correlated

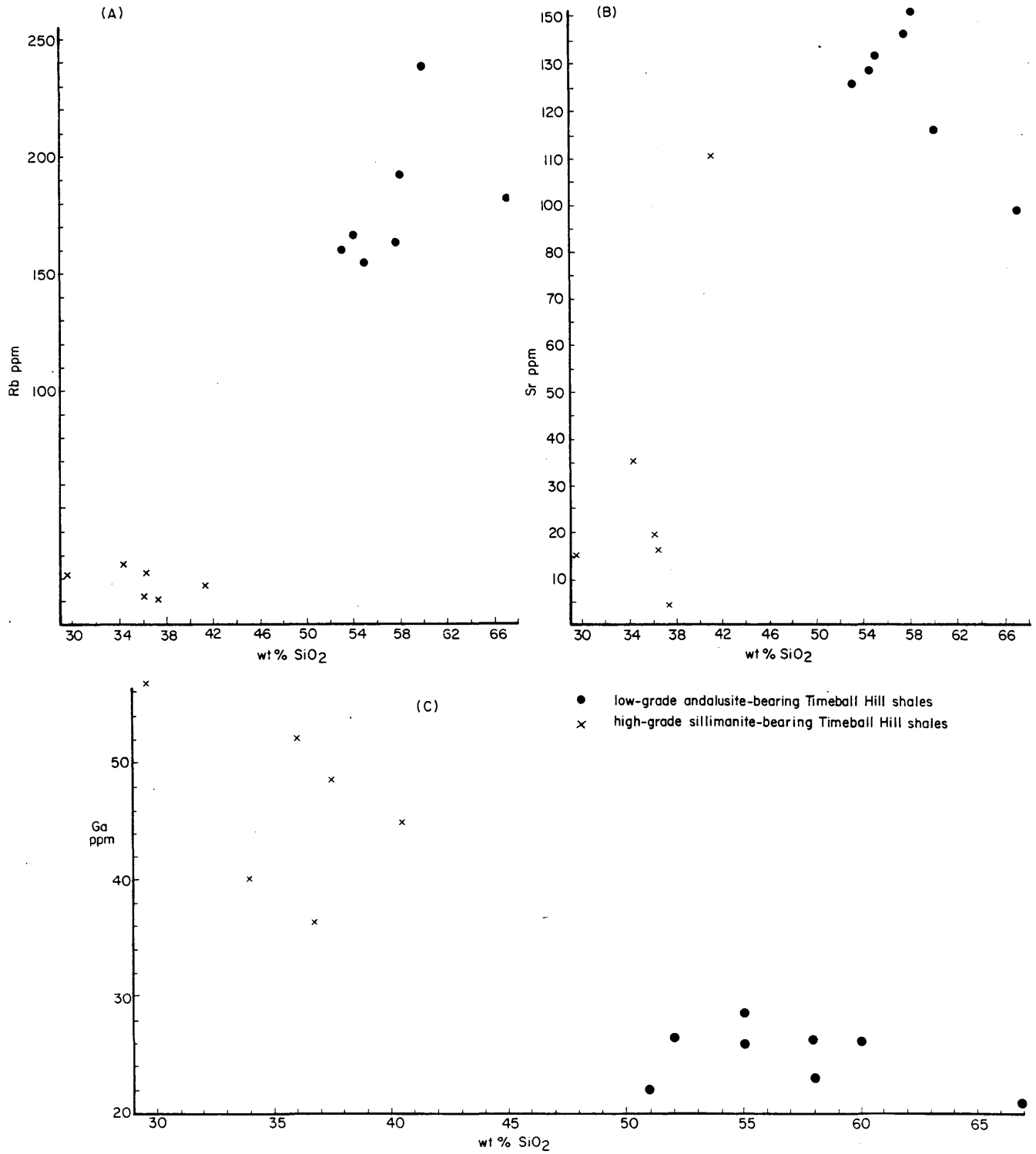

Fig. 14: Plot of the concentrations of Rb, Sr and Ga against wt percent SiO_2 for the low- and high-grade Timeball Hill pelites

(Heier, 1966), since both the low- and high-grade shales have similar Ca concentrations. Sr is reported to be more mobile in contact metamorphism than in regional metamorphism and the rate of Sr exchange in contact metamorphism appears to depend on the chemical nature of the rock and on temperature (Ghose, 1966).

The mean Y concentration in the low grade samples (about 28 ppm) is similar to the values reported for shales (Wedepohl, 1978), while the high-grade samples have values below 4 ppm.

The mean Zr content of about 180 ppm in the low-grade samples agrees closely with the values reported for shales (Wedepohl, 1978). The Zr is mainly accomodated by zircon although ilmenite and rutile may also contain Zr due to the Zr^{4+} - Ti^{4+} substitution. The depletion of Zr in the high-grade samples ($\leq$ 10 ppm) is surprising in view of the relative stability of zircon in the metamorphic environment. The behaviour of Zr in this system appears to be anomalous and a satisfactory explanation cannot be given.

The low-grade samples have a mean Nb concentration of 17 ppm which is identical to the average value reported for argillaceous rocks by Wedepohl (1978). The high-grade samples have concentrations below 5 ppm. A decrease of Nb during metamorphism has also been found by Drury (1973) in a study of pyroxene gneisses from the Lewisian Complex, Inner Hebrides.

The mean Hf concentration of 7 ppm in the low-grade samples agrees with the average value reported for shales (Wedepohl, 1978). Due to the high lower limit of detection (4 ppm) the values for the high-grade samples could not be evaluated.

The low-grade samples have a mean Ga content of 28 ppm which is in agreement with the value for schists and hornfelses (Wedepohl, 1978). The concentration in the high-grade samples varies between 37 and 56 ppm with a mean value of 45 ppm due to the Ga^{3+} - Al^{3+} substitution. An increase of Ga with metamorphic grade was also noted by Borisenok and Saukov (1960) in a study of idocrase skarns, while Evans (1964) also noted an increase in the Ga content and the Ga/Al

ratio in a study of Connemara rocks.

It is believed that the differences in trace element abundances between the high-and low-grade rocks are too big to be caused by cation diffusion and that only the removal of a melt of granitic composition could have changed the trace element concentrations to the extent observed in the Timeball Hill pelites.

4.4 Chemistry of the calcareous formations.

The composition of the calcareous rocks vary essentially in the concentrations of the elements Ca, Mg, Si and Al although Fe and Mg may also display considerable variations in some of the samples. Most calc- silicates contain significant proportions of Al_2O_3 and SiO_2 (Fig. 15) and no chemical distinction between the units is possible.

The low alkali concentrations in most samples indicate that clay minerals rather than feldspars are responsible for the Al_2O_3 in the calc-silicates, while the low K_2O and high CaO concentrations of the rocks further argue against the presence of significant volumes of evaporite material in the area.

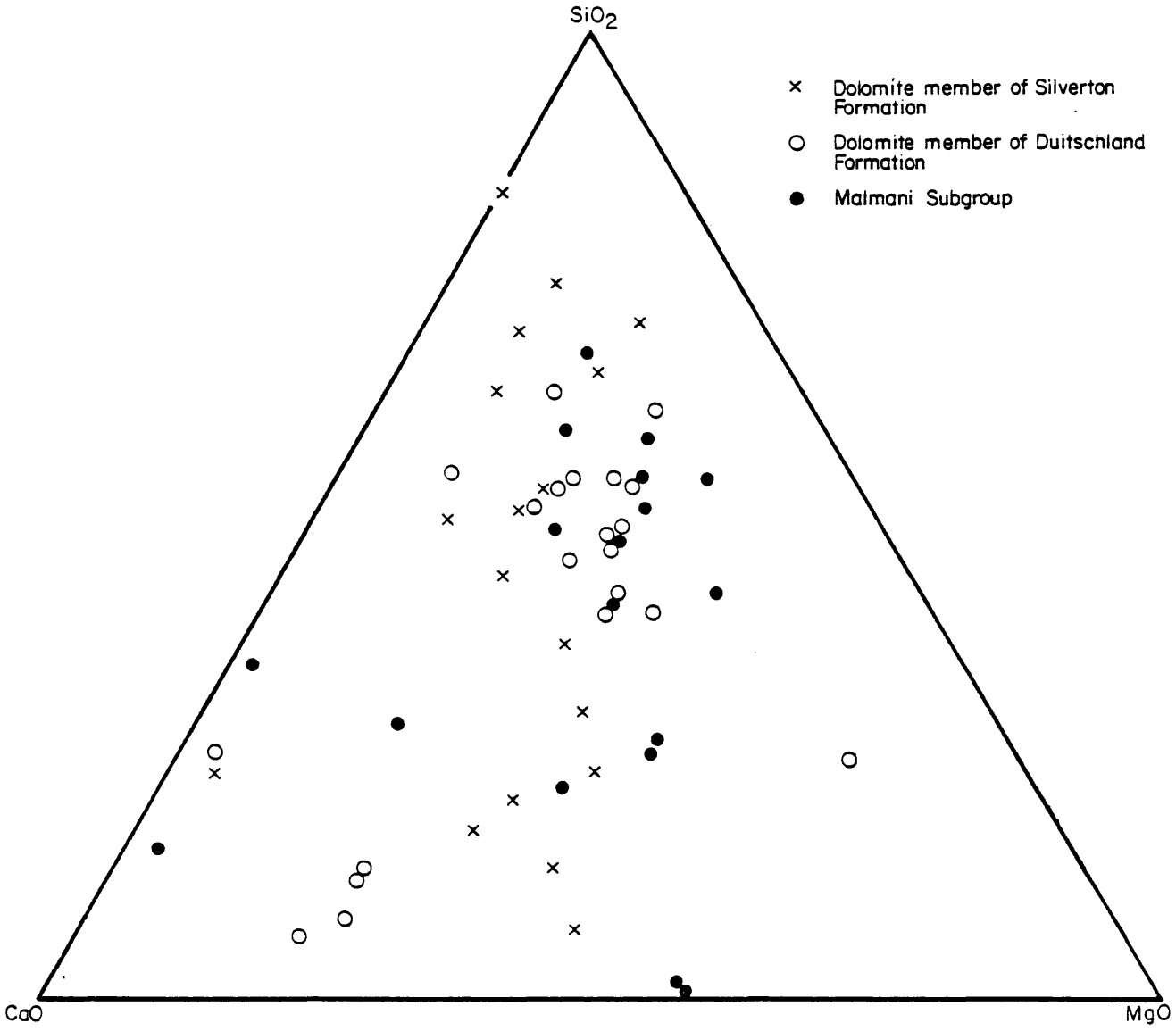

Fig. 15: The composition of the calcareous rocks from the Potgietersrus area in terms of the molecular quantities SiO_2, CaO and MgO

5. MINERAL CHEMISTRY

5.1 Introduction

Mineral analyses obtained for representative samples from the various pelitic and calcareous assemblage groups are tabulated in Appendices 2 - 15. The partitioning of Mg and Fe between the ferromagnesian minerals from the pelitic assemblages is presented in Figure 16 as a log - MgO/FeO_T plot in which the variation of partition coefficients can be discerned by visual comparison of the lenghts (in log units) of line segments between the positions of coexisting ferromagnesian minerals (Albee, 1972). Equal partition coefficients (K_D) between sample points are represented by equal segments because

$$\log K_{D\,\alpha-\beta}^{Mg-Fe} = \log \left[\frac{(Mg/Fe)_\alpha}{(Mg/Fe)_\beta}\right]$$

$$= \log (Mg/Fe)_\alpha - \log (Mg/Fe)_\beta \quad ....5(1)$$

where α and β represent mineral phases.

The relative Mg/Fe ratios for the minerals are: ilmenite < magnetite < garnet ≤ hercynite < olivine < orthoamphibole ≤ orthopyroxene < biotite < cordierite. Chloritoid appears to be more magnesian than garnet but its position relative to olivine and hercynite is uncertain. In two samples (PH - 321 and PH - 330) biotite is more Fe-rich than coexisting orthopyroxene. This is a reversal of the general Mg/Fe enrichment and will be discussed in Chapter 6. Zoning is restricted to rare cases where garnet rims are more magnesian than the cores and cordierite porphyroblasts (PH - 75) which have more ferruginous rims than cores. In general line segments between mineral pairs have approximately equal lengths while the relative Mg/Fe ratios agree with the results of similar studies by Albee (1972), Hensen (1971), Grant (1973) and references therein.

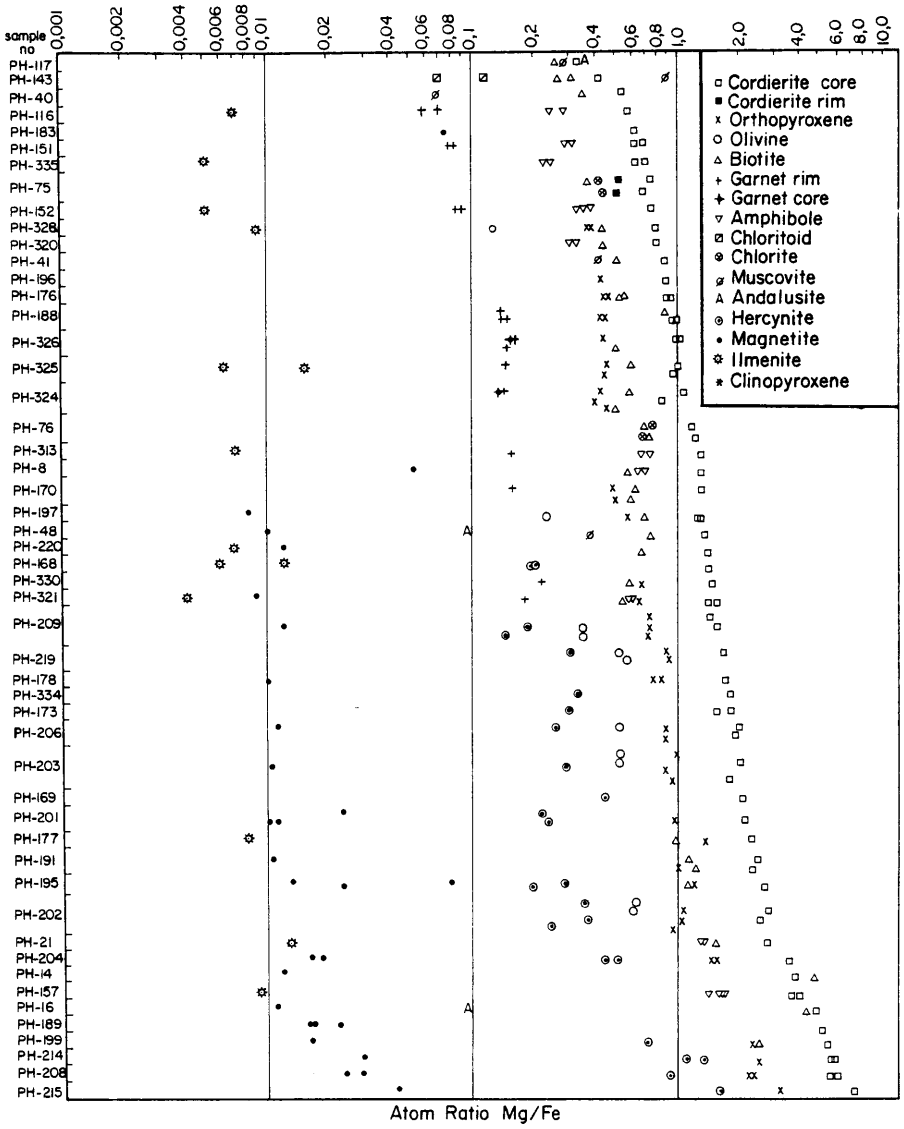

Atom Ratio Mg/Fe for individual grains of coexisting phases. Equal distances between points represent equal partition coefficients. Only samples containing cordierite represented on this diagram.

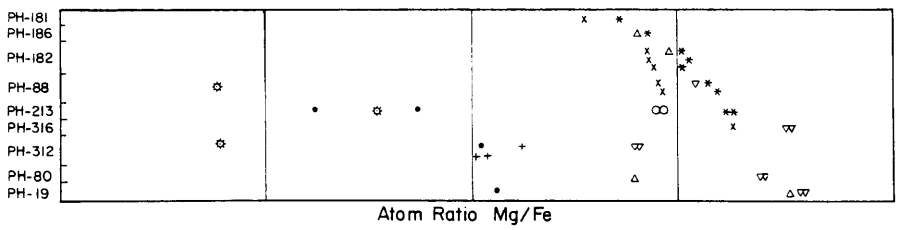

Cpx, Opx and Amphibole assemblages that do not contain cordierite.

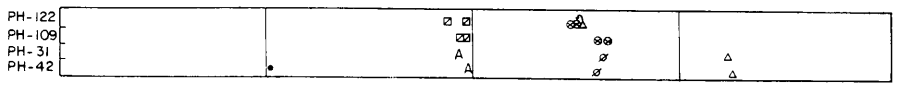

Low grade assemblages that do not contain cordierite or where no cordierite analyses are available.

Fig. 16: Atom ratio Mg/Fe for individual grains of coexisting phases. Equal distances between points represent equal partition coefficients

5.2 Analytical methods.

Polished thin sections and standards were vacuum coated with carbon to a thickness of about 20 µm. All minerals were then analysed on a JEOL J X A - 50 A electron probe micro-analyser housed at the Geological Survey of South-Africa. The normal acceleration voltage was 15 KV and the typical specimen current was 20 nA. Online data reduction based on the procedure after Bence and Albee (1968) was performed. Anhydrous multi-element silicates and oxides were used as standards.

For minerals that may contain substantial amounts of Fe^{3+}, the Fe_2O_3 content was calculated from stoichiometry using the method of Finger (1972) as computerized by M.R. Sharpe (pers. comm.). In order to overcome the problem of local or mosaic equilibrium (Korzhinskii,1959), only mineral pairs that were in contact with, or in close proximity to, one another were analysed. Garnet crystals, in particular, were checked for zoning. The analytical error is estimated to be approximately 2 percent relative for all elements analysed on all samples.

5.3 Mineral compositions

5.3.1 Biotite

If a theoretical 4 wt percent H_2O is added to the oxide analyses in Appendix 2, most totals lie within 1 percent of 100 percent. Structural formulae were calculated on the assumption that the tetrahedral sites were completely filled with Si^{iv} and Al^{iv} with the remainder of the Al occupying octahedral sites.

Biotite coexisting with chloritoid and chlorite plus cordierite (i.e. low-grade assemblages) are more aluminous than the biotite coexisting with orthopyroxene plus garnet and spinel plus olivine from high-grade assemblages (Fig. 17), with the siderophyllite component being particularly important in the low-grade assemblages. Biotites from pelitic rocks plot in the meroxene and lepidomelane fields of Tröger (1971),(Fig. 18), while phlogopites from the calc-silicates are enriched in Al + Ti relative to the

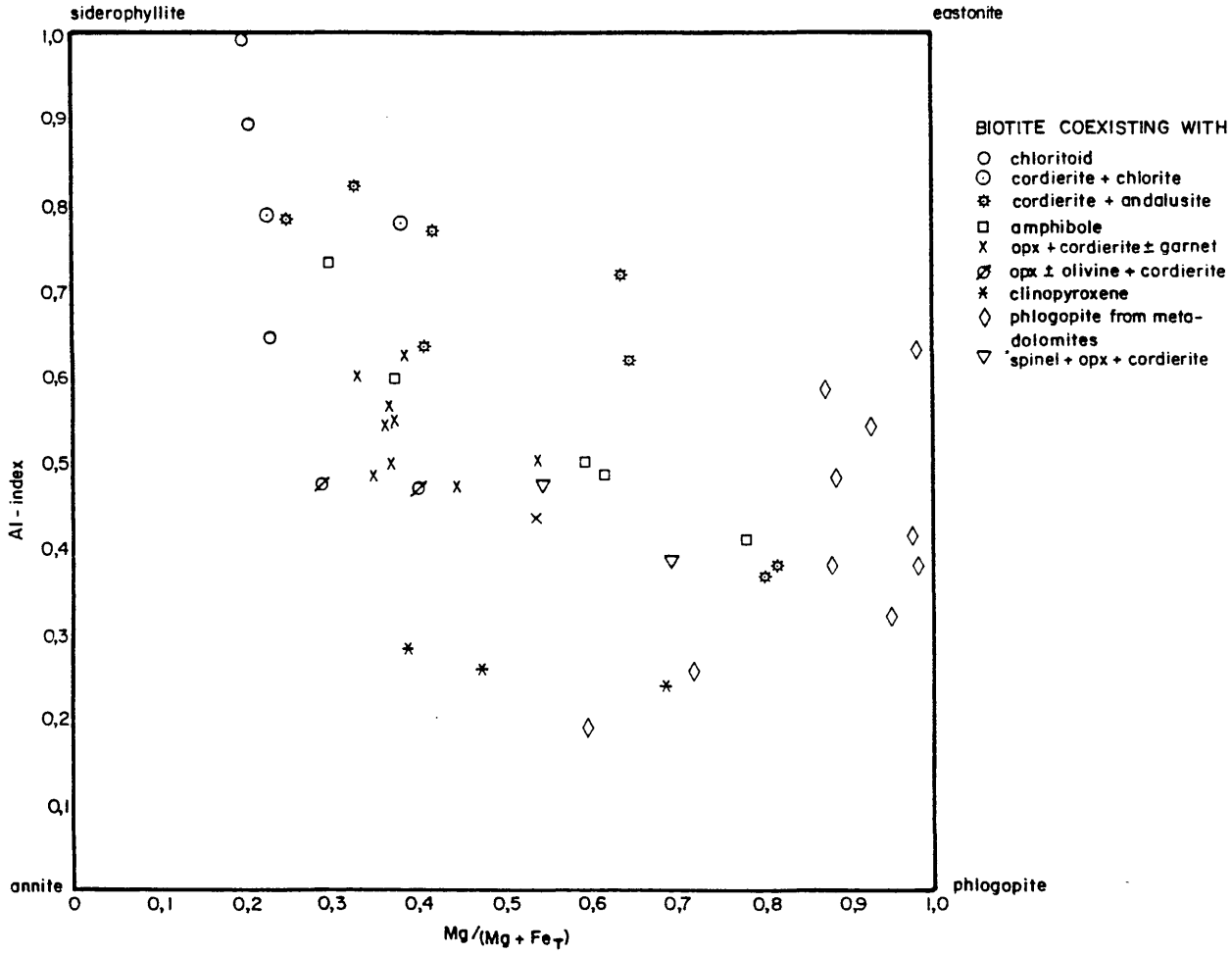

Fig. 17: The four most important biotite end-members expressed in terms of the Al-index (see text) and the Mg/(Mg+Fe$_T$) ratio

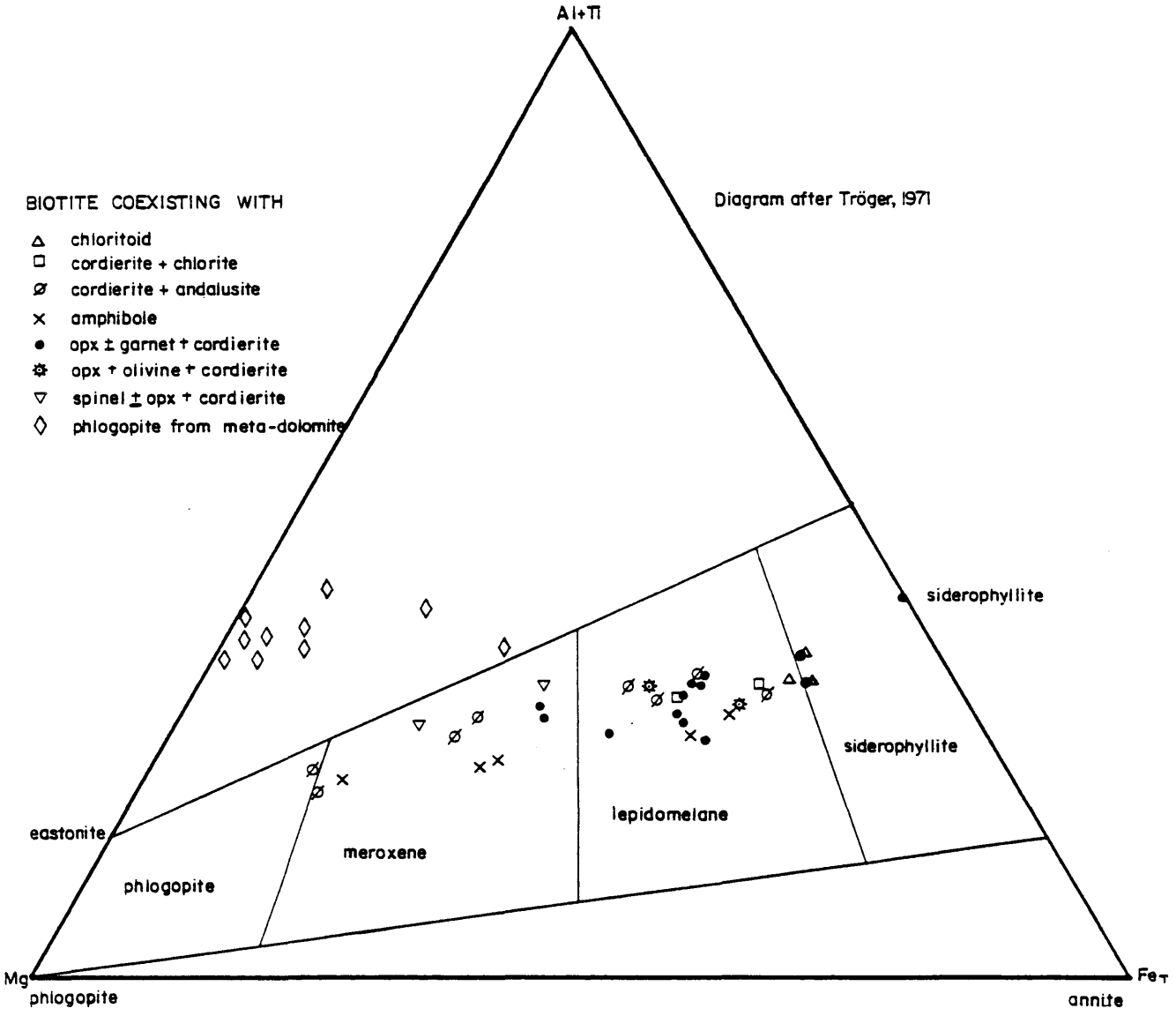

Fig. 18: Biotite from the Potgietersrus area classified according to the nomenclature of Tröger (1971)

phlogopite field of Tröger (1971).

Biotite compositions can be adequately expressed in terms of the end-members phlogopite, annite, eastonite and siderophyllite. The following reasoning was adopted for the calculation of the end-members. The low - Al end-members (annite and phlogopite) and the high - Al end-members (eastonite and siderophyllite) contains 2 Al plus 6 Si and 4 Al plus 5 Si atoms per formula unit respectively. In order to express a biotite analysis in terms of Al substitution, a scale with the low- Al end-members at the 0 percent point and the high-Al end-members at 100 percent was constructed. To accomplish this the amount of Al in the Al-poor end-members must be subtracted from the alumina content of the analysis to be evaluated and the remaining Al must then be multiplied with a constant that will express the Al substitution in terms of a percentage in such a way that the high- Al end-members plot at 100 percent. The low-Al end-members have an Al/(Al + Si) ratio of 0,25 ($^2/_8$) and the high-Al end-members have a ratio of 0,444 ($^4/_9$). The Al-index is now defined as:

$$\text{Al-index} = \left[(\text{Al}/(\text{Al}+\text{Si})\ bi - 0{,}25) \times \frac{1}{(0{,}444 - 0{,}25)}\right] \quad ..5(2)$$

The four end-member molecules are given by:

$$\% \text{ Phlogopite} = \left[\text{Mg}/(\text{Mg} + \text{Fe})\ bi\right] \left[1 - \text{Al-index}\right] \times 100$$
$$\% \text{ Annite} = \left[\text{Fe}/(\text{Mg} + \text{Fe})\ bi\right] \left[1 - \text{Al-index}\right] \times 100$$
$$\% \text{ Eastonite} = \left[\text{Mg}/(\text{Mg} + \text{Fe})\ bi\right] \left[\text{Al-index}\right] \times 100$$
$$\% \text{ Siderophyllite} = \left[\text{Fe}/(\text{Mg} + \text{Fe})bi\right] \left[\text{Al-index}\right] \times 100$$

Controls on biotite composition

Hörmann et al. (1980) concluded that biotite compositions in Lapland granulites depend on the bulk composition as well as the mineral assemblage while Fletcher and Greenwood (1979) found that biotite chemistry from a metamorphic belt in British Columbia depends essentially on metamorphic grade. If, however, a sample contains fewer than the maximum number of phases for the number of components, not all the chemical potentials will be fixed by pressure, temperature and mineral assemblage so that the bulk composition of the individual

rocks will affect the compositions of the minerals, even at constant pressure and temperature.

There is an inverse relationship between the annite and siderophyllite components and metamorphic grade as defined by a number of index minerals or mineral assemblages (Fig. 19 A and B) but no relationship between the phlogopite or eastonite components and metamorphic grade could be detected. Despite a fair amount of scatter there appears to be a correlation between the $Mg/(Mg + Fe_T)$ ratio in the bulk rock and that in biotite (Fig. 20), while Figure 17 indicates that the $Mg/(Mg + Fe_T)$ ratio does not depend on metamorphic grade. Lapinsky (1981) and Hörmann et al. (1980) made similar observations, but Fletcher and Greenwood (1979) found an increase in Mg with increasing metamorphic grade in British Columbia.

Chinner (1960) pointed out that the Al content of biotite may be controlled by the oxygen fugacity. The minimum chemical potential of Al that is needed for the nucleation of an Al_2SiO_5 polymorph increases with increasing fO_2. Where the chemical potential of Al is lower than the minimum value required for the nucleation of an Al_2SiO_5 polymorph, the other Al - bearing minerals in the sample will become enriched in Al_2O_3. With increasing metamorphic grade the chemical potential of Al will also increase since the entropy of Al^{3+} is negative. When the chemical potential of Al exceeds the minimum value required for the formation of an Al_2SiO_5 polymorph, the Al will be partitioned in favour of the polymorph. This may explain the more aluminous biotites in the chloritoid and chlorite plus cordierite -bearing assemblages relative to the andalusite-bearing assemblages (Fig. 17).

The Ti content of biotite increases with increasing metamorphic grade (Fig. 21). Various other workers, e.g. Fletcher and Greenwood (1979) found a similar ralationship. The high TiO_2 values (up to 5,4 wt percent, sample PH - 197) compare well with the highest values recorded in the literature (Deer et al., 1962 c).

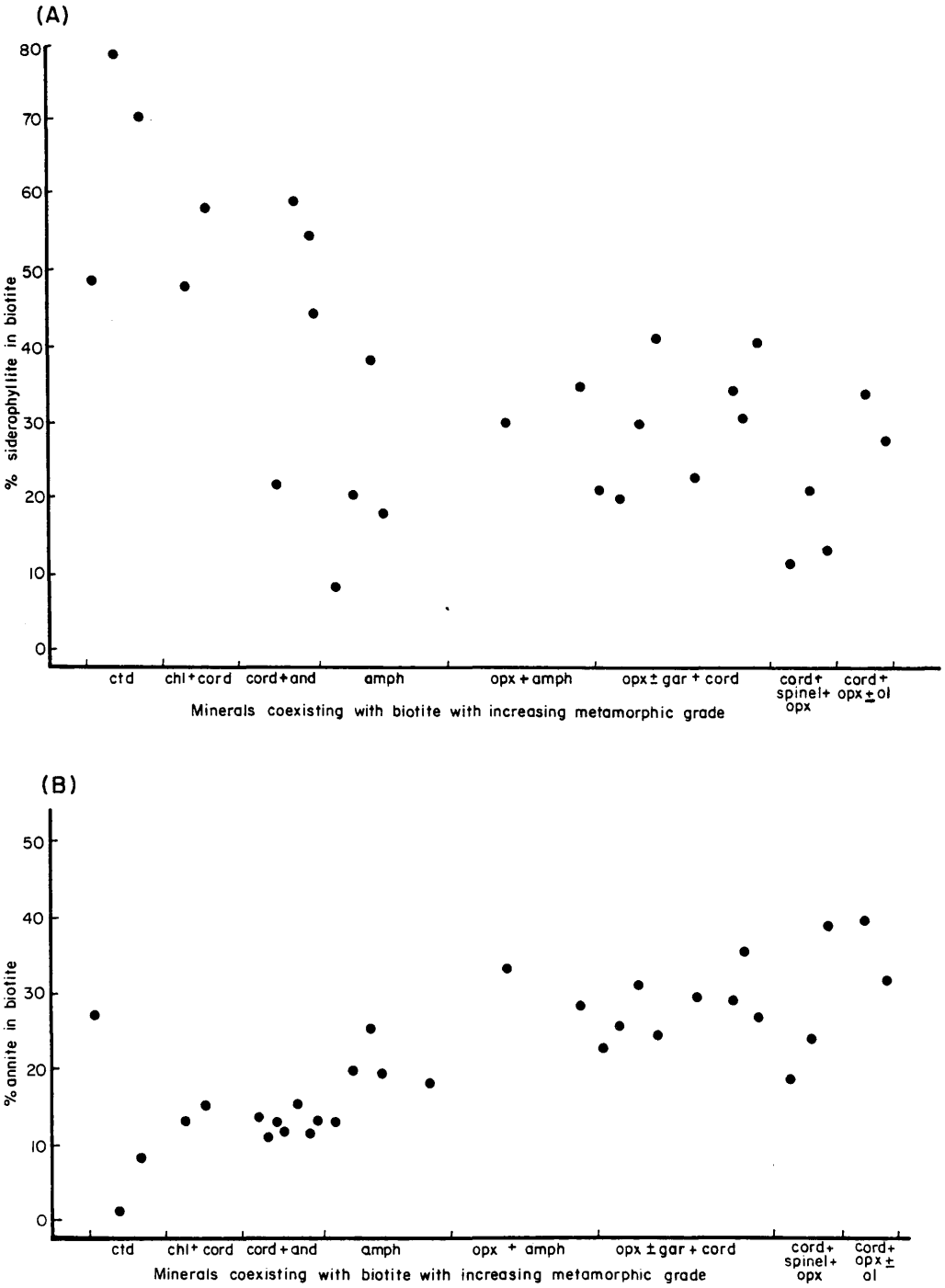

Fig. 19: Siderophyllite (A) and annite (B) end-members in biotite from the Potgietersrus area as a function of metamorphic grade

Fig. 20: Relationship between the $Mg/(Mg + Fe_T)$ ratio in biotite and the molecular $Mg/(Mg + Fe_T)$ ratio in the bulk rock

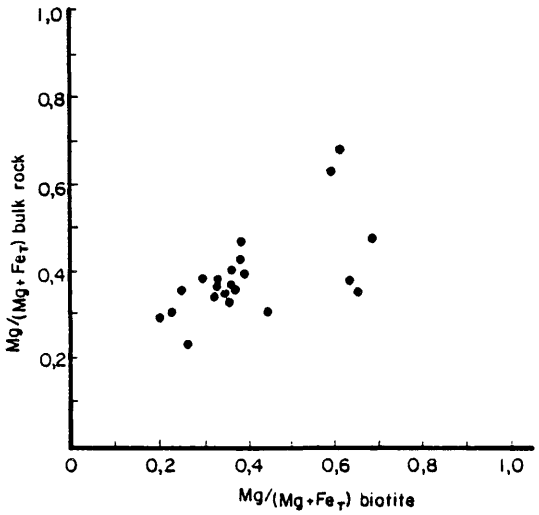

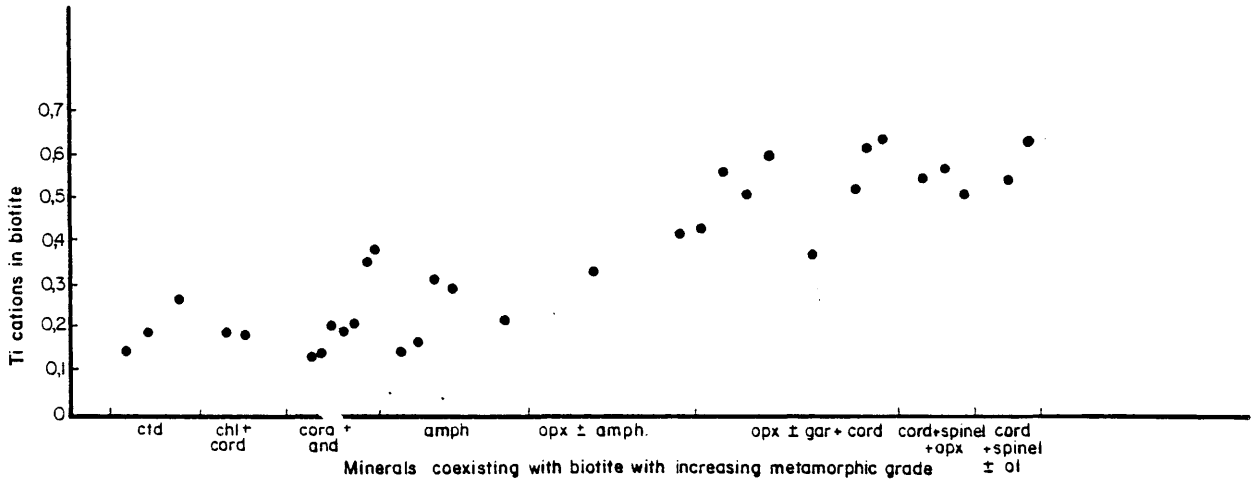

Fig. 21: The number of Ti cations in biotite as a function of metamorphic grade

Substitutions in biotite

The well established substitution (Hörmann et al., 1980):

$$(Mg, Fe) + Si^{4+} \rightleftharpoons Al^{iv} + Al^{vi} \quad \text{.....5(4)}$$

accounts for the introduction of Al into biotite. The negative correlation between Ti and $\sum(Al^{vi} + Mg + Fe)$ (Fig. 22 A) indicates the substitution of Ti into the octahedral sites in biotite, while the negative correlation between Al^{vi} and Ti (Fig. 22 B) suggests that Al^{vi} is the most likely element to be replaced through the substitution:

$$Si^{4+} + Al^{vi} \rightleftharpoons Al^{iv} + Ti^{vi} \quad \text{.....5(5)}$$

5.3.2 Cordierite

Cordierite analyses (Appendix 3) have totals between 96,2 and 98,4 wt percent, indicating a significant water content. In the calculation of the structural formula it was assumed that the tetrahedral sites were completely filled by Si^{iv} and Al^{iv} with the remainder of the Al occupying octahedral sites. The deviation from stoichiometry in some analyses may be due to the structure of cordierite being more complex than is generally believed.

Influence of host rock composition on occurrence

Many workers commented on the occurrence of cordierite as a function of host rock composition. Dallmeyer (1972), for example, argued that cordierite is only stable in rocks with a MgO/(MgO + FeO) ratio greater than 0,6 and that the $K_2O/(K_2O + MgO + FeO)$ ratio of the bulk rock may also influence cordierite stability.

Cordierite occurrence in the study area is not influenced by the MgO/(MgO + FeO) ratio of the bulk rock over the range represented (Fig. 23) but all cordierite-bearing rocks contain more than 10 wt percent Al_2O_3. The cordierite-free samples come from the Ca-rich, Al-poor shale members of the Duitschland- and Silverton Formations and the formation of

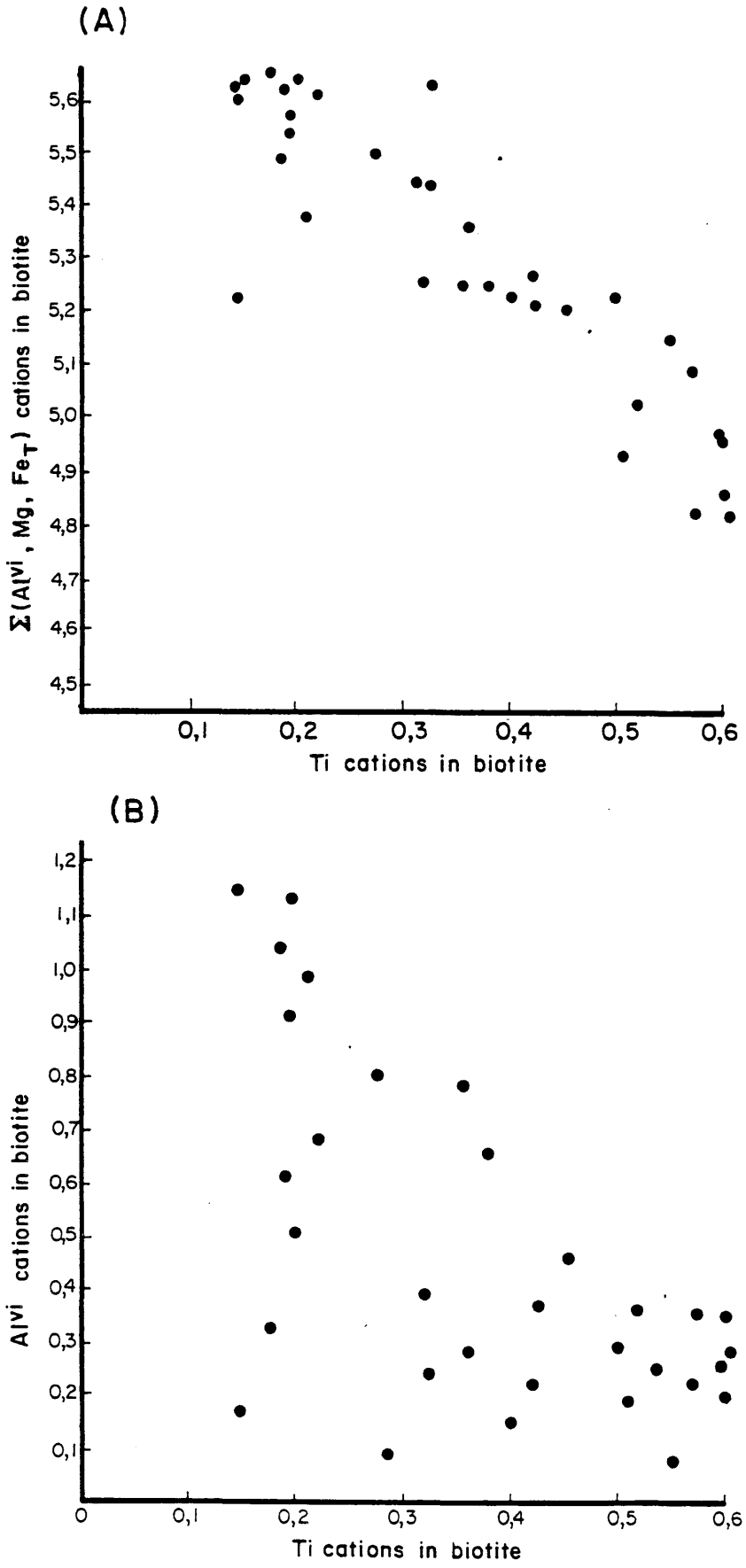

Fig. 22: Plot illustrating the substitution of Ti into octahedral sites in biotite (A), with Al^{vi} being the most likely species to be replaced (B)

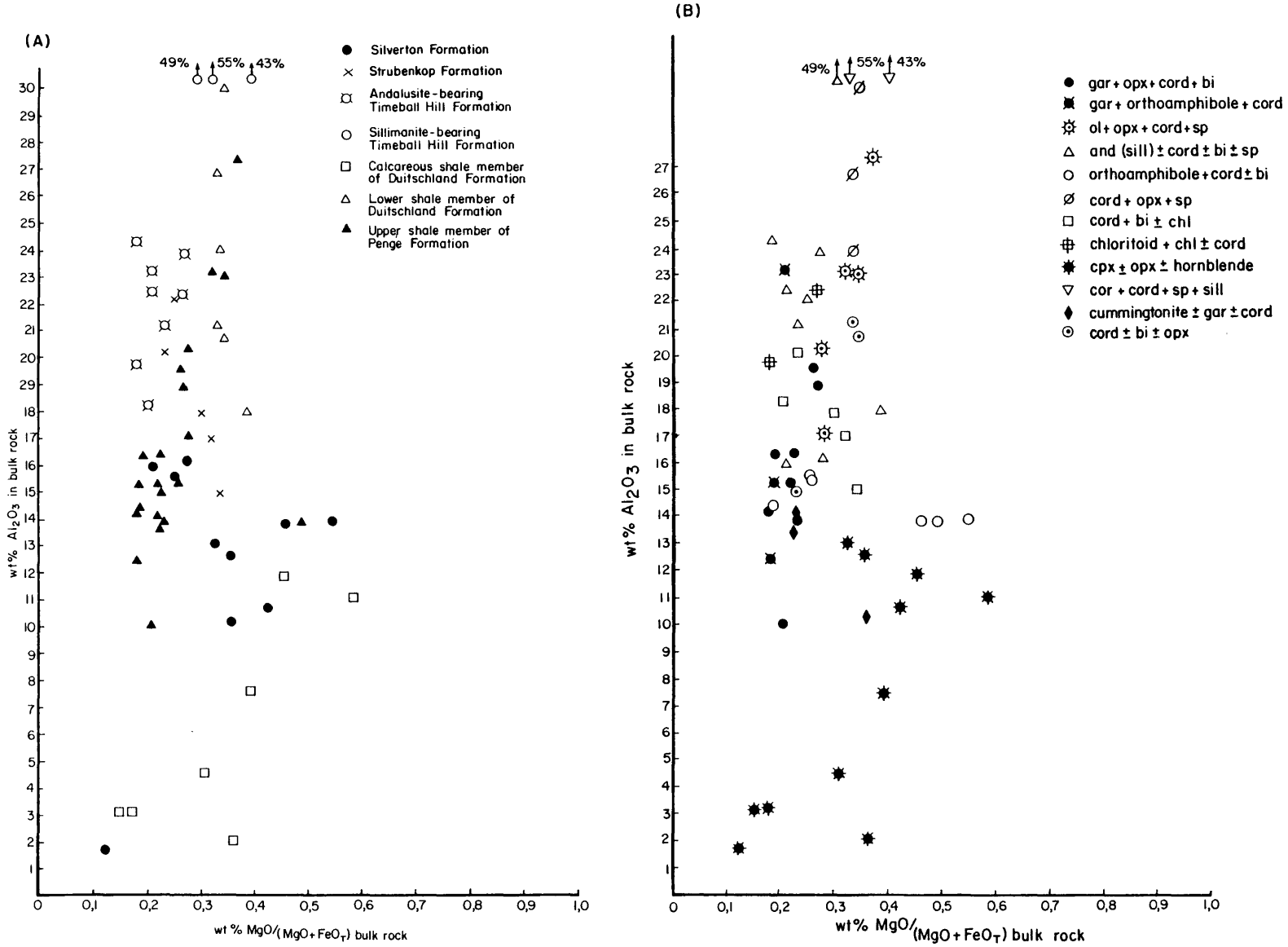

Fig. 23: Relationship between the pelitic unit (A) as well as the mineral assemblage (B) and the Al_2O_3 content and $MgO/(MgO + FeO_T)$ ratio of the bulk rock

cordierite, therefore, appears to be inhibited by high Ca and low Al bulk rock compositions.

Dallmeyer and Dodd (1971) also found that cordierite-free gneisses are enriched in Ca and K and depleted in Al relative to cordierite-bearing gneisses. The following reaction (Henry, 1974) explains the formation of plagioclase, rather than cordierite in Ca-rich rocks.

$$\text{cordierite} + \text{quartz} + Na^{+} + Ca^{2+} + K^{+} \rightleftharpoons \text{plagioclase} + Fe^{2+} + Mg^{2+} \quad \text{.....5(6)}$$

Variation in cordierite chemistry

The $Mg/(Mg + Fe_T)$ ratio in cordierite is clearly a function of host rock composition (Fig. 24). A possible explanation for the Fe- enrichment of the cordierite rims in sample PH - 75 will be provided in Chapter 6.

5.3.3 Orthoamphibole

The Fe - Mg amphiboles have been classified according to the method of Leake (1978) (Fig. 25). It is difficult to estimate the Fe_2O_3 content of the amphiboles since calculation of the analyses (Appendix 4) to a fixed number of cations is undesirable (Leake, 1978). For Fe - Mg amphiboles the sum of the cations, excluding Na and K should equal 15 and this sum is therefore an indication of the Fe^{3+}/Fe^{2+} ratio.

Robinson et al. (1971) proposed a test of the quality of ortho-amphibole analyses based on the charge balance that must be maintained through certain common amphibole substitutions. In order to apply this test the two end-members anthophyllite and gedrite are given the respective formulae:

$\square R_2^{2+}R_5^{2+}Si_8O_{22}(OH)_2$ and $Na_xR_2^{2+}(R_{5-y}^{2+}R_y^{3+})(Al_{x+y}Si_{8-x-y})O_{22}(OH)_2$. Na occupies the otherwise vacant A-site; R^{2+} = Mg,Ni,Fe^{2+}, Mn,Ca; R^{3+} = Al,Fe^{3+},Cr^{3+},(Ti^{4+} + $R^{2+}_{0,5}$). $\square$ = vacancy; X = A-site occupancy and Y = $\sum$(Al^{vi},Fe^{3+},Cr^{3+}, $2(Ti^{4+})$).
The X and Y subscripts further refer to the edenite ($NaAl^{iv} \rightleftharpoons \square Si^{+}$) and tschermakite ($Al^{iv}Al^{vi} \rightleftharpoons MgSi$)

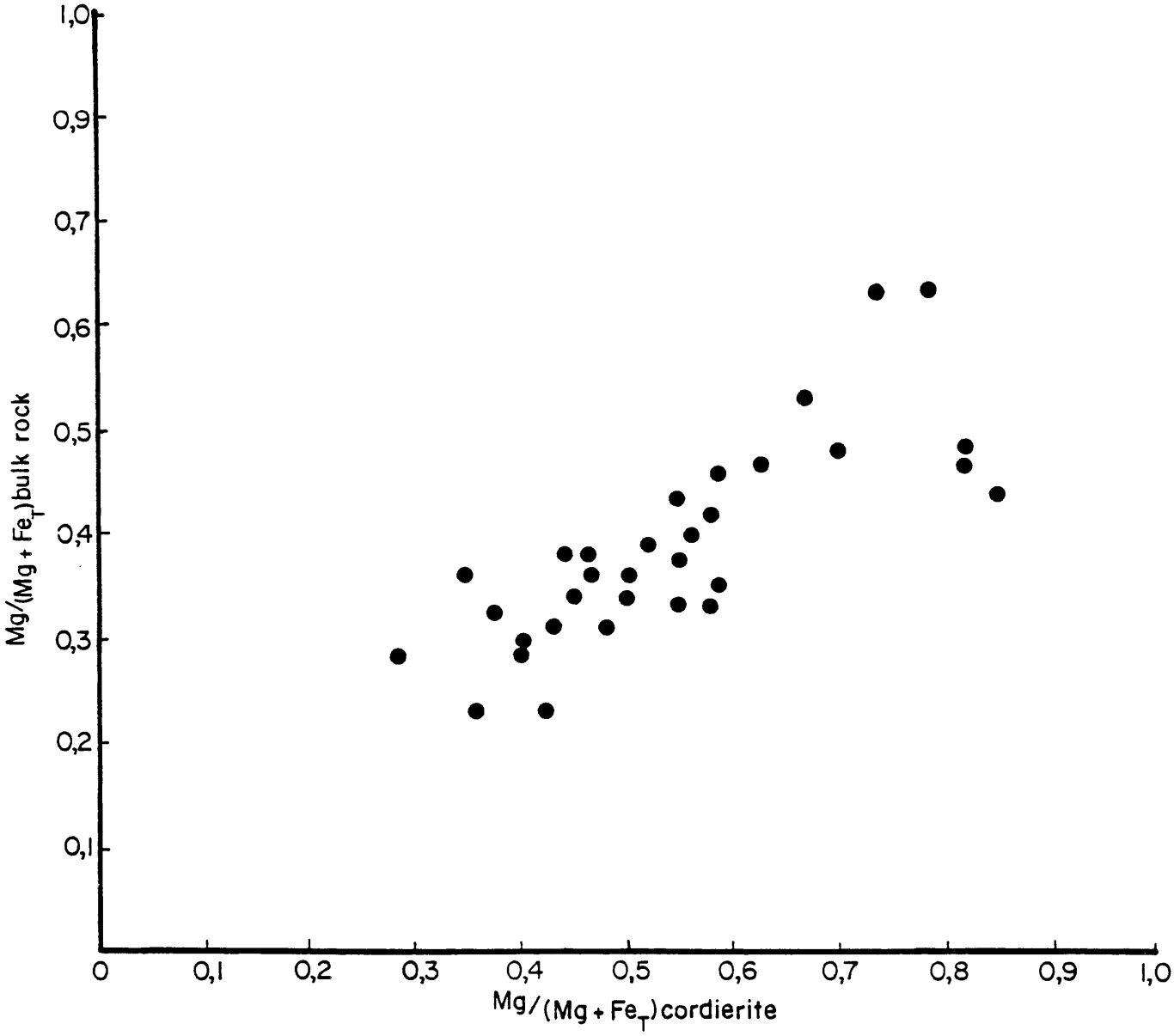

Fig. 24: The composition of cordierite as a function of the molecular Mg/(Mg + Fe$_T$) ratio in the bulk rock

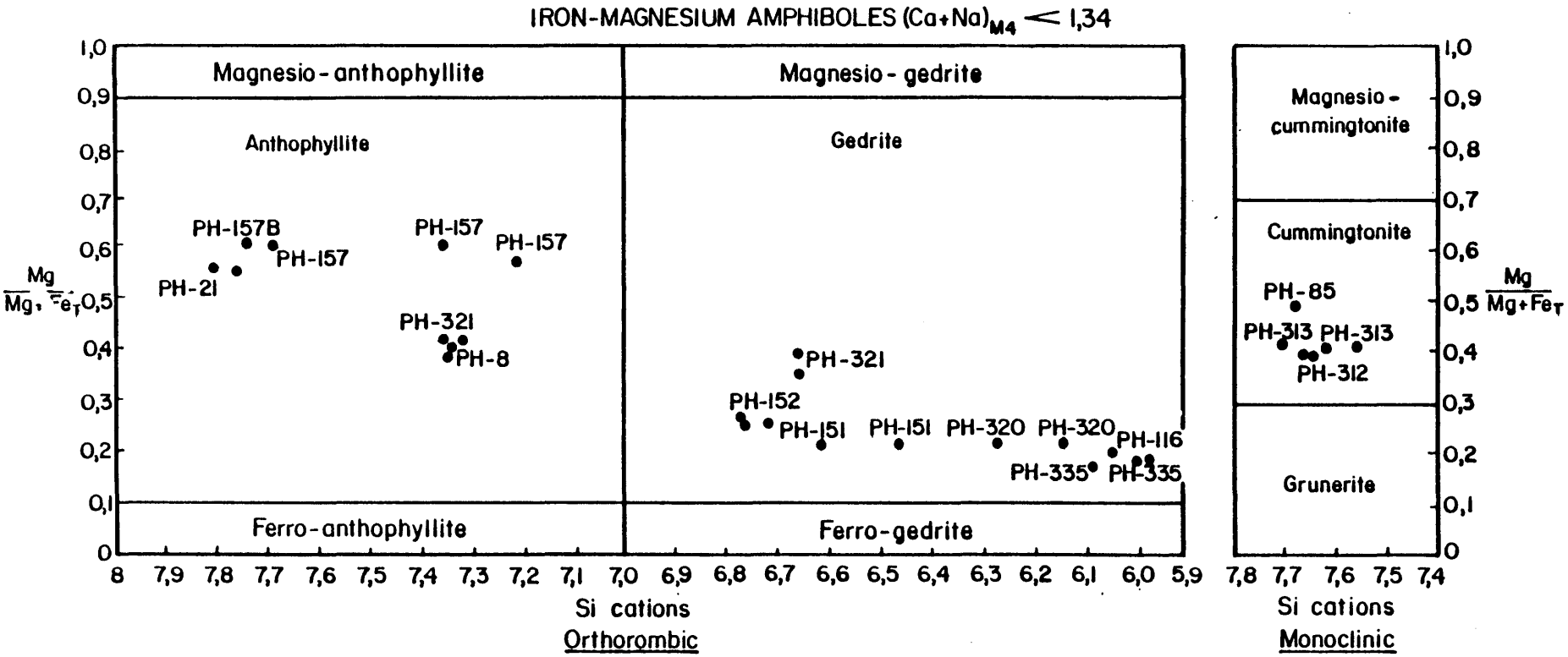

Fig. 25: Classification of the Fe-Mg amphiboles from the Potgietersrus area according to Leake (1978)

substitutions respectively (Spear, 1980). From charge balance restrictions it follows that $\sum(x,y) = Al^{iv}$. The difference between $\sum(x+y)$ and Al^{iv}, i.e. $(x + y) - Al^{iv}$ is called the "residual value" (Robinson et al., 1971) and is indicative of additional substitutions or analytical errors. Positive residual values may indicate glaucophane - or richterite-substitutions or analytical errors. Negative residual values could result from the amount of (Na + k) being less than the calculated A-site occupancy, leading to the substitution of divalent cations in the A-site, or from errors. Underestimation of the Fe^{3+} content will also cause a too low Y - value and thus a negative residual value. Analyses with large negative residuals in the study area also have cation sums in excess of 15, while analyses with residuals close to 0 have cation sums smaller than 15 (Appendix 5), suggesting that the analyses with large negative residuals may contain significant amounts of Fe_2O_3.

Influence of host rock composition on occurrence

The bulk rock composition has been shown to be important in the formation of orthoamphiboles by Lal and Moorhouse (1969) as well as Lal and Shukla (1975). The criteria recognized by the former authors are also applicable to the study area (Fig. 26).

First, the alkali content of the bulk rock must be low in order to prevent the incorporation of Al, Mg and Fe in biotite, or the formation of calcic- or sodic amphiboles.

Secondly, the $(FeO+MgO+MnO) / [Al_2O_3 - (Na_2O + 2CaO)]$ ratio must be greater than 1. Even though the Al_2O_3 component was not corrected for CaO and Na_2O (Fig. 26) all the orthoamphibole-bearing samples have $(FeO_T + MgO)/Al_2O_3$ ratios greater than 1, except for one Ca-rich sample which has a ratio equal to 1.

Thirdly, the FeO/(FeO + MgO) ratio of the host rock must fall in the orthoamphibole - cordierite - garnet stability field or on the orthoamphibole - garnet or orthoamphibole - cordierite tie-lines.

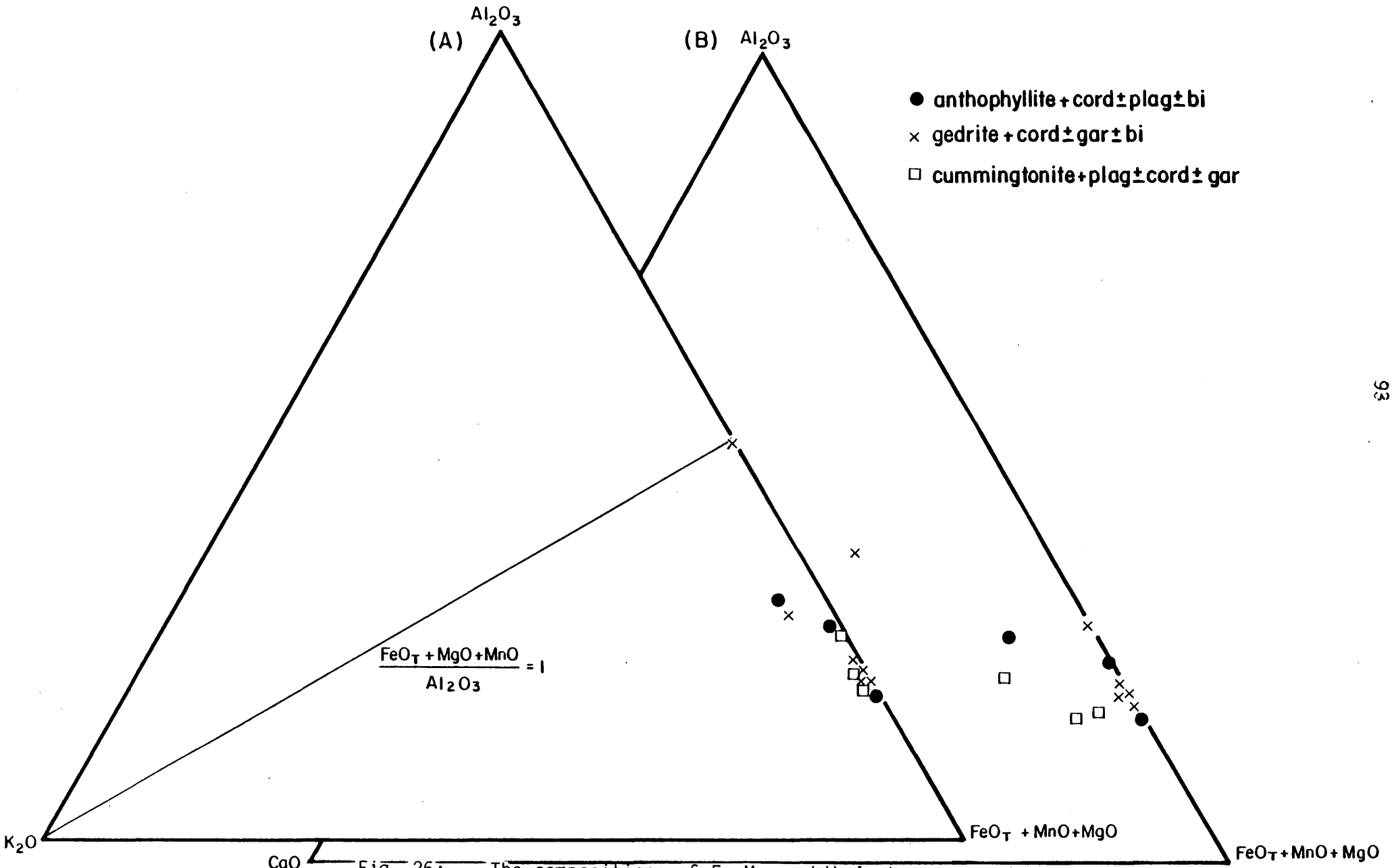

Fig. 26: The compositions of Fe-Mg amphibole-bearing rocks in terms of the molecular quantities Al_2O_3; K_2O; CaO and FeO_T + MgO + MnO

Variation in orthoamphibole chemistry

Anthophyllite - bearing rocks in the study area are more magnesian than gedrite-bearing rocks, while the composition of anthophyllite also appears to be a function of the $Mg/(Mg + Fe_T)$ ratio in the bulk rock (Fig. 27).

The chemical variation in orthoampiboles can essentially be described in terms of the composition of anthophyllite ($Mg_7Si_8O_{22}(OH)_2$) and the following three substitutions:

Fe $\rightleftharpoons$ Mg ..... 5(7)
the tschermaks exchange: Mg+ Si $\rightleftharpoons$ $Al^{iv} + Al^{vi}$.... 5(8)
and the edenite exchange: Na + Al^{iv} $\rightleftharpoons$ □ + Si ... 5(9)

Spear (1980) used several chemical parameters to distinguish between anthophyllite and gedrite. On one of his plots (Fig. 28), data from the study area is combined with data from Sharma and MacRae (1981) in order to illustrate the miscibility gap between anthophyllite and gedrite as well as the importance of the tschermaks substition relative to its Fe-analogue.

Papike and Ross (1970) and Finger (1970) provided a crystal chemical explanation for the preferential replacement of Mg, rather than Fe^{2+}, by Al^{3+}. Al^{vi} is confined to the smaller M2 site of orthoamphibole while the small Mg^{2+} cation also partitions strongly into this site relative to the larger M1 and M3 sites, which accommodate the larger Fe^{2+} cation. The introduction of Al can thus only take place at the expense of Mg in the M2 site while the Fe^{2+} in the M1 and M3 sites remains unaffected.

5.3.4 Calcic Amphiboles

The calcic amphiboles were also classified according to the method of Leake (1978) (Fig. 29). Amphibole analyses (Appendix 5) were recalculated to fill 8 tetrahedral sites with Si and Al. The remaining Al was allocated to octahedral sites and where the total octahedral occupancy was less than 7, Na was used to account for the difference. Only two analyses have A-site occupancies greater than 0,5.

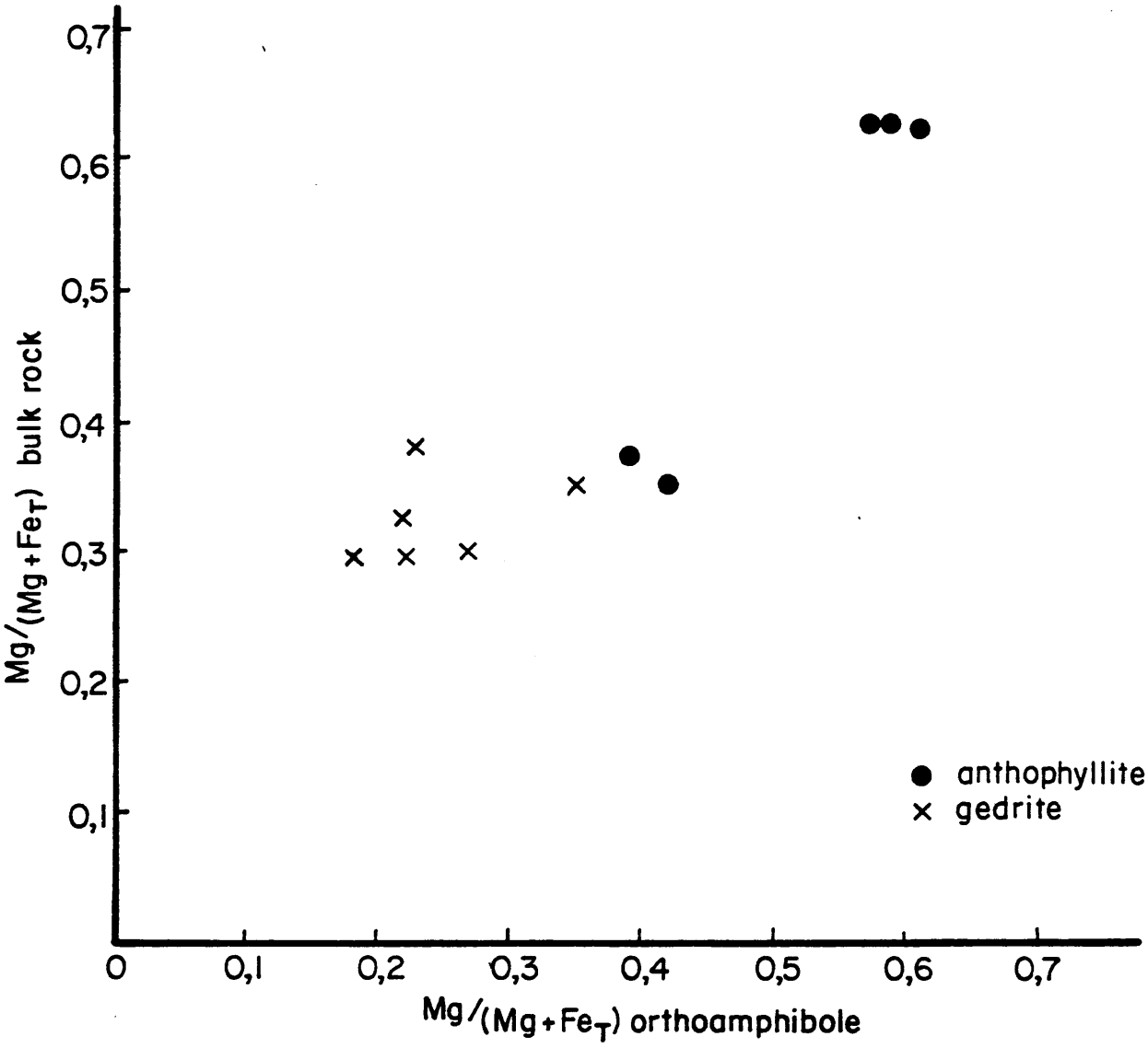

Fig. 27: Orthoamphibole composition as a function of the molecular Mg/(Mg + Fe_T) ratio of the bulk rock

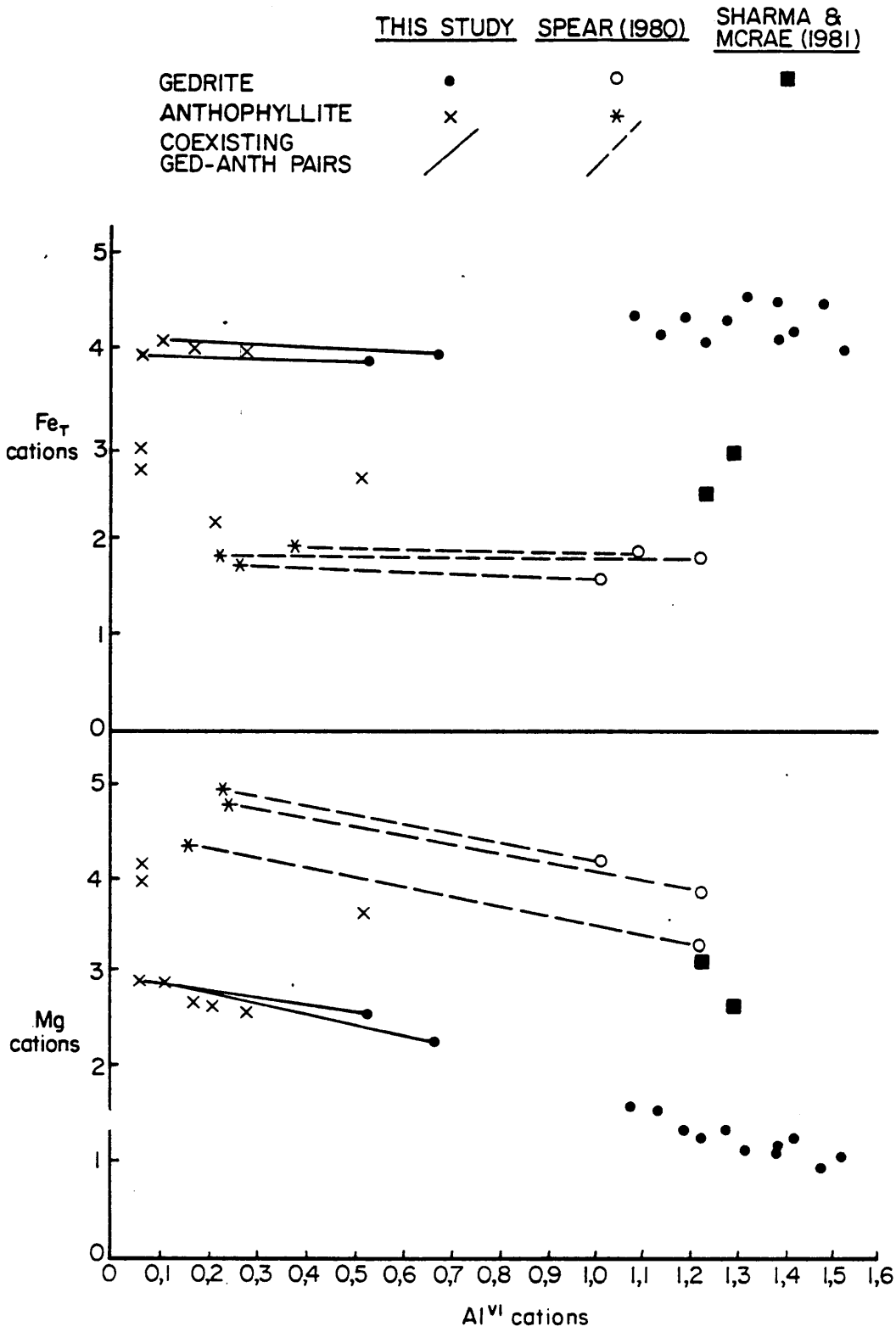

Fig. 28: The negative correlation between Mg and Al^{VI} for orthoamphiboles from the study area and from the literature suggests the substitution of Al^{VI} for Mg rather than for Fe^{2+}

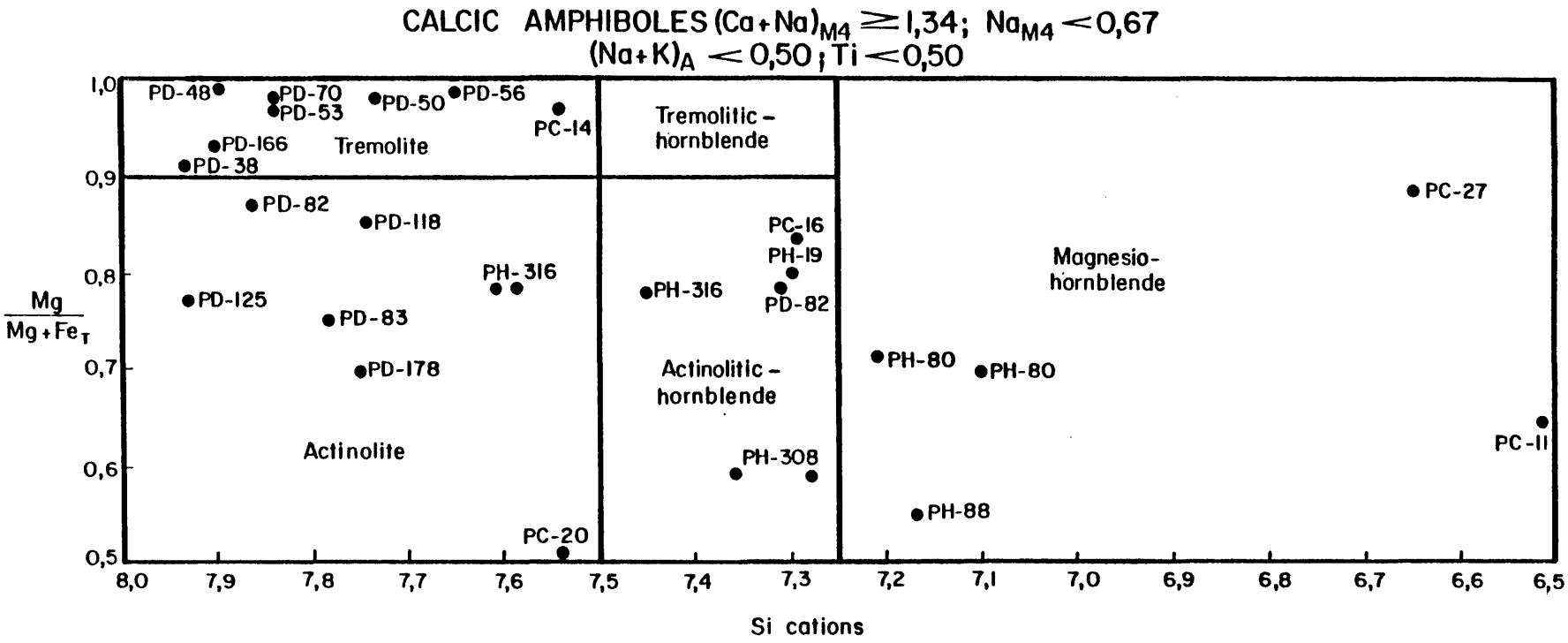

Fig. 29: Classification of the calcic-amphiboles from the Potgietersrus area according to Leake (1978)

The total number of cations in the M1, M2 and M3 sites (assuming all the Ca and Na in octahedral coordination occupy the M4 site) should be equal to 13 and deviations from this number give an indication of the Fe_2O_3 content of the amphibole.

Influence of host rock composition on occurrence

Calcic amphiboles are common in calc-silicates but in pelitic rocks they are restricted to the high Ca, low Al units of the Silverton- and Duitschland Formations (Fig. 23 A and B).

Variation in chemistry

Compositional variations can be expressed in terms of a few substitutions or combinations of substitutions into tremolite ($\square^{A}\ Ca_2^{M4}\ Mg_5^{vi}Si_8^{iv}O_{22}(OH)_2$) . Except for $Mg - Fe^{2+}$; $Al - Fe^{3}$ and Na - K exchanges, the four major substitutions are: the tschermaks substitution (eqn. 5(8)); the edenite substitution (eqn. 5(9)); the glaucophane substitution: $Na^{M4} + Al^{vi} \rightleftharpoons Ca^{M4} + Mg^{vi}$ ...5(10) and the richterite substitution: $Na^{A} + Na^{M4} \rightleftharpoons \square^{A} + Ca^{M4}$ ...5(11) Ti^{4+} substitutes in the octahedral sites in the same way as Al or Fe^{3+} but each Ti cation requires twice as much compensation as a trivalent cation.

The relative importance of the edenite- and tschermakite-substitutions are illustrated in Figure 30 (after Ernst, 1968), while the glaucophane- and richterite-substitutions are of minor importance in the study area.

The $Mg/(Mg + Fe_T)$ ratio of the calcic amphiboles is a strong function of the bulk rock composition (Fig. 31), but the $Al/(Al + Si)$ ratio does not show any correlation with rock composition.

5.3.5 Cummingtonite

According to the classification of Leake (1978) all the clino - Fe - Mg amphiboles fall in the cummingtonite field (Fig. 25). Two cummingtonite analyses (Appendix 5) have

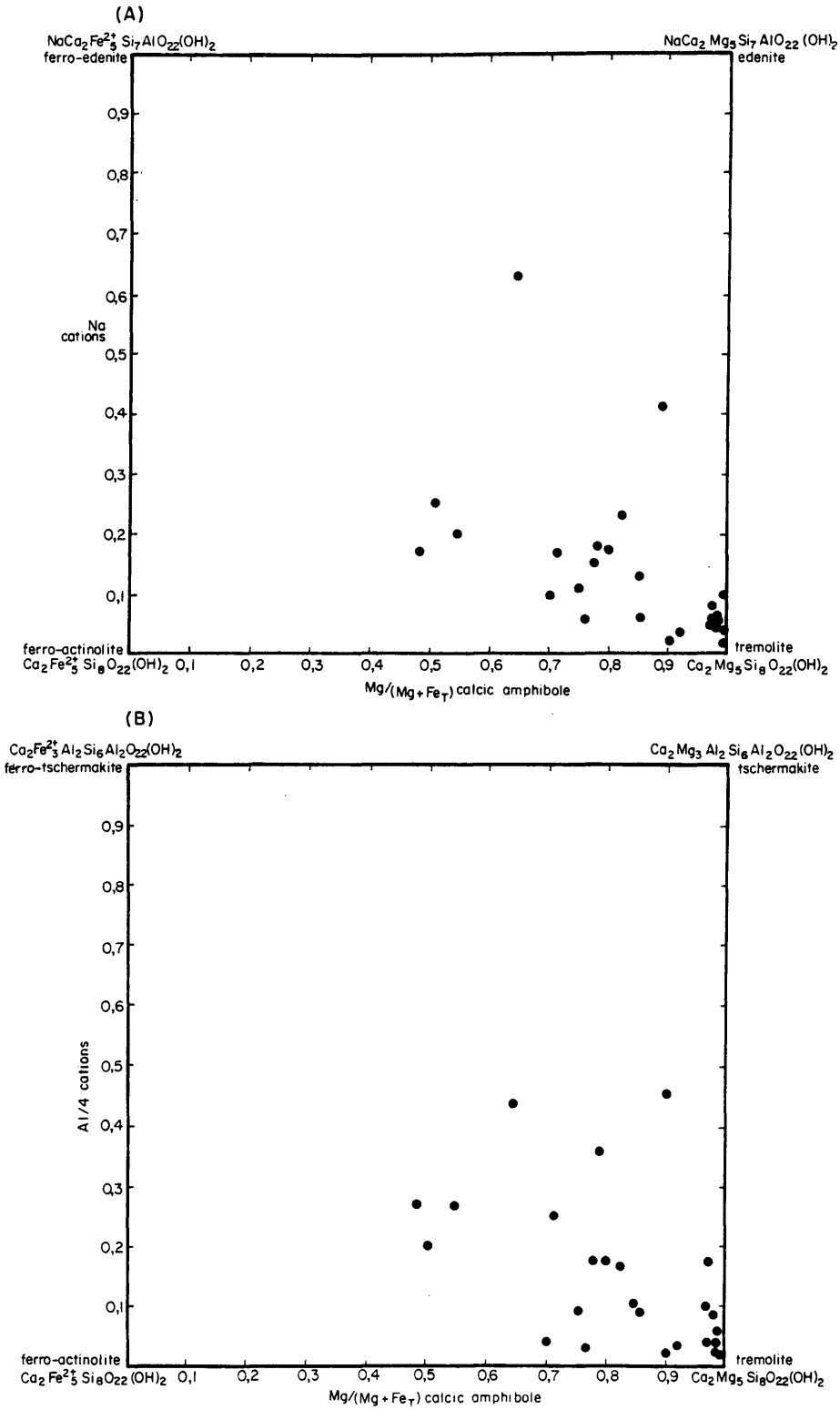

Fig. 30: Plot illustrating the importance of the edenite - (A) and tschermakite (B) - substitutions in the calcic amphiboles from the Potgietersrus area

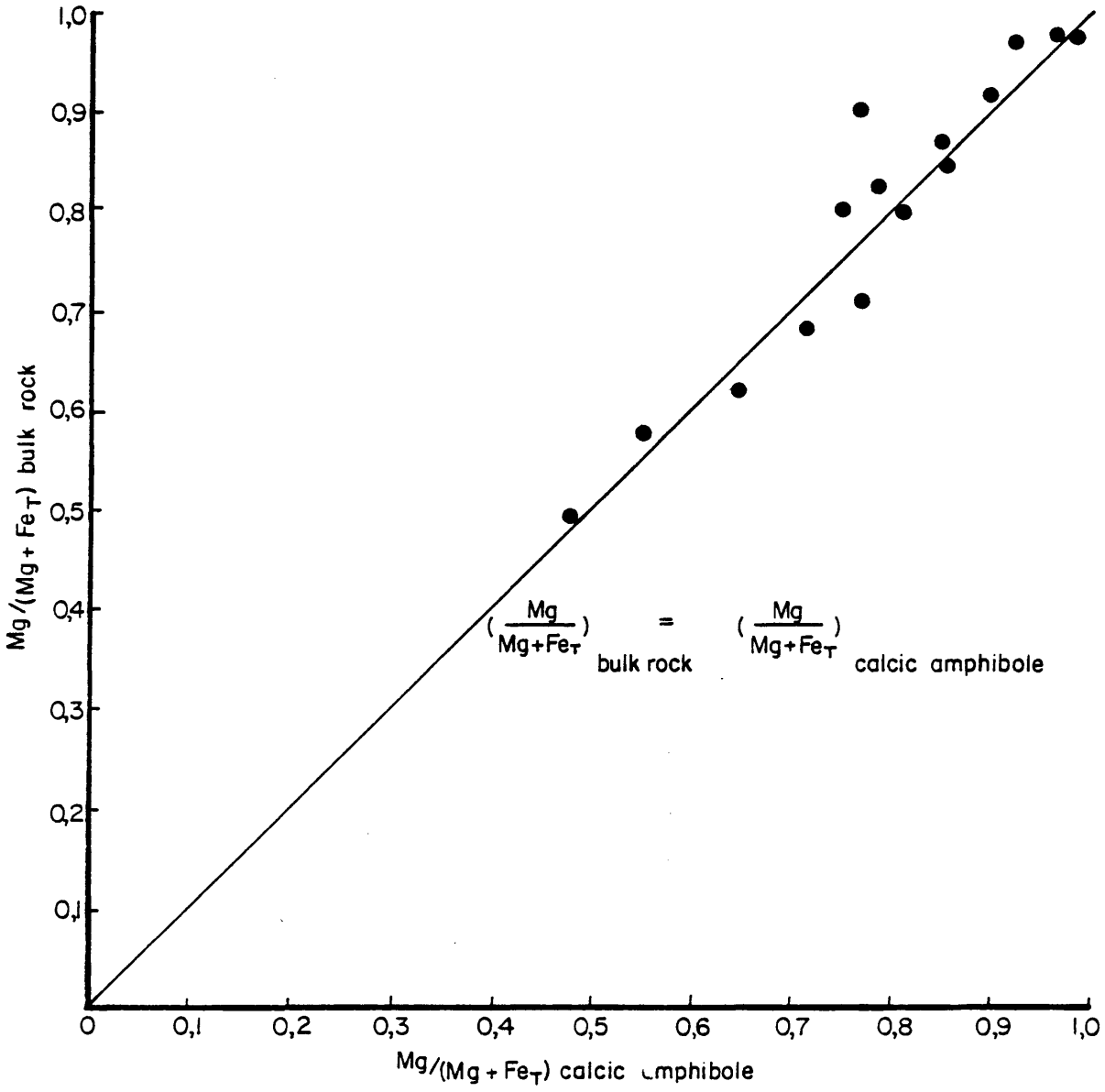

Fig. 31: Calcic-amphibole composition as a function of the molecular Mg/(Mg + Fe_T) ratio in the bulk rock

insufficient Al to fill 8 tetrahedral sites and the total tetrahedral site occpancy may be as low as 0,78.

Influence of host rock composition on occurrence

It has been suggested that a small amount of CaO is required to stabilize cummingtonite (Ernst, 1968 and references therein), but many cummingtonite analyses, however, have negligible amounts of CaO or contain similar amounts to orthoamphiboles (Deer et al., 1962 b). A definite Ca-enrichment in the cummingtonite-bearing samples relative to the majority of orthoamphibole-bearing samples in the study area is suggested in Figure 26, and it seems plausible therefore that the presence of Ca may facilitate the nucleation of cummingtonite as proposed by Cameron(1975).

5.3.6 Garnet

Garnet analyses are given in Appendix 6. Fe_2O_3 was calculated for the grandite-, schlorlomite- and spessartine-rich garnets. In the calculation of the end-members for schlorlomite-rich garnet, $(Ca_3Ti_2(Fe^{3+}_2Ti)O_{12}$ being the schlorlomite molecule (Rickwood, 1968)), the almandine, pyrope and spessartine components were grouped together. The end-members are then given by the following molecular proportions:

almandine + pyrope + spessartine = (Fe + Mg + Mn)/3 ;
grossularite = $^1/_2$ [Al - 2 (alm + py + spess)] ;
schlorlomite = Ti/3 and
andradite = [Fe^{3+} - 2 (schl)]/2 or [Ca - 3(gros) - 3(schl)]/3

When the andradite molecule was calculated according to the second equation a "residual" Fe^{3+} component often remains (Residual Fe^{3+} = [Fe^{3+} - 2(schl) - 2(andr)]. This may be due to tiny magnetite or hematite inclusions in garnet or to analytical errors since Fe^{3+} is calculated from stoichiometry.

For grandite garnets, the almandine, pyrope and spessartine components are also grouped together and the andradite

and grossularite molecules are then given by the molecular quantities $Fe^{3+}/2$ and $\left[Al-2(alm + pyr + spes)\right]/2$ respectively.

Influence of host rock composition on occurrence

Garnet-bearing rocks are low in CaO and MnO but are enriched in $FeO_T + MgO$ and have $(FeO_T + MgO)/Al_2O_3$ ratios greater than 1 (Fig. 32). Under relatively low-pressure thermal metamorphic conditions the cordierite solid solution is complete (Chinner, 1962) and garnet is then restricted to rocks less aluminous than the cordierite solid solution. Higher pressures will decrease the extent of solid solution in cordierite, making it possible for garnet to crystallize in a wider range of rock compositions. The almandine-rich garnets are further restricted to bulk rocks with a $Mg/(Mg + Fe_T)$ ratio lower than 0,3 (Fig. 23).

The factors controlling the formation of the schlorlomite-rich garnet are uncertain but it is suspected that relatively high concentrations of both TiO_2 and Fe_2O_3 are required in the rock. The occurrence of grandite garnet is controlled by both the bulk rock composition and the H_2O/CO_2 ratios of the fluid phase present at the time of metamorphism (Gordon and Greenwood, 1971).

Variation in garnet chemistry

No relationship was found between garnet composition and the $Mg/(Mg + Fe_T)$ ratio of the bulk rock, possibly because of the narrow range of the latter in the study area. The Ca content, however, is a function of rock composition since the three most calcic rocks (Fig. 32) host the garnets with the highest grossularite components (Fig. 33).

The garnets coexisting with orthopyroxene are more magnesian than those coexisting with orthoamphibole (Fig. 33).

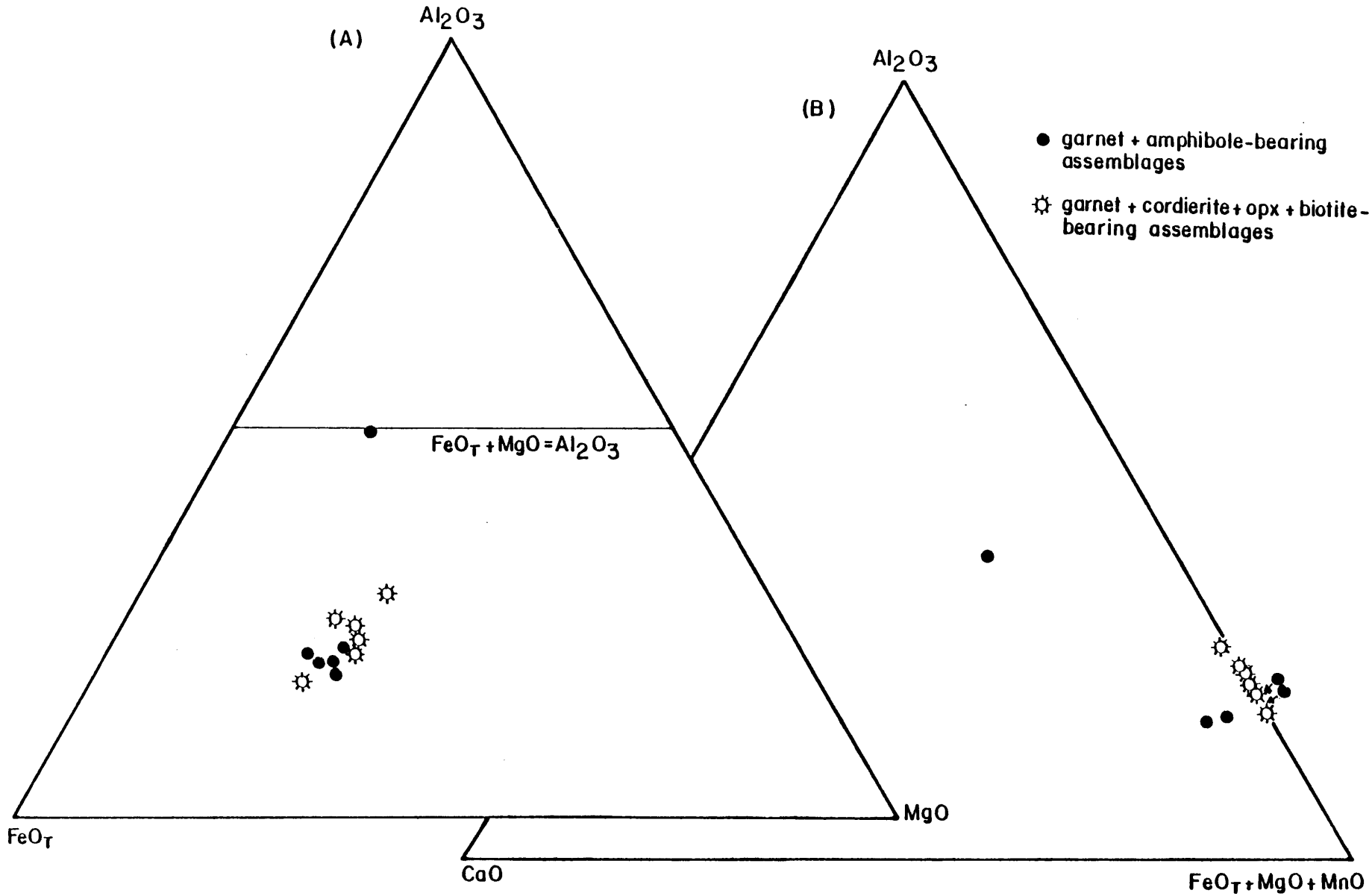

Fig. 32: Bulk rock compositions of the garnet-bearing rocks in terms of the molecular quantities Al_2O_3; CaO; FeO_T and $FeO_T + MgO + MnO$

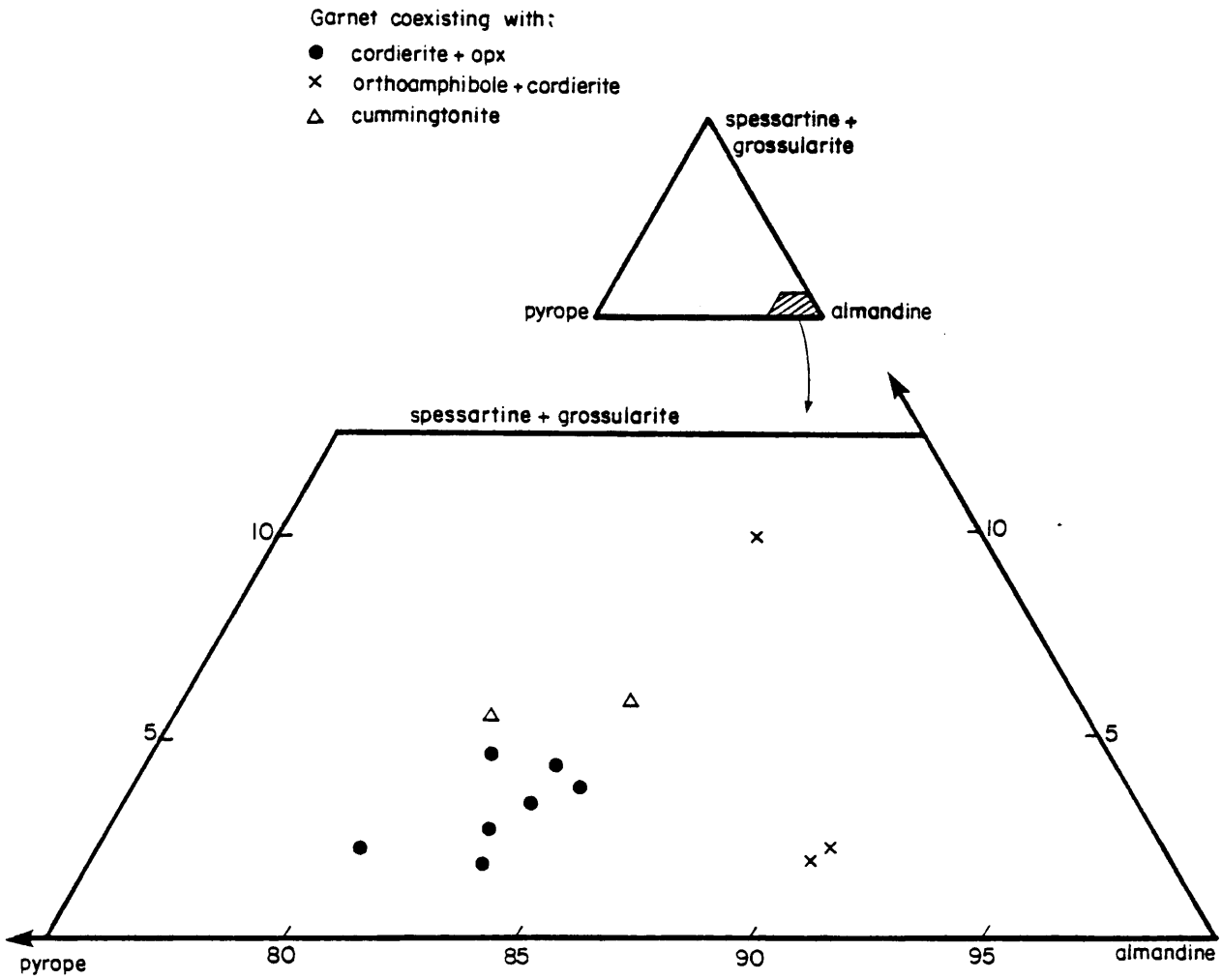

Fig. 33: The compositions of garnets from pelitic assemblages expressed in terms of the almandine, pyrope and spessartine plus grossular molecules

Various workers, e.g. Hollister (1969) found a similar increase of the pyrope content with increasing temperature, although it is more often an indication of increasing pressure (Yoder and Chinner, 1960).

Garnet zoning is restricted to rare cases where the rims are more magnesian than the cores. The rarity of zoning may be ascribed to the high equilibration temperatures (> 600°C) of most garnet-bearing samples (Woodsworth, 1977).

The compositions of the Ti - garnets from the study area are compared with those from other metamorphic rocks on a variation diagram (Fig. 34) which represents a plane of the enstatite - wollastonite - perovskite - hematite tetrahedron (Huckenholz, 1969). The various garnet molecules in the tetrahedron are defined by:

schlorlomite = 3 perovskite + 1 hematite
andradite = 3 wollastonite + 1 hematite
khoharite = 3 enstatite + 1 hematite
Mg-melanite = 1 enstatite + 2 wollastonite + 1 perovskite.

Grossularite is the most important end-member in most other grandite garnets from the study area. Since no data on the Fe_2O_3 concentrations in the bulk rock samples is available it is difficult to determine which factors control the formation of andradite and grossularite, although the fluid phase composition at the time of metamorphism is also known to be important in this respect (Taylor and Liou, 1978).

The anisotropic garnets described in chapter 3 are chemically homogenous and have spessartine, grossularite and almandine as major constituents, while anisotropic garnets from Japan with a similar tatami texture belong to the grandite-garnet series (Takēuchi et al., 1982). These authors concluded that anisotropism in grandite garnets may be caused by straining due to the ordering of octahedrally coordinated cations as a result of differences in ionic radii (Ionic radius of Al^{3+} = 0,5 Å ; radius of Fe^{3+} = 0,64 Å). Maximum ordering is

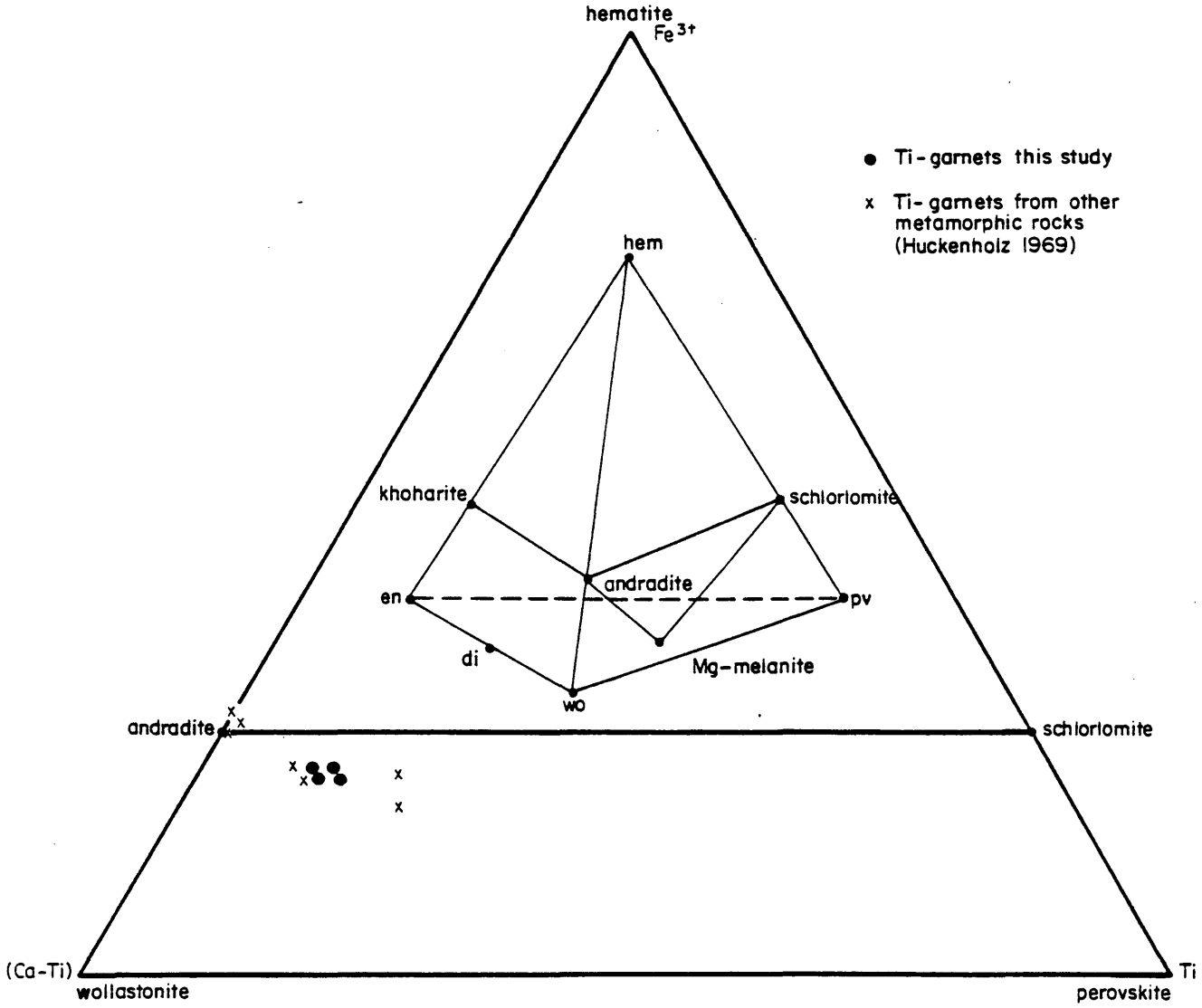

Fig. 34: The compositions of Ti-garnets from the Potgietersrus area and other metamorphic rocks in terms of the hematite (hem); enstatite (en); wollastonite (wo) and perovskite (pv) molecules.

a function of the chemical composition of the garnet and occurs at a composition $gross_{60}$ $andr_{40}$. It is suspected that the anisotropism of the garnets in the study area may be the result of the ordering of both the tri- and divalent cations because of the considerable difference in the ionic radii of Ca (0,99Å) and Mn(0,8Å). Ordering of the trivalent cations in the octahedral sites will cause a distortion of the octahedra in the crystal lattice. Since the divalent cations are situated in the interstices within the Si-Al-Fe^{3+} framework (Deer et al., 1962 a) the distortion of the network may enhance the ordering of the divalent cations, causing an additional strain on the lattice. This may account for the anisotropism of the crystals despite the relatively small andradite component.

5.3.7 Orthopyroxene

The Al_2O_3 content of orthopyroxene analyses (Appendix 7) can be evaluated in terms of the "Al-value", which is calculated on the basis of a maximum of 25 mol percent substitution of Al into orthopyroxene which leads to an end-member stoichiometry of $Mg_3Al_2Si_3O_{12}$ instead of $MgAl_2SiO_5$ for aluminous Mg-orthopyroxene (Ganguly and Ghose, 1979). The pyrope end-member has a Al/(Al + Si) ratio of 0,4, while enstatite has a ratio of 0.
In order to develop a scale that will have enstatite at 0 percent and pyrope at 100 percent, the Al/(Al + Si) ratio of an analysis must be multiplied by 250. The value obtained, referred to as the "Al-value", indicates the percentage pyrope in the orthopyroxene analysis.

Control of bulk rock composition on occurrence

Orthopyroxene is absent from Al-silicate polymorph-bearing samples since the orthopyroxene - Al_2SiO_5 - polymorph tie-line is only stable at high pressures (Hess, 1969). Orthopyroxene-bearing samples therefore have effective bulk compositions less aluminous than the cordierite solid solution under low-pressure conditions.

Variation in orthopyroxene chemistry

Although there is a correlation between orthopyroxene composition and the $Mg/(Mg + Fe_T)$ ratio as well as the Al_2O_3 concentration of the bulk rock (Fig. 35 A and B), a few points show significant deviation from the relationships and a possible correlation between orthopyroxene composition and the metamorphic grade and or mineral assemblage was therefore examined (Fig. 36). This plot suggests a relationship between the $Mg/(Mg + Fe_T)$ ratio and the mineral assemblage with garnet-and olivine-bearing assemblages having the lowest, and spinel-bearing assemblages the highest ratio respectively.

The temperature dependence of the solubility of Al in orthopyroxenes from olivine- and spinel-bearing assemblages has been shown by several workers e.g. Obata (1976). Although the higher grade samples in the study area generally have more aluminous orthopyroxenes, the most important factor determining the Al_2O_3 concentration appears to be the mineral assemblage (Fig. 36). The orthopyroxenes from spinel $\pm$ olivine-bearing assemblages are notably enriched in Al_2O_3 relative to the orthopyroxenes from hornblende- and clinopyroxene-bearing assemblages. Berg (1977 a) also found a relationship between alumina solubility and the mineral assemblage, as well as the $Mg/(Mg + Fe_T)$ ratio of orthopyroxenes from the Nain contact aureoles, Labrador.

5.3.8 Muscovite

Muscovite analyses (Appendix 8) usually have octahedral site occupancies greater than 4 and interlayer occupancies less than 2. Similar results were obtained by Fletcher and Greenwood (1979) in a study of metamorphic muscovites from British Columbia.

Muscovite can undergo two major substitutions, viz. towards phengite ($K_2Al_2(Mg,Fe)_2Si_8O_{20}(OH)_4$) and ferrimuscovite ($K_2(Al, Fe^{3+})_4[Si_6Al_2O_{20}](OH)_2$). The phengite- and ferrimuscovite substitutions involve

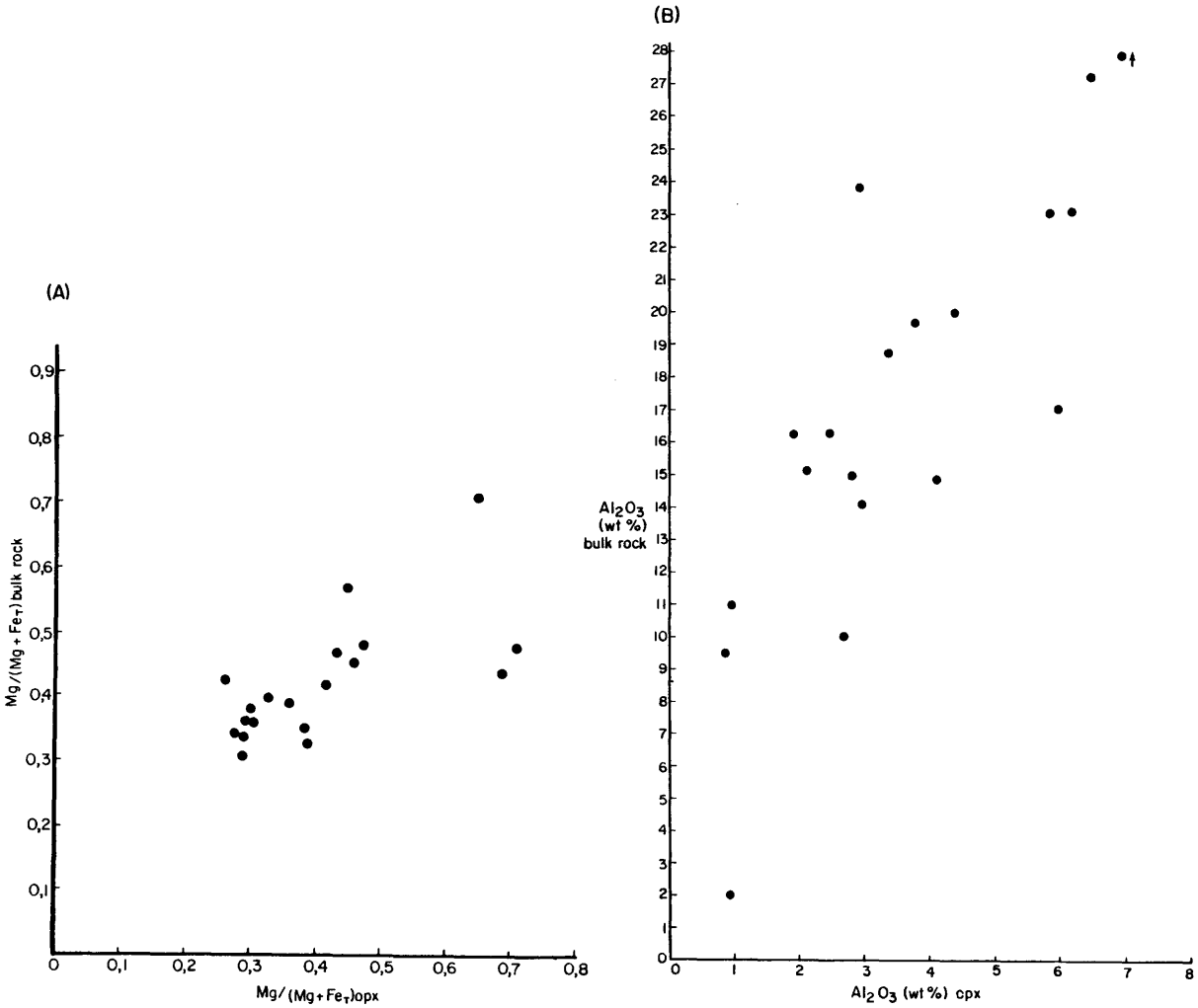

Fig. 35: Orthopyroxene composition as a function of the molecular Mg/(Mg + Fe_T) ratio (A) and wt percent Al_2O_3 (B) content of the bulk rock

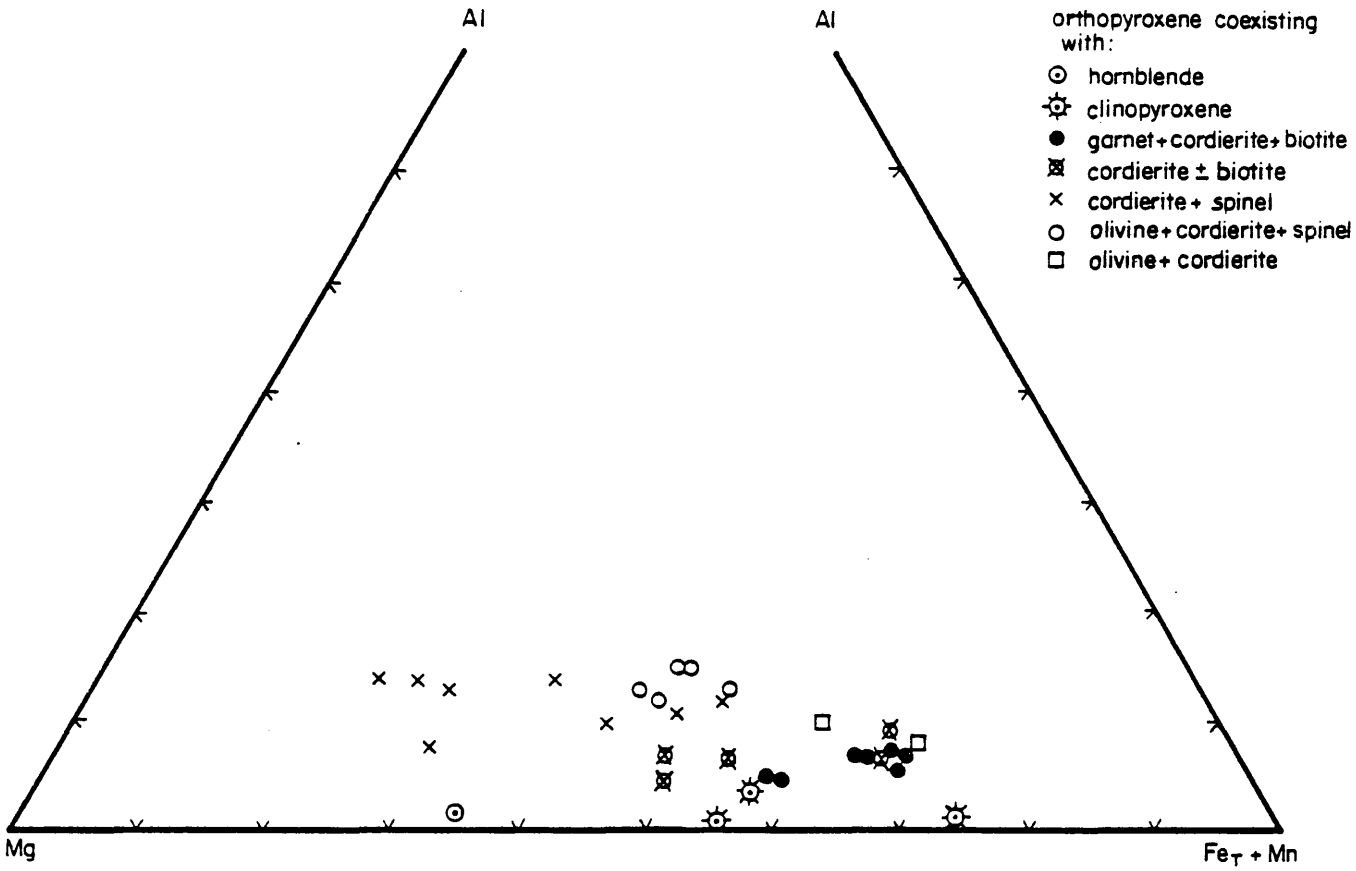

Fig. 36: The Al, Mg and Fe_T concentrations in orthopyroxene as a function of mineral assemblage

the $2\ Al^{iv} + 2\ Al^{vi} \rightleftharpoons 2\ Mg^{vi} + 2\ Si^{iv}$ and $Al^{vi} \rightleftharpoons (Fe^{3+})^{vi}$ exchanges respectively. The magnitude of the phengite substitution cannot be calculated by assuming that $(Fe_T + Mg)$ represents the phengite molecule since some Fe may be present as Fe^{3+}. The muscovite and phengite end-members were thus calculated on the basis of Si, Al substitution in a similar way as the biotite end-members. Muscovite has a Al/(Al + Si) ratio of 0,5 while phengite has a ratio of 0,2. Phengite was plotted at the 0 point of the substitution scale and muscovite at the 100 point. The percentage muscovite in an analysis can then be calculated from the formula:

$$\% \text{ musc} = \left[Al/(Al + Si) - 0,2 \right] \times 3,333 \times 100 \quad \ldots\ldots\ldots\ldots 5(12)$$

The percentage phengite is then equal to 100- % muscovite.

Variation in muscovite chemistry

Not enough data points are available to draw conclusive evidence regarding the control of the bulk rock composition on muscovite composition, but a relationship between the $Mg/(Mg + Fe_T)$ ratio in the bulk rock and in muscovite is suspected. The following well established trends were detected in the muscovites from the study area:

1) a negative correlation between Na and Fe as well as between Na and $(Mg + Fe_T)$.
2) a positive correlation between Fe and Mg and
3) a negative correlation between $(Mg + Fe_T)$ and Al.

Cipriani et al. (1971) showed that the $(Mg + Fe_T)$ concentration and therefore the phengite content, decreases with increasing temperature, causing a "purification" of muscovite with increasing metamorphic grade.

5.3.9 Chlorite

The chlorites (analyses Appendix 8) have been classified according to the nomenclature of Hey (1954) (Fig. 37).

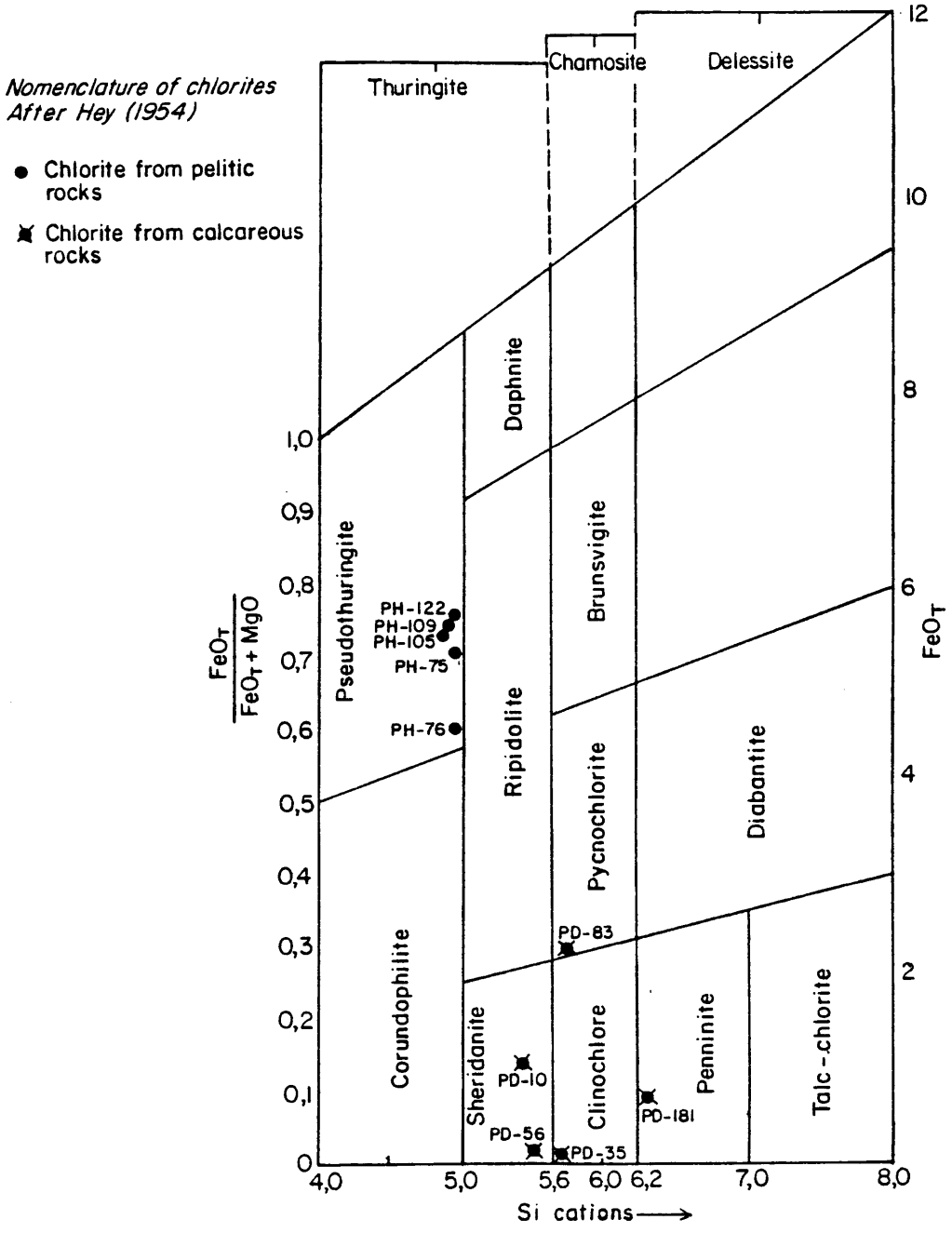

Fig. 37: Classification of the chlorites from the Potgietersrus area according to Hey (1954)

Both the $Mg/(Mg + Fe_T)$ and $Al/(Al + Si)$ ratio of chlorite appears to depend on the rock composition. The chlorites from calcareous rocks contain more Si than those from pelitic rocks (Fig. 37) although their bulk rock compositions are less siliceous than the pelitic rocks. Their higher Si content is, however, the result of a higher $Si/(Si + Al)$ ratio in the calc-silicates compared to the pelites.

5.3.10 Clinopyroxene

The Fe_2O_3 content was calculated for all analyses (Appendix 9) as it may be an important component in clinopyroxene (Deer et al., 1962 b). Clinopyroxenes in pelitic formations is restricted to low Al_2O_3 (< 13 wt percent), high CaO bulk rocks (Fig. 23) while it is common in calcareous rocks.

There is a positive correlation between the enstatite content of clinopyroxene and the bulk rock composition (Fig. 38) while no relationship between clinopyroxene composition and mineral assemblage could be detected.

The maximum Al_2O_3 content of clinopyroxene is 10 wt percent (PH - 207) but these clinopyroxenes are not fassaites since they contain less than 25 wt percent CaO.

5.3.11 Fassaite

The Fe_2O_3 content was calculated for all fassaite analyses (Appendix 10). Since no mathematical unique scheme exists for the calculation of the fassaite end-members the procedure used by Powell and Powell (1974) according to which Ti-pyroxene ($Tp = CaTiAl_2O_6$) is calculated first, was employed. Sodium is then divided equally between jadeite ($NaAlSi_2O_6$) and acmite ($NaFe^{3+}Si_2O_6$) followed by the calculation of the Fe-tschermaks ($FaTs = CaFe^{3+}AlSiO_6$), Ca-tschermaks ($CaTs = CaAl_2SiO_6$) and diopside ($CaMgSi_2O_6$) molecules. With all elements expressed as molecular quantities the end-member molecules are then calculated from the following formulae:

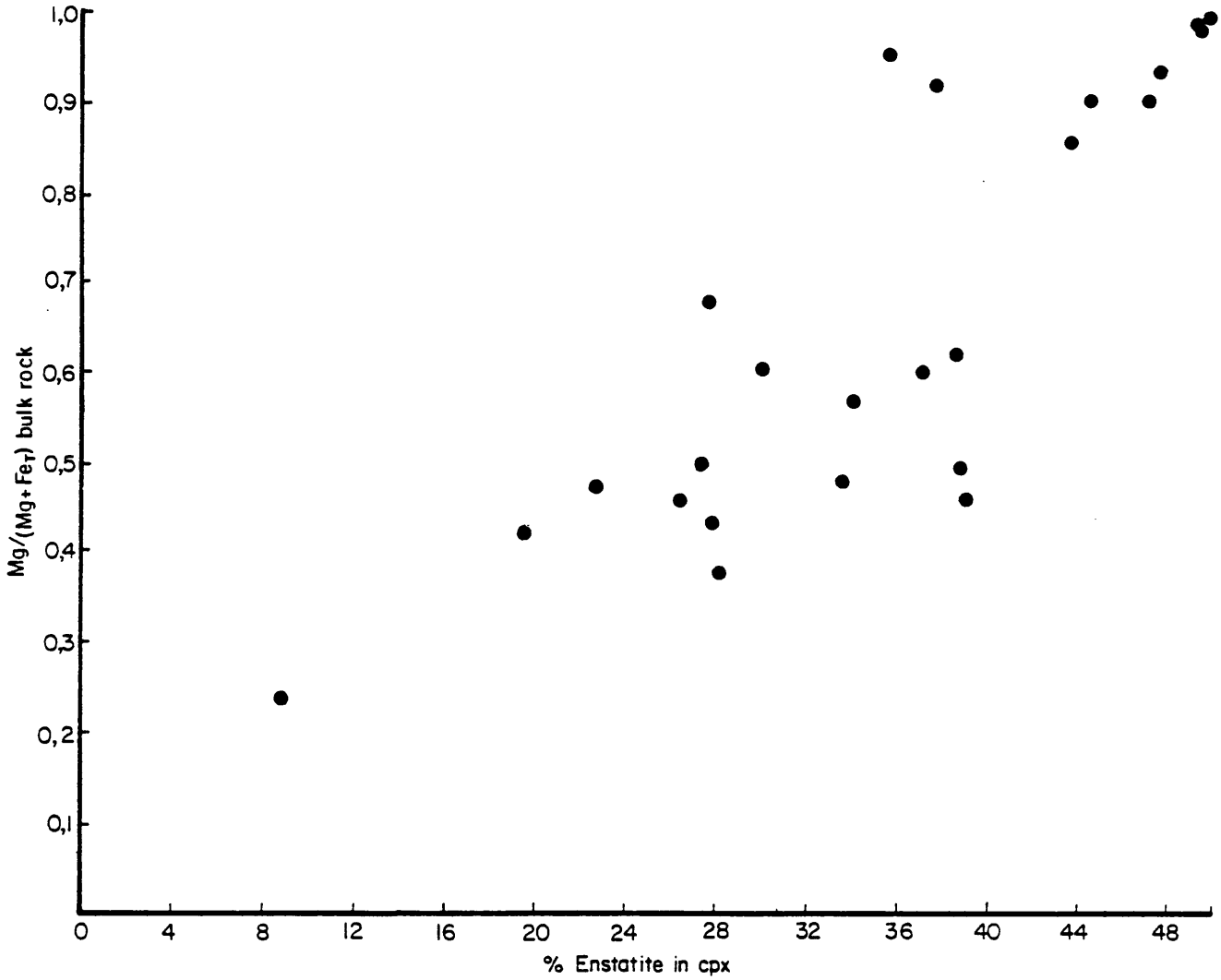

Fig. 38: The enstatite content of clinopyroxene as a function of the molecular Mg/(Mg + Fe$_T$) ratio of the bulk rock

diopside (di) = Mg + Fe^{2+} Ti-pyroxene (Tp) = Ti

jadeite (ja) = Acmite (ac) = $^1/_2$ Na^+

Fe - tshermaks (FaTs) = Fe^{3+} - $^1/_2$ Na

Ca-tshermaks (CaTs) = $^1/_2$ [Al-2(Ti)- $^1/_2$(Na)-(Fe^{3+} - $^1/_2$ Na)]

= $^1/_2$ [Al-2(Ti)-Fe^{3+}]

Variation in fassaite composition

Fassaites are characterized by a high CaO concentration (about 25 wt percent or 1 ion per formula unit), a high but variable Al_2O_3 content and a high Fe^{3+}/Fe^{2+} ratio, while the TiO_2 content may also be high (Deer et al. 1962 b). No relationship between bulk rock composition and fassaite composition could be detected in the study area.

The fassaite crystals in sample PD - 96 show concentric zoning with respect to TiO_2 with cores containing up to 4,5 wt percent TiO_2 and rims containing less than 0,4 wt percent TiO_2. The core compositions of these crystals are similar to the composition of Ti-pyroxenes from Hocheifel (Huckenholz, 1965 a and b) (Fig. 39). The core-rim tie-lines are almost parallel to the diopside-Ca-tschermaks side of the diagram (Fig. 39), suggesting that the fO_2 remained constant during the period of pyroxene growth. The zoning of the crystals is probably the result of the strong partitioning of Ti into the growing clinopyroxene porphyroblasts after nucleation, thereby depleting the matrix in TiO_2.

The following two substitutions are important in terrestrail pyroxenes (Shedlock and Essene, 1979):

$(Al^{3+}, Fe^{3+}) + Al^{iv} \rightleftharpoons (R^{2+})^{vi} + Si^{iv}$ .....5(13)

and

$(Ti^{4+})^{vi} + 2(Al^{3+})^{iv} \rightleftharpoons (R^{2+})^{vi} + 2(Si)^{iv}$ .....5(14)

The latter substitution explains the high Al_2O_3 and low SiO_2 concentrations in the TiO_2 - rich pyroxene cores and the low Al_2O_3, high SiO_2 and MgO values in the TiO_2-poor rims.

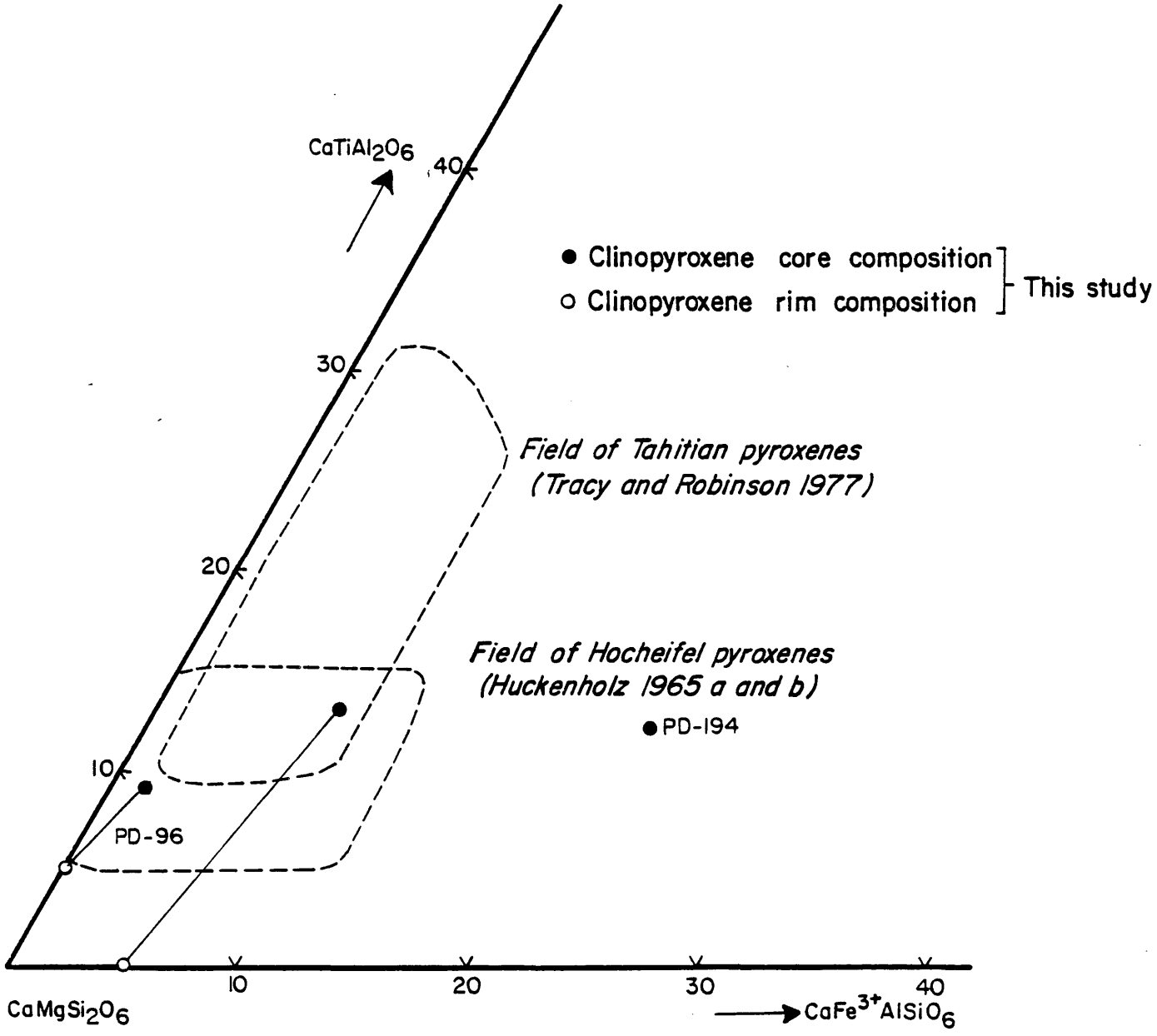

Fig. 39: The compositions of Ti - rich clinopyroxenes from the Potgietersrus area compared with the compositional fields of Tahitian pyroxenes (Huckenholz, 1965 a and b)

The compositions of the low-TiO_2 fassaites from the study area are compared with the compositions of fassaites from various other localities in Figure 40 A - C. The position of the proposed solvus between fassaite and diopside (Ginzburg, 1969) is also indicated. Various workers, e.g. Shedlock and Essene (1979) have since showed that there is no evidence for the existence of a solvus in the system di - FaTs - CaTs at subsolvus temperatures, and this study is in agreement with their observations.

Fassaites from sample PD - 184, which contains 36 wt percent Al_2O_3, are with 19,4 and 20,1 wt percent Al_2O_3 the most aluminous pyroxenes so far described from terrestrial rocks. The previous highest value recorded is 19,66 wt percent for a fassaite from a calc-silicate nodule from the La Soufriere volcano, on the island of St. Vincent in the Lesser Antilles (Devine and Sigurdsson, 1980).

5.3.12 Iron-titanium oxide minerals

Magnetite and ilmenite analyses are presented in Appendix 11. There is no mathematically unique scheme for recasting opaque mineral analyses into end-member molecules. Buddington and Lindsley (1964) as well as Carmichael (1967) proposed procedures for treating di- and trivalent cations in opaque minerals, but for the purpose of this study it was decided to use the method of Powell and Powell (1977) according to which maximum and minimum values of X_{mt}; X_{ulv}; X_{ilm} and X_{hem} are calculated. (X_{mt} denotes the fraction of magnetite in a particular solid solution series , etc.).

Variation in iron-titanium mineral chemistry

The ulvospinel content of most magnetite grains is low while the substitution of Al_2O_3 and Cr_2O_3 is likewise limited to a maximum of 6,4 and 3,5 wt percent respectively.

The TiO_2 content of the bulk rock does not control the TiO_2 content of magnetite. When magnetite is the only oxide phase in a rock the TiO_2 content depends on the modal

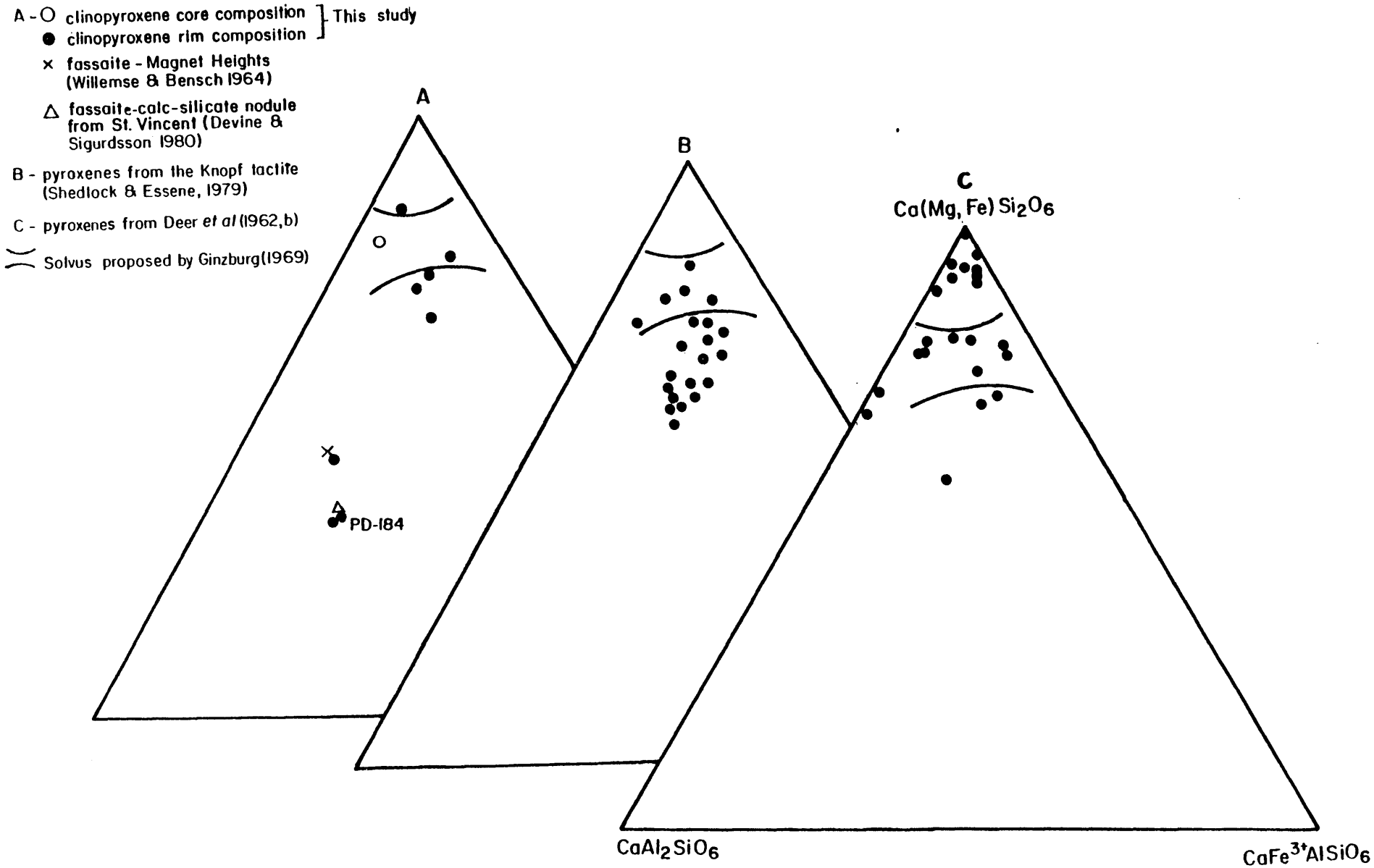

Fig. 40: Fassaite compositions from the Potgietersrus area (A) compared with fassaites from other localities (B) and (C)

concentration of magnetite since TiO_2 enters magnetite preferentially at metamorphic temperatures (Abdullah, 1965). When ilmenite is also present the partitioning of TiO_2 between magnetite and ilmenite will depend entirely on the temperature of formation.

Ilmenite analyses have negligible hematite concentrations while the MnO and MgO substitutions are also very low.

5.3.13 Plagioclase

Total Fe has been calculated as Fe_2O_3 for the plagioclase analyses in Appendix 12. The analyses do not always fit such a stoichiometry although this may be due to analytical difficulties in determening SiO_2.

Plagioclase composition in metamorphic rocks is a function of bulk rock composition (Hörmann et al., 1980) and metamorphic grade (Fletcher and Greenwood, 1979). Although there is a correlation between plagioclase - and bulk rock-composition in the study area (Fig. 41), the plagioclase from sample PH - 79 do not conform to the predicted relationship. Not enough data is available to test a possible relationship between plagioclase composition and metamorphic grade.

The occurrence of two texturally and chemically different types of plagioclase in sample PH - 79 has been described in Chapter 3. The first type (An_{17}) occurs in the groundmass of the sample as small subidioblastic crystals riddled with inclusions. The second type (An_3) forms large rounded aggregates devoid of any inclusions. The compositions of the two types define the limbs of the peristerite gap (solvus) which has been taken as the transition from low- to medium metamorphic grade or the almandine and oligoclase zones (Mason, 1962).

Brown (1965) summarized the reasons that could lead to the presence of two feldspars in a rock:

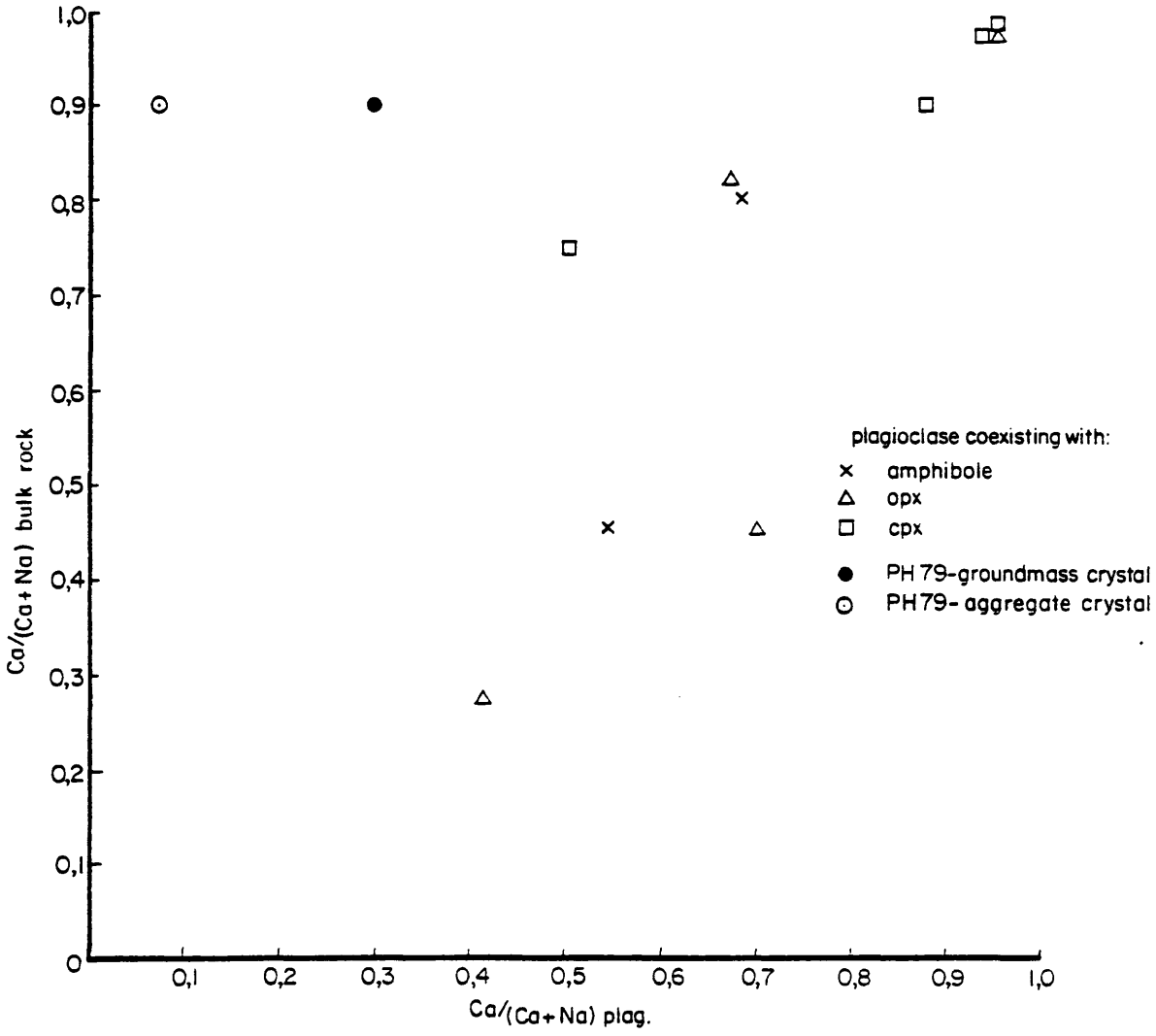

Fig. 41: The composition of plagioclase as a function of the molecular Ca/(Ca + Na) ratio in the bulk rock and the mineral assemblage

1) The plagioclase represents, in part, original detrital grains;
2) The grains were converted to albite in areas now in a low metamorphic grade;
3) Albite was in the process of transformation into oligoclase. Some crystals were fully transformed and others untransformed. The compositional jump was controlled by the peristerite solvus and the two plagioclases could be in equilibrium.

These explanations cannot, however, account for the textural difference between the two plagioclases in sample PH - 79. The texture seems to suggest that albite crystallized early in isolated aggregates in which the crystals grew slowly, expelling inclusions which were then concentrated along the boundaries of the aggregates. The period of albite growth was followed by a period of rapid oligoclase growth which took place at a higher temperature. At 6 kbar pressure the crest of the peristerite solvus lies at about 500°C (Crawford, 1966) which indicates that sample PH - 79 must have equilibrated at a temperature lower than 500°C.

Zoning

Plagioclase commonly shows reversed zoning although the difference in composition between core and rim rarely exceeds 2 percent Ab. A possible cause of the zoning is a CaO - Na_2O exchange reaction with the fluid phase present at the time of metamorphism.

5.3.14 Aluminosilicate polymorphs

Andalusite and sillimanite analyses are presented in Appendix 12. Although Al_2SiO_5 polymorphs occur in rocks with a variety of bulk compositions, Figure 23 suggests that at least 15 wt percent Al_2O_3 is needed in the bulk rock for the crystallization of an Al_2SiO_5 polymorph. The average FeO concentrations in both andalusite and sillimanite

are slightly lower than the values reported by Hörrmann et al. (1980), while the MgO and MnO concentrations are similar to values reported by Deer et al. (1962 a).

5.3.15 Olivine

Olivine analyses from the study area are presented in Appendix 13. Forsterite-rich olivine is common in calc-silicates whereas the fayalitic olivine comes from the shale member of the Penge Formation. Fayalitic olivine is usually found in metamorphosed iron-formations (Berg 1977 a and b; Vaniman et al., 1980) and the only other known terrestrial occurrence of olivine in a meta-pelite is the Riekensglück hornfels (Abraham and Schreyer, 1973).

The compositions of the olivine-bearing pelites have the following characteristics (Fig. 42):1)The $(MgO + FeO_T)/(Al_2O_3 + SiO_2)$ ratio is greater than 0,5 while this ratio is less than 0,25 for the average pelites (Fig. 11) and 2) The $SiO_2/(Al_2O_3 + FeO_T + MgO)$ ratio is less than 1 while it is greater than 1,5 for average pelites (Fig. 11). The rarity of rocks with a similar composition in nature is partially responsible for the paucity of olivine in metapelites.

Variation in olivine chemistry

There is a relationship between the $Mg/(Mg + Fe_T)$ ratio in olivine and the bulk rock composition (Fig. 43). Olivines from meta-pelites are enriched in Fe-relative to the corresponding bulk rocks because Fe is partitioned into olivine relative to the coexisting ferromagnesian minerals (orthopyroxene and cordierite).

5.3.16 Spinel

Considerable uncertainty is involved in the Fe_2O_3 values calculated for spinel analyses (Appendix 14) since the

Fig. 42: The bulk rock compositions of various olivine-bearing rocks from the Potgietersrus area compared with the compositions of other olivine-bearing rocks cited in the literature

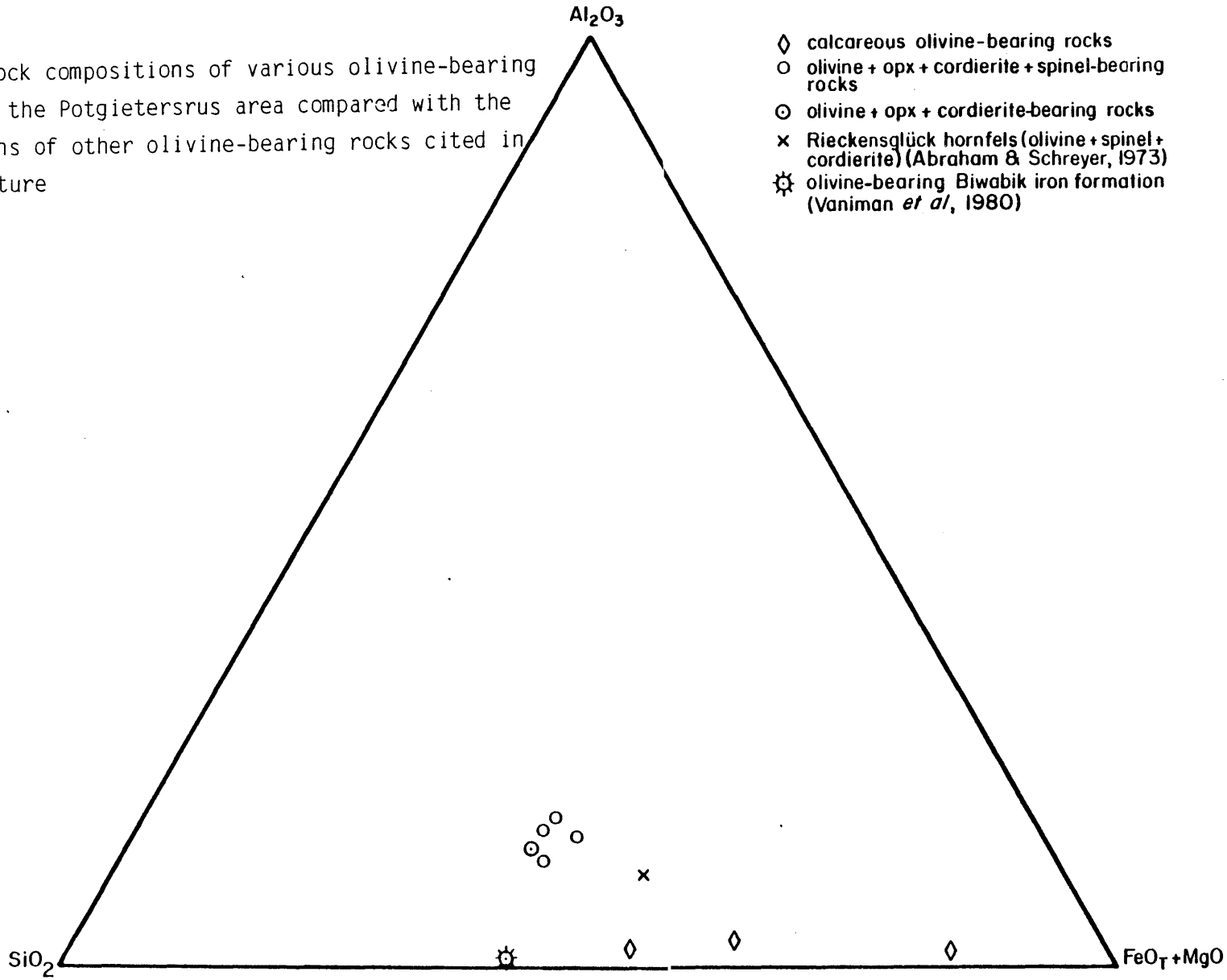

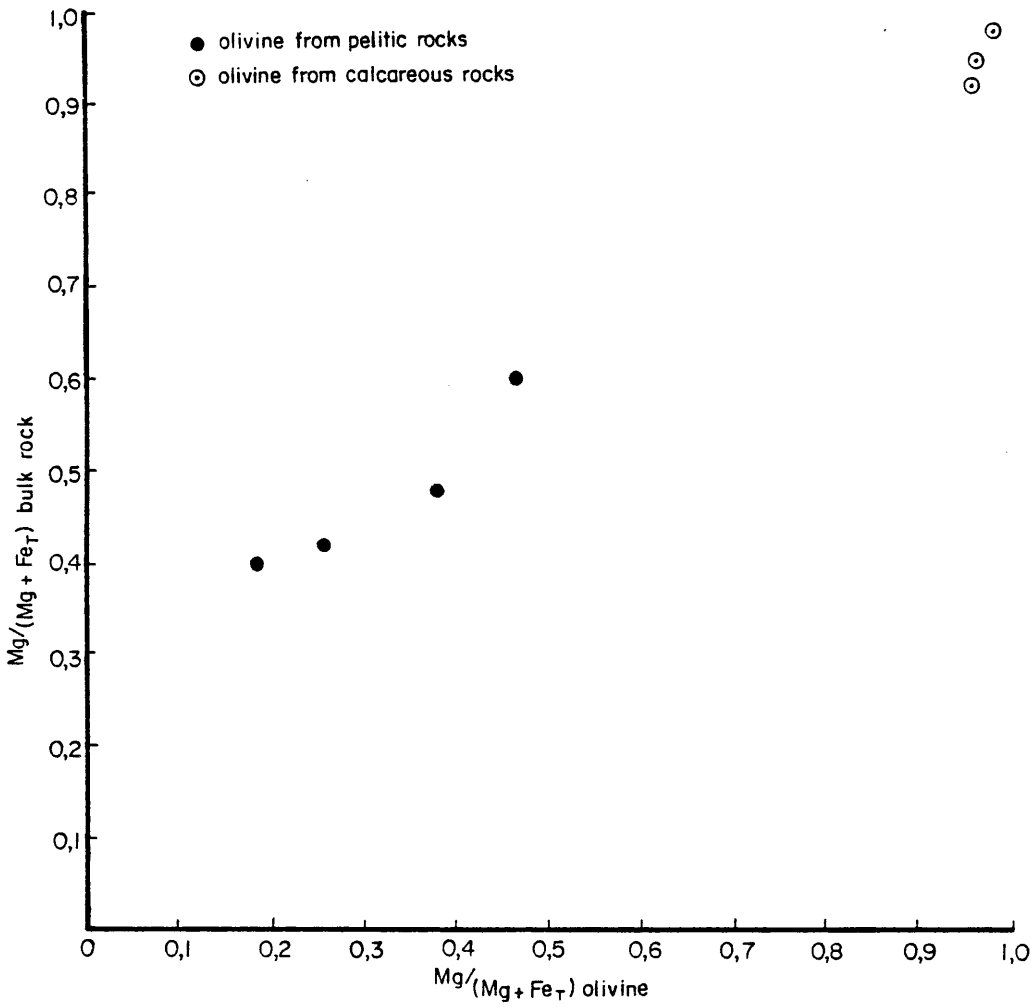

Fig. 43: Olivine composition as a function of the molecular Mg/(Mg + Fe_T) ratio in the bulk rock

deviation of the structural formulae from stoichiometry prior to the calculation of Fe_2O_3 depends largely on the accuracy determined for the Al_2O_3 concentration.

Control of bulk rock composition on occurrence

According to Turnock and Eugster (1962) hercynite is restricted to an environment rich in Fe and Al, while low silica activities and oxygen fugacities are also required in order to prevent the oxidation of hercynite to ferrian hercynite or magnetite plus corundum. Spinel-bearing rocks from the study area have variable Al_2O_3 / (FeO_T + MgO) ratios but rather similar SiO_2 concentrations (Fig. 44). The $SiO_2/(Al_2O_3 + FeO_T + MgO)$ ratio for all, but one sample, is lower than 1 (Fig. 44), while the ratio for average pelites is higher than 1,5 (Fig 11). This relationship suggests that a low SiO_2, rather than a high Al_2O_3 concentration is required for the crystallization of spinel in a particular rock.

Variation in spinel chemistry

Spinel displays a wide range of Mg/(Mg + Fe) ratios and no ralationship between the composition of spinel and the bulk rock composition could be detected. Due to the refractory nature of spinel the crystals within single samples display a significant variation in composition, e.g. two crystals in sample PH - 195 have Mg/(Mg + Fe) ratios of 0,21 and 0,16 respectively. The crystals are unzoned, indicating that they homogenized even if they did not equilibrate with one another. The example illustrates the principle of local-or mosaic equilibrium (Korzhinskii, 1959) where the system as a whole is not necesseraly in equilibrium although equilibrium is attained locally.

Spinels from the study area are either colourless to light green (calc-silicates), dark green (orthopyroxene-bearing assemblages) or brownish-grey (sillimanite-bearing assemblages) in colour. The colourless spinels have high Mg/(Mg+Fe)ratios and the brownish-grey spinels low

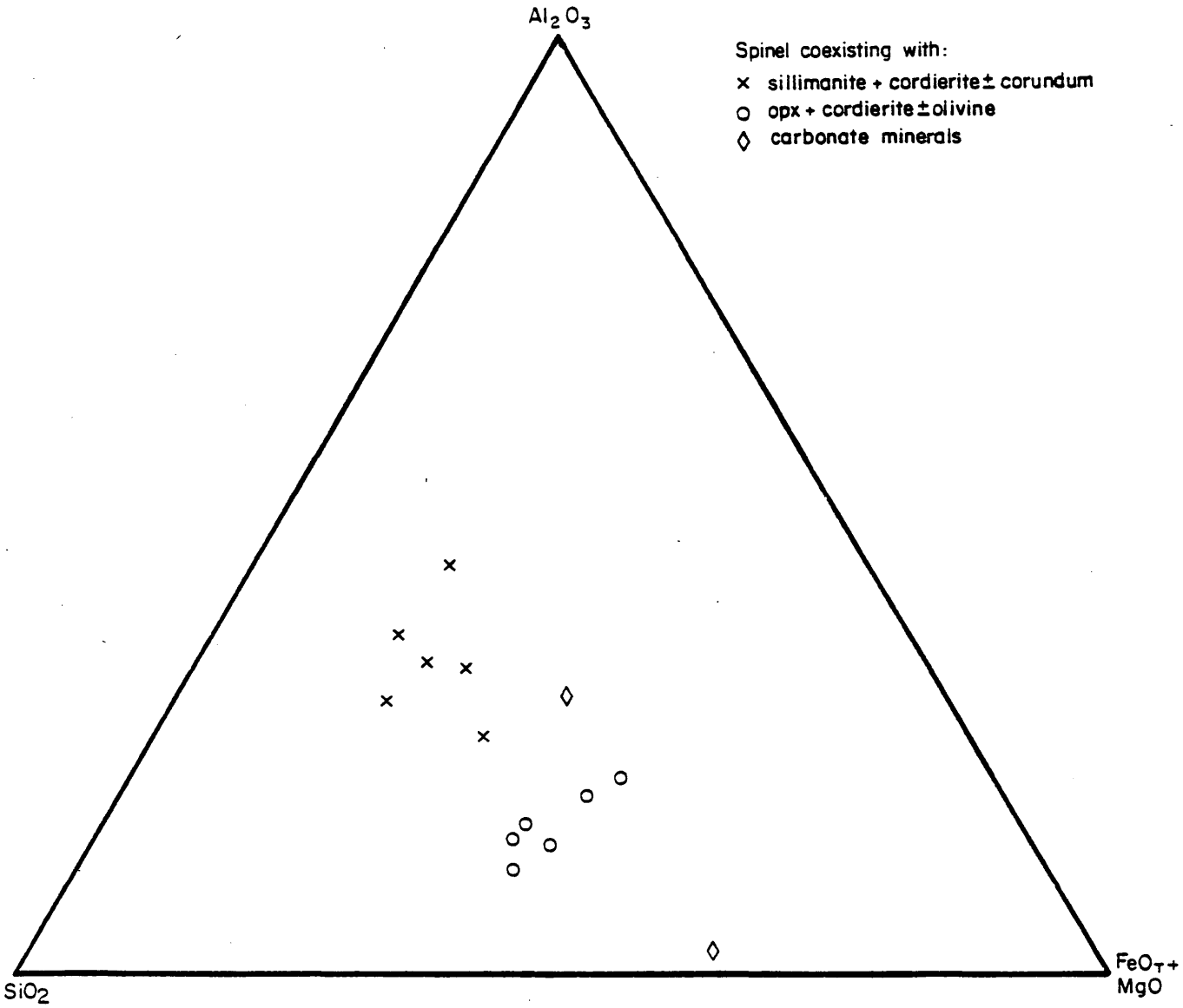

Fig. 44: The bulk rock compositions of spinel-bearing rocks from the Potgietersrus area illustrating the low molecular $SiO_2/(Al_2O_3 + FeO_T + MgO)$ ratio of these rocks

Fe^{2+}/Fe^{3+} ratios. The relatively oxidized nature of the brownish-grey spinels is confirmed by the presence of corundum (which may be an oxidation product of spinel) in some of these samples.

5.3.17 Additional minerals

A number of minerals from the study area do not show a meaningful compositional range or are relatively rare so that only a few analyses of such minerals are available (Appendix 15)

a) Chloritoid

Chloritoid appears to be confined to relatively Al_2O_3 and FeO-rich rocks (Fig. 23). The $Mg/(Mg + Fe_T)$ ratios are low and constant, which is in agreement with the observation by Deer et al. (1962 a) on the limited substitution of Mg for Fe^{2+} in chloritoid compared to other ferromagnesian silicates with a similar crystal structure.

b) K-feldspar

The identification of K-feldspar in cordierite-plagioclase-bearing rocks was difficult due to the similarities of the optical properties of these minerals. The analyses are characterized by high orthoclase - (86 - 98 percent) and low anorthite (0 - 2 percent) components. Similar compositions are common in metamorphic rocks (Hörmann et al., 1980).

c) Calcite and Dolomite

Only tree coexisting carbonate pairs were analyses. Mn and Fe substitutions are limited and a maximum MgO content of 6,5 wt percent was recorded for calcite.

d) Epidote

Epidote is common in many calc-silicates where it is believed to be of retrograde origin. The chemical composition

varies between the end-members clinozoisite ($Ca_2Al.Al_2O.OH[Si_2O_7][SiO_4]$) and pistacite ($Ca_2Fe^{3+}Al_2O.OH[Si_2O_7][SiO_4]$) The pistacite content varies between 3,8 and 33 percent. A similar range has been found by Holdaway (1972) who showed that the bulk rock composition as well as the fO_2 determines the Fe-content of epidote. Only when epidote coexists with a Fe- excess mineral, e.g. magnetite or hematite, will the Fe-content be a function of fO_2 alone. Rambaldi (1973) however, showed that the CO_2/H_2O ratio of the fluid phase will also influence the amount of Fe in epidote. Clinozoisite will be stable in a more H_2O-rich fluid phase, thus explaining the Al-rich rims of zoned epidote crystals in sample PD - 158. This is in agreement with the suggested retrograde growth of epidote, since the fluid phase was believed to have become increasingly H_2O-rich with dropping temperatures at the end of the metamorphic event (Chapter 6).

e) Wollastonite

Wollastonite is a rare mineral in the study area. The maximum MnO and FeO concentrations in the analysed crystals are 1,2 and 0,8 wt percent respectively.

f) Monticellite

This mineral has been found in only one sample from the study area. It has a very unusual composition because of its high Mn and Fe concentrations. Despite the existence of an isomorphous series between monticellite ($CaMgSiO_4$) , glaucochroite ($CaMnSiO_4$) and kirschsteinite ($CaFeSiO_4$) , monticellite analyses very seldom depart from the ideal composition (Deer et al., 1962 a). The rarity of minerals with intermediate compositions in the isomorphous series is usually ascribed to the limited availability of Fe and Mn in the host rock. The host rock of the monticellite in the study area does not have an unusual composition since it only contains 2,1 and 0,86 wt percent FeO and MnO respectively More work is needed to establish why monticellite with such an unusual

composition occurs in this particular rock.

The only natural Mn-rich monticellite seems to have been described by Schaller (1935) from California. This therefore seems to be the first account of monticellite with high quantities of both the Mn - and Fe-end-members in natural rocks.

g) Sphene

Sphene is common in the calc-silicates from the study area. An antipathetic relationship between Ti and Al was noted in the analysed grains.

h) Prehnite

Prehnite is common in the calc-silicates where it occurs as veinfillings, idioblastic crystals in quartz aggregates and as pseudomorphs after clinopyroxene and plagioclase. All types are believed to be of retrograde origin.

i) Idocrase

Idocrase occurs together with clinopyroxene and garnet in some calc-silicates from the study area. The analyses often deviate significantly from stoichiometry.

j) Ni- minnesotaite (Willemseite)

This very unusual mineral occurs as irregular aggregates of acicular or tabular crystals with a radial arrangement in sample PD - 178. It has a distinct yellowish-brown colour in plane polarized light and shows weak pleochroism. The birefringence appears low although the colour of the mineral may mask the true birefringence. Unfortuanately too little material is persent in the sample to make the separation of enough, and sufficiently pure material possible for determening the optical properties of the mineral or to obtain an X-ray diffractogram, and the mineral had to be identified on the basis of its chemical composition alone.

The Mg - Ni silicates described in the literature resemble either talc or chlorite in composition. The Ni-silicate from the study area differs from the Ni-chlorites, nimite and nickeloan clinochlore, in that it contains more FeO than MgO, too much SiO_2 and too little Al_2O_3 to be classified as a chlorite.

Ni-rich talc, willemseite, has been described by De Waal (1970) from Bon Accord near Barberton. The chemical composition resembles that of minnesotaite and its cell formula is: $(Fe, Ni, Mg, H_2O)_3$ $(Si, Al, Fe)_4$ $O_{10}(OH)_2$. He also suggested that this name should be used for all talc minerals having Ni as the major element in octahedral coordination. The kerolite-pimelite mineral series, which is a series of Mg - Ni hydrous silicates with talc-like compositions, have Al_2O_3, SiO_2, NiO and (MgO + FeO) values which correspond closely to the composition of willemseite (Brindley et al., 1979). The Ni-silicate from the study area therefore appears to be a ferruginous equivalent of willemseite or the kerolite-pimelite mineral series, i.e. a Ni-Fe-talc or Ni-minnesotaite. Comparison with a minnesotaite analysis (Appendix 15) verifies this theory.

The mineral is suspected to be of retrograde origin, probably involving a Fe-Ni sulphide introduced as an immiscible sulphide liquid into the rock during crystallization of the richly mineralized Platreef which constitutes the base of the Bushveld Complex closeby.

k) Pumpellyite

The two suspected pumpellyite analyses deviate considerably from stoichiometry so that the analyses are only semi-quantitative.

6. PHASE EQUILIBRIA AND METAMORPHIC MINERAL REACTIONS

A brief explanation of some of the theoretical considerations applied in this chapter is given in Appendix 16.

6.1 The paragenetic sequence for pelitic mineral assemblages

6.1.1 Chlorite and chloritoid-bearing assemblages

The assemblages chlorite + chloritoid + white mica + detrital minerals and chlorite + andalusite + white mica + detrital minerals are sporadically developed in pelites from the Timeball Hill Formation and represent the lowest metamorphic grade recorded in the study area (Fig. 45).

Andalusite formed through the discontinuous reaction:

pyrophyllite $\rightleftharpoons$ andalusite + quartz + H_2O .....6(1)

in the system SiO_2 - Al_2O_3 - H_2O, with excess quartz and with water as a boundary value component. The reaction may, however, be continuous if water is an initial value component or if Fe^{3+} substitutes for Al in the Al-silicates.

Model reactions in the system SiO_2 - Al_2O_3 - FeO - MgO -K_2O - H_2O with excess quartz and muscovite and where water is a boundary value component are presented in Figure 46. Hoschek (1969) suggested the following continuous chloritoid-forming reaction (Fig. 46 B):

chlorite + Al-silicate (pyrophyllite/kaolinite)
$\rightleftharpoons$ chloritoid + quartz + H_2O .....6(2)

Because the relative order of Mg/Fe is chlorite > chloritoid, the chlorite - chloritoid - Al-silicate triangle will become more Mg-rich with increasing metamorphic grade.

In the absence of such an Al-silicate mineral or after it has been consumed through reactions 6(1) and 6(2), the chlorite-muscovite assemblage may break up according to one of the following continuous reactions:

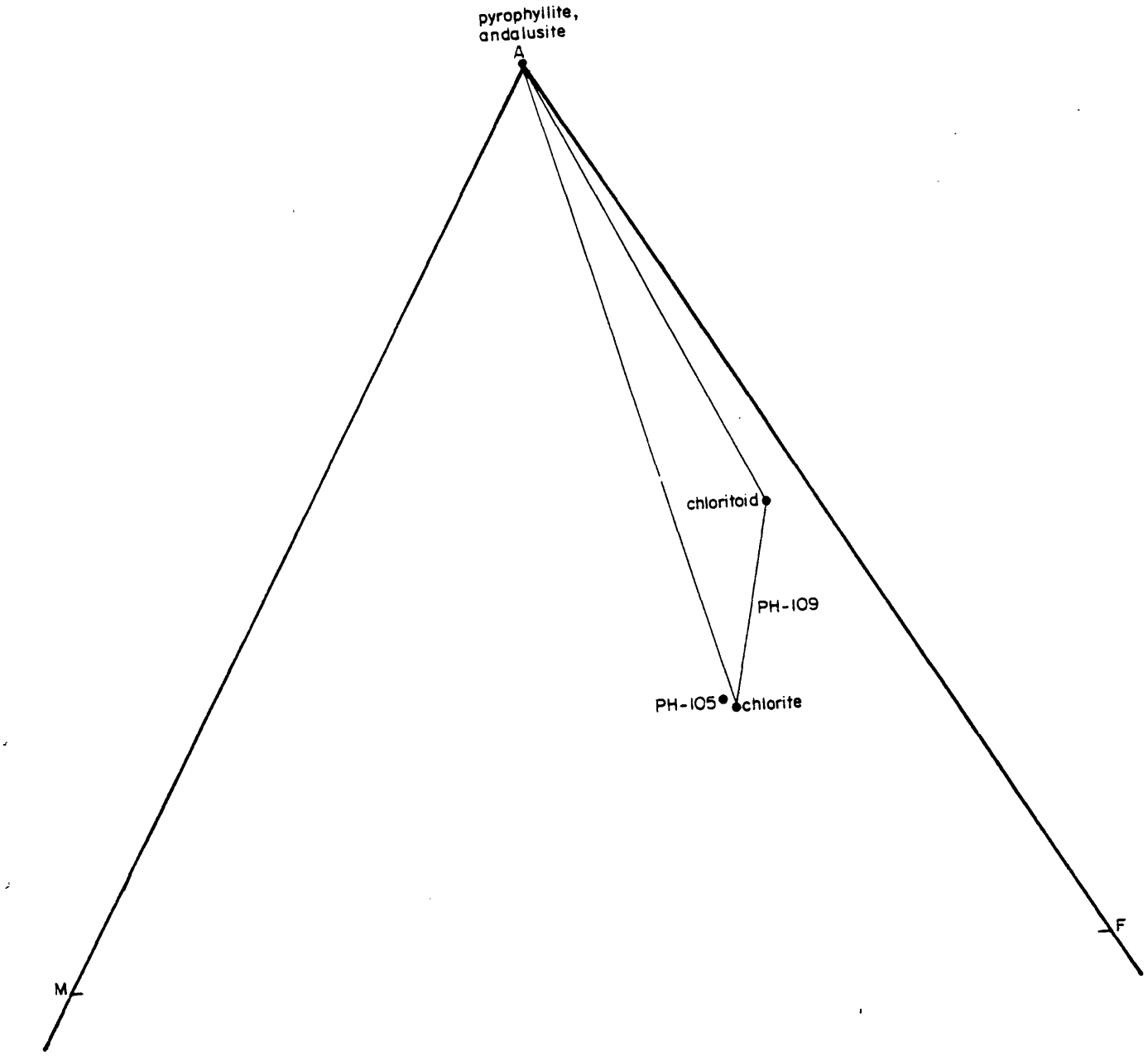

Fig. 45: AFM projection of the chlorite + chloritoid + pyrophyllite assemblage in the Timeball Hill pelites

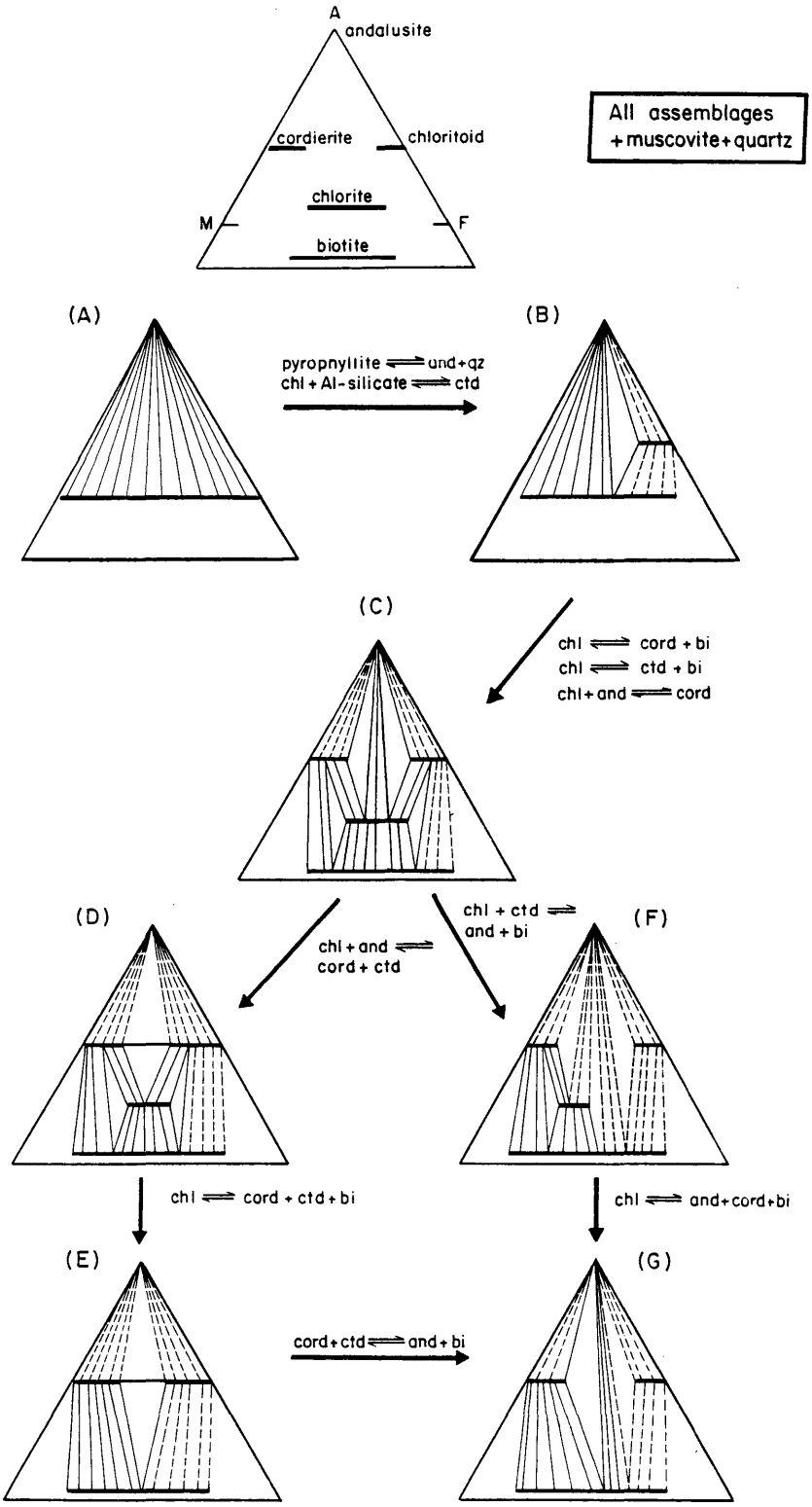

Fig. 46: Facies series for the breakdown of chlorite-bearing assemblages. The Timeball Hill pelites followed the route A,B,C,D,E,G, while the route A,B,C,F,G is representative of higher pressures. Dashed tie-lines are possible, but not observed assemblages

chlorite + muscovite + quartz ⇌ cordierite + biotite + H_2O..6(3)

or chlorite + muscovite + quartz ⇌ chloritoid + biotite + H_2O .....6(4)

Reaction 6(3) takes place in the more magnesian bulk rocks, and reaction 6(4) in the more ferruginous bulk rocks from the study area (Fig. 46C and Fig. 47A).

Because the relative order of Mg/Fe is chloritoid < biotite < chlorite < cordierite, the three-phase triangle chlorite-chloritoid-biotite will become more Mg-rich with increasing metamorphic grade, while the cordierite-chlorite-biotite triangle will become more Fe-rich with increasing grade, thereby explaining the Fe-enrichment in cordierite rims in sample PH - 75 (Fig. 47 A).

It is suggested that the discontinuous reaction (Fig. 46 C,D):

chlorite + andalusite + quartz ⇌ cordierite + chloritoid + H_2O .....6(5)

was responsible for the formation of the cordierite-chloritoid assemblage in the study area. Since the Mg/Fe enrichment is such that chlorite always occurs on the Fe-rich side of the cordierite-biotite tie-line and the Mg-rich side of the chloritoid - biotite tie-line, the terminal breakdown of chlorite must be the discontinuous reaction (Fig. 46 D,E):

chlorite + muscovite + quartz ⇌ cordierite + chloritoid + biotite + H_2O .....6(6)

The terminal, discontinuous chlorite breakdown reaction found by Labotka (1981) (Fig. 46 F,G):

chlorite + muscovite + quartz ⇌ cordierite + andalusite + biotite + H_2O .....6(7)

did not occur in the study area because the stable chlorite-chloritoid join prevented the coexistence of andalusite and biotite.

The stability of the cordierite-chloritoid join is terminated by the discontinuous reaction (Fig. 46 E,G):

cordierite + chloritoid + muscovite ⇌ andalusite + biotite + quartz + H_2O .....6(8)

The assemblage cordierite + chloritoid + muscovite + andalusite + biotite + quartz has been found in sample PH - 143

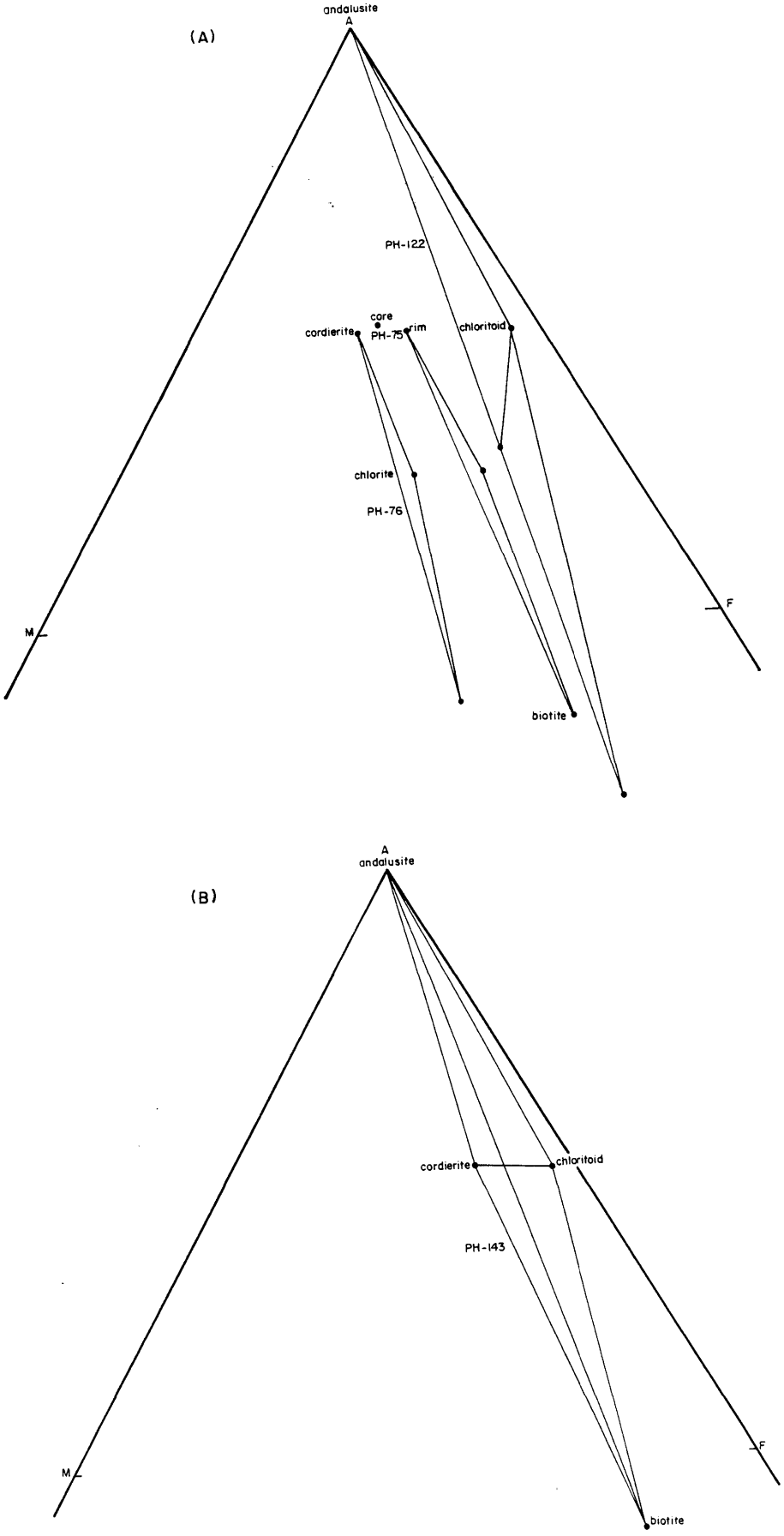

Fig. 47: AFM projection of the chlorite + cordierite + biotite and chlorite + chloritoid + biotite + andalusite assemblages (A). Note the Fe-enrichment of the cordierite rims in sample PH - 75 relative to the cores. AFM projection of the tie-line flip chloritoid + cordierite to andalusite + biotite (B)

(Fig 47 B) and reaction 6(8) may therefore be continuous. This situation could arise if the water activity was buffered by the mineral assemblage or if minor elements, e.g. Ti were substituted into biotite. Reaction 6(8) explains the resorbed appearance of chloritoid crystals enclosed by cordierite in sample PH - 143 as well as the absence of typical chloritoid breakdown minerals (staurolite and garnet) in rocks with the appropriate bulk compositions.

At higher metamorphic grades the cordierite + biotite + andalusite + muscovite + quartz assemblage is stable in the study area (Fig. 46 G and 48). The cordierite-andalusite-biotite triangle would move towards more magnesian compositions with increasing metamorphic grade as a result of the continuous reaction:

cordierite + muscovite $\rightleftharpoons$ biotite + andalusite + quartz + H_2O .....6(9)

The more Fe-rich assemblages , (e.g. sample PH - 117) were collected at a greater distance away from the contact with the Bushveld Complex relative to the more magnesian assemblages (Fig. 48), thereby verifying the displacement of the three-phase triangle.

Schreinemakers analysis

A Schreinemakers analysis of the phases andalusite, cordierite, chloritoid, chlorite and biotite was undertaken to examine the stability field of the cordierite-chloritoid assemblage and the position of reaction 6(8) in P,T space.

For a three component system with 5 phases there will be one invariant point from which 5 univariant lines (reactions) will radiate. The disposition of these lines around the invariant point can be deduced according to the method of Schreinemakers as outlined by Zen (1966). Every univariant reaction is labelled by the phase that does not take part in that reaction, as is customary for the treatment of petrogenetic grids. The absent phase is always written in parentheses. The five univariant reactions, together with their estimated slopes, are given in Table 6. These reactions were deduced for the system SiO_2 - Al_2O_3 -

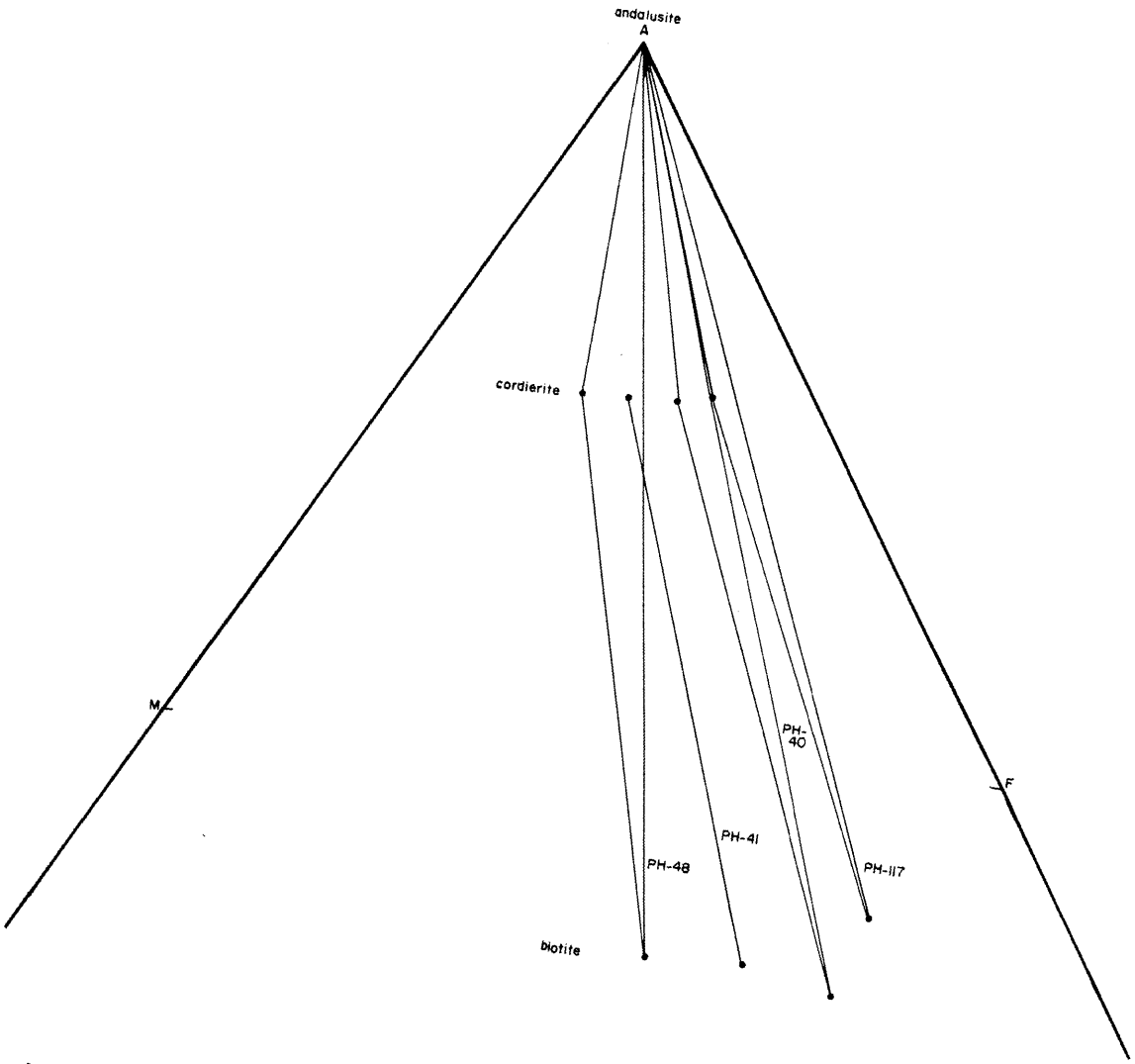

Fig. 48: AFM projection of the andalusite + cordierite + biotite assemblage

TABLE 6 Reactions and calculated slopes of univariant lines for cordierite ± chloritoid-bearing assemblages in muscovite + quartz-bearing AKFM pelites

Univariant line	Reaction	$\Delta S/n_{H_2O}$ (dj/deg mole)	$\Delta V_s/n_{H_2O}$ (cc/ mole)	$\frac{dP}{dT}$ (bar/deg)
(and)	3,07 chl + 2,87 musc + 5,53 qz ⇌ 2,67 cord + 2,87 bi + ctd + 11,28 H_2O	584	- 4,1	+ 29
(cord)	1,20 chl + ctd + 2,46 musc ⇌ 4,28 and + 2,46 bi + 0,70 qz + 5,80 H_2O	578	-10,3	+ 41
(ctd)	1,60 chl + 2,00 musc + 1,80 qz ⇌ cord + 1,60 and + 2,00 bi + 6,40 H_2O	582	- 6,2	+ 32
(bi)	chl + 3,00 and + 3,80 qz ⇌ 1,60 cord + 1,30 ctd + 2,70 H_2O	593	+ 5,1	+ 20
(chl)	cord + 1,33 ctd + 1,28 musc ⇌ 4,11 and + 1,28 bi + 2,73 qz + 1,33 H_2O	560	-29,5	-107

Volume data from Appendix 17

FeO - MgO - K_2O - H_2O in which quartz and muscovite are excess phases and where water is a boundary value component. The chemographic relations between the phases was obtained through a projection from muscovite, water and quartz onto the A F M plane (Fig. 49). Univariant reactions were balanced and the slopes of the boundaries calculated by using the mineral formulas and molar volumes given in Appendix 17. V_{H_2O} was taken as 24,3 cc/mole at P = 3 kbar and T = 500°C (Albee, 1965 a). The reaction slopes were estimated from the Clausius Clapeyron equation after Albee (1965 a):

$$\left|\frac{dP_s}{dT}\right|_{\Delta G = 0} = \frac{\Delta S}{\Delta V_s + n_{H_2O} V_{H_2O} \dfrac{dP_{H_2O}}{dP_s}} \qquad \ldots\ldots\ldots\ldots 6(10)$$

where ΔV_s = volume change for the solid phases involved in the reaction, ΔS = entropy change of the reaction and V_{H_2O} = molar volume of water. The term $n_{H_2O} V_{H_2O} \left|\frac{dP_{H_2O}}{dP_s}\right|$ constitutes the fluid contribution to the volume change of the reaction and is equal to zero for reactions that do not involve fluid phases. Reaction slopes were calculated by assuming that the fluid phase consists of pure H_2O at the same pressure as the solid phases, i.e. $P_{H_2O} \sim P_s$ and $\left|\frac{dP_{H_2O}}{dP_s}\right| \sim 1$

The ΔS is small for reactions that do not involve hydration or dehydration and that do not cause a change in the coordination numbers of cations with 4 - or 6-fold coordination. The entropy change in a dehydration reaction is approximately 590 dj/deg. mole at P = 2,5 kbar and and T = 500°C (Albee, 1965 a and references therein).

A further correction to the ΔS was made for reactions that involve a first-order coordination change of Al from six to four and vice versa. A value of ΔS ($Al^{vi} \rightarrow Al^{iv}$) of + 80

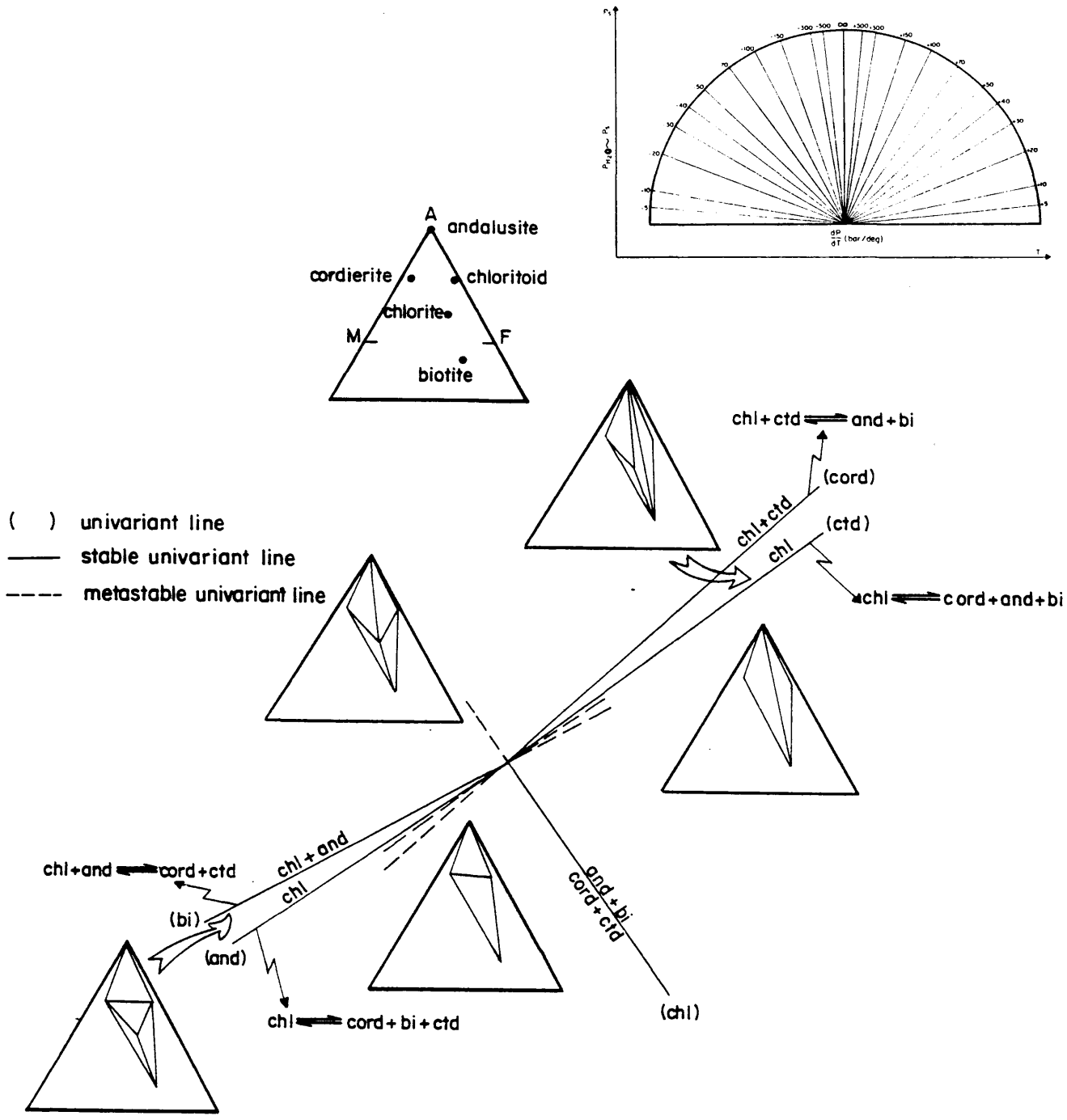

Fig. 49: Schreinemakers diagram illustrating the breakdown of chlorite-bearing assemblages and the tie-line flip between cordierite + chloritoid to andalusite + biotite

dj/deg.mole was assumed (Albee, 1965 a). When these approximations are applied, the Clausius Clapeyron equation simplifies to:

$$\frac{dP_s}{dT} = \frac{590 + [(\Delta \text{ Al coordination})(80)]}{\Delta V_s / n_{H_2O} + 24,3} / n_{H_2O} \quad \ldots\ldots 6(11)$$

Since we are mainly interested in the relative slopes of the lines the error in the ΔS and ΔV values are insignificant because they are the same or proportional for all reactions. When the value of $\Delta V_s/n_{H_2O}$ approaches -24,3, however, large slopes are obtained and the uncertainty of the value of the slope may be significant to the extent that even the sign of the slope may be wrong. Small slopes are obtained for many cordierite-breakdown reactions because the value of $\Delta S/n_{H_2O}$ is greatly decreased by the entropy change for $Al^{iv} \rightarrow Al^{vi}$, while $\Delta V_s/n_{H_2O}$ is also large and negative. For such reactions the value of the slope is uncertain but its sign is correct.

Having calculated the slopes of the univariant lines, the grid was orientated in P,T space by assuming that dehydration reactions have water on the high-temperature side of the boundary. This orientation also results in cordierite occurring on the low-pressure side of the boundaries, which is compatible with its high molar volume, and is in agreement with most petrogenetic grids.

From Figure 49 it is clear that the cordierite-chloritoid join is only stable at pressures lower than the invariant point. Reaction 6(8) (univariant line (and)), has a negative slope and will therefore take place in response to either increasing temperature or pressure. At pressures greater than the invariant point the reaction route A,B,C,F,G in Figure 46 will be followed and the cordierite-chloritoid assemblage will therefore not be encountered.

Although the pressure coordinate of the invariant point (Fig. 49) is unknown, Labotka (1981) presented a petrogenetic grid in which the terminal discontinuous chlorite reactions (6(6) and 6(7)), i.e the univariant lines (and) and (ctd)

meet in an invariant point which is situated at a pressure that is about 1,5 kbar lower than the Al_2SiO_5 triple point. If the invariant point in Figure 49 is equivalent to Labotka's invariant point, its pressure coordinate must be between 2,5 and 4,5 kbar. This is in agreement with Albee's (1965 a) observation that the cordierite-chloritoid assemblage is only stable under low pressure contact metamorphic conditions.

6.1.2 Phase relations of the Fe-Mg amphiboles and the orthopyroxene + garnet-bearing assemblages

Amphibole phase relations are illustrated in a projection from K-feldspar, plagioclase, quartz and water onto the plane Al_2O_3 - MgO - FeO_T + MnO in Figure 50. The orthopyroxene + garnet + cordierite + biotite assemblages are presented in a projection from K-feldspar , quartz and water onto the Al_2O_3 - MgO - FeO_T + MnO plane in Figure 51. The orthoamphibole + cordierite assemblages probably originated through reactions similar to those proposed by Lal and Shukla (1975) and Akella and Winkler (1966):

Al-chlorite + quartz $\rightleftharpoons$ gedrite + cordierite + H_2O .....6(12)

and garnet + Al-chlorite + quartz $\rightleftharpoons$gedrite + cordierite + H_2O .....6(13)

Garnet crystallized as the result of a reaction similar to the one proposed by Hsu (1968):

Fe-chlorite + fluid + quartz $\rightleftharpoons$almandine + fluid .....6(14)

Some samples from the study area show a reversal in the relative Fe/Mg ratios of biotite relative to anthophyllite (Fig. 50 A) and orthopyroxene (Fig. 51). Grant (1981) quoted many workers who found that biotite is always more magnesian than coexisting orthoamphibole and orthopyroxene. It is not known why one biotite analysis (Fig. 50 A) is more rich than the coexisting anthophyllite but it is apparently not an unique situation since Lal et al. (1978) also published a biotite analysis that is more ferruginous than coexisting gedrite.

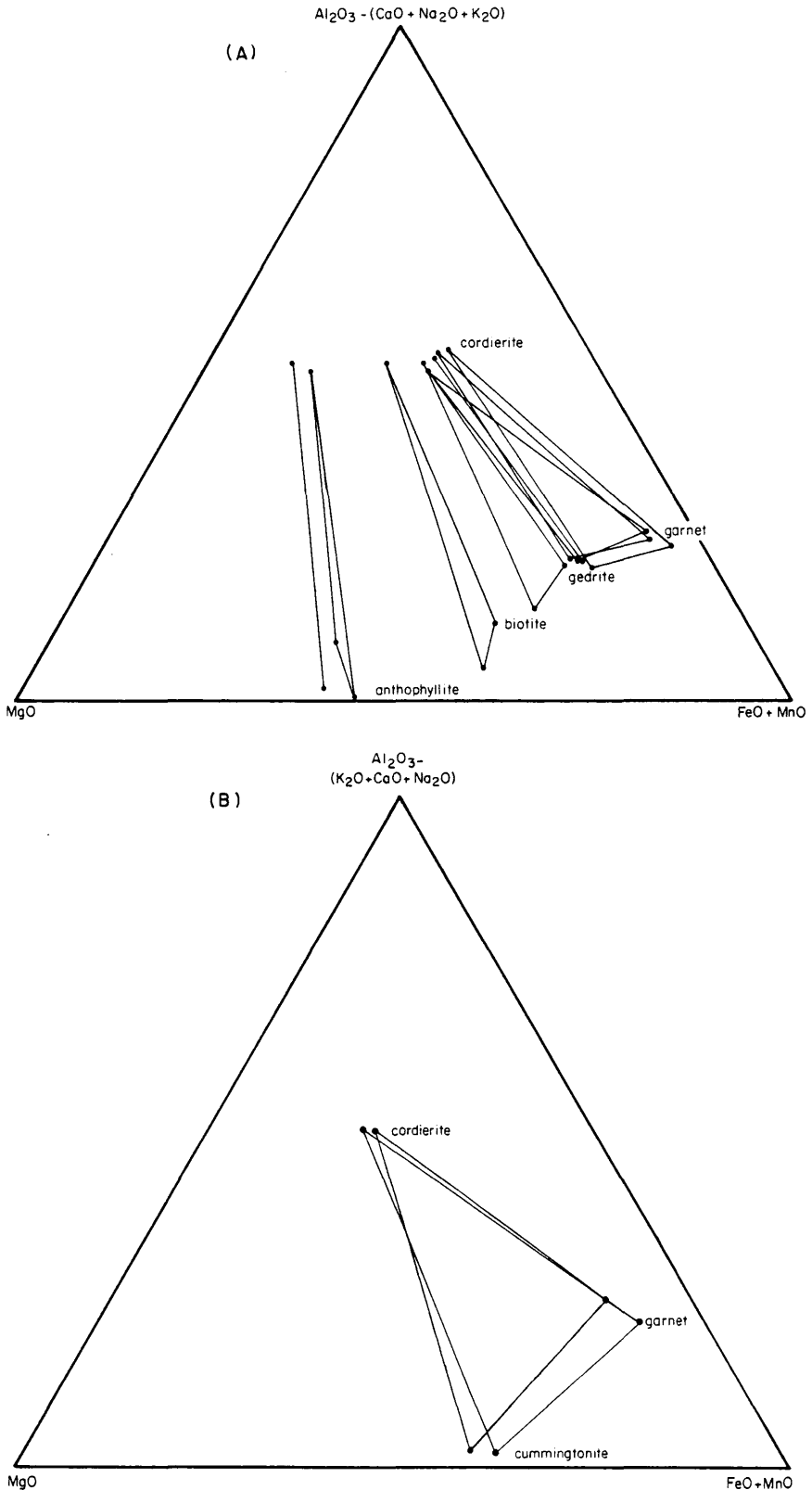

Fig. 50: Projection from K-feldspar, plagioclase, quartz and water illustrating the gedrite and anthophyllite-bearing assemblages (A) and the cummingtonite-bearing assemblages (B)

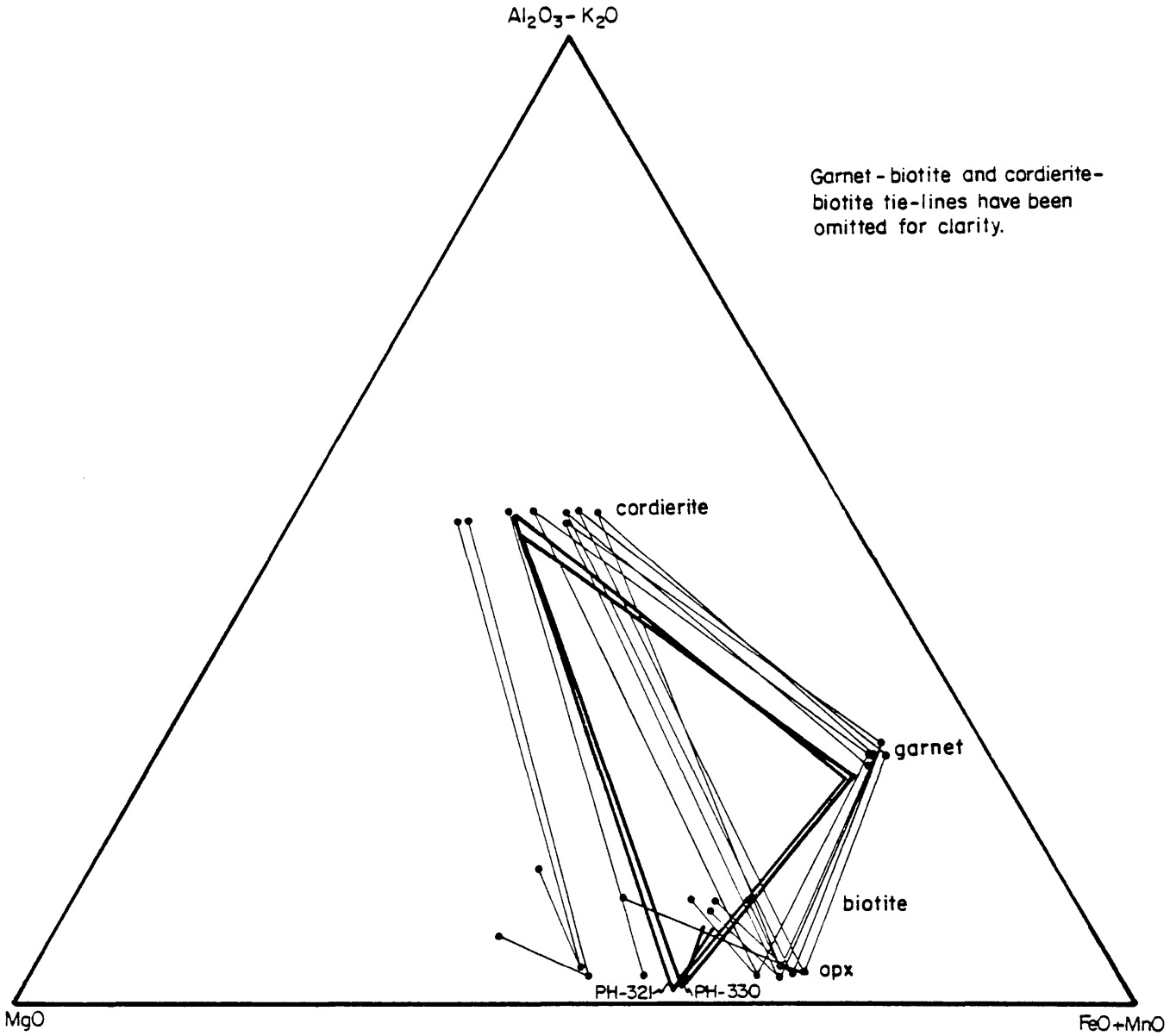

Fig. 51: AFM projection of garnet + orthopyroxene-bearing assemblages. Tie-lines for samples PH - 321 and PH - 330 are in bold in order to accentuate the Fe/Mg ratio of biotite relative to that in orthopyroxene

Two samples (PH - 321 and PH - 330) contain biotite that is more ferruginous than coexisting orthopyroxene (Fig. 51). This is apparently the first time that such a relationship has been chemically verified. The two samples represent the lowest-grade orthopyroxene-bearing samples in the study area. Sample PH -321 contains both orthoamphibole and minute orthopyroxene crystals, while sample PH - 330, that was collected within metres of sample PH -321, contains tiny orthopyroxene grains in a poorly recrystallized matrix.

The reversal in the Fe/Mg ratios of orthopyroxene and biotite is believed to be a disequilibrium situation. At lower grades than the orthopyroxene-in isograd, biotite is in equilibrium with gedrite that is more ferruginous than the former mineral (Fig. 50). On the isograd gedrite reacts to produce orthopyroxene, that is much more magnesian than the reacting gedrite (Fig. 50, 51), as well as the biotite in equilibrium with gedrite. This is a disequilibrium situation and the Fe-Mg exchange reaction:

Mg-orthopyroxene + Fe-biotite $\rightleftharpoons$ Fe-orthopyroxene + Mg-biotite .....6(15)

now takes place to restore equilibrium, when biotite will be more magnesian than the coexisting orthopyroxene.

For the purpose of the Schreinemakers analysis of the orthopyroxene- in isograd, the relative order of Fe/Mg was assumed to be garnet < gedrite < biotite < orthopyroxene < cordierite. Despite the controversial position of biotite relative to orthopyroxene it is believed that the relative Fe,Mg ratios of the phases when orthopyroxene starts to crystallize will determine the phase relations at the isograd.

Lastly, it is interesting to note the absence of K-feldspar from the orthoamphibole -bearing assemblages. This has also been observed by Grant (1981) who ascribed it to the reaction:

gedrite + K-feldspar $\rightleftharpoons$ cordierite + biotite + garnet .....6(16)

Schreinemakers analysis

The univariant reactions between the phases sillimanite, cordierite, garnet, gedrite, orthopyroxene, K-feldspar, biotite, albite, quartz and water were determined for the mineral compositions given in Appendix 17. These phases form part of the system SiO_2 - Al_2O_3 - FeO - MgO - K_2O - Na_2O - H_2O. Quartz, K-feldspar and plagioclase are assumed to be excess phases and water is a boundary value component. Chemographic ralations are then obtained by a projection from quartz, plagioclase and water onto the system Al_2O_3 - FeO - MgO - K_2O (Fig. 52).

The number of invariant points, univariant lines and divariant surfaces in a system can be calculated through the formula:

$$\frac{P!}{\emptyset\ !\ (P - \emptyset)!} \qquad \text{.....6(17)}$$

where p = number of all the phases to be considered and $\emptyset$ = number of coexisting phases present in the equilibrium (Mueller and Saxena, 1977). $\emptyset$ can be obtained from the phase rule. In the 4 component system there are 7 phases and there will thus be 7! / 6! (7-6)! = 7 invariant points. Each invariant point will involve 6 phases. The invariant points are identified by the absent phase which is written in brackets (Table 7, Fig 52). Every univariant reaction involves 4 or 5 phases and connects two invariant points. The univariant reactions radiating from every invariant point are labelled by writing the absent phase in parentheses (Table 7). At an invariant point, pressure, temperature and the composition of all phases are uniquely fixed. In the case of a univariant reaction one variable can be chosen (P,T or the composition of one phase) whereby all other variables are determined uniquely.

Both terminal and non-terminal univariant reactions occur in the system under consideration (Table 7, Fig. 52). Biotite and K-feldspar are the only K-bearing phases, i.e. the

TABLE 7 Reactions and slopes of univariant lines for orthoamphibole and orthopyroxene-bearing assemblages in K-feldspar + quartz-bearing AKFM pelites

Invariant point	Univariant line	Reaction	$\Delta S/n_{H_2O}$ (dj/deg.mole)	$\Delta V_{s/n_{H_2O}}$ (cc/mole)	$\frac{dP}{dT}$ (bar/deg)
[cord]	(gar)	7,22 bi + 1,65 sill + 1,00 ab + 17,93 qz ⇌ 2,00 ged + 8,69 opx + 7,22 K-spar + 5,22 H_2O	615	-17,2	+ 87
	(ged)	6,25 bi + 20,31 qz ⇌ gar + 13,31 opx + 1,50 sill + 6,25 K-spar + 6,25 H_2O	558	-18,8	+101
	(opx)	5,00 bi + gar + 4,20 sill + 1,60 ab + 7,60 qz ⇌ 3,20 ged + 5,00 K-spar + 1,80 H_2O	821	- 9,7	+ 56
	(bi)	2,00 ged + 5,39 qz ⇌ 6,67 opx + 3,39 sill + 1,11 gar + 1,00 ab + 2,00 H_2O	410	-23,9	+1025
	(sill)	13,88 bi + 1,00 ab + 39,65 qz ⇌ 2,00 ged + 22,95 opx + 1,05 gar + 13,88 K-spar + 11,88 H_2O	583	-17,9	+ 91
	(K-spar)	2,00 ged + 5,39 qz ⇌ 6,67 opx + 3,39 sill + 1,11 gar + 1,00 ab + 2,00 H_2O	410	-23,9	+1025
[opx]	(cord)	5,00 bi + gar + 4,20 sill + 1,60 ab + 7,60 qz ⇌ 3,20 ged + 5,00 K-spar + 1,80 H_2O	821	-9,7	+56
	(gar)	6,68 bi + 6,25 sill + 1,54 ab + 13,74 qz ⇌ 3,08 ged + 1,00 cord + 6,68 K-spar + 3,60 H_2O	707	-2,1	+32
	(ged)	1,95 bi + 2,30 sill + 6,68 qz ⇌ 1,00 gar + 1,14 cord + 1,95 K-spar + 1,95 H_2O	600	+4,6	+20

Invariant point	Univariant line	Reaction	$\Delta S/n_{H_2O}$ (dj/deg.mole)	$\Delta V_{s/n_{H_2O}}$ (cc/mole)	$\frac{dP}{dT}$ (bar/deg)
	(bi)	2,00 ged + 1,07 sill + 5,94 qz ⇌ 1,67 cord + 2,22 gar + 1,00 ab + 2,00 H_2O	477	+12,5	+ 13
	(sill)	2,25 ged + 1,00 K-spar + 3,24 qz ⇌ 1,34 cord + 1,98 gar + 1,00 bi + 1,13 ab + 1,25 H_2O	442	+19,0	+ 10
	(K-spar)	2,00 ged + 1,07 sill + 5,94 qz ⇌ 1,67 cord + 2,22 gar + 1,00 ab + 2,00 H_2O	477	+12,5	+ 13
[ged]	(cord)	6,25 bi + 20,31 qz ⇌ gar + 13,31 opx + 1,50 sill + 6,25 K-spar + 6,25 H_2O	558	-18,8	+101
	(gar)	1,00 cord + 4,29 bi + 13,59 qz ⇌ 13,15 opx + 3,72 sill + 4,29 K-spar + 4,29 H_2O	539	-29,0	-115
	(opx)	1,95 bi + 2,30 sill + 6,68 qz ⇌1,00 gar + 1,04 cord + 1,95 K-spar + 1,95 H_2O	600	+ 4,6	+ 20
	(bi)	5,97 opx + 3,99 sill +0,49 qz ⇌ 1,49 cord + 1,00 gar	120	+65	+ 1,8
	(sill)	10,98 bi + 35,93 qz ⇌ 19,40 opx + 1,00 cord + 2,38 gar + 10,98 K-spar + 10,98 H_2O	565	-14,9	+ 60
	(K-spar)	5,97 opx + 3,99 sill + 0,49 qz ⇌ 1,49 cord + 1,00 gar	120	+65	+ 1,8

Invariant point	Univariant line	Reaction	$\Delta S/n_{H_2O}$ (dj/deg.mole)	$\Delta V_s/n_{H_2O}$ (cc/mole)	$\frac{dP}{dT}$ (bar/deg)
[gar]	(cord)	7,22 bi + 1,65 sill + 1,00 ab + 17,93 qz ⇌ 2,00 ged + 8,69 opx + 7,22 K-spar + 5,22 H_2O	615	-17,2	+ 87
	(ged)	1,00 cord + 4,29 bi + 13,59 qz ⇌ 13,15 opx + 3,72 sill + 4,29 K-spar + 4,29 H_2O	539	-29,0	-115
	(opx)	6,68 bi + 6,25 sill + 1,54 ab + 13,74 qz ⇌ 3,08 ged + 1,00 cord + 6,68 K-spar + 3,60 H_2O	707	- 2,1	+32
	(bi)	2,00 ged + 1,67 cord + 4,81 qz ⇌ 13,33 opx + 7,83 sill + 1,00 ab + 2,00 H_2O	343	-60,7	- 9
	(sill)	20,43 bi + 1,00 cord + 2,26 ab + 53,77 qz ⇌ 32,52 opx + 4,52 ged + 20,43 K-spar + 15,91 H_2O	595	-20,1	+142
	(K-spar)	2,00 ged + 1,67 cord + 4,81 qz ⇌ 13,33 opx + 7,83 sill + 1,00 ab + 2,00 H_2O	343	-60,7	- 9
[sill]	(cord)	13,88 bi + 1,00 ab + 39,65 qz ⇌ 2,00 ged + 22,95 opx + 1,05 gar + 13,88 K-spar + 11,88 H_2O	583	-17,9	+ 91
	(gar)	20,43 bi + 1,00 cord + 2,26 ab + 53,77 qz ⇌ 32,52 opx + 4,52 ged + 20,43 K-spar + 15,91 H_2O	595	-20,1	+142
	(ged)	10,98 bi + 35,93 qz ⇌ 19,40 opx + 1,00 cord + 2,38 gar + 10,98 K-spar + 10,98 H_2O	565	-14,9	+ 60

Invariant point	Univariant line	Reaction	$\Delta S/n_{H_2O}$ (dj/deg.mole)	$\Delta V_s/n_{H_2O}$ (cc/mole)	$\frac{dP}{dT}$ (bar/deg)
	(opx)	2,25 ged + 1,00 K-spar + 3,24 qz ⇌1,34 cord + 1,98 gar + 1,00 bi + 1,13 ab + 1,25 H_2O	442	+19,0	+ 10
	(bi)	2,00 ged + 5,80 qz ⇌ 1,27 cord + 1,96 gar + 1,57 opx + 1,00 ab + 2,00 H_2O	460	+3,8	+ 16
	(K-spar)	2,00 ged + 5,80 qz ⇌ 1,27 cord + 1,96 gar + 1,57 opx + 1,00 ab + 2,00 H_2O	460	+3,8	+ 16
[bi] and [K-spar]	(gar)	2,00 ged + 1,67 cord + 4,81 qz ⇌ 13,33 opx + 7,83 sill + 1,00 ab + 2,00 H_2O	343	-60,7	- 9
	(ged)	5,97 opx + 3,99 sill + 0,49 qz ⇌ 1,49 cord + 1,00 gar	120	+65	+ 1,8
	(opx)	2,00 ged + 1,07 sill + 5,94 qz ⇌ 1,67 cord + 2,22 gar + 1,00 ab + 2,00 H_2O	477	+12,5	+ 13
	(sill)	2,00 ged + 5,80 qz ⇌ 1,27 cord + 1,96 gar + 1,57 opx + 1,00 ab + 2,00 H_2O	460	+3,8	+ 16
	(cord)	2,00 ged + 5,39 qz ⇌ 6,67 opx + 3,39 sill + 1,11 gar + 1,00 ab + 2,00 H_2O	+410	-23,9	+1025

Volume data from Appendix 17

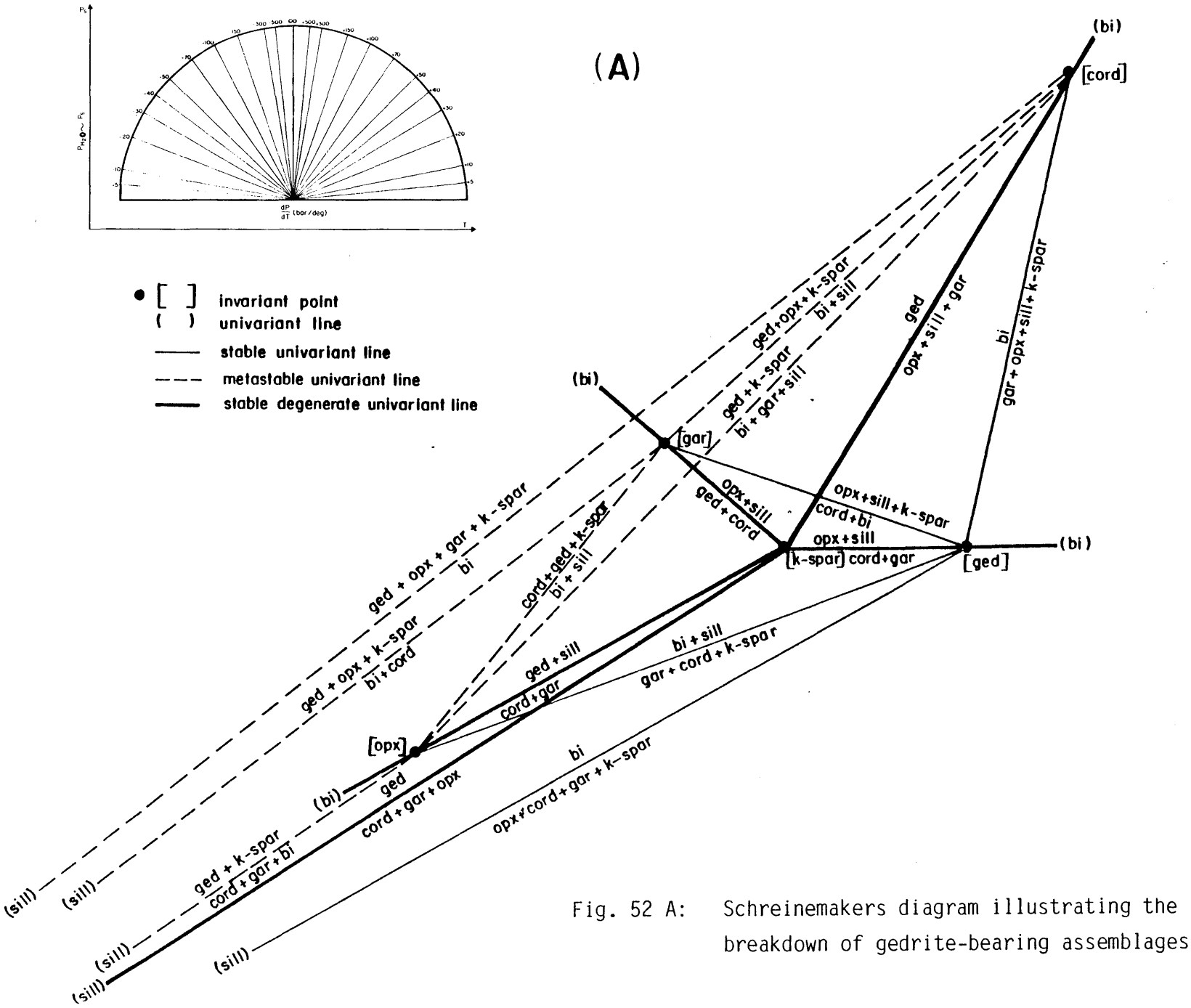

Fig. 52 A: Schreinemakers diagram illustrating the breakdown of gedrite-bearing assemblages

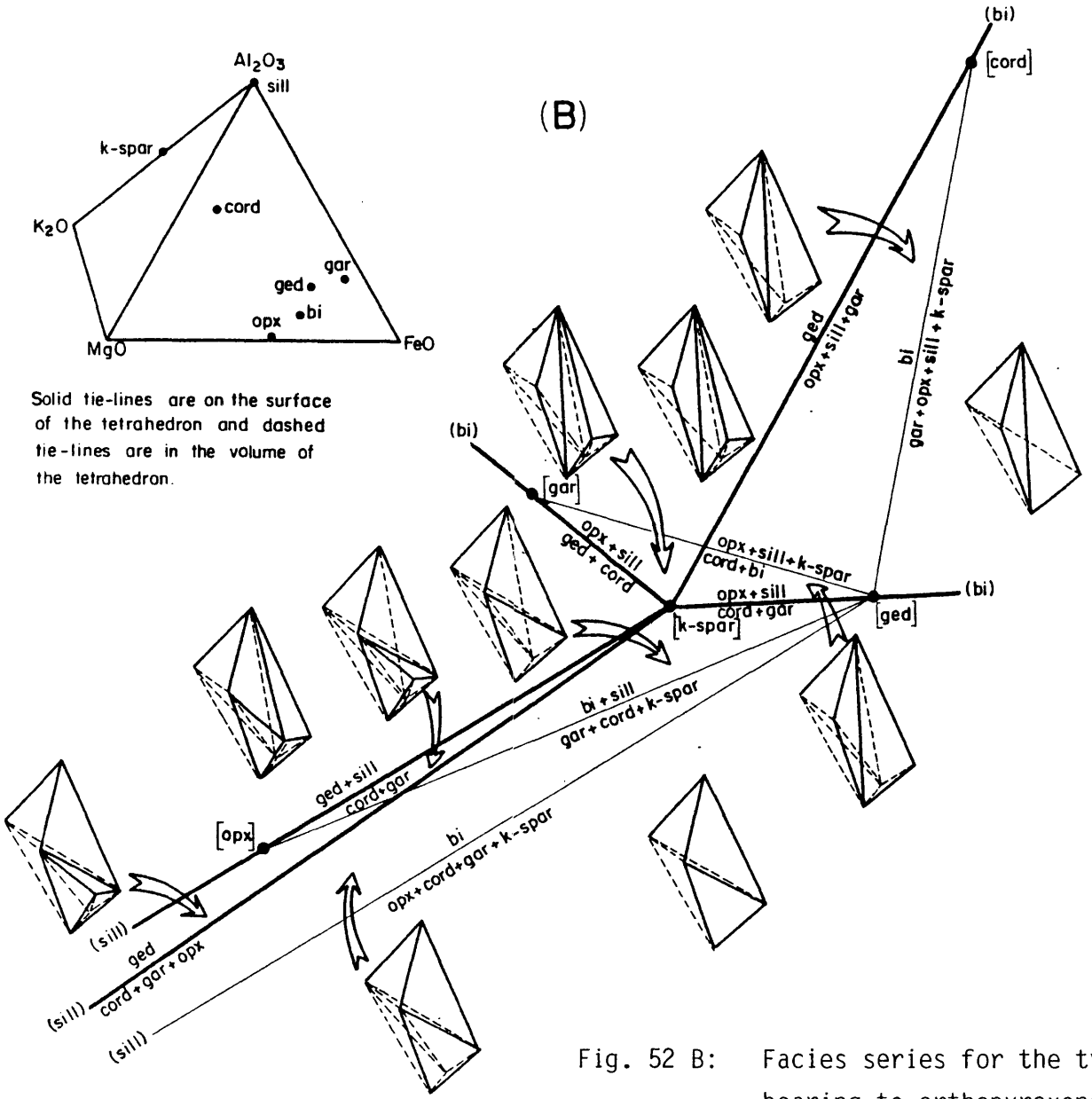

Fig. 52 B: Facies series for the transition from gedrite-bearing to orthopyroxene-bearing assemblages

only phases that do not plot on the Al_2O_3 - MgO - FeO plane of the tetrahedron and are therefore necessarily similtaneously involved or absent from any mineral reaction. Such systems are said to be degenerate (Zen, 1966). Univariant reactions in which K-bearing phases do not take part are known as degenerate equilibria, while those in which they do take part are called non degenerate equilibria. The phases that plot on the Al_2O_3 - FeO - MgO plane of the tetrahedron are the singular phases and they are related to one another by fewer than n components. Biotite and K-feldspar are the indifferent phases but because they take part in some univariant equilibria they are only "relatively indifferent" (Zen, 1966), and this causes the coincidence of two univariant curves around the invariant points.

Because the two indifferent phases plot chemographically on the same side (about a point in a binary system, about a line in a ternary system about a plane in a quartenary system) of the singular phases, the univariant curves bearing the labels of the indifferent phases intersect stable to metastable. The stable to metastable coincidence of the (K-spar) and (bi) univariant curves (Fig. 52) implies that either the [K-spar] or [bi] invariant points will be undefined in the petrogenetic grid. The topology of the grid (Fig. 52) renders the [bi] invariant point undefined.

Univariant reactions were balanced and the slopes of the boundaries calculated by using the mineral formulae and molar volumes in Appendix 17. P_{H_2O} was assumed to be equal to P_s and the method outlined in section 6.1.1. was adopted in the calculation of the slopes (Table 7).

In order to orientate the grid in P,T space it is necessary to have the relative positions of two invariant points since the rest of the grid will then be constrained by the Schreinemakers rules. The relative positions of two invariant points may be obtained from experimental or field evidence. Since gedrite is stable at lower temperatures than orthopyroxene it follows that the [ged] invariant point must be situated at a higher temperature than the [opx] invariant point. The (opx, ged) univariant reaction

has a slope of +20 bar /deg (Table 7) which is in agreement with slopes obtained for this reaction by Grant (1981), Hess (1969) and Holdaway and Lee (1977). The positive slope of the reaction boundary causes the [ged] invariant point to be situated at a higher pressure and temperature than the [opx] invariant point. This arrangement leads to the liberation of water on the high-temperature side of the reaction boundary, while it also causes cordierite to be stable on the low-pressure side of the reaction boundary. Most dehydration reactions in Figure 52 display the same characteristics, the only exceptions being the (cord, sill); (cord, gar); (gar, sill); (gar, opx); (opx, sill); and (opx, cord) equilibria. All six reactions are apparently metastable since they imply the stable assemblages gedrite + orthopyroxene and gedrite + K-feldspar at low temperatures. The assemblage gedrite + orthopyroxene can only be stable on the orthopyroxene- in isograd which is given by the (K-spar, sill) and (K-spar, cord) equilibria in Figure 52, while the gedrite + K-feldspar assemblage is apparently extrinsically metastable since it has never been observed in natural assemblages.

The (ged, K-spar) univariant reaction is completely anhydrous and a slope of + 1,8 bar/deg has been calculated for this boundary (Table 7). Grant (1981) also obtained a small positive slope for this reaction. The orthopyroxene-sillimanite assemblages, which is stable at pressures higher than the univariant boundary, is rare in nature and pressures as great as 8 kbar may be required for the formation of this assemblage. The (K-spar, sill) and (K-spar, cord) reactions account for the terminal breakdown of gedrite. The former reaction, i.e.

gedrite + quartz $\rightleftharpoons$ cordierite + garnet + orthopyroxene + albite + H_2O .....6(18)

was responsible for the formation of orthopyroxene in the study area.

The stability field of the assemblage gedrite + sillimanite (andalusite) is important in estimating the pressure coordinate of the [opx] invariant point. The univariant reaction

(K-spar, opx) defines the lower pressure stability limit of the gedrite-sillimanite assemblage. Robinson and Jaffe (1969) concluded that gedrite + kyanite (sillimanite)-bearing rocks from Massachusetts and New Hampshire crystallized at about 5,5 kbar, while Sharma and McRae(1981) calculated an equilibrium pressure of 6 kbar for a gedrite + sillimanite + kyanite + garnet + staurolite + cordierite assemblage from India. The (K-spar, opx) reaction has a flat slope (about + 13 bar/deg) and the [opx] invariant point must therefore be situated at between 5 and 6 kbar pressure. This value is consitent with the calculated pressures of 4 to 5 kbar for the study area and the absence of the orthoamphibole - Al_2SiO_5 polymorph assemblage from rocks with the appropriate bulk composition.

Figure 52 predicts a terminal biotite breakdown reaction within the orthopyroxene stability field (reaction (ged, cord)), that is not realized in the facies series of the study area, where in fact, biotite reacts with garnet to produce cordierite and orthopyroxene (reaction 6(19)). The discrepancy is caused by the assumption that biotite is more Fe-rich than orthopyroxene when it is actually more magnesian than the orthopyroxene-cordierite tie-line in the high grade samples where biotite has equilibrated with orthopyroxene.

Phase ralations of garnet + orthopyroxene-bearing assemblages

The AFM phase relations of the garnet+ orthopyroxene + biotite + cordierite assemblage (Fig. 51) suggest the following discontinuous reaction

biotite + 2 garnet + 6 quartz $\rightleftharpoons$ cordierite + orthopyroxene + K-feldspar + H_2O .....6(19)

in the system SiO_2 - Al_2O_3 - FeO -MgO - K_2O - H_2O with water behaving as a boundary value component. Field evidence however, indicates that this assemblage occurs over about 3 km strike length parallel to the metamorphic gradient, which indicates that the assemblage is stable over a temperature interval of about 50°C assuming a fixed pressure. The reaction is therefore divariant.

There may be several reasons for this: First the very low Ca and Mn concentrations in garnet are unlikely to have stabilized this phase, but the high Ti, up to about 5,2 wt percent TiO_2, in biotite from this assemblage could have caused the univariant boundary to become divariant. The rarity or absence of ilmenite and rutile in most samples from this assemblage could be a further indication that Ti cannot be treated as an excess component in this system. Hensen (1971) reached a similar conclusion and also suggested substitution of fluorine and chlorine for the hydroxyl group cause this reaction boundary to become multivariant. Secondly, H_2O may not have behaved as a boundary value component, i.e. the metamorphic fluid was not pure H_2O and had its composition buffered internally by the mineral assemblage.

In the study area, garnet is completely consumed before biotite through reaction 6(19). Biotite coexisting with orthopyroxene and cordierite will eventually break down according to a reaction terminal to biotite:

biotite + quartz $\rightleftharpoons$ orthopyroxene + K-feldspar + H_2O .....6(20)

6.1.3 Phase relations of the high-grade Timeball Hill pelites

The following textures of the cordierite + spinel $\pm$ sillimanite $\pm$ corundum $\pm$ biotite-bearing rocks must be explained:

1) sillimanite inclusions in spinel
2) K-feldspar grains that appear to be replacing spinel
3) large cordierite crystals in contact with spinel and
4) the abundance of biotite in sillimanite-absent assemblages.

Phase relations are illustrated in a projection from sillimanite, K-feldspar and water onto the plane SiO_2 - (0,75 MgO + 0,25 Al_2O_3) - (0,75 FeO + 0,25 Al_2O_3) (Fig. 53). The two corundum-bearing samples (PH - 169 and PH - 334) are notably more magnesian than the samples in which corundum is absent.

The andalusite + cordierite + biotite assemblage is stable in the low-grade Timeball Hill pelites. With increasing

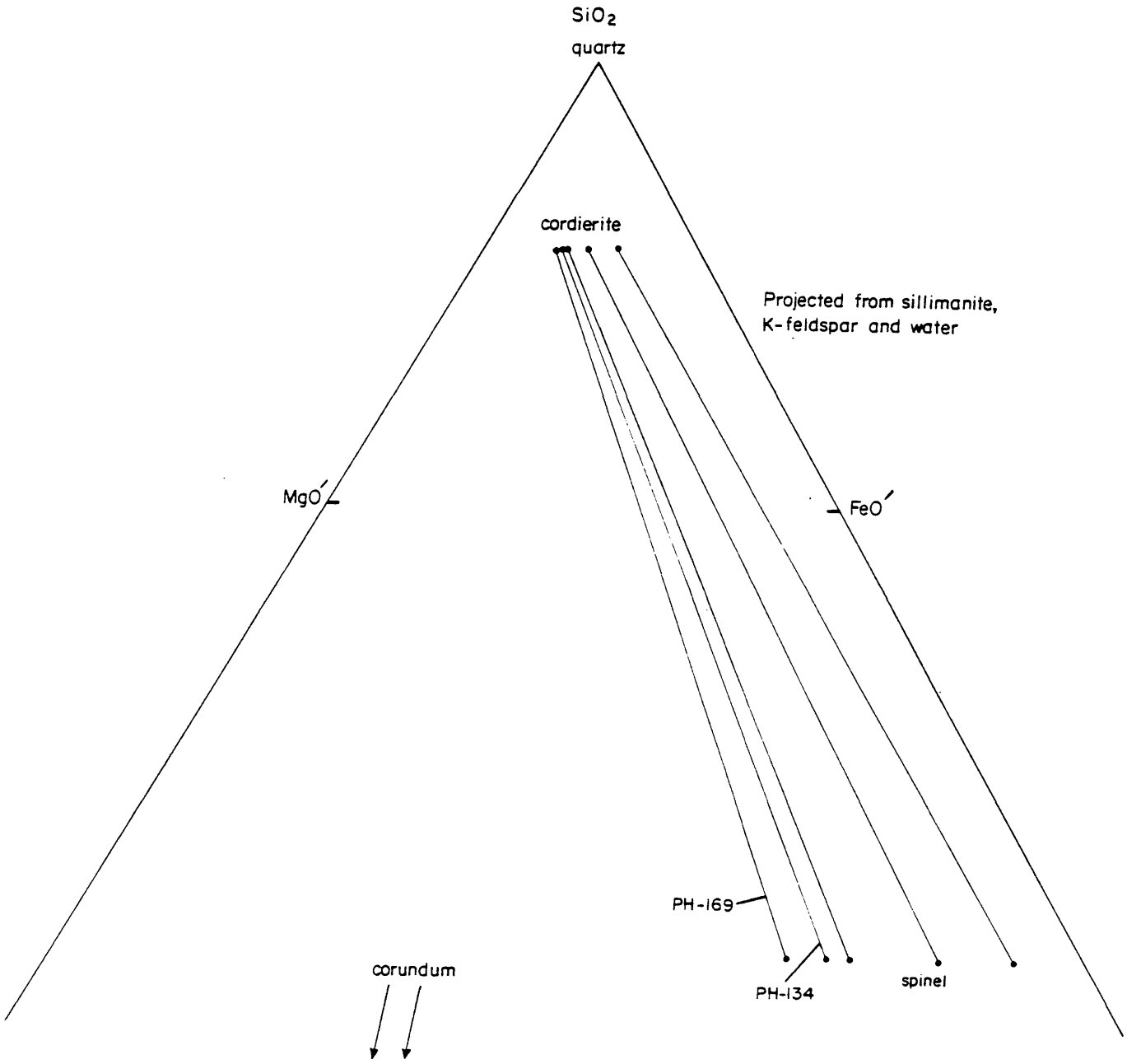

Fig. 53: Projection from sillimanite, K-feldspar and water onto the plane SiO_2 - MgO´ - FeO´ for sillimanite + cordierite + spinel ± corundum-bearing assemblages. Note the more magnesian compositions of the two corundum-bearing samples (PH - 169; PH - 334) MgO´ = 0,75 MgO + 0,25 Al_2O_3 and FeO´ = 0,75 FeO + 0,25 Al_2O_3

metamorphic grade the andalusite + sillimanite phase boundary is crossed and biotite reacts with sillimanite according to the discontinuous reaction:

biotite + sillimanite ⇌ cordierite + spinel + K-feldspar + H_2O .....6(21)

A similar reaction was responsible for the formation of gahnite-rich spinel in meta-pelites from Finland (Dietvorst, 1980). Whenever the phases biotite, sillimanite, cordierite and spinel were found together, the biotite displayed ragged, resorbed outlines which may be of a retrograde origin. In the study area, biotite is consumed before sillimanite in all but one low-Al_2O_3 sample, which plots on the biotite side of the cordierite-spinel tie-line. With a further increase in temperature the terminal breakdown of cordierite takes place according to a reaction proposed by Richardson (1968):

cordierite ⇌ spinel + quartz + H_2O .....6(22)

The corundum laths that cut into spinel crystals indicate that the reaction:

2 spinel + 5 sillimanite + H_2O ⇌ cordierite + corundum ...6(23)

occured in a few samples. This reaction boundary has a small negative slope (Harris, 1981 ; Wells and Richardson, 1979) and spinel + sillimanite is stable on the high-pressure, high temperature side of the boundary. Where reaction 6(23) has taken place in the study area, it is believed to have been in response to a drop in temperature at the end of the metamorphic episode. Further evidence for a hydration reaction in the formation of cordierite + corundum is the composition of cordierite from two corundum-bearing samples. They have oxide totals between 96 and 97 wt percent. A hydration reaction is compatible with a drop in temperature during the late stages of the metamorphic event.

Schreinemakers analysis

A Schreinemakers diagram was constructed in order to examine

the phase ralations between the phases spinel, sillimanite, cordierite, biotite and corundum in the system SiO_2 - Al_2O_3 - Fe_2O_3 - MgO - FeO - K_2O - H_2O where water is assumed to be a boundary value component. The mineral phases in the high-grade Timeball Hill pelites are related through a number of divariant reactions that can be illustrated by treating Al_2O_3 and Fe_2O_3 as well as MgO and FeO as isomorphous components, thereby creating the effective system SiO_2 - Al_2O_3 + Fe_2O_3 - MgO + FeO - K_2O. K-feldspar is assumed to be an excess phase.

All the reactions encountered in the study area can be deduced from a study of the [bi] and [qz] invariant points, and only the univariant reactions pertaining to these invariant points are therefore given in Table 8. The chemographic relations indicate two sets of colinear phases in the SiO_2 - Al_2O_3 + Fe_2O_3 - MgO + FeO system. In the first colinearity, quartz, cordierite and spinel are the singular phases while biotite, sillimanite and corundum are relatively indifferent. In the second colinearity the singular phases are quartz, corundum and sillimanite while cordierite, biotite and spinel are relatively indifferent.

Equation 6(11) cannot be used to estimate the slopes of the univariant reactions in Table 8 because of large uncertainties in the thermodynamical constants of anhydrous reactions as well as reactions involving spinel when the simplified Clausius Clapeyron equation is applied. The grid (Fig. 54) was orientated in P,T space by using the small negative slope obtained for the (qz, bi) reaction by Harris (1981) as well as Wells and Richardson (1979). The topology of the grid was further constrained by adopting a negative slope for the (bi, cor) univariant line (Harris, 1981) and by assuming that spinel and cordierite occur on the high-and-low-pressure sides of the univariant curves respectively (Hensen, 1971). The (qz, cor), (qz, sill), (qz, sp) and (qz, cord) curves are dehydration reactions that have water on the high-temperature side of the reaction boundaries.

TABLE 8 Discontinuous reactions araound the [qz] and [bi] invariant points in the system SiO_2 - Al_2O_3+ Fe_2O_3- MgO + FeO for spinel + sillimanite-bearing assemblages

Invariant point	Univariant line	Reaction
[bi]	(cor)	cord ⇌ 2 sp + 5 qz
	(sill)	cord ⇌ 2 sp + 5 qz
	(qz)	cord + 5 cor ⇌ 2 sp + 5 sill
	(cord)	sill ⇌ cor + qz
	(sp)	sill ⇌ cor + qz
[qz]	(cor)	6,11 sill + 2,78 bi ⇌ 1,00 cord + 5,22 sp + 2,78 K-spar + 2,78 H_2O
	(sill)	1,00 cord + 27,50 cor + 12,50 bi ⇌ 34,50 sp + 12,50 K-spar + 12,50 H_2O
	(cord)	4,50 cor + 2,50 bi + 1,00 sill ⇌ 6,50 sp + 2.50 K-spar + 2,50 H_2O
	(sp)	6,90 sill + 1,00 bi ⇌ 4,70 cor + 1,30 cord + 1,00 K-spar + 1,00 H_2O
	(bi)	1,00 cord + 5,00 cor ⇌ 2,00 sp + 5,00 sill

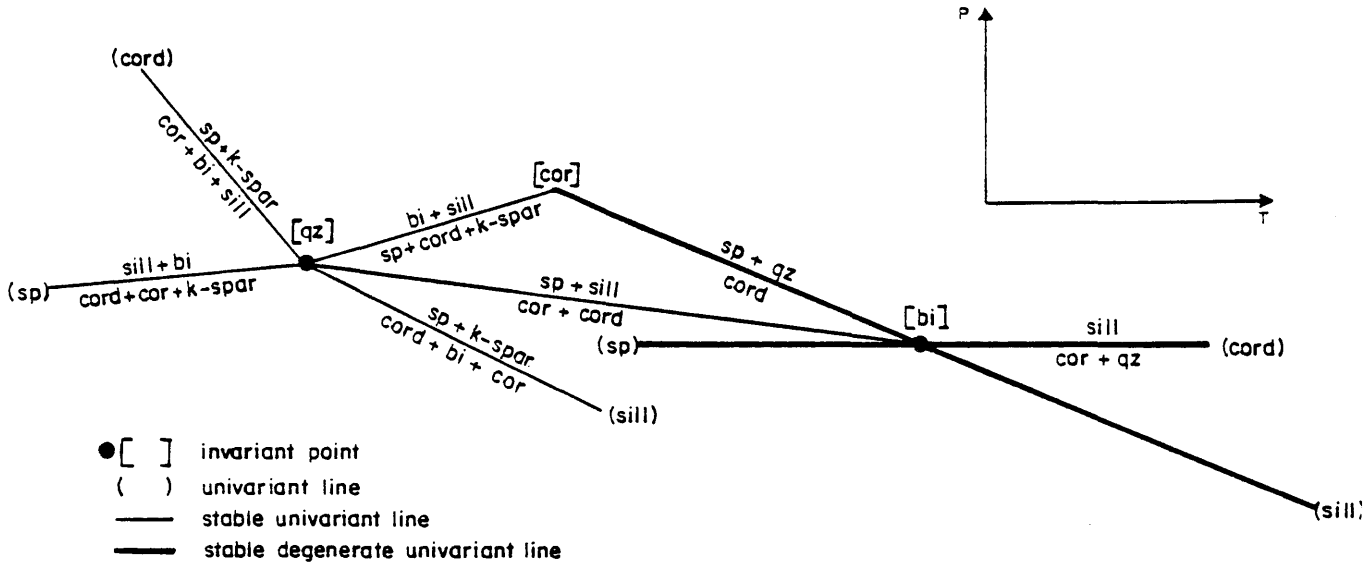

Fig. 54: Schreinemakers diagram illustrating the phase relations of the high-grade Timeball Hill pelites

The univariant lines around the [bi] invariant point have a relatively simple disposition due to the colinearities between quartz, cordierite and spinel on the one hand and quartz, sillimanite and corundum on the other. For both colinearities the relatively indifferent phases lie on the same side of the lines connecting the singular phases and the (bi,cor) and (bi,sill) as well as the (bi,cord) and (bi,sp) lines therefore intersect stable to metastable.

The phase relations of the high-grade Timeball Hill pelites can be explained by a facies series that passes on the high-pressure side of the [qz] and [bi] invariant points but on the low-pressure side of the [cor] invariant point. Such a reaction route explains the stable biotite-andalusite (sillimanite) assemblage at low temperatures and the subsequent tie-line flip, sillimanite + biotite to cordierite + spinel with increasing metamorphic grade. At the highest grades the breakdown of cordierite to spinel and quartz was therefore also possible. The (bi,qz) univariant line was intersected when temperatures and pressures dropped at the end of the metamorphic event.

The petrogenetic grid can be approximately orientated with respect to the Al_2SiO_5 triple point. The assemblage biotite + andalusite + sillimanite + cordierite + spinel (sample PH - 184) indicates the intersection of the (qz,cor) reaction boundary with the sillimanite + andalusite phase boundary. The [qz] invariant point is therefore situated in the andalusite stability field.

6.1.4 Melting reactions in the high-grade Timeball Hill pelites

The melting reactions can be schematically illustrated in an Al_2O_3 - MgO - FeO - SiO_2 tetrahedron (Fig. 55). The initial composition of the pelites lie in the cordierite - sillimanite - biotite - quartz space at an approximate position X. Anatexis reduces the concentrations of SiO_2 and the alkalis

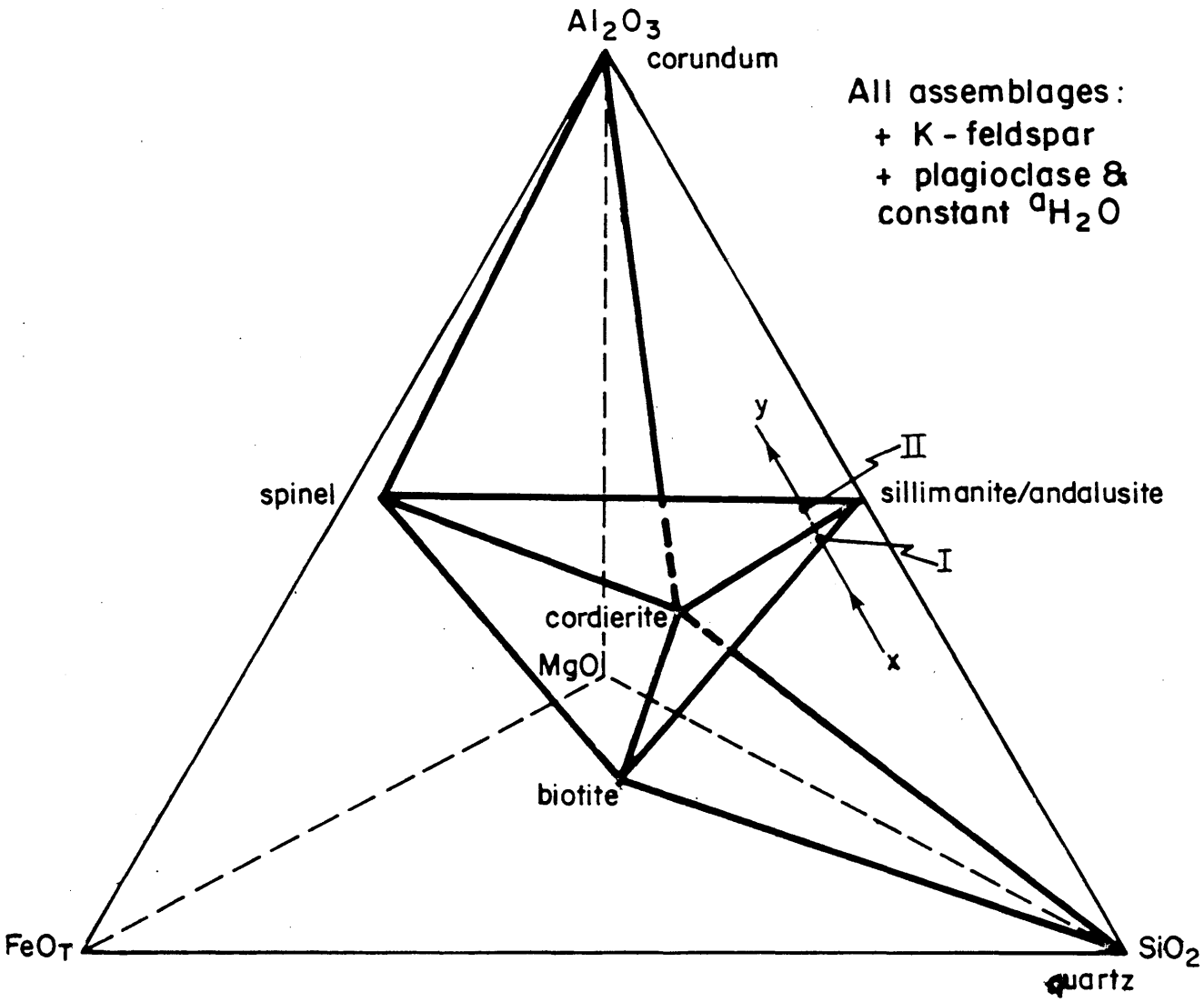

Fig. 55: Change in bulk rock composition of the Timeball Hill pelites with increasing partial melting. X represents the initial composition of the low-grade Timeball Hill shales. All free quartz will be consumed at point I and corundum will be a possible phase at compositions less siliceous than point II. Point Y represents the composition of the high-grade Timeball Hill pelites

to such an extent that the composition of the restite migrates away from the SiO_2 apex along the line x - y. At position I all free quartz is consumed and the restite lies in the plane cordierite - biotite - sillimanite. Further melting causes the SiO_2 - undersaturated phase, spinel, to join the paragenesis. With further melting point II on the spinel- cordierite - sillimanite plane is reached. Continuous melting causes the restite composition to move into the corundum - cordierite- spinel - sillimanite space It is clear that extensive melting is required for the original SiO_2 saturated rocks to reach a composition where the corundum + sillimanite + spinel + cordierite assemblage will be stable.

At point X the melting reaction is believed to be:
sillimanite + plagioclase + K-feldspar + quartz + H_2O $\rightleftharpoons$ liquid .....6(24)
The temperature at which reaction 6(24) will proceed is a function of the Ab/An ratio in the rock, as well as the water pressure (Von Platen, 1965). There is a dramatic rise in the temperature at which anatexis begins with a decrease in the Ab/An ratio of the pelite at a fixed water pressure. In the Ca-poor Timeball Hill pelites, plagioclase is the first phase to be completely consumed. The next melting reaction to take place will be:
sillimanite + K-feldspar + quartz + H_2O $\rightleftharpoons$ liquid .....6(25)
According to Thompson and Tracy (1979) this reaction takes place at a temperature of about 50°C higher than reaction 6(24) at a fixed P_{H_2O}. Reaction 6(25) will proceed until the K-feldspar is completely consumed after which melting will proceed according to a reaction proposed by Von Platen (1965):
biotite + sillimanite + quartz $\rightleftharpoons$ cordierite + $\underbrace{KAlSi_3O_8 + H_2O}_{\text{liquid}}$ .....6(26)

This reaction will proceed until the plane cordierite -biotite- sillimanite is reached, position I in Figure 55. At this point all free quartz has been consumed and melting will take

place through the reaction:

biotite + sillimanite ⇌ cordierite + spinel + $\underbrace{KAlSi_3O_8 + SiO_2 + H_2O}_{\text{liquid}}$ .....6(27)

Petrographic support for reaction 6(27) is found in the form of large xenoblastic K-feldspar grains next to spinel in some cordierite + spinel + sillimanite-bearing rocks from the study area. When biotite is completely consumed through reaction 6(27) the restite composition will move into the corundum - spinel - sillimanite - cordierite space and melting will take place through the reaction:

cordierite ⇌ spinel + $\underbrace{SiO_2 + H_2O}_{\text{liquid}}$ .....6(28)

The melting curve for anhydrous silicate systems has a very steep positive slope in P,T space because there is an increase in the total volume of the system when melting occurs. Addition of water to the system will lower the melting temperature at any given pressure until the amount of water exceeds its solubility in the melt. At this point the melting curve will have a negative slope until very high pressures are encountered because the melting reaction will now be:

solid + vapor (H_2O) ⇌ liquid .....6(29)

At low pressures reaction 6(29) causes a reduction of the total volume on melting due to the greater volume of water in the vapor state compared with when it is dissolved in a silicate melt.

In general, anatexis results in a decrease of P_{H_2O} in the restite and $P_{H_2O} = 0,2\ P_{total}$ is typical for pelitic restites (Harris, 1981 ; Wells, 1979). The melting curve for $P_{H_2O} = 0,2\ P_{total}$ is almost vertical in P,T space and is situated at a temperature of about 800°C (Thompson and Tracy, 1979). Melting of the high-grade Timeball Hill pelites probably took place under greatly reduced water pressures during the second stage of the metamorphic event (Chapter 8). During the first part of the metamorphic event

temperatures were probably not high enough to cause large scale anatexis, but the dehydration reactions that took place lowered P_{H_2O} significantly. The lowering of P_{H_2O} caused the melting curve to be displaced towards higher temperatures so that anatexis during the second part of the metamorphic event took place at elevated temperatures.

6.1.5 Phase relations of olivine-bearing assemblages

In assemblage group 11, olivine occurs together with cordierite and orthopyroxene, while thin quartz layers sometimes separate olivine and orthopyroxene grains. In assemblage group 12, olivine is commonly enclosed by orthopyroxene and spinel porphyroblasts, while thin quartz layers may be developed between cordierite and orthopyroxene grains.

Both assemblage groups are regarded as being silica under-saturated since the thin quartz layers are believed to be reaction products in otherwise silica-deficient rocks. The phase relations of assemblage group 12 are illustrated in a stereoscopic phase diagram projected from K-feldspar and water into the SiO_2 - Al_2O_3 - MgO - FeO tetrahedron (Fig. 56).

The reaction that is responsible for the appearance of olivine in assemblage group 11 is uncertain because none of the samples show any textures which may be related to such a reaction. A possible reaction can be inferred from the low-grade assemblages in rocks of similar bulk composition and from the chemographic relations between the relevant phases. The order of Fe/Mg for the phases concerned is garnet > olivine > orthopyroxene > biotite > cordierite and the relative Al_2O_3 concentrations are olivine < orthopyroxene < biotite < garnet < cordierite. From the relative Al_2O_3 concentrations it is clear that olivine could only have formed through a non-terminal reaction, i.e. a change in tie-lines among four ferromagnesian phases. The following reaction is suggested:

garnet + orthopyroxene + quartz $\rightleftharpoons$ cordierite + olivine ...6(30)

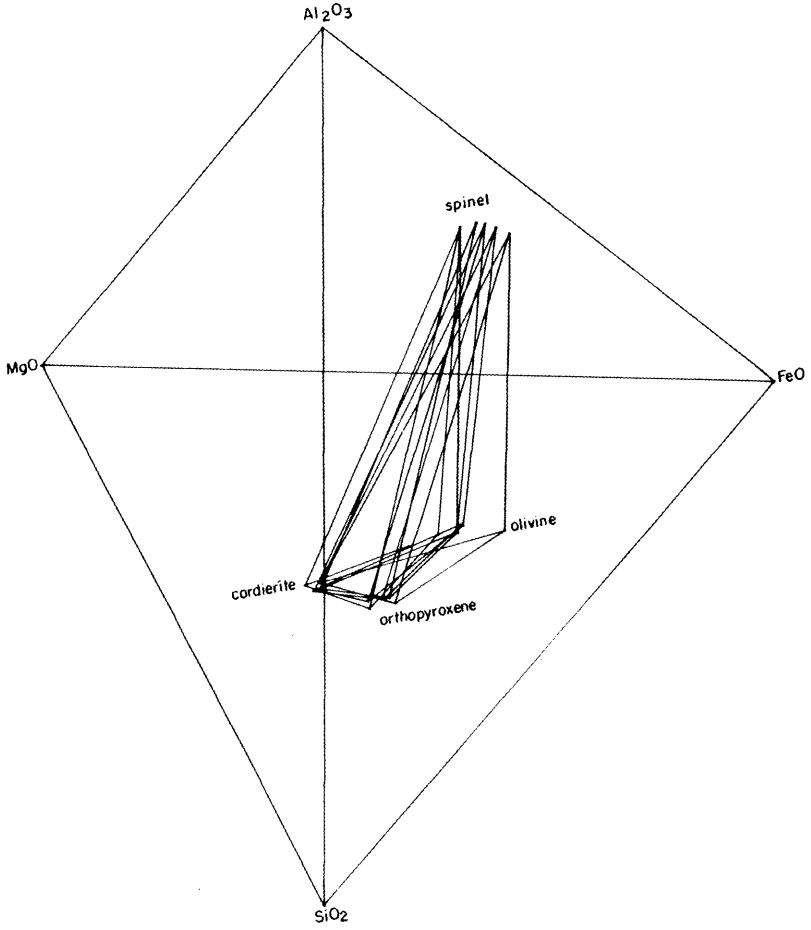

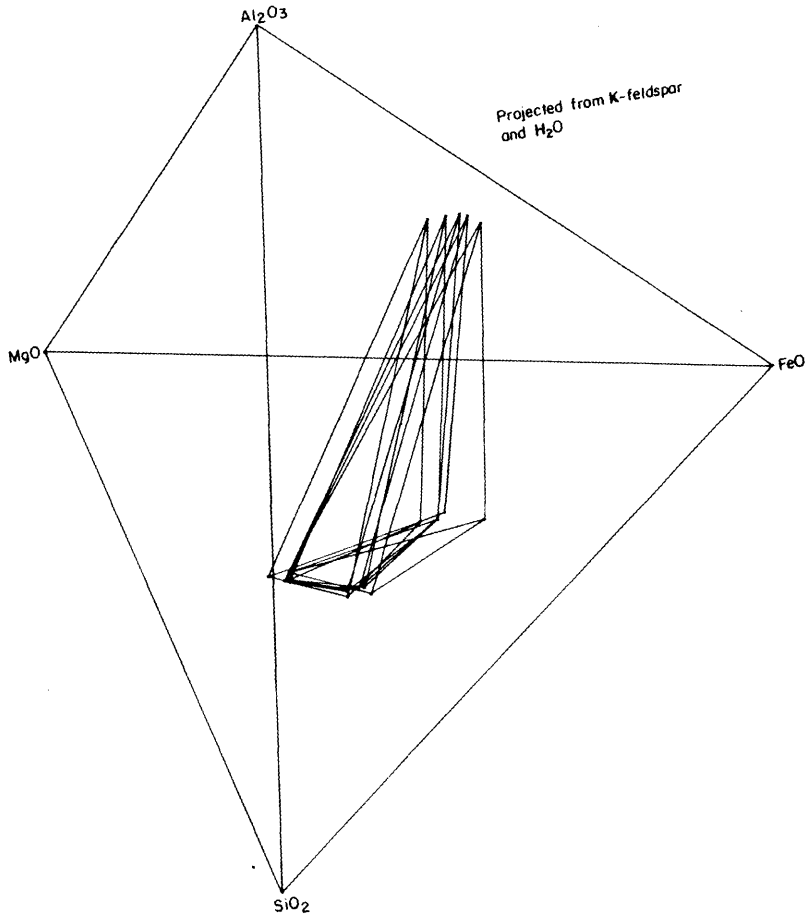

Fig. 56: Stereoscopic projection from K-feldspar and water into the Al_2O_3 - MgO - FeO - SiO_2 tetrahedron for the spinel + cordierite + olivine + orthopyroxene assemblage

The reaction is univariant in the system SiO_2-Al_2O_3-MgO-FeO with excess quartz Reaction 6(30) will proceed until garnet is completely consumed after which any excess quartz will equilibrate with olivine and orthopyroxene. In garnet-absent assemblages olivine may be produced according to the reaction:

biotite + quartz ⇌ olivine + K-feldspar + H_2O .....6(31)

Spinel is introduced into assemblage group 12 through the reaction:

cordierite + olivine ⇌ spinel + orthopyroxene .....6(32)

The reaction is divariant in the system SiO_2-Al_2O_3+ Fe_2O_3-MgO-FeO where Fe_2O_3 and Al_2O_3 are treated as isomorphous components and where quartz is not in excess. The stability of the four phase assemblage over a temperature interval at a fixed pressure has been verified by the spread in the localities of the samples that contain this assemblage.

The olivine - K-feldspar intergrowth that replaced spinel in assemblage group 12 is difficult to explain. The presence of K-feldspar indicates that biotite was a reactant in the reaction that produced the texture. The relatively low SiO_2 and alkali content of the samples containing this intergrowth (PH - 202, PH - 203) suggests that the samples have undergone limited anatexis. The following reaction is suggested:

biotite + 3 orthopyroxene ⇌ 3 olivine + $\underbrace{KAlSi_3O_8 + H_2O}_{\text{liquid}}$ .....6(33)

This may also explain the resorbed appearance of the spinel in contact with the intergrowth as it may well have been unstable in the presence of a SiO_2- rich liquid.

The intergrowth between orthopyroxene and spinel may be accounted for by reaction 6(32) or it may be the result of the reaction:

olivine + Al-orthopyroxene ⇌ spinel + orthopyroxene .....6(34)

The involvement of olivine in the formation of the texture could, however, not be confirmed beyond all doubt.

6.1.6 The orthopyroxene + cordierite + spinel + magnetite assemblage

Samples belonging to assemblage group 10 can be divided into three textural types (Chapter 3). The minerals from this assemblage group cover a wide compositional range, but no relationship between mineral composition and textural type could be detected.

Orthopyroxene is never in contact with the oxide minerals in the first textural type, thereby indicating that orthopyroxene and one or both of the oxide phases are unstable together, while cordierite is stable together with both orthopyroxene and the oxide minerals. In the second textural type, orthopyroxene is freely in contact with composite oxide grains, while the third textural type is characterized by intergrowths between orthopyroxene and oxide grains.

The third textural type probably resulted from the tie-line flip between olivine and cordierite to orthopyroxene and spinel (reaction 6 (32)), but it is not clear which reaction introduced spinel in the two former textural types. The assemblages orthopyroxene + cordierite $\pm$ biotite and orthopyroxene + cordierite + garnet $\pm$ biotite occur in rocks of similar bulk composition at lower metamorphic grades. It was shown that the garnet-bearing assemblage produced olivine with increasing grade according to reaction 6(30). This olivine-bearing assemblage subsequently reacted to produce the third textural type. The most likely spinel-producing reaction is therefore reaction 6(22). This is, however, also a quartz-producing reaction and since the spinel-bearing assemblages only contain very small amounts of quartz, the problem cannot be satisfactoraly resolved at this stage.

The essential difference between the first- and second-textural types lies in the fact that both textural types

contain the same number of phases that appear to be in disequilibrium in the first type and in equilibrium in the second textural type. Therefore the number of components must be different for the two textural types if the Gibbs phase rule is observed and if the samples equilibrated under similar P,T conditions. Identical physical conditions of metamorphism are suggested by the proximity of the localities of the samples containing the two textural types.

The system under consideration contains the components SiO_2-Al_2O_3-Fe_2O_3-FeO-MgO with water as a boundary value component. The following phases are present: quartz, orthopyroxene, cordierite, spinel and magnetite. Since there are 5 phases and 5 immobile components the system will have two degrees of freedom and the 5 phases will coexist over a P,T interval. This is the situation in the second textural type.

Under equilibrium conditions the fO_2 of the system, and therefore the activity of Fe_2O_3 will be controlled by the reaction:

$$2\ FeAl_2O_4 + {}^1/_2\ O_2 \rightleftharpoons Fe_3O_4 + 2\ Al_2O_3 \quad \text{.....6(35)}$$

hercynite magnetite corundum

In the natural Mg-bearing system a $spinel_{ss}$ will take the place of hercynite and Mg will be liberated by reaction 6(35) since magnetite can only accomodate small amounts of Mg. The Mg and Al released by reaction 6(35) will combine with silica to form cordierite as a reaction product. For the natural system reaction 6(35) may then be rewritten as:

Al-rich $spinel_{ss}$ + quartz + $O_2 \rightleftharpoons Fe^{3+}$-rich $spinel_{ss}$ + cordierite .....6(36)

Reaction 6(36) will control the exsolution of two oxide phases from one another and at the same time control the activity of Fe_2O_3 in spinel.

Variation in the fO_2 will cause fluctuations in the activity of Fe_2O_3 in the Fe^{3+}-rich $spinel_{ss}$. Many workers

e.g. Klein (1966) and Butler (1969), pointed to the immobility of oxygen during metamorphism, i.e. oxygen is an initial value component. Fe_2O_3 will therefore be an immobile component and Fe_3O_4 activity will be buffered by the mineral assemblage. In the first textural type the number of immobile components is believed to be less than in the second textural type. This can be achieved if the water activity is buffered by the mineral assemblage in the second textural type, by the influence of minor components or by the behaviour of oxygen. On the basis of textural evidence (as outlined below) it is suggested that the activity of Fe_2O_3 was externally controlled in the first textural type, i.e. oxygen behaved as a boundary value component. The number of immobile components will then be reduced to 4 and the system will have one degree of freedom. This will cause the establishment of the following reaction relationship:

orthopyroxene + Al-rich spinel$_{ss}$ + O_2 ⇌ cordierite + Fe^{3+} -rich spinel$_{ss}$ .....6(37)

Since the two spinel solid solutions occur together in a single grain, reaction 6(37) is consistent with the texture where cordierite occurs between orthopyroxene and the oxide grain as well as inclusions and embayments in oxide grains which are in close proximity to orthopyroxene.

It is not clear why oxygen appears to have been inert in the second- and mobile in the first textural types. The second textural type might be the result of local equilibrium where the oxygen fugacity was controlled by the mineral assemblage, while the first textural type might be the result of macro buffering of the fO_2 through a retrograde reaction in falling temperature conditions at the end of the metamorphic event.

6.2 Metamorphism of calcareous rocks.

6.2.1 Metamorphism of siliceous dolomite and limestone.

With increasing metamorphic grade clinochlore, phlogopite, tremolite, diopside, forsterite and spinel are typical

silicate minerals that appear in siliceous dolomites. The metamorphic reactions in such rocks liberate CO_2, and the fluid phase composition is usually buffered by the mineral assemblage. The system may, however, also be open to one or more fluid phase species, causing the composition of the fluid phase to be only partially buffered by the mineral assemblage. The paragenetic sequence for the siliceous dolomites is defined by the first 5 assemblage groups in Tables 2 and 4. Spinel and clinochlore are only stable in rocks that are sufficiently enriched in Al_2O_3 and depleted in SiO_2 to plot on the Al-side of the diopside- forsterite-calcite plane in the system SiO_2 - Al_2O_3 - CaO- MgO + FeO_T.

An isobaric T- X_{CO_2} diagram was constructed to illustrate the various mineral reactions in the siliceous dolomites from the study area (Fig. 57). The positions of the reaction equilibria (Table 9) were determined after the method of Powell (1978 b). The standard states of the minerals and fluid species are the pure phases at the pressure and temperature of interest. The chemical potential of a species in the fluid phase is then given by:

$$\mu_i = G_{i\,(P,T)} + RT \ln f_i + RT \ln X_i \gamma_i \qquad \text{.....6(37)}$$

where μ_i is the chemical potential of species i in the fluid phase, $G_{i\,(P,T)}$ is the Gibbs energy of species i at the pressure and temperature of interest; f_i is the fugacity of species i ; X_i is the mole fraction of species i and γ_i is the activity coefficient of species i in the fluid phase. A positive deviation from ideality for H_2O - CO_2 mixtures has been shown by Greenwood (1973) and a regular solution model has been adopted in the calculation of γ_{H_2O} and γ_{CO_2} (Powell, 1978 b):

$$RT \ln \gamma_{CO_2} = (20{,}8 - 0{,}015\ T)\ X^2_{H_2O}$$

$$\text{and } RT \ln \gamma_{H_2O} = (20{,}8 - 0{,}015\ T)\ X^2_{CO_2} \qquad \text{.....6(38)}$$

TABLE 9 Reactions in siliceous dolomites from the Potgietersrus area as illustrated in Figure 57

Number	Reaction	$\Delta(\Delta H_{f(1,298)})$ KJ	$\Delta S_{(1,298)}$ KJK^{-1}	$\Delta V_{S(1,298)}$ $KJK\ bar^{-1}$
1	3 do + K-spar + H_2O ⇌ phlog + 3 cc + 3 CO_2	159,6	0,3615	-4,125
2	2,5 phlog + 3 cc + 12 qz ⇌ 1,5 trem + 2,5 K-spar + H_2O + 3 CO_2	298	0,6369	-7,614
3	5 dol + 8 qz + H_2O ⇌ trem + 3 cc + 7 CO_2	464,6	1,0271	-11,5
4	trem + 3 cc ⇌ 4 di + do + CO_2 + H_2O	160,2	0,3029	-5,50
5	trem + 3cc + 2 qz ⇌ 5 di + 3 CO_2 + H_2O	316,4	0,6354	-0,86
6	trem + 11 dol ⇌ 8 fo + 13 cc + 9 CO_2 + H_2O	1043	1,822	-15,03
7	di + 3 do ⇌ 2 fo + 4 cc + 2 CO_2	220,6	0,380	-2,38
8	chl + 2 do ⇌ sp + 3 fo + 2 cc + 2 CO_2 + 4 H_2O	549	0,967	-9,13
9	cc + qz ⇌ wo + CO_2	94,6	0,162	-1,969

Thermodynamic data from Powell (1978 b)

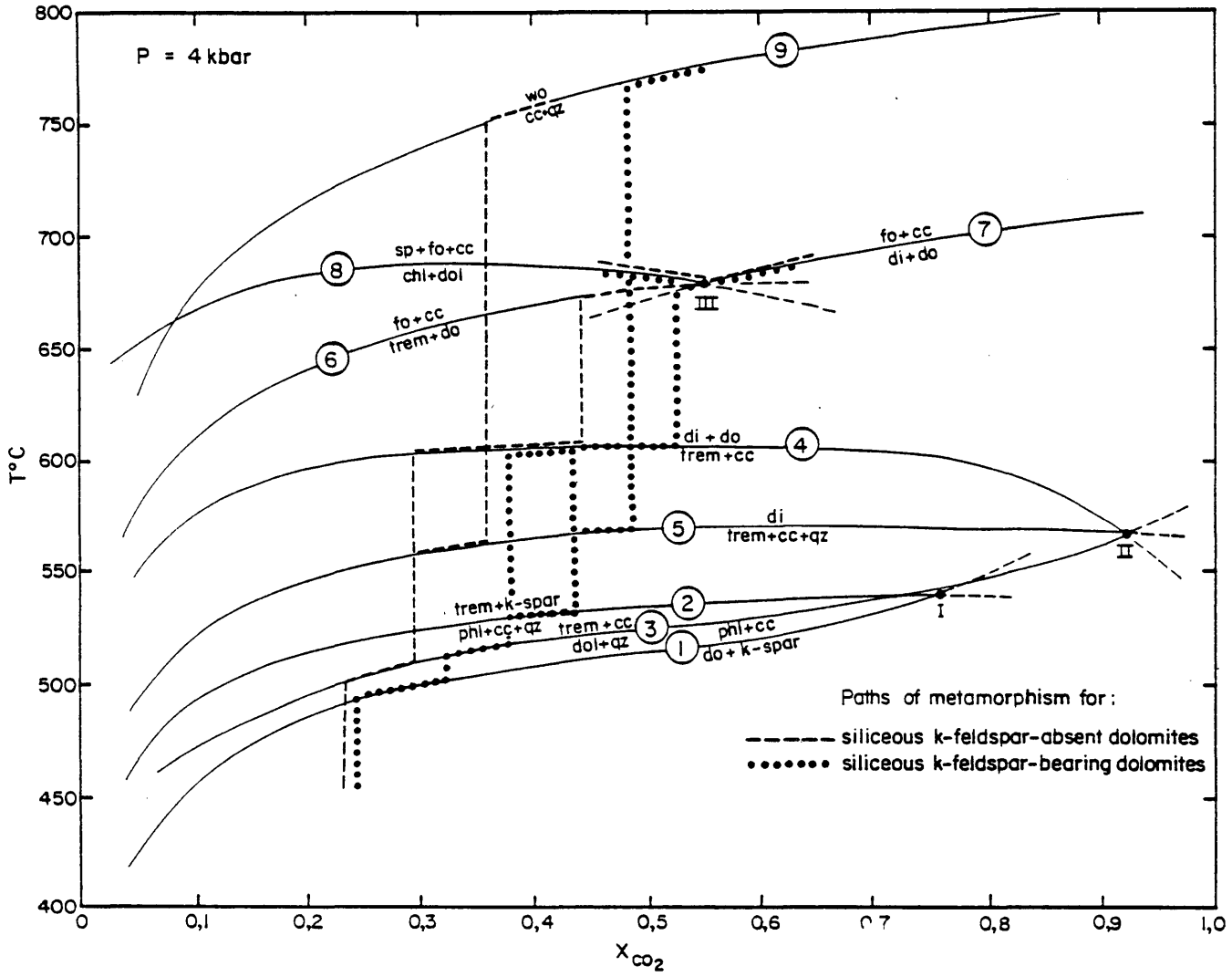

Fig. 57: T - X_{CO_2} relations for the reactions in siliceous dolomites, illustrating metamorphic paths for K-feldspar-bearing and -absent assemblages

Powell (1978 b) defined ΔG° for a solid-fluid reaction as:

$$\Delta G^{\circ} = \Delta(\Delta H_f(1,298)) - T\Delta S(1,298) + P\Delta V_s(1,298) + nF_{H_2O} + mF_{CO_2} \quad \ldots\ldots 6(39)$$

The F terms contain the volume expressions for each of the fluid end-members together with the heat capacity integral for the difference in heat capacity of fluid species structurally bound in a solid state relative to the free fluid species. F_{H_2O} and F_{CO_2} are linear functions of temperature and have been tabulated for a range of temperatures and pressures, covering 100 K intervals, at each pressure (Powell, 1978 b). The stoichiometric reaction coefficients for H_2O and CO_2 are given by n and m respectively. T is the absolute temperature in K and P is in kbar. $\Delta H_{f(1,298)}$ is the enthalpy of formation from the elements at 1bar and 298K; $\Delta S(1,298)$ is the entropy at 1bar and 298 K while $\Delta V_{s(1,298)}$ is the volume change for the solid phases in the reaction at 1 bar and 298 K.

The position of a reaction in T - X_{CO_2} space can be calculated by assuming equilibrium conditions, i.e.

$$\Delta\mu = 0 = \Delta G^{\circ} + RT\ln K$$

$$\therefore\ 0 = \Delta(\Delta H_{f(1,298)}) - T\Delta S_{(1,298)} + P\Delta V_{s(1,298)} + F_{H_2O} + F_{CO_2} + RT\ln K \quad \ldots\ldots 6(40)$$

where $RT\ln K = RT\ln \frac{(^a\text{solid})\text{prod}}{(^a\text{solid})\text{react}} + nRT\ln X_{H_2O} + mRT\ln XCO_2 + nRT\ln \gamma_{H_2O} + mRT\ln \gamma_{CO_2}$ $\ldots\ldots 6(41)$

In the construction of the T - X_{CO_2} diagram the activities of the solid phases were assumed to be unity, i.e.

$RT\ln (^a\text{solid})\text{ prod} / (^a\text{solid})\text{react} = 0.$

Thermodynamic data was obtained from Powell (1978 b) including F_{H_2O} and F_{CO_2} values for the temperature interval 773 - 873 K and 4 kbar pressure. An incorrect choice of the temperature interval in the calculation of F values has a minimal influence on the T - X_{CO_2} relations

of the reactions (Powell, 1978 b).

The constructed T - X_{CO_2} diagram (Fig. 57) is in good agreement with similar grids published in the literature. Three invariant points, I, II and III are present. (Note that only the univariant reactions that were recognized in the study area are presented in Figure 57, and that several more univariant reactions will meet in the invariant points when all the possible reactions are considered). Invariant point I involves K-feldspar and phlogopite - bearing assemblages, while invariant point II is equivalent to the [forsterite, talc] invariant point in the system SiO_2 - CaO - MgO - CO_2 - H_2O (Metz and Trommsdorff, 1968). The exact X_{CO_2} coordinate of invariant point III is uncertain because of the flat slopes of the reactions that intersect at this point. The X_{CO_2} coordinate of 0,55 is, however, in excellent agreement with the value of the equivalent 1P2 invariant point of Buchner-Nurminen (1982).

The metamorphic paths for K-feldspar-bearing and -absent siliceous dolomites are schematically outlined in Figure 57. At the lowest grades reaction 1 (reaction numbers refer to Table 9) will introduce phlogopite into potassic dolomites. When all K-feldspar has been consumed, reaction 3 will be intersected with increasing metamorphic grade. This will also be the first reaction to take place in K-feldspar-absent dolomites. At equivalent metamorphic grades clinochlore is produced in sufficiently aluminous dolomites as a breakdown product of clay minerals. Phlogopite breaks down according to reaction 2, providing that quartz has not been completely consumed by reaction 3. Any quartz that may be present after the termination of reactions 2 and 3 reacts according to reaction 5 in both K-feldspar-bearing and -absent systems. If tremolite is completely consumed before quartz through reaction 5, the resulting calcite + quartz + diopside assemblage remains stable until wollastonite is eventually formed through reaction 9. The diopside + calcite + tremolite assemblage that usually remains after the ceasation of reaction 5 breaks down according to reaction 4 with increasing metamorphic grade.

The presence of the forsterite + dicpside + tremolite + calcite + dolomite assemblage (PC - 27), which is stable at invariant point III, suggests that the fluid phase, at this stage, must have had a composition close to the X_{CO_2} of invariant point III (0,55 in Fig. 57). At temperatures lower than invariant point III, reaction 6 will terminate the stability field of the tremolite-dolomite join and at the same time buffer the fluid phase composition towards the invariant point. At invariant point III reaction 7 will cause the breakdown of the diopside-dolomite join. Spinel will be formed in clinochlore-bearing assemblages through reaction 8. If clinochlore is completely consumed before diopside at invariant point III, reaction 7 will buffer the fluid phase composition towards a higher X_{CO_2} with increasing grade. If, however, diopside is completely consumed before clinochlore, reaction 8 will buffer the fluid phase composition towards a lower X_{CO_2} with increasing grade and the spinel + forsterite + calcite + dolomite assemblage will result. Unreacted phlogopite from reaction 2 will still be stable, explaining the presence of phlogopite in some forsterite- and spinel-bearing assemblages.

The fluid phase composition is believed to have been buffered by the mineral reactions during the prograde metamorphic event. No evidence could be found for the dilution of the fluid phase by H_2O while the assemblages travelled through the isobaric divariant fields. The K-feldspar-bearing assemblages apparently followed a slightly more CO_2-rich path during the lower metamorphic grades because they underwent two more decarbonization reactions (1 and 2) than the K-feldspar-absent system. The eventual fluid phase composition is, however, believed to have been rather similar to the X_{CO_2} value of invariant point III for both the K-feldspar- bearing and -absent systems. If, as has been postulated by Greenwood (1975), the bulk of the reactions occur at isobaric invariant points then most of the forsterite - and spinel-bearing samples crystallized at X_{CO_2} = 0,55. The T - X_{CO_2} paths further suggest that the fluid phase composition was never more CO_2-rich than X_{CO_2} = 0,55 at lower metamorphic grades than invariant

point III. This postulation is confirmed by the absence of the clinochlore breakdown reaction to tremolite and spinel in the study area, since this reaction takes place at higher X_{CO_2} values and lower temperatures than invariant point III (Buchner - Nurminen, 1982).

The rarity of wollastonite in the study area can be attributed to two reasons. First, the bulk rock must be quartz- and calcite-rich to prevent either or both from being completely consumed through reaction 5. Secondly, a temperature of at least 750°C at 4 kbar pressure and a fluid phase composition with $X_{CO_2} \sim 0,5$ is required (Fig. 57). This temperature estimate is in good agreement with temperatures calculated from geothermometres in pelitic rocks collected in close proximity to the wollastonite-bearing samples.

The wollastonite + monticellite + garnet + diopside (fassaite) + calcite assemblage (PD - 194) remains difficult to explain. Although no akermanite was detected, the intergrowth between monticellite and wollastonite may be ascribed to the following retrograde reaction proposed by Willemse and Bensch (1964) to account for a similar texture in carbonate xenoliths from the eastern Bushveld Complex:

akermanite $\rightleftharpoons$ monticellite + wollastonite .....6(42)

The garnet that is sometimes intergrown with monticellite and wollastonite is more inigmatic. The garnet has a composition $Ca_{2,7}(Fe^{2+}, Mn)_{0,3}(Al, Fe^{3+})_2 Si_3O_{12}$ and another Al, Fe^{3+}-bearing mineral was therefore a reactant in the garnet-producing reaction. The most likely mineral is diopside ($CaMg_{0,5}(Al, Fe^{3+})_{1,0}Si_{1,5}O_6$), which was never seen in contact with the garnet-bearing symplectite. The following reaction is suggested:

0,5 akermanite + diopside + 0,5 calcite $\rightleftharpoons$ 0,5 garnet + monticellite + 0,5 CO_2 .....6(43)

The successive breakdown of akermanite and diopside and akermanite may thus be responsible for the complex symplectites in the specimen.

6.2.2. Metamorphism of "impure dolomites"

6.2.2.1 Phase relations between garnet and clinopyroxene

Two textural types of clinopyroxene and garnet are present in the impure dolomite mineral assemblages (Chapter 3). The first type occurs as individual garnet and clinopyroxene crystals, while the second type gives rise to a symplectic intergrowth between the two phases. Chemically, the single crystal clinopyroxenes are distinctly enriched in Al_2O_3 relative to the clinopyroxene intergrown with garnet (Fig. 58). Fibrous clinopyroxene from Magnet Heights is similarly enriched in Al_2O_3 relative to granular clinopyroxene (Willemse and Bensch, 1964). Both textural types of garnet have,however, similar chemical compositions.

Figure 58 suggests the following reaction between the relevant phases:

granular clinopyroxene + calcite $\rightleftharpoons$ garnet + intergrown clinopyroxene .....6(44)

Willemse and Bensch (1964) proposed a similar reaction between fibrous- and granular clinopyroxene from Magnet Heights.

Assuming that the intergrown clinopyroxene is pure diopside in composition, reaction 6 (44) will consume quartz for granular clinopyroxene compositions more aluminous than $CaMg_{0,67}Al_{0,63}Si_{1,7}O_6$. This fassaite composition will be a limiting one in the sense that more aluminous fassaite will be unstable together with quartz and calcite relative to diopside and grossularite, while less aluminous clinopyroxene will be stable together with quartz and calcite. The reaction could then explain the observation that fassaite-quartz assemblages are unknown or very rare in nature (Deer et al., 1962 b).

6.2.2.2 Mineral reactions in the impure dolomites

The metamorphism of the impure dolomites can be described in terms of the system SiO_2- Al_2O_3 - MgO - FeO - CaO - K_2O

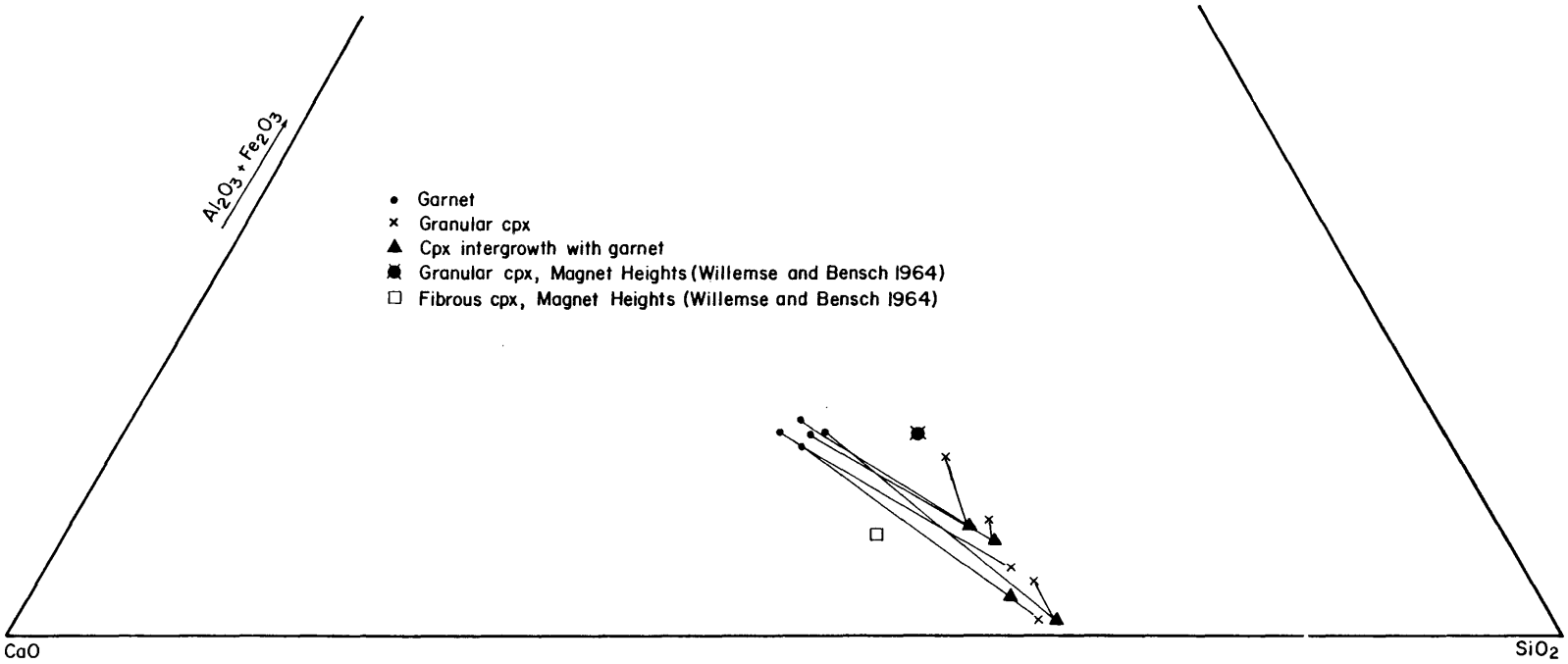

Fig. 58: Plot illustrating the difference in composition between "granular"- and "intergrowth" clinopyroxene coexisting with garnet. Garnet-granular-clinopyroxene tie-lines have been omitted for clarity

- H_2O - CO_2. The phases chlorite, biotite-phlogopite, calcic amphibole, clinopyroxene, plagioclase, K-feldspar, grandite-rich garnet, sphene, idocrase, spinel and fassaite are encountered with increasing metamorphic grade. Epidote and prehnite are retrograde minerals that may be present in the impure dolomites.

A number of possible mineral reactions in the impure dolomites (Table 10) are graphically illustrated in Figure 59. The reactions were balanced for pure end-member mineral compositions. The T - X_{CO_2} curves were calculated according to the method outlined in section 6.2.1 for a total pressure of 4 kbar. In the following discussion reaction numbers refer to Table 10.

Chlorite and phlogopite break down according to reactions 11 and 13 respectively. Field evidence indicates that chlorite and phlogopite are completely consumed through the respective reactions and that unreacted quartz and calcite reacts with calcic amphibole to produce clinopyroxene (reaction 5). At higher metamorphic grades unreacted calcic amphibole reacts with calcite to produce clinopyroxene and dolomite. The rarity of the clinopyroxene + dolomite assemblage suggests, however, that reaction 4 was relatively unimportant in the study area. Both clinopyroxene-producing reactions fall in the sphene stability field, explaining the ubiquity of sphene in clinopyroxene-bearing assemblages. Wollastonite has not been observed in the impure dolomites, indicating that calcite reacted with plagioclase to produce grandite garnet (reaction 12). Spinel may be the product of a chlorite breakdown reaction, or the result of the breakdown of fassaite to spinel, garnet and clinopyroxene (Onuma et al., 1981).

Idocrase is believed to have formed through one of the following reactions:

plagioclase + diopside + calcite + quartz $\rightleftharpoons$ idocrase .....6(45)

grossularite + plagioclase + diopside + calcite $\rightleftharpoons$ idocrase .....6(46)

TABLE 10 Reactions in "impure dolomites" from the Potgietersrus area as illustrated in Figure 59

Number	Reaction	$\Delta(\Delta H_{f(1,298)})$	$\Delta S_{(1,298)}$	$\Delta V_{S(1,298)}$
		KJ	KJK^{-1}	$KJKbar^{-1}$
4	trem + 3 cc ⇌ 4 di + do + CO_2 + H_2O	160,2	0,3029	- 5,50
5	trem + 3 cc + 2 qz ⇌ 5 di + 3 CO_2 + H_2O	316,4	0,6354	- 0,86
9	cc + qz ⇌ wo + CO_2	94,6	0,162	- 1,969
10	ru + cc + qz ⇌ spn + CO_2	73,5	0,158	- 2,279
11	chl + 3 cc + 7 qz ⇌ trem + an + 3 CO_2 + 3 H_2O	426,8	0,935	-10,35
12	an + 2 cc + qz ⇌ gr + 2 CO_2	122,6	0,239	- 7,20
13	5 phl + 6 cc + 24 qz ⇌ 3 tr + 5 or + 6 CO_2 + 2 H_2O	595,8	1,274	-15,23
14	2 zo + CO_2 ⇌ 3 an + cc + H_2O	63,2	0,108	6,63
15	4 zo + qz ⇌ 5 an + gr + 2 H_2O	249,0	0,455	6,064
16	2 zo + 5 cc + 3 qz ⇌ 3 gr + 5 CO_2 + H_2O	431,0	0,825	-14,98

Thermodynamic data from Powell (1978 b)

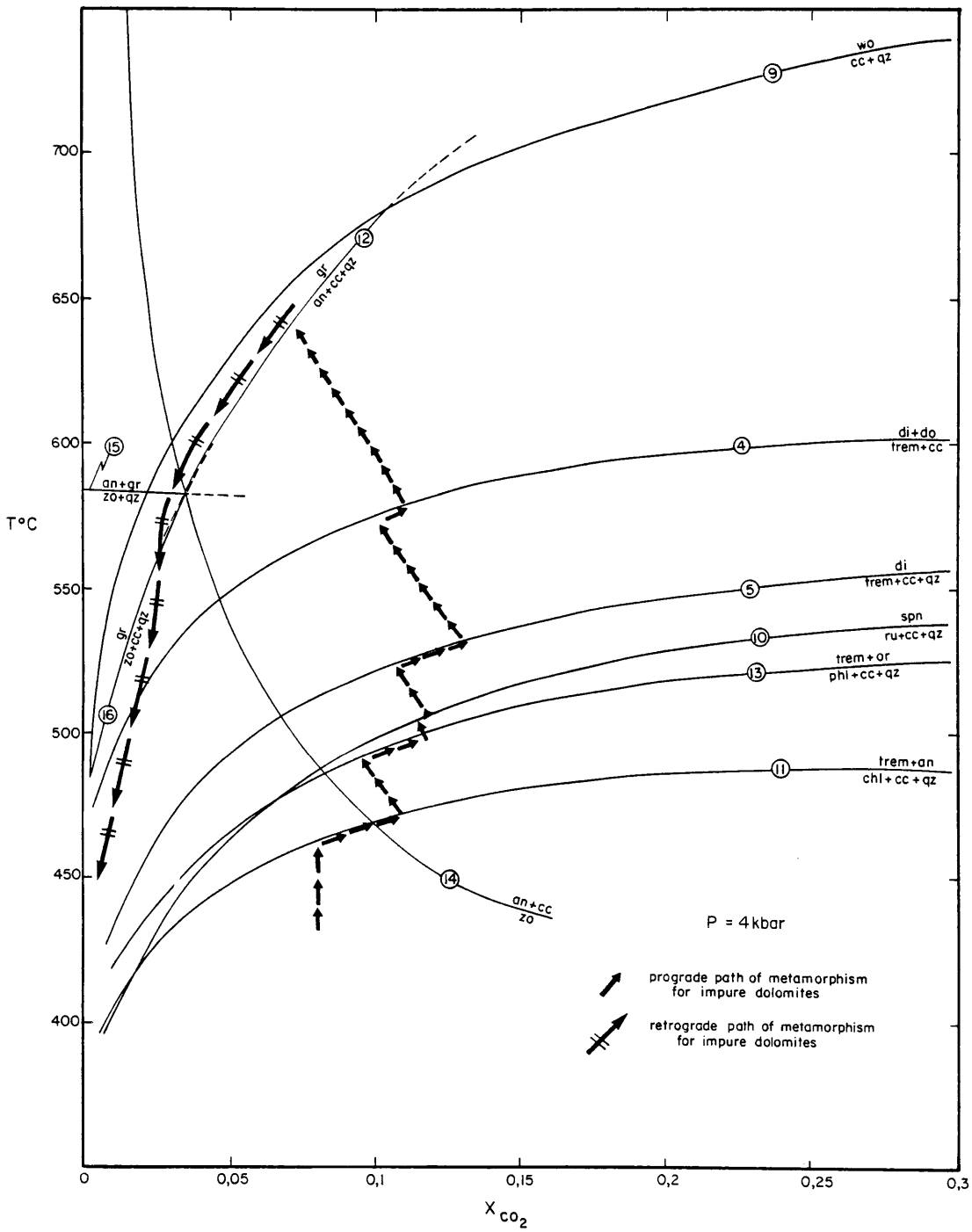

Fig. 59: T - X_{CO_2} relations for the reactions in impure dolomites, illustrating the proposed prograde and retrograde metamorphic paths for the study area

and grossularite + diopside ⇌ idocrase + anorthite + quartz ..... 6(47)

Figure 59 constrains the T - X_{CO_2} conditions of formation of the impure dolomites. The topology of the grid agrees closely with similar published grids (e.g. Kerrick, 1974). Invariant point I is situated at a higher temperature and a lower X_{CO_2} compared with Kerrick's (1974) grid, while invariant point II could be as H_2O-rich as $X_{CO_2} \sim 0{,}03$ (Kerrick, 1974).

Figure 59 cannot be directly applied to natural assemblages because of the substitution of Fe^{2+} for Mg and Fe^{3+} for Al in natural assemblages. It has been shown, for example, that the substitution of Fe^{3+} for Al in grandite garnet causes it to be stable to higher X_{CO_2} values while it also extends the thermal stability field of garnet to both higher and lower temperatures (Taylor and Liou, 1978). There has further been disagreement about the location and slope of reaction 14 in Figure 59. Some workers e.g. Storre (1970) have considered this reaction to have a positive slope, while others derived a negative slope (Gordon and Greenwood, 1971). Storre and Nitsch (1972) proposed a vertical slope in the 450 - 550°C range. Kerrick (1974) found little incompatibility with the Storre and Nitsch (1972) boundary and used a steep negative slope (similar to Figure 59) in the 400 - 600°C range. The theoretically-derived curve in Figure 59 is in good agreement with the curve by Kerrick (1974) at temperatures greater than about 500°C, but it is probably too shallow at lower temperatures.

A schematic reaction route has been suggested for the impure dolimites in Figure 59. Since the garnet ± calcite ± plagioclase ± quartz assemblage is confined to relatively water-rich fluid phase compositions and the low-temperature chlorite, phlogopite and calcic-amphibole breakdown reactions are all decarbonization reactions that will buffer the fluid phase composition towards higher X_{CO_2} values, it follows that the fluid phase composition in the system was not determined by the mineral assemblage only but also by the environment. A metamorphic path is suggested where the fluid phase was buffered

along the isobaric univariant curves, but was diluted with H_2O from an external source while the assemblages travelled through the isobaric divariant fields in Figure 59. Although no evidence for the influx of water into the siliceous dolomites could be found, it must be noted that the influx of water on the scale proposed for the impure dolomites would not have altered the reaction paths proposed for the siliceous dolomites and would, therefore, not have been detected.

6.2.2.3 Retrograde metamorphism in the impure dolomites

Many garnet + diopside $\pm$ plagioclase $\pm$ calcite $\pm$ quartz assemblages contain epidote and prehnite as additional minerals. Although epidote could have formed in garnet- and clinopyroxene - bearing assemblages during the prograde metamorphic event , this is considered unlikely because of the extremely low X_{CO_2} required in the fluid phase and the close association between epidote and prehnite in most epidote-bearing samples. Since there is no evidence for the breakdown of garnet to plagioclase, calcite and quartz (reaction 12) during the retrograde event it is suggested that the T - X_{CO_2} path that was followed during the retrograde event was restricted by reactions 9 and 12 (Fig. 59) until, at least, reaction 14 was intersected. At lower temperatures both reactions 16 and 4 probably took place until the prehnite stability field was reached at about 400°C (Schiffman and Liou, 1980). The T - X_{CO_2} path during the retrograde event suggests the continuous influx of water into the fluid phase. Such a path is consistent with the eventual formation of prehnite which is only stable in calcareous rocks when the chemical potential of water is increased relative to that of CO_2. The following prehnite-forming reactions might have been important:

calcite + quartz + plagioclase + $H_2O \rightleftharpoons$ prehnite + CO_2....6(48)

zoisite + grossular + quartz + $H_2O \rightleftharpoons$ prehnite .....6(49)

and zoisite + calcite + quartz + $H_2O \rightleftharpoons$ prehnite + CO_2....6(50)

In two samples prehnite appears to have formed in cracks that developed in the calc-silicate host rock. The

first example is a 15cm thick prehnite + epidote layer that cuts through a spinel + fassaite-bearing outcrop in a vein-like fashion. The second example is a clinopyroxene + calcic amphibole-bearing rock where prehnite occurs as idioblastic crystals in quartz aggregates. The cracks probably resulted from the drastic volume reduction of the calc-silicates during metamorphism. The source of the water-rich fluid that was introduced into the impure dolomites is uncertain. Gabbroic magmas like the Bushveld Complex magma are believed to have been relatively dry, therefore it would have been unlikely that the magma could have provided the fluids. The only other source is the associated pelitic rocks which were relatively dry at the end of the metamorphic event as is suggested by the absence of hydrous minerals, e.g. biotite. The water that was originally present in the rocks was therefore driven off during the metamorphic event, and this water could have entered the cracks that developed in the calc-silicates.

7. INTENSIVE PARAMETERS

7.1 The distribution of elements between phases

A rigorous test of equilibrium requires that each component has the same chemical potential in all coexisting phases in an assemblage. At a fixed pressure and temperature the chemical potential of a component in a phase is a function of its concentration, and in the case of non-ideal crystals also a function of other chemical changes which take place in a crystal. If the chemical potential of a component in two coexisting phases is dependent on concentration only, then the component must be regularly partitioned between the two phases, provided that equilibrium conditions exist. Since the ferromagnesian minerals are of paramount importance in this section, the distribution of FeO and MgO between the coexisting phases will be examined in some detail.

The molecular MgO/FeO ratios of two ferromagnesian minerals will define a straight line on a distribution diagram if:

1) equilibrium was achieved;
2) the distribution is ideal;
3) The pressure and temperature was either constant, or had no significant effect on the distribution.

The distribution of two components (A and B) between two phases (α and β) may be expressed as:

$$A\alpha + B\beta \rightleftharpoons B\alpha + A\beta \quad \text{.....7(1)}$$

for which the equilibrium constant is:

$$K = \frac{X_B^{\alpha} \cdot X_A^{\beta} \cdot \gamma_B^{\alpha} \cdot \gamma_A^{\beta}}{X_A^{\alpha} \cdot X_B^{\beta} \cdot \gamma_A^{\alpha} \cdot \gamma_B^{\beta}} \quad \text{.....7(2)}$$

where X_B^{α} = mole ratio B/(A + B) in phase α and γ_B^{α} = activit

coefficient of B in phase α. If A and B are the only miscible species present, equation 7(2) may be re-written:

$$K = \frac{(1 - X_A^{\alpha}) . X_A^{\beta} . \gamma_B^{\alpha} . \gamma_A^{\beta}}{(1 - X_A^{\beta}) . X_A^{\alpha} . \gamma_A^{\alpha} . \gamma_B^{\beta}} \quad \text{.....7(3)}$$

For an ideal distribution of A and B between α and β the values of the activity coefficients are equal to unity and equation 7(3) simplifies to

$$K = \frac{(1 - X_A^{\alpha}) X_A^{\beta}}{(1 - X_A^{\beta}) X_A^{\alpha}} \quad \text{.....7(4)}$$

Exchange reactions such as 7(1), which involve solid phases, only have very small ΔV values and are therefore very suitable for calibration as geothermometers.

7.1.1 The distribution of Mg and Fe between garnet and coexisting biotite, orthopyroxene and cordierite

The calculated distribution coefficients between the relevant phases are tabulated in Table 11 and illustrated in Figure 60. The Mg, Fe distribution between garnet and orthopyroxene shows very little scatter and the mean K_D value is in good agreement with values reported in the literature, e.g. Van Reenen and du Toit (1978).

The distribution of Mg and Fe between garnet and biotite is erratic. The value of the distribution coefficient increases with metamorphic grade. Albee (1965 b) illustrated this increase when he obtained values of 0,2 for assemblages in the garnet zone; 0,215 in the staurolite zone; 0,23 in the kyanite zone and 0,3 to 0,24 in the sillimanite- K-feldspar zone. The mean value for the study area is similar to the range typical of the sillimanite-K-feldspar zone, which is also consistent with the presence of orthopyroxene in most garnet + biotite assemblages. There appears to be a positive correlation between $K_{D_{Mg,Fe}}^{gar - bi}$

TABLE 11 $K_{D_{Mg-Fe}}$ values for the distribution of Mg and Fe between garnet and coexisting opx, cordierite and biotite

Sample #	$(Mg/Fe)_{gar}$	$(Mg/Fe)_{opx}$	$(Mg/Fe)_{cord}$	$(Mg/Fe)_{biot}$	$K_{D_{Mg-Fe}}^{gar-opx}$	$K_{D_{Mg-Fe}}^{gar-cord}$	$K_{D_{Mg-Fe}}^{gar-bi}$
PH - 116	0,057		0,587			0,097	
PH - 151	0,078		0,69			0,113	
PH - 152	0,088		0,748			0,118	
PH - 170	0,159	0,489	1,272	0,615	0,325	0,125	0,259
PH - 188	0,139	0,416	0,960	0,840	0,334	0,154	0,165 a
PH - 313	0,157		1,256			0,125	
PH - 321	0,176	0,611	1,394	0,538	0,288	0,126	0,327
PH - 324	0,169	0,419	1,029	0,574	0,403	0,164	0,294
PH - 325	0,143	0,444	0,986	0,591	0,322	0,145	0,242
PH - 326	0,144	0,437	0,872	0,499	0,359	0,165	0,289
PH - 330	0,216	0,659	1,411	0,583	0,328	0,153	0,370
					0,337	$0,151 \pm 0,015$b	0,297
			Mean $K_{D_{Mg-Fe}}$		$\pm 0,036$	$0,116 \pm 0,012$c	$\pm$ 0,046

a not used in calculation of mean $K_{D_{Mg-Fe}}$

b mean for opx-bearing assemblages

c mean for amphibole-bearing assemblages

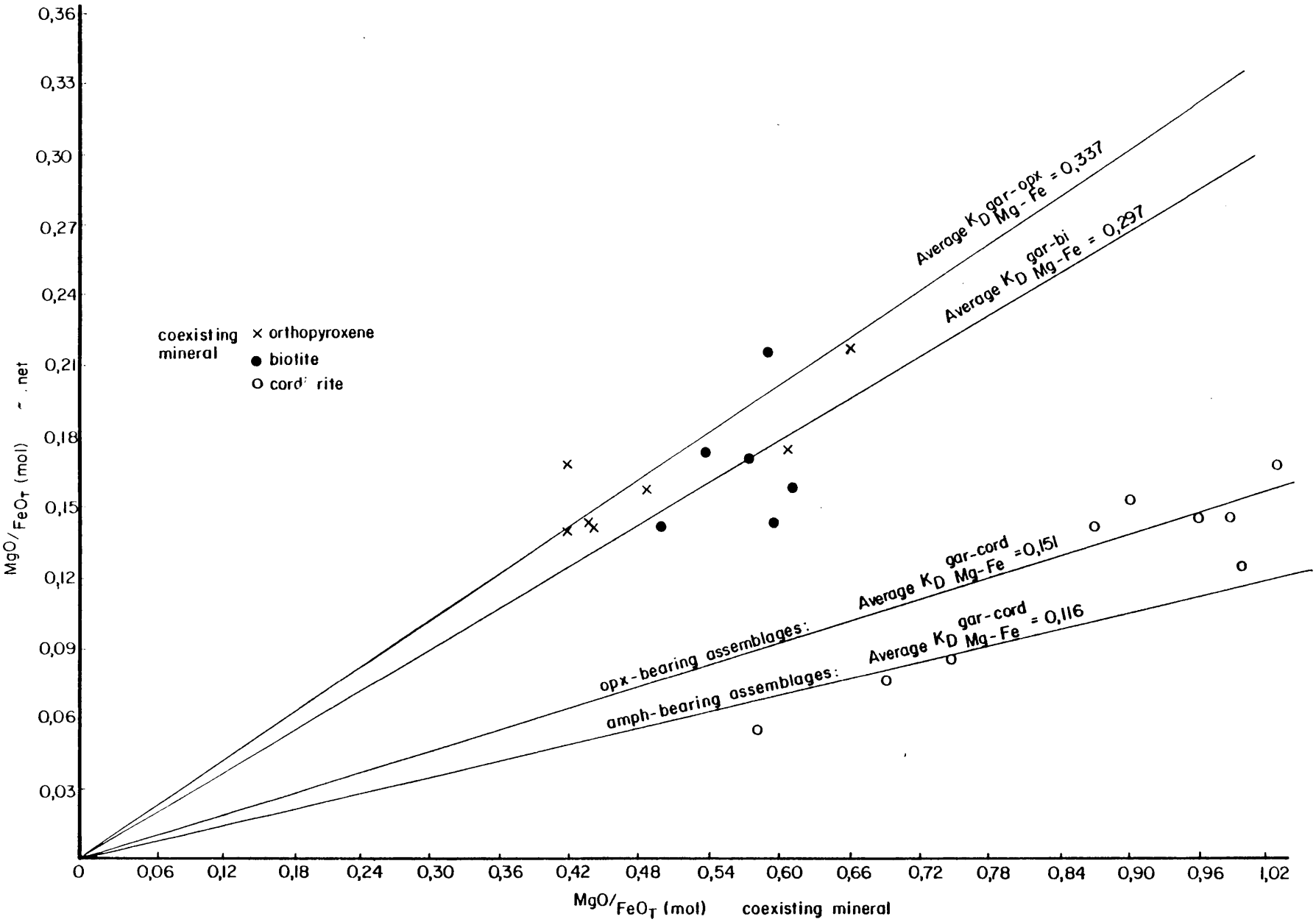

Fig. 60: The distribution of Fe and Mg between garnet and coexisting orthopyroxene, biotite and cordierite

and the number of Ti cations in biotite as well as a negative correlation between $K_{D_{Mg,Fe}}^{gar\text{-}bi}$ and the number of Ca cations in garnet. Rollinson (1981) noted a similar departure from ideality in the Fe, Mg distribution between garnet and biotite. This non-ideality as well as variations in the equilibration temperatures of the samples are responsible for the scatter evident in Figure 60.

The value of $K_{D_{Mg,Fe}}^{gar\text{-}cord}$ is a function of temperature. Distribution curves for amphibole- and orthopyroxene-bearing assemblages are therefore distinguished in Figure 60. The former assemblage equilibrated between 650° and 700° C, while the latter assemblage equilibrated at about 750 °C. The $K_{D\ Mg,Fe}^{gar\text{-}cord}$ values obtained for the two groups are in agreement with values obtained by Kamineni (1975) for gedrite-bearing samples (0,08 to 0,12), and by Holdaway and Lee (1977) for samples that crystallized at between 680° and 760°C (0,156). Various other workers e.g. Berg (1977 a and b) and Hensen (1977) also observed an increase in $K_{D_{Mg,\ Fe}}^{gar\text{-}cord}$ with increasing temperature

7.1.2 The distribution of Mg and Fe between orthopyroxene and coexisting cordierite, spinel and biotite

The Mg, Fe distribution curves, based on the data in Table 12 are presented in Figure 61. The mean $K_{D\ Mg,Fe}^{opx\text{-}sp}$ value, which has been calculated by omitting the samples where orthopyroxene is not in contact with spinel, is higher than the values calculated for four pairs from the Nain Complex using the data of Berg (1977 a). The Mg, Fe distribution coefficient is a function of the MgO/FeO ratios of both orthopyroxene and spinel (Fig. 62) and this non-ideal behaviour is partially responsible for the difference in the distribution coefficient between the Nain and Potgietersrus samples. Both the MgO/FeO ratio of orthopyroxene and spinel have a similar effect on $K_{D\ Mg,Fe}^{opx\text{-}sp}$ with the result

TABLE 12 $K_{D_{Mg-Fe}}$ values for the distribution of Mg and Fe between opx and coexisting cordierite, spinel and biotite

Sample #	$(Mg/Fe)_{opx}$	$(Mg/Fe)_{cord}$	$(Mg/Fe)_{sp}$	$(Mg/Fe)_{bi}$	$K_{D_{Mg-Fe}}^{opx-cord}$	$K_{D_{Mg-Fe}}^{opx-sp}$	$K_{D_{Mg,Fe}}^{opx-bi}$
PH - 170	0,489	1,272		0,615	0,384		0,795
PH - 176	0,446	0,876		0,514	0,509		0,868
PH - 177	0,952	2,195		1,343	0,434		0,709
PH - 178	0,777	1,665			0,467		
PH - 188	0,416	0,96		0,840	0,433		0,495 a
PH - 191	0,961	2,119		1,206	0,454		0,797
PH - 195	1,168	2,566	0,271	1,198	0,455	4,310 a	0,975
PH - 196	0,416	0,845			0,492		
PH - 197	0,377	0,760		0,414	0,496		0,911
PH - 199	2,228	5,106	0,982	2,319	0,463	2,269 a	0,961
PH - 201	0,925	2,052	0,224		0,451	4,129	
PH - 202	1,007	2,379	0,352		0,423	2,860	
PH - 203	0,851	1,716	0,281		0,495	3,028	
PH - 204	1,428	3,405	0,484		0,419	2,950	
PH - 206	0,866	1,878	0,250		0,461	3,464	
PH - 208	2,195	5,808	0,868		0,378	2,53 a	
PH - 209	0,730	1,412	0,146		0,517	5,000	
PH - 212	0,765	1,744	0,213		0,439	3,59	
PH - 214	2,454	5,256	1,027		0,467	2,389	

TABLE 12 (Continued)

Sample #	$(Mg/Fe)_{opx}$	$(Mg/Fe)_{cord}$	$(Mg/Fe)_{sp}$	$(Mg/Fe)_{bi}$	$K_{D_{Mg-Fe}}^{opx-cord}$	$K_{D_{Mg-Fe}}^{opx-sp}$	$K_{D_{Mg-Fe}}^{opx-bi}$
PH - 215	2,857	7,015	1,516		0,407	1,885	
PH - 219	0,859	1,630	0,296		0,527	2,902	
PH - 321	0,611	1,394		0,538	0,438		1,136 a
PH - 324	0,397	0,814		0,574	0,488		0,692
PH - 325	0,444	0,986		0,591	0,450		0,751
PH - 326	0,437	0,872		0,499	0,501		0,876
PH - 328	0,377	0,760		0,414	0,496		0,911
PH - 330	0,659	1,411		0,583	0,467		1,130 a
			Mean $K_{D_{Mg-Fe}}$		0,462 ± 0,039	3,215 ± 0,882	0,844 ± 0,098

a not used in calculation of mean $K_{D_{Mg-Fe}}$

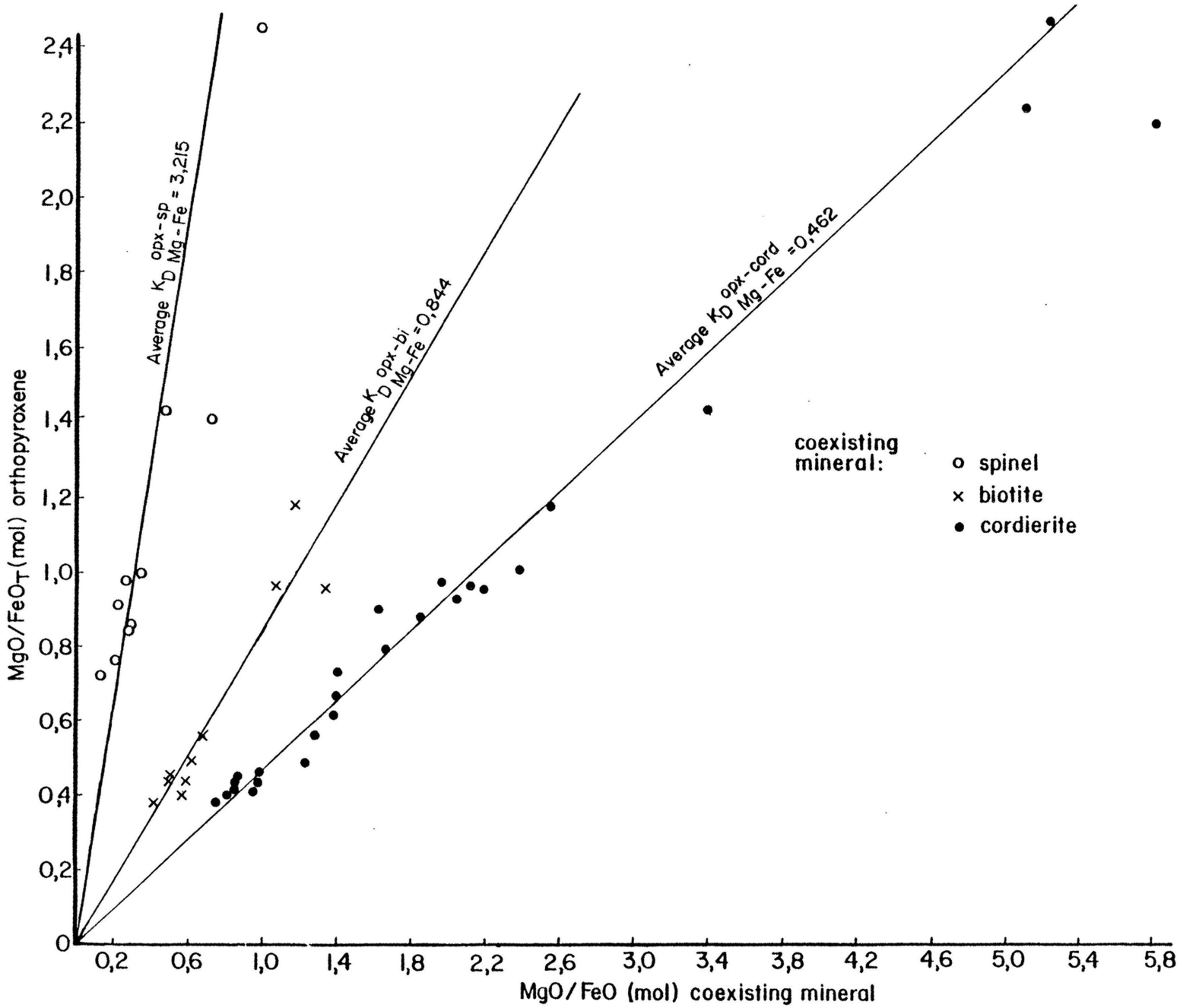

Fig. 61: The distribution of Fe and Mg between orthopyroxene and coexisting spinel, biotite and cordierite

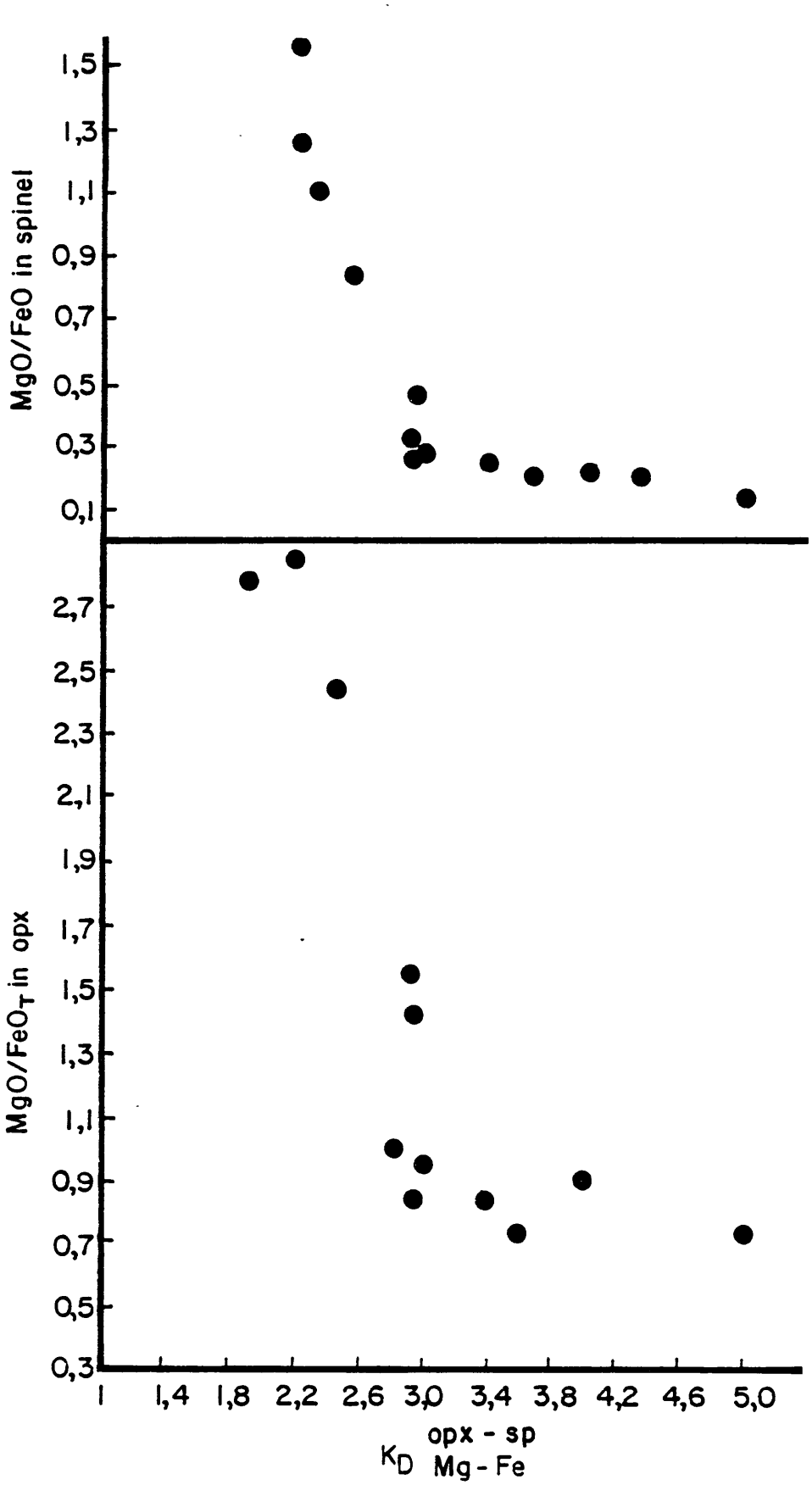

Fig. 62: $K_{D_{Mg-Fe}}^{opx-sp}$ as a function of the MgO/FeO ratios of spinel and orthopyroxene

that the K_D is very sensitive to changes in the compositions of the phases.

The scatter around the mean $K_{DMg,Fe}^{opx-bi}$ value of 0,844 may be due to differences in the equilibration temperatures of the samples or to non-ideal distribution of Mg and Fe between orthopyroxene and biotite, since there appears to be a positive correlation between $K_{D\ Mg,Fe}^{opx-bi}$ and the number of Ti cations in biotite.

There is little scatter around the mean $K_{D\ Mg,Fe}^{opx-cord}$ value of 0,462 which is lower than the mean of values reported by Hensen and Green (1972)(0,59 to 0,43) and that of Holdaway (1976)(0,70).

7.1.3 The distribution of Mg and Fe between amphibole (gedrite, anthophyllite and cummingtonite) and coexisting garnet, biotite and cordierite

The calculated Mg, Fe distribution coefficients are presented in Table 13 and illustrated in Figure 63. The $K_{D_{Mg,Fe}}^{cord-ged}$ and $K_{D_{Mg,Fe}}^{cord-anth}$ values show considerable scatter around the respective mean values of 2,489 and 2,04. Various workers found a wide range of distribution coefficients and values as low as 2,3 (Lal and Moorhouse, 1969) and as high as 4,08 (Sharma and MacRae, 1981) were reported. There appears to be a positive correlation between $K_{D_{Mg,Fe}}^{cord-amph}$ and the number of Al^{vi} cations in the amphibole which is the result of the Tschermaks substitution where Al^{vi} as well as Mg^{2+} partition strongly into the small M2 site in amphibole. A high Al^{vi} occupation causes the MgO/FeO ratio in the amphibole to be lower compared to the low Al amphiboles, and the $K_{D_{Mg,Fe}}^{cord-amph}$ value therefore increases. Since all the cordierite + amphibole-bearing assemblages crystallized over a small temperature interval this non-ideal Mg,Fe distribution may be responsible for the observed scatter in the distribution coefficient.

TABLE 13 $K_{D_{Mg-Fe}}$ values for the distribution of Mg and Fe between amphibole and coexisting cordierite, biotite and garnet

Sample #	$(Mg/Fe)_{ged}$	$(Mg/Fe)_{anth}$	$(Mg/Fe)_{cumm}$	$(Mg/Fe)_{cord}$	$(Mg/Fe)_{bi}$	$(Mg/Fe)_{gar}$	$K_{D_{Mg-Fe}}^{cord-ged}$	$K_{D_{Mg-Fe}}^{cord-anth}$	$K_{D_{Mg-Fe}}^{bi-ged}$	$K_{D_{Mg-Fe}}^{bi-anth}$	$K_{D_{Mg-Fe}}^{gar-ged}$	$K_{D_{Mg-Fe}}^{gar-cumm}$
PH - 8		0,650		1,238	0,562			1,905		0,865		
PH - 21		1,310		2,674	1,468			2,041		1,121		
PH - 116	0,249			0,587		0,057	2,357				0,229	
PH - 151	0,297			0,690		0,078	2,323				0,263	
PH - 152	0,367			0,748		0,088	2,038				0,240	
PH - 157		1,599		3,670				2,300				
PH - 312			0,649			0,115						0,177
PH - 313			0,687	1,256		0,157		1,828 a				0,229
PH - 320	0,300			0,790	0,439		2,633		1,463			
PH - 321	0,559	0,732		1,394	0,538	0,176	2,494	1,900	0,962	0,735	0,315	
PH - 335	0,220			0,680			3,091					
					Mean $K_{D_{Mg-Fe}}$		2,489	2,040	1,212	0,907	0,262	0,200
							± 0,355	± 0,187	+ 0,354	+ 0,196	+ 0,038	+ 0,037

a This value = $K_{D_{Mg-Fe}}^{cumm-cord}$ and was not included in the calculation of the mean $K_{D_{Mg-Fe}}^{anth-cord}$ value

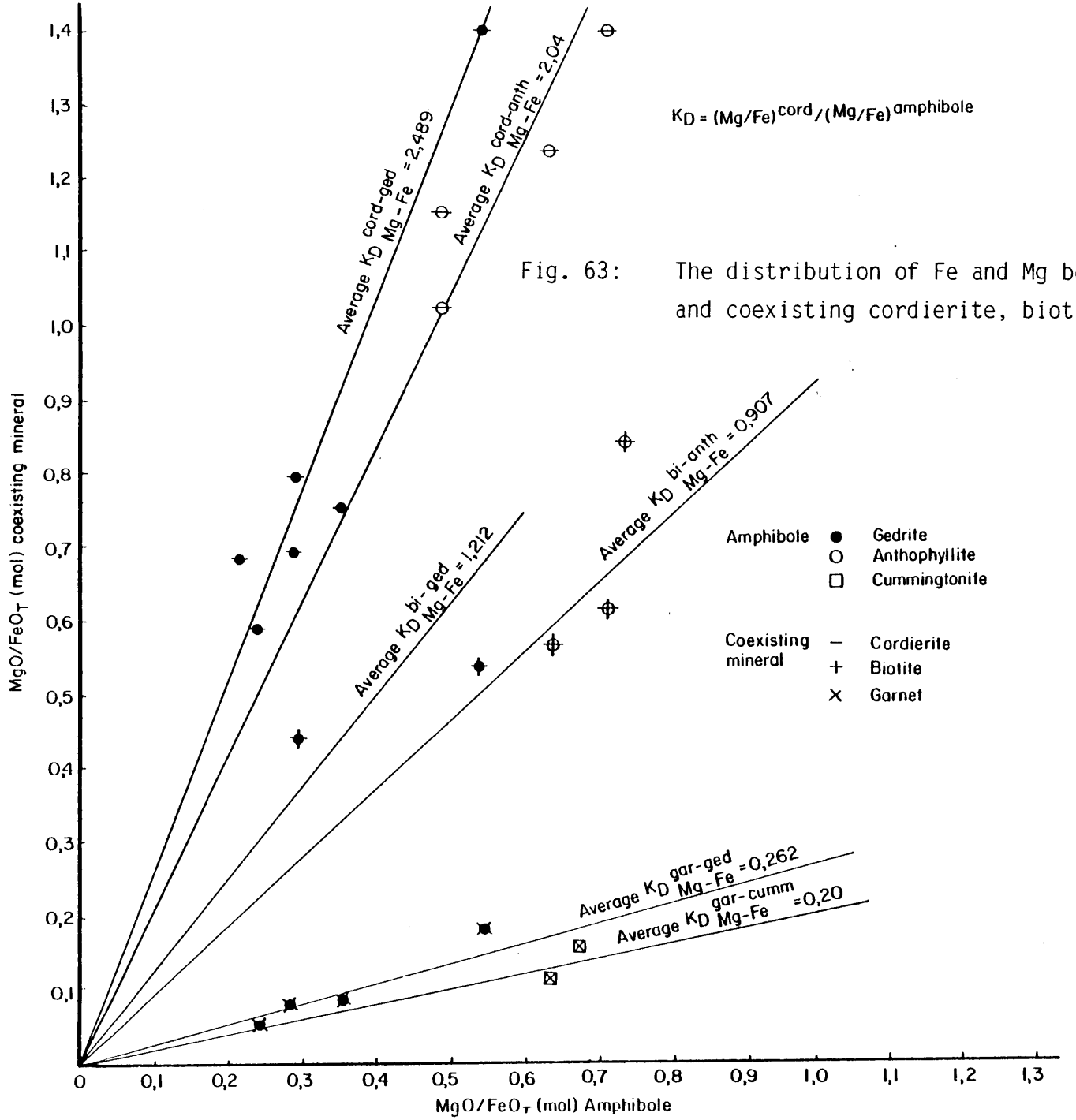

Fig. 63: The distribution of Fe and Mg between the Fe, Mg amphiboles and coexisting cordierite, biotite and garnet

7.1.4 The distribution of Mg and Fe between olivine and coexisting spinel, orthopyroxene and cordierite

The Mg, Fe distribution curves, based on the data in Table 14 are presented in Figure 64. There is very little scatter of data points around the mean $K_{D_{Mg,Fe}}^{ol-sp}$ value of 1,943. Distribution coefficients calculated for more ferruginous rocks from the Nain Complex (Berg, 1977 a) range between 1,75 and 2,45, thereby suggesting a non-ideal Mg,Fe distribution between olivine and spinel. The non-ideality is confirmed by the negative correlation between $K_{D_{Mg-Fe}}^{ol-sp}$ and the MgO/FeO ratios of both olivine and spinel (Fig. 65 A).

The distribution of MgO and FeO between olivine and orthopyroxene shows a large amount of scatter around the mean $K_{D_{Mg,Fe}}^{ol-opx}$ value of 0,5 since this distribution coeffient is, apparently, non-ideal (Fig.65 B). There is thus little significance in the calculated mean $K_{D_{Mg,Fe}}^{ol-opx}$ value and a visual estimate of the change in $K_{D_{Mg,Fe}}^{ol-opx}$ as a function of mineral composition is therefore indicated in Figure 64.

The mean $K_{D_{Mg,Fe}}^{ol-cord}$ value is also of little significance because of the non-ideality of the Mg,Fe distribution between the two phases and a visual estimate of the change in $K_{D_{Mg,Fe}}^{ol-cord}$ is therefore presented in Figure 64. There is, however, also a significant amount of scatter of the data points around this curve, suggesting that the mineral pair may not be in chemical equilibrium. In view of the rarity of the olivine-cordierite assemblage a separate distribution has been compiled by using data from this study, the experimental system of Hsu and Burnham (1969) and the Riekensglück hornfels (Abraham and Schreyer, 1973) (Fig. 66 A). Eyeball estimates of the best fit curves through the data points intersect the lines of ideal $K_{D_{Mg,Fe}}^{cord-ol}$, thereby suggesting non-ideal Mg-Fe distribution between

TABLE 14 $K_{D_{Mg-Fe}}$ values for the distribution of Mg and Fe between olivine and coexisting spinel, opx and cordierite

Sample #	$(Mg/Fe)_{ol}$	$(Mg/Fe)_{sp}$	$(Mg/Fe)_{opx}$	$(Mg/Fe)_{cord}$	$K_{D_{Mg-Fe}}^{ol-sp}$	$K_{D_{Mg-Fe}}^{ol-opx}$	$K_{D_{Mg-Fe}}^{ol-cord}$
PH - 197	0,228		0,561	1,285		0,406	0,177
PH - 202	0,613	0,339	1,007	2,379	1,808	0,609	0,258
PH - 203	0,528	0,281	0,968	1,993	1,879	0,545	0,265
PH - 206	0,512	0,250	0,866	1,878	2,048	0,591	0,273
PH - 209	0,325	0,146	0,73	1,412	2,226	0,445	0,230
PH - 219	0,519	0,296	0,859	1,630	1,753	0,604	0,318
PH - 328	0,127		0,377	0,76		0,337	0,167
					1,943	0,500	0,240
			Mean $K_{D_{Mg-Fe}}$		$\pm$ 0,193	$\pm$ 0,109	$\pm$ 0,054

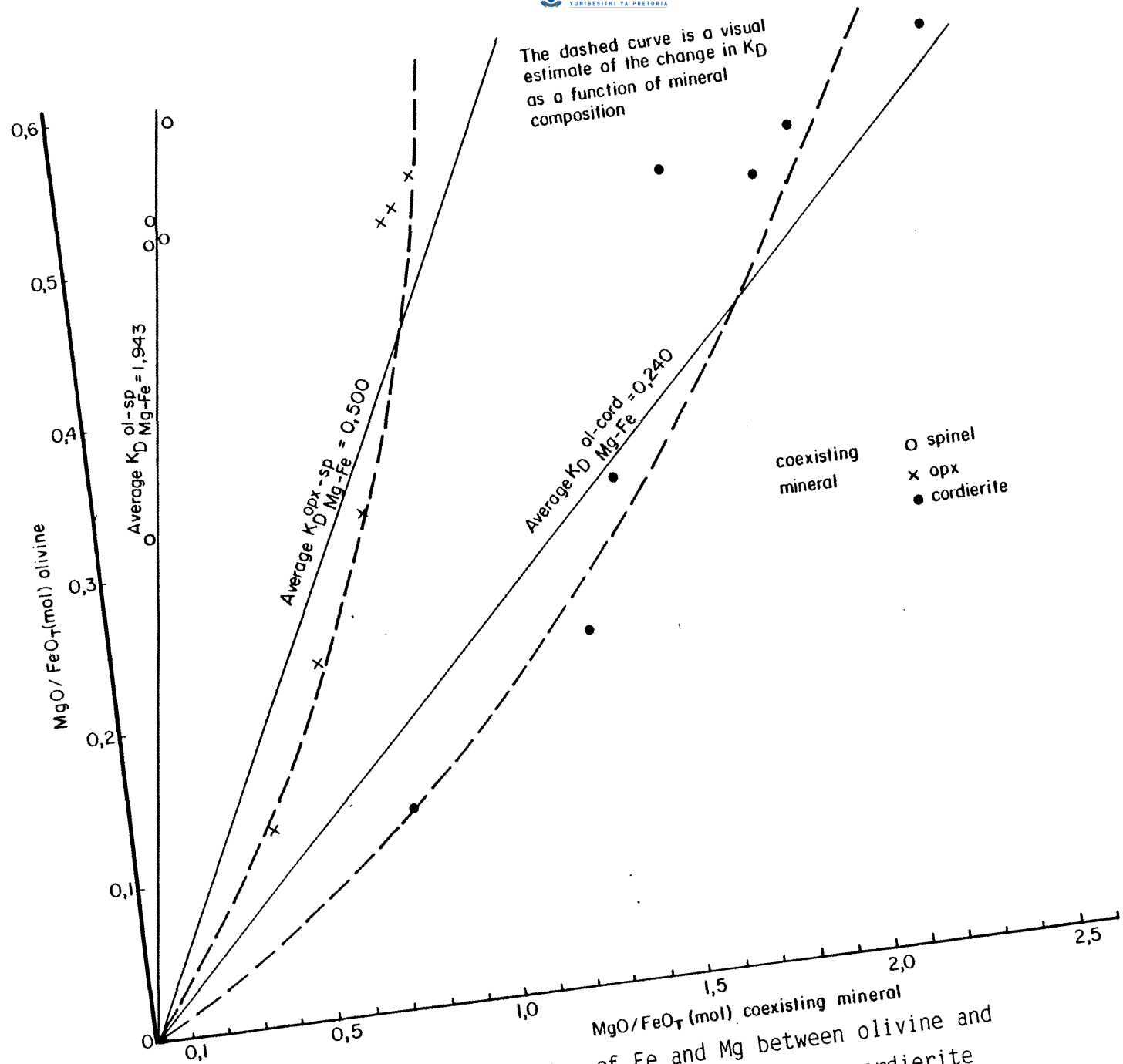

Fig. 64: The distribution of Fe and Mg between olivine and coexisting spinel, orthopyroxene and cordierite

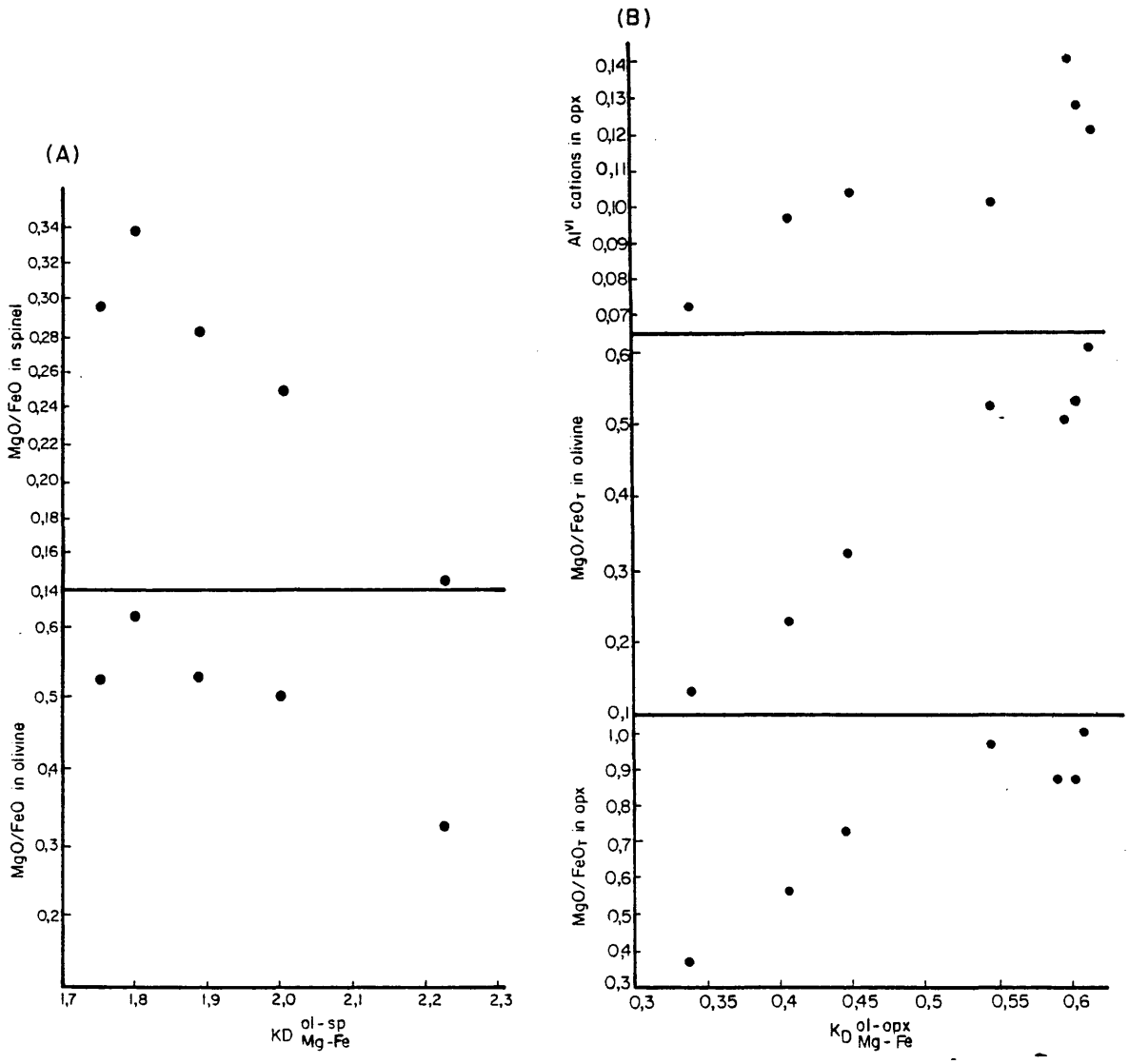

Fig. 65: $K_{D_{Mg-Fe}}^{ol-sp}$ (A) and $K_{D_{Mg-Fe}}^{ol-opx}$ (B) as functions of certain compositional variables in olivine, spinel and orthopyroxene

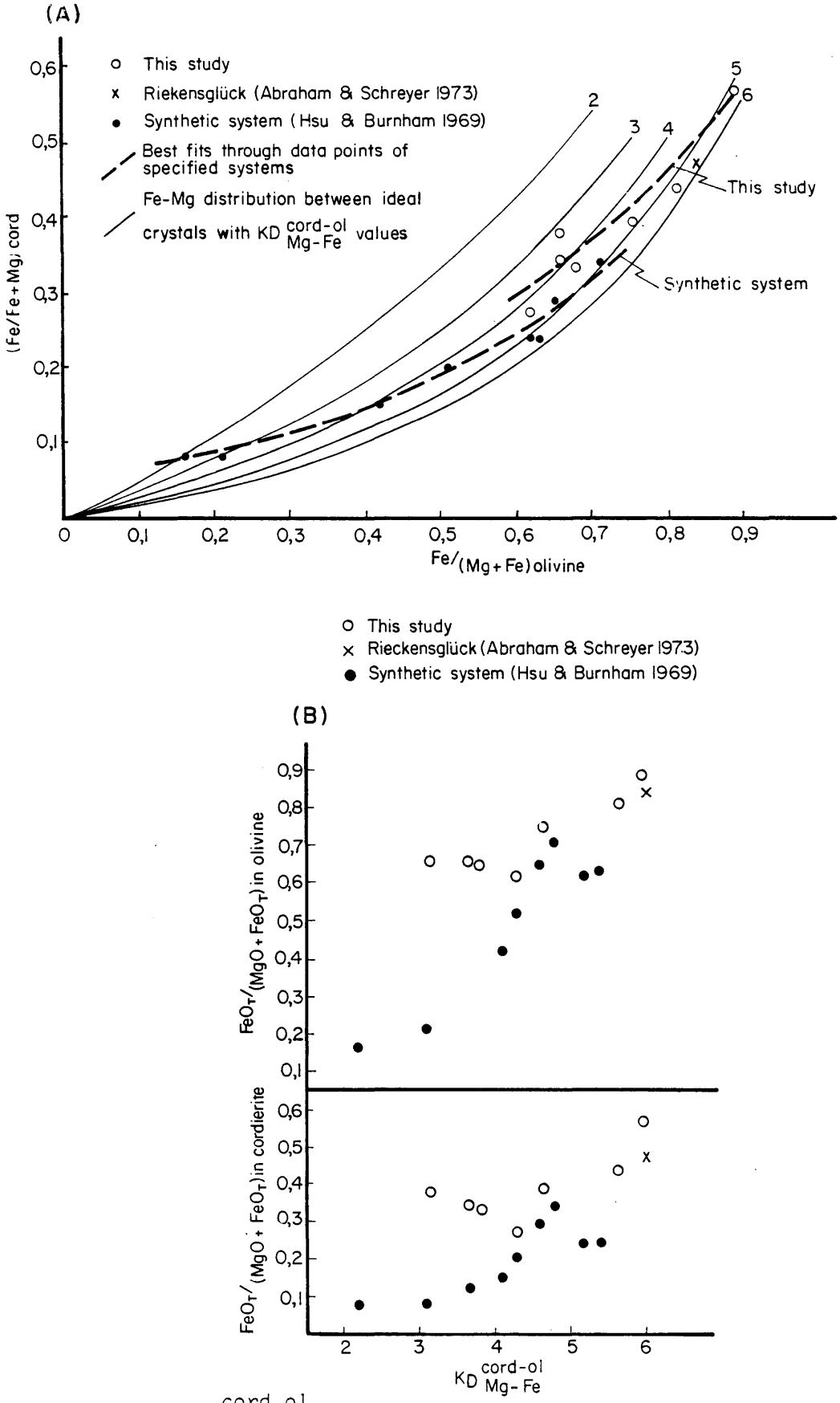

Fig. 66: $K_{D_{Mg-Fe}}^{cord-ol}$ for the synthetic system of Hsu and Burnham (1969) as well as for the data points from the study area (A). The relationship between $K_{D_{Mg-Fe}}^{cord-ol}$ and the mineral composition illustrates the non-ideal distribution of Mg and Fe between olivine and cordierite (B)

olivine and cordierite. The non-ideal element distribution is illustrated in Figure 66 B which reveals a positive correlation between $K_{D_{Mg,Fe}}^{cord-ol}$ and the $FeO_T/(MgO + FeO_T)$ ratios of both olivine and cordierite. Data points from the synthetic system cluster rather tightly around the best fit curve (Fig. 66 A) and also yield a better defined correlation in Figure 66 B. Since the samples from the study area are believed to have crystallized over a relatively small temperature interval the scatter in $K_{D_{Mg,Fe}}^{ol-cord}$ values (Fig. 66 A) is considered to be the result of non-equilibrium between olivine and cordiertie. This conclusion is in agreement with the proposed breakdown of the olivine + cordierite assemblage to spinel and orthopyroxene (Chapter 6).

7.1.5 The distribution of Mg and Fe between cordierite and coexisting spinel and biotite

The Mg, Fe distribution data is summarized in Table 15 and illustrated in Figure 67 A. A large amount of scatter is present in the $K_{D_{Mg,Fe}}^{cord-bi}$ values. No relationship between $K_{D_{Mg,Fe}}^{cord-bi}$ and mineral composition could be detected and the scatter is probably due to differences in the equilibration temperatures of the samples, or to non-equilibrium between cordierite and biotite. The mean $K_{D_{Mg,Fe}}^{cord-bi}$ value for the study area is however, in good agreement with values obtained form the literature e.g. 1,75 to 2,38 (Dallmeyer and Dodd, 1971).

Most data points cluster tightly around the mean $K_{D_{Mg,Fe}}^{cord-sp}$ value of 7,24 (Fig. 67 A). Because of the possible application of this mineral pair to geothermometry the samples from the stydy area are compared with data published by Kars et al. (1980)(Fig. 67 B). Eyeball estimates of the best-fit curves through the data sets in Figure 67 B intersect the lines of constant $K_{D_{Mg,Fe}}^{sp-cord}$ at low Mg/(Mg + Fe) ratios for spinel, suggesting slight non-ideality

TABLE 15 $K_{D_{Mg-Fe}}$ values for the distribution of Mg and Fe between cordierite and coexisting spinel and biotite

Sample #	$(Mg/Fe)_{cord}$	$(Mg/Fe)_{sp}$	$(Mg/Fe)_{bi}$	$K_{D_{Mg-Fe}}^{cord-sp}$	$K_{D_{Mg-Fe}}^{cord-bi}$
PH - 8	1,238		0,562		2,203
PH - 14	3,608		4,428		0,815 a
PH - 16	4,371		4,075		1,073 a
PH - 21	2,674		1,568		1,822
PH - 40	0,528		0,342		1,544
PH - 41	0,869		0,496		1,752
PH - 48	1,309		0,742		1,764
PH - 75	0,509		0,358		1,422
PH - 76	1,170		0,677		1,728
PH - 117	0,338		0,254		1,331
PH - 143	0,391		0,254		1,539
PH - 168	1,394	0,192		7,260	
PH - 169	2,000	0,413		4,843	
PH - 170	1,272		0,615		2,068
PH - 173	1,506	0,288		5,229	
PH - 176	0,876		0,514		1,704
PH - 177	2,195		1,343		1,634
PH - 183	0,618	0,071		8,704	
PH - 184	1,052	0,163		6,454	

TABLE 15 (Continued)

Sample #	$(Mg/Fe)_{cord}$	$(Mg/Fe)_{sp}$	$(Mg/Fe)_{bi}$	$K_{D_{Mg-Fe}}^{cord-sp}$	$K_{D_{Mg-Fe}}^{cord-bi}$
PH - 188	0,960		0,840		1,143
PH - 191 A	2,319		1,090		2,128
PH - 191 B	2,119		1,206		1,757
PH - 195	2,566	0,271		9,467	
PH - 197	1,285		0,679		1,892
PH - 199	5,106	0,693		7,367	
PH - 201	2,052	0,224		9,161	
PH - 202	2,637	0,352		7,491	
PH - 203	1,993	0,281		7,093	
PH - 204	3,405	0,484		7,035	
PH - 206	1,878	0,250		7,512	
PH - 208	5,808	0,868		6,691	
PH - 209	1,412	0,146		9,671	
PH - 212	1,744	0,213		8,188	
PH - 214	5,410	1,027		5,270	
PH - 215	7,015	1,516		4,627	
PH - 219	1,630	0,296		5,507	
PH - 320	0,790		0,439		1,800
PH - 321	1,394		0,538		2,591
PH - 324	1,029		0,574		1,793
PH - 325	0,986		0,591		1,668

TABLE 15 (Continued)

Sample #	$(Mg/Fe)_{cord}$	$(Mg/Fe)_{sp}$	$(Mg/Fe)_{bi}$	$K_{D_{Mg-Fe}}^{cord-sp}$	$K_{D_{Mg-Fe}}^{cord-bi}$
PH - 326	0,872		0,499		1,747
PH - 328	0,760		0,414		1,836
PH - 330	1,411		0,583		2,420
PH - 334	1,748	0,304		5,750	
		Mean $K_{D_{Mg-Fe}}$		6,373 b	1,824
				± 1,433	± 0,327
				7,314 c	
				± 1,571	

a not used in calculation of mean $K_{D_{Mg-Fe}}$

b $K_{D_{Mg-Fe}}$ for sillimanite ± corundum bearing assemblages

c $K_{D_{Mg-Fe}}$ for opx ± olivine-bearing assemblages

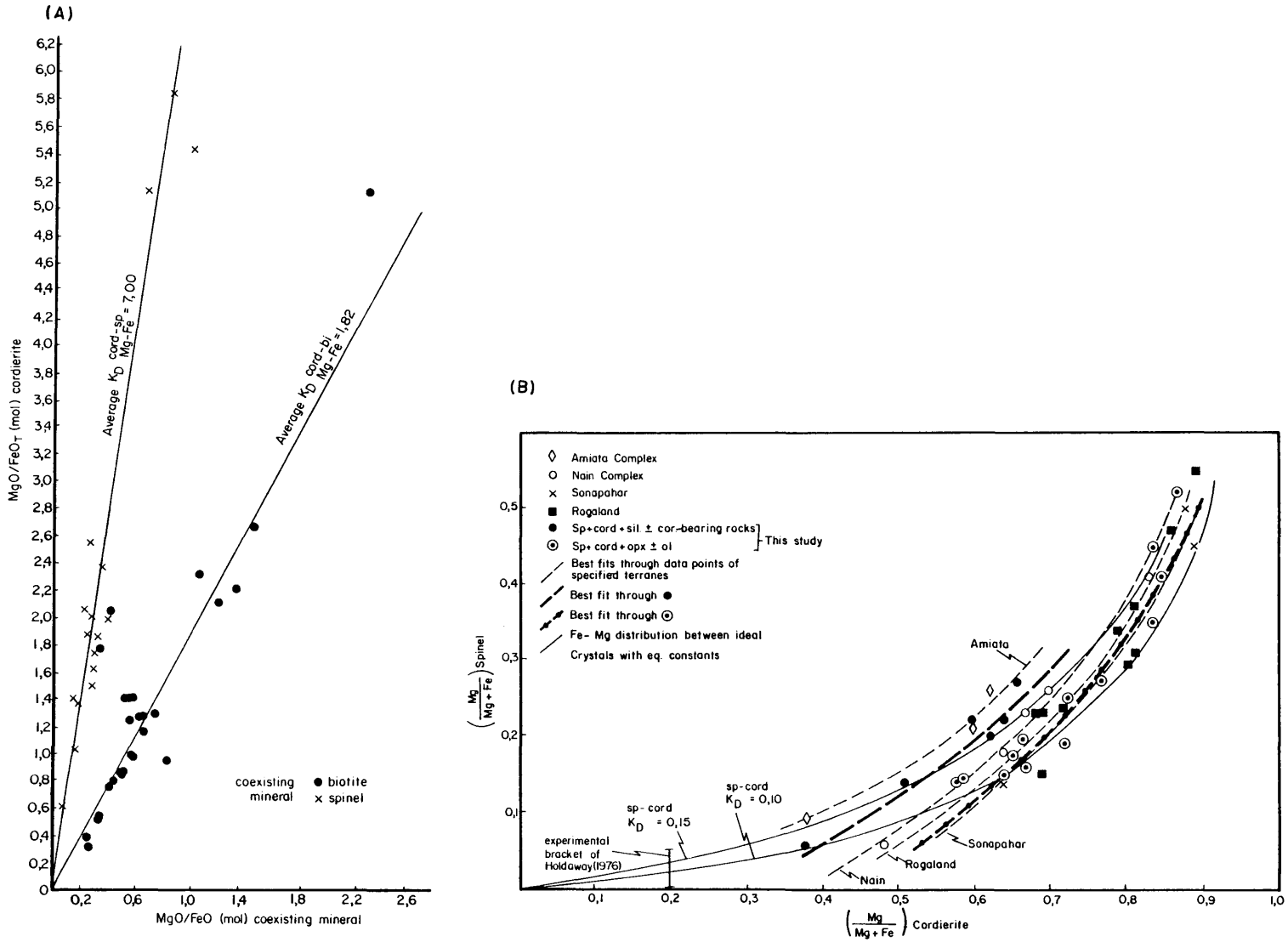

Fig. 67: The distribution of Fe and Mg between cordierite and coexisting biotite and spinel (A). The cordierite-spinel data points from the study area compared to data points cited in the literature (B)

in the system. Figure 67 B further suggests a lower $K_{D_{Mg,Fe}}^{cord-sp}$ value (6,41) for the sillimanite ± corundum-bearing assemblage from the high-grade Timeball Hill Formation than for the orthopyroxene ± olivine-bearing assemblage from the Penge Formation (7,30). This difference is believed to be mainly due to different equilibration temperatures for the two assemblages.

Kars et al. (1980) obtained $K_{D_{Mg,Fe}}^{cord-sp}$ values ranging between 12,50 and 6,67 for granulite facies migmatites with a similar composition to the Potgietersrus samples, that have re-equilibrated at about 700°C from Rogaland, Norway. Berg (1977 a) reported $K_{D_{Mg,Fe}}^{cord-sp}$ values ranging between 14,29 and 6,67 for slightly more ferruginous pelites that are believed to have equilibrated at between 650° and 820°C from the Nain Complex, Labrador. Cordierite-spinel pairs from Sonapahar, India have $K_{D_{Mg,Fe}}^{cord-sp}$ values in the range 7,35 to 11,0 and come from samples that have equilibrated at 600°C under 5 kbar pressure in rocks with a similar composition to the Potgietersrus rocks (Lal et al., 1978). Kars et al. (1980) also reported on cordierite + spinel ± andalusite ± sillimanite ± hypersthene ± biotite-bearing metamorphic xenoliths in acid volcanic rocks from the Amiata Complex, Tuscany, Italy which have equilibrated at about 800°C and 3 kbar pressure. $K_{D_{Mg,Fe}}^{cord-sp}$ values from this locality range between 6,25 and 4,65 with a mean value of 5,43. Little experimental data is available on the value of $K_{D_{Mg,Fe}}^{cord-sp}$ but Holdaway (1976) found mineral compositions in the system SiO_2 - Al_2O_3-MgO-FeO, at 830 °C and 3 kbar pressure, which are compatible with distribution data from natural systems and with the ideal distribution of Fe and Mg between cordierite and spinel (Fig. 67 B).

The intersection of the best-fit curves with the ideal $K_{D_{Mg,Fe}}^{cord-sp}$ lines in Figure 67 B suggests a non-ideal Mg,Fe distribution between cordierite and spinel.

No relationship could, however, be detected in a plot of $K_{D_{Mg,Fe}}^{cord-sp}$ against the possible compositional variables and the crossing of tie-lines are considered to be the result of an unjustified extrapolation of the $K_{D_{Mg,Fe}}^{cord-sp}$ lines for the various localities. It may thus be concluded that the distribution of Mg and Fe between cordierite and spinel is ideal and that $K_{D_{Mg,Fe}}^{cord-sp}$ decreases with increasing temperature.

7.2 Calculation of the physical conditions of metamorphism

For the thermodynamic basis of the derivation of geothermometers and geobarometers the interested reader is referred to Appendix 16.

7.2.1 Geothermometry

7.2.1.1 The garnet-biotite geothermometer

The geothermometer is based on the Mg,Fe exchange reaction:

Fe-garnet + Mg-biotite $\rightleftharpoons$ Mg-garnet + Fe-biotite .....7(5)

Thompson (1976 b) found that $K_{D_{Mg,Fe}}^{bi-gar}$ is relatively independent of pressure and a_{H_2O} but that it is a function of temperature. Using theoretical arguments and temperature estimates from other sources Thompson (1976 b) and Holdaway and Lee (1977) calibrated the linear relationship of ln K_D^{bi-gar} to reciprocal temperature, while Ferry and Spear (1978) conducted cation exchange experiments on synthetic annite-phlogopite micas and almandine-pyrope garnets between 550° and 800°C at 2,07 kbar pressure. Ferry and Spear suggested that the experimentally-derived geothermometer can be applied to natural systems where the biotites and garnets do not deviate significantly from the binary solutions. They also claimed a resolution of about $\pm$ 50° for the geothermometer which corresponds to the error in temperature that results when $\pm$ 0,001 error in Xann, Xphl, Xalm and Xpy are propagated through the various equations.

The amounts of Al^{vi} and Ti in biotite as well as Ca and Mn in garnet are known to affect $K_{D_{Mg,Fe}}^{bi\text{-}gar}$ (Ferry and Spear, 1978). Dallmeyer (1974) discussed possible structural adjustments in garnet and biotite caused by the substitution of other cations for Mg and Fe^{2+}. Because of the substitution of Ti, Al and Fe^{3+} for Mg and Fe^{2+} in biotite the positive charge on the octahedral layer is increased. This excess positive charge is partially compensated for by increased tetrahedral substitution of Al for Si, resulting in an expansion of the tetrahedral layer. Complete charge balance is achieved by having unoccupied octahedral positions. These vacancies together with the smaller size of the substituting cations reduce the dimensions of the octahedral layer. The resultant structural mismatch between the layers may be compensated for if the larger Fe^{2+} cation is preferentially accomodated over Mg in the octahedral position. This also explains why high Al biotites from the study area have low Mg/(Mg + Fe) ratios (Chapter 5). The substitution of Ca and Mn in garnet may likewise cause local structural expansions that may lead to the preferential substitution of Fe^{2+} into the garnet octahedral sites. There may, therefore be a competition between garnet and biotite for Fe^{2+}, causing a non-ideal Fe, Mg distribution between the two minerals.

The Thompson (1976 b), Holdaway and Lee (1977) as well as the Ferry and Spear (1978) equations according to which the garnet-biotite temperatures were calculated (Table 16) assume ideal mixing in the garnet and biotite solid solutions. Although both solid solutions are probably non-ideal, Mueller (1972) concluded that the available data from natural assemblages favours a model for biotite in which a_{Fe} is close to the mole fraction, X_{Fe}^{bi}. Garnet non-ideality increases with increasing grossularite and spessartine components (Ganguly and Kennedy, 1974). Since the garnets from the study area have low Ca and Mn concentrations, it is believed that omitting activity coefficients does not introduce serious errors in the calculated temperatures.

The temperatures calculated from the Ferry and Spear calibration are substantially higher than those obtained from the other two calibrations (Table 16). In addition to the large amount of scatter in the calculated temperatures for every sample, there is also a considerable temperature range between the samples that is not compatible with field relations or with the results of other geothermometers present in those samples.

The scatter in the results obtained from this geothermometer may be due to:

1) The influence of minor elements in garnet and biotite;
2) retrograde equilibration;
3) analytical uncertainty and
4) Disequilibrium between garnet and biotite.

Disequilibrium is also suggested by the scatter in $K_{D_{Mg,Fe}}^{gar\text{-}bi}$ values (section 7.1.1) and by the proposed reaction relationship between the two phases (Chapter 6). It is therefore concluded that this geothermometer does not provide a reliable estimate of metamorphic temperatures in the study area.

7.2.1.2) The garnet-cordierite geothermometer

This geothermometer is based on the Fe,Mg exchange reaction:

Fe-cordierite + Mg-garnet $\rightleftharpoons$ Mg-cordierite + Fe-garnet ..7(6)

Using theoretical considerations and temperature estimates from other sources Thompson (1976 b) as well as Holdaway and Lee (1977) calibrated the linear relationship between ln $K_D^{gar\text{-}cord}$ and reciprocal temperature for garnet-cordierite pairs, while Wells (1976 a) calibrated a geothermometer based on the experimental work of Hensen and Green (1971, 1972). The Fe, Mg distribution between the two phases has been shown to be relatively insensitive to compositional variations although the Ca content of garnet may cause the garnet solid solutic to be non-ideal. The garnets from the study area are, however, low in Ca and Mn and both the garnet and cordierite solid solutions are assumed

TABLE 16 Summary of temperatures calculated according to the garnet biotite geothermometer

Sample	X_{Mg}^{gar}	X_{Mg}^{bi}	A	B			C		
			all P	3kbar	4kbar	5kbar	3kbar	4kbar	5kbar
PH - 170	0,137	0,381	668	674	678	682	727	732	737
PH - 188	0,140	0,456	584	600	603	606	610	613	616
PH - 324	0,143	0,365	711	707	712	717	786	790	764
PH - 325	0,125	0,371	647	658	661	664	700	704	708
PH - 326	0,133	0,333	705	728	731	734	816	821	826

A: Thompson (1976 b) $$T = \frac{2739,7}{1,56 + \ln ({}^{1}/K_D)}$$

B: Holdaway and Lee (1977) $$T = \frac{6150 + 24,6\ P}{3,93 - R\ln K_D}$$

C: Ferry and Spear (1978) $$T = \frac{12454,0 + 57,0\ P}{4,662 - 3\ R\ln K_D}$$

where $$K_D = \frac{(1-X_{Mg}^{bi})\ (X_{Mg}^{gar})}{(X_{Mg}^{bi})\ (1 - X_{Mg}^{gar})}$$

to be ideal in the temperature calculations (Table 17).

The Thompson (1976 b) calibration yielded temperatures that are almost identical to the results of the Wells (1976 a) calibration while the Holdaway and Lee (1977) method gave temperatures that are slightly higher than those obtained from the other calibrations (Table 17).

Sample PH-116 has the lowest equilibration temperature which is in agreement with its locality that is further away from the contact with the Bushveld Complex than the other amphibole-bearing samples (PH - 151, -152 and -313). They were collected within metres of each other and while the two former samples give almost identical equilibration temperatures, the slightly higher value calculated for sample PH - 313 may be due to the higher Ca concentration in its garnets. The amphibole + orthopyroxene-bearing sample (PH - 321) give a temperature bracket of 645° to 660°C.

The temperatures calculated for the orthopyroxene-bearing samples can be evaluated against the degree of recrystallization of the samples and their localities relative to the contact between the Bushveld Complex and the Transvaal Sequence. The temperatures conform to the relative expected temperatures with sample PH - 330 yielding a lower value than sample PH - 170 while the remaining samples equilibrated at slightly higher, but similar temperatures.

On the basis of this geothermometer it may be concluded that amphibole-bearing assemblages equilibrated at between 550° and 630°C while the orthopyroxene - in isograd is situated at about 650°C. The orthopyroxene-bearing assemblages are stable up to about 760°C.

7.2.1.3 The garnet-orthopyroxene geothermometer

Due to the shortcumings of the Mg - Fe exchange garnet-orthopyroxene as geothermometer (Dahl, 1980), Powell

TABLE 17 Summary of temperatures calculated according to the garnet-cordierite geothermometer

Sample	X_{Mg}^{gar}	X_{Mg}^{cord}	A	B		C	
			all P	4kbar	5kbar	4kbar	5kbar
PH - 116	0,054	0,370	570	569	564	584	588
PH - 151	0,075	0,408	612	618	613	629	634
PH - 152	0,078	0,428	625	617	612	627	632
PH - 170	0,141	0,560	642	646	641	654	658
PH - 188	0,140	0,489	712	741	736	737	741
PH - 313	0,130	0,557	643	646	641	653	658
PH - 321	0,150	0,582	645	653	648	660	664
PH - 324	0,143	0,507	735	731	726	729	733
PH - 325	0,125	0,488	691	697	692	700	703
PH - 326	0,135	0,478	737	761	756	754	759
PH - 330	0,178	0,585	710	713	708	712	717

A: Thompson (1976 b) $T = \dfrac{2724,9}{\ln K_D + 0,896}$

B: Wells (1976 a) $T = \dfrac{40261,0 - 176,8\,P}{6\,R\,\ln K_D + 15,88}$

C: Holdaway and Lee (1977) $T = \dfrac{6150,0 + 30,3\,P}{2,69 - R\,\ln (1/K_D)}$

where $K_D = \dfrac{(X_{Mg}^{cord})\,(1 - X_{Mg}^{gar})}{(X_{Mg}^{gar})\,(1 - X_{Mg}^{cord})}$

(1978 a) calibrated the following reaction as a geothermometer:

$^1/_3\ Ca_3Al_2Si_3O_{12} + Mg_2Si_2O_6 \rightleftharpoons {}^1/_3\ Mg_3Al_2Si_3O_{12} + CaMgSi_2O_6$ .....7(7)

Ca and Na are assumed to occupy the M_2 site and Al^{3+}, Ti^{4+} and Cr^{3+} the M_1 site of orthopyroxene. The distribution of Mg and Fe between the M_1 and M_2 sites was further assumed to be ideal. By using experimentally-derived interaction parameters for Ca and Mg in both orthopyroxene and garnet, Powell (1978 a) derived an equation that is believed to be accurate within $\pm$ 75°C at a given pressure (Table 18). The accuracy of the geothermometer is, however, hampered by small amounts of Ca as well as large amounts of Fe in both garnet and orthopyroxene from natural assemblages since the Ca and Mg interaction parameters were derived from experimental work in the CMAS system.

Temperatures calculated from this geothermometer (Table 18) are well within the bracket obtained from the garnet-cordierite geothermometer when the uncertainty of the calibration is considered. The values obtained for sample PH - 330 are, however, believed to be wrong since they are higher than most values obtained from the other, better recrystallized, samples (section 7.2.1.2).

7.2.1.4 The orthopyroxene-clinopyroxene geothermometer

The miscibility gap between diopside and enstatite has been applied by several workers, e.g. Wood and Banno (1973) as well as Wells (1977) as a geothermometer. Both calibrations assume ideal distribution of Mg and Fe between the M_1 and M_2 sites of both orthopyroxene and clinopyroxene, i.e. the activity of $Mg_2Si_2O_6$ in both ortho- and clinopyroxene is equal to $X_{Mg}^{M1} \cdot X_{Mg}^{M2}$. Both equations (Table 19) were derived from experimental work in the Mg-end member system which were then extended into the natural Fe-bearing system. Both calibrations are believed to be accurate within $\pm$ 60°C.

TABLE 18 SUMMARY OF TEMPERATURES CALCULATED ACCORDING TO THE METHOD OF POWEL (1978a)FOR GARNET-ORTHOPYROXENE PAIRS

Sample	$\left(\frac{Ca}{Ca + Mg}\right)^{gar}$	$\left(\frac{Ca}{Ca + Mg}\right)^{opx}$	3kb	4kb	5kb
PH-170	0,183	0,011	654	664	673
PH-188	0,200	0,014	663	673	682
PH-321	0,095	0,004	619	629	637
PH-324	average of 4 values		719	729	739
PH-325	average of 2 values		665	675	685
PH-326	0,146	0,012	693	703	713
PH-330	0,073	0,005	706	716	726

$$T = \frac{7500 + 63 \times P - (2870 + 50 \times P)\,(X_{Mg} - X_{Ca})^{gar} - 1900\,(X_{Fe}^{M_2})^{opx}}{4{,}58 - \ln K_D - 2{,}16\,(X_{Mg} - X_{Ca})^{gar}}$$

where $K_D = \dfrac{(X_{Mg}^{gar})\,(X_{Ca}^{M_2})^{opx}}{(X_{Ca}^{gar})\,(X_{Mg}^{M_2})^{opx}}$

(The distribution of Mg and Fe between the M_1 and M_2 sites in opx is assumed to be ideal)

TABLE 19 Summary of temperatures calculated according to the two-pyroxene method

Sample	A	B	C	
	all P	all P	4kbar	5kbar
PH - 88	818	870	917	918
PH - 181	742	765	887	889
PH - 182	800	850	998	1000

A: Wood and Banno (1973) $T = \dfrac{-10202}{\ln K_D - 7{,}65\,(X_{Fe}^{opx}) + 3{,}88\,(X_{Fe}^{opx})^2 - 4{,}6}$

B: Wells (1977) $T = \dfrac{7341}{3{,}355 + 2{,}44\,(X_{Fe}^{opx}) - \ln K_D}$

where $K_D = a^{cpx}_{Mg_2Si_2O_6} \;/\; a^{opx}_{Mg_2Si_2O_6}$

C: Powell (1978 a) $-\dfrac{\left[1600 + 80\,P + (X_{Ca}^{M2} - X_{Mg}^{M2})^{cpx}(6670 - 88\,P) - 1900 \cdot (X_{Fe}^{M2})^{opx}\right]}{\ln K_D}$

where $K_D = \dfrac{(X_{Ca}^{M2})^{opx}\,(X_{Mg}^{M2})^{cpx}}{(X_{Mg}^{M2})^{opx}\,(X_{Ca}^{M2})^{cpx}}$

Powell (1978 a) argued that the assumption of ideality in ortho- and clinopyroxene may introduce larger errors than was previously expected and he then introduced the following reaction as a possible geothermometer:

$$CaMgSi_2O_6 + Mg_2Si_2O_6 \rightleftharpoons CaMgSi_2O_6 + Mg_2Si_2O_6 \quad \ldots\ldots 7(8)$$

clinopyroxene orthopyroxene orthopyroxene clinopyroxene

The geothermometer was calibrated against experimental data in the CMAS system that was extended into natural multi component pyroxenes using rather limited published data. A regular solution model was adopted for the pyroxene M_2 site, and an accuracy of about $\pm$ 75°C is suspected.

The Powell (1978 a) method yields values that are significantly higher than those calculated by way of the two other methods when applied to two pyroxene pairs from the study area (Table 19). The calculated temperatures show a large amount of scatter and are also higher than the temperatures obtained from geothermometers in pelitic rocks collected in close proximity to the localities of the two pyroxene-bearing samples. It is concluded that this geothermometer has a limited application in the study area, especially in the light of its unreliability at temperatures lower than 900°C (J.M. Ferry, pers. comm).

7.2.1.5 The cordierite-spinel geothermometer

The reaction:

Fe-cordierite + Mg-spinel $\rightleftharpoons$ Mg-cordierite + Fe-spinel ...7(9)

has been calibrated as a geothermometer since it has been shown that $K_{D_{Mg,Fe}}^{cord\text{-}sp}$ is a function of temperature. The Mg, Fe distribution also appears to be ideal (section 7.1.5). No experimental data are available for this mineral pair and the thermodynamic constants of reaction 7(9) were derived from a plot of $RlnK_D$ against $\frac{1}{T} \times 10^4$ for natural mineral pairs (Table 20). A linear regression line calculated through the least squares method has the form (Fig. 68):

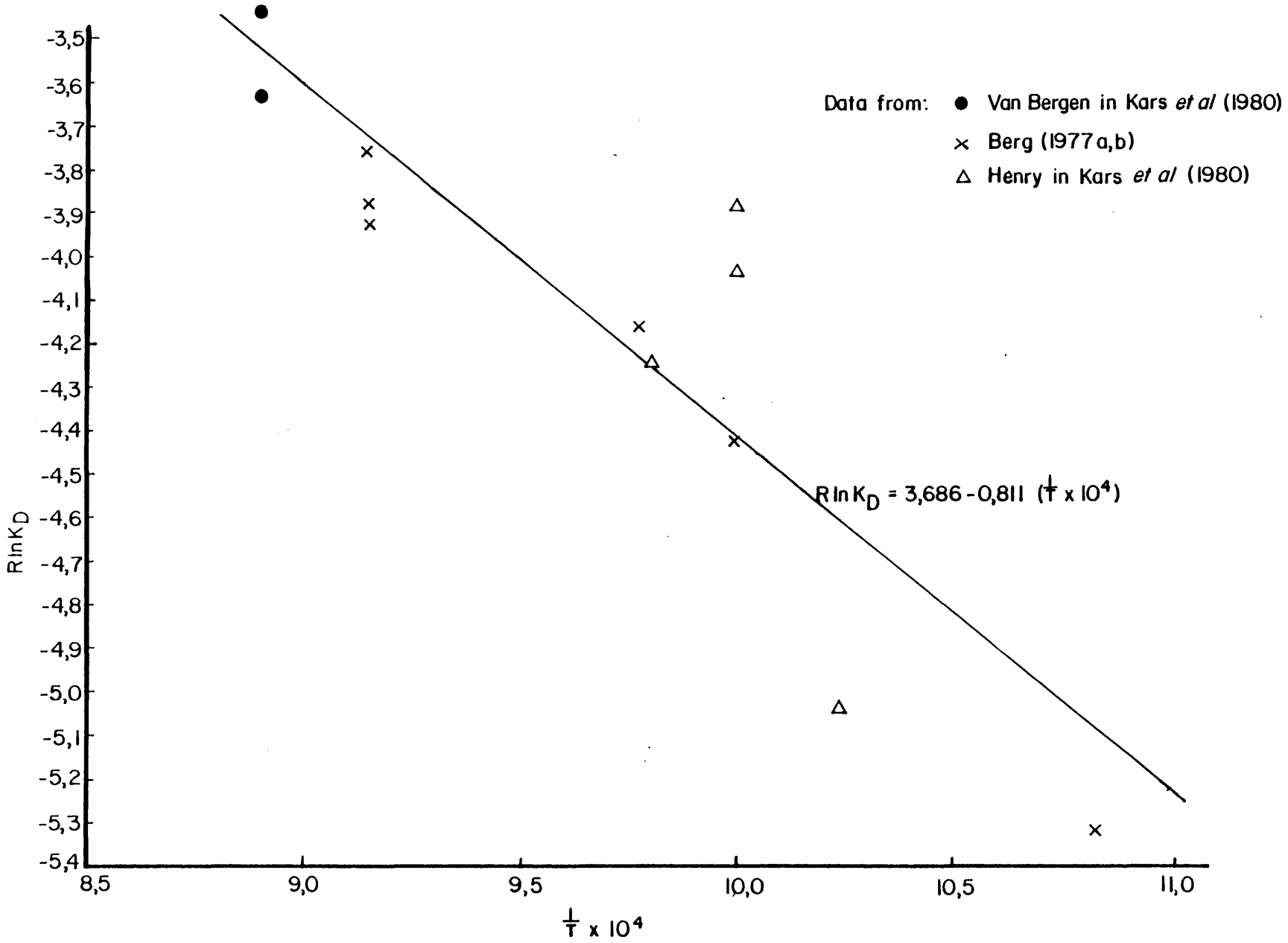

Fig. 68: Plot of $R\ln K_{D_{Mg-Fe}}^{sp-cord}$ vs. $\frac{1}{T}$ for the calibration of the cordierite-spinel geothermometer

TABLE 20 Data used for the calculation of the thermodynamic constants of the cordierite-spinel geothermometer

locality	$\ln K_D$	$\frac{1}{T} \times 10^4$	Data Source
Rogaland	- 2,040	10	Henry in Kars et al. (1980)
	- 1,959	10	
	- 2,137	9 ,804	
	- 2,538	10,235	
Nain contact	- 1,952	9 ,1491	Berg (1977 a & b)
aureoles	- 1,890	9 ,1491	
	- 1,973	9 ,1491	
	- 2,096	9 ,775	
	- 2,674	10,834	
Amiata	- 1,732	8 ,90	Van Bergen in Kars et al. (1980)
Complex	- 1,826	8 ,90	

$$R\ln K_D = 3{,}686 - 8110\ (\tfrac{1}{T}) \quad \ldots\ldots\ldots\ldots\ldots\ldots 7(10)$$

$\Delta S°_{reaction}$ and $\Delta H°_{reaction}$ are therefore equal to 3,686 cal mole^{-1} K^{-1} and 8110 cal mole^{-1} respectively. An expression for the geothermometer was derived (Table 21) in which ideal mixing of the cordierite and spinel solid solutions are assumed. Note that the spinel solid solution will only mix ideally when Cr^{3+} and Fe^{3+} concentrations are low. The accuracy of the geothermometer is difficult to estimate since the thermodynamic constants were derived from natural minerals for which the equilibration temperatures are only approximately known.

Vielzeuf (1983) also calibrated a cordierite-spinel geothermometer against natural data and the results of the two calibrations as applied to the study area are presented in Table 21. Two cordierite + spinel-bearing assemblages are distinguished. The first contains sillimanite $\pm$ corundum and comes from the high-grade Timeball Hill pelites which have been shown to have undergone anatexis under dry, granulite-type conditions. The second assemblage contains orthopyroxene and olivine and come from the largely unaltered Penge Formation shales. The mean temperatures and standard deviations calculated for the two assemblages using my geothermometer are 864° $\pm$ 54°C and 804° $\pm$ 34°C respectively. Vielzeuf's (1983) geothermometer yields 1035 ° $\pm$ 158°C and 902° $\pm$ 155°C respectively. With my geothermometer it is possible to distinguish meaningfully between the two assemblages, while it is not possible with Vielzeuf's geothermometer because the mean temperature of the two assemblages are within $\pm$ 1 standard deviation of each other.

The temperatures calculated from my geothermometer are believed to be geologically more reasonable than those calculated from Vielzeuf (1983) for the following reasons:

1) An equilibration temperature of 864° $\pm$ 54°C for the high-grade Timeball Hill pelites is in

TABLE 21 Spinel-cordierite temperatures calculated for the Potgietersrus area

	Sample #	$(\frac{Mg}{Mg + Fe})_{sp}$	$(\frac{Mg}{Mg + Fe})_{cord}$	A	B
assemblage 1	PH - 168	0,162	0,582	790	825
	PH - 169	0,270	0,668	916	1195
	PH - 173	0,224	0,642	890	1108
	PH - 334	0,234	0,636	860	1013
assemblage 2	PH - 184	0,141	0,512	824	912
	PH - 199	0,410	0,836	785	815
	PH - 202	0,254	0,704	782	805
	PH - 203	0,220	0,665	797	842
	PH - 204	0,326	0,773	800	848
	PH - 206	0,200	0,653	780	803
	PH - 208	0,465	0,853	813	885
	PH - 209	0,159	0,602	764	763
	PH - 214	0,506	0,873	810	1100
	PH - 215	0,571	0,875	888	1255

A: This study $T = \frac{8110}{3,686 - 1,987 \ln K_D}$

B: Vielzeuf (1983) $T = \frac{-1763}{\ln K_D + 0,378}$

where $K_D = \frac{(X_{Mg}^{sp})(1 - X_{Mg}^{cord})}{(X_{Mg}^{cord})(1 - X_{Mg}^{sp})}$

agreement with anatexis under dry conditions ($P_{H_2O} \sim 0,2\ P_{total}$) when the melting curve is situated at about 800°C and has an almost vertical slope in P,T space (Thompson and Tracy, 1979). A temperature of 1035° ± 158°C for these rocks is too high because that is similar to the temperature estimates for the Thorncliffe inclusions in the critical zone of the Bushveld Complex (Hulbert, 1983) where mullite, rather than sillimanite is stable. The Thorncliffe rocks are also more aluminous than the high-grade Timeball Hill pelites (Hulbert, pers. comm.) thereby suggesting that these rocks were melted at rather higher temperatures.

2) An equilibration temperature of 804° ± 34°C for the Penge Formation shales is in agreement with:
   a) the lack of evidence for extensive anatexis if dry granulite-type conditions ($P_{H_2O} \sim 0,2\ P_{total}$) can be assumed;
   b) the equilibration temperature of about 750°C calculated for the low-grade equivalent assemblage (garnet + orthopyroxene + cordierite + biotite).

   The temperature of 902° ± 155°C calculated from Vielzeuf's geothermometer is believed to be too high because it would imply rather extensive anatexis even under completely anhydrous conditions.

Vielzeuf (1983) assumed that the spinel-cordierite pairs from the xenoliths that he examined were in equilibrium with a basaltic magma at a temperature of about 1100°C. He published a $K_{D_{Mg,Fe}}^{cord\text{-}sp}$ value of 5,18 (which was then thought to be the lowest on record), that yielded an equilibration temperature of 1118°C according to his geothermometer. When this $K_{D_{Mg,Fe}}^{cord\text{-}sp}$ is applied to my geothermometer, a temperature of about 900°C is obtained. This study has produced $K_{D_{Mg,Fe}}^{cord\text{-}sp}$ values as low as 4,63 for rocks that could not possibly have equilibrated at temperatures exceeding 1100°C and it must therefore be concluded that his geothermometer overreads metamorphic

temperatures by as much as 200°C at high temperatures (> 900°C). At lower temperatures (~ 800°C) there is, however, a good agreement between my geothermometer and Vielzeuf's (Table 21).

It is concluded that the cordierite-spinel geothermometer derived in this study can distinguish between samples that equilibrated at about 800°C and 860°C respectively and a resolution of about $\pm$ 60°C is probably realistic despite the uncertainty in the thermodynamic constants. The successful application of this geothermometer depends however, on the use of mineral pairs that are in chemical equilibrium only. Spinel compositions in the same rock may vary significantly over short distances due to the refractory nature of spinel and the slow kinetics of the system. In order to assume chemical equilibrium only cordierites and spinels which are in direct contact with one another may be used for temperature calculations.

7.2.2 Geobarometry

7.2.2.1 Stability of the olivine + cordierite + orthopyroxene + spinel assemblage

To my knowledge this is the first description of the assemblage cordierite + olivine + orthopyroxene + spinel although Abraham and Schreyer (1973) described the assemblage olivine + cordierite + spinel from a ferruginous hornfels near Riekensglück, West Germany.

A number of workers have, however, examined the P,T,X_{Mg} relations of the four-phase assemblage experimentally and theoretically. Hensen (1971) as well as Hensen and Green (1972) examined the chemographic relations of the four phases, while Hsu and Burnham (1969) found a stability field for the assemblage at about 800°C in rock compositions more magnesian than 35 mole percent pyrope in an experimental investigation of the system $Fe_3Al_2Si_3O_{12}$ - $Mg_3Al_2Si_3O_{12}$ under 2 kbar water pressure. They also found an increase in the equilibrium temperature of the divariant assemblage with increasing magnesium content of the bulk composition.

In the Fe-free system Schreyer (1976) and Lal and Seifert (1979) found a stability field for the divariant assemblage at a pressure of 3,25 kbar and at temperatures above about 700°C. There is a drastic reduction in the pressure stability of the assemblage with decreasing $Mg/(Mg + Fe_T)$ ratio of the bulk rock and no stability field could be found for the assemblage in compositions more Fe-rich than Mg/(Mg + Fe) = 5. At this composition equilibrium was attained at a pressure of 1,5 kbar and 780°C under quartz-fayalite-magnetite (QFM) buffer conditions (Fig. 69). According to their work, the stability of the assemblage decreases rapidly with increasing oxygen fugacity. Under hematite-magnetite (HM) buffer conditions the assemblage could not be stabilized in compositions with Mg/(Mg + Fe) < 0,85. Frost (1975) predicted an identical behaviour of the system with respect to Mg/(Mg + Fe) ratio and confining pressure and he also noted a strong positive correlation between equilibrium pressure and the aluminium content of spinel. A 20 percent substitution of Fe^{3+} or Cr^{3+} for Al^{3+} in spinel is sufficient to shift equilibrium pressures below 1,8 kbar at a temperature of 730°C in the pure Mg end-member system.

The bulk compositions of the olivine-bearing rocks from the study area are compared with the composition of the experimental system of Lal and Seifert (1979) and the Riekensglück hornfels in Figure 69. The oxygen fugacity in the olivine-bearing rocks was buffered by QFM (quartz occurs as rare thin rims between orthopyroxene and cordierite grains) which is also the buffer employed by Lal and Seifert (1979). The Cr^{3+} and Fe^{3+} concentrations in the spinel (as estimated from stoichiometry) are low and it is probably reasonable to assume that a temperature similar to the 780°C under which Lal and Seifert (1979) performed their experiments, prevailed during the metamorphic event. From Figure 69 it is clear that a cordierite + olivine assemblage could only have been stable in the study area at pressures of about 1,5 kbar. The implication of this will be discussed in a later section.

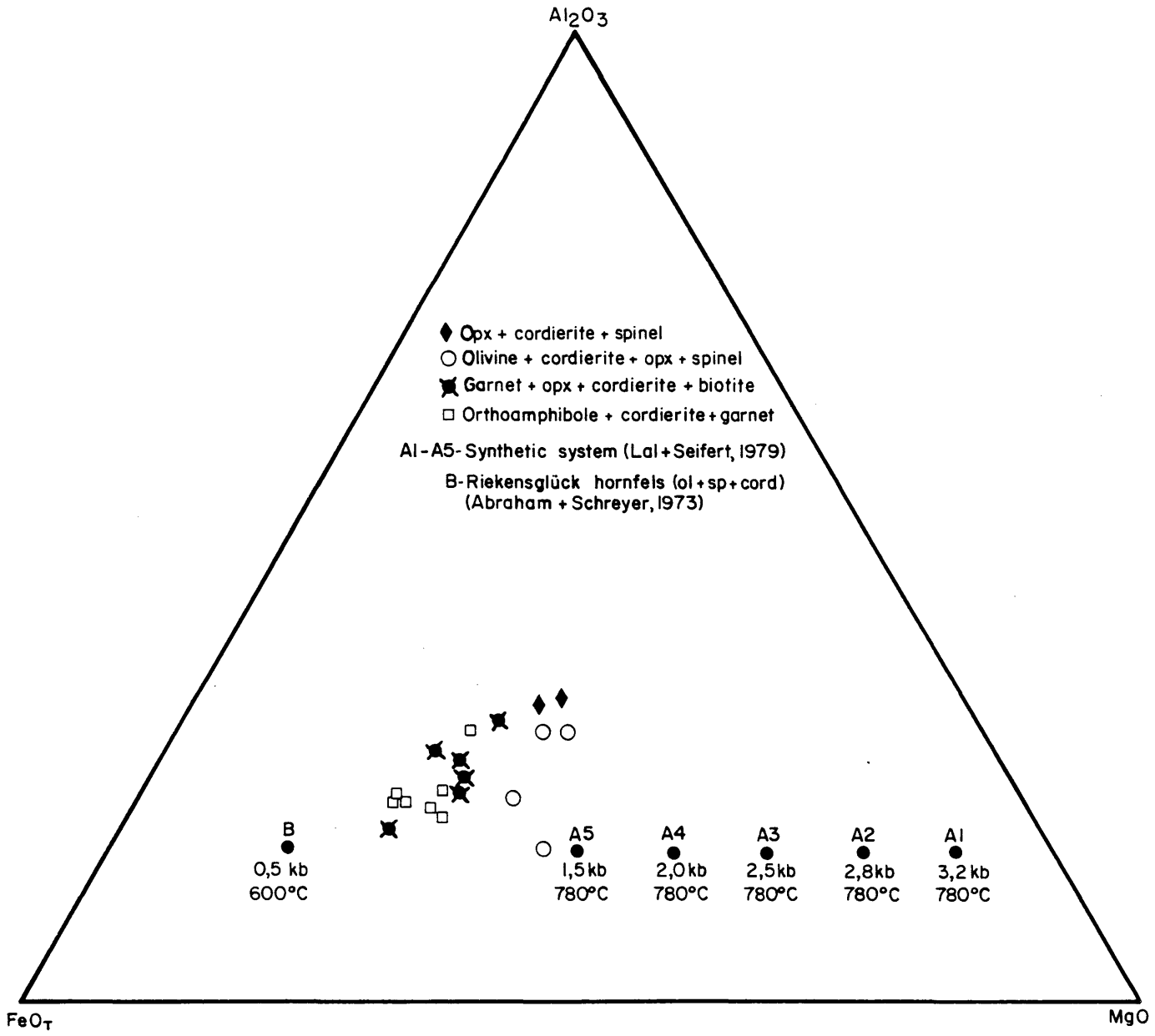

Fig. 69: Plot comparing the compositions of various samples of the shale member of the Penge Formation (including the olivine + cordierite-bearing samples) with the synthetic system of Lal and Seifert (1979) and the Riekensglück hornfels (Abraham and Schreyer, 1973). Equilibration P,T conditions for the synthetic system and the estimated conditions of formation of the Riekensglück sample are also presented

7.2.2.2 The orthopyroxene + olivine + quartz geobarometer

The geobarometer,which is based on the reaction:
ferrosilite ⇌ fayalite + quartz .....7(11)
has recently been investigated by Bohlen and Boettcher (1981) as well as Berg (1977 b). The results of both studies regarding the breakdown of ferrosilite-rich orthopyroxene are in good agreement and a P,T diagram from Berg (1977 b) has been used to estimate equilibration pressures for the study area.

Most orthopyroxene + olivine-bearing samples from the study area contain spinel and no quartz and can therefore not be used to estimate metamorphic conditions. Only one sample (PH - 328) contains the assemblage orthopyroxene(En_{73}) + olivine + quartz + cordierite. Garnet + cordierite and spinel + cordierite pairs in nearby outcrops suggest an equilibration temperature of between 750°C and 800°C for this sample. According to Berg's (1977 b) diagram the equilibrium pressures were 1,5 and 2,0 kbar at the two respective temperatures. These values are in excellent agreement with the estimated equilibrium pressure of about 1,5 kbar at which the cordierite + olivine assemblage was stable in the study area.

7.2.2.3 The reaction: cordierite + orthopyroxene ⇌ garnet + quartz

Hensen and Green (1973) constructed a P,T diagram (Fig. 70), on which the compositions of coexisting cordierite and garnet have been contoured for the divariant reaction. Both the contours for cordierite and garnet have very shallow slopes which gives rise to a high degree of accuracy for the pressure coordinate.

In order to meaningfully evaluate the accuracy of the estimated pressures, some factors that may influence P-T-X_{Mg} relations must be evaluated. First, the accuracy in slope and the position of the contours are limited by uncertainties in the pressure, temperature calibration of the experimental system on which the

contours are based (Hensen and Green, 1972). Towards the low-temperature part of the diagram problems inherent in extrapolating from high temperature results to lower temperatures may also be encountered.

Secondly, high Ca and Mn concentrations in garnet will extend the stability of garnet in the various assemblages (Hensen and Green, 1972). The garnets used in this study have low Ca and Mn concentrations and this factor may, therefore, be disregarded.

Thirdly, the oxygen fugacity may influence P,T relations. Graphite capsules were used in the original experiments and oxygen fugacities were therefore low. Higher oxygen fugacities in natural rocks will result in an increase of the Fe_2O_3 concentration of the system. The Fe_2O_3 may be incorporated into aluminous orthopyroxene, thereby extending the stability field of orthopyroxene (Hensen and Green, 1973). These authors concluded, however, that providing variations in fO_2 do not eliminate either garnet or cordierite in favour of magnetite, the experimentally - derived P,T,X_{Mg} relations will be valid for natural assemblages in the presence or absence of magnetite as an additional phase.

Fourthly, it has been shown that P_{H_2O} significantly influences cordierite stability (Newton and Wood, 1979). These authors examined the influence of the hydration state of cordierite on the Mg,Fe isopleths of coexisting cordierite and garnet for the breakdown of cordierite to garnet, sillimanite and quartz, and concluded that a difference of up to 3 kbar in the calculated pressure exists between the conditions $P_{H_2O} = 0$ and $P_{H_2O} = P_{total}$, with cordierite stable to higher pressures in the latter situation. Hensen and Green (1973), however, quoted a personal communication from Newton that the effect of P_{H_2O} on cordierite stability is non-linear and that the effect of cordierite hydration may only be significant under extremely dry conditions ($P_{H_2O} \rightarrow 0$).

Hensen and Green's (1972) experimental work, in which $P_{H_2O} < P_{tot}$, agrees with Newton's (1972) "wet" cordierite stability suggesting that sufficient water was present in the experimental system to stabilize cordierite to conditions very close to the maximum stability limit under conditions of $P_{H_2O} = P_{total}$. The presence of biotite in the rocks from the study area suggests that conditions were not completely anhydrous and that the data of the experimental system may therefore be applied to the natural rocks.

Fifthly, the influence of biotite on the P,T,X_{Mg} relations must be considered. Hensen (1971) pointed out that the presence of biotite does not affect the divariant equilibrium between garnet, cordierite, orthopyroxene and quartz, although it may change the relative proportions of the phases in divariant equilibrium. One phase, e.g. garnet, may even be completely eliminated through the reaction between garnet and biotite that produces orthopyroxene, cordierite and K-feldspar. The presence of biotite can, however, not change the compositions of the phases in divariant equilibrium since these compositions are unique functions of P and T (Hensen, 1971).

Results obtained from this geobarometer (Table 22) give a mean pressure of 4,3 kbar and a standard deviation of 0,35 kbar. Although Hensen and Green (1973) did not specify the uncertainty in the pressure calculation, it is probably in the order of 0,5 kbar so that it is realistic to assume a pressure bracket of 4 to 5 kbar for the study area.

Garnet, cordierite, orthopyroxene pairs from the study area are compared with similar pairs from other metamorphic terranes in Figure 71, from which it is clear that the Potgietersrus samples are indistinguishable from the Nain samples for which Berg (1977 b) calculated an equilibrium pressure of 4 to 5 kbar. Both Schreyer and

TABLE 22 Summary of pressures calculated for the garnet + cordierite + orthopyroxene + quartz assemblage

Sample	X_{Mg}^{gar}	X_{Mg}^{cord}	Pressure (kbar)
PH - 170	0,140	0,560	4,8
PH - 188	0,129	0,488	4,0
PH - 321	0,150	0,580	4,6
PH - 324	0,145	0,500	4,1
PH - 325	0,125	0,495	4,0
PH - 326	0,135	0,478	4,1
PH - 330	0,178	0,585	4,7

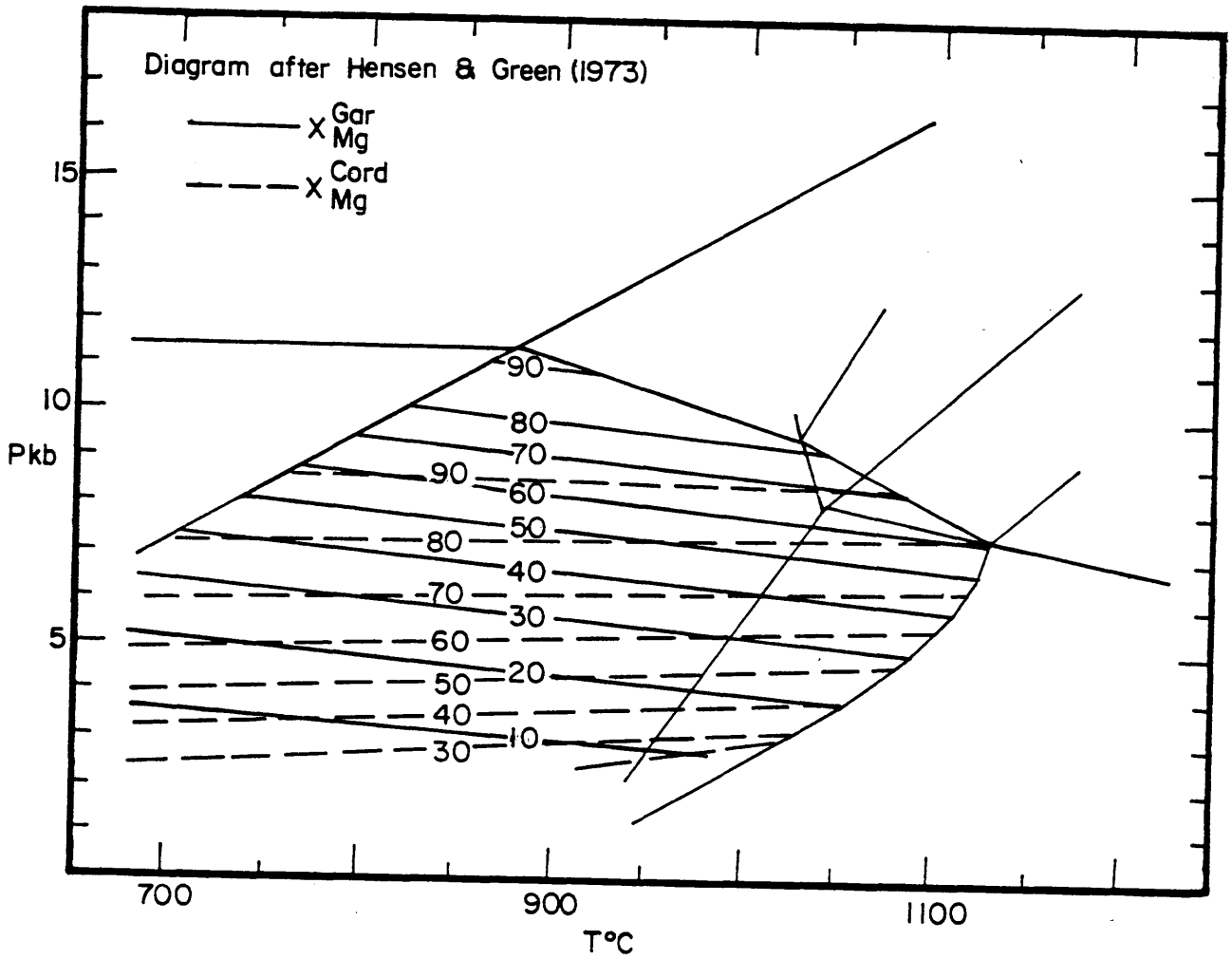

Fig. 70: P,T diagram with X_{cord} and X_{gar} contours for the divariant reaction cordierite + orthopyroxene ⇌ garnet + quartz (Hensen and Green, 1973)

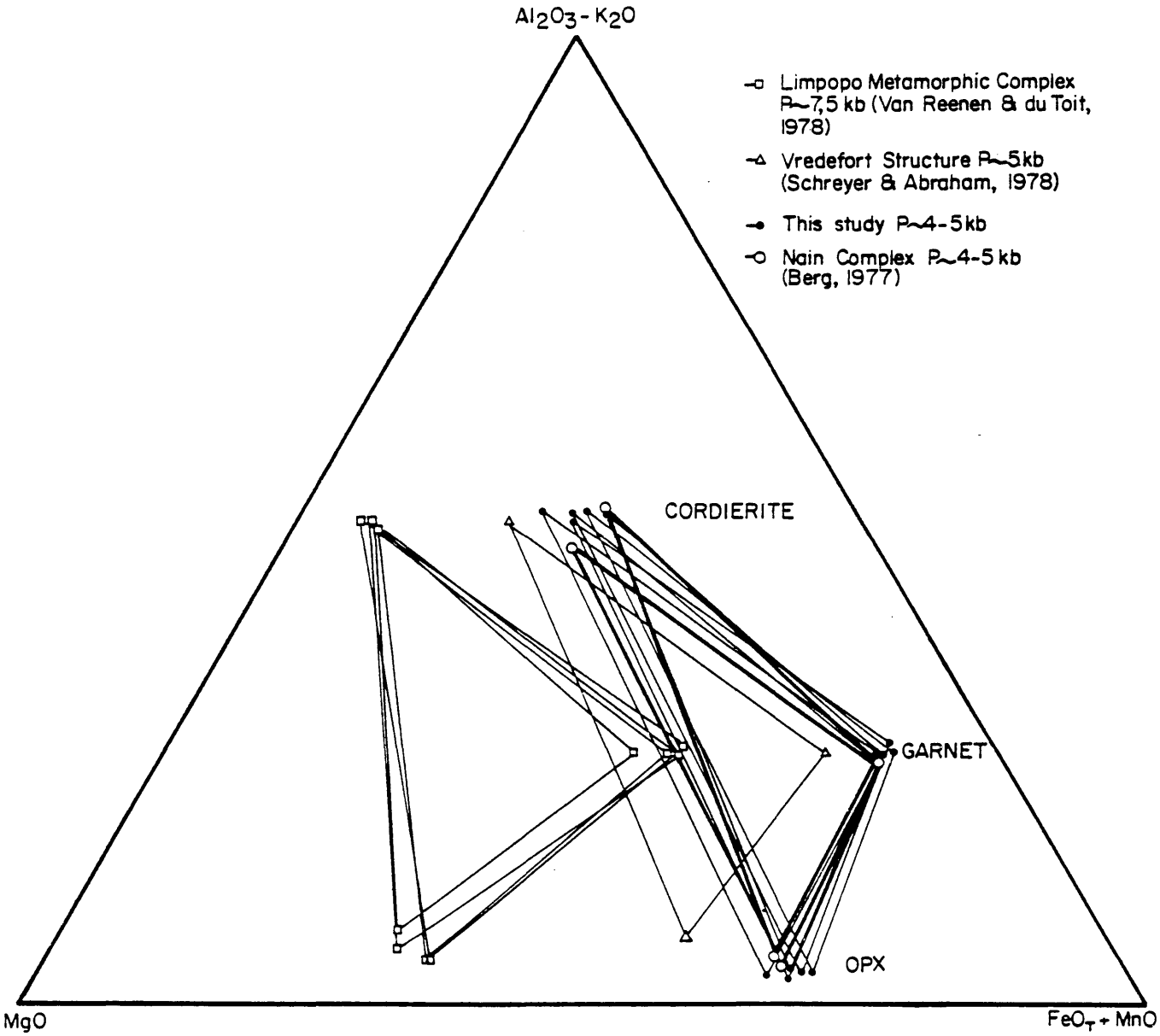

Fig. 71: AFM diagram comparing the compositions of garnet, cordierite and orthopyroxene from various localities, illustrating the Fe-enrichment of those minerals with increasing pressure

Abraham (1978) as well as Berg (1977 b) concluded that this geobarometer is rather trustworthy and a considerable amount of confidence is placed on the pressures calculated from this method.

7.2.2.4 The garnet-orthopyroxene geobarometer

The potential of using the distribution of Al between garnet and orthopyroxene as a geobarometer has first been recognized by Wood (1974) who calibrated a geobarometer based on the reaction:

$Mg_2Si_2O_6 + MgAl_2SiO_6 \rightleftharpoons Mg_3Al_2Si_3O_{12}$ .....7(12)

orthopyroxene Mg-Tschermaks garnet

Wood (1974) assumed that the Tschermaks substitution in orthopyroxene takes place with complete coupling of octahedral and tetrahedral aluminium atoms thereby maintaining local charge balance in the structure. The volume change of reaction 7(12) is a function of the X_{Al}^{M1} in orthopyroxene and is given by:

$$\Delta V_r = -\frac{(X_{Al}^{opx} + 156{,}25)}{20} \times \frac{1}{41{,}84} \quad \text{.....7(13)}$$

where $X_{Al}^{opx} = \frac{Al \times 100}{2(Si + Ti) + 0{,}67(Al + Fe^{3+})}$ .....7(14)

X_{Al}^{M1} is assumed to be equal to Al/2. This is an arbitrary assumption that eliminates the dependence of the quality of the X_{Al}^{M1} value on the accuracy of the Si determination. Unfortuanately the dP/dT of the geobarometer is steep (1 kbar / 20°C)(Table 23) which means that the equilibration temperature must be accurately known before a meaningful pressure value can be obtained.

Finnerty and Boyd (1984) evaluated a number of garnet-orthopyroxene geothermobarometers applied to a suite of garnet lherzolites from Lesotho and concluded that only the MacGregor (1974) geobarometer satisfies all the petrological constraints of the lherzolites, while

TABLE 23 SUMMARY OF PRESSURES CALCULATED ACCORDING TO THE GARNET-ORTHOPYROXENE ASSEMBLAGE. WHERE TWO MINERAL PAIRS IN THE SAME SAMPLE GAVE SIGNIFICANTLY DIFFERENT RESULTS, BOTH PRESSURES ARE PRESENTED (LABELLED A AND B)

Sample	Pressure (kbar) at		
	650°C	700°C	750°C
PH-170	0,8	3,2	5,5
PH-188A	0,6	3,0	5,3
PH-188B	0,0	2,4	4,6
PH-321A	4,6	7,2	9,7
PH-321B	3,8	6,3	9,0
PH-324A	1,6	3,5	5,9
PH-324B	1,1	3,1	5,4
PH-325A	2,4	5,0	7,3
PH-325B	1,5	3,9	6,3
PH-326	0,7	3,0	4,9
PH-330	4,2	6,6	9,1

$$P = \frac{RT}{\Delta V_r} \ln K_D + \frac{(7012 - 3{,}89 \times T)}{\Delta V_r} - 10450\, X_{Fe}^{opx} (1 - 2\, X_{Al}^{M1})$$

where $$K_D = \frac{(X_{Al}^{M1})^{opx} (1 - X_{Al}^{M1})^{opx}}{(X_{Fe}^{gar} + X_{Mg}^{gar})^3 (X_{Al}^{gar})^2}$$

and $$\Delta V_r = \frac{-(X_{Al}^{opx} + 156{,}25)}{20} \times \frac{1}{41{,}84}$$

they consider the Wood (1974) method to be both inaccurate and imprecise. The MacGregor (1974) method as applied by Finnerty and Boyd (1984) gives, however, pressure values that are 8 to 9 kbar higher than the Wood (1974) calibration at 700°C when applied to orthopyroxenes from garnet-bearing samples in the study area, and only the Wood (1974) calibration has therefore been used in the eventual compilation of P,T data.

It is difficult to appreciate the significance of the pressure values calculated from this geobarometer (Table 23) because of the steep slope of the geobarometric curve. It will, however, be shown in a later section that there is a good agreement between the Hensen and Green (1973) geobarometer and this one when a more exact equilibration temperature for each sample is applied.

Despite Finnerty and Boyd's (1984) observations regarding the application of the Wood (1974) and MacGregor (1974) calibrations, it must be concluded that the former method gives far more reliable results in the relatively low pressure Potgietersrus area than the latter method. Despite the success of this geobarometer, caution must still be exercised when it is applied to rocks that differ in composition from the Mg-rich garnet peridotites for which it was initially intended.

7.2.2.5 The Ca-Tschermaks molecule + plagioclase + quartz geobarometer

This geobarometer is based on the pressure stability of the Ca-Tschermaks molecule (CaTs) in clinopyroxene coexisting with plagioclase and quartz:

$$CaAl_2SiO_6 + SiO_2 \rightleftharpoons CaAl_2Si_2O_8 \quad \text{.....7(15)}$$

Ca-Tschermaks quartz anorthite

There are a few problems when this geobarometer is applied to natural mineral assemblages. First, there is no unique way of calculating the mole fraction of

$CaAl_2SiO_6$ in a clinopyroxene. The mole fraction of CaTs depends on the order in which the other molecules are made in the recalculation scheme. Two different methods are followed. In the first method (Powell and Powell, 1974), the Ti in the analysis is assigned to the $CaTiAl_2O_6$ molecule which is based on the Al: Ti ratio of 2 : 1 observed in lavas. Some of the excess Al is then assigned to the jadeite molecule, with the balance of the Al evenly distributed between the tetrahedral and M_1 sites in the CaTs molecule. The recalculation scheme may be summarized as:

cpx analysis → $CaTiAl_2O_6$ → $NaAlSi_2O_6$ → $CaAl_2SiO_6$

It becomes impossible to build the CaTs molecule into this scheme when 2 Ti > Al in the clinopyroxene analysis. The activity of CaTs is given by the amount of Al assigned to jadeite plus the amount of octahedral Al in $CaAl_2SiO_6$ (Powell quoted in Buchanan, 1976). Using this scheme the total amount of Al in the M_1 site is given by:

$$Al^{M1} = {}^1/_2\,(Al-2Ti-Na) + Na \quad \text{.....7(16)}$$

In an alternative recalculation procedure (Wood quoted in Buchanam, 1976) the Ti in clinopyroxene is assigned to the $NaTiAlSiO_6$ molecule with excess Na accomodated in the jadeite molecule. Only the excess Al allocated evenly between the M_1 and tetrahedral sites is, however, now used to obtain the amount of octahedral Al. This recalculation scheme may be summarized as:

cpx analysis → $NaTiAlSiO_6$ → $NaAlSi_2O_6$ → $CaAl_2SiO_6$

with the amount of Al in the M_1 site given by:

$$Al^{M1} = {}^1/_2\,(Al - Na) \quad \text{.....7(17)}$$

In this scheme it will be impossible to build the CaTs molecule when Ti > Na in the original clinopyroxene analysis.

Neither of the two schemes accounts for Fe^{3+} in clinopyroxene. The acmite molecule will cause an increase in the amount of Al in M_1 equal to half the amount of acmite according to the Wood mixing model, while the amount of Al in M_1 will decrease by half the amount of acmite according to the Powell mixing model.

Secondly, the relationship between the mole fraction of CaTs and its activity is not fully understood. Wood (1976) studied the mixing properties of CaTs and showed that in $CaMgSi_2O_6$ - $CaAl_2SiO_6$ solid solutions the activity of CaTs is greater than its mole fraction and in $CaFeSi_2O_6$ - $CaAl_2SiO_6$ solid solutions the activity of CaTs is less than its mole fraction and that the two are approximately equal when the Mg/(Mg + Fe) ratio of clinopyroxene equals 0,6. If $a_{CaTs} \approx X_{CaTs}$ it would indicate considerable short-range Al-Si order in clinopyroxene, similar to what has been observed for $Mg_2Si_2O_6$ - $MgAl_2SiO_6$ orthopyroxenes (Wood, 1979), so that the relationship will be due to near-ideal mixing of ordered units in the clinopyroxene structure. Okamura et al. (1974), however, proved from X-ray crystallographic studies of synthetic CaTs a high degree of Si,Al tetrahedral disorder , while Newton (1976) also showed that there must be a significant positive enthalpy of mixing in CaTs.

Herzberg (1978) discussed clinopyroxene mixing models and concluded that the CaTs molecule is neither completely ordered ($a^{cpx}_{CaTs} = X^{cpx}_{CaTs}$), nor is it completely disordered ($a^{cpx}_{CaTs} = 4.X^{M2}_{Ca} \cdot X^{M1}_{Al} \cdot X^{Tet}_{Al} \cdot X^{Tet}_{Si}$). He therefore proposed two local charge balance models. In the first (charge balance I) Al and Mg mix randomly in M_1, and Al in the tetrahedral site is coupled to its nearest neighbour Al in M_1 in order to preserve local charge balance. The activity expression for this model is:

$$a^{cpx}_{CaTs} = (X^{M2}_{Ca}).(X^{M1}_{Al}). \gamma^{cpx}_{CaAl_2Si0_6} \quad \text{.....7(18)}$$

The second model (charge balance II) assumes that Al and Si are disordered in the tetrahedral sites and that Al in M_1 will be coupled to its nearest neighbour Al in tetrahedral sites in order to maintain local charge balance. The following activity model is then obtained:

$$a^{cpx}_{CaTs} = 4.(X^{M2}_{Ca}).(X^{Tet}_{Al}).(X^{Tet}_{Si}). \gamma^{cpx}_{CaAl_2SiO_6} \quad \text{.....7(19)}$$

Herzberg (1978) then went further to show that the charge balance I model is the most representative of the mixing properties of diopside - enstatite - CaTs solutions.

The pressures were calculated (Table 24) using the method of S. Reed (pers. comm. to M.R. Sharpe, 1980), who adopted the charge balance I model in his calibration. Pyroxene activity coefficients are from Wells (1976 b), who used a regular solution model for γ_{Ca}^{M2} and γ_{Al}^{M1} while plagioclase activity coefficients are from Orville (1972). The expression for the geobarometer as well as the results obtained for three samples are presented in Table 24. Pressures calculated from the Powell mixing model are higher than those calculated from the Wood mixing model, perhaps because of the presence of some acmite in the clinopyroxenes that will increase the Wood mixing model pressures and decrease the Powell mixing model pressures. In the eventual compilation of the P,T data for the study area it will be shown that the pressures calculated from this geobarometer fall in the 4 to 5 kbar range when more exact temperatures are applied, thus yielding results that are in good agreement with the Hensen and Green (1973) and Wood (1974) geobarometers.

7.2.2.6 The spinel + sillimanite + cordierite + corundum geobarometer

Wells and Richardson (1979) calibrated the reaction:

5 sillimanite + 2 spinel $\rightleftharpoons$ 5 corundum + cordierite ...7(20)

as a geobarometer. Sillimanite and corundum are assumed to be pure and they therefore have activities equal to 1, while ideal mixing is assumed for cordierite and spinel, i.e. $a^{cord}_{Fe_2Al_4Si_5O_{18}} = (X^{cord}_{Fe})^2$ and $a^{spinel}_{FeAl_2O_4} = (X^{sp}_{Fe})^2$. An uncertainty of $\pm$ 0,6 kbar is assumed for this geobarometer, while Wells (pers. comm. to L. Hulbert, 1980) warned that when spinel is Cr-rich the assumption of ideal mixing is incorrect.

TABLE 24 Pressures calculated from the CaTs - plagioclase - quartz geobarometer according to the method of S. Reed (see text)

Sample	Powell mixing model Pressure (kbar) at		Wood mixing model Pressure (kbar) at	
	700°C	800°C	700°C	800°C
PH - 88	6,5	5,3	1,5	0,0
PH - 182	7,2	6,2	5,5	4,4
PH - 186	6,0	4,9	4,6	3,4

$$P = \frac{\left[(3{,}97\ T) + 3295 + RT \ln K_D\right]}{349{,}1}$$

where $K_D = \dfrac{(X_{Ca}^{M2})\,(X_{Al}^{M1})\,.\,\gamma_{Ca}^{M2}\,.\,\gamma_{Al}^{M1}\,.}{X_{An}^{plag}\,.\,\gamma_{An}^{plag}}$

and $RT \ln \gamma_{Ca}^{M2} = (X_{Mg}^{M2})^2\,(8416{,}0 - 1{,}7\ T) + (X_{Fe}^{M2})^2\ 1400 + \left[X_{Mg}^{M2}.X_{Fe}^{M2}(9816-1{,}7T)\right]$

and $RT \ln \gamma_{Al}^{M1} = (X_{Mg}^{M1})^2\ 2500 + (X_{Fe}^{M1})^2\ 3000 + (X_{Mg}^{M1})\,(X_{Fe}^{M1})\,(2500 + 3000)$

Only two samples contain this assemblage (Table 25). The geobarometer has an almost horizontal slope, making it insensitive to even large temperature variations. The calculated pressures for both samples are well within the 4 - 5 kbar range obtained from other geobarometers when the uncertainty of 0,6 kbar is considered.

7.2.2.7 The cordierite + spinel + quartz geobarometer

Harris (1981) derived a geobarometer based on the reaction:
cordierite $\rightleftharpoons$ 2 spinel + 5 quartz .....7(21)
Experimental data of Richardson (1968) was used for the calibration. Both cordierite and spinel are assumed to form ideal solid solutions
($a^{spinel}_{FeAl_2O_4} = (X^{sp}_{Fe})^2$ and $a^{cordierite}_{Fe_2Al_4Si_5O_{18}} = (X^{cord}_{Fe})^2$),
while quartz is assumed to be pure SiO_2.

The pressures calculated for the study area (Table 26) show some scatter (up to 2,5 kbar at a given temperature), but when the data are combined with more accurate temperature estimates (section 7.2.3.3) the values conform well with the 4 to 5 kbar bracket obtained from other well established geobarometers.

Many spinel + cordierite-bearing samples from the study area, in particular those from the high-grade Timeball Hill pelites, contain very little or no quartz at all. In the case of the Timeball Hill Formation, it has been suggested that reaction 7 (21) was in fact a melting reaction, in which case the quartz liberated by the reaction was actually SiO_2 contained in a granitic melt. In that case $a^{quartz}_{SiO_2}$ should rather be $a^{melt}_{SiO_2}$, that will be less than 1,0 since other elements, (e.g. alkalis) and water are also present in the granitic melt. If $a^{melt}_{SiO_2}$ is less than 1,0; K_D will also be lower than when quartz accomodates the SiO_2. The decrease in the value of K_D will be pronounced even if $a^{melt}_{SiO_2}$ is only slightly less than unity, because a_{SiO_2} is raised to the fifth power in the formulation of K_D. A silica activity of 0,99

TABLE 25 Pressures calculated from the assemblage cordierite + spinel + corundum + sillimanite according to the method of Wells and Richardson (1979)

Sample	X_{Fe}^{cord}	$X_{Fe^{2+}}^{spinel}$	Pressure (kbar) at	
			800°C	1000°C
PH - 169	0,333	0,707	5,6	5,4
PH - 334	0,377	0,750	5,3	5,0

$$P = 1 + \frac{2814 - 1,95T - T \ln K_D}{0,4084}$$

where $$K_D = \frac{(a^{cord}_{Fe_2Al_4Si_5O_{18}})\ (a^{cor}_{Al_2O_3})^5}{(a^{sp}_{FeAl_2O_4})\ (a^{sill}_{Al_2SiO_5})}$$

TABLE 26 Pressures calculated from the assemblage cordierite + spinel + quartz according to the method of Harris (1981)

Sample	X_{Fe}^{cord}	X_{Fe}^{spinel}	Pressure (kbar) at		
			700°C	800°C	850°C
PH - 168	0,418	0,838	4,0	3,2	2,5
PH - 169	0,332	0,730	4,5	3,7	3,0
PH - 173	0,358	0,776	4,4	3,6	2,9
PH - 199	0,164	0,504	6,0	5,3	4,6
PH - 202	0,275	0,742	5,3	4,6	3,9
PH - 203	0,334	0,780	4,7	4,0	3,3
PH - 204	0,227	0,674	5,8	5,1	4,4
PH - 206	0,340	0,800	4,7	4,0	3,3
PH - 208	0,163	0,535	6,3	5,6	4,9
PH - 209	0,398	0,841	4,2	3,5	2,8
PH - 214	0,160	0,494	6,0	5,3	4,6
PH - 215	0,125	0,429	6,5	5,8	5,1
PH - 334	0,364	0,766	4,2	3,5	2,8

$$P = 1 + \frac{8720 + (\ln K_D - 8{,}18)\,T}{0{,}4446}$$

where $$K_D = \frac{(a_{FeAl_2O_4}^{sp})^2 \; (a_{SiO_2}^{quartz})^5}{(a_{Fe_2Al_4Si_5O_{18}}^{cord})}$$

for example, will cause the value of K_D to be only 95 percent of the value obtained when a_{SiO_2} equals unity. This decrease in the value of K_D will cause a drop of 0,2 kbar in the calculated pressure at a given temperature.

Inspection of Table 26 reveals that all the samples which are believed to have undergone extensive anatexis (PH - 168; - 169; - 173; - 173 and - 334) give pressure values which are noticeably lower than most other samples. It is therefore suggested that the lower pressures calculated for these samples is the result of $a^{melt}_{SiO_2}$ values which were less than unity.

7.2.3 Evaluation of the P,T data for the study area

7.2.3.1 Amphibole-bearing assemblages. (Fig. 72)

Temperatures for these assemblages were calculated with the garnet-cordierite geothermometer. Sample PH - 116 yielded the lowest calculated temperatures in the study area (570° to 585°C at 4 kbar pressure). This is geologically reasonable since the PH - 116 sample locality is more distant from the basal contact with the Bushveld Complex than the other sample localities where temperatures of between 610° and 655°C were calculated. It may thus be concluded that the amphibole + garnet + cordierite-bearing samples in the Potgietersrus area were stable over a temperature interval of 570° to 655°C at about 4 kbar pressure.

7.2.3.2 Garnet + cordierite + orthopyroxene + biotite-bearing assemblages. (Fig. 73)

Several geothermometers and geobarometers may be applied to samples containing this assemblage and P,T boxes were therefore constructed for every sample by calculating mean temperatures from the intersections of the various geothermometer curves with the temperature - independent geobarometer curve of Hensen and Green (1973). Curve G in PH - 188 and curve F in PH - 334, PH - 326 and PH - 170 were, however, not used in the calculation of

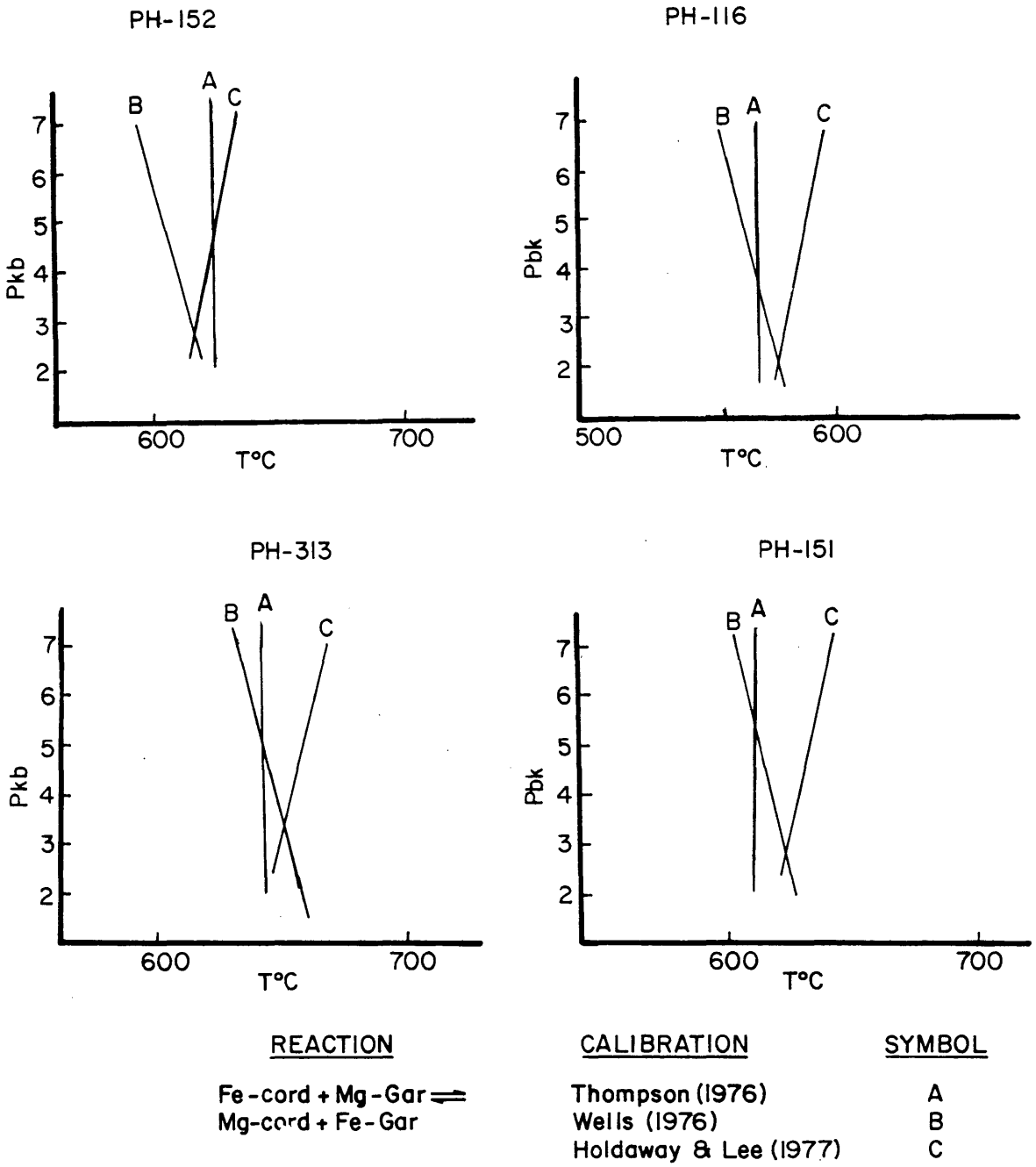

REACTION	CALIBRATION	SYMBOL
Fe-cord + Mg-Gar ⇌ Mg-cord + Fe-Gar	Thompson (1976)	A
	Wells (1976)	B
	Holdaway & Lee (1977)	C

Fig. 72: Temperatures calculated from three calibrations of the garnet-cordierite geothermometer for the amphibole-bearing assemblages from the Potgietersrus area

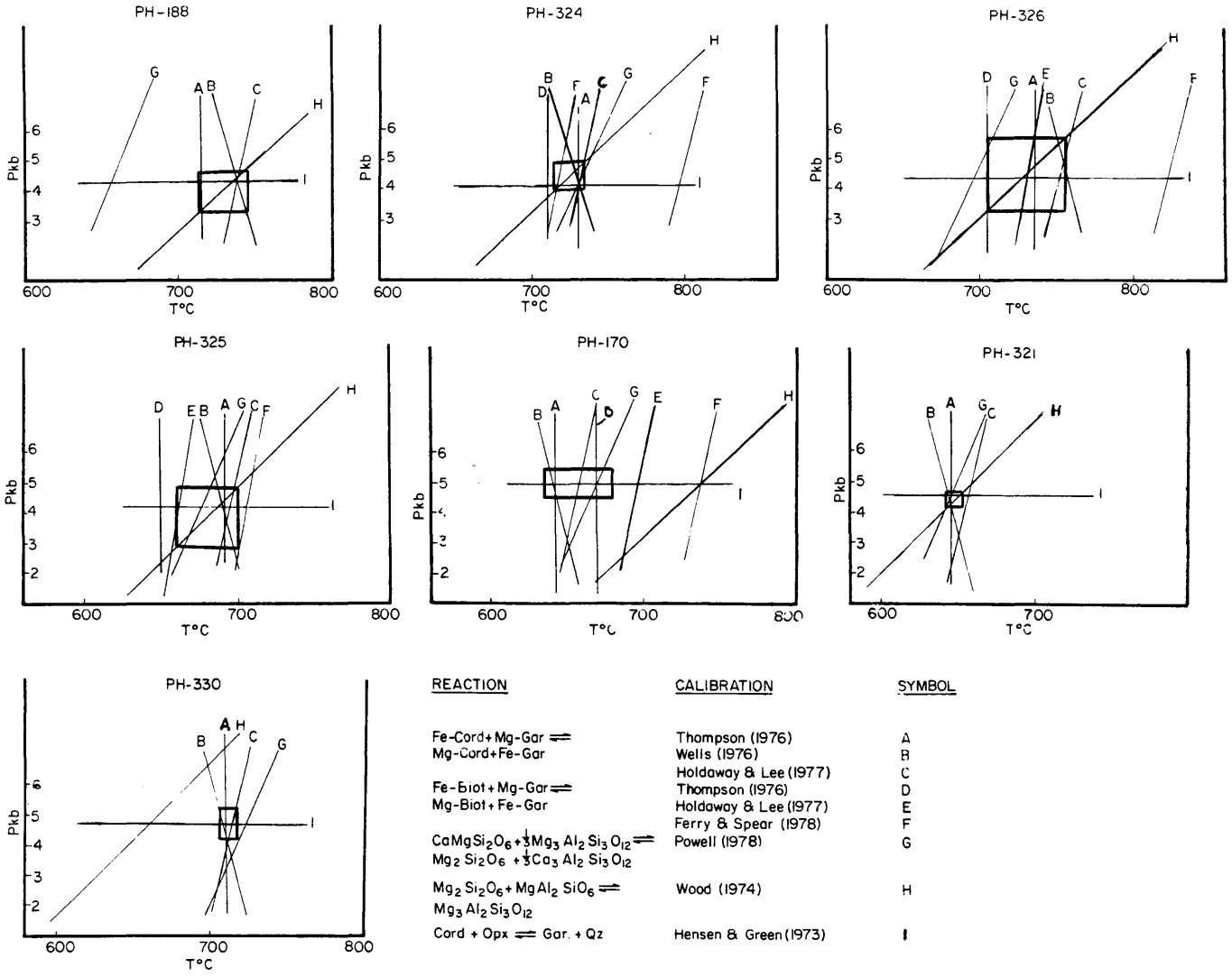

Fig. 73: Compilation of P,T data for the garnet + cordierite + orthopyroxene + biotite assemblage. The construction of the P,T boxes is discussed in the text

mean temperatures because they yield temperatures that are more than two standard deviations away from the calculated mean temperatures at the pressure of curve I (Fig. 73). In 5 of the 7 samples the Wood (1974) geobarometer curve intersects curve I at a temperature that falls within one standard deviation of the mean temperature. For these samples the pressure bracket of the P,T boxes were obtained by reading of the maximum pressure at the mean temperature plus 1σ and the minimum pressure at the mean temperature minus 1σ . For the two remaining samples the pressure bracket is given by the pressure of curve I $\pm$ 0,5 kbar at the mean temperature $\pm$ 1σ .

Sample PH - 321 contains both orthopyroxene and ortho-amphibole and the mean temperature of 647° $\pm$ 5°C is in good agreement with the stability field calculated for the amphibole-bearing assemblages. Sample PH - 330 is relatively poorly recrystallized and contains small xenoblastic orthopyroxene grains. Its locality is also close to that of sample PH - 321. A mean temperature of 713° $\pm$ 6° C is obtained for this sample. Field and textural evidence suggest that the difference in the equilibration temperatures between this sample and PH - 321 should be less tnan 66°C and it is suggested that the temperatures obtained for samples PH - 321 and PH -330 are too low and or too high respectively.

The remaining samples are expected to yield very similar results. Samples PH - 188, PH - 324 and PH - 326, in fact, give respective values of 732° $\pm$ 14°C; 725° $\pm$ 9°C and 730° $\pm$ 24°C while samples PH - 325 and PH - 170 give slightly lower values of 680° $\pm$ 20°C and 660° $\pm$ 20°C respectively. These lower values are probably due to retrograde equilibration.

It may be concluded that this assemblage group crystallized at temperatures ranging between 650° to 700°C near the orthopyroxene- in isograd and at about 750°C near the spinel $\pm$ olivine- in isograd at a pressure of 4 to 5 kbar.

7.2.3.3 Spinel + cordierite-bearing assemblages. (Fig. 74)

Pressure - temperature conditions for the two sillimanite-bearing, corundum-absent assemblages are illustrated in Figure 74 A, while the corundum-bearing samples are presented in Figure 74 B. Pressures calculated according to the Harris (1981) geobarometer are relatively low at the temperatures estimated from the spinel-cordierite geothermometer possibly because of the reduced activity of SiO_2 in the granitic melt, which was presumably present in these samples, relative to the activity of SiO_2 in quartz. The calculated temperatures of the corundum-bearing samples are lower than the mullite stability field (Cameron, 1976), and therefore in agreement with the petrographic observation, while the temperatures calculated from the Vielzeuf (1983) geobarometer (Table 21) fall within the mullite stability field. His geothermometer was therefore not used in the compilation of the P,T conditions of the study area.

The metamorphic conditions for the spinel + orthopyroxene + cordierite assemblage where the former two minerls are not in contact with one another, and where they are in contact, are illustrated in Figures 74 C and D respectively. The P,T coordinates for the samples (heavy dots) are very similar although sample PH - 215 produces a rather higher temperature.

The samples containing the olivine- K-feldspar and spinel-orthopyroxene intergrowths are illustrated in Figure 74 E, while the remaining olivine + spinel-bearing samples are plotted in Figure 74 F. The P,T conditions for the olivine-bearing samples are very similar and also indistinguishable from the olivine-absent, orthopyroxene-bearing samples.

It may be concluded that sillimanite $\pm$ corundum-bearing samples crystallized at 864° $\pm$ 54°C, while sillimanite-absent samples crystallized at 804° $\pm$ 34°C. Equilibrium pressures for the latter samples ranges between 4,0

REACTION	CALIBRATION	SYMBOL
Fe- cord + Mg- sp ⇌ Mg- cord + Fe- sp	This study	(i)
cord ⇌ sp + qz	Harris (1981)	(ii)
cord + cor ⇌ sill + sp	Wells + Richardson (1979)	(iii)

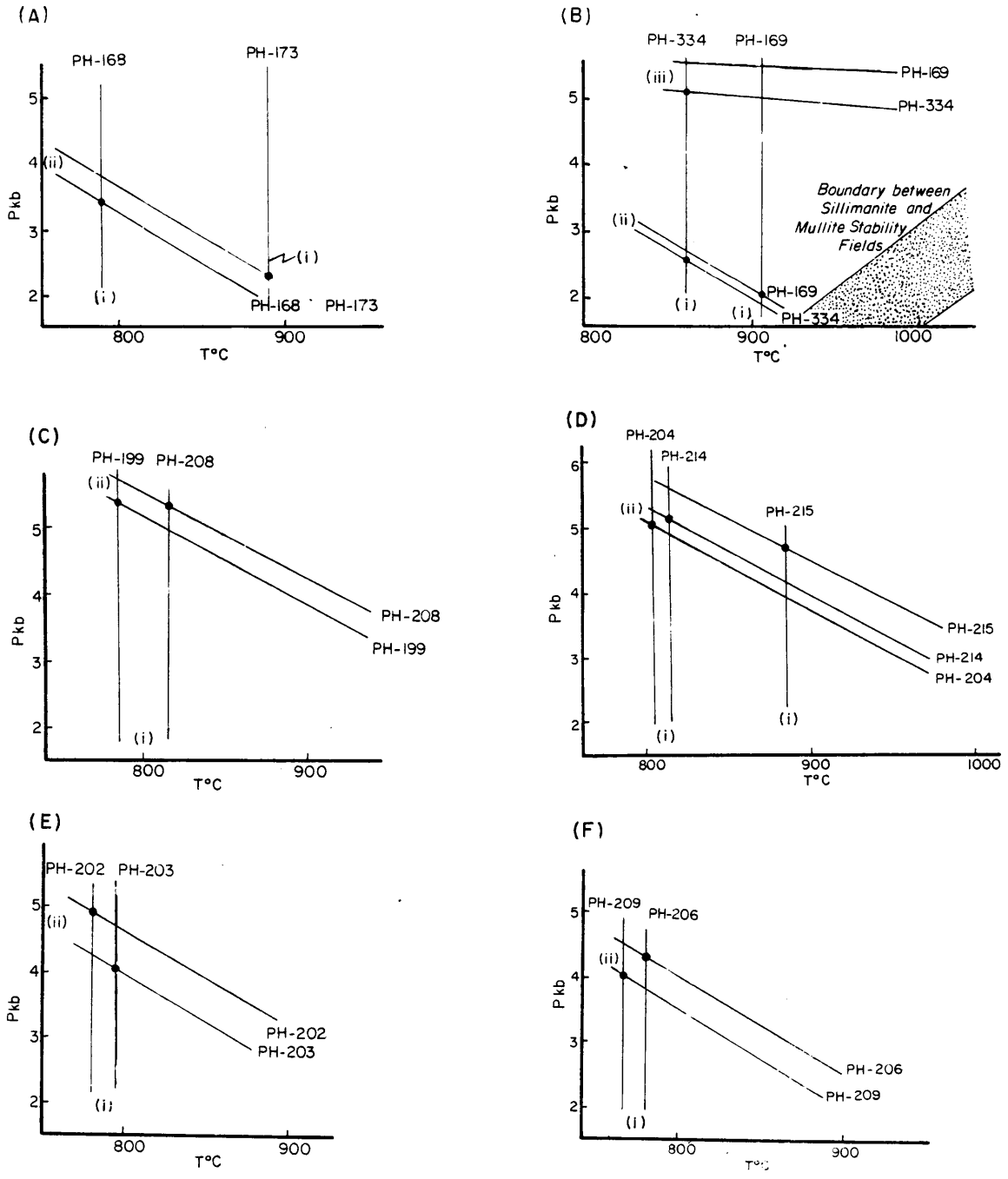

Fig. 74: Compilation of P,T data for spinel-bearing assemblages. Dots represent the intersection of a geobarometer curve with a geothermometer curve in a particular sample

and 5,3 kbar, but the pressures calculated from the Harris (1981) geobarometer for the former samples are apparently too low. The values of 5,1 and 5,5 kbar obtained for the two corundum-bearing samples from the Wells and Richardson (1979) geobarometer are, however, in good agreement with the pressure bracket of the sillimanite-absent assemblages.

7.2.3.4 Orthopyroxene + clinopyroxene + plagioclase + quartz assemblages.(Fig. 75)

The temperatures calculated from the two-pyroxene method are unreliable at temperatures lower than 900° C (J.M. Ferry, pers. comm.) and the temperatures calculated for the relevant samples are therefore uncertain. Pressures calculated from the Wood mixing model are about 1,5 kbar lower than those obtained from the Powell mixing model, the difference probably being due to some Fe^{3+} in the clinopyroxene. It will be shown in the next section that the Powell mixing model is apparently more accurate than the Wood mixing model, in which case the pressures obtained for samples PH - 186 and PH - 88 are in good agreement with the values calculated for other assemblages at a temperature of about 800°C. The pressure calculated for sample PH - 182, however, appears to be too high.

7.3 Silica activities in clinopyroxene + plagioclase ± quartz assemblages

The purpose of this investigation was to determine whether the Powell or Wood mixing models for the CaTs molecule in clinopyroxene give the most reliable results.

The silica activity may be calculated according to the general formula:

$$(\log a_i)^{P,T} = \frac{A}{\ } + B + \frac{C}{T}(P-1) + \Sigma \log a_{products} - \Sigma \log a_{reactants} \quad \ldots\ldots\ldots\ldots\ldots\ldots\ldots\ldots 7(22)$$

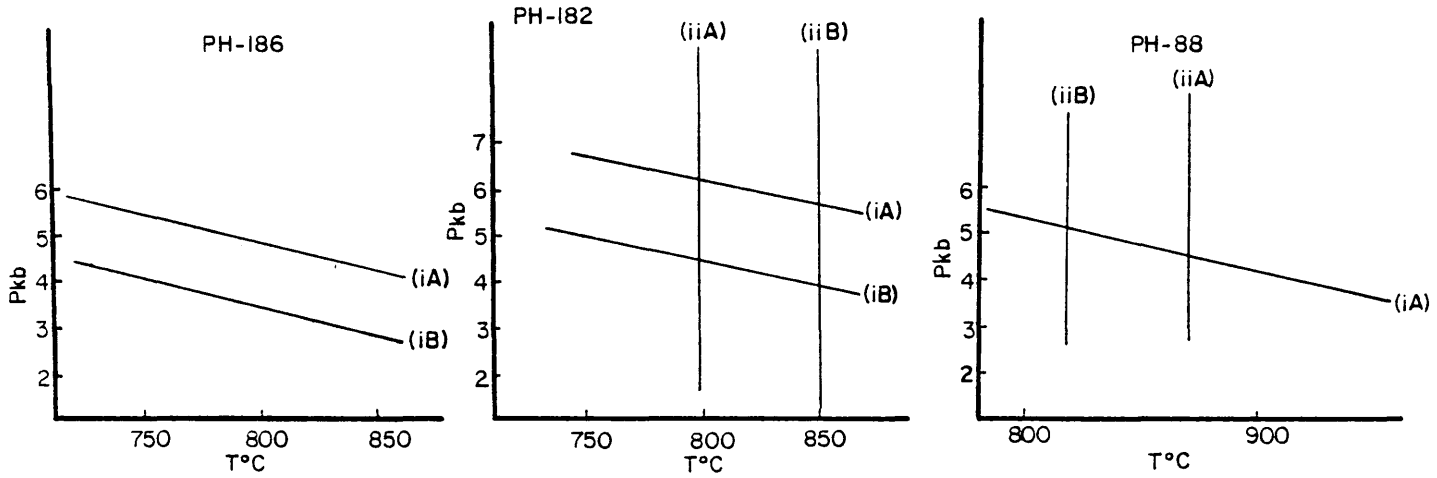

REACTION	CALIBATION	SYMBOL
$CaAl_2Si_2O_8 \rightleftharpoons CaAl_2SiO_6 + SiO_2$	Reed (1980) Powell mixing model	iA
	Wood mixing model	iB
$(Mg_2Si_2O_6)_{opx} \rightleftharpoons (Mg_2Si_2O_6)_{cpx}$	Wells (1977)	iiA
	Wood and Banno (1973)	iiB

Fig. 75: Compilation of P,T data for plagioclase + clinopyroxene + quartz-bearing assemblages from the Potgietersrus area

At a fixed 1 bar pressure the temperature sensitivity of a_{SiO_2} in a plagioclase + clinopyroxene + quartz assemblage is given by:

$$\log a_{SiO_2} = -\frac{1410}{T} - 0{,}532 + \log a^{plag}_{CaAl_2Si_2O_8} - \log a^{cpx}_{CaAl_2SiO_6} \quad \text{.....7(23)}$$

The activity coefficient of plagioclase was obtained from Orville (1972) while $a^{cpx}_{CaAl_2SiO_6}$ was calculated according to the method outlined in section 7.2.2.5. The values for coefficients A and B were obtained form Nicholls et al. (1971). Silica activities as a function of pressure and temperature are illustrated in Figure 76 and tabulated in Table 27. The Wood mixing model yields higher silica activities than the Powell mixing model for the quartz-bearing assemblages, while the situation is reversed for the quartz-absent sample (PH - 213, Fig. 76). There is further a distinct break in the 1 bar silica activities of the quartz-present and -absent samples.

Isobaric log a_{SiO_2} vs. temperature relations at 1 bar, 2 kbar, 4 kbar and 5 kbar were calculated by adding the factor $\frac{C}{T}$ (P - 1) to the 1 bar activities calculated from equation 7(23). The value of C is equal to + 0,052 (Nicholls et al., 1971) and the results are presented in Figures 76 B - D.

Rocks that contain free quartz must have silica activities of unity and since the P,T conditions of crystallization of each sample are fairly well established, it will be possible to decide which of either the Powell or Wood mixing models give the best approximation of the crystallization conditions. Inspection of Figures 76 B - D shows that the Powell mixing model yields silica activities of unity at temperatures ranging between about 700° - 830°C and a pressure of 4 to 5 kbar. For the Wood mixing model,

TABLE 27 log a_{SiO_2} as a function of P and T for plagioclase + cpx ± quartz-bearing assemblages

Sample #	mixing model	log a^{plag}_{An}	log a^{cpx}_{CaTs}	log a_{SiO_2} at 1bar			log a_{SiO_2} at 1073 K		
				973 K	1073 K	1173 K	2 kbar	4 kbar	5 kbar
PH - 88	Powell	-0,1979	-1,8981	-0,2809	-0,1459	-0,0338	-0,0489	0,0479	0,0963
	Wood	-0,1979	-2,2466	0,0676	0,2026	0,3147	0,2996	0,3964	0,4448
PH - 182	Powell	-0,0867	-1,700	-0,3678	-0,2328	-0,1207	-0,1358	-0,039	0,009
	Wood	-0,0867	-1,8967	-0,1711	-0,0361	0,0760	0,0609	0,1577	0,2061
PH - 186	Powell	-0,0545	-1,7816	-0,254	-0,119	-0,007	-0,022	0,0748	0,1232
	Wood	-0,0545	-1,9746	-0,061	0,074	0,1861	0,171	0,2678	0,3162
PH - 213	Powell	-0,0501	-1,3935	-0,6377	-0,5027	-0,3906	-0,4057	-0,3089	-0,2605
	Wood	-0,0501	-1,3326	-0,6986	-0,5636	-0,4515	-0,4666	-0,3698	-0,3214

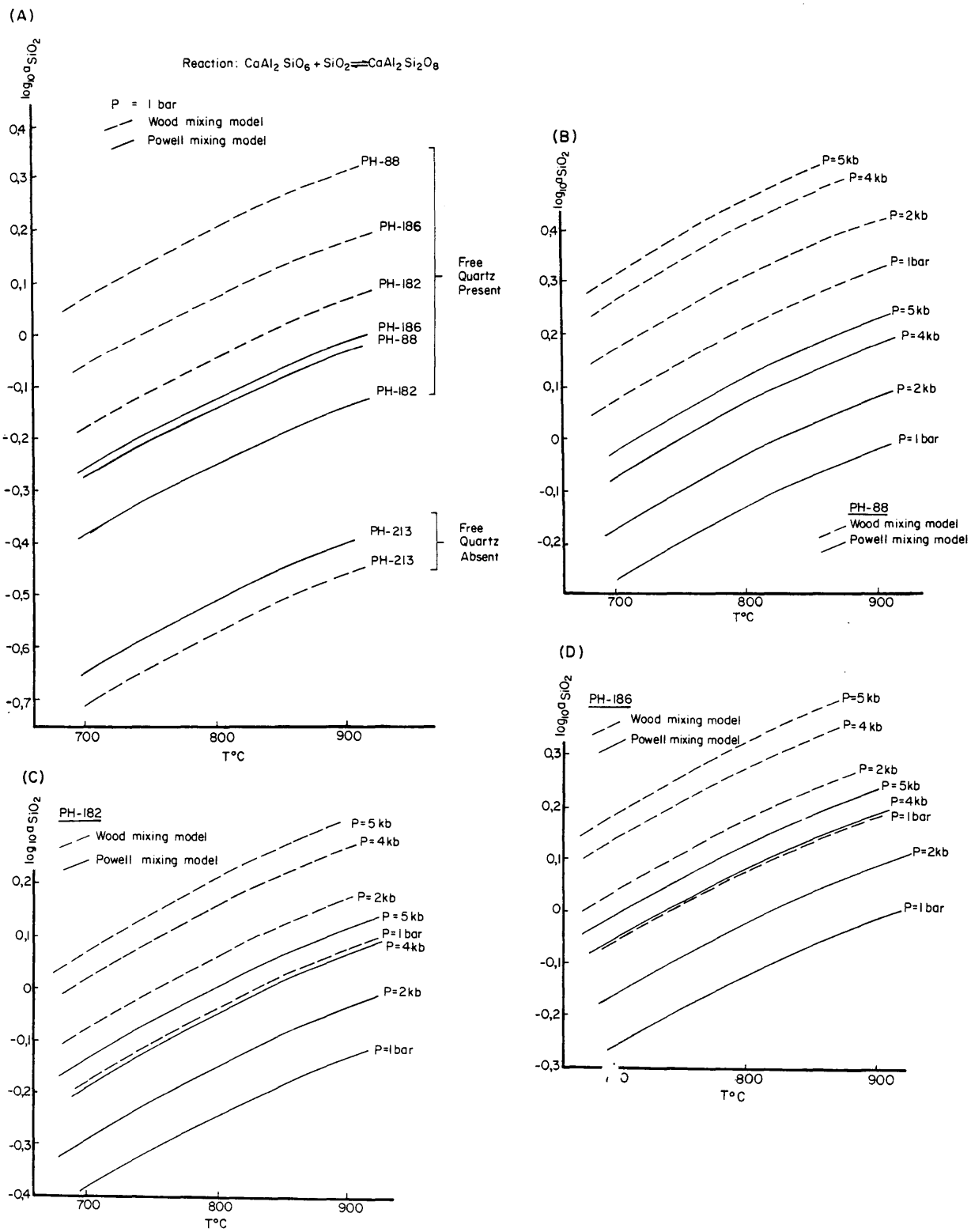

Fig. 76: Silica-activities for the plagioclase + clinopyroxene + quartz-bearing assemblages from the study area

on the other hand, only the 1 bar curve sometimes gives silica activities of unity at similar temperatures. The silica-deficient sample (PH - 213) has silica activities below unity at all geologically reasonable P,T conditions for both mixing models.

It may be concluded that the Powell mixing model fits the observed intensive parameters better than the Wood mixing model and the pressures calculated from this mixing model for the CaTs - plagioclase - quartz geobarometer is therefore preferred to the values calculated from the Wood mixing model.

7.4 Oxygen fugacities

7.4.1 Garnet-bearing assemblages

Several workers,e.g. Chinner (1962) have shown that almandine-rich garnet is only stable in relatively Fe-rich bulk compositions. In the study area, however, some garnet-free samples have almost identical compositions to garnet-bearing samples at equivalent metamorphic conditions.

Garnet-bearing samples contain either Fe-Mg amphiboles or orthopyroxene together with cordierite, biotite and K-feldspar. Opaque minerals are rare and no coexisting ilmenite-magnetite pairs were detected. All the garnet-bearing samples, however, contain ilmenite as an accessory phase while the garnet-absent samples may contain either ilmenite or magnetite. The ilmenite-bearing, garnet-absent samples are, however, Mg-rich and this may account for the absence of garnet. Rumble (1976) suggested that the presence of ilmenite alone in a pelitic rock is indicative of low fO_2 values, and it is therefore suspected that the garnet-bearing samples crystallized at relatively low oxygen fugacities.

Oxygen fugacities were estimated by assuming the ilmenite in garnet-bearing samples and the magnetite in garnet-absent samples were in equilibrium with magnetite and ilmenite respectively. Oxygen fugacities were then

obtained from Buddington and Lindsley (1964) at 600°C for the amphibole-bearing samples and at 750°C for the orthopyroxene-bearing samples. These results are presented in Figure 77 A together with the almandine stability field as determined by Hsu (1968).

With the exception of one Mg-rich sample all the garnet-bearing rocks have oxygen fugacities that plot within the almandine stability field, while the remaining garnet-absent samples plot outside the almandine stability field. It is therefore concluded that the presence of garnet in the pelitic rocks from the study area is a function of both the bulk rock composition and the oxygen fugacity.

7.4.2 Spinel + magnetite-bearing assemblages

The oxygen fugacities of coexisting spinel + magnetite pairs may be estimated from isothermal plots of fO_2 vs. spinel composition (Turnock and Eugster, 1962). At 800°C, which is a reasonable equilibration temperature for the orthopyroxene + spinel $\pm$ olivine-bearing samples from the study area, the two oxide phases coexist for oxygen fugacities between about 10^{-17} and 10^{-13} bars. This range covers the Ni-NiO, QFM and MW buffers at 800°C and is in agreement with the presence of olivine, quartz and magnetite in sample PH - 328.

The oxygen fugacity brackets of the spinel-bearing as well as the garnet-bearing samples are presented in Figure 77 B. The figure illustrates how the fO_2 brackets conform to the buffer curves with increasing temperature, confirming the behaviour of oxygen as an initial value component (Butler, 1969 and Klein, 1966).

Fig. 77: Estimated oxygen fugacities for garnet-bearing and garnet-absent samples (A). Compilation of oxygen fugacities for various assemblages from the study area, illustrating how the oxygen fugacity is buffered with increasing metamorphic grade (B)

(A)

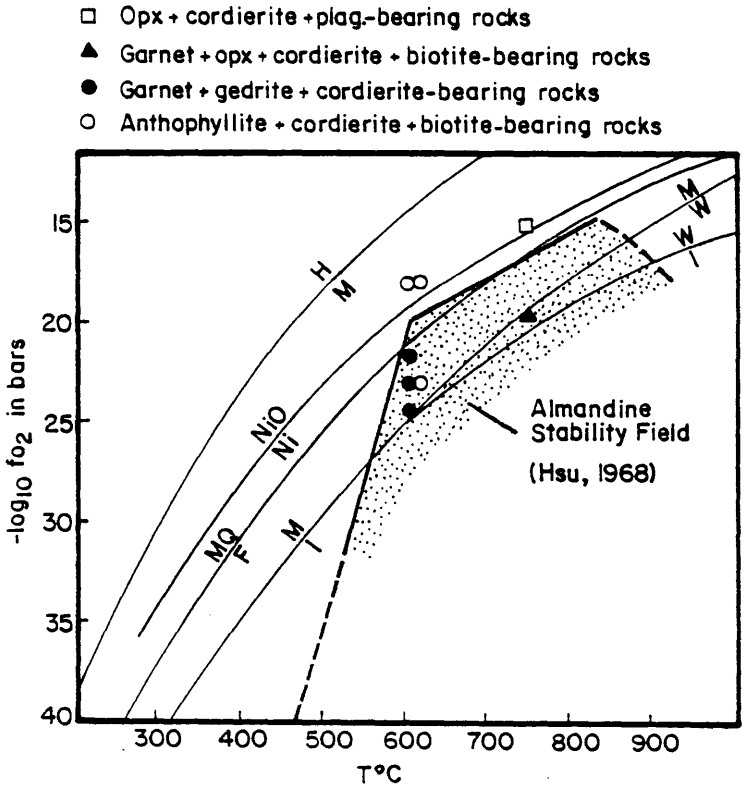

(B)

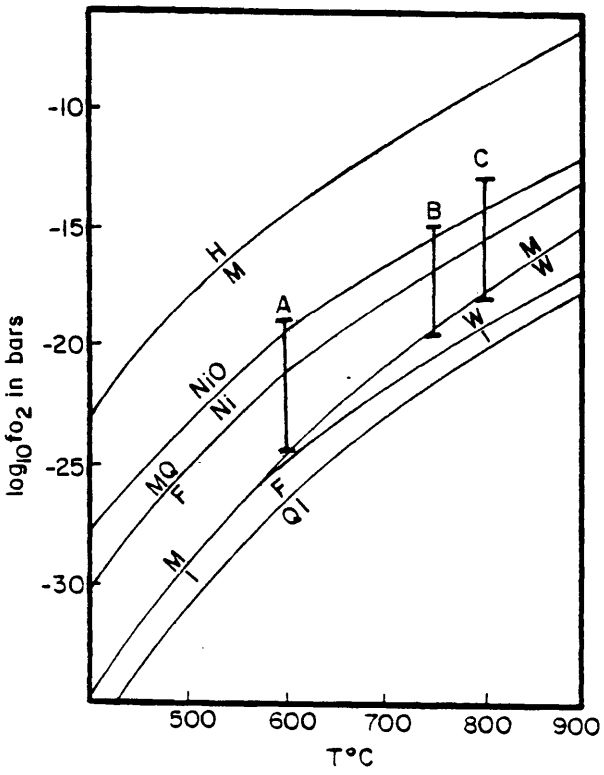

oxygen fugacity bracket for:

A amphibole-bearing assemblages

B orthopyroxene ± garnet-bearing assemblages

C spinel-bearing assemblages

8 CONCLUSION

The formation of the metamorphic aureole of the Bushveld Complex in the Potgietersrus area can be divided into two stages based on the change in the physical conditions during metamorphism. It is suggested that the following minerals and mineral assemblages formed during the early stage: the cores of the zoned cordierite crystals in pelitic assemblage group (2); the rounded, inclusion-free, cordierite crystals in pelitic assemblage group (4); the large plagioclase crystals (An_3) in calcareous assemblage group (11), as well as the olivine + cordierite assemblage. The chloritoid + cordierite assemblage might also have been stable during this stage.

The second stage is characterized by the formation of the cordierite rims in pelitic assemblage group (2); the cordierite-orthoamphibole intergrowths in pelitic assemblage group (4); the small plagioclase crystals (An_{17}) in calcareous assemblage group (11), as well as the breakdown of the olivine + cordierite assemblage to spinel + orthopyroxene, the breakdown of cordierite + orthopyroxene to garnet and quartz, the breakdown of the chloritoid + cordierite assemblage to andalusite and biotite and the formation of the cordierite + spinel + sillimanite ± corundum assemblage.

The estimated P,T conditions of the two stages of the metamorphic event are illustrated in Figure 78. The first stage took place at a pressure of about 1,5 kbar and temperatures of up to about 700°C were attained. During the second stage a pressure of between 4 and 5 kbar was reached while maximum temperatures were approximately 850° to 900°C.

Two stages for the metamorphic event are consistent with a model whereby the lower zone magma was intruded earlier than the magma from which the critical-, main- and upper zones crystallized. This early magma was intruded as an irregularly outlined sheet-like body. To the north of Potgietersrus, where the present erosion surface has exposed the lower zone at six localities, the level of the intrusion was controlled by the contact between the Transvaal Sequence and the floor granites, with smaller magma "fingers" penetrating the Transvaal Sequence (Uitloop 2 body) and the

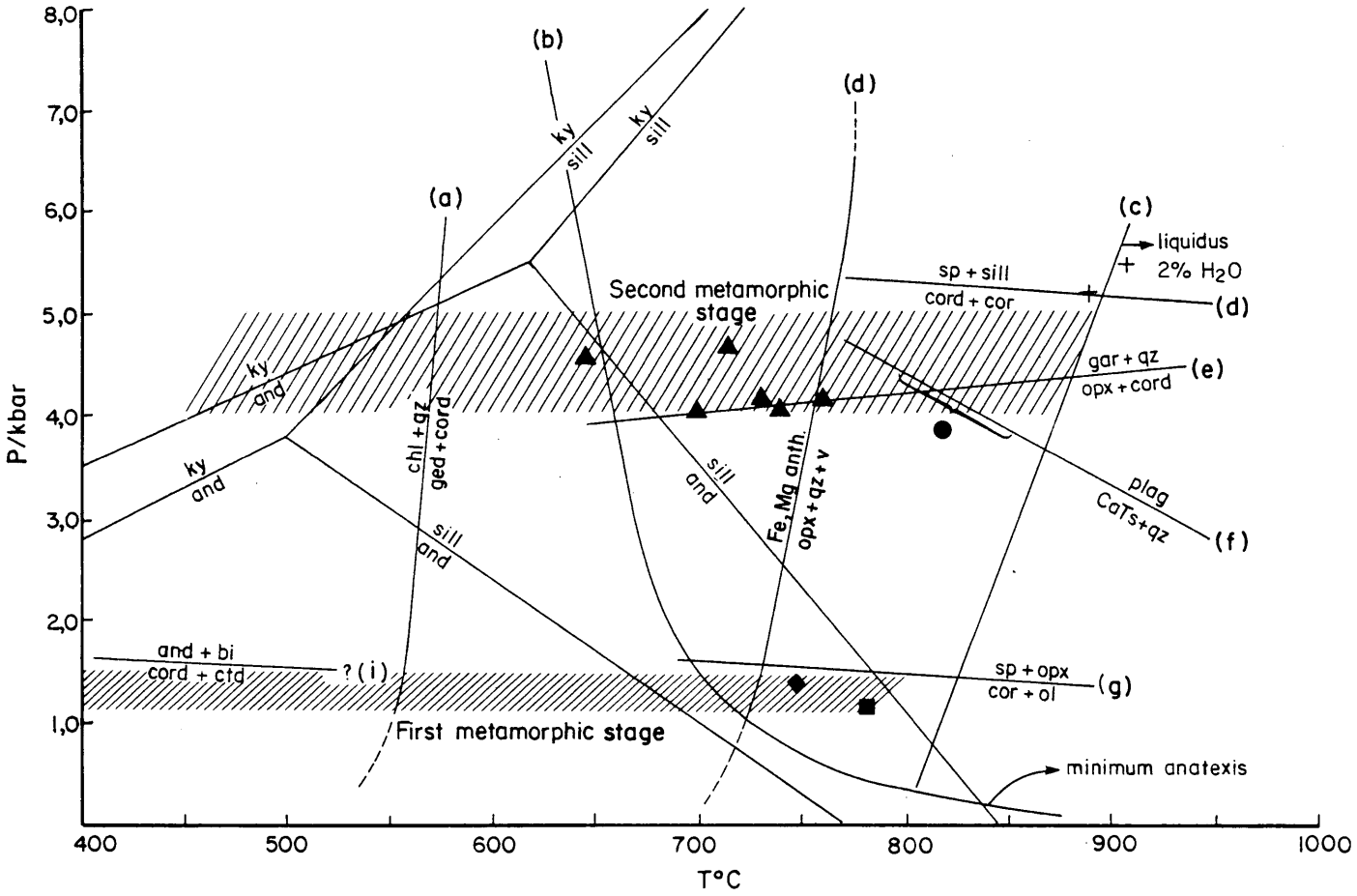

Figure 78

P-T diagram showing experimentally determined mineral equilibria and geothermometry-geobarometry data. Aluminosilicate triple points at higher and lower PT are from Richardson et al. (1969) and Holdaway (1971) respectively. The curves of the mineral equilibria are (a) from Akella and Winkler (1966), (b) and (c) from Winkler (1979), (d) Ravior and Hinrichson (1975), (e) Wells and Richardson (1979) curve is for X_{Fe}^{cord} (= Fe/Fe + Mg) ~ 0,35, (f) Hensen and Green (1973) curve is for X_{Mg}^{cord} (= Mg/Mg + Fe) ~ 0,50, (g) Reed (pers. comm. to M.R. Sharpe, 1980), (h) Lal and Seifert (1979) curve is for Mg/(Mg + Fe) bulk rock ~ 0,45, (i) estimated position (this study)

+ : calculated P,T conditions based on reaction (e) and spinel-cordierite pairs

• : calculated P,T conditions based on reaction (g) and opx-cpx pairs

▲ : calculated P,T conditions based on reaction (f) and gar-cord pairs

■ : estimated P,T condition based on bulk rock composition and reaction (h)

♦ : calculated P,T condition based on the olivine + orthopyroxene + quartz assemblage

Hatched areas illustrate the P-T conditions for the two metamorphic stages. Abbreviations: ky = kyanite; sill = sillimanite; and = andalusite; bi = biotite; cord = cordierite; ctd = chloritoid; chl = chlorite; qz = quartz; ged = gedrite; anth = anthophyllite; opx = orthopyroxene; cpx = clinopyroxene; ol = olivine; sp = spinel; gar = garnet; plag = plagioclase; CaTs = Ca-Tschermaks molecule; v = vapour

floor granites (Bultongfontein bodies).

(1) The extent of the lower zone is unknown and impossible to estimate from gravitational data because of the pronounced signature of the Penge Formation. To the south of Potgietersrus, for instance, the lower zone appears to be restricted to the Grasvally area, although the localities of the samples that contain evidence for two stages of metamorphism suggest that there may by more lower zone material present than is currently exposed in the Grasvally body. This postulated part of the lower zone is apparently intruded into the Transvaal Sequence at a level that is not presently exposed. This model for the emplacement of the Bushveld Complex in the Potgietersrus area is consistent with:

1) The low pressure attained during the early stage. Because the lower zone was intruded into or below the Transvaal Sequence, the metamorphic pressure was equal to a lithostatic pressure beneath the approximately 5 km thick pile of Transvaal Sequence sediments and Rooiberg Felsites,which is equal to about 1,5 kbar. This estimated lithostatic pressure is in excellent agreement with the calculated equilibrium pressure for the cordierite + olivine assemblage and with the value obtained from the olivine + orthopyroxene + quartz geobarometer.

2) The high temperatures reached during the early stage to the north of Potgietersrus where the level of the Transvaal Sequence exposed is only about 0,7 to 1,0 km from the contact with the floor granites and therefore with the proposed level of intrusion of the lower zone. Since the heat loss from the ultramafic lower zone magma would have been through the roof, a temperature of about 750°C should have been relatively easy to attain so close to the contact with the lower zone.

3) A sheet-like shape for the lower zone is in accord with the relative wide-spread distribution of samples that show evidence for two metamorphic stages. This would not have been the case if the lower zone outcrops were in fact sattelite bodies.

(9) The latter stage of the metamorphic event took place with the intrusion of magma from which the critical-, main- and upper zones crystallized. There was apparently a sufficient hiatus between the two magma intrusions to permit the complete or almost complete crystallization of the lower zone magma as is evident from mineral geochemistry and the transgression of the Grasvally body by the critical and main zones of the Bushveld Complex (Van der Merwe, 1978). The second magma was intruded at a higher stratigraphic level than the lower zone magma, viz. the contact between the Transvaal Sequence and the Rooiberg Felsites.

A pressure of 4 to 5 kbar was calculated for the second stage of the metamorphic event. This bracket is in good agreement with values of about 5 kbar calculated by Hulbert and Sharpe (1981) for the Bushveld contact aureole in the eastern Transvaal as well as with the presence of kyanite in pelitic xenoliths in the Bushveld Complex from the south of Potgietersrus (Hall and Gardthausen, 1911). Van Rooyen (1950) recorded the cordierite + garnet + sillimanite + quartz assemblage in Timeball Hill pelites to the north of Potgietersrus. This assemblage is only stable at pressures greater than about 4 kbar (Hensen and Green, 1973).

Assuming a thickness of about 8 km for the critical-, main- and upper zones of the Bushveld Complex and the Rooiberg Felsites, the lithostatic pressure at the level of contact between the Transvaal Sequence and the main body of the Bushveld Complex could not have exceeded 2,5 kbar at the present level of exposure. The calculated pressures therefore exceeds the lithostatic pressure by about 2 kbar. This difference may be the result of one, or a combination of the following factors:

1) gas overpressure, i.e. $P_{fluid} > P_{solid}$;
2) tectonic overpressure or
3) an underestimation of the lithostatic pressure that operated during the second stage of the metamorphic event.

The value of the fluid pressure is unlikely to be more than 100 bar greater than the lithostatic pressure (Rickard and Wickman, 1980). Evidence for gas overpressure in the form of tension gashes, hydraulic fractures or brittle failure is further more absent in the study area and this factor could therefore

not have contributed significantly to the high pressures calculated for the second stage of the metamorphic event.

Evidence for the presence of tectonic overpressure or directed stress is provided by a large fold in the Dwaalheuwel Formation which has a roughly N - S fold axis that is parallel to the contact between the Bushveld Complex and the floor rocks as well as to the 010° lineament set identified by Sharpe and Chadwick (1981) in several floor-attached structures in the eastern compartment of the Bushveld Complex, which they interpreted as the result of regional compression related to the subsidence of the floor and the intrusion of the Bushveld Complex.

The strength of rocks under directed stress conditions in the presence of a fluid is negligible. The rocks in the study area may however provide a unique case. If most of the water in the rocks was driven off during the first, lower temperature, pressure stage, the rocks must have been relatively desiccated during the second stage of the metamorphic event. It is therefore possible that the rocks might have been able to sustain some directed stress over a relatively short period of time during the second stage of the metamorphic event. Even under these special conditions is it, however, unlikely that directed stress could have contributed more than about 1,0 kbar to the maximum pressure calculated for the metamorphic event (Brace et al., 1970).

It is therefore proposed that the lithostatic pressure on the present level of exposure of the floor rocks during the second stage of the metamorphic event was about 1,0 kbar higher than the calculated value. According to the model suggested the critical-, main- and upper zones had the shape of a funnel with an elliptic cone, similar to the funnel-shaped feeder areas in the eastern- and western compartments of the Bushveld Complex. Such a model is also in agreement with the proposed sill-like shape of the Potgietersrus limb in the Villa Nora area (Van der Merwe, 1978) where a higher stratigraphic level of the complex may be exposed. The volume of critical-, main- and critical zone magma present during the second stage of the metamorphic event was therefore significantly greater than what is suggested by the current dyke-like shape of the Potgietersrus limb of the Bushveld Complex near the study area which is believed to be an artifact of the present erosion level.

The 2 kbar difference between the calculated maximum pressures and the estimated lithostatic pressure can thus be accounted for by a directed stress contribution and by assuming that the lithostatic pressure during the second stage of the metamorphic event was about 1,0 kbar higher than the value suggested by the current field relations, brought about by superincumbent load of layered rocks.

The high temperature at which partial melting took place during the second stage of the metamorphic event is consistent with low PH_2O ($PH_2O \sim 0{,}2\ P_{total}$) in these rocks at the time of melting. This observation can be explained by two stages in the metamorphic event where most of the water in the rock was driven off during the first, lower temperature stage when temperatures were not high enough at that stratigraphic level to cause partial melting. The rocks were, however, then dry when the second, high temperature stage took place so that melting was only possible at very high temperatures.

ACKNOWLEDGEMENTS

The author would like to thank the Institute for Geological Research on the Bushveld Complex and the Council for Scientific and Industrial Research for sponsoring this study.

Sincere thanks are due to Dr. C. Frick of the Geological Survey of South Africa for making his microprobe facilities available and to many farmers in the Potgietersrus area for their generous hospitality.

I would also like to express my sincere gratitude to Dr. M.R. Sharpe of the Institute for Geological Research on the Bushveld Complex for supervising this study as well as for his assistance in the data processing. His friendship and continued interest in this study is also deeply appreciated.

Prof. G.Von Gruenewaldt and Mr J.P.Engelbrecht are thanked for reading early drafts of the manuscript. Helpful comments by Drs J.M. Ferry and P.R.A. Wells are also greatefully acknowledged.

I am also indebted to Miss V. Van den Berg for her able typing and to Mrs M. Potgieter for drafting the diagrams.

REFERENCES

ABDULLAH, M.I., 1965.
The iron-titanium oxide phases in metamorphism, p.274-280. In, Pitcher, W.S. and Flinn, G.W.(Eds.), Controls of Metamorphism. Oliver and Boyd, Edinburgh, 368 p.

ABRAHAM, K.and SCHREYER, W., 1973.
Petrology of a ferruginous hornfels from Riekensglück, Harz Mountains, Germany. Contrib. Mineral. Petrol., v.40, p.275-292.

AKELLA, J. and WINKLER, H.G.F., 1966.
Orthorhombic amphibole in some metamorphic reactions. Contrib. Mineral. Petrol., v.12, p. 1-12.

ALBEE, A.L., 1965 a.
A petrogenetic grid for the Fe-Mg silicates of pelitic schists. Am. J. Sci., v.263, p.512-536.

ALBEE, A.L., 1965 b.
Distribution of Fe, Mg and Mn between garnet and biotite in natural mineral assemblages. J.Geol., v.73, p.155-164.

ALBEE,A.L., 1972.
Pelitic schists: Reaction relations of chloritoid and staurolite. Geol. Soc. Am. Bull., v.83, p.3249-3268.

BENCE, A.E. and ALBEE, A.L., 1968.
Empirical correction factors for the electron microanalysis of silicates and oxides. J. Geol., v.76, p.382-403.

BERG, J.H., 1977 a.
Dry granulite mineral assemblages in the contact aureoles of the Nain Complex, Labrador. Contrib. Mineral. Petrol., v.64, p.33-52.

BERG, J.H., 1977 b.
Regional geobarometry in the contact aureoles of the anorthositic Nain Complex, Labrador. J.Petrol., v.18, p.399-430.

BLATT, H. MIDDLETON, G. and MURRAY, R., 1972.
Origin of sedimentary rocks. Englewood Cliffs, New Jersey, 634p.

BOHLEN, S.R. and BOETTCHER, A.L., 1981.
Experimental investigation and geological applications of orthopyroxene geobarometry. Am. Mineral., v.66, p.951-964.

BORISENOK, L.A. and SAUKOV, A.A., 1960.
Geochemical cycle of gallium. Intern. Geol. Congr., 21st, Rept.Session, Norden Part 1,96.

BOWEN, N.L., 1928.
The evolution of the igneous rocks. Princeton University press, Princeton, 332p.

BRACE, W.F., ERNST, W.G. and KALLBERG, R.W., 1970.
An experimental study of tectonic overpressure in Franciscan rocks. Geol. Soc. Am. Bull., v.81, p.1325-1338.

BRINDLEY, G.W., BISH, D.L. and WAN, HSIENG-MING, 1979.
Compositions, structures and properties of nickel-containing minerals in the kerolite-pimelite series. Am.Mineral., v.64, p.615-625.

BROWN, G.C. and FYFE, W.S., 1970.
The production of granitic melts during ultrametamorphism. Contrib. Mineral. Petrol., v.28, p.310-318.

BROWN, W.L., 1965.
Crystallographic aspects of feldspars in metamorphism, p.342-351. In, Pitcher, W.S. and Flinn,G.W. (Eds.), Controls of metamorphism, Oliver and Boyd, Edinburgh, 368 p.

BUCHANAN, D.L., 1976.
The phase chemistry of the Bushveld Complex in the Bethal area. Ph.D. thesis (unpublished), Imperial College of Science and Technology, London, 163 p.

BUCHNER-NURMINEN, K., 1982.
On the mechanism of contact aureole formation in dolomitic country rock by the Adamello intrusion (northern Italy). Am. Mineral., v.67, p.1101-1117.

BUDDINGTON , A.F. and LINDSLEY, D.H., 1964.
Iron-titanium oxide minerals and synthetic equivalents. J. Petrol., v.5, p. 310-357.

BUTLER, P., 1969.
Mineral compositions and equilibria in the metamorphosed iron formation of the Gagnon region, Quebec, Canada. J. Petrol., v.10, p.56-101.

BUTTON, A., 1973.
A regional study of the stratigraphy and development of the Transvaal basin in the eastern and northeastern Transvaal. Ph.D. thesis (unpublished), University of the Witwatersrand, 510 p.

CAMERON, K.L., 1975.
An experimental study of actinolite-cummingtonite phase relations with notes on the synthesis of Fe-rich anthophyllite. Am. Mineral., v.60, p. 375-390.

CAMERON, W.E., 1976.
Coexisting sillimanite and mullite. Geol. Mag. v. 113, p. 497-514.

CARMICHAEL, I.S.E., 1967.
The iron-titanium oxides of salic volcanic rocks and their associated ferromagnesian silicates. Contrib. Mineral. Petrol., v. 14, p. 36-64.

CHINNER, G.A., 1960.
Pelitic gneisses with varying ferrous/ferric ratios from Glen Cova, Angus, Scotland. J.Petrol., v. 1, p. 178-217.

CHINNER, G.A., 1962.
Almandine in thermal aureoles. J. Petrol., v. 3, p. 316-340.

CIPRIANI, C., SASSI, F.P. and SCOLARI, A., 1971.
Metamorphic white micas: Determination of paragenetic fields. Schweitz. Min. Petr. Mitt., v. 51, p. 259-296.

COUSINS, C.A., 1959.
The structure of the mafic portion of the Bushveld Igneous Complex. Trans. Geol. Soc. S. Afr., v. 62, p. 179-189.

CRAWFORD, M.L., 1966.
Composition of plagioclase and associated minerals in some schists from Vermont, U.S.A. and South Westland, New Zeeland, with inferences about the peristerite solvus. Contrib. Mineral. Petrol., v. 13, p. 269-294.

DAHL, P.S., 1980.
The thermal-compositional dependence of Fe^{2+}- Mg distribution between coexisting garnet and pyroxene: applications to geothermometry. Am. Mineral., v. 65, p. 854-866.

DALLMEYER, R.D., 1972.
Compositional controls on cordierite-bearing assemblages in high-grade regional metamorphism. Intern. Geol. Congr., 24th, Section 2, p. 52-63.

DALLMEYER, R.D., 1974.
The role of crystal structure in controlling the partitioning of Mg and Fe^{2+} between coexisting garnet and biotite. Am. Mineral., V. 59, p. 201-203.

DALLMEYER, R.D. and DODD, R.T., 1971.
Distribution and significance of cordierite in paragneisses of the Hudson Highlands, southeastern New York. Contrib. Mineral. Petrol., v. 33, p. 289-308.

DAVIDSON, L.R. and MATHISON, C.I., 1974.
Aluminous orthopyroxene and associated cordierites, garnets and biotites from granulites of the Quairading district, Western Australia. Neues. Jb. Mineral. Mh., v. 6, p. 272-287.

DEER, W.A., HOWIE, R.A. and ZUSSMAN, J., 1962 a.
Rock forming minerals, volume 1 (ortho- and ring silicates). Longmans, Green, London, 333p.

DEER, W.A., HOWIE, R.A. and ZUSSMAN, J., 1962 b.
Rock forming minerals, volume 2 (chain silicates). Longmans, Green, London, 379 p.

DEER, W.A. , HOWIE, R.A. and ZUSSMAN, J., 1962 c.
Rock forming minerals, volume 3 (sheet silicates). Longmans, Green, London, 270 p.

DEVINE, J.D. and SIGURDSSON, H., 1980.
Garnet- fassaite calc-silicate nodule from La Soufriére, St. Vincent. Am. Mineral., V.65, p. 302-305.

DIETVORST, E.J.L., 1980.
Biotite breakdown and the formation of gahnite in metapelitic rocks from Kemio, southwest Finland. Contrib. Mineral. Petrol., V.75, p. 327-337.

DRURY, S.A., 1973.
The geochemistry of Precambrian granulite facies rocks from the Lewisian Complex of Tiree, Inner Hebrides, Scotland. Chem. Geol., v.11, p. 167-188.

ERNST, W.G., 1968.
Amphiboles: crystal chemistry, phase relations and occurrence Springer-Verlag, New York, 125 p.

EVANS, B.W., 1964.
Fractionation of elements in the pelitic hornfelses of the Cashel-Lough Wheelaun intrusion, Connemara, Eire. Geochim. Cosmochim. Acta, V.28, p. 127-156.

FERRY, J.M. and SPEAR, F.S., 1978.
Experimental calibration of the partitioning of Fe and Mg between biotite and garnet. Contrib. Mineral. Petrol., v.66, p. 113-117.

FINGER, L.W., 1970.
Refinement of the crystal structure of anthophyllite. Carnegie Inst. Wash., Yb. 68, p. 283-288.

FINGER, L.W., 1972.
The uncertainty in the calculated ferric iron content of microprobe analyses. Carnegie Inst. Wash., Yb. 71, p. 600-603.

FINNERTY, A.A. and BOYD, F.R., 1984.
Evaluation of thermobarometers for garnet peridotites. Geochim. Cosmochim. Acta, v.48, p. 15-27.

FLETCHER, C.J.N. and GREENWOOD, H.J., 1979.
Metamorphism and structure of the Penfold Creek area, near Quesnel Lake, British Columbia. J. Petrol., v.20, p. 743-794.

FROST, B.R., 1975.
Contact metamorphism of serpentinite, chloritic Blackwall and Rodingite at Paddy - Go - Easy Pass, central Cascades, Washington. J. Petrol., v.16, p. 272-313.

GANGULY, J. and GHOSE, S., 1979.
Aluminous orthopyroxene: order-disorder, thermodynamic properties, and petrological implications. Contrib. Mineral. Petrol., v. 69, p. 375-385.

GANGULY, J. and KENNEDY, G.C., 1974.
The energetics of natural garnet solid solutions. I Mixing of the aluminosilicate end-members. Contrib. Mineral. Petrol., v. 48, p. 137-148.

GHOSE, N.C., 1966.
Behaviour of trace elements during thermal metamorphism and or granitization of the metasediments and basic igneous rocks. Geol. Rundsch., v.55, p. 608-617.

GINZBURG, I.V., 1969.
Immiscibility of the natural pyroxenes diopside and fassaite and the criterion for it. Dok. Akad. Nauk. SSSR., v. 186, p. 423-426.

GORDON, T.M. and GREENWOOD, H.J., 1971.
The stability of grossularite in H_2O - CO_2 mixtures. Am. Mineral., v. 56, p. 1674-1688.

GRANT, J.A., 1973.
Phase equilibria in high-grade metamorphism and partial melting of pelitic rocks. Am. J. Sci., v. 273, p. 289-317.

GRANT, J.A., 1981.
Orthoamphibole and orthopyroxene relations in high-grade metamorphism of pelitic rocks. Am. J. Sci., v. 281, p. 1127-1143.

GREENWOOD, H.J., 1973.
Thermodynamic properties of gaseous mixtures of H_2O and CO_2 between 450° and 800°C and 0 to 500 bars. Am. J. Sci., v. 273, p. 561-571.

GREENWOOD, H.J., 1975.
Buffering of pore fluids by metamorphic reactions. Am. J. Sci., v. 275, p. 573-593.

HALL, A.L., 1909.
On calcareous beds in the Pretoria Series, east of Potgietersrust, and their metamorphism. Trans. Geol. Soc. S. Afr., v. 12, p. 1-9.

HALL, A.L. and GARDTHAUSEN, C., 1911.
Note on some remarkable xenoliths of altered shale from the norite of Potgietersrust and Mapoch's country. Trans. Geol. Soc. S. Afr., v. 14, p. 74-78.

HARRIS, N., 1981.
The application of spinel-bearing metapelites to P/T determinations : An example from south India. Contrib. Mineral. Petrol., v. 76, p. 229-233.

HEIER, K.S., 1960.
Petrology and geochemistry of high-grade metamorphic and igneous rocks on Langöy, northern Norway. Norg. Geol. Undersokelse, v. 207, p. 246.

HEIER, K.S., 1966.
Some crystallochemical relations of nephelines and feldspars on Stjernöy, north Norway. J. Petrol., v. 7, p. 95-113.

HENRY, J., 1974.
Garnet-cordierite gneisses near the Egersund-Ogna anorthositic intrusion, soathwestern Norway. Lithos, v. 7, p. 207-216.

HENSEN, B.J., 1971.
Theoretical phase relations involving cordierite and garnet in the system MgO - FeO - Al_2O_3 - SiO_2. Contrib. Mineral. Petrol., v. 33, p. 191-214.

HENSEN, B.J., 1977.
Cordierite - garnet bearing assemblages as geothermometers and barometers in granulite facies terranes Tectonophysics, v. 43, p. 73-88.

HENSEN, B.J. and GREEN, D.H., 1971.
Experimental study of the stability of cordierite and garnet in pelitic compositions at high pressures and temperatures. I. Compositions with excess aluminosilicate. Contrib. Mineral. Petrol., v. 33, p. 309-330.

HENSEN, B.J. and GREEN, D.H., 1972.
Experimental study of the stability of cordierite and garnet in pelitic compositions at high pressures and temperatures. II. Compositions without excess aluminosilicate. Contrib. Mineral. Petrol., v. 35, p. 331-354.

HENSEN, B.J. and GREEN, D.H., 1973.
Experimental study of the stability of cordierite and garnet in pelitic compositions at high pressures and temperatures. III. Synthesis of experimental data and geological applications. Contrib. Mineral. Petrol., v. 38, p. 151-166.

HERZBERG, C.T., 1978.
Pyroxene geothermometry and geobarometry : an experimental and thermodynamic evaluation of some subsolidus phase relations involving pyroxenes in the system CaO - MgO - Al_2O_3 - SiO_2. Geochim. Cosmochim. Acta, v. 42, p. 945-957.

HESS, P.C., 1969.
The metamorphic paragenesis of cordierite in pelitic rocks. Contrib. Mineral. Petrol., v. 24, p. 191-207.

HEY, M.H., 1954.
A new review of chlorites. Mineral. Mag., v. 30, p. 277-292.

HOLDAWAY, M.J., 1971.
Stability of andalusite and the aluminium silicate phase diagram. Am. J. Sci., v. 271, p. 97-131.

HOLDAWAY, M.J., 1972.
Thermal stability of Al - Fe epidote as a function of fO_2 and Fe content. Contrib. Mineral. Petrol., v. 37, p. 307-340.

HOLDAWAY, M.J., 1976.
Mutual compatibility relations of the Fe^{2+} - Mg - Al silicates at 800°C and 3 kb. Am. J. Sci., v. 276, p. 285-308.

HOLDAWAY, M.J. and LEE, S.M., 1977.
Fe-Mg cordierite stability in high-grade pelitic rocks based on experimental, theoretical and natural observations. Contrib. Mineral. Petrol., v. 63, p. 175-198.

HOLLISTER, L.S., 1969.
Contact metamorphism in the Kwoiek area of British Columbia: an end member of the metamorphic process. Geol. Soc. Am. Bull., v.80, p. 2465-2494.

HÖRMANN, P.K., RAITH, M., RAASE, P., ACKERMAND, D. and SEIFERT, F., 1980.
The granulite complex of Finnish Lapland: petrology and metamorphic conditions in the Ivatojoki-Inarijärui area. Geol. Survey Finland Bull. 308, 95 p.

HOSCHEK, G., 1969.
The stability of staurolite and chloritoid and their significance in metamorphism of pelitic rocks. Contrib. Mineral. Petrol., v.22, p. 208-232.

HSU, L.C., 1968.
Selected phase relationships in the system Al-Mn-Fe-Si-O: a model for garnet equilibria. J. Petrol., v. 9, p. 40-83.

HSU, L.C. and BURNHAM, C.W., 1969.
Phase relationships in the system $Fe_3Al_2Si_3O_{12}$ - $Mg_3Al_2Si_3O_{12}$- H_2O at 2,0 kilobars. Geol. Soc. Am. Bull., v.80, p. 2393-2408.

HUCKENHOLZ, H.G., 1965 a.
Der petrogenetische Werdegang der klinopyroxene in den tertiären vulkaniten der Hocheifel. I. Beitr. Mineral. Petrog., v. 11, p. 138-195.

HUCKENHOLZ, H.G., 1965 b.
Der petrogenetische werdegang der klinopyroxene in den tertiären vulkaniten der Hocheifel. II. Beitr. Mineral. Petrog., v. 11, p. 415-448.

HUCKENHOLZ, H.G., 1969.
Synthesis and stability of Ti-andradite. Am. J. Sci., v. 267 A, p. 209-232.

HULBERT, L.J., 1983.
A petrological investigation of the Rustenburg Layered Suite and associated mineralization south of Potgietersrus. Ph.D. thesis (unpublished), University of Pretoria, 511 p.

HULBERT, L.J. and SHARPE, M.R., 1981.
Stop 1: andalusite - biotite - cordierite - muscovite hornfels, Faugha Ballagh. Third International Platinum Symposium - excursion guidebook, p. 39-41. Vermaak, C.F. and Von Gruenewaldt, G. (Eds.).

HUNTER, D.R., 1970.
The geology of the Usushwana Complex in Swaziland. Geol. Soc. S. Afr., Spec. Publ. 1, p. 645-660.

HUNTER, D.R., 1975.
The regional geological setting of the Bushveld Complex. (An adjunct to the provisional tectonic map of the Bushveld Complex). Econ. Geol. Res. Unit, Univ. Witwatersrand, 18p.

HUTCHISON, C.S., 1974.
Laboratory handbook of petrographic techniques. John Wiley and Sons, Inc., New York, 527 p.

IIJIMA, A. and MATSUMOTO, R., 1982.
Berthierine and chamosite in coal measures of Japan. Clays and Clay Minerals, v.30, p. 264-274.

JAMES, H.L., 1966.
Chemistry of the iron-rich sedimentary rocks. U.S. Geol. Survey, Prof. Pap., 440 - W, 60 p.

KAMINENI, D.C., 1975.
Chemical mineralogy of some cordierite-bearing rocks near Yellowknife, Northwest Territories, Canada. Contrib. Mineral. Petrol., v. 53, p. 293-310.

KARS, H., JANSEN, J.B.J., TOBI, A.C. and POORTER, R.P.E., 1980.
The metapelitic rocks of the polymetamorphic Precambrain of Rogaland, SW Norway. Part II. Mineral relations between cordierite, hercynite and magnetite within the osumilite - in isograd. Contrib. Mineral. Petrol., v.74, p.235-244.

KERRICK, D.M., 1974.
Review of metamorphic mixed-volatile (H_2O - CO_2) equilibria. Am. Mineral., v. 59, p. 729-762.

KLEIN, C., 1966.
Mineralogy and petrology of the metamorphosed Wabush iron formation, southwestern Labrador. J. Petrol., v. 7, p. 246-305.

KORZHINSKII, D.S., 1950.
Phase rule and geochemical mobility of elements. Intern. Geol. Congr., 18th, Part II.

KORZHINSKII, D.S., 1959.
Physicochemical basis of the analysis of the paragenesis of minerals. Consultants bureau, inc., New York, 142 p.

KRETZ, R., 1966.
Interpretation of the shape of mineral grains in metamorphic rocks. J. Petrol., v. 7, p. 68-94.

KYNASTON, H. and HALL, A.L., 1911.
The geology of the country round Potgietersrust. An explanation of sheet 7, Geol. Survey of South Africa.

LABOTKA, T.C., 1981.
Petrology of an andalusite-type regional metamorphic terrane, Panamint Mountains, California. J. Petrol., v. 22, p. 261-296.

LAL, R.K., ACKERMAND, D., SEIFERT, F. and HALDAR, S.K., 1978.
Chemographic relationships in sapphirine-bearing rocks from Sonapahar, Assam, India. Contrib. Mineral. Petrol., v. 67, p. 169-187.

LAL, R.K. and MOORHOUSE, W.W., 1969.
Cordierite-gedrite rocks and associated gneisses of Fishtail Lake, Harcourt Township, Ontario. Can. J. Earth Sci., v. 6, p. 154-165.

LAL, R.K. and SEIFERT, F., 1979.
The reaction cordierite + olivine ⇌ orthopyroxene + spinel in the system Mg-Fe-Al-Si-O-H. Neues. Jb. Mineral. Mh., v.5, p. 225-232.

LAL, R.K. and SHUKLA, R.S., 1975.
Genesis of cordierite - gedrite - cummingtonite rocks of the northern portion of the Khetri Copper Belt, Rajasthan, India. Lithos, v. 8, p. 175-186.

LAMBERT, I.B. and HEIER, K.S., 1968.
Geochemical investigation of high-grade regional metamorphic and associated rocks in the Australian Shield. Lithos, v. 1, p. 30-53.

LAPINSKY, L., 1981.
An electron microprobe investigation of some rocks from the Bushveld Complex contact aureole. M.Sc. thesis (unpublished), University of Natal, 222 p.

LEAKE, B.E., 1978.
Nomenclature of amphiboles. Am. Mineral., v. 63, p. 1023-1052.

MARTINI, J.E.J., 1977.
A copper-bearing bed in the Pretoria Group in northeastern Transvaal. Geol. Soc. S. Afr., Spec. Publ. 6, p. 65-72.

MASON, B., 1962.
Metamorphism in the southern Alps of New Zeeland. Bull. Am. Museum Nat. History, v. 123, p. 215-247.

MERWE, M.J., VAN DER, 1978.
The geology of the basic and ultramafic rocks of the Potgietersrus limb of the Bushveld Complex. Ph.D. thesis (unpublished), University of the Witwatersrand, 176 p.

METZ, P. and TROMMSDORFF, V., 1968.
On phase equilibria in metamorphosed siliceous dolomites. Contrib. Mineral. Petrol., v. 18, p. 305-309.

MOLENGRAAFF, G.A.F., 1901.
Géologie de la Republique Sud-Africaine du Transvaal. Bull. Soc. Géol. de France, 4 Sér Tome 1, p. 13-92.

MOORE, B.R. and DENNEN, W.H., 1970.
A geochemical trend in silicon-aluminum -iron ratios and the classification of clastic sediments. J. Sed. Petrol., v. 40, p. 1147-1152.

MUELLER, R.F., 1972.
Stability of biotite: a discussion. Am. Mineral., v. 57, p. 300-316.

MUELLER, R.F. and SAXENA, S.K., 1977.
Chemical petrology with application to the terrestrial planets and meteorites. Springer-Verlag, New York, 394 p.

MacGREGOR, I.D., 1974.
The system $MgO-Al_2O_3-SiO_2$: solubility of Al_2O_3 in enstatite for spinel and garnet peridotite compositions. Am. Mineral., v. 59, p. 110-119.

NEWTON, R.C., 1972.
An experimental determination of the high-pressure stability limits of magnesian cordierite under wet and dry conditions. J. Geol., v.80, p. 398-420.

NEWTON, R.C., 1976.
Thermochemistry of garnets and aluminous pyroxenes in the CMAS system, p. 29-56. In, Fraser, D.G.(Ed.), Thermodynamics in geology. D. Reidel Publishing Company, Dordrecht, 410 p.

NEWTON, R.C. and WOOD, B.J., 1979.
Thermodynamics of water in cordierite and some petrologic consequences of cordierite as a hydrous phase. Contrib. Mineral. Petrol., v. 68, p. 391-405.

NICHOLLS, J., CARMICHAEL, I.S.E. and STORMER, J.C., 1971.
Silica activity and P_{total} in igneous rocks. Contrib. Mineral. Petrol., v. 33, p. 1-20.

NORRISH, K. and HUTTON, J.J., 1969.
An accurate X-ray spectrographic method for analysis of a wide range of geological samples. Geochim. Cosmochim. Acta, v. 33, p. 431-453.

OBATA, M., 1976.
The solubility of Al_2O_3 in orthopyroxene in spinel and plagioclase peridotites and spinel pyroxenite. Am. Mineral., v. 61, p. 804-816.

OKAMURA, F.P., GHOSE, S. and OHASHI, H., 1974.
Structure and crystal chemistry of calcium Tschermak's pyroxene, $CaAl_2SiO_6$. Am. Mineral., v. 59, p. 549-577.

ONUMA, K., AKASAKA, M. and YAGI, K., 1981.
The bearing of the system $CaMgSi_2O_6$- $CaAl_2SiO_6$ - $CaFeAlSiO_6$ on fassaitic pyroxene. Lithos, v. 14, p. 173-182.

ORVILLE, P.M., 1972.
Plagioclase cation exchange equilibria with aqueous chloride solution. Results at 700°C and 200 bars in the presence of quartz. Am. J. Sci., v. 272, p. 234-272.

PAPIKE, J.J. and ROSS, M., 1970.
Gedrites: crystal structures and intercrystalline cation distributions. Am. Mineral., v. 55, p. 1945-1972.

PLATEN, H., VON, 1965.
Experimental anatexis and genesis of migmatites, p. 203-218. In, Pitcher, W.S. and Flinn, G.W.(Eds.), Controls of metamorphism. Oliver and Boyd, Edinburgh, 368 p.

POWELL, M. and POWELL, R., 1974.
An olivine - clinopyroxene geothermometer. Contrib. Mineral. Petrol., v. 48, p. 249-263.

POWELL, R., 1978 a.
The thermodynamics of pyroxene geotherms. Phil. Trans. R. Soc. London, v.288, p. 457-469.

POWELL, R., 1978 b.
Equilibrium thermodynamics in petrology. An introduction. Harper and Row Publishers, London, 284 p.

POWELL, R. and POWELL, M., 1977.
Geothermometry and oxygen barometry using coexisting iron-titanium oxides: a reappraisal. Mineral. Mag., v. 41, p. 257-263.

RAMBALDI, E.R., 1973.
Variation in the composition of plagioclase and epidote in some metamorphic rocks near Bancroft, Ontario. Can. J. Earth Sci., v. 10, p. 852-868.

RAVIOR, E. and HINRICHSEN, Th., 1975.
Upper stability of synthetic anthophyllite mixed crystals. Neues. Jb. Mineral. Mh., v. 4, p. 162-166.

REENEN, D.D., VAN and DU TOIT, M.C.,1978.
The reaction garnet + quartz ⇌ cordierite + hypersthene in granulites of the Limpopo Metamorphic Complex in northern Transvaal. Geol. Soc. S. Afr., Spec. Publ. 4, p. 149-177.

REINHARD, E.W., 1968.
Phase relations in cordierite-bearing gneisses from the Gananoque area, Ontario. Can. J. Earth Sci., v. 5, p. 455-482.

RICHARDSON, S.W., 1968.
Staurolite stability in a part of the system Fe-Al-Si-O-H. J. Petrol., v. 9, p. 467-488.

RICHARDSON, S.W., GILBERT, M.C. and BELL, P.M., 1969.
Experimental determination of the kyanite-andalusite and andalusite-sillimanite equilibria, the alumino-silicate triple point. Am. J. Sci., v. 267, p. 259-272.

RICKARD, D. and WICKMAN, F.E., 1980.
General discussion. In,Chemistry and geochemistry of solutions at high temperatures and pressures. Physics and Chemistry of the earth, v. 13 and 14, p. 537-541.

RICKWOOD, P.C., 1968.
On recasting analyses of garnet into end-member molecules. Contrib. Mineral. Petrol., v. 18, p. 175-198.

ROBIE, R.A., HEMINGWAY, B.S. and FISHER, J.R., 1978.
Thermodynamic properties of minerals and related substances at 298,15 K and 1bar (10^5 Pascals) pressure and at higher temperature. Geol. Survey Am. Bull. 1452, 456 p.

ROBINSON, P. and JAFFE, H.W., 1969.
Aluminous enclaves in gedrite-cordierite gneiss from southwestern New Hampshire. Am. J. Sci., v. 267, p. 389-421.

ROBINSON, P., ROSS, M. and JAFFE, H.W., 1971.
Composition of the anthophyllite-gedrite series, compositions of gedrite and hornblende, and the anthophyllite-gedrite solvus. Am. Mineral., v. 56, p. 1005-1040.

ROHRLICH,V.R., PRICE, N.B. and CALVERT, S.E., 1969.
Chamosite in the recent sediments of Loch Etive, Scotland. J. Sed. Petrol., v. 39, p. 624-631.

ROLLINSON, H.R. 1981.
Garnet-pyroxene thermometry and barometry in the Scourie-granulites, N.W. Scotland. Lithos, v. 14, p. 225-238.

ROOYEN, D.P., VAN, 1950.
The metamorphic rocks constituting the floor of the Bushveld Igneous Complex, north of Potgietersrus. Trans. Geol. Soc. S. Afr., v. 53, p. 65-71.

RUMBLE, D. III, 1976.
Oxide minerals in metamorphic rocks, R1-R20. In, Rumble, D. (Ed.), Mineral. Soc. Am. Short course notes on Oxide Minerals.

SCHALLER, W.T., 1935.
Monticellite from San Bernardino county California, and the monticellite series. Am. Mineral., v. 20, p. 815-827.

SCHIFFMAN, P. and LIOU, J.G., 1980.
Synthesis and stability relations of Mg-Al pumpellyite, $Ca_4Al_5MgSi_6O_{21}(OH)_7$. J. Petrol., v. 21, p. 441-474.

SCHREYER, W., 1976.
Experimental metamorphic petrology at low pressures and high temperatures, p. 261-331. In, Bailey, D.K. and MacDonald, R. (Eds.), The evolution of the crystalline rocks. Academic Press, London.

SCHREYER, W. and ABRAHAM, K., 1978.
Symplectitic cordierite-orthopyroxene-garnet assemblages as products of contact metamorphism of pre-existing basement granulites in the Vredefort Structure, South Africa, and their relations to pseudotachylite. Contrib. Mineral. Petrol., v. 68, p. 53-62.

SHARMA, R.S. and MacRAE, N.D., 1981.
Paragenetic relations in gedrite-cordierite-staurolite-biotite-sillimanite-kyanite gneisses at Ajitpura, Rajasthan, India. Contrib. Mineral. Petrol., v. 78, p. 48-60.

SHARPE, M.R. and CHADWICK, B., 1981.
The geometry and origin of structures in certain Transvaal Sequence rocks within and adjacent to the eastern compartment of the Bushveld Complex. Inst. Geol. Res. Bushveld Complex, Univ. Pretoria, Res. Rept. 27, 19 p.

SHAW, D.M., 1956.
Geochemistry of pelitic rocks. Part III: Major elements and general geochemistry. Geol. Soc. Am. Bull., v. 67, p. 919-934.

SHEDLOCK, R.J. and ESSENE, E.J., 1979.
Mineralogy and petrology of a tactite near Helena, Montana. J. Petrol., v. 20, p. 71-97.

SMIT, P.J., HALES, A.L. and GOUGH, D.I., 1962.
The gravity survey of the Republic of South Africa. Geol. Surv. S. Afr., Handbook 6, 422 p.

SPEAR, F.S., 1980.
The gedrite-anthophyllite solvus and the composition limits of orthoamphibole from the Post Pond Volcanics, Vermont. Am. Mineral., v. 65, p. 1103-1118.

STORRE, B., 1970.
Stabilitatsbedingungen grossular - führenden paragenesen in system $CaO-Al_2O_3-SiO_2-CO_2-H_2O$. Contrib. Mineral. Petrol., v. 29, p. 145-162.

STORRE, B. and NITSCH, K-H., 1972.
Die reaktion 2 zoisit + 1 CO_2 ⇌ 3 anorthit + 1 calcit + 1 H_2O. Contrib. Mineral. Petrol., v. 35, p. 1-10.

STRAUSS, C.A., 1954.
The geology and mineral deposits of the Potgietersrust Tin-Fields. Geol. Survey S. Afr. Mem.46, 241 p.

TAKéUCHI, Y., HAGA, N., UMIZU,S. and SATO, G., 1982.
The derivative structure of silicate garnets in grandite. Z. Kristallographie, v. 158, p. 53-99.

TAYLOR, B.E. and LIOU, J.G., 1978.
The low temperature stability of andradite in C-O-H fluids. Am. Mineral., v. 63, p. 378-393.

THOMPSON, A.B., 1976 a.
Mineral reactions in pelitic rocks: I. Prediction of P-T-X (Fe-Mg) phase relations. Am. J. Sci., v. 276, p. 401-424.

THOMPSON, A.B., 1976 b.
Mineral reactions in pelitic rocks: II Calculation of some P-T-X (Fe-Mg) phase relations. Am. J. Sci., v. 276, p. 425-454.

THOMPSON, A.B. and TRACY, R.J., 1979.
Model system for anatexis of pelitic rocks. II Facies series melting and reactions in the system $CaO-KAlO_2-NaAlO_2-Al_2O_3-SiO_2-H_2O$. Contrib. Mineral. Petrol., V. 70, p. 429-438.

THOMPSON, J.B., Jr., 1957.
The graphical analysis of mineral assemblages in pelitic schists. Am. Mineral., v. 42, p. 842-858.

TRACY, R.J. and ROBINSON, P., 1977.
Zoned titanium augite in alkali olivine basalt from Tahiti and the nature of titanium substitutions in augite. Am. Mineral., v. 62, p. 634-645.

TRÖGER, W.E., 1971.
Optische bestimmung der gesteinsbildenden minerale. Teil 1, Bestimmungstabellen, 4 Aufl. Schweizerbart'sche Verlagsbuchhandlung, Stuttgart, 188 p.

TRUTER, F.C., 1947.
A remarkable transcurrent fault near Potgietersrus, Transvaal. Trans. Geol. Soc. S. Afr., v. 50, p. 1-15.

TURNOCK, A.C. and EUGSTER, H.P., 1962.
Fe-Al oxides: Phase relationships below 1000°C. J. Petrol., v. 3, p. 533-565.

VANIMAN, D.T., PAPIKE, J.J. and LABOTKA, T., 1980.
Contact-metamorphic effects of the Stillwater Complex, Montana: the concordant iron formation. Am. Mineral., v. 65, p. 1087-1102.

VIELZEUF, D., 1983.
The spinel and quartz associations in high grade zenoliths from Tallante (S.E. Spain) and their potential use in geothermometry and barometry. Contrib. Mineral. Petrol., v. 82, p. 301-311.

WAAL, S.A., DE, 1970.
Nickel minerals from Barberton, South Africa, III Willemseite, a nickel-rich talc. Am. Mineral., v. 55, p. 31-42.

WEDEPOHL, K.H., (Ed.), 1978.
Handbook of geochemistry. Springer-Verlag, New York.

WELLS, P.R.A., 1976 a.
Late Archaean metamorphism in the Buksefjorden region, southwest Greenland. Contrib. Mineral. Petrol., v. 56, p. 229-242.

WELLS, P.R.A., 1976 b.
The metamorphic petrology of high grade Archaean rocks, Buksefjorden,southern west Greenland. Ph.D. thesis (unpublished), University of Exeter.

WELLS, P.R.A., 1977.
Pyroxene thermometry in simple and complex systems. Contrib. Mineral. Petrol., v. 62, p. 129-139.

WELLS, P.R.A., 1979.
Chemical and thermal evolution of Archaean sialic crust, S.W. Greenland. J. Petrol., v. 20, p. 187-226.

WELLS, P.R.A. and RICHARDSON, S.W., 1979.
Thermal evolution of metamorphic rocks in the central Highlands of Scotland. In, Harris, A.L., Holland, C.H. and Leake, B.E. (Eds.), Caledonides of the British Isles-reviewed. Geol. Soc. London Spec. Publ., v. 8, p. 339-344.

WILLEMSE, J. and BENSCH, J.J., 1964.
Inclusions of original carbonate rocks in gabbro and norite of the eastern part of the Bushveld Complex. Trans. Geol. Soc. S. Afr., v. 67, p. 1-87.

WINKLER, H.G.F., 1979.
Petrogenesis of metamorphic rocks, 5 th edition. Springer-Verlag, New York, 348 p.

WOOD, B.J., 1974.
The solubility of alumina in orthopyroxene coexisting with garnet. Contrib. Mineral. Petrol., v. 46, p. 1-15.

WOOD, B.J., 1976.
Mixing properties of tschermakitic clinopyroxenes. Am. Mineral., v. 61, p. 599-602.

WOOD, B.J., 1979.
Activity-composition relations in $Ca(Mg, Fe)Si_2O_6$-$CaAl_2SiO_6$ clinopyroxene solid solution. Am. J. Sci., v. 279, p. 854-887.

WOOD,B.J. and BANNO, S., 1973.
Garnet-orthopyroxene and orthopyroxene-clinopyroxene relationships in simple and complex systems. Contrib. Mineral. Petrol., v. 42, p. 109-124.

WOODSWORTH, G.J., 1977.
Homogenization of zoned garnets from pelitic schists. Can. Mineral., v.15, p. 230-242.

YODER, H.S. and CHINNER, G.A., 1960.
Almandine-pyrope water systems at 10 000 bars Carnegie Inst. Wash., Yb. 59, p. 81-84.

ZAGT, S., 1942.
Die geologie rondom Potgietersrus. M.Sc. thesis (unpublished), University of Pretoria, 35 p.

ZEN, E - An., 1963.
Components, phases and criteria of chemical equilibrium in rocks. Am. J. Sci., v. 261, p. 929-942.

ZEN, E - An., 1966.
Construction of pressure-temperature diagrams for multicomponent systems after the method of Schreinemakers - a geometric approach. U.S. Geol. Survey Bull. 1225, 56 p.

Appendix 1

ANALYSES AND MODES OF PELITIC ROCKS FROM THE TRANSVAAL SEQUENCE NEAR POTGIETERSRUS

Sample #	PH-5	PH-8	PH-21	PH-30	PH-31	PH-40	PH-42	PH-50	PH-75	PH-76	PH-79	PH-80	PH-85	PH-88	PH-109	PH-116	PH-122	PH-124	PH-138 -And
Formation	T3SiH	T3siH	T3siH	pre-B. sill	T3siH	T3sSh	T3siH	T3sSh	T3sSH	T3sSh	T3siH	T3siH	T3siH	T3siH	T3tSh	T3tH	T3tH	T3tH	T3tH
SiO_2	66,95	54,33	63,19	58,27	62,92	60,22	62,55	64,77	60,83	62,95	48,19	60,69	64,67	61,48	60,15	51,14	53,10	58,15	67,95
TiO_2	0,10	0,90	0,82	1,02	1,06	0,86	0,95	0,59	0,76	0,67	0,74	0,69	1,09	0,94	0,79	0,99	0,98	0,93	0,60
Al_2O_3	1,78	15,63	13,85	15,02	16,22	22,31	15,99	17,03	20,14	17,96	13,11	13,89	10,09	9,60	22,25	23,11	22,80	21,31	18,19
FeO[a]	22,88	19,60	7,83	10,06	8,32	6,21	9,60	5,65	7,16	6,50	9,70	5,24	10,24	9,48	5,30	10,94	10,49	8,23	3,60
MnO	0,17	0,10	0,09	0,17	0,02	0,03	0,05	0,08	0,07	0,05	0,21	0,02	0,16	0,14	0,03	0,21	0,07	0,06	0,02
MgO	3,18	6,59	7,63	5,14	2,89	2,02	2,93	2,64	2,12	2,77	4,73	6,23	5,69	6,96	1,73	3,00	2,61	2,81	1,39
CaO	1,97	0,20	2,63	5,99	0,16	0,17	1,10	1,39	0,14	0,73	9,61	3,43	3,06	9,06	0,16	6,64	0,40	0,50	0,07
Na_2O	0,15	0,50	0,56	1,12	0,22	1,45	0,92	1,87	1,03	1,83	1,26	0,90	4,12	2,19	1,00	3,29	1,13	0,85	1,02
K_2O	0,03	0,18	2,17	1,84	5,12	4,67	4,86	3,49	3,25	2,68	8,09	6,37	0,02	0,25	4,10	0,05	2,76	3,66	3,12
P_2O_5	0,12	0,02	0,11	0,22	0,08	0,08	0,09	0,07	0,09	0,11	0,87	0,09	0,08	0,05	0,09	0,07	0,18	0,21	0,05
Cr_2O_3	0,04	0,23	0,04	0,02	0,05	0,03	0,07	0,03	0,02	0,03	0,01	0,04	0,04	0,04	0,02	0,04	0,03	0,04	0,02
NiO	0,03	0,18	0,03	0,01	0,02	0,01	0,02	0,01	0,01	0,01	0,01	0,02	0,02	0,01	0,01	0,02	0,02	0,01	-
L.O.I.	0,76	0,60	1,06	0,65	2,01	1,47	0,61	1,45	3,35	2,47	3,23	1,16	-0,30	0,06	3,63	0,08	5,02	2,24	3,58
H_2O^-	0,16	0,09	0,14	0,05	0,20	0,15	0,10	0,18	0,25	0,24	0,11	0,19	0,05	0,13	0,30	0,09	0,28	0,22	0,22
Total	98,32	99,15	100,15	99,58	99,29	99,68	99,84	99,25	99,22	99,00	99,87	98,96	99,03	100,39	99,56	99,67	99,87	99,22	99,83
Zn	62	268	105	206	27	52	35	70	141	101	195	29	100	109	37	161	118	109	57
Cu	8	95	18	4	0	5	0	2	1	16	18	0	99	4	16	2	19	45	27
Nb	0	0	9	21	12	19	9	12	18	15	45	8	7	4	20	17	16	20	17
Zr	27	91	171	371	231	251	181	140	231	216	414	158	116	141	246	154	153	193	177
Y	9	17	23	49	23	31	22	19	29	26	44	15	42	32	31	29	25	33	23
Sr	445	17	124	435	50	152	113	251	182	164	1971	225	90	167	116	324	126	151	98
Rb	0	7	110	94	222	237	214	157	153	135	329	224	0	5	239	2	160	192	182
Ga	3	15	16	17	21	25	20	18	22	21	15	16	12	13	26	23	26	27	22
Hf	0	2	7	9	6	4	9	4	9	8	10	2	1	6	8	5	6	8	6
mode	cpx mt qz	cord anth bi mt qz	cord anth bi ilm qz	hbl plag mt qz	cord and bi musc k-spar mt qz	cord and bi musc mt qz	cord and bi musc k-spar plag qz	cord bi musc mt qz	cord bi musc chl mt qz	cord bi musc chl mt qz	gar cpx cc plag mt apatite qz	hbl bi plag qz	cumm plag mt ilm qz	opx cpx hbl plag mt qz	ctd chl mt qz	gar ged cord plag ilm qz	cord ctd chl and bi mt qz	cord and bi musc mt ilm qz	chl musc mt qz

a Total Fe as FeO

pre-B.sill = pre-Bushveld sill

ANALYSES AND MODES OF PELITIC ROCKS FROM THE TRANSVAAL SEQUENCE NEAR POTGIETERSRUS

Sample #	PH-138 +And.	PH-143	PH-151	PH-152	PH-157	PH-164	PH-166	PH-167	PH-168	PH-169	PH-170	PH-172	PH-176	PH-178	PH-179	PH-180	PH-181	PH-182	PH-186
Formation	T3tH	T3tH	T2pH	T2pH	T2pH	T2dH.m3	T2dH.m3	T2dH.m3	T3tH	T3tH	T2pH	T2tH	T2pH	T2dH.m1	T2dH.m1	T2dH.m1	T2dH.m3	T2dH.m3	T2dH.m3
SiO_2	54,68	58,52	56,91	47,56	50,45	59,04	45,48	53,69	36,61	34,50	48,38	36,30	47,48	48,06	48,66	52,56	49,57	52,16	47,43
TiO_2	0,82	0,83	0,38	0,48	1,32	0,12	0,33	0,77	1,44	0,04	0,92	0,16	0,82	0,98	0,87	0,83	0,28	0,77	0,40
Al_2O_3	24,62	19,85	12,56	15,47	13,81	3,23	7,49	21,09	34,77	43,06	18,92	45,20	19,78	23,87	23,00	20,78	1,98	14,45	4,53
FeO[a]	7,39	10,57	23,15	27,33	16,03	23,05	14,43	11,94	15,63	11,07	19,93	13,22	21,58	14,37	13,77	11,69	24,25	14,36	22,07
MnO	0,03	0,06	0,08	0,09	0,23	0,25	0,44	0,08	0,08	0,06	0,09	0,06	0,08	0,10	0,12	0,14	0,48	0,15	0,70
MgO	1,68	2,51	5,41	6,85	15,42	4,77	9,36	5,74	7,61	7,27	7,37	3,66	7,36	7,23	7,22	6,42	9,92	4,98	10,96
CaO	0,21	0,29	0,24	0,38	0,43	8,89	20,50	0,59	0,21	0,22	0,16	0,08	0,08	0,77	0,76	0,83	13,97	8,65	15,03
Na_2O	1,01	0,87	0,54	0,40	0,31	0,36	0,29	0,47	0,37	0,49	0,52	0,28	0,36	1,03	1,46	0,80	0,37	1,03	0,25
K_2O	2,80	2,87	0,02	0,03	0,03	0,32	0,42	3,01	0,18	0,65	2,20	0,09	1,43	2,38	1,99	2,45	0,23	2,07	0,12
P_2O_5	0,15	0,21	0,15	0,27	0,12	0,00	0,00	0,26	0,00	0,00	0,05	0,00	0,03	0,28	0,29	0,17	0,00	0,12	0,00
Cr_2O_3	0,03	0,03	0,03	0,04	0,09	0,05	0,03	0,06	0,10	0,16	0,06	0,10	0,05	0,07	0,07	0,06	0,02	0,06	0,02
NiO	0,02	0,02	0,03	0,03	0,07	0,03	0,03	0,04	0,06	0,05	0,04	0,05	0,04	0,04	0,05	0,04	0,03	0,04	0,03
L.O.I.	5,80	3,48	-0,49	0,69	0,76	-0,51	0,54	1,80	3,20	2,25	0,66	1,09	-0,07	0,73	1,57	2,52	-1,02	0,38	-1,03
H_2O^-	0,93	0,20	0,11	0,25	0,05	0,15	0,14	0,15	0,13	0,12	0,19	0,09	0,10	0,09	0,19	0,44	0,09	0,16	0,09
Total	100,17	100,31	99,12	98,49	99,12	99,75	99,48	99,69	100,39	99,94	99,49	100,38	99,12	100,00	100,02	99,73	100,17	99,38	100,60
Zn	104	122	66	84	99	52	58	109	146	108	99	172	93	105	113	114	43	102	44
Cu	42	8	1	8	142	7	1	412	4	18	9	7	3	11	2	90	3	77	5
Nb	18	16	8	16	6	0	8	17	5	0	17	0	17	12	10	18	4	10	7
Zr	166	208	95	123	86	30	69	147	4	0	148	4	138	155	137	149	32	126	69
Y	28	26	29	35	25	18	26	36	0	0	32	3	24	35	39	32	20	27	21
Sr	128	142	6	10	7	75	152	15	17	36	31	19	14	112	67	33	24	170	60
Rb	167	164	0	0	0	12	17	188	23	27	126	12	90	119	100	185	8	81	7
Ga	26	24	16	19	17	4	10	27	36	41	26	52	26	32	30	28	4	7	7
Hf	3	6	3	5	5	3	4	4	4	7	3	1	3	1	7	5	0	6	6
mode	and chl musc mt qz	cord ctd and bi mt qz	gar cord ged ilm qz	gar cord ged ilm qz	cord anth ilm qz	cpx hbl mt qz	cpx mt qz	cord bi plag k-spar mt qz	cord sp bi mt	cord sp sill cor	gar opx cord bi plag qz	cord sp sill mt	opx cord plag mt qz	opx cord plag mt qz	cord sp sill ilm	cord bi plag k-spar mt qz	opx cpx hbl mt qz	opx cpx bi plag qz	cpx mt qz

a Total Fe as FeO

ANALYSES AND MODES OF PELITIC ROCKS FROM THE TRANSVAAL SEQUENCE NEAR POTGIETERSRUS

Sample #	PH-188	PH-189	PH-190	PH-192	PH-196	PH-197	PH-202	PH-208	PH-209	PH-213	PH-214	PH-218	PH-219	PH-302	PH-304	PH-308	PH-312	PH-313	PH-316
Formation	T2pH	T2dH.m1	T3tH	T2dH.m3	T2pH	T2pH	T2pH	T2pH	T2pH	T2dH.m3	T2pH	T2pH	T2pH	T3siH	T3tH	T3tH	T2pH	T2pH	T2dH.m3
SiO_2	61,55	38,91	41,11	61,39	46,96	44,55	42,97	32,25	45,45	44,33	29,91	40,54	41,51	46,35	55,31	54,94	47,93	49,20	54,25
TiO_2	0,31	1,05	0,09	0,07	0,16	0,75	0,21	1,24	0,18	0,44	1,01	0,11	0,19	0,75	0,92	0,62	0,92	0,87	0,48
Al_2O_3	10,03	26,66	39,33	3,19	14,85	20,24	23,20	28,39	17,13	11,83	30,41	21,61	23,11	12,55	23,81	14,76	13,73	14,12	11,01
FeO[a]	21,87	20,15	10,48	22,41	28,64	24,59	21,28	23,98	25,75	15,11	24,19	26,94	22,95	9,23	10,04	9,30	25,10	26,04	10,40
MnO	0,06	0,13	0,08	0,21	0,09	0,08	0,06	0,10	0,11	0,41	0,11	0,10	0,08	0,16	0,07	0,18	0,16	0,18	0,16
MgO	5,43	9,93	4,19	3,95	8,41	8,89	11,12	10,62	10,60	12,45	12,59	9,85	10,73	5,63	3,08	8,49	7,62	7,32	14,62
CaO	0,32	0,11	0,73	8,45	0,14	0,02	0,02	0,07	0,02	14,45	0,07	0,08	0,00	10,25	0,30	8,29	3,43	2,12	7,76
Na_2O	0,31	0,61	1,10	0,17	0,39	0,33	0,35	0,32	0,37	0,39	0,33	0,44	0,27	3,69	1,23	1,36	0,92	0,50	0,47
K_2O	0,13	0,57	0,24	0,16	0,04	0,16	0,27	0,24	0,08	0,13	0,25	0,22	0,33	4,03	2,92	0,64	0,13	0,24	0,40
P_2O_5	0,10	0,01	0,00	0,00	0,00	0,01	0,00	0,00	0,00	0,00	0,00	0,03	0,01	0,82	0,15	0,03	0,11	0,10	0,00
Cr_2O_3	0,05	0,11	0,09	0,04	0,04	0,07	0,10	0,12	0,07	0,06	0,15	0,08	0,10	0,01	0,04	0,06	0,08	0,10	0,20
NiO	0,02	0,08	0,04	0,02	0,05	0,05	0,06	0,09	0,05	0,05	0,11	0,05	0,05	0,01	0,02	0,04	0,05	0,05	0,07
L.O.I.	-1,23	0,60	2,11	-0,32	-1,23	-0,66	-0,44	0,73	-0,86	0,36	0,13	-0,68	-0,35	6,49	1,61	1,14	-1,07	-1,34	0,15
H_2O^-	0,07	0,09	0,13	0,16	0,15	0,07	0,07	0,13	0,10	0,13	0,10	0,19	0,07	0,05	0,07	0,13	0,05	0,08	0,09
Total	99,02	99,01	99,72	99,90	98,69	99,15	99,27	98,28	99,05	100,14	99,36	99,56	99,05	100,02	99,57	99,98	99,16	99,58	100,06
Zn	59	116	82	31	75	94	70	75	84	59	102	70	48	126	109	79	73	97	74
Cu	16	6	154	5	7	45	5	4	7	2	8	20	10	71	2	87	39	21	2
Nb	7	5	0	3	0	6	0	0	0	0	0	0	45	45	16	6	12	11	3
Zr	74	32	8	43	7	25	5	7	4	12	5	5	410	410	171	103	142	138	66
Y	19	7	3	18	7	10	5	5	5	17	5	4	44	44	26	20	23	23	15
Sr	3	12	111	103	15	0	0	0	0	138	0	0	1343	1343	133	132	81	40	149
Rb	4	50	17	6	5	19	36	28	11	5	39	28	218	218	155	27	6	10	13
Ga	12	43	45	2	17	27	25	48	19	13	52	19	21	14	29	14	18	18	11
Hf	1	4	3	0	2	4	3	1	0	0	2	1	0	4	8	1	3	6	6
mode	gar opx cord bi plag ilm qz	cord plag mt	cord sp sill plag ilm	cpx mt qz	opx cord qz	ol opx cord bi mt qz	ol opx cord sp	ol opx cord sp mt	ol opx cord mt	ol cpx plag mt ilm	opx cord sp mt	ol opx cord sp	ol opx cord sp mt	cpx bi cc plag mt qz	cord and bi musc mt qz	hbl plag qz	cumm cord plag ilm qz	cumm cord plag ilm qz	opx hbl plag mt qz

a Total Fe as FeO

ANALYSES AND MODES OF PELITIC AND CALCAREOUS ROCKS FROM THE TRANSVAAL SEQUENCE NEAR POTGIETERSRUS

Sample #	PH-317	PH-319	PH-320	PH-321	PH-324	PH-325	PH-326	PH-327	PH-330	PH-334	PH-335	PD-18	PD-20	PD-59	PD-61 Sil	PD-61+Sil	PD-70	PD-72	PD-76
Formation	T2dH.m1	T3tH	T2pH	T2pH	T2pH	T2pH	T2pH	T2pH	T2pH	T3tH	T2pH	T2dD.m4	T2dD.m4	T2D	T2D	T2D	T2D	T2D	T2D
SiO_2	58,04	37,21	55,83	46,78	54,49	51,17	52,87	46,95	52,49	29,59	48,82	28,91	50,58	0,62	0,96	22,58	21,09	39,32	40,40
TiO_2	0,57	0,08	0,49	0,45	0,49	0,66	0,53	0,88	0,47	0,07	0,74	0,17	0,49	0,00	0,00	0,00	0,01	0,00	0,10
Al_2O_3	17,83	48,45	15,58	16,49	14,37	16,34	15,21	19,81	15,48	55,30	14,74	5,14	12,25	0,09	0,06	0,20	0,23	0,00	2,09
FeO^a	9,06	8,94	16,44	27,08	22,82	22,54	22,47	21,63	20,86	8,76	27,99	1,36	4,59	0,21	0,43	0,34	0,57	0,23	2,39
MnO	0,04	0,05	0,07	0,16	0,06	0,09	0,07	0,10	0,10	0,06	0,09	0,20	0,05	0,22	0,22	0,15	0,19	0,19	0,29
MgO	5,67	3,77	5,63	8,09	6,65	7,05	7,19	7,70	5,86	4,22	6,53	17,08	14,41	25,96	26,26	23,68	23,03	25,03	20,17
CaO	0,78	0,09	0,26	0,32	0,07	0,10	0,12	0,18	0,40	0,13	0,24	16,84	10,98	25,40	25,86	24,45	24,64	16,36	25,06
Na_2O	2,17	0,45	0,67	0,54	0,19	0,45	0,43	0,48	0,66	0,50	0,53	0,07	0,68	0,00	0,05	0,05	0,06	0,05	0,01
K_2O	4,72	0,22	2,52	0,24	0,78	1,15	0,93	1,88	1,54	0,25	0,01	1,60	3,36	0,00	0,00	0,00	0,02	0,00	0,03
P_2O_5	0,16	0,00	0,11	0,05	0,02	0,04	0,03	0,04	0,10	0,00	0,13	0,00	0,04	0,00	0,00	0,00	0,00	0,00	0,00
Cr_2O_3	0,05	0,13	0,03	0,05	0,05	0,05	0,04	0,06	0,05	0,15	0,05	0,01	0,02	0,00	0,00	0,00	0,00	0,01	0,00
NiO	0,03	0,03	0,02	0,03	0,04	0,03	0,03	0,04	0,03	0,07	0,04	0,01	0,02	0,00	0,00	0,00	0,00	0,00	0,02
CO_2	-	-	-	-	-	-	-	-	-	-	-	25,13	0,28	35,80	35,09	24,75	24,99	14,83	7,49
L.O.I.	1,16	0,77	1,82	-1,01	-0,67	-0,33	-0,37	0,03	0,60	1,12	-0,65	3,58[b]	2,41[b]	10,78[b]	10,99[b]	3,73[b]	5,32[b]	3,41[b]	2,53[b]
H_2O^-	0,08	0,06	0,16	0,07	0,11	0,09	0,08	0,08	0,11	0,09	0,04	0,21	0,24	0,04	0,04	0,06	0,22	0,15	0,25
Total	100,36	100,25	99,63	99,34	99,47	99,43	99,63	99,86	98,75	100,31	99,30	100,31	100,40	99,12	99,96	99,99	100,37	99,58	100,83
Zn	9	41	78	88	87	94	83	88	82	50	104	14	12	2	1	1	8	2	120
Cu	0	6	22	5	4	5	3	7	13	15	29	2	1	1	3	0	2	0	8
Nb	14	0	11	10	13	13	12	17	11	0	13	4	6	0	0	0	0	0	0
Zr	117	2	103	104	103	132	107	140	104	0	132	105	118	2	0	0	2	0	14
Y	14	0	24	18	28	29	33	33	24	0	26	11	16	2	3	0	0	0	10
Sr	61	4	31	9	3	10	8	15	56	15	12	66	245	9	9	7	12	10	44
Rb	209	12	125	15	48	70	53	96	89	21	0	69	134	0	0	0	0	0	0
Ga	22	49	20	22	18	23	19	28	20	57	17	n.d.	n.d.	n.d.	n.d.	n.d.	n.d.	n.d.	n.d.
Hf	3	5	5	1	4	2	3	3	5	2	8	n.d.	n.d.	n.d.	n.d.	n.d.	n.d.	n.d.	n.d.
mode	cord sp bi k-spar	cord sp sill k-spar	cord ged bi ilm qz	gar opx cord ged anth bi mt ilm qz	gar opx cord bi plag ilm qz	gar opx cord bi plag ilm qz	gar opx cord bi plag ilm qz	gar opx cord bi plag ilm qz	gar opx cord bi plag mt qz	cord sp sill cor	cord ged mt qz	phlog chl dol cc qz	epidote cc dol qz	trem cc dol qz	trem cpx cc dol qz	cc dol qz	cpx trem cc dol	trem cc dol	cpx Fo (serp) cc dol

a Total Fe as FeO
b L.O.I. - CO_2

ANALYSES AND MODES OF CALCAREOUS ROCKS FROM THE TRANSVAAL SEQUENCE NEAR POTIGETERSRUS

Sample #	PD-81	PD-82 Amph	PD-82 Cpx	PD-83	PD-86	PD-88	PD-89	PD-91	PD-118	PD-125	PD-128	PD-131	PD-132	PD-150	PD-156	PD-157	PD-158	PD-159	PD-161
Formation	T2D	T2dD.m2	T2dD.m2	T2dD.m2	T2D	T2D	T2D	T2D	T2D	T2dD.m4	T2D	T2dD.m2	T2dD.m2	T2dD.m2	T2dD.m4	T2dD.m4	T2dD.m4	T2dD.m4	T2dD.m4
SiO_2	47,97	49,68	51,18	48,50	49,67	50,92	55,76	23,22	50,07	48,64	40,74	9,33	54,63	52,11	44,27	6,26	39,99	46,26	8,52
TiO_2	0,26	0,30	0,10	0,18	0,21	0,23	0,05	0,06	0,17	0,26	0,03	0,12	0,19	0,46	0,45	0,07	0,14	0,45	0,11
Al_2O_3	10,34	5,67	1,95	9,84	5,22	11,02	1,15	1,74	8,68	11,62	0,14	2,70	14,12	14,05	11,05	1,70	23,94	8,75	2,48
FeO[a]	7,82	5,91	3,80	6,47	1,77	4,38	5,68	1,81	4,93	2,19	0,51	1,14	2,58	2,09	4,33	0,90	5,45	3,76	1,03
MnO	0,40	0,17	0,16	0,19	0,11	0,15	0,18	0,47	0,16	0,09	0,28	0,28	0,08	0,04	0,11	0,17	0,10	0,19	0,16
MgO	10,04	17,17	19,33	15,26	19,64	15,00	22,55	9,48	16,38	12,25	20,06	9,77	8,65	8,65	17,64	9,78	4,74	17,13	9,92
CaO	17,03	17,63	22,45	16,99	22,88	12,98	12,53	39,16	15,84	23,07	26,51	40,24	12,75	16,38	22,33	41,85	24,00	23,01	41,81
Na_2O	1,66	0,89	0,21	0,22	0,07	1,24	0,24	0,04	0,47	0,04	0,08	0,15	4,87	4,08	0,05	0,17	0,00	0,02	0,02
K_2O	1,80	0,37	0,08	0,05	0,05	1,17	0,05	0,45	0,91	0,03	0,00	0,47	1,31	0,82	0,00	0,43	0,00	0,00	0,00
P_2O_5	0,00	0,00	0,00	0,00	0,00	0,00	0,00	0,00	0,00	0,00	0,00	0,00	0,00	0,78	0,00	0,00	0,00	0,00	0,00
Cr_2O_3	0,01	0,11	0,02	0,17	0,03	0,16	0,01	0,01	0,28	0,01	0,00	0,01	0,02	0,02	0,03	0,01	0,02	0,03	0,01
NiO	0,02	0,03	0,02	0,09	0,01	0,09	0,04	0,01	0,05	0,01	0,00	0,01	0,04	0,01	0,01	0,01	0,01	0,02	0,02
CO_2	1,91	0,78	1,00	0,22	0,26	0,28	0,20	21,67	0,41	0,22	11,23	28,86	0,22	0,20	0,09	29,45	0,07	0,18	27,89
L.O.I.-CO_2	1,18	1,12	0,37	2,44	0,47	2,16	1,79	1,87	2,08	2,11	0,00	7,21	1,19	1,46	0,42	8,96	2,52	0,99	7,91
H_2O^-	0,23	0,10	0,06	0,12	0,10	0,14	0,08	0,10	0,12	0,05	0,14	0,17	0,17	0,14	0,07	0,07	0,07	0,09	0,08
Total	100,67	99,93	100,73	100,74	100,49	99,92	100,31	100,09	100,55	100,59	99,72	100,46	100,82	101,29	100,85	99,83	101,05	100,88	99,96
Zn	61	41	25	349	34	37	39	6	40	60	4	5	14	12	16	8	5	18	46
Cu	6	13	5	50	1	2	2	7	3	2	2	0	0	0	3	116	6	3	156
Nb	3	0	0	0	0	0	0	3	0	0	0	0	4	40	7	0	4	0	3
Zr	62	27	21	16	44	25	6	25	18	113	14	27	95	219	133	20	74	165	26
Y	10	11	6	7	12	9	5	14	8	44	3	17	13	31	22	17	25	20	22
Sr	224	49	22	12	23	146	7	85	86	10	48	668	460	178	10	1061	259	38	972
Rb	67	7	0	0	0	31	0	12	26	0	0	30	80	30	0	19	0	0	0
Mode	cpx cc sphene plag(ser)	act qz?	cpx qz?	trem chl prh	cpx	act cpx bi qz	act cpx	Fo(serp) cc dol	act cpx plag (ser)	act cpx prehn qz	cpx cc	cpx cc sp	cpx plag (ser) sphene qz?	cpx plag (ser) sphene prehn	cpx	cpx cc k-spar	cz prehn	cpx	cpx cc

a Total Fe as FeO

ANALYSES AND MODES OF CALCAREOUS ROCKS FROM THE TRANSVAAL SEQUENCE NEAR POTGIETERSRUS

Sample #	PD-163	PD-166	PD-171	PD-172	PD-175	PD-184	PD-185	PD-186A	PD-186C	PD-191	PD-194	PD-200	PD-210	PD-212	PD-217	PC-10	PC-11	PC-12	PC-13
Formation	T2D	T2D	T2dD.m2	T2dD.m2	T2dD.m4	T2dD.m4	T2dD.m4	T2dD.m2	T2dD.m2	T2D	T2D	T2D	T2D	T2D	T2D	T3SiD	T2SiD	T2SiD	T2SiD
SiO_2	17,33	54,98	17,47	4,46	11,89	23,81	40,15	40,25	47,11	26,43	10,19	42,66	34,88	62,95	44,63	12,73	49,98	52,78	15,86
TiO_2	0,01	0,00	0,20	0,04	0,12	0,17	1,47	0,14	0,19	0,08	0,11	0,46	0,46	0,31	0,54	0,06	0,72	0,73	0,17
Al_2O_3	0,10	0,07	4,58	0,94	50,05	36,45	13,15	2,94	4,33	2,40	1,24	6,43	14,81	11,57	9,36	2,08	13,02	12,73	3,88
FeO[a]	0,30	0,87	2,29	0,46	9,10	8,06	7,04	17,48	15,03	2,28	2,09	12,80	3,69	0,61	4,47	1,97	9,85	9,75	2,99
MnO	0,15	0,37	0,49	0,07	0,53	0,45	0,16	0,48	0,35	0,51	0,86	0,32	0,39	0,06	0,15	0,05	0,32	0,26	0,08
MgO	18,89	21,09	1,55	8,46	19,58	12,45	14,78	10,23	12,61	1,21	1,37	13,31	18,11	9,02	13,45	13,99	9,29	4,90	1,59
CaO	30,63	20,19	43,91	43,63	6,86	15,71	22,99	21,43	21,27	44,05	48,68	22,46	22,09	4,13	24,88	34,68	12,55	10,95	45,53
Na_2O	0,24	0,02	0,42	0,29	0,11	0,18	0,02	0,28	0,15	0,26	0,51	0,17	0,01	2,10	0,23	0,26	2,70	5,88	0,30
K_2O	0,01	0,01	0,00	0,00	0,00	0,01	0,01	0,56	0,06	0,57	0,00	0,01	0,00	6,40	0,00	0,00	0,45	0,59	0,03
P_2O_5	0,00	0,00	0,05	0,00	0,00	0,00	0,00	0,00	0,00	0,00	0,00	0,00	0,00	0,00	0,00	0,00	0,10	0,14	0,04
Cr_2O_3	0,01	0,01	0,02	0,01	0,09	0,05	0,05	0,02	0,03	0,02	0,01	0,03	0,02	0,03	0,06	0,01	0,25	0,21	0,03
NiO	0,01	0,00	0,03	0,02	0,11	0,11	0,04	0,03	0,02	0,02	0,01	0,03	0,02	0,00	0,02	0,01	0,08	0,06	0,02
CO_2	-	0,44	-	-	1,91	-	0,12	4,26	0,27	-	-	0,83	1,93	6,87	-	-	-	-	-
L.O.I.-CO_2	31,92[b]	2,48	28,55[b]	40,93[b]	0,23	1,83[b]	0,27	2,25	-0,63	21,10[b]	34,01[b]	0,62	4,52	-4,06	1,75[b]	33,14[b]	-0,41[b]	0,96[b]	28,44[b]
H_2O^-	0,22	0,18	0,11	0,14	0,15	0,08	0,05	0,09	0,07	0,07	0,20	0,31	0,32	0,13	0,09	0,23	0,10	0,21	0,15
Total	99,88	100,71	99,67	99,45	100,73	99,36	100,30	100,44	100,86	99,00	99,28	100,44	101,25	100,12	99,63	99,21	99,00	100,15	99,11
Zn	2	18	9	1	526	260	13	41	31	6	n.d.	38	14	10	53	13	120	72	40
Cu	1	0	1	22	5	11	604	5	3	15	n.d.	5	3	2	10	2	106	0	20
Nb	0	0	0	0	0	4	4	3	0	0	n.d.	3	10	5	3	0	3	4	0
Zr	5	2	35	11	37	54	304	39	55	41	n.d.	73	109	64	93	19	66	76	33
Y	4	2	24	13	11	10	49	15	10	11	n.d.	13	24	5	16	11	19	27	10
Sr	30	10	497	70	6	36	19	26	7	68	n.d.	19	4	36	30	124	236	463	928
Rb	0	0	0	0	0	0	0	11	0	19	n.d.	0	0	123	0	0	16	27	0
mode	fo(serp) cc dol	trem cpx cc qz	cpx gar cc prehn	fo(serp) cc dol	cpx sp	cpx sp epidote	cpx gar	act k-spar cc	cpx cc	cpx wo cc	monti wo gar cpx cc	cpx gar prehn	idocrase cpx cc	act cpx mt qz	cpx sp cc	Fo(serp) sp cc dol	act cpx plag	cpx ep plag prehn mt qz?	gar cpx cc

a Total Fe as FeO

b CO_2 not determined i.e. L.O.I.-CO_2 = L.O.I.

A = Amph
C = Cpx

ANALYSES AND MODES OF CALCAREOUS ROCKS FROM THE TRANSVAAL SEQUENCE NEAR POTGIETERSRUS

Sample #	PC-14	PC-16	PC-18	PC-25	PC-27-Fo	PC-27+Fo	PC-30	PC-34	PC-45	PC-50	PC-52A	PC-52+Ga	PC-52-Ga	PC-53
Formation	T3SiD	T3SiD	T3SiD	T3SiD	T3SiD	T3SiD	T3SiD	T3SiD	T3SiD	T3SiD	T3SiD	T3SiD	T3SiD	T3SiD
SiO_2	9,50	59,52	50,28	68,30	31,65	24,91	49,67	5,27	46,01	15,63	18,22	42,57	45,80	39,06
TiO_2	0,05	0,41	1,10	0,38	0,17	0,04	0,62	0,06	0,37	0,07	0,19	0,32	0,38	0,35
Al_2O_3	1,13	9,56	18,22	7,05	3,81	1,63	10,94	1,18	10,83	2,14	4,05	11,97	9,65	6,27
FeO[a]	0,70	4,74	3,57	8,46	2,28	1,83	9,05	0,70	6,27	0,90	1,58	5,16	5,02	3,39
MnO	0,09	0,04	0,25	0,19	0,07	0,08	0,32	0,05	0,22	0,02	0,02	0,22	0,19	0,30
MgO	18,26	10,87	4,56	0,00	16,66	18,61	5,16	19,96	11,11	15,79	19,56	6,88	10,65	11,93
CaO	30,24	8,54	14,38	13,22	27,51	27,81	19,97	30,62	22,39	32,91	27,17	29,73	26,33	28,93
Na_2O	0,26	2,76	3,08	0,17	0,45	0,28	1,86	0,26	0,28	0,25	0,22	0,21	0,21	0,24
K_2O	0,18	2,03	1,79	0,00	0,75	0,05	0,35	0,06	0,45	0,00	0,00	0,02	0,04	0,01
P_2O_5	0,02	0,10	0,13	0,37	0,12	0,04	0,09	0,01	0,09	0,00	0,00	0,00	0,03	0,05
Cr_2O_3	0,01	0,02	0,21	0,07	0,02	10,01	0,06	0,01	0,03	0,01	0,01	0,03	0,03	0,02
NiO	0,01	0,02	0,04	0,01	0,01	0,01	0,01	0,02	0,02	0,02	0,01	0,02	0,02	0,01
L.O.I.	38,99	1,25	2,55	1,18	16,04	23,47	0,73	40,91	1,68	31,66	28,60	1,71	1,23	9,02
H_2O^-	0,13	0,09	0,13	0,06	0,25	0,52	0,13	0,18	0,20	0,34	0,31	0,09	0,16	0,37
Total	99,56	99,95	100,29	99,46	99,79	99,29	98,96	99,29	99,95	99,74	99,94	98,93	99,74	99,95
Zn	19	66	126	10	47	62	127	22	212	24	38	114	167	14
Cu	30	7	0	4	0	1	0	0	8	2	5	3	4	36
Nb	3	9	5	0	0	0	6	0	8	2	6	8	9	4
Zr	22	129	127	147	44	13	96	19	79	29	99	69	88	126
Y	6	20	13	47	13	12	21	5	20	12	12	34	19	18
Sr	151	287	506	1207	171	187	211	261	135	234	97	29	31	157
Rb	12	59	88	0	43	0	17	4	27	0	0	3	5	0
Mode	trem	act	cpx	gar	Fo	cpx	cpx	Fo	cpx	Fo(serp)	cpx	Ga	cpx	cpx
	phlog	plag(ser)	plag	ep	cpx	trem	act	phlog	sp	trem	sp	cpx	cc	sp
	cc	bi	sphene	qz	trem	cc	phlog	cc		cc		cc		phlog
	dol				cc	dol	plag(ser)	dol		dol				cc
					dol									

a Total Fe as FeO

Appendix 2

ELECTRON MICROPROBE ANALYSES OF BIOTITE

Sample ##	PH-8	PH-14	PH-16	PH-19	PH-21	PH-31	PH-40	PH-41	PH-42	PH-48	PH-75	PH-76	PH-79	PH-80	PH-117	PH-122	PH-143	PH-170	PH-176
SiO_2	34,46	39,11	39,04	38,02	36,53	36,17	34,51	33,69	36,52	34,14	35,11	35,06	37,31	34,98	32,09	36,86	32,36	34,61	33,14
TiO_2	2,74	1,35	1,25	1,37	1,57	1,74	1,78	3,06	1,81	3,33	1,63	1,71	2,91	2,53	2,31	1,25	1,65	4,45	5,10
Al_2O_3	16,98	15,94	15,04	15,92	16,52	19,59	19,82	19,90	18,25	19,39	20,17	19,95	13,31	15,63	20,08	18,79	22,57	16,24	16,68
FeO_T	25,64	8,30	9,25	10,34	17,75	14,87	25,14	23,16	14,69	20,76	25,41	22,54	13,90	17,44	28,24	23,99	27,25	22,65	23,64
MnO	0,16	0,10	0,15	0,11	0,16	0,15	0,15	0,11	0,18	0,14	0,14	0,20	0,38	0,16	0,19	0,18	0,16	0,16	0,15
MgO	8,09	20,63	21,14	20,98	14,62	14,69	4,82	6,44	15,16	8,64	5,10	7,68	17,34	15,76	4,03	4,10	3,88	7,34	6,82
CaO	0,03	0,04	0,08	0,17	0,12	0,06	0,08	0,03	0,06	0,08	0,07	0,09	0,37	0,05	0,08	0,18	0,08	0,09	0,09
Na_2O	0,39	0,15	0,30	0,39	0,61	0,22	0,19	0,26	0,19	0,32	0,21	0,33	0,15	0,20	0,29	0,34	0,22	0,34	0,44
K_2O	7,87	9,82	10,10	7,99	8,28	8,61	9,63	9,42	9,75	9,41	8,47	8,37	10,13	9,96	8,75	9,08	8,53	9,16	9,27
Cr_2O_3	0,19	0,13	0,17	0,42	0,23	0,18	0,09	0,30	0,17	0,18	0,00	0,26	0,09	0,27	0,26	0,23	0,22	0,23	0,31
NiO	0,53	0,31	0,26	0,51	0,33	0,38	0,21	0,28	0,35	0,46	0,31	0,23	0,21	0,19	0,25	0,22	0,23	0,30	0,28
Total	97,08	95,88	96,78	96,22	96,72	96,66	96,42	96,65	97,13	96,85	96,62	96,42	96,10	97,17	96,57	95,22	97,15	95,57	95,92
Numbers of ions on the basis of 22(O)																			
Si	5,309	5,622	5,608	5,473	5,433	5,293	5,356	5,180	5,356	5,184	5,393	5,332	5,561	5,246	5,065	5,715	5,014	5,384	5,188
Al	2,691	2,378	2,392	2,527	2,567	2,707	2,644	2,820	2,644	2,816	2,607	2,668	2,337	2,754	2,935	2,285	2,986	2,616	2,812
	8,000	8,000	8,000	8,000	8,000	8,000	8,000	8,000	8,000	8,000	8,000	8,000	7,898	8,000	8,000	8,000	8,000	8,000	8,000
Al	0,392	0,322	0,153	0,173	0,328	0,671	0,980	0,785	0,509	0,652	1,044	0,907	-	0,008	0,799	1,148	1,135	0,361	0,265
Ti	0,318	0,146	0,135	0,148	0,175	0,191	0,208	0,354	0,200	0,381	0,188	0,195	0,326	0,286	0,274	0,145	0,193	0,521	0,600
Fe^{2+}	3,304	0,998	1,111	1,244	2,207	1,819	3,262	2,977	1,801	2,635	3,264	2,866	1,732	2,188	3,727	3,110	3,530	2,946	3,095
Mn	0,021	0,013	0,018	0,014	0,020	0,018	0,020	0,014	0,022	0,018	0,018	0,025	0,048	0,021	0,025	0,024	0,020	0,021	0,020
Mg	1,857	4,419	4,527	4,502	3,240	3,205	1,115	1,476	3,314	1,956	1,167	1,741	3,853	3,524	0,947	0,947	0,896	1,702	1,591
Cr	0,023	0,014	0,019	0,048	0,027	0,021	0,011	0,036	0,020	0,021	0,000	0,031	0,010	0,031	0,032	0,028	0,026	0,028	0,039
Ni	0,066	0,035	0,030	0,059	0,040	0,045	0,026	0,035	0,042	0,056	0,039	0,028	0,025	0,023	0,032	0,027	0,028	0,037	0,035
Ca	0,005	0,006	0,012	0,027	0,018	0,009	0,013	0,005	0,009	0,013	0,012	0,014	0,059	0,008	0,014	0,030	0,013	0,014	0,014
Na	0,117	0,042	0,084	0,108	0,176	0,063	0,056	0,078	0,054	0,094	0,063	0,098	0,044	0,057	0,090	0,101	0,067	0,103	0,134
K	1,550	1,805	1,855	1,470	1,575	1,611	1,910	1,851	1,828	1,826	1,662	1,627	1,931	1,909	1,766	1,800	1,690	1,821	1,855
	7,653	7,800	7,944	7,793	7,806	7,653	7,601	7,611	7,799	7,652	7,457	7,532	8,028	8,055	7,706	7,360	7,598	7,554	7,648
$Mg/(Mg+Fe_T)$	0,359	0,815	0,802	0,783	0,594	0,637	0,255	0,331	0,647	0,426	0,263	0,378	0,689	0,616	0,202	0,233	0,202	0,366	0,339
MOLECULAR PROPORTIONS																			
Phlogopite	14,3	50,4	54,6	46,1	29,5	17,8	5,3	5,9	24,5	9,5	5,5	8,4	52,6	31,5	2,1	8,3	0,3	16,7	12,6
Annite	25,5	11,5	13,5	12,8	20,1	10,2	15,5	11,8	13,3	12,8	15,3	13,9	23,7	19,6	8,4	27,4	1,12	28,8	24,6
Eastonite	21,6	31,1	25,6	32,2	29,9	45,9	20,2	27,2	40,2	33,1	20,8	29,3	16,3	30,1	18,1	15,0	19,9	19,9	21,3
Siderophyllite	38,6	7,0	6,3	8,9	20,5	26,1	59,0	55,0	22,0	44,6	58,4	48,3	7,4	18,8	71,4	49,3	78,7	34,6	41,4

ELECTRON MICROPROBE ANALYSES OF BIOTITE

Sample #	PH-177	PH-182	PH-186	PH-188	PH-191	PH-195	PH-197	PH-199	PH-220	PH-320	PH-321	PH-324	PH-325	PH-326	PH-328	PH-330
SiO_2	36,16	37,11	36,30	35,88	36,45	36,21	35,56	36,74	34,63	33,81	34,39	35,27	33,94	33,42	34,35	33,23
TiO_2	5,00	4,38	3,33	3,19	3,79	5,02	5,42	4,89	3,94	1,85	2,76	5,24	4,23	5,37	4,53	3,47
Al_2O_3	15,56	13,56	13,58	15,83	16,48	15,96	15,59	15,00	17,57	18,61	15,28	15,56	15,39	16,54	15,25	15,71
FeO_T	17,30	19,24	23,58	21,65	17,56	15,91	20,93	12,24	21,86	26,32	25,74	22,95	23,85	24,33	25,66	23,90
MnO	0,14	0,18	0,24	0,20	0,19	0,15	0,12	0,17	0,17	0,11	0,14	0,18	0,10	0,23	0,17	0,20
MgO	11,75	9,74	8,54	10,20	11,75	10,69	7,97	15,92	8,49	6,49	7,77	6,32	7,91	6,81	5,97	7,82
CaO	0,09	0,11	0,17	0,08	0,07	0,07	0,07	0,06	0,05	0,08	0,08	0,06	0,11	0,06	0,08	0,08
Na_2O	0,09	0,49	0,27	0,53	0,17	0,08	0,20	0,08	0,13	0,37	0,74	0,32	0,43	0,51	0,24	0,36
K_2O	8,70	9,43	9,19	8,39	9,40	10,03	9,48	9,59	9,26	8,30	8,74	8,59	8,17	9,33	9,19	9,55
Cr_2O_3	0,31	0,24	0,36	0,43	0,20	0,28	0,29	0,19	0,17	0,19	0,13	0,28	0,29	0,26	0,19	0,39
NiO	0,33	0,24	0,29	0,49	0,45	0,41	0,24	0,18	0,30	0,20	0,24	0,23	0,22	0,38	0,20	0,23
Total	95,43	94,72	95,85	96,87	96,51	94,81	95,87	95,06	96,57	96,33	96,01	95,00	94,64	97,24	95,83	94,94
							Numbers of ions on the basis of 22(0)									
Si	5,456	5,724	5,654	5,448	5,458	5,503	5,464	5,458	5,296	5,268	5,408	5,500	5,351	5,180	5,416	5,281
Al	2,544	2,276	2,346	2,552	2,542	2,497	2,536	2,542	2,704	2,732	2,592	2,500	2,649	2,820	2,584	2,719
	8,000	8,000	8,000	8,000	8,000	8,000	8,000	8,000	8,000	8,000	8,000	8,000	8,000	8,000	8,000	8,000
Al	0,223	0,189	0,147	0,281	0,365	0,361	0,287	0,084	0,462	0,684	0,240	0,359	0,209	0,200	0,249	0,222
Ti	0,567	0,508	0,390	0,365	0,426	0,573	0,626	0,546	0,453	0,217	0,327	0,615	0,502	0,626	0,536	0,415
Fe^{2+}	2,183	2,482	3,071	2,748	2,199	2,022	2,689	1,520	2,795	3,429	3,385	2,993	3,145	3,153	3,383	3,176
Mn	0,018	0,024	0,032	0,026	0,024	0,019	0,015	0,022	0,022	0,015	0,018	0,023	0,014	0,030	0,022	0,027
Mg	2,641	2,241	1,983	2,307	2,622	2,422	1,826	3,525	1,934	1,507	1,822	1,469	1,859	1,572	1,404	1,852
Cr	0,036	0,029	0,044	0,052	0,023	0,033	0,035	0,023	0,021	0,023	0,016	0,035	0,036	0,031	0,024	0,049
Ni	0,040	0,029	0,036	0,060	0,054	0,050	0,030	0,022	0,037	0,025	0,030	0,029	0,028	0,047	0,025	0,030
Ca	0,014	0,018	0,028	0,014	0,012	0,012	0,011	0,009	0,008	0,013	0,013	0,010	0,019	0,011	0,014	0,014
Na	0,027	0,146	0,083	0,156	0,050	0,023	0,060	0,022	0,039	0,111	0,226	0,097	0,130	0,152	0,072	0,112
K	1,678	1,860	1,830	1,628	1,800	1,948	1,862	1,821	1,811	1,653	1,757	1,712	1,647	1,848	1,851	1,941
	7,427	7,526	7,644	7,637	7,575	7,463	7,441	7,594	7,582	7,677	7,834	7,342	7,589	7,670	7,580	7,838
$Mg/(Mg+Fe_T)$	0,547	0,474	0,392	0,456	0,543	0,544	0,404	0,698	0,409	0,305	0,350	0,329	0,371	0,332	0,293	0,368
							MOLECULAR PROPORTIONS									
Phlogopite	30,5	35,0	27,9	24,0	26,9	28,7	21,5	42,9	14,8	8,1	18,1	17,3	18,4	13,0	15,3	16,4
Annite	25,3	38,8	43,3	28,7	22,7	24,0	31,7	18,5	21,4	18,4	33,6	35,4	31,2	26,3	36,9	28,1
Eastonite	24,2	12,4	11,3	21,6	27,4	25,7	18,9	26,9	26,1	22,4	16,8	15,6	18,7	20,2	14,0	20,4
Siderophyllite	20,0	13,8	17,5	25,7	23,0	21,6	27,9	11,7	37,7	51,1	31,4	31,7	31,7	40,5	33,8	35,1

ELECTRON MICROPROBE ANALYSES OF PHLOGOPITE

Sample #	PD-10	PD-18	PD-35	PD-56	PD-124	PD-214	PD-216	PC-14	PC-16	PC-34
SiO_2	39,97	39,91	40,68	42,05	36,80	39,47	38,38	41,75	39,04	37,97
TiO_2	0,61	0,69	0,50	0,57	5,01	0,40	6,20	0,74	5,22	1,59
Al_2O_3	16,79	17,53	16,46	16,73	12,60	18,43	15,62	17,37	14,21	19,00
FeO_T	5,74	5,25	0,88	2,43	16,81	3,14	5,22	1,34	10,91	0,88
MnO	0,12	0,10	0,13	0,15	0,25	0,22	0,16	0,23	0,29	0,19
MgO	22,39	22,10	25,42	23,90	13,73	24,42	20,01	24,19	15,90	25,22
CaO	0,20	0,09	0,28	0,19	0,06	0,06	0,07	0,19	0,10	0,09
Na_2O	0,20	0,14	0,50	0,25	0,34	0,59	0,93	0,47	0,33	0,26
K_2O	9,35	9,90	10,47	10,45	10,12	10,08	10,03	9,60	10,38	10,56
Cr_2O_3	0,17	0,15	0,14	0,00	0,15	0,12	0,22	0,17	0,13	0,19
NiO	0,22	0,22	0,22	0,00	0,24	0,17	0,20	0,19	0,18	0,25
Total	95,76	96,08	95,68	96,72	96,11	97,10	97,04	96,24	96,69	96,20
				Numbers of ions on the basis of 22(O)						
Si	5,652	5,622	5,673	5,802	5,570	5,473	5,419	5,747	5,671	5,290
Al	2,348	2,378	2,327	2,198	2,247	2,527	2,581	2,253	2,329	2,710
	8,000	8,000	8,000	8,000	7,817	8,000	8,000	8,000	8,000	8,000
Al	0,449	0,532	0,377	0,523	-	0,484	0,018	0,564	0,103	0,409
Ti	0,065	0,074	0,053	0,059	0,570	0,042	0,658	0,077	0,570	0,166
Fe^{2+}	0,679	0,618	0,102	0,280	2,127	0,364	0,617	0,154	1,325	0,102
Mn	0,014	0,011	0,015	0,017	0,032	0,025	0,019	0,027	0,035	0,023
Mg	4,720	4,641	5,284	4,915	3,098	5,045	4,210	4,963	3,442	5,238
Cr	0,019	0,016	0,015	0,000	0,017	0,013	0,024	0,018	0,015	0,021
Ni	0,025	0,024	0,025	0,000	0,029	0,019	0,022	0,021	0,021	0,028
Ca	0,030	0,014	0,042	0,027	0,009	0,009	0,011	0,028	0,015	0,013
Na	0,055	0,039	0,135	0,067	0,099	0,158	0,254	0,124	0,092	0,069
K	1,690	1,782	1,866	1,844	1,958	1,787	1,811	1,689	1,928	1,880
	7,746	7,751	7,914	7,732	7,939	7,946	7,644	7,665	7,546	7,949
$Mg/(Mg+Fe_T)$	0,873	0,882	0,980	0,945	0,592	0,932	0,871	0,969	0,721	0,980
				MOLECULAR PROPORTIONS						
Phlogopite	51,4	47,6	60,8	60,5	48,2	43,3	54,4	57,8	53,8	36,8
Annite	7,1	6,1	1,0	3,8	32,8	2,7	7,6	2,2	20,2	1,2
Eastonite	36,2	5,0	37,2	32,8	10,9	50,2	33,1	38,6	18,6	60,7
Siderophyllite	5,3	41,3	1,0	2,9	8,1	3,8	4,9	1,4	7,4	1,3

Appendix 3

ELECTRON MICROPROBE ANALYSES OF CORDIERITE

Sample #	PH-8	PH-14	PH-16	PH-21	PH-40	PH-41	PH-48	PH-75(core)	PH-75(rim)	PH-76	PH-116	PH-117	PH-143	PH-151	PH-152	PH-157	PH-168	PH-169	PH-170
SiO_2	47,30	48,24	48,66	48,33	46,74	47,91	47,05	46,84	46,42	46,45	47,24	44,90	47,83	46,44	45,69	48,26	46,79	46,75	46,46
TiO_2	0,09	0,11	0,10	0,11	0,14	0,13	0,13	0,14	0,14	0,11	0,12	0,10	0,12	0,14	0,12	0,12	0,12	0,09	0,12
Al_2O_3	32,46	32,94	34,22	32,59	31,70	31,84	32,59	31,11	30,81	32,09	31,78	32,00	32,75	31,94	32,67	33,34	32,52	32,85	33,23
FeO_T	10,13	5,25	3,98	6,23	14,70	11,62	9,93	12,82	15,02	10,46	12,66	15,87	13,79	12,51	13,44	4,91	9,81	7,93	9,66
MnO	0,18	0,12	0,18	0,24	0,15	0,19	0,09	0,20	0,18	0,34	0,21	0,34	0,14	0,14	0,10	0,16	0,24	0,12	0,14
MgO	7,03	10,62	9,78	9,34	4,35	5,66	7,30	5,23	4,28	6,92	4,17	3,01	3,02	4,84	5,64	10,11	7,67	8,90	6,90
CaO	0,08	0,06	0,10	0,08	0,06	0,07	0,08	0,07	0,16	0,07	0,13	0,07	0,07	0,06	0,06	0,06	0,08	0,08	0,09
Na_2O	0,22	0,22	0.09	0,31	0,09	0,23	0,19	0,29	0,13	0,18	0,21	0,16	n.d.	0,14	0,19	0,22	0,28	0,25	0,25
K_2O	0,05	0,07	0,08	0,06	0,06	0,06	0,06	0,05	0,02	0,06	0,04	0,06	n.d.	0,06	0,06	0,06	0,07	0,14	0,05
Total	97,54	97,63	97,19	97,29	97,99	97,71	97,42	96,75	97,16	96,68	96,56	96,51	96,72	96,27	97,97	97,24	97,58	97,11	96,90
Numbers of ions on the basis of 18(O)																			
Si	4,951	4,393	4,961	4,984	4,974	5,037	4,929	5,009	4,993	4,927	5,045	4,888	5,064	4,978	4,851	4,947	4,897	4,878	4,889
Al	1,049	1,061	1,039	1,016	1,026	0,963	1,071	0,991	1,007	1,073	0,955	1,112	0,936	1,022	1,149	1,053	1,103	1,122	1,111
	6,000	6,000	6,000	6,000	6,000	6,000	6,000	6,000	6,000	6,000	6,000	6,000	6,000	6,000	6,000	6,000	6,000	6,000	6,000
Al	2,956	2,913	3,072	2,943	2,949	2,981	2,952	2,929	2,898	2,937	3,044	2,993	3,153	3,012	2,938	2,974	2,907	2,916	3,009
Ti	0,007	0,009	0,008	0,009	0,011	0,010	0,010	0,012	0,012	0,008	0,009	0,008	0,010	0,012	0,009	0,009	0,009	0,006	0,009
Fe^{2+}	0,886	0,449	0,340	0,537	1,308	1,021	0,890	1,146	1,350	0,927	1,130	1,445	1,221	1,121	1,193	0,421	0,858	0,692	0,849
Mn	0,016	0,010	0,016	0,021	0,013	0,017	0,008	0,018	0,016	0,030	0,019	0,031	0,012	0,013	0,009	0,014	0,021	0,011	0,012
Mg	1,097	1,620	1,486	1,436	0,690	0,887	1,139	0,833	0,687	1,094	0,663	0,488	0,477	0,773	0,892	1,545	1,196	1,384	1,081
Ca	0,009	0,007	0,011	0,009	0,007	0,007	0,009	0,008	0,018	0,008	0,015	0,008	0,007	0,006	0,007	0,006	0,008	0,009	0,010
Na	0,045	0,043	0,018	0,062	0,019	0,046	0,038	0,059	0,026	0,036	0,044	0,035	0,000	0,028	0,039	0,044	0,058	0,051	0,050
K	0,006	0,009	0,011	0,008	0,008	0,008	0,008	0,007	0,003	0,007	0,006	0,009	0,000	0,008	0,007	0,007	0,009	0,018	0,006
	5,022	5,060	4,962	5,025	5,005	4,977	5,054	5,012	5,010	5,047	4,930	5,017	4,880	4,973	5,094	5,020	5,066	5,087	5,026
$Mg/(Mg+Fe_T)$	0,553	0,783	0,814	0,728	0,345	0,465	0,567	0,421	0,337	0,541	0,369	0,253	0,281	0,408	0,428	0,786	0,582	0,667	0,560

ELECTRON MICROPROBE ANALYSES OF CORDIERITE

Sample #	PH-173	PH-176	PH-177	PH-178	PH-183	PH-184	PH-188	PH-189	PH-191	PH-195	PH-196	PH-197	PH-199	PH-201	PH-202	PH-203	PH-204	PH-206	PH-208
SiO_2	47,49	45,89	47,95	47,21	45,86	46,24	47,08	48,82	47,24	48,47	46,90	48,21	49,45	47,69	48,35	48,12	48,35	47,79	49,21
TiO_2	0,11	0,12	0,14	0,10	0,14	0,15	0,13	0,13	0,13	0,12	0,12	0,13	0,12	0,10	0,12	0,11	0,12	0,14	0,11
Al_2O_3	33,20	33,33	32,71	33,58	31,68	33,00	31,62	33,29	33,13	33,03	31,63	32,82	31,84	32,44	33,45	32,61	33,26	32,71	33,03
FeO_T	8,99	11,98	7,25	8,30	14,18	11,09	10,84	4,04	6,85	6,39	12,27	9,81	3,99	7,54	6,58	8,08	5,03	8,28	3,52
MnO	0,12	0,11	0,23	0,29	0,18	0,19	0,25	0,22	0,23	0,14	0,13	0,19	0,22	0,13	0,16	0,16	0,13	0,11	0,15
MgO	7,60	5,88	8,93	7,75	4,91	6,54	5,83	11,02	8,90	9,20	5,82	7,07	11,41	8,67	8,79	9,04	9,60	8,73	11,44
CaO	0,07	0,05	0,07	0,08	0,07	0,08	0,09	0,05	0,07	0,09	0,07	0,05	0,05	0,05	0,07	0,06	0,08	0,08	0,09
Na_2O	0,23	0,10	0,12	0,15	0,22	0,15	0,12	0,22	0,17	0,14	0,15	0,12	0,16	0,32	0,17	0,25	0,15	0,12	0,13
K_2O	0,15	0,08	0,06	0,04	0,13	0,06	0,08	0,06	0,04	0,17	0,06	0,17	0,39	0,09	0,16	0,06	0,45	0,32	0,37
Total	97,96	97,54	97,46	97,50	97,37	97,50	96,04	97,85	96,76	97,75	97,15	98,57	97,63	97,03	97,85	98,49	97,17	98,28	98,05
Numbers of ions on the basis of 18(O)																			
Si	4,918	4,850	4,958	4,878	4,915	4,875	5,014	4,952	4,914	4,973	4,980	4,984	5,032	4,960	4,964	4,949	4,970	4,931	4,979
Al	1,082	1,150	1,042	1,122	1,085	1,125	0,986	1,048	1,086	1,027	1,020	1,016	0,968	1,040	1,036	1,051	1,030	1,069	1,021
	6,000	6,000	6,000	6,000	6,000	6,000	6,000	6,000	6,000	6,000	6,000	6,000	6,000	6,000	6,000	6,000	6,000	6,000	6,000
Al	2,970	2,999	2,944	2,967	2,916	2,974	2,982	2,932	2,975	2,967	2,938	2,982	2,849	2,936	3,011	2,900	3,000	2,908	2,917
Ti	0,009	0,009	0,011	0,008	0,011	0,012	0,011	0,010	0,010	0,009	0,009	0,010	0,009	0,008	0,009	0,009	0,009	0,011	0,008
Fe^{2+}	0,779	1,058	0,627	0,717	1,271	0,977	0,965	0,343	0,595	0,548	1,089	0,848	0,339	0,655	0,565	0,695	0,432	0,715	0,297
Mn	0,010	0,010	0,019	0,025	0,016	0,017	0,023	0,018	0,019	0,012	0,012	0,017	0,019	0,011	0,014	0,014	0,011	0,009	0,012
Mg	1,173	0,927	1,376	1,194	0,785	1,028	0,926	1,665	1,380	1,406	0,921	1,090	1,731	1,344	1,344	1,385	1,471	1,343	1,725
Ca	0,008	0,006	0,007	0,009	0,007	0,009	0,010	0,006	0,008	0,010	0,007	0,006	0,006	0,006	0,008	0,007	0,008	0,008	0,009
Na	0,046	0,021	0,024	0,030	0,045	0,029	0,025	0,042	0,035	0,028	0,030	0,023	0,031	0,064	0,034	0,050	0,030	0,024	0,026
K	0,019	0,011	0,008	0,005	0,017	0,009	0,010	0,007	0,005	0,023	0,007	0,023	0,051	0,012	0,021	0,008	0,059	0,042	0,048
	5,014	5,041	5,016	4,955	5,068	5,055	4,952	5,023	5,027	5,003	5,013	4,999	5,035	5,036	5,006	5,068	5,020	5,060	5,042
$Mg/(Mg+Fe_T)$	0,601	0,467	0,687	0,625	0,382	0,513	0,488	0,829	0,699	0,720	0,458	0,562	0,836	0,672	0,704	0,665	0,773	0,653	0,853

ELECTRON MICROPROBE ANALYSES OF CORDIERITE

Sample #	PH-209	PH-212	PH-214[a]	PH-214[b]	PH-215	PH-219	PH-220	PH-313	PH-320	PH-321	PH-324[c]	PH-324[d]	PH-325	PH-326	PH-328	PH-330	PH-334	PH-335
SiO_2	47,73	47,27	48,99	48,97	48,26	47,84	47,30	47,98	46,56	46,60	46,72	46,74	48,18	46,96	46,33	47,04	46,75	46,73
TiO_2	0,13	0,14	0,13	0,13	0,12	0,12	0,14	0,12	0,13	0,14	0,11	0,11	0,10	0,10	0,13	0,10	0,12	0,15
Al_2O_3	32,70	32,84	33,37	32,61	33,63	31,89	31,83	32,45	32,01	33,20	31,83	31,77	31,06	32,40	31,58	32,31	33,46	32,47
FeO_T	9,09	7,99	4,06	3,04	3,14	8,98	9,84	9,73	12,33	9,21	11,77	10,48	11,10	11,88	12,97	9,56	8,39	12,82
MnO	0,22	0,11	0,13	0,13	0,15	0,14	0,24	0,11	0,16	0,14	0,22	0,22	0,13	0,14	0,15	0,16	0,23	0,08
MgO	7,20	8,40	11,95	11,68	12,31	8,21	7,39	6,86	5,46	7,48	5,38	6,05	6,14	5,81	5,53	7,56	8,23	4,89
CaO	0,05	0,09	0,08	0,06	0,10	0,06	0,09	0,07	0,08	0,06	0,06	0,07	0,07	0,06	0,09	0,06	0,10	0,07
Na_2O	0,39	0,16	0,26	0,26	0,38	0,29	0,21	0,48	0,42	0,33	0,09	0,09	0,12	0,19	0,18	0,14	0,13	0,18
K_2O	0,07	0,09	0,39	0,39	0,63	0,34	0,05	0,06	0,09	0,06	0,05	0,05	0,06	0,05	0,07	0,07	0,21	0,04
Total	97,58	97,09	99,36	97,27	98,72	97,87	97,09	97,86	97,24	97,22	96,23	95,58	96,96	97,59	97,03	97,00	97,62	97,43
							Numbers of ions on the basis of 18(O)											
Si	4,966	4,927	4,916	4,988	4,868	4,976	4,974	4,996	4,950	4,884	4,986	4,993	5,084	4,945	4,947	4,944	4,863	4,954
Al	1,034	1,073	1,084	1,012	1,132	1,024	1,026	1,004	1,050	1,116	1,014	1,007	0,916	1,055	1,053	1,056	1,137	1,046
	6,000	6,000	6,000	6,000	6,000	6,000	6,000	6,000	6,000	6,000	6,000	6,000	6,000	6,000	6,000	6,000	6,000	6,000
Al	2,975	2,960	2,862	2,902	2,865	2,885	2,919	2,977	2,960	2,983	2,989	2,992	2,946	2,965	2,920	2,945	2,965	3,009
Ti	0,010	0,011	0,010	0,009	0,009	0,010	0,011	0,009	0,010	0,011	0,009	0,009	0,008	0,008	0,010	0,008	0,009	0,012
Fe^{2+}	0,791	0,697	0,340	0,258	0,264	0,781	0,865	0,847	1,096	0,807	1,051	0,936	0,979	1,046	1,158	0,840	0,730	1,136
Mn	0,019	0,010	0,011	0,011	0,012	0,012	0,021	0,010	0,014	0,012	0,020	0,020	0,012	0,012	0,014	0,014	0,020	0,007
Mg	1,117	1,305	1,787	1,774	1,852	1,273	1,158	1,064	0,866	1,168	0,856	0,963	0,965	0,912	0,880	1,185	1,276	0,773
Ca	0,006	0,011	0,009	0,007	0,010	0,007	0,010	0,008	0,009	0,007	0,007	0,008	0,008	0,007	0,010	0,007	0,011	0,007
Na	0,079	0,033	0,051	0,051	0,075	0,059	0,042	0,098	0,087	0,066	0,018	0,018	0,024	0,039	0,039	0,029	0,026	0,037
K	0,009	0,011	0,049	0,050	0,082	0,045	0,007	0,008	0,013	0,008	0,007	0,007	0,008	0,007	0,009	0,010	0,028	0,005
	5,006	5,038	5,119	5,062	5,169	5,072	5,033	5,021	5,055	5,062	4,957	4,953	4,950	4,996	5,039	5,038	5,065	4,986
$Mg/(Mg+Fe_T)$	0,586	0,652	0,838	0,871	0,873	0,620	0,572	0,557	0,441	0,591	0,449	0,506	0,495	0,466	0,432	0,585	0,636	0,405

a cordierite inclusion in opx
b cordierite in contact with opx and hercynite
c cordierite in contact with opx
d cordierite in contact with garnet

Appendix 4

ELECTRON MICROPROBE ANALYSES OF ORTHO-AMPHIBOLE

Sample #	PH-8	PH-21	PH-116A	PH-116B	PH-151A	PH-151B	PH-152A	PH-152B	PH-157A	PH-157B	PH-320A	PH-320B	PH-321A	PH-321B	PH-321C	PH-321D	PH-335
type	anth	anth	ged	ged	ged	ged	ged	ged	anth	anth	ged	ged	ged	ged	anth	anth	ged
SiO_2	48,45	52,77	38,17	38,48	42,09	43,38	44,64	43,99	49,41	53,22	39,75	40,39	43,59	43,36	47,68	47,73	39,17
TiO_2	0,36	0,16	0,28	0,18	0,30	0,32	0,27	0,26	0,28	0,18	0,29	0,25	0,49	0,34	0,40	0,29	0,19
Al_2O_3	5,23	1,08	18,00	17,09	16,91	15,41	13,24	12,63	7,65	1,25	18,02	16,03	11,19	10,39	3,81	4,34	18,50
FeO_T	31,34	23,95	34,34	34,25	31,08	32,03	32,41	33,69	21,61	22,07	31,94	33,15	31,28	30,19	30,89	31,35	34,17
MnO	0,23	0,49	0,28	0,46	0,21	0,22	0,28	0,28	0,39	0,31	0,32	0,32	0,24	0,19	0,14	0,12	0,22
MgO	11,42	17,61	4,80	5,41	5,18	5,16	6,87	6,95	16,67	19,80	5,39	5,73	9,82	11,33	12,69	12,80	4,22
CaO	0,33	0,28	0,36	0,33	0,15	0,16	0,09	0,10	0,55	0,31	0,23	0,26	0,18	0,08	0,12	0,13	0,18
Na_2O	0,51	0,11	1,04	0,85	0,80	1,03	0,47	1,00	0,57	0,14	1,42	1,59	1,20	1,05	0,83	0,63	1,08
K_2O	0,07	0,06	0,06	0,05	0,06	0,07	0,07	0,07	0,06	0,06	0,09	0,07	0,07	0,06	0,06	0,06	0,05
NiO	0,46	0,00	0,00	0,00	0,00	0,00	0,00	0,00	0,00	0,00	0,00	0,00	0,00	0,92	0,00	0,00	0,00
Total	98,40	96,51	97,33	97,10	96,78	97,78	98,34	98,97	97,19	97,34	97,45	97,79	98,06	97,91	96,62	97,45	97,78
Numbers of ions on the basis of 23(0)																	
Si	7,346	7,818	5,989	6,058	6,464	6,619	6,770	6,706	7,209	7,746	6,143	6,267	6,662	6,659	7,364	7,318	6,088
Al	0,654	0,182	2,011	1,942	1,536	1,381	1,230	1,294	0,791	0,215	1,857	1,733	1,338	1,341	0,636	0,682	1,912
	8,000	8,000	8,000	8,000	8,000	8,000	8,000	8,000	8,000	7,961	8,000	8,000	8,000	8,000	8,000	8,000	8,000
Al	0,281	0,006	1,317	1,227	1,523	1,390	1,136	0,976	0,524	-	1,425	1,198	0,677	0,539	0,057	0,101	1,476
Ti	0,041	0,018	0,033	0,021	0,034	0,036	0,031	0,030	0,030	0,020	0,033	0,029	0,056	0,040	0,046	0,034	0,022
Fe^{2+}	3,973	2,967	4,505	4,508	3,991	4,086	4,110	4,295	2,636	2,686	4,127	4,301	3,997	3,877	3,990	4,020	4,441
Mn	0,029	0,062	0,037	0,060	0,028	0,029	0,036	0,036	0,048	0,038	0,042	0,042	0,031	0,025	0,019	0,015	0,028
Mg	2,581	3,888	1,123	1,269	1,186	1,174	1,553	1,578	3,625	4,296	1,240	1,326	2,236	2,594	2,921	2,927	0,977
Ca	0,053	0,044	0,060	0,055	0,024	0,025	0,014	0,016	0,086	0,048	0,038	0,044	0,029	0,013	0,021	0,021	0,030
Ni	0,057	0,000	0,000	0,000	0,000	0,000	0,000	0,000	0,000	0,000	0,000	0,000	0,000	0,113	0,000	0,000	0,000
Na	-	0,015	-	-	0,214	0,260	0,120	0,069	0,051	-	0,095	0,060	-	-	-	-	0,026
	7,015	7,000	7,075	7,140	7,000	7,000	7,000	7,000	7,000	7,088	7,000	7,000	7,026	7,201	7,054	7,118	7,000
Na	0,151	0,018	0,315	0,261	0,024	0,046	0,019	0,227	0,111	0,040	0,331	0,419	0,355	0,311	0,247	0,186	0,298
K	0,014	0,011	0,012	0,010	0,012	0,013	0,014	0,013	0,011	0,012	0,017	0,014	0,013	0,011	0,011	0,012	0,011
	0,165	0,029	0,327	0,271	0,036	0,059	0,033	0,240	0,122	0,052	0,348	0,433	0,368	0,322	0,258	0,198	0,309
$Mg/(Mg+Fe_T)$	0,394	0,567	0,199	0,220	0,229	0,223	0,274	0,269	0,579	0,615	0,231	0,235	0,359	0,401	0,422	0,421	0,180
x	0,17	0,03	0,33	0,27	0,04	0,06	0,03	0,24	0,12	0,05	0,35	0,43	0,37	0,32	0,26	0,20	0,31
y	0,36	0,04	1,38	1,27	1,59	1,46	1,20	1,04	0,58	0,04	1,49	1,26	0,79	0,62	0,15	0,17	1,52
$(x+y)-Al^{iv}$	-0,12	-0,11	-0,301	-0,40	0,09	0,14	0,00	-0,01	-0,09	-0,13	-0,02	-0,04	-0,18	-0,40	-0,23	-0,31	-0,08

anth = anthophyllite
ged = gedrite

Appendix 5

ELECTRON MICROPROBE ANALYSES OF CALCIC AMPHIBOLE

Sample #	PH-19	PH-80	PH-88	PH-316[a]	PD-34	PD-38	PD-48	PD-50	PD-53	PD-56	PD-70	PD-82	PD-83[b]	PD-89	PD-118	PD-125	PD-130	PD-166	PD-128[c]
SiO_2	51,05	48,55	48,05	52,22	57,75	57,45	57,83	56,98	58,05	55,40	57,96	51,94	54,61	56,91	55,39	56,28	58,03	57,88	53,83
TiO_2	0,27	0,45	1,29	1,00	0,14	0,14	0,15	0,22	0,15	0,18	0,14	0,25	0,16	0,23	0,17	0,15	0,16	0,14	0,15
Al_2O_3	4,14	5,80	5,99	4,14	1,45	0,58	0,57	2,28	0,94	2,41	1,05	8,64	2,05	2,31	2,37	0,77	0,60	0,73	2,12
FeO_T	8,81	11,94	17,58	8,68	0,84	4,12	0,44	0,72	1,15	1,42	0,82	7,73	9,99	5,95	6,49	9,75	0,53	3,46	12,02
MnO	0,18	0,13	0,21	0,18	0,25	0,48	0,15	0,14	0,16	0,15	0,09	0,25	0,42	0,30	0,26	0,11	0,63	0,58	0,31
MgO	19,78	16,63	11,91	17,16	24,04	22,07	23,36	23,85	24,09	23,80	24,56	15,52	16,77	19,41	20,31	17,88	23,41	22,50	15,58
CaO	11,83	12,33	10,83	12,21	13,14	12,52	14,41	13,52	13,92	13,15	13,42	12,65	12,20	12,62	11,78	12,71	14,34	12,72	12,53
Na_2O	0,61	0,56	0,70	0,56	0,24	0,08	0,10	0,26	0,20	0,25	0,23	0,49	0,40	0,50	0,24	0,24	0,15	0,14	0,35
K_2O	0,15	0,42	0,45	0,24	0,10	0,09	0,16	0,16	0,06	0,04	0,08	0,08	0,17	0,16	0,16	0,08	0,08	0,12	0,12
Total	96,82	96,81	97,01	96,39	97,95	97,53	97,17	98,13	98,72	96,80	98,35	97,55	96,77	98,39	97,17	97,97	97,93	98,27	97,01
Numbers of ions on the basis of 23(0)																			
Si	7,315	7,098	7,157	7,451	7,835	7,930	7,909	7,735	7,849	7,647	7,841	7,311	7,776	7,862	7,741	7,930	7,898	7,902	7,753
Al	0,685	0,902	0,843	0,549	0,165	0,070	0,091	0,265	0,149	0,353	0,159	0,689	0,224	0,138	0,259	0,070	0,097	0,098	0,247
	8,000	8,000	8,000	8,000	8,000	8,000	8,000	8,000	7,998	8,000	8,000	8,000	8,000	8,000	8,000	8,000	7,995	8,000	8,000
AL	0,014	0,097	0,208	0,146	0,066	0,024	0,002	0,100	-	0,039	0,009	0,744	0,120	0,237	0,132	0,058	-	0,019	0,113
Ti	0,029	0,050	0,145	0,107	0,014	0,015	0,015	0,022	0,015	0,018	0,014	0,027	0,018	0,024	0,018	0,016	0,016	0,014	0,016
Fe^{2+}	1,056	1,459	2,190	1,036	0,096	0,475	0,050	0,082	0,130	0,164	0,093	0,910	1,190	0,687	0,758	1,149	0,060	0,395	1,447
Mn	0,021	0,016	0,027	0,022	0,029	0,056	0,018	0,016	0,018	0,017	0,010	0,029	0,050	0,035	0,031	0,013	0,072	0,067	0,038
Mg	4,224	3,624	2,643	3,650	4,861	4,541	4,762	4,826	4,854	4,896	4,952	3,257	3,559	3,996	4,231	3,756	4,749	4,579	3,344
Ca	1,816	1,930	1,728	1,866	1,909	1,851	2,111	1,966	2,016	1,944	1,946	1,907	1,861	1,867	1,763	1,919	2,091	1,860	1,934
Na	-	-	0,059	0,154	0,025	0,022	0,028	-	-	-	-	0,126	0,109	0,133	0,065	0,064	0,012	0,037	0,099
	7,160	0,236	7,000	6,981	7,000	6,984	6,986	7,012	7,033	7,078	7,024	7,000	6,907	6,979	6,998	6,975	7,000	6,971	6,991
Na	0,170	0,158	0,144	-	0,037	-	-	0,069	0,051	0,068	0,061	0,007	-	-	-	-	0,026	-	-
K	0,027	0,078	0,086	0,044	0,017	0,017	0,027	0,027	0,011	0,007	0,013	0,014	0,031	0,029	0,028	0,014	0,013	0,021	0,021
	0,197	0,236	0,230	0,044	0,054	0,017	0,027	0,096	0,062	0,075	0,074	0,021	0,031	0,029	0,028	0,014	0,039	0,021	0,021
$Mg/(Mg+Fe_T$,	0,799	0,712	0,546	0,778	0,981	0,905	0,990	0,983	0,974	0,968	0,982	0,782	0,750	0,853	0,848	0,766	0,987	0,921	0,698
Σ(M1,M2,M3)	5,344	5,246	5,213	4,961	5,066	5,111	4,847	5,046	5,017	5,134	5,078	4,967	4,937	4,979	5,170	4,992	4,897	5,074	4,958

a Contains 0,82% Cr_2O_3 (0,093 atom fraction)

b Contains 1,23% NiO (0,141 atom fraction)

ELECTRON MICROPROBE ANALYSES OF CALCIC AMPHIBOLE

Sample # type	PC-11	PC-14	PC-16	PC-20	PC-27	PC-30
SiO_2	43,46	54,72	50,99	50,66	47,22	47,90
TiO_2	1,33	0,60	0,82	0,24	0,45	0,28
Al_2O_3	10,02	4,31	4,10	4,57	10,75	6,02
FeO_T	13,81	1,35	7,87	17,64	4,34	19,28
MnO	0,47	0,25	0,26	1,19	0,29	1,06
MgO	14,05	22,00	19,63	10,24	19,41	9,90
CaO	12,09	13,28	12,12	11,96	13,00	11,82
Na_2O	2,20	0,32	0,85	0,54	1,51	0,57
K_2O	0,19	0,13	0,40	0,15	0,63	0,36
Total	97,62	96,96	97,04	97,19	97,60	97,19
Numbers of ions on the basis of 23(0)						
Si	6,431	7,535	7,291	7,539	6,657	7,229
Al	1,569	0,465	0,691	0,461	1,343	0,771
	8,000	8,000	7,982	8,000	8,000	8,000
Al	0,178	0,235	-	0,341	0,443	0,299
Ti	0,148	0,062	0,088	0,027	0,048	0,031
Fe^{2+}	1,708	0,156	0,941	2,195	0,511	2,433
Mn	0,059	0,029	0,031	0,151	0,034	0,135
Mg	3,098	4,515	4,184	2,272	4,078	2,226
Ca	1,917	1,959	1,856	1,907	1,964	1,911
Na	-	0,044	-	0,107	-	-
	7,108	7,000	7,100	7,000	7,078	7,035
Na	0,630	0,042	0,235	0,049	0,412	0,166
K	0,036	0,022	0,073	0,029	0,113	0,069
	0,666	0,064	0,308	0,078	0,525	0,235
$Mg/(Mg+Fe_T)$	0,645	0,967	0,817	0,509	0,889	0,478
Σ (M1;M2;M3)	5,191	4,997	5,244	4,986	5,114	5,124

ELECTRON MICROPROBE ANALYSES OF CUMMINGTONITE

Sample #	PH-85	PH-312	PH-313
SiO_2	51,12	50,18	49,89
TiO_2	0,18	0,23	0,20
Al_2O_3	0,55	1,76	2,47
FeO_T	28,75	32,96	31,91
MnO	0,30	0,14	0,17
MgO	15,82	12,00	12,31
CaO	1,05	0,33	0,32
Na_2O	0,17	0,27	0,26
K_2O	0,06	0,06	0,06
	98,00	97,93	97,59
Numbers of ions on the basis of 23(0)			
Si	7,685	7,674	7,617
Al	0,097	0,317	0,383
	7,782	7,991	8,000
Al	-	-	0,060
Ti	0,020	0,027	0,023
Fe^{2+}	3,614	4,215	4,075
Mn	0,038	0,018	0,022
Mg	3,545	2,734	2,801
Ca	0,168	0,054	0,053
Na	-	-	-
	7,385	7,048	7,034
Na	0,048	0,071	0,075
K	0,011	0,012	0,012
	0,059	0,083	0,087
$Mg/(Mg+Fe_T)$	0,495	0,393	0,407

Appendix 6

ELECTRON MICROPROBE ANALYSES OF GARNET

Sample #	PH-79 A	PH-79 B	PH-79 C	PH-79 D	PH-116	PH-151	PH-152	PH-170	PH-188	PH-312	PH-313	PH-321	PH-324	PH-325	PH-326	PH-330	PH-L(rim)	PH-L(core
SiO_2	32,38	31,72	31,92	31,83	36,69	35,89	35,61	37,80	36,22	36,55	36,43	36,53	36,58	36,46	36,13	36,70	35,53	36,11
TiO_2	5,74	7,23	7,48	6,50	0,20	0,17	0,16	0,18	0,16	0,14	0,13	0,15	0,14	0,14	0,15	0,15	0,37	0,47
Al_2O_3	3,73	2,66	3,24	3,39	20,90	20,63	21,14	20,95	21,26	20,60	21,02	21,44	21,04	21,61	21,29	20,80	20,32	19,68
Fe_2O_3[a]	25,74	25,29	24,19	24,04	-	-	-	-	-	-	-	-	-	-	-	-	3,48	3,62
FeO	0,00	1,19	1,36	1,37	36,99	38,74	39,36	35,83	37,00	37,73	35,83	36,91	36,38	35,78	36,44	35,40	6,37	6,41
MnO	0,31	0,32	0,32	0,30	1,65	0,32	0,18	0,69	0,29	0,21	0,32	0,27	0,31	0,55	0,47	0,42	26,43	26,52
MgO	0,49	0,63	0,4[illegible]	0,55	1,19	1,68	1,87	3,20	2,73	2,44	3,15	3,65	3,40	2,88	2,95	4,29	0,51	0,50
CaO	32,60	31,65	32,28	31,43	2,01	0,54	0,39	1,05	0,94	1,88	1,63	0,45	0,73	0,95	0,74	0,47	5,90	6,59
Na_2O	0,15	0,16	0,13	0,11	0,10	0,14	0,12	0,10	0,17	0,11	0,11	0,12	0,10	0,12	0,09	0,10	0,15	0,12
Cr_2O_3	0,17	0,19	0,16	0,19	0,15	0,16	0,15	0,21	0,25	0,24	0,28	0,11	0,25	0,19	0,22	0,25	0,17	0,16
NiO	0,30	0,28	0,26	0,33	0,24	0,21	0,23	0,23	0,27	0,17	0,18	0,19	0,24	0,26	0,38	0,18	0,24	0,28
Total	101,61	101,32	101,80	100,04	100,12	98,48	99,21	100,24	99,29	100,07	99,08	99,82	99,17	98,94	98,86	98,76	99,47	100,46
Numbers of ions on the basis of 24(O)																		
Si	5,333	5,275	5,270	5,338	5,975	5,948	5,869	6,049	5,905	5,941	5,927	5,898	5,943	5,928	5,904	5,959	5,806	5,856
Al	0,667	0,521	0,630	0,662	0,025	0,052	0,131	-	0,095	0,059	0,073	0,102	0,057	0,072	0,096	0,041	0,194	0,144
	6,000	5,796	5,900	6,000	6,000	6,000	6,000	6,049	6,000	6,000	6,000	6,000	6,000	6,000	6,000	6,000	6,000	6,000
Al	0,044	-	-	0,009	3,985	3,977	3,974	3,953	3,988	3,887	3,956	3,977	3,970	4,069	3,994	3,938	3,719	3,616
Cr	0,023	0,029	0,021	0,026	0,020	0,021	0,018	0,027	0,032	0,030	0,036	0,014	0,033	0,024	0,027	0,032	0,022	0,020
Fe^{3+}	3,189	3,165	3,005	3,034	-	-	-	-	-	-	-	-	-	-	-	-	0,428	0,442
Ti	0,711	0,904	0,929	0,820	0,024	0,022	0,019	0,022	0,019	0,017	0,015	0,018	0,017	0,017	0,018	0,018	0,046	0,057
	3,967	4,098	3,955	3,889	4,029	4,020	4,011	4,002	4,039	3,934	4,007	4,009	4,020	4,110	4,039	3,988	4,215	4,135
Mg_{2+}	0,121	0,157	0,112	0,138	0,288	0,416	0,460	0,765	0,664	0,591	0,764	0,878	0,824	0,697	0,718	1,039	0,123	0,122
Fe^{2+}	0,000	0,166	0,189	0,192	5,038	5,369	5,424	4,803	5,043	5,128	4,875	4,983	4,942	4,865	4,980	4,806	0,872	0,870
Mn	0,044	0,044	0,045	0,042	0,227	0,045	0,025	0,095	0,039	0,029	0,045	0,037	0,042	0,076	0,064	0,058	3,659	3,643
Ca	5,733	5,638	5,711	5,647	0,351	0,096	0,069	0,181	0,164	0,327	0,283	0,078	0,127	0,165	0,128	0,081	1,033	1,144
Na	0,049	0,050	0,041	0,035	0,032	0,046	0,039	0,032	0,052	0,034	0,035	0,039	0,033	0,038	0,031	0,031	0,047	0,038
Ni	0,040	0,038	0,035	0,045	0,032	0,029	0,030	0,030	0,032	0,023	0,023	0,025	0,031	0,034	0,050	0,024	0,022	0,036
	6,007	6,093	6,133	6,099	5,968	6,001	6,047	5,906	5,994	6,132	6,025	6,040	5,999	5,875	5,971	6,039	5,756	5,853
MOLECULAR PROPORTIONS																		
Almandine					85,3	90,6	90,7	82,2	85,3	84,4	81,7	83,4	83,3	83,8	84,6	80,3	15,3	15,1
Pyrope	5,6	13,2	12,6	13,4	4,9	7,0	7,7	13,1	11,2	9,7	12,8	14,7	13,9	12,0	12,2	17,4	2,2	2,1
Spessartine					3,8	0,8	0,4	1,6	0,7	0,5	0,8	0,6	0,7	1,3	1,1	1,0	64,3	63,0
Grossular	12,9	1,0	4,9	4,7	5,9	1,6	1,2	3,1	2,8	5,4	4,7	1,3	2,1	2,8	2,2	1,4	12,5	14,0
Andradite	57,3	53,2	48,5	52,4	-	-	-	-	-	-	-	-	-	-	-	-	5,6	5,8
Schlorlomite	24,2	32,6	34,0	29,4	-	-	-	-	-	-	-	-	-	-	-	-	-	-

a. calculated from stoichiometry

ELECTRON MICROPROBE ANALYSES OF GARNET

Sample #	PD-19	PD-152	PD-158A	PD-158B	PD-162b	PD-162c	PD-171b	PD-171c	PD-176b	PD-176c	PD-194	PC-13	PC-25	PC-52b	PD-52c	OV-4C
SiO_2	36,88	37,20	36,34	37,51	37,82	37,94	38,39	38,45	37,51	37,96	38,44	36,83	35,22	38,59	38,70	36,75
TiO_2	0,47	0,94	2,55	1,29	0,93	0,86	1,19	1,08	0,72	0,78	0,72	1,34	2,01	0,49	0,69	0,25
Al_2O_3	12,87	16,76	11,36	13,84	16,20	16,52	15,12	16,16	16,05	14,91	20,33	18,20	4,74	19,70	19,63	6,01
Fe_2O_3 [a]	15,24	10,54	13,57	10,99	9,88	8,87	9,06	8,65	10,40	11,48	3,53	7,84	24,26	5,21	5,09	23,06
FeO	0,14	0,62	2,37	1,67	0,00	0,00	0,84	1,16	0,00	0,08	0,90	0,00	0,00	0,46	0,65	0,00
MnO	2,30	0,50	0,20	0,24	0,44	0,37	1,61	0,84	0,47	0,32	2,35	0,29	1,84	0,80	0,56	0,21
MgO	0,31	0,73	0,57	0,55	0,63	0,67	0,94	0,96	0,67	0,52	1,00	0,78	0,56	0,75	0,87	0,54
CaO	31,67	32,51	31,88	32,83	34,20	34,25	31,74	31,86	33,67	34,11	32,43	34,98	31,04	33,83	33,86	33,62
Na_2O	0,13	0,24	0,18	0,14	0,11	0,12	0,39	0,43	0,15	0,16	0,00	0,00	0,33	0,09	0,10	0,10
Cr_2O_3	0,12	0,17	0,23	0,23	0,08	0,17	0,18	0,16	0,15	0,19	0,00	0,00	0,24	0,17	0,18	0,19
NiO	0,16	-	0,23	0,21	0,11	0,12	0,19	0,19	0,23	0,20	0,00	0,00	0,21	0,16	0,21	0,10
Total	100,29	100,21	99,48	99,50	100,40	99,89	99,65	99,94	100,02	100,71	99,70	100,26	100,45	100,25	100,54	100,83
Numbers of ions on the basis of 24(O)																
Si	5,850	5,773	5,824	5,921	5,852	5,878	5,992	5,957	5,830	5,891	5,881	5,664	5,792	5,882	5,881	5,950
Al	0,150	0,227	0,176	0,079	0,148	0,122	0,008	0,043	0,170	0,109	0,119	0,336	0,208	0,118	0,119	0,050
	6,000	6,000	6,000	6,000	6,000	6,000	6,000	6,000	6,000	6,000	6,000	6,000	6,000	6,000	6,000	6,000
Al	2,255	2,838	1,969	2,495	2,806	2,893	2,772	2,907	2,769	2,619	3,547	2,961	0,711	3,420	3,394	1,096
Cr	0,015	0,021	0,029	0,029	0,009	0,021	0,023	0,019	0,019	0,091	0,000	0,000	0,031	0,020	0,022	0,024
Fe^{3+}	1,819	1,231	1,636	1,306	1,150	1,033	1,064	1,009	1,216	1,341	0,407	0,907	3,001	0,597	0,582	2,809
Ti	0,056	0,109	0,307	0,153	0,108	0,100	0,140	0,125	0,084	0,023	0,083	0,155	0,248	0,056	0,078	0,030
	4,145	4,199	3,941	3,983	4,073	4,047	3,999	4,060	4,088	4,074	4,037	4,023	3,991	4,093	4,076	3,959
Mg	0,073	0,168	0,136	0,130	0,145	0,156	0,218	0,222	0,154	0,121	0,229	0,178	0,138	0,171	0,197	0,131
Fe^{2+}	0,019	0,081	0,318	0,221	0,000	0,000	0,110	0,150	0,000	0,011	0,115	0,000	0,000	0,058	0,082	0,000
Mn	0,309	0,066	0,027	0,033	0,057	0,049	0,212	0,110	0,062	0,041	0,305	0,037	0,257	0,103	0,072	0,029
Ca	5,383	5,405	5,475	5,551	5,669	5,684	5,306	5,289	5,606	5,672	5,315	5,762	5,467	5,524	5,511	5,832
Na	0,041	0,073	0,056	0,043	0,034	0,035	0,117	0,128	0,046	0,048	0,000	0,000	0,105	0,025	0,028	0,030
Ni	0,020	-	0,030	0,027	0,014	0,015	0,024	0,024	0,028	0,025	0,000	0,000	0,027	0,019	0,025	0,013
	5,845	5,793	6,042	6,005	5,919	5,939	5,987	5,923	5,896	5,918	5,964	5,977	5,994	5,900	5,915	6,035
MOLECULAR PROPORTIONS																
Almandine Pyrope Spessartine	12,7	9,8	16,9	13,2	6,5	6,7	18,7	16,3	6,9	5,7	21,2	6,9	13,5	10,7	11,4	5,4
Grossular	44,2	61,6	39,8	53,1	65,4	67,7	53,6	58,5	63,8	61,3	68,8	71,6	9,8	74,8	74,4	23,6
Andradite	43,1	28,7	43,3	33,7	28,1	25,6	27,7	25,2	29,3	33,0	10,0	21,5	76,7	14,5	14,2	71,0

a calculated from stoichoimetry
b "massive" garnet
c garnet intergrowth with cpx.

Appendix 7

ELECTRON MICROPROBE ANALYSES OF ORTHOPYROXENE

Sample #	PH-88	PH-170	PH-176	PH-177	PH-178	PH-181	PH-182	PH-188	PH-191	PH-195	PH-196	PH-197	PH-199	PH-201	PH-202[a]	PH-202[b]	PH-203[a]	PH-203[b]	PH-204
SiO_2	49,71	47,10	45,88	48,77	49,21	48,29	49,72	47,31	48,13	48,73	46,09	47,27	51,48	47,37	47,96	47,94	48,12	47,44	47,46
TiO_2	0,17	0,31	0,30	0,23	0,26	0,20	0,28	0,25	0,14	0,35	0,42	0,40	0,36	0,13	0,46	0,29	0,47	0,45	0,13
Al_2O_3	0,45	2,88	3,28	2,28	2,91	0,62	2,94	2,72	3,04	4,45	4,10	4,42	3,51	5,31	5,89	5,39	5,38	6,05	6,79
FeO_T	32,04	37,38	39,15	30,13	32,34	40,33	31,40	39,28	30,30	26,74	38,31	35,52	18,64	30,37	28,24	29,13	29,37	29,59	24,30
MnO	0,59	0,27	0,32	0,55	0,48	0,89	0,59	0,28	0,59	0,23	0,19	0,15	0,57	0,23	0,18	0,23	0,20	0,19	0,19
MgO	14,92	10,24	9,80	16,09	14,10	8,06	12,40	9,17	16,33	17,53	8,93	11,18	23,27	15,76	15,94	15,00	15,95	14,12	19,46
CaO	1,06	0,17	0,14	0,24	0,24	0,99	1,15	0,16	0,05	0,29	0,08	0,11	0,28	0,20	0,06	0,08	0,08	0,07	0,31
Na_2O	0,10	0,12	0,13	0,15	0,12	0,11	0,12	0,10	0,10	0,13	0,14	0,12	0,08	0,11	0,12	0,13	0,13	0,13	0,10
Cr_2O_3	0,13	0,18	0,12	0,18	0,25	0,18	0,22	0,40	0,17	0,20	0,23	0,25	0,19	0,15	0,28	0,24	0,20	0,19	0,15
NiO	0,22	0,29	0,32	0,21	0,25	0,22	0,26	0,43	0,24	0,28	0,22	0,24	0,26	0,08	0,22	0,26	0,25	0,25	0,24
Total	99,39	98,94	99,44	98,83	100,16	99,89	99,08	100,10	99,09	98,93	98,71	99,66	98,64	99,71	99,35	98,69	100,15	98,48	99,13
Numbers of ions on the basis of 6(O)																			
Si	1,967	1,919	1,881	1,920	1,926	1,983	1,961	1,922	1,892	1,881	1,891	1,888	1,915	1,845	1,853	1,874	1,855	1,862	1,809
Al	0,021	0,081	0,119	0,080	0,074	0,017	0,039	0,078	0,108	0,119	0,109	0,112	0,085	0,155	0,147	0,126	0,145	0,138	0,191
	1,988	2,000	2,000	2,000	2,000	2,000	2,000	2,000	2,000	2,000	2,000	2,000	2,000	2,000	2,000	2,000	2,000	2,000	2,000
Al	-	0,057	0,039	0,025	0,060	0,013	0,098	0,052	0,033	0,083	0,089	0,096	0,069	0,089	0,121	0,122	0,099	0,142	0,114
Ti	0,005	0,009	0,009	0,007	0,008	0,006	0,008	0,007	0,004	0,010	0,013	0,012	0,010	0,004	0,013	0,009	0,014	0,013	0,004
Fe^{2+}	1,060	1,273	1,342	0,992	1,058	1,385	1,035	1,335	0,996	0,863	1,314	1,186	0,580	0,990	0,912	0,952	0,947	0,971	0,774
Mn	0,020	0,009	0,011	0,018	0,016	0,031	0,020	0,010	0,020	0,007	0,007	0,005	0,018	0,007	0,006	0,008	0,006	0,006	0,006
Mg	0,880	0,622	0,599	0,944	0,822	0,493	0,729	0,555	0,957	1,008	0,546	0,666	1,290	0,915	0,918	0,874	0,917	0,826	1,105
Ca	0,045	0,007	0,006	0,010	0,010	0,044	0,049	0,007	0,002	0,012	0,003	0,005	0,011	0,008	0,002	0,003	0,003	0,003	0,012
Na	0,007	0,010	0,010	0,011	0,009	0,009	0,009	0,008	0,007	0,010	0,011	0,009	0,006	0,008	0,009	0,010	0,010	0,010	0,007
Cr	0,004	0,006	0,003	0,005	0,008	0,006	0,007	0,013	0,005	0,006	0,007	0,008	0,006	0,004	0,008	0,007	0,006	0,006	0,004
Ni	0,007	0,009	0,010	0,006	0,008	0,007	0,008	0,014	0,007	0,009	0,007	0,008	0,008	0,002	0,007	0,008	0,008	0,008	0,007
	2,028	2,002	2,029	2,018	1,999	1,994	1,963	2,001	2,031	2,008	1,997	1,995	1,998	2,027	1,996	1,993	2,010	1,985	2,033
$Mg/(Mg+Fe_T)$	0,454	0,328	0,309	0,488	0,437	0,262	0,412	0,294	0,490	0,539	0,294	0,359	0,688	0,481	0,502	0,477	0,492	0,458	0,588
Al-value	2,6	16,8	19,4	13,1	16,3	3,7	16,3	15,8	17,3	24,2	23,7	24,8	18,6	29,2	31,6	29,2	29,1	32,7	36,1

a orthopyroxene in contact with spinel

b orthopyroxene intergrowth with spinel

ELECTRON MICROPROBE ANALYSES OF ORTHOPYROXENE

Sample #	PH-206	PH-208	PH-209	PH-212[a]	PH-212[b]	PH-214	PH-215	PH-219	PH-316	PH-321	PH-324	PH-325	PH-326	PH-328	PH-330
SiO_2	46,41	49,37	46,09	47,06	46,84	48,74	49,40	47,35	53,64	47,73	47,72	48,22	47,31	46,59	48,17
TiO_2	0,49	0,31	0,47	0,24	0,30	0,25	0,50	0,57	0,24	0,18	0,25	0,25	0,26	0,25	0,19
Al_2O_3	6,90	6,52	5,73	5,68	6,16	7,06	7,15	6,26	0,98	1,97	2,85	2,44	2,81	3,36	2,12
FeO_T	29,74	19,01	32,40	31,73	31,18	17,40	16,12	30,19	20,66	35,51	38,70	37,94	37,98	39,84	34,92
MnO	0,24	0,32	0,18	0,22	0,19	0,37	0,22	0,22	0,47	0,30	0,10	0,17	0,31	0,19	0,24
MgO	14,44	23,37	13,28	13,63	14,15	23,96	25,77	14,54	22,07	12,47	8,61	9,45	9,36	8,41	12,90
CaO	0,07	0,35	0,07	0,24	0,23	0,28	0,10	0,07	0,95	0,07	0,15	0,17	0,16	0,23	0,10
Na_2O	0,13	0,07	0,12	0,25	0,20	0,11	0,10	0,13	0,10	0,12	0,14	0,12	0,12	0,17	0,09
Cr_2O_3	0,10	0,15	0,17	0,24	0,13	0,13	0,25	0,18	0,19	0,22	0,30	0,18	0,25	0,20	0,34
NiO	0,22	0,22	0,26	0,21	0,23	0,21	0,28	0,26	0,26	0,37	0,32	0,26	0,31	0,24	0,25
Total	98,74	99,69	98,77	99,50	99,61	98,51	99,89	99,77	99,56	98,94	99,14	99,20	98,87	99,48	99,32
Numbers of ions on the basis of 6(0)															
Si	1,821	1,822	1,835	1,851	1,835	1,809	1,796	1,840	1,993	1,928	1,947	1,957	1,933	1,910	1,929
Al	0,179	0,178	0,165	0,149	0,165	0,191	0,204	0,160	0,007	0,072	0,053	0,043	0,067	0,090	0,071
	2,000	2,000	2,000	2,000	2,000	2,000	2,000	2,000	2,000	2,000	2,000	2,000	2,000	2,000	2,000
Al	0,140	0,106	0,104	0,114	0,119	0,118	0,102	0,127	0,036	0,022	0,084	0,074	0,068	0,072	0,029
Ti	0,015	0,009	0,014	0,007	0,009	0,007	0,014	0,017	0,007	0,005	0,008	0,008	0,008	0,008	0,006
Fe^{2+}	0,976	0,587	1,079	1,044	1,021	0,540	0,490	0,981	0,642	1,199	1,320	1,287	1,298	1,365	1,169
Mn	0,008	0,010	0,006	0,007	0,006	0,012	0,007	0,007	0,015	0,010	0,003	0,006	0,011	0,007	0,008
Mg	0,845	1,286	0,788	0,799	0,826	1,325	1,396	0,843	1,222	0,751	0,524	0,572	0,570	0,514	0,770
Ca	0,003	0,014	0,003	0,010	0,010	0,011	0,004	0,003	0,038	0,003	0,007	0,007	0,007	0,010	0,004
Na	0,010	0,005	0,009	0,019	0,015	0,008	0,007	0,010	0,007	0,009	0,011	0,009	0,010	0,013	0,007
Cr	0,003	0,004	0,005	0,007	0,004	0,004	0,007	0,006	0,006	0,007	0,010	0,006	0,008	0,006	0,011
Ni	0,007	0,006	0,008	0,007	0,007	0,006	0,008	0,008	0,008	0,012	0,010	0,008	0,010	0,008	0,008
	2,007	2,027	2,016	2,014	2,017	2,031	2,035	2,002	1,981	2,018	1,977	1,977	1,990	2,003	2,012
$Mg/(Mg+Fe_T)$	0,464	0,687	0,422	0,434	0,447	0,711	0,740	0,462	0,654	0,385	0,283	0,307	0,304	0,273	0,397
Al-value	37,3	33,7	32,0	31,1	33,5	36,5	36,4	33,7	5,3	11,6	16,4	14,1	16,3	19,5	12,3

a. orthopyroxene intergrowth with spinel

b. orthopyroxene not in contact with spinel

Appendix 8

ELECTRON MICROPROBE ANALYSES OF MUSCOVITE

Sample #	PH-31	PH-40	PH-41	PH-42	PH-48	PH-117	PH-143
SiO_2	46,58	46,46	45,92	44,25	44,28	44,21	47,11
TiO_2	0,51	0,30	0,52	0,62	0,10	0,20	0,17
Al_2O_3	32,33	35,44	33,81	32,33	34,02	38,51	36,11
FeO_T	4,35	1,35	3,29	3,90	3,98	1,27	0,66
MnO	0,12	0,08	0,10	0,16	0,11	0,11	0,10
MgO	1,03	0,51	0,76	0,85	0,82	0,19	0,32
CaO	0,06	0,06	0,07	0,05	0,04	0,06	0,07
Na_2O	0,29	0,69	0,59	0,34	0,38	1,06	1,30
K_2O	10,74	10,58	10,35	11,43	10,56	8,83	8,29
Total	96,01	95,47	95,41	93,93	94,29	94,44	94,13
Numbers of ions on the basis of 22(0)							
Si	6,253	6,165	6,161	6,109	6,052	5,879	6,230
Al	1,747	1,835	1,839	1,891	1,948	2,121	1,770
	8,000	8,000	8,000	8,000	8,000	8,000	8,000
Al	3,367	3,705	3,506	3,368	3,529	3,913	3,857
Ti	0,052	0,029	0,053	0,064	0,010	0,020	0,017
Fe^{2+}	0,489	0,150	0,369	0,450	0,455	0,141	0,073
Mn	0,014	0,008	0,011	0,018	0,012	0,012	0,011
Mg	0,206	0,100	0,152	0,175	0,167	0,038	0,064
	4,128	3,992	4,091	4,075	4,173	4,124	4,022
Ca	0,009	0,008	0,009	0,008	0,006	0,009	0,010
Na	0,075	0,178	0,154	0,090	0,102	0,272	0,333
K	1,844	1,795	1,775	2,017	1,845	1,501	1,401
	1,928	1,981	1,938	2,116	1,953	1,783	1,744
$Mg/(Mg+Fe_T)$	0,297	0,400	0,292	0,278	0,266	0,208	0,451

MOLECULAR PROPORTIONS

Muscovite	83,3	91,0	88,3	87,7	91,7	100,0	91,7
Phengite	16,7	9,0	11,7	12,3	8,3	0,0	8,3

ELECTRON MICROPROBE ANALYSES OF CHLORITE

Sample #	PH-75	PH-76	PH-105	PH-109	PH-122	PD-10	PD-18	PD-35	PD-56	PD-83	PD-181
SiO_2	22,58	23,25	21,97	22,23	22,01	27,37	27,88	31,09	29,71	29,54	33,29
TiO_2	0,20	0,20	0,12	0,19	0,16	0,14	0,13	0,14	0,13	0,14	0,41
Al_2O_3	22,81	23,84	24,96	23,61	24,12	22,89	22,14	23,90	23,83	21,54	20,70
FeO_T	33,94	29,02	30,59	32,69	35,73	9,38	30,10	1,06	2,21	16,59	3,59
MnO	0,15	0,21	0,21	0,26	0,18	0,08	0,14	0,19	0,19	0,34	0,22
MgO	7,93	11,86	7,59	7,33	6,03	25,92	4,88	31,33	31,14	21,39	25,23
CaO	0,07	0,06	0,05	0,08	0,06	0,12	0,12	0,26	0,17	0,10	1,21
Na_2O	0,11	0,11	0,10	0,25	0,13	0,12	0,09	0,21	0,18	0,31	0,22
K_2O	0,05	0,07	0,08	0,14	0,04	0,11	0,08	0,16	0,09	0,10	1,03
NiO	0,25	0,32	0,30	0,24	0,28	0,22	0,20	0,16	0,16	0,30	2,04
Total	88,09	88,94	85,97	87,02	88,74	86,35	85,76	88,50	87,81	90,35	87,94
Numbers of ions on the basis of 28(0)											
Si	4,990	5,278	4,885	4,948	4,868	5,370	6,090	5,677	5,511	5,724	6,275
Al	3,010	2,722	3,115	3,052	3,132	2,630	1,910	2,323	2,489	2,276	1,725
	8,000	8,000	8,000	8,000	8,000	8,000	8,000	8,000	8,000	8,000	8,000
Al	2,930	3,249	3,424	3,140	3,156	2,661	3,787	2,819	2,719	2,643	2,873
Ti	0,032	0,031	0,020	0,032	0,027	0,021	0,021	0,019	0,018	0,020	0,058
Fe^{2+}	6,272	5,158	5,688	6,084	6,609	1,539	5,498	0,162	0,343	2,687	0,565
Mn	0,028	0,038	0,040	0,048	0,033	0,012	0,025	0,029	0,030	0,055	0,035
Mg	2,612	3,758	2,517	2,432	1,989	7,578	1,590	8,526	8,609	6,178	7,087
Ca	0,017	0,013	0,012	0,020	0,014	0,026	0,028	0,050	0,034	0,021	0,243
Na	0,048	0,045	0,044	0,108	0,057	0,047	0,039	0,075	0,064	0,116	0,081
K	0,014	0,019	0,022	0,040	0,012	0,027	0,023	0,038	0,020	0,025	0,247
Ni	0,044	0,054	0,053	0,043	0,049	0,035	0,035	0,024	0,024	0,047	0,309
	11,997	12,365	11,820	11,947	11,946	11,946	11,046	11,742	11,861	11,792	11,498
$Mg/(Mg+Fe_T)$	0,294	0,422	0,307	0,285	0,231	0,831	0,224	0,981	0,962	0,697	0,926

Appendix 9

ELECTRON MICROPROBE ANALYSES OF CLINOPYROXENE

Sample	PH-79	PH-88	PH-161	PH-166	PH-181	PH-182	PH-186	PH-192	PH-207	PH-213	PH-315	PD-19	PD-38	PD-48	PD-53	PD-81	PD-82
SiO_2	51,33	51,11	48,55	48,00	48,27	49,41	49,85	46,99	44,12	49,60	47,59	52,40	54,21	54,54	54,18	51,00	52,81
TiO_2	0,27	0,18	0,26	0,46	0,27	0,29	0,32	0,16	1,50	0,96	0,24	0,10	0,16	0,15	0,17	0,18	0,26
Al_2O_3	1,07	0,54	0,95	2,08	0,94	1,03	0,94	1,44	9,75	2,85	0,77	0,74	0,53	0,50	0,86	1,67	1,65
Fe_2O_3[a]	7,82	1,94	2,43	3,71	3,07	2,73	0,42	3,81	4,50	2,96	2,90	2,40	1,38	0,26	0,83	0,00	2,46
FeO	8,30	11,26	18,26	12,58	18,16	13,39	17,93	21,15	5,62	9,87	19,99	5,24	0,00	0,00	0,00	13,11	1,94
MnO	0,65	0,32	0,97	0,39	0,57	0,41	0,82	0,67	1,10	0,65	0,63	0,96	0,60	0,19	0,13	0,92	0,24
MgO	8,28	11,70	5,43	6,75	6,38	9,52	7,36	2,91	9,40	12,62	3,75	14,01	18,28	18,26	18,74	8,93	15,77
CaO	19,98	21,52	22,03	24,80	20,56	21,37	20,66	22,05	22,89	19,81	22,43	23,94	24,39	25,24	24,69	22,68	23,90
Na_2O	2,57	0,18	0,15	0,13	0,24	0,16	0,18	0,14	0,19	0,28	0,15	0,10	0,12	0,12	0,23	0,34	0,43
K_2O	0,05	0,08	0,07	0,06	0,04	0,07	0,15	0,07	0,07	0,06	0,06	0,06	0,07	0,06	0,06	0,10	0,08
Cr_2O_3	0,17	0,16	0,17	0,14	0,16	0,32	0,24	0,16	0,23	0,34	0,20	0,18	0,00	0,00	0,00	0,13	0,00
NiO	0,26	0,19	0,21	0,23	0,26	0,21	0,24	0,23	0,21	0,33	0,23	0,24	0,20	0,24	0,17	0,17	0,23
Total	100,75	99,18	99,48	99,33	98,92	98,91	99,11	99,78	99,58	100,33	98,94	100,37	99,94	99,56	100,06	99,23	99,77
							Numbers of ions on the basis of 6(O)										
Si	1,950	1,961	1,938	1,888	1,931	1,931	1,969	1,907	1,679	1,874	1,934	1,950	1,965	1,977	1,951	1,971	1,940
Al	0,048	0,024	0,045	0,096	0,044	0,047	0,031	0,069	0,321	0,126	0,037	0,032	0,023	0,021	0,037	0,029	0,060
	1,998	1,985	1,983	1,984	1,975	1,978	2,000	1,976	2,000	2,000	1,971	1,982	1,988	1,998	1,988	2,000	2,000
Al	-	-	-	-	-	-	0,013	-	0,116	0,001	-	-	-	-	-	0,047	0,011
Ti	0,008	0,005	0,008	0,014	0,008	0,008	0,010	0,005	0,043	0,027	0,007	0,003	0,004	0,004	0,005	0,005	0,007
Fe^{3+}	0,223	0,056	0,073	0,110	0,092	0,080	0,012	0,116	0,129	0,084	0,089	0,067	0,038	0,007	0,022	0,000	0,068
Fe^{2+}	0,264	0,362	0,611	0,414	0,609	0,438	0,593	0,719	0,179	0,312	0,680	0,163	0,000	0,000	0,000	0,424	0,060
Mn	0,021	0,011	0,033	0,013	0,019	0,013	0,027	0,023	0,036	0,021	0,022	0,030	0,018	0,006	0,004	0,030	0,007
Mg	0,469	0,669	0,323	0,395	0,380	0,555	0,433	0,176	0,533	0,711	0,227	0,777	0,988	0,987	1,006	0,515	0,864
Ca	0,813	0,884	0,942	1,045	0,881	0,895	0,874	0,958	0,933	0,801	0,976	0,954	0,947	0,980	0,953	0,939	0,941
Na	0,189	0,013	0,012	0,010	0,019	0,012	0,014	0,011	0,014	0,020	0,011	0,007	0,008	0,008	0,016	0,025	0,031
K	0,002	0,004	0,004	0,003	0,002	0,004	0,008	0,003	0,003	0,003	0,003	0,003	0,003	0,003	0,003	0,004	0,004
Cr	0,005	0,005	0,005	0,004	0,005	0,010	0,008	0,005	0,007	0,010	0,006	0,005	0,000	0,000	0,000	0,004	0,000
Ni	0,008	0,006	0,007	0,007	0,008	0,007	0,008	0,008	0,006	0,010	0,007	0,007	0,006	0,007	0,005	0,005	0,007
	2,002	2,015	2,018	2,015	2,023	2,022	2,000	2,024	1,999	2,000	2,028	2,016	2,012	2,002	2,014	1,998	2,000
$Mg/(Mg+Fe^{2+})$	0,640	0,649	0,346	0,488	0,385	0,559	0,422	0,197	0,749	0,695	0,250	0,826	1,000	1,000	1,000	0,548	0,935
							MOLECULAR PROPORTIONS										
Wollastonite[b]	46,0	44,9	48,3	53,2	44,9	45,5	45,7	48,7	52,6	42,0	49,5	48,6	47,9	49,5	48,0	50,0	48,7
Enstatite[b]	26,5	33,9	16,6	20,1	19,4	28,2	22,6	8,9	30,1	37,2	11,5	39,6	50,0	49,9	50,7	27,4	44,7
Ferrosilite[b]	27,6	21,2	35,1	26,7	35,7	26,3	31,6	42,4	17,3	20,8	39,0	11,8	2,2	0,6	1,4	22,6	6,6

a Calculated from stoichiometry

b End-members calculated with total Fe as Fe^{2+}

ELECTRON MICROPROBE ANALYSES OF CLINOPYROXENE

Sample #	PD-97	PD-124	PD-125	PD-128	PD-131	PD-157	PD-158	PD-162[c]	PD-162[d]	PD-166	PD-171[d]	PD-171[c]	PD-178	PD-181	PD-191	PD-205	PD-214
SiO_2	52,99	51,66	51,94	53,58	51,68	47,72	51,01	51,21	53,04	54,44	49,14	53,66	53,24	54,17	47,72	51,41	49,27
TiO_2	0,39	0,25	0,44	0,19	0,22	0,62	0,19	0,31	0,16	0,16	0,46	0,21	0,46	0,17	0,80	0,31	0,38
Al_2O_3	1,50	1,26	2,03	1,13	1,81	5,47	1,44	3,11	0,51	0,47	4,07	2,24	1,85	0,92	5,90	4,50	7,63
Fe_2O_3[a]	1,78	2,56	4,31	0,69	1,85	7,10	0,81	1,36	1,40	0,64	6,78	0,00	0,00	0,28	1,84	0,46	1,87
FeO	0,00	9,32	0,00	0,00	6,80	2,05	11,11	3,78	4,59	0,00	0,00	5,12	6,07	1,10	9,22	3,46	2,15
MnO	0,33	0,38	0,12	0,34	0,61	0,85	0,31	0,40	1,19	0,26	1,43	1,45	0,16	0,24	1,31	0,18	0,24
MgO	17,24	13,21	16,71	18,13	12,90	11,96	10,29	13,05	13,79	18,03	13,03	13,36	13,68	17,35	8,85	14,53	13,13
CaO	25,29	20,74	23,29	25,31	23,43	23,40	23,14	25,51	25,01	25,12	23,96	23,17	23,11	24,72	23,45	24,44	24,27
Na_2O	0,12	0,37	0,60	0,20	0,27	0,66	0,24	0,21	0,17	0,14	0,38	0,39	0,40	0,12	0,21	0,10	0,41
K_2O	0,07	0,06	0,08	0,06	0,11	0,12	0,13	0,06	0,05	0,08	0,09	0,09	0,06	0,08	0,07	0,07	0,08
Cr_2O_3	0,13	0,17	0,00	0,20	0,00	0,00	0,23	0,13	0,20	0,20	0,26	0,17	0,22	0,15	0,18	0,17	0,18
NiO	0,12	0,27	0,00	0,19	0,00	0,00	0,29	0,21	0,23	0,16	0,20	0,20	0,25	0,21	0,23	0,25	0,22
Total	99,96	100,25	99,52	100,02	99,68	99,95	99,19	99,34	100,34	99,70	99,80	100,06	99,50	99,51	99,78	99,88	99,83
Numbers of ions on the basis of 6(O)																	
Si	1,927	1,941	1,904	1,935	1,940	1,788	1,959	1,911	1,969	1,975	1,831	1,980	1,976	1,976	1,825	1,890	1,812
Al	0,064	0,056	0,087	0,048	0,060	0,212	0,041	0,089	0,022	0,020	0,169	0,020	0,024	0,024	0,175	0,110	0,188
	1,991	1,997	1,991	1,983	2,000	2,000	2,000	2,000	1,991	1,995	2,000	2,000	2,000	2,000	2,000	2,000	2,000
Al	-	-	-	-	0,020	0,030	0,024	0,048	-	-	0,010	0,077	0,057	0,016	0,091	0,085	0,143
Ti	0,011	0,007	0,012	0,005	0,006	0,017	0,006	0,009	0,004	0,004	0,013	0,006	0,013	0,005	0,023	0,008	0,010
Fe^{3+}	0,049	0,072	0,119	0,019	0,052	0,200	0,023	0,038	0,039	0,018	0,190	0,000	0,000	0,008	0,053	0,013	0,052
Fe^{2+}	0,000	0,293	0,000	0,000	0,214	0,064	0,357	0,118	0,143	0,000	0,000	0,158	0,188	0,033	0,295	0,106	0,066
Mn	0,010	0,012	0,004	0,010	0,019	0,027	0,010	0,013	0,038	0,008	0,045	0,045	0,005	0,008	0,042	0,006	0,007
Mg	0,935	0,740	0,912	0,976	0,722	0,668	0,589	0,726	0,763	0,975	0,724	0,735	0,757	0,943	0,504	0,796	0,720
Ca	0,985	0,835	0,914	0,979	0,942	0,940	0,952	1,020	0,995	0,976	0,957	0,916	0,919	0,966	0,960	0,963	0,957
Na	0,008	0,027	0,043	0,014	0,020	0,048	0,018	0,015	0,012	0,010	0,027	0,028	0,029	0,008	0,016	0,007	0,029
K	0,003	0,003	0,004	0,003	0,005	0,006	0,006	0,003	0,003	0,003	0,004	0,004	0,003	0,004	0,004	0,003	0,004
Cr	0,004	0,005	0,000	0,006	0,000	0,000	0,007	0,004	0,006	0,006	0,008	0,005	0,006	0,004	0,005	0,005	0,005
Ni	0,004	0,008	0,000	0,006	0,000	0,000	0,009	0,006	0,007	0,005	0,006	0,006	0,007	0,006	0,007	0,007	0,006
	2,009	2,002	2,008	2,018	2,000	2,000	2,001	2,000	2,010	2,005	1,984	1,980	1,984	2,001	2,000	1,999	1,999
$Mg/(Mg+Fe^{2+})$	1,000	0,716	1,000	1,000	0,771	0,912	0,622	0,860	0,842	1,000	1,000	0,823	0,801	0,966	0,631	0,882	0,916
MOLECULAR PROPORTIONS																	
Wollastonite[b]	49,9	43,0	46,9	49,5	48,8	50,2	49,5	53,6	51,3	49,5	51,1	50,6	49,3	49,5	53,0	51,3	53,3
Enstatite[b]	47,4	38,1	46,8	49,3	37,4	35,7	30,6	38,2	39,3	49,4	38,7	40,6	40,6	48,4	27,8	42,4	40,1
Ferrosilite[b]	2,7	18,8	6,4	1,2	13,8	14,1	19,8	8,2	9,4	1,1	10,2	8,7	10,1	2,1	19,2	6,3	6,6

a Calculated from stoichiometry
b End-memebers calculated with total Fe as Fe^{2+}
c Cpx intergrowth with garnet
d Cpx single crystal

ELECTRON MICROPROBE ANALYSES OF CLINOPYROXENE

Sample #	PD-216	PC-11	PC-12	PC-13	PC-20	PC-27	PC-30	PC-32	PC-36
SiO_2	50,81	50,38	51,79	49,69	53,65	53,54	50,50	50,75	53,49
TiO_2	1,20	0,38	0,17	0,41	0,19	0,28	0,18	0,15	0,18
Al_2O_3	5,33	2,70	1,30	3,91	0,93	1,82	1,01	1,32	1,29
Fe_2O_3[a]	1,89	5,32	4,49	4,24	1,54	2,45	2,56	2,86	1,23
FeO	1,74	3,03	2,75	4,20	0,00	0,07	11,04	10,37	0,00
MnO	0,39	0,68	0,83	0,33	0,54	0,33	1,28	0,70	0,37
MgO	15,31	13,29	13,72	11,42	17,06	16,77	9,11	10,12	17,55
CaO	21,98	23,30	24,26	25,05	25,26	24,13	23,69	23,28	24,78
Na_2O	0,81	0,62	0,54	0,50	0,21	0,58	0,25	0,30	0,28
K_2O	0,09	0,08	0,07	0,09	0,07	0,07	0,06	0,08	0,08
Cr_2O_3	0,21	0,28	0,16	0,17	0,14	0,18	0,24	0,23	0,17
NiO	0,22	0,22	0,28	0,21	0,18	0,21	0,27	0,23	0,23
Total	99,98	100,28	100,36	100,22	99,77	100,43	100,19	100,39	99,65
				Numbers of ions on the basis of 6(O)					
Si	1,855	1,876	1,923	1,861	1,956	1,939	1,942	1,935	1,944
Al	0,145	0,118	0,057	0,139	0,040	0,061	0,046	0,059	0,055
	2,000	1,994	1,980	2,000	1,996	2,000	1,988	1,994	1,999
Al	0,084	-	-	0,033	-	0,017	-	-	-
Ti	0,033	0,011	0,005	0,011	0,005	0,008	0,005	0,004	0,005
Fe^{3+}	0,052	0,149	0,125	0,119	0,042	0,067	0,074	0,082	0,034
Fe^{2+}	0,053	0,094	0,085	0,132	0,000	0,002	0,356	0,331	0,000
Mn	0,012	0,021	0,026	0,011	0,017	0,010	0,042	0,023	0,011
Mg	0,833	0,738	0,759	0,638	0,927	0,905	0,522	0,575	0,951
Ca	0,859	0,929	0,965	1,005	0,986	0,936	0,976	0,951	0,965
Na	0,058	0,045	0,039	0,037	0,014	0,040	0,019	0,022	0,020
K	0,004	0,004	0,003	0,004	0,003	0,003	0,003	0,004	0,004
Cr	0,006	0,008	0,005	0,005	0,004	0,005	0,007	0,007	0,005
Ni	0,006	0,007	0,008	0,006	0,005	0,006	0,008	0,007	0,007
	2,000	2,006	2,020	2,001	2,003	1,999	2,012	2,006	2,002
$Mg/(Mg+Fe^{2+})$	0,940	0,887	0,899	0,829	1,000	0,998	0,595	0,635	1,000
				MOLECULAR PROPORTIONS					
Wollastonite[b]	47,8	48,7	49,9	53,1	50,3	49,0	50,6	49,0	49,4
Enstatite[b]	46,3	38,6	39,2	33,7	47,3	47,4	27,1	29,7	48,7
Ferrosilite[b]	5,8	12,7	10,9	13,3	2,4	3,6	22,3	21,3	2,0

a Calculated from stoichiometry

b End members calculated with total Fe as Fe^{2+}

Appendix 10

ELECTRON MICROPROBE ANALYSES OF FASSAITE

Sample #	PD-96 (core)	PD-96 (rim)	PD-148	PD-152	PD-174A	PD-174B	PD-176[b]	PD-176[c]	PD-177	PD-184A	PD-184B	PD-194	PC-52[d]	PC-52[c]
SiO_2	42,98	50,16	44,42	44,88	40,61	40,52	46,65	43,21	44,70	39,49	39,16	39,70	47,82	48,66
TiO_2	4,33	0,33	0,63	0,86	0,68	0,72	0,55	0,73	0,52	0,52	0,39	3,45	0,69	0,35
Al_2O_3	12,17	6,86	10,22	10,52	16,43	17,03	7,63	12,82	11,44	19,42	20,11	14,90	8,08	6,40
Fe_2O_3[a]	3,03	1,87	5,38	7,08	5,95	5,96	5,50	6,96	5,29	6,79	6,28	6,36	4,13	4,64
FeO	0,00	0,00	0,00	0,09	0,00	0,00	1,43	0,00	0,00	0,00	0,55	0,00	0,60	0,22
MnO	0,33	0,40	0,19	0,33	0,25	0,29	0,20	0,21	0,16	0,29	0,16	1,70	0,36	0,64
MgO	12,55	15,57	13,49	12,04	10,33	10,12	11,41	10,90	12,70	8,01	7,43	9,28	13,12	13,54
CaO	24,09	24,42	25,30	24,27	25,01	24,83	25,79	24,71	24,69	24,98	25,01	23,69	24,90	25,09
Na_2O	0,37	0,31	0,17	0,28	0,16	0,15	0,17	0,17	0,14	0,16	0,17	0,18	0,24	0,25
K_2O	0,06	0,07	0,10	0,05	0,08	0,08	0,08	0,08	0,08	0,06	0,08	0,00	0,09	0,03
Cr_2O_3	0,12	0,12	0,29	0,00	0,16	0,12	0,14	0,17	0,20	0,13	0,25	0,18	0,13	0,10
NiO	0,14	0,14	0,21	0,00	0,26	0,19	0,24	0,25	0,12	0,21	0,19	0,22	0,17	0,10
Total	100,17	100,25	100,40	100,40	99,92	100,01	99,79	100,21	100,04	100,06	99,78	99,66	100,33	100,02
					Numbers of ions on the basis of 6(O)									
Si	1,582	1,816	1,627	1,660	1,503	1,498	1,745	1,604	1,645	1,470	1,463	1,496	1,758	1,795
Al	0,418	0,814	0,373	0,340	0,497	0,502	0,255	0,396	0,355	0,530	0,537	0,504	0,242	0,205
	2,000	2,000	2,000	2,000	2,000	2,000	2,000	2,000	2,000	2,000	2,000	2,000	2,000	2,000
Al	0,110	0,108	0,068	0,118	0,219	0,240	0,081	0,165	0,141	0,322	0,348	0,157	0,108	0,073
Ti_{3+}	0,120	0,009	0,017	0,024	0,019	0,020	0,016	0,020	0,014	0,014	0,011	0,100	0,019	0,010
Fe^{2+}	0,084	0,051	0,148	0,197	0,166	0,166	0,155	0,194	0,147	0,190	0,177	0,180	0,114	0,129
Fe	0,000	0,000	0,000	0,003	0,000	0,000	0,045	0,000	0,000	0,000	0,017	0,000	0,019	0,007
Mn	0,010	0,012	0,006	0,010	0,008	0,009	0,006	0,007	0,005	0,009	0,005	0,054	0,011	0,020
Mg	0,689	0,840	0,736	0,664	0,570	0,558	0,636	0,603	0,697	0,445	0,414	0,521	0,719	0,745
Ca	0,950	0,947	0,993	0,961	0,991	0,983	1,034	0,983	0,973	0,996	1,001	0,956	0,980	0,992
Na	0,026	0,022	0,012	0,020	0,012	0,011	0,012	0,012	0,010	0,011	0,012	0,014	0,017	0,018
K	0,003	0,003	0,005	0,002	0,004	0,004	0,004	0,004	0,004	0,003	0,004	0,000	0,004	0,001
Cr	0,004	0,003	0,008	0,000	0,005	0,003	0,004	0,005	0,006	0,004	0,007	0,005	0,004	0,003
Ni	0,004	0,004	0,006	0,000	0,008	0,006	0,007	0,007	0,003	0,006	0,006	0,007	0,005	0,003
	2,000	1,999	1,999	1,999	2,002	2,000	2,000	2,000	2,000	2,000	2,002	1,994	2,000	2,001
					MOLECULAR PROPORTIONS									
Diopside	70	76	72	68	57	55	73	62	68	46	45	56	76	79
CaTs	10	20	13	11	25	27	9	17	16	33	36	15	10	7
FATs	7	4	14	19	16	16	17	19	14	19	18	19	11	13
Tp	12	1	2	2	2	2	2	2	1	2	1	10	2	1

a Calculated from stoichiometry
b cpx intergrowth with garnet
c cpx single crystal
d cpx intergrowth with garnet
e cpx single crystal inclusion in garnet

Appendix 11

ELECTRON MICROPROBE ANALYSES OF MAGNETITE

Sample #	PH-8	PH-14	PH-16	PH-19	PH-42	PH-48	PH-79	PH-189	PH-191[b]	PH-191[c]	PH-192	PH-195	PH-197	PH-199	PH-201[d]	PH-201[e]	PH-203	PH-204
TiO_2	0,65	10,94	10,33	0,18	14,06	21,34	0,36	5,61	2,09	9,97	0,62	6,11	12,39	2,86	4,74	2,34	23,46	0,81
Al_2O_3	2,68	1,25	0,88	0,67	0,66	0,12	0,53	2,69	2,37	3,18	1,45	3,95	6,40	2,10	5,00	2,15	3,79	1,28
Fe_2O_3[a]	63,29	46,59	49,64	66,65	42,07	27,93	69,19	55,20	63,08	46,58	66,18	51,18	36,21	60,98	53,68	61,05	16,96	65,31
FeO	31,07	40,71	40,81	30,40	44,00	50,09	31,56	35,51	33,11	40,12	30,92	36,12	42,46	33,56	35,94	33,33	51,84	30,92
MnO	0,23	0,23	0,14	0,00	0,18	0,20	0,19	0,57	0,21	0,37	0,26	0,21	0,21	0,20	0,16	0,22	0,25	0,16
MgO	0,90	0,27	0,26	0,23	0,26	0,29	0,23	0,32	0,24	0,23	0,25	0,46	0,19	0,30	0,46	0,23	0,25	0,32
Cr_2O_3	3,48	0,51	0,56	0,40	0,17	0,28	0,16	0,55	0,73	0,58	0,15	1,92	1,79	0,60	1,69	1,77	1,03	0,61
NiO	0,10	0,27	0,32	0,10	0,30	0,27	0,00	0,37	0,35	0,44	0,30	0,51	0,89	0,00	0,00	0,00	0,36	0,34
Total	102,40	100,77	102,94	98,63	101,70	100,52	102,22	100,82	102,18	101,47	100,13	100,13	100,54	100,60	101,67	101,09	97,94	99,75
Numbers of ions on the basis of 4(0)																		
Ti	0,018	0,308	0,286	0,005	0,400	0,600	0,010	0,157	0,058	0,276	0,018	0,171	0,340	0,081	0,130	0,066	0,662	0,023
Al	0,116	0,055	0,038	0,031	0,032	0,005	0,023	0,118	0,104	0,138	0,065	0,173	0,275	0,093	0,215	0,095	0,168	0,058
Fe^{3+}	1,748	1,314	1,374	1,947	1,164	0,786	1,952	1,551	1,759	1,292	1,895	1,430	0,994	1,727	1,476	1,721	0,479	1,877
Cr	0,101	0,015	0,016	0,012	0,005	0,008	0,005	0,016	0,021	0,017	0,004	0,056	0,052	0,018	0,049	0,053	0,030	0,018
	1,983	1,692	1,714	1,995	1,601	1,399	1,990	1,842	1,942	1,723	1,982	1,830	1,661	1,919	1,870	1,935	1,339	1,976
Fe^{2+}	0,958	1,278	1,258	0,988	1,371	1,569	0,991	1,110	1,028	1,239	0,986	1,123	1,297	1,058	1,100	1,046	1,629	0,989
Mn	0,007	0,007	0,004	0,000	0,006	0,006	0,006	0,018	0,007	0,012	0,008	0,007	0,006	0,006	0,005	0,007	0,008	0,005
Mg	0,049	0,015	0,014	0,013	0,014	0,016	0,013	0,018	0,013	0,013	0,014	0,026	0,010	0,017	0,025	0,013	0,014	0,018
Ni	0,003	0,008	0,009	0,003	0,009	0,008	0,000	0,011	0,011	0,013	0,009	0,015	0,026	0,000	0,000	0,000	0,011	0,010
	1,017	1,308	1,285	1,004	1,400	1,599	1,010	1,157	1,059	1,277	1,017	1,171	1,339	1,081	1,130	1,066	1,662	1,022
MOLECULAR PROPORTIONS																		
max. usp.	2,1	32,9	30,2	0,5	41,1	62,3	1,0	17,72	6,4	31,2	2,0	20,4	42,8	8,8	15,53	7,3	76,2	2,5
min. mt.	97,9	67,1	69,8	99,5	58,9	37,7	99,0	82,28	93,6	68,8	98,0	79,6	57,2	91,2	84,47	92,7	23,8	97,5
min. usp.	0,0	30,8	28,4	0,0	39,3	59,8	0,0	14,73	4,7	28,5	0,4	17,1	39,0	7,5	13,48	6,1	72,9	1,0
max. mt.	100,0	69,2	71,6	100,0	60,7	40,2	100,0	85,27	95,3	71,5	99,6	82,9	61,0	92,5	86,52	93,9	27,1	99,0

a Claculated from stoichiometry
b Magnetite rimmed by biotite
c No biotite rim
d Magnetite intergrowth with hercynite
e Magnetite next to orthopyroxene

ELECTRON MICROPROBE ANALYSES OF MAGNETITE

Sample #	PH-206	PH-298[b]	PH-208[c]	PH-209	PH-213	PH-214	PH-215	PH-220	PH-321
TiO_2	25,48	2,33	5,71	27,37	2,69	6,09	6,62	0,21	0,36
Al_2O_3	3,52	4,02	2,14	4,31	2,03	3,59	2,17	1,40	0,77
Fe_2O_3[a]	14,24	59,56	53,25	8,65	60,54	53,47	55,52	68,24	67,17
FeO	53,90	32,76	35,00	55,27	33,65	36,18	36,59	31,47	31,13
MnO	0,22	0,21	0,21	0,27	0,22	0,20	0,23	0,21	0,10
MgO	0,35	0,43	0,19	0,38	0,32	0,56	0,84	0,21	0,17
Cr_2O_3	1,02	0,67	0,44	1,13	2,84	0,30	0,53	0,72	0,90
NiO	0,38	0,36	0,36	0,39	0,27	0,26	0,30	0,29	0,27
Total	99,11	100,34	97,30	97,77	102,66	100,65	102,80	102,75	100,87
				Numbers of ions on the basis of 4(0)					
Ti	0,710	0,065	0,167	0,768	0,074	0,170	0,182	0,006	0,010
Al	0,154	0,177	0,098	0,189	0,088	0,157	0,093	0,061	0,034
Fe^{3+}	0,397	1,673	1,555	0,243	1,680	1,494	1,527	1,906	1,918
Cr	0,030	0,020	0,014	0,033	0,083	0,009	0,015	0,021	0,027
	1,291	1,935	1,834	1,233	1,925	1,830	1,817	1,994	1,989
Fe^{2+}	1,672	1,024	1,138	1,726	1,039	1,125	1,120	0,979	0,989
Mn	0,007	0,007	0,007	0,009	0,007	0,006	0,007	0,007	0,003
Mg	0,019	0,024	0,011	0,021	0,018	0,031	0,046	0,012	0,009
Ni	0,011	0,011	0,011	0,012	0,011	0,008	0,009	0,009	0,008
	1,709	1,066	1,167	1,768	1,075	1,170	1,182	1,007	1,009
				MOLECULAR PROPORTIONS					
max. usp.	81,4	7,6	18,2	90,6	9,0	19,5	20,6	0,6	1,0
min. mt.	18,6	92,4	81,8	9,4	91,0	80,5	79,4	99,4	99,0
min. usp.	78,0	5,0	16,4	86,0	7,0	16,5	16,5	0,0	0,0
max. mt.	22,0	95,0	83,6	14,0	93,0	83,5	83,5	100,0	100,0

a Calculated from stoichiometry
b Large magnetite grain not in contact with opx
c Small magnetite grain in contact with opx

ELECTRON MICROPROBE ANALYSES OF ILMENITE

Sample #	PH-21	PH-85	PH-88	PH-116	PH-157	PH-168	PH-177	PH-184	PH-213	PH-220	PH-312	PH-313	PH-321	PH-325	PH-328	PH-335
TiO_2	51,56	51,66	51,74	49,95	50,88	51,66	52,13	53,44	50,53	49,95	51,92	51,03	50,89	51,31	51,83	51,55
Al_2O_3	0,41	0,38	0,33	1,43	0,39	0,34	0,47	0,49	0,42	0,40	0,41	0,40	0,44	0,42	0,44	0,35
Fe_2O_3[a]	2,11	1,18	0,80	3,30	3,48	1,48	0,61	0,00	3,64	5,32	0,01	3,43	3,25	1,69	1,71	1,34
FeO	44,80	44,93	44,82	43,66	44,45	45,01	45,20	44,53	42,49	43,14	46,10	45,02	44,98	44,98	45,65	45,80
MnO	0,76	0,34	1,08	0,34	0,57	0,50	1,01	0,77	1,13	1,12	0,19	0,19	0,28	0,17	0,46	0,22
MgO	0,35	0,50	0,17	0,35	0,23	0,29	0,20	0,64	0,83	0,19	0,17	0,19	0,11	0,38	0,23	0,14
Cr_2O_3	0,24	0,21	0,18	0,19	0,27	0,23	0,35	0,18	0,86	0,23	0,16	0,21	0,19	0,21	0,20	0,16
NiO	0,10	0,23	0,24	0,21	0,25	0,35	0,24	0,26	0,27	0,24	0,00	0,26	0,24	0,25	0,00	0,00
Total	100,33	99,43	99,36	99,43	100,52	99,86	100,21	100,31	100,17	100,59	98,96	100,73	100,38	99,41	100,52	99,56
Numbers of ions on the basis of 3(O)																
Ti	0,972	0,981	0,986	0,946	0,959	0,979	0,984	1,000	0,951	0,942	0,992	0,960	0,961	0,976	0,975	0,981
Al	0,012	0,011	0,010	0,042	0,012	0,010	0,014	0,014	0,012	0,012	0,012	0,012	0,013	0,012	0,013	0,010
Fe^{3+}	0,040	0,022	0,015	0,063	0,066	0,028	0,012	0,000	0,069	0,100	0,000	0,064	0,061	0,032	0,032	0,026
Cr	0,005	0,004	0,004	0,004	0,005	0,005	0,007	0,004	0,017	0,005	0,003	0,004	0,004	0,004	0,004	0,003
	1,029	1,018	1,015	1,055	1,042	1,022	1,017	1,018	1,049	1,059	1,007	1,040	1,039	1,024	1,024	1,020
Fe^{2+}	0,940	0,950	0,951	0,921	0,933	0,950	0,950	0,927	0,891	0,906	0,981	0,943	0,946	0,953	0,957	0,970
Mn	0,016	0,007	0,023	0,007	0,012	0,011	0,021	0,016	0,024	0,024	0,004	0,004	0,006	0,004	0,010	0,005
Mg	0,013	0,019	0,006	0,013	0,009	0,011	0,008	0,024	0,031	0,007	0,006	0,007	0,004	0,014	0,009	0,005
Ni	0,002	0,005	0,005	0,004	0,005	0,007	0,005	0,005	0,006	0,005	0,000	0,005	0,005	0,005	0,000	0,000
	0,971	0,981	0,985	0,945	0,959	0,979	0,984	0,972	0,952	0,942	0,991	0,959	0,961	0,976	0,976	0,980
MOLECULAR PROPORTIONS																
max. hem.	2,1	1,0	1,0	3,3	3,4	1,5	1,0	0,0	4,0	5,2	0,0	3,3	3,2	2,0	1,6	1,3
min. ilm.	97,9	99,0	99,0	96,7	96,6	98,5	99,0	100,0	96,0	94,8	100,0	96,7	96,8	98,0	98,4	98,7
min. hem.	1,0	0,0	0,0	1,0	2,6	0,7	0,0	0,0	2,0	4,5	0,0	2,5	2,3	1,0	0,0	0,7
max. ilm.	99,0	100,0	100,0	99,0	97,4	99,3	100,0	100,0	98,0	95,5	100,0	97,5	97,7	99,0	100,0	99,3

Appendix 12

ELECTRON MICROPROBE ANALYSES OF PLAGIOCLASE

Sample #	PH-19	PH-79[b]	PH-79[c]	PH-85	PH-88A	PH-88B	PH-170 (core)	PH-170 (rim)	PH-177 (core)	PH-177 (rim)	PH-178 (core)	PH-178 (rim)	PH-182A	PH-182B	PH-186A (core)	PH-186B (rim)	PH-220	PH-213 (core)	PH-213 (rim)
SiO_2	48,56	63,27	66,08	58,99	54,82	54,92	61,76	61,98	58,27	58,50	54,41	54,40	48,95	47,35	45,08	45,47	54,92	45,42	45,42
Al_2O_3	32,49	22,81	20,41	25,47	28,24	28,31	23,82	24,07	26,34	26,15	28,64	28,66	32,23	33,56	34,36	34,56	27,97	34,05	34,07
Fe_2O_3[a]	0,00	0,92	0,21	0,00	0,25	0,23	0,31	0,24	0,00	0,00	0,15	0,00	0,00	0,00	0,00	0,00	0,26	0,21	0,52
FeO	0,38	0,00	0,00	0,30	0,00	0,00	0,00	0,00	0,30	0,22	0,16	0,53	0,39	0,29	0,38	0,17	0,00	0,23	0,00
CaO	16,16	3,53	0,70	7,71	10,11	9,86	5,33	4,90	7,96	7,97	10,96	11,08	15,14	16,62	17,84	18,16	9,95	18,09	18,09
Na_2O	2,14	9,03	10,85	7,13	5,48	5,57	8,35	8,74	6,30	6,84	5,10	4,91	2,50	1,82	0,94	0,89	5,79	1,02	1,15
K_2O	0,24	0,85	0,86	0,08	0,28	0,32	0,11	0,14	0,32	0,31	0,27	0,27	0,23	0,15	0,09	0,10	0,16	0,15	0,15
Total	99,97	100,41	99,11	99,68	99,18	99,21	99,68	100,07	99,49	99,99	99,69	99,85	99,44	99,79	98,69	99,35	99,05	99,17	99,40
Numbers of ions on the basis of 32(O)																			
Si	8,910	11,178	11,679	10,577	9,957	9,965	10,995	10,980	10,464	10,472	9,858	9,852	9,004	8,711	8,421	8,432	9,971	8,453	8,429
Al	7,024	4,748	4,251	5,382	6,044	6,053	4,996	5,025	5,574	5,515	6,115	6,115	6,985	7,276	7,563	7,552	5,984	7,467	7,451
Fe^{3+}	0,000	0,122	0,028	0,000	0,034	0,032	0,047	0,032	0,000	0,000	0,020	0,000	0,000	0,000	0,000	0,000	0,035	0,030	0,072
	15,934	16,048	15,958	15,959	16,035	16,050	16,038	16,037	16,038	15,987	15,993	15,967	15,989	15,987	15,984	15,984	15,990	15,950	15,952
Fe^{2+}	0,058	0,000	0,000	0,044	0,000	0,000	0,000	0,000	0,045	0,033	0,025	0,081	0,060	0,045	0,059	0,026	0,000	0,036	0,000
Ca	3,176	0,667	0,132	1,481	1,968	1,916	1,016	0,930	1,531	1,527	2,128	2,150	2,982	3,275	3,570	3,608	1,936	3,607	3,596
Na	0,759	3,092	3,716	2,477	1,930	1,960	2,882	3,000	2,194	2,374	1,791	1,722	0,890	0,650	0,340	0,320	2,036	0,369	0,414
K	0,057	0,192	0,193	0,019	0,065	0,073	0,025	0,031	0,072	0,072	0,062	0,062	0,054	0,036	0,022	0,024	0,037	0,036	0,035
	4,050	3,951	4,041	4,021	3,963	3,949	3,923	3,961	3,842	4,006	4,006	4,015	3,986	4,006	3,991	3,978	4,009	4,048	4,045
MOLECULAR PROPORTIONS																			
Albite	19,0	78,3	92,0	62,3	48,7	49,6	73,5	75,7	57,8	59,8	45,0	43,8	22,7	16,4	8,6	8,1	50,8	9,2	10,2
Anorthite	79,5	16,9	3,3	37,2	49,7	48,5	25,9	23,5	40,3	38,4	53,5	54,7	76,0	82,7	90,8	91,3	48,3	89,9	88,9
Orthoclase	1,4	4,9	4,8	0,5	1,6	1,9	0,6	0,8	1,9	1,8	1,6	1,6	1,4	0,9	0,6	0,6	0,9	0,9	0,9

a Calculated from stoichiometry
b Small "groundmass" feldspar crystal
c Feldspar from "clear patch"

ELECTRON MICROPROBE ANALYSES OF PLAGIOCLASE

Sample #	PH-312	PH-316	PH-320	PD-124	PC-16
SiO_2	54,86	45,95	60,49	56,90	58,40
Al_2O_3	28,39	34,70	24,79	26,79	25,76
Fe_2O_3[a]	0,00	0,00	0,00	0,24	0,20
FeO	0,79	0,26	0,19	0,00	0,00
CaO	10,35	18,09	6,49	9,17	6,93
Na_2O	5,25	1,00	7,86	6,19	7,49
K_2O	0,07	0,11	0,15	0,48	0,21
Total	99,71	100,11	99,97	99,77	98,99
Numbers of ions on the basis of 32(O)					
Si	9,930	8,456	10,777	10,245	10,511
Al	6,055	7,525	5,204	5,683	5,464
Fe^{3+}	0,000	0,000	0,000	0,033	0,026
	15,985	15,981	15,981	15,961	16,001
Fe^{2+}	0,120	0,040	0,029	0,000	0,000
Ca	2,006	3,566	1,238	1,769	1,337
Na	1,842	0,358	2,713	2,160	2,614
K	0,016	0,025	0,033	0,109	0,048
	3,984	3,989	4,013	4,038	3,999
MOLECULAR PROPORTIONS					
Albite	47,7	9,1	68,1	53,5	65,4
Anorthite	51,9	90,3	31,1	43,8	33,4
Orthoclase	0,4	0,6	0,8	2,7	1,2

a Calculated from stoichiometry

ELECTRON MICROPROBE ANALYSES OF ANDALUSITE AND SILLIMANITE

Sample #	PH-16 and.	PH-31 and.	PH-42 and.	PH-48 and.	PH-117 and.	PH-143 and.	PH-184 and.	PH-173 sill.	PH-183 sill.
SiO_2	37,06	36,94	36,34	36,36	36,96	37,00	36,38	36,33	37,08
TiO_2	0,11	0,16	0,19	0,11	0,13	0,13	0,14	0,00	0,21
Al_2O_3	59,51	59,93	60,81	60,81	61,69	62,27	61,86	63,47	60,51
FeO_T	2,68	2,41	2,17	1,73	0,41	0,37	0,22	0,38	1,24
MnO	0,13	0,22	0,13	0,09	0,13	0,05	0,12	0,00	0,11
MgO	0,14	0,12	0,11	0,09	0,08	0,08	0,35	0,08	0,07
CaO	0,07	0,07	0,05	0,06	0,06	0,06	0,06	0,06	0,06
Cr_2O_3	0,21	0,12	0,16	0,18	0,12	0,19	0,16	0,00	0,28
NiO	0,15	0,16	0,13	0,16	0,17	0,22	0,18	0,00	0,15
Total	100,06	100,13	100,09	99,59	99,75	100,37	99,47	100,32	99,71
Numbers of ions on the basis of 20(O)									
Si	4,062	4,042	3,971	3,984	4,013	3,995	3,962	3,920	4,048
Ti	0,009	0,013	0,016	0,009	0,010	0,010	0,011	0,000	0,017
Al	7,686	7,727	7,830	7,851	7,891	7,923	7,938	8,071	7,784
Fe^{2+}	0,246	0,221	0,198	0,158	0,037	0,034	0,020	0,034	0,113
Mn	0,012	0,020	0,012	0,009	0,012	0,005	0,011	0,000	0,011
Mg	0,023	0,019	0,018	0,015	0,013	0,013	0,057	0,012	0,011
Ca	0,008	0,008	0,006	0,007	0,007	0,007	0,007	0,007	0,007
Cr	0,018	0,011	0,013	0,016	0,010	0,016	0,014	0,000	0,024
Ni	0,013	0,014	0,011	0,014	0,015	0,019	0,016	0,000	0,013
	12,077	12,075	12,075	12,063	12,008	12,022	12,036	12,044	12,028
$Mg/(Mg+Fe_T)$	0,080	0,074	0,075	0,075	0,182	0,199	0,589	0,186	0,079

Appendix 13

ELECTRONMICROPROBE ANALYSES OF OLIVINE

Sample #	PH-197	PH-202	PH-203	PH-206	PH-209	PH-213	PH-219[a]	PH-219[b]	PH-328	PD-140	PD-208	PD-214	PD-216	PC-1	PC-10	PC-27	PC-34	PC-36
SiO_2	31,28	33,33	33,04	30,84	31,32	33,66	32,91	32,70	32,24	41,19	41,77	40,55	39,76	41,87	40,54	41,14	41,43	41,61
TiO_2	0,14	0,16	0,16	0,18	0,18	0,15	0,18	0,16	0,17	0,11	0,15	0,12	0,15	0,13	0,16	0,14	0,14	0,14
Al_2O_3	0,92	0,35	0,37	0,35	0,34	0,34	0,33	0,30	0,32	0,54	1,24	1,23	1,46	0,26	0,90	0,84	0,86	0,79
FeO_T	57,97	47,64	50,42	52,02	56,48	43,18	49,61	49,10	61,87	3,26	1,16	9,76	9,66	0,75	4,02	3,43	1,55	3,45
MnO	0,28	0,27	0,22	0,30	0,27	1,17	0,27	0,24	0,26	1,29	0,94	1,14	1,13	0,15	0,31	0,41	0,32	0,45
MgO	7,41	16,38	14,94	14,95	10,84	21,02	14,45	15,28	4,42	53,03	53,75	45,99	46,84	55,81	53,44	52,72	55,41	53,20
CaO	0,08	0,10	0,08	0,08	0,08	0,12	0,08	0,08	0,08	0,08	0,20	0,37	0,09	0,16	0,23	0,06	0,10	0,10
Na_2O	0,16	0,12	0,16	0,15	0,20	0,15	0,13	0,15	0,18	0,14	0,29	0,31	0,30	0,22	0,10	0,14	0,17	0,15
Cr_2O_3	0,20	0,18	0,28	0,14	0,23	0,21	0,22	0,17	0,14	0,17	0,16	0,15	0,09	0,17	0,13	0,18	0,00	0,15
NiO	0,26	0,32	0,27	0,34	0,33	0,10	0,30	0,29	0,31	0,18	0,22	0,19	0,20	0,21	0,13	0,22	0,18	0,20
Total	98,70	98,85	99,94	99,35	100,27	100,10	98,48	98,47	99,99	99,99	99,88	99,81	99,68	99,73	99,96	99,28	100,16	100,24
Numbers of ions on the basis of 4(O)																		
Si	1,002	1,004	0,998	0,954	0,979	0,981	1,007	0,999	1,035	0,987	0,990	1,000	0,983	0,990	0,972	0,989	0,980	0,991
Al	-	-	0,002	0,013	0,013	0,012	-	0,001	-	0,013	0,010	-	0,017	0,007	0,025	0,011	0,020	0,009
	1,002	1,004	1,000	0,967	0,992	0,993	1,007	1,000	1,035	1,000	1,000	1,000	1,000	0,997	0,997	1,000	1,000	1,000
Al	0,035	0,013	0,011	-	-	-	0,012	0,010	0,012	0,002	0,025	0,036	0,025	-	-	0,013	0,004	0,013
Ti	0,003	0,004	0,004	0,004	0,004	0,003	0,004	0,004	0,004	0,002	0,003	0,002	0,003	0,002	0,003	0,003	0,003	0,002
Fe^{2+}	1,552	1,200	1,274	1,345	1,476	1,052	1,270	1,254	1,661	0,065	0,023	0,201	0,200	0,015	0,081	0,069	0,031	0,069
Mn	0,008	0,007	0,006	0,008	0,007	0,029	0,007	0,006	0,007	0,026	0,019	0,024	0,024	0,003	0,006	0,008	0,006	0,009
Mg	0,354	0,736	0,673	0,689	0,505	0,913	0,659	0,696	0,211	1,894	1,899	1,691	1,725	1,967	1,910	1,889	1,953	1,888
Ca	0,003	0,003	0,003	0,003	0,003	0,004	0,002	0,003	0,003	0,002	0,005	0,010	0,002	0,004	0,006	0,002	0,002	0,003
Na	0,010	0,007	0,009	0,009	0,012	0,009	0,007	0,009	0,011	0,006	0,013	0,015	0,015	0,010	0,005	0,007	0,008	0,007
Cr	0,005	0,004	0,007	0,003	0,006	0,005	0,005	0,004	0,003	0,003	0,003	0,003	0,002	0,003	0,003	0,003	0,000	0,003
Ni	0,007	0,008	0,007	0,008	0,008	0,002	0,007	0,007	0,008	0,003	0,004	0,004	0,004	0,004	0,003	0,004	0,003	0,004
	1,977	1,982	1,974	2,069	2,021	2,017	1,973	1,993	1,920	2,003	1,994	1,986	2,000	2,008	2,017	1,998	2,010	1,998
$Mg/(Mg+Fe_T)$	0,185	0,379	0,345	0,339	0,255	0,465	0,341	0,356	0,113	0,967	0,988	0,894	0,896	0,990	0,960	0,965	0,985	0,965

a Olivine in contact with cordierite

b Olivine inclusion in spinel

Appendix 14

ELECTRONMICROPROBE ANALYSES OF SPINEL

Sample ##	PH-168	PH-169(core)	PH-173	PH-183	PH-184	PH-195A	PH-195B	PH-199A	PH-199B	PH-201A	PH-201B	PH-202[b]	PH-202[c]	PH-203[b]	PH-204A	PH-204B	PH-206
TiO_2	0,28	0,25	0,31	0,32	0,27	0,35	0,25	0,23	0,28	0,17	0,24	0,28	0,55	0,63	0,16	0,13	0,53
Al_2O_3	53,81	59,63	59,17	50,41	59,21	52,05	53,83	55,66	55,35	51,52	52,39	58,88	57,11	53,75	53,05	52,01	54,00
Fe_2O_3[a]	6,39	1,94	0,34	9,15	0,06	5,31	4,39	8,54	7,35	6,40	6,22	0,98	0,38	5,74	9,81	10,38	6,27
FeO	34,66	30,40	32,84	37,50	35,94	31,89	33,83	21,81	25,15	33,16	33,35	31,61	33,64	32,56	28,18	29,27	33,37
MnO	0,22	0,28	0,17	0,21	0,19	0,27	0,24	0,43	0,48	0,18	0,20	0,18	0,13	0,17	0,18	0,17	0,23
MgO	3,75	7,07	5,31	1,50	3,30	4,84	3,63	12,05	9,79	4,00	4,21	6,18	4,43	5,16	7,66	6,88	4,68
Cr_2O_3	0,70	0,59	0,82	1,16	0,44	4,19	2,35	1,31	1,31	2,26	2,10	0,95	0,75	1,48	0,75	0,97	1,05
NiO	0,00	0,31	0,26	0,31	0,28	0,88	0,89	0,35	0,32	0,00	0,00	0,00	0,00	0,32	0,39	0,28	0,31
Total	99,81	100,47	99,22	100,56	99,69	99,78	99,41	100,38	100,03	97,69	98,71	99,06	97,00	99,81	100,18	100,09	100,44
						Numbers of ions on the basis of 4(O)											
Ti	0,006	0,005	0,006	0,007	0,006	0,008	0,005	0,005	0,006	0,004	0,005	0,006	0,012	0,014	0,003	0,003	0,011
Al	1,833	1,937	1,962	1,755	1,977	1,773	1,840	1,787	1,807	1,797	1,804	1,946	1,951	1,815	1,768	1,750	1,819
Fe^{3+}	0,139	0,040	0,007	0,204	0,001	0,116	0,096	0,175	0,153	0,142	0,137	0,021	0,008	0,124	0,209	0,223	0,135
Cr	0,016	0,013	0,018	0,027	0,010	0,096	0,054	0,028	0,029	0,053	0,048	0,021	0,017	0,034	0,017	0,022	0,024
	1,994	1,995	1,993	1,993	1,994	1,993	1,995	1,995	1,995	1,996	1,994	1,994	1,988	1,987	1,997	1,998	1,989
Fe^{2+}	0,839	0,702	0,774	0,928	0,853	0,772	0,822	0,498	0,583	0,822	0,817	0,743	0,817	0,782	0,667	0,700	0,799
Mn	0,005	0,006	0,004	0,005	0,004	0,007	0,006	0,010	0,011	0,005	0,005	0,004	0,003	0,004	0,004	0,004	0,006
Mg	0,161	0,290	0,223	0,066	0,139	0,209	0,157	0,489	0,404	0,177	0,183	0,259	0,191	0,220	0,323	0,293	0,200
Ni	0,000	0,007	0,006	0,007	0,006	0,020	0,021	0,008	0,007	0,000	0,000	0,000	0,000	0,007	0,009	0,006	0,007
	1,005	1,005	1,007	1,006	1,002	1,008	1,006	1,005	1,005	1,004	1,005	1,006	1,011	1,013	1,003	1,003	1,012
$Fe^{3+}/(Fe^{3+}+Al+Cr)$	0,070	0,020	0,004	0,103	0,001	0,058	0,048	0,088	0,077	0,072	0,069	0,010	0,004	0,063	0,105	0,112	0,068
$Mg/(Mg+Fe^{2+})$	0,161	0,293	0,224	0,067	0,141	0,213	0,161	0,496	0,409	0,177	0,184	0,258	0,190	0,220	0,326	0,295	0,200

a Calculated from stoichiometry

b Core composition at a crystal next to olivine

c Intergrowth with orthopyroxene

ELECTRONMICROPROBE ANALYSES OF SPINEL

Sample #	PH-208	PH-209	PH-212[b]	PH-212[c]	PH-214	PH-215	PH-219	PH-334A	PH-334B	PD-148	PD-174	PD-177	PD-184	PD-208	PD-214	PC-1	PC-10
TiO_2	0,18	0,65	0,35	0,52	0,17	0,21	0,43	0,23	0,27	0,14	0,16	0,12	0,13	0,48	0,21	0,50	0,38
Al_2O_3	56,71	51,65	51,18	51,97	58,70	59,08	53,88	58,51	58,55	63,26	66,70	65,18	65,15	70,32	62,32	60,72	63,35
Fe_2O_3[a]	6,86	7,32	10,47	8,65	6,86	6,68	6,53	1,85	2,46	5,80	0,83	3,38	2,88	0,00	6,00	11,15	6,20
FeO	23,02	34,60	34,23	33,90	20,03	17,76	32,18	32,34	31,98	8,01	10,55	8,25	9,32	1,24	10,70	1,45	6,76
MnO	0,18	0,20	0,17	0,16	0,17	0,19	0,21	0,19	0,23	0,61	0,79	0,90	1,25	0,40	0,79	0,15	0,10
MgO	11,23	3,66	3,72	4,06	13,67	15,13	5,32	5,53	5,98	21,61	20,21	21,45	20,46	26,43	19,78	26,18	22,96
CaO	0,00	0,00	0,10	0,09	0,00	0,00	0,00	0,00	0,00	0,07	0,07	0,08	0,08	0,19	0,10	0,26	0,12
Cr_2O_3	0,47	1,83	0,19	0,55	0,35	0,43	1,21	0,69	0,79	0,14	0,20	0,27	0,18	0,45	0,21	0,17	0,17
NiO	0,35	0,35	0,29	0,24	0,35	0,28	0,32	0,37	0,30	0,27	0,27	0,29	0,36	0,17	0,20	0,19	0,25
Total	99,00	100,26	100,70	100,14	100,30	99,76	100,08	99,71	100,56	99,91	99,78	99,92	99,81	99,68	100,31	100,77	100,29
						Numbers of ions on the basis of 4(O)											
Ti	0,004	0,014	0,008	0,011	0,003	0,004	0,009	0,005	0,006	0,003	0,003	0,002	0,002	0,009	0,004	0,009	0,007
Al	1,840	1,769	1,752	1,776	1,848	1,849	1,814	1,936	1,920	1,882	1,974	1,926	1,937	1,989	1,873	1,771	1,866
Fe^{3+}	0,142	0,160	0,229	0,189	0,138	0,134	0,140	0,039	0,051	0,110	0,016	0,064	0,055	0,000	0,115	0,208	0,117
Cr	0,010	0,042	0,004	0,013	0,007	0,009	0,027	0,015	0,017	0,003	0,004	0,005	0,004	0,008	0,004	0,003	0,003
	1,996	1,985	1,993	1,989	1,996	1,996	1,990	1,995	1,994	1,998	1,997	1,997	1,998	2,006	1,996	1,991	1,993
Fe^{2+}	0,531	0,842	0,833	0,823	0,448	0,395	0,770	0,761	0,745	0,169	0,222	0,173	0,197	0,025	0,228	0,030	0,142
Mn	0,004	0,005	0,004	0,004	0,004	0,004	0,005	0,005	0,006	0,013	0,017	0,019	0,027	0,008	0,017	0,003	0,002
Mg	0,461	0,158	0,161	0,175	0,544	0,599	0,227	0,231	0,248	0,813	0,757	0,802	0,769	0,945	0,752	0,966	0,855
Ca	0,000	0,000	0,003	0,003	0,000	0,000	0,000	0,000	0,000	0,002	0,002	0,002	0,002	0,005	0,003	0,007	0,003
Ni	0,008	0,008	0,007	0,006	0,007	0,006	0,007	0,008	0,007	0,005	0,005	0,006	0,007	0,003	0,004	0,004	0,005
	1,004	1,013	1,008	1,011	1,003	1,004	1,009	1,005	1,006	1,002	1,003	1,002	1,002	0,986	1,004	1,010	1,007
$Fe^{3+}/(Fe^{3+}+Al+Cr)$	0,071	0,081	0,115	0,095	0,069	0,067	0,071	0,020	0,026	0,055	0,008	0,032	0,027	0,000	0,058	0,105	0,059
$Mg/(Mg+Fe^{2+})$	0,465	0,158	0,162	0,176	0,548	0,603	0,228	0,233	0,250	0,828	0,773	0,882	0,796	0,974	0,767	0,970	0,858

a Calculated from stoichiometry

b Spinel intergrown with opx

c Spinel not in contact with opx

Appendix 15

ELECTRON MICROPROBE ANALYSES OF CHLORITOID

Sample #	PD-109	PH-122	PH-143A	PH-143B
SiO_2	24,62	24,68	24,56	24,13
TiO_2	0,15	0,13	0,17	0,26
Al_2O_3	39,88	40,00	39,96	39,52
FeO_T	25,48	26,14	26,69	27,45
MnO	0,40	0,46	0,19	0,21
MgO	1,30	1,33	1,69	1,07
CaO	0,06	0,05	0,07	0,07
Na_2O	0,09	0,12	0,10	0,10
K_2O	0,09	0,05	0,07	0,05
Total	92,07	92,96	93,50	92,86
Numbers of ions on the basis of 12(O)				
Si	2,050	2,041	2,025	2,012
Al	0,950	0,959	0,975	0,988
	3,000	3,000	3,000	3,000
Al	2,961	2,937	2,908	2,895
Ti	0,009	0,008	0,010	0,016
Fe^{2+}	1,774	1,807	1,841	1,914
Mn	0,028	0,032	0,013	0,015
Mg	0,161	0,164	0,207	0,133
Ca	0,006	0,005	0,006	0,006
Na	0,014	0,018	0,016	0,016
K	0,009	0,006	0,007	0,006
	4,962	4,977	5,008	5,001
$Mg/(Mg+Fe_T)$	0,083	0,083	0,101	0,065

a Calculated from stoichiometry.

ELECTRON MICROPROBE ANALYSES OF K-FELDSPAR

Sample #	PH-14	PH-16	PH-40	PH-42	PH-48	PH-80	PD-157	PH-182	PH-202	PH-203
SiO_2	63,43	63,49	63,49	63,81	62,38	64,89	63,47	63,60	64,00	62,54
Al_2O_3	19,86	19,67	19,67	19,34	20,25	18,03	19,56	19,38	18,61	18,84
Fe_2O_3[a]	0,32	0,26	0,00	0,20	0,24	0,00	0,14	0,19	0,71	0,69
FeO	0,00	0,00	0,74	0,00	0,00	0,77	0,00	0,00	0,00	0,00
CaO	0,12	0,14	0,08	0,07	0,02	0,41	0,30	0,10	0,00	0,04
Na_2O	1,48	1,41	0,81	1,22	0,98	0,29	0,82	1,22	0,59	0,22
K_2O	14,51	14,64	14,54	15,51	15,79	15,58	15,66	14,75	15,92	17,32
Total	99,72	99,61	99,33	100,51	99,66	99,97	99,95	99,24	99,83	99,65
Numbers of ions on the basis of 32(O)										
Si	11,680	11,708	11,777	11,705	11,496	12,004	11,695	11,788	11,854	11,595
Al	4,310	4,273	4,298	4,181	4,398	3,930	4,248	4,231	4,062	4,116
Fe^{3+}	0,044	0,036	0,000	0,028	0,034	0,000	0,020	0,026	0,098	0,096
	16,034	16,017	16,075	15,914	15,928	15,934	15,963	16,045	16,014	15,807
Fe^{2+}	0,000	0,000	0,114	0,000	0,000	0,119	0,000	0,000	0,000	0,000
Ca	0,023	0,028	0,016	0,014	0,004	0,081	0,058	0,019	0,000	0,008
Na	0,527	0,505	0,291	0,434	0,350	0,105	0,292	0,439	0,213	0,079
K	3,417	3,450	3,447	3,637	3,719	3,685	3,688	3,495	3,770	4,105
	3,967	3,983	3,868	4,085	4,073	3,990	4,038	3,953	3,983	4,192
MOLECULAR PROPORTIONS										
Albite	13,3	12,7	7,8	10,6	8,6	2,7	7,2	11,1	5,3	1,9
Anorthite	0,6	0,7	0,4	0,3	0,1	2,1	1,4	0,5	0,0	0,2
Orthoclase	86,1	86,6	91,8	89,0	91,3	95,2	91,3	88,4	94,7	97,9

ELECTRON MICROPROBE ANALYSES OF CALCITE AND DOLOMITE

Sample #	PH-79	PH-207	PD-10	PD-18	PD-19	PD-34	PD-34	PD-35	PD-48	PD-50	PD-50	PD-53	PD-56	PD-70	PD-70	PD-81	PD-128	PD-130	PD-131
	cal	cal	dol	dol	cal	cal	dol	dol	dol	cal	dol	cal	dol	cal	dol	cal	cal	cal	cal
FeO_T	0,31	0,36	3,61	0,90	0,22	0,21	0,54	0,54	0,22	0,15	0,48	0,10	1,00	0,27	0,58	0,19	0,20	0,14	0,26
MnO	0,48	2,60	0,19	0,63	0,47	0,29	0,71	0,30	0,12	0,21	0,14	0,13	1,16	0,40	0,40	0,18	0,31	0,14	0,46
MgO	0,31	0,17	19,45	20,14	0,49	6,50	21,38	21,85	21,51	1,03	22,02	0,46	21,53	3,73	20,74	0,53	4,07	0,21	0,60
CaO	54,70	52,83	29,73	31,93	53,74	43,95	31,36	31,02	29,78	54,04	32,01	54,32	30,55	52,00	30,31	54,00	53,07	55,30	54,02
Total	55,80	55,96	52,98	53,60	54,92	50,95	53,99	53,71	51,63	55,43	54,65	55,01	54,24	56,40	52,03	54,90	57,65	55,79	55,34

Numbers of ions on the basis of 2(0)

Fe^{2+}	0,009	0,010	0,094	0,023	0,006	0,006	0,013	0,014	0,056	0,004	0,012	0,003	0,025	0,007	0,015	0,005	0,005	0,004	0,007
Mn	0,014	0,074	0,005	0,016	0,013	0,009	0,018	0,008	0,003	0,006	0,004	0,004	0,030	0,011	0,011	0,005	0,008	0,004	0,013
Mg	0,016	0,008	0,906	0,917	0,025	0,339	0,958	0,979	0,972	0,051	0,970	0,023	0,962	0,180	0,963	0,027	0,191	0,011	0,030
Ca	1,962	1,907	0,995	1,044	1,955	1,646	1,010	0,999	0,969	1,938	1,014	1,970	0,983	1,802	1,011	1,963	1,795	1,982	1,950
	2,001	1,999	2,000	2,000	1,999	2,000	1,999	2,000	2,000	1,999	2,000	2,000	2,000	2,000	2,000	2,000	1,999	2,001	2,000

Sample #	PD-140	PD-157	PD-176	PD-177	PD-191	PC-34
	cal	cal	cal	cal	cal	dol
FeO_T	0,15	0,21	0,24	0,17	0,15	0,26
MnO	0,52	0,30	0,13	0,18	0,17	0,33
MgO	3,41	0,45	0,14	0,74	0,23	21,93
CaO	52,38	53,66	54,71	55,66	53,38	31,23
Total	56,46	54,62	55,22	56,75	53,93	53,75

Numbers of ions on the basis of 2(0)

Fe	0,004	0,006	0,007	0,005	0,004	0,007
Mn	0,014	0,009	0,004	0,005	0,005	0,008
Mg	0,164	0,023	0,007	0,036	0,012	0,981
Ca	1,817	1,963	1,982	1,954	1,979	1,004
	1,999	2,001	2,000	2,000	2,000	2,000

cal = calcite
dol = dolomite

ELECTRON MICROPROBE ANALYSES OF EPIDOTE

Sample #	PD-82	PD-152	PD-158 (core)	PD-158 (rim)	PD-158A	PD-176	PD-178	PD-184	PC-12	PC-25
SiO_2	39,82	39,10	36,70	37,05	38,08	38,17	37,95	38,29	37,80	36,91
TiO_2	0,16	0,16	0,16	0,18	0,19	0,16	0,19	0,15	0,17	0,21
Al_2O_3	28,71	32,55	23,07	24,78	21,60	28,13	25,05	31,90	21,12	22,76
Fe_2O_3[a]	5,36	1,90	1,90	13,22	15,56	7,53	12,25	1,96	15,71	14,81
MnO	0,42	0,18	0,18	0,23	0,18	0,14	0,16	0,27	0,56	0,27
MgO	0,41	0,31	0,31	0,38	0,24	0,34	0,21	0,22	0,59	0,43
CaO	23,54	23,34	23,34	22,49	22,21	22,67	22,83	24,73	21,77	22,48
Na_2O	0,25	0,21	0,21	0,24	0,13	0,13	0,13	0,14	0,12	0,00
	98,67	97,75	97,75	98,57	98,19	97,27	98,77	97,66	97,84	97,87
Numbers of ions on the basis of 12(0)										
Si	2,930	2,863	2,843	2,812	2,917	2,867	2,860	2,807	2,913	2,839
Al	0,070	0,137	0,157	0,188	0,083	0,133	0,140	0,193	0,087	0,161
	3,000	3,000	3,000	3,000	3,000	3,000	3,000	3,000	3,000	3,000
Al	2,419	2,669	1,947	2,025	1,867	2,355	2,081	2,596	1,830	1,901
Fe^{3+}	0,300	0,105	0,834	0,753	0,895	0,424	0,693	0,110	0,909	0,856
	2,719	2,774	2,781	2,778	2,762	2,779	2,774	2,706	2,739	2,757
Ti	0,009	0,009	0,009	0,011	0,011	0,009	0,011	0,009	0,009	0,011
Mn	0,026	0,009	0,009	0,014	0,014	0,009	0,009	0,018	0,037	0,018
Mg	0,044	0,035	0,046	0,041	0,028	0,036	0,022	0,022	0,069	0,051
Ca	1,853	1,832	1,813	1,831	1,825	1,826	1,845	1,970	1,799	1,851
Na	0,036	0,026	0,037	0,036	0,018	0,018	0,018	0,009	0,018	0,000
	1,968	1,911	1,914	1,933	1,896	1,898	1,905	2,028	1,932	1,931
MOLECULAR PROPORTIONS										
Pistacite	11,0	3,8	30,0	27,1	32,4	15,3	25,0	4,1	33,2	31,0
Clinozoisite	89,0	96,2	70,0	72,9	67,6	84,7	75,0	95,9	66,8	69,0

a Total Fe as Fe_2O_3

ELECTRON MICROPROBE ANALYSES OF WOLLASTONITE

Sample #	PD-191A	PD-191B	PD-194A	PD-194B
SiO_2	51,14	51,28	50,60	50,67
TiO_2	0,17	0,16	0,20	0,19
Al_2O_3	0,53	0,51	0,79	0,83
FeO_T	0,52	0,80	0,39	0,21
MnO	1,17	1,17	1,04	0,91
MgO	0,24	0,30	0,47	0,38
CaO	45,40	44,98	46,49	46,69
Na_2O	0,12	0,13	0,00	0,00
Total	99,29	99,33	99,98	99,88
Numbers of ions on the basis of 18(0)				
Si	5,960	5,974	5,891	5,880
Al	0,072	0,070	0,109	0,113
	6,032	6,044	6,000	5,993
Ti	0,015	0,014	0,017	0,017
Fe^{2+}	0,050	0,078	0,038	0,021
Mn	0,116	0,115	0,103	0,090
Mg	0,042	0,051	0,082	0,065
Ca	5,668	5,614	5,798	5,801
Na	0,027	0,029	0,000	0,000
	5,918	5,901	6,038	5,994

ELECTRON MICROPROBE ANALYSES OF ADDITIONAL MINERALS

Mineral	Monticellite		Sphene			Prehnite				Idocrase		
Sample #	PD-194A	PD-194B	PH-L	PD-81	PC-32	PD-125	PD-158	PD-162	PD-205	PD-97A	PD-97B	PD-158
SiO_2	34,93	35,18	29,65	30,62	29,13	42,76	42,64	42,89	42,85	38,38	38,19	37,16
TiO_2	0,22	0,18	34,22	37,15	37,78	0,09	0,14	0,17	0,21	0,40	0,46	0,14
Al_2O_3	0,73	0,96	6,03	2,12	2,38	24,87	24,94	24,62	25,47	16,66	17,51	22,26
FeO_T	14,49	14,86	0,28	0,57	0,80	0,19	0,34	0,97	0,25	3,40	3,08	1,34
MnO	6,99	6,81	0,17	0,11	0,31	0,10	0,11	0,12	0,09	0,16	0,30	0,18
MgO	10,82	11,76	Mg 0,12	0,46	0,43	0,42	0,35	0,22	0,32	3,51	2,93	0,58
CaO	30,61	30,50	29,11	27,29	27,69	26,82	26,74	26,46	25,60	34,64	34,70	36,20
Na_2O	0,00	0,00	0,12	0,27	0,31	0,10	0,09	0,09	0,12	0,13	0,12	0,29
Total	98,79	100,25	99,70	98,59	98,83	95,35	95,35	95,54	94,91	97,28	97,29	98,15

Numbers of ions on the basis of:

	4(0)		19.5(0)			23(0)				72(0)		
Si	1,009	1,000	Si 3,665	3,826	3,655	Si 5,869	5,862	5,894	5,905	Si 18,106	17,981	17,210
Ti	0,004	0,004	Al 0,335	0,174	0,345	Al 0,131	0,138	0,106	0,095	Al 0,000	0,019	0,790
Al	0,025	0,032	4,000	4,000	4,000	6,000	6,000	6,000	6,000	18,106	18,000	18,000
Fe^{2+}	0,350	0,353	Al 0,543	0,138	0,007	Al 3,890	3,902	3,881	4,041	Al 9,262	9,693	11,358
Mn	0,171	0,164	Ti 3,181	3,491	3,564	Ti 0,009	0,015	0,018	0,021	Ti 0,142	0,164	0,047
Mg	0,466	0,498	Fe^{2+} 0,029	0,059	0,084	Fe^{3+} 0,020	0,035	0,101	0,026	Fe^{2+} 1,339	1,212	0,521
Ca	0,948	0,929	3,753	3,688	3,655	Mn 0,012	0,013	0,014	0,011	Mn 0,065	0,120	0,071
Na	0,000	0,000	Mn 0,017	0,011	0,033	Mg 0,086	0,072	0,044	0,067	Mg 2,465	2,053	0,397
	2,973	2,980	Mg 0,023	0,085	0,081	4,017	4,037	4,058	4,166	13,273	13,242	12,394
MOLECULAR PROPORTIONS			Ca 3,855	3,654	3,722	Ca 3,944	3,939	3,895	3,780	Ca 17,506	17,501	17,964
Monticellite	47,2	49,1	Na 0,029	0,064	0,076	Na 0,027	0,024	0,024	0,031	Na 0,122	0,108	0,261
Kirschsteinite	35,5	34,7	3,924	3,814	3,912	3,971	3,963	3,919	3,811	17,628	17,609	18,225
Glaucochroite	17,3	16,2										

a Total Fe as Fe_2O_3

ELECTRON MICROPROBE ANALYSES OF ADDITIONAL MINERALS

Mineral	Ni-minnesotaite			Pumpellyite	
Sample #	PD-178A	PD-178B	D.H. & Z[a]	PH-LA	PH-LB
SiO_2	48,74	50,60	51,29	38,57	38,49
TiO_2	0,17	0,16	0,04	0,12	0,10
Al_2O_3	1,28	1,62	0,61	27,34	27,29
FeO_T	21,06	11,30	35,46	1,80	1,77
MnO	0,15	0,19	0,12	2,22	2,12
MgO	2,85	4,60	6,26	4,46	4,27
CaO	0,56	0,69	0,00	22,89	22,81
Na_2O	0,60	0,34	0,08	0,13	0,12
K_2O	0,98	0,31	0,03	0,08	0,07
NiO	18,31	30,15	0,00		
Total	94,70	99,96	93,89	97,61	97,04
			Numbers of ions on the basis of:		
	22(0)			26.5(0)	
Si	7,745	7,614	7,874	6,374	6,393
Al	0,241	0,289	0,074	0,000	0,000
	7,986	7,903	7,948	6,374	6,393
Al	0,000	0,000	0,000	5,321	5,335
Ti	0,019	0,018	0,000	0,015	0,015
				5,336	5,350
Fe^{2+}	2,793	1,417	4,554	0,248	0,249
Mn	0,019	0,027	0,016	0,307	0,289
Mg	0,677	1,029	1,432	1,100	1,056
Ni	2,335	3,647	0,000		
	5,843	6,138	6,002	1,655	1,594
Ca	0,095	0,108	0,000	4,055	4,056
Na	0,190	0,090	0,024	0,040	0,039
K	0,190	0,054	0,006	0,020	0,020
	0,475	0,252	0,030	4,115	4,115

a minnesotaite analysis from Deer, Howie and Zussman (1962c)

Appendix 16 A brief review of some theoretical considerations

A) The Gibbs phase rule

The application of the Gibbs phase rule to metamorphic mineral assemblages assumes that chemical equilibrium can be attained in a small volume of the rock, which forms a thermodynamic system comprising of phases (minerals) and components. Components are the minimum number of indepenently variable chemical constituents that must be specified in order that their combination will yield all possible phases of a chemical system (Reinhard, 1968). A "closed" system can only exchange energy with its surroundings while an "open" system can exchange both energy and matter with its surroundings.

Three factors are significant in determining the state of a metamorphic system, viz. temperature, pressure and the chemical potentials of the components (Reinhard, 1968). These factors are "intensive" properties because their magnitudes are not dependent on the size of the system (Korzhinskii, 1959). The number of properties that can be varied without changing the number of phases in a system, or the number of components in any phase, is the number of degrees of freedom or the variance (F) of that system. It is clear that the number of intensive properties that may vary for any phase are the chemical potentials, of all components in the system (C) plus the pressure and temperature, viz. the total number of variable intensive properties are (C + 2) where C denotes the number of components. Equilibrium at constant pressure and temperature requires that the change in Gibbs free energy (dG) of the system be equal to zero. This means that the free energy change in each phase of the system must also be equal to zero. There will therefore be Ø equations stating that the change in free energy for Ø phases will be equal to zero. The variance of a system may then be defined as follows:

The number of variable properties which must be specified to describe the state of the system	-	The number of equations which must be specified to satisfy the requirement of thermodynamic equilibrium	= variance

or $(C + 2) - \emptyset = F$. This is the Gibbs phase rule.

When the phase rule is applied it is important to distinguish between open and closed systems. Korzhinskii (1950) defined perfectly mobile components (C_m) as those chemical species that have their chemical potentials (μ_i) as independent variables while the "inert" components (C_i) are those whose amounts (n_i) are the independent variables. In a broad way the perfectly mobile components are open to the system whereas the inert components are closed to the system. It is important to note, however, that these concepts are not synonymous since it is possible, for example, that throughout the metamorphic episode a particular component, i, was added to, or subtracted from the system, yet because of the rapidity of reaction rates the value of μ_i in the rock was at all times buffered by the mineral assemblage, rather than controlled by the value of the potential in the environment (Korzhinskii, 1959). Because the amount of component i did not remain constant, the system is by definition open to this component, yet at the same time component i is inert because its chemical potential is not controlled by the environment of the system. Zen (1963) suggested that the two types of components should be called "initial value components" and "boundary value components" instead of "inert" and "mobile" components respectively, because the values of their chemical potentials are determined either by their initial proportions or by the values of the potentials at the boundary of the system respectively.

The presence of each mobile component adds another variable to the system so that for a system open to certain components the phase rule becomes:

$F = C_i - \emptyset + (C_m + 2)$

Where the term in parentheses can be regarded as the externally controlled variables, viz. pressure, temperature and the chemical potentials of the mobile components. When these variables are fixed, the maximum number of equilibrium mineral phases will be given by $\emptyset = C_i$. Chemical species in the fluid phase (e.g. H_2O and CO_2) can behave in a mobile or immobile manner. It is clear that when a fluid phase species becomes immobile the number of equilibrium mineral phases will increase by one relative to when the component is mobile.

Derivation of components

Certain components are more important than others in a certain rock type, e.g. pelites or carbonates. Minerals like quartz, alkali feldspars and opaque minerals are common to virtually all pelitic assemblages and for this reason some of the components involved in these phases are not essential in determining the mineral assemblage of a rock. Chemical species that determine the presence and the composition of phases in a particular rock are of greater importance in the system. For these reasons Reinhard (1968) classified the components in the rock into groups:

1) Trace components

   These include all the trace elements in a rock as well as the major elements, e.g. P_2O_5 and MnO that do not determine the presence of any major phases in a paragenesis. These elements may be ignored in the paragenetic analysis.

2) Excess components

   These components are present in minerals that are common to all assemblages. An increase in their concentrations only results in the increase of the modal amounts of the corresponding phases. The minerals quartz, K-feldspar or muscovite, magnetite and ilmenite or rutile are present in almost all the pelitic assemblages and therefore the elements SiO_2, K_2O, Fe_2O_3 and TiO_2 may be considered

excess components. The number of effective components may further be reduced by treating Na_2O and CaO as isomorphous excess components that occur in the mineral plagioclase, which is also common to most pelitic assemblages.

3) Inert components

These components are critical in dertermining the appearance and composition of certain minerals in a metamorphic mineral paragenesis. They include Al_2O_3 , FeO and MgO which are essential in controlling the presence and composition of the ferromagnesian minerals. The Mg/(Mg + Fe) ratios of the ferromagnesian minerals are also important in this respect. When two minerals have the same, or similar Mg/(Mg + Fe) ratios the number of effective components in the system is reduced by 1 since Fe and Mg then behave as 1 component (Hollister, 1969).

4) Mobile elements

H_2O and CO_2 are usually assumed to be mobile or boundary value components, which means that their chemical potentials are fixed externally to the system and that mass movement of these components could have occured.

B) Graphical representation of components and phases

Since Al_2O_3 , FeO and MgO are the most important inert components in pelitic rocks, the AFM diagram of Thompson (1957) is usually used for the graphical display of pelitic parageneses. The diagram, which is actually a projection onto the AFM plane of all points in a tetrahedron of which the fourth corner is K_2O, is only intended for SiO_2-saturated rocks that have K-feldspar or muscovite as additional minerals. Depending on whether muscovite or K-feldspar is present in a rock, all points in the tetrahedrom are projected from either the muscovite or K-feldspar points. The "A" coordinate of any point is then given by:

$$A = \frac{Al_2O_3 - 3\,K_2O}{Al_2O_3 - 3K_2O + MgO + FeO_T} \quad \text{or} \quad A = \frac{Al_2O_3 - K_2O}{Al_2O_3 - K_2O + MgO + FeO_T}$$

for projections from muscovite and K-feldspar respectively. (The amount of K_2O in the correction of the A-coordinate is determined by the molecular $Al_2O_3 : K_2O$ ratio in muscovite and K-feldspar). The M coordinate in the projection is given by the $Mg/(Mg + Fe_T)$ ratio of a particular point.

A metamorphic system with three inert components (e.g. Al_2O_3 , MgO and FeO) will have three phases in divariant equilibium (F = 2). The three phases will form a triangle in the three component diagram (e.g. AFM), of which the exact position will depend on the external conditions (P,T) under which the assemblage has crystallized. The shifting or displacement of a three-phase triangle, due to changing metamorphic conditions, is not an indefinite process and after a certain amount of displacement a reaction will take place to form new mineral assemblages which will define new three-phase triangles in the diagram.

The displacement of a three-phase triangle is the result of a continuous reaction. Petrographically these reactions are manifested by changing proportions of the phases involved in the reaction. Continuous reactions take place over a pressure, temperature interval and both parameters have to be specified in order to define the position of the triangle in the projection. When a continuous reaction in a three-component system is examined in terms of only two components(i.e. when MgO or FeO is equal to zero), the reaction loses 1 degree of freedom and it now takes place along a line in P,T space.

This is the limiting case of a continuous reaction and it may now be balanced using stoichiometric coefficients appropriate to the mineral formulae of the participating phases. Since both MgO and FeO are present in natural systems, a continuous reaction may be thought of as a

combination of either end-member reaction and a Fe-Mg exchange reaction (Thompson, 1976 a).

The displacement of any three-phase triangle in response of changing temperature or a_{H_2O} may be predicted from a knowledge of the relative Fe/Mg ratios of the phases involved, while the displacement due to changing pressure may be predicted from the relative Fe/Mg ratios and the $\Delta \bar{V}^\circ$ for the end-member reactions (Thompson 1976 a).

Discontinuous reactions reflect a distinct change in the topology of the AFM diagram. These reactions generally affect a large range of bulk compositions and are independent of the proportions of the relevant phases. They therefore produce easily observed changes in the mineral assemblage of the host rock and are thus suitable as isograds (Thompson, 1976 a). Discontinuous reactions involve 4 or 5 phases in 3 and 4 component systems respectively. Such reactions have 1 degree of freedom and take place at a fixed temperature and pressure until one or more of the reactants are completely consumed.

The expression of discontinuous reactions can be deduced from the relative positions of mineral compositions in the AFM diagram and two types can be distinguished. Terminal discontinuous reactions cause the appearance or disappearance of a phase in the AFM diagram and have the general form: $A \rightleftharpoons B + C + D\ (+ E)$. Chemographically A lies within the triangle BCD or inside the tetrahedron BCDE (in four component systems). If the reaction proceeds from left to right with increasing temperature, it is clearly not possible for A to exist at temperatures higher than the temperature at which the reaction takes place at constant pressure. Non-terminal discontinuous reactions cause a tie-line flip between 4 or 5 mineral phases, and have the general form: $A + B \rightleftharpoons C + D\ (+ E)$. Chemographically the A B tie-line crosses tie-line C D, or A lies outside the tetrahedron BCDE and the line AB intersects the plane CDE (in the four component system). If the reaction proceeds from left to right it is now possible for A or B to coexist together with CD(E) at

higher temperatures than the temperature at which the reaction takes place at a fixed pressure. It is also evident that non-terminal reactions involving A or B must take place at lower temperatures than the terminal breakdown reaction of A or B.

C) Schreinemakers analysis

The study of mineral reactions is facilitated by the geometric analysis of phase equilibria based on Schreinemakers' rules as outlined by Zen (1966). The rules are the topological expressions of the fact that a given phase can not take part in an equilibrium reaction outside its own stability field (Mueller and Saxena, 1977). The rules are:

Rule 1: When two divariant assemblages each of n phases meet along an univariant curve of n + 1 phases, then on one side of the univariant curve, the divariant assemblage 1 is relatively less metastable than assemblage 2, whereas on the other side of the curve assemblage 2 is relatively less metastable than assemblage 1.

Rule 2 (Morey-Schreinemakers rule): The P - T region in the neighbourhood of each invariant point is divided by univariant curves into n + 2 sectors ($n > 1$), each of which is $< 180°$ in angular extent and is occupied by one or more divariant assemblages one of which is unique for the sector.

The application of Schreiemakers analysis are explained in more detail in chapter 6.

Derivation of geothermometers and geobarometers

The basis of the thermodynamic calibration of geothermometers and geobarometers is as follows:

1) Experiments involving pure end-member components;
2) Bracketed equilibria of the mineral reactions being examined and
3) Application of fundamental equilibrium conditions.

For any reaction involving components of minerals, fluids or melts:

$$WA + XB \rightleftharpoons YC + ZD \quad \ldots\ldots\ldots\ldots\ldots\ldots (1)$$

phases a b c d

the condition of equilibrium at any pressure and temperature is:

$$Y\mu_C^c + Z\mu_D^d - W\mu_A^a - X\mu_B^b = \Delta G = 0 \quad \ldots\ldots\ldots\ldots (2)$$

where μ_C^c refers to the chemical potential of component C in phase c etc. and Y etc. refers to the number of moles of components involved in the reaction. If the phases are pure then the μ's can be replaced by molar free energies (G c etc) of the phases at the pressure and temperature of interest. This is true because G is defined as the sum of the chemical potentials of each component times the number of moles of each for all the components in a phase or system:

$$G_{Tot} = \Sigma_i \mu_i n_i \quad \ldots\ldots\ldots\ldots\ldots\ldots\ldots\ldots (3)$$

where μ_i is the chemical potential of component i, n_i is the number of moles of component i in the phase of interest and the summation extends over all components. G is therefore a function of the number of moles of components present in the phase, or system of interest. The chemical potential of any component i may be obtained by the partial differentiation of G with respect to n_i for constant amounts of all other components (n_j):

$$\left(\frac{\partial G_{Tot}}{\partial n_i}\right)_{P,T,n_j} = \mu_i \quad \ldots\ldots\ldots\ldots\ldots\ldots\ldots (4)$$

For a pure one component phase it is clear that $G = \mu n$ and

$$\mu = G/n \quad \ldots\ldots\ldots\ldots\ldots\ldots\ldots\ldots\ldots\ldots (5)$$

Therefore, for a pure phase the chemical potential of its constituent component is equal to the molar free energy of the phase. The chemical potentials or free energies can be calculated at any pressure and temperature given molar (or partial molar) enthalpies H, entropies S, heat capacities Cp and volumes V.

$$G_{P,T} = H_{(1,298)} + \int_{298}^{T} CpdT - T\left(S_{298} + \int_{298}^{T} \frac{Cp}{T} dT\right) + \int_{1}^{P} VdP \quad (6)$$

For reactions involving solid phases only it is generally valid to make the assumption ΔCp (Σ(Cp) products - Σ(Cp) reactants) equals 0, and that ΔV is a constant. With these assumptions equatic (6) becomes

$$\Delta G^\circ_{reaction} = \Delta H^\circ_{reaction} - T\Delta S^\circ_{reaction} + (P-1)$$

$$\Delta V^\circ_{reaction} \quad \ldots\ldots\ldots\ldots\ldots\ldots\ldots\ldots\ldots\ldots\ldots\ldots (7)$$

where $\Delta G^\circ_{reaction}$ = free energy of the reaction; $\Delta H^\circ_{reaction}$ = enthalpy of reaction at standard state P,T: $\Delta S^\circ_{reaction}$ = entropy of reaction at standard state P,T, $\Delta V^\circ_{reaction}$ = volume change of reaction at standard state P,T. For solid phases the standard state of pure solids at the pressure and temperature of interest is often used. For vapor phases the assumption that the volume is independent of pressure and temperature is invalid and it is often convenient to use a standard state of pure vapor at 1 bar and the temperature of interest.

The general expression for the chemical potential of a component i in any multicomponental phase (A) is:

$$\mu_i^A = \mu_i^{\circ A} + RT\ln a_i^A \quad \ldots\ldots\ldots\ldots\ldots\ldots\ldots\ldots\ldots\ldots(8)$$

where $\mu_i^{\circ A}$ is the standard chemical potential of component i in phase A, a_i^A is the activity of component i in phase A, R is the gas constant and T is the temperature in K. The standard state to which the standard chemical potential refers is some temperature, pressure and composition of that phase. The activity a_i^A is a function of the composition of phase A and also often of pressure and temperature. When the phase is in the standard state the activity must be equal to 1 and ln a is equal to 0. The activity can be defined as:

$$a_i^A = X_i^A \cdot \gamma_i^A \quad \ldots\ldots\ldots\ldots\ldots\ldots\ldots\ldots\ldots\ldots\ldots(9)$$

where X_i^A is the mole fraction of component i in phase A and γ_i^A is the activity coefficient of component i in phase A. For ideal solid solutions γ is equal to 1 and $a_i^A = X_i^A$.

Substituting equation (8) into (2) leads to the expression:

$$Y\,\mu^{\circ C}_C + Z\,\mu^{\circ d}_D - W\,\mu^{\circ a}_A - X\,\mu^{\circ b}_B + YRT\ln a_C^c + ZRT\ln a_D^d$$

$$- WRT\ln a_A^a - XRT\ln a_B^b = 0 \quad \ldots\ldots\ldots\ldots\ldots\ldots\ldots\ldots(10)$$

ΔG° (standard Gibbs energy of reaction) is now introduced to signify the change in Gibbs energy for the reaction with each of the end-members in its standard state, i.e.

$$\Delta G^\circ = Y\,\mu^{\circ C}_C + Z\,\mu^{\circ d}_D - W\,\mu^{\circ a}_A - X\,\mu^{\circ b}_B \quad \ldots\ldots\ldots\ldots\ldots\ldots\ldots\ldots(11)$$

similarly the activity terms can be summed. Using RTlnK to mean the change of the RTlna terms for the reaction, then:

$$RT\ln K = YRT\ln a_C^c + ZRT\ln a_D^d - WRT\ln a_A^a - XRT\ln a_B^b \quad \ldots\ldots(12)$$

Equation (12) can be simplified to:

$$RT\ln K = RT\ln \frac{(a_C^c)^Y (a_D^d)^Z}{(a_A^a)^W (a_B^b)^X} \quad \ldots\ldots\ldots\ldots\ldots\ldots\ldots\ldots(13)$$

K is called the equilibrium constant. By substituting equations(13) and (11) into (10) the following equation is obtained:

$$0 = \Delta G^\circ + RT\ln K \quad \ldots\ldots\ldots\ldots\ldots\ldots\ldots\ldots\ldots\ldots\ldots\ldots(14)$$

This expression is a restatement of $\Delta\mu = 0$ for a reaction at equilibrium using a standard state for each phase.

Equation (14) may now be combined with eqn (7) to give the following expression:

$$-RT\ln K = \Delta H^\circ_{reaction} - T\,\Delta S^\circ_{reaction} + (P-1)\,\Delta V^\circ_{reaction}$$

$$\Rightarrow 0 = \Delta H^\circ_{reaction} - T\Delta S^\circ_{reaction} + (P-1)\Delta V^\circ_{reaction} + RT\ln K$$

$$\Rightarrow 0 = \Delta H^\circ_{reaction} + (P-1)\,\Delta V^\circ_{reaction} + T\,(R\ln K - \Delta S^\circ_{reaction}) \quad \ldots\ldots\ldots\ldots(15)$$

Equation (15) is generally used to calculate pressures and temperatures for an equilibrium mineral assemblage, using ΔH°, ΔS° and ΔV° values obtained from experimental work or natural mineral assemblages.

APPENDIX 17 Mineral compositions and molar volumes used in the calculation of univariant lines

Mineral	Formula	Molar volume[c] at 25° C
		(cc)
albite (ab)	$NaAlSi_3O_8$	100,0
almandine (gar)	$Mg_{0,3}Fe_{2,7}Al_2Si_3O_{12}$	115,3
andalusite (and)	Al_2SiO_5	51,5
biotite[a] (bi)	$KMg_{1,3}Fe_{1,3}Al_{0,4}(Al_{1,4}Si_{2,6}O_{10})(OH)_2$	151,0
biotite[b] (bi)	$KMg_{0,9}Fe_{1,7}Al_{0,4}(Al_{1,4}Si_{2,6}O_{10})(OH)_2$	151,0
chlorite (chl)	$Mg_{2,5}Fe_{2,0}Al_{1,5}(Al_{1,5}Si_{2,5}O_{10})\ (OH)_8$	209,0
chloritoid (ctd)	$Mg_{0,2}Fe_{0,8}Al_2SiO_5\ (OH)_2$	69,7
cordierite (cord)	$Mg_{1,4}Fe_{0,6}Al_3(AlSi_5O_{18})$	233,0
corundum (cor)	Al_2O_3	25,6
gedrite (ged)	$Na_{0,5}Mg_{1,5}Fe_{3,5}Al_2(Al_{2,5}Si_{5,5}O_{22})\ (OH)_2$	265,9
K-feldspar (K-spar)	$KAlSi_3O_8$	108,9
muscovite (musc)	$KAl_2(AlSi_3O_{10})\ (OH)_2$	141,0
orthopyroxene (opx)	$Mg_{0,4}Fe_{0,6}SiO_3$	31,3
quartz (qz)	SiO_2	22,7

APPENDIX 17 (Continued)

Mineral	Formula	Molar volume[c] at 25°C
		(cc)
sillimanite (sill)	Al_2SiO_5	49,9
spinel (sp)	$Mg_{0,3}Fe_{0,7}Al_2O_4$	40,7

a : compositon of biotite used in section 6.1.1.

b : composition of biotite used in section 6.1.2.

c : volumes from Albee (1965 a) and Robie et al. (1978)